

Crystal Engineering with 2,2':6',2''- Terpyridine Derivatives and their Metal Complexes:

From simple building blocks to coordination
polymers and networks

Inauguraldissertation

zur
Erlangung der Würde eines Doktors der Philosophie
Vorgelegt der
Philosophisch-Naturwissenschaftlichen Fakultät
Der Universität Basel

Von

Jonathon Edward Beves
aus Australien

Genehmigt von der Philosophisch-Naturwissenschaftlichen Fakultät der auf
Antrag

von:

Prof. Dr. E. C. Constable

Prof. Dr. T. R. Ward

Basel, den 9 December, 2008.

Prof Dr. Eberhard Parlow
Dekan der Philosophisch-
Naturewissenschaftlichen Fakultät

Open up your mind and go your own way.

Max Cavalera, Brazilian genius

Table of Contents

<i>Acknowledgements</i>	<i>vii</i>
<i>Abstract</i> ix	
<i>Compound Numbering</i>	<i>xiii</i>
Chapter 1 Introduction	1
1.1. <i>Supramolecular Chemistry</i>	1
1.2. <i>Terpyridine in supramolecular chemistry</i>	8
1.3. ‘ <i>Crystal Engineering</i> ’ as <i>Supramolecular Chemistry</i>	10
1.4. <i>This thesis</i>	16
Chapter 2 Preparation and characterisation of 4'-functionalised-hydrazone-2,2':6',2''-terpyridine ligands	17
2.1. <i>Introduction</i>	17
2.2. <i>4'-Hydrazone functionalised-2,2':6',2''-terpyridine ligands</i>	17
2.3. <i>Neutral ligands: solution behaviour</i>	20
2.3.1. <i>Variable temperature NMR</i>	22
2.4. <i>Identification of dynamic processes</i>	25
2.5. <i>Protonated ligands</i>	27
2.6. <i>Identification of dynamic processes of protonated ligands</i>	30
2.7. <i>Where is the site of protonation and how does this restrict rotation?</i>	31
2.8. <i>Substituent Effects</i>	37
2.8.1. <i>¹H and ¹³C NMR spectroscopy</i>	37
2.8.2. <i>UV-Vis spectra of select ligands</i>	39
2.9. <i>Deprotonation</i>	41
2.10. <i>X-ray structure characterisation</i>	42
2.11. <i>X-Ray crystal structures of neutral ligands</i>	43
2.12. <i>X-Ray crystal structures of mono protonated ligands</i>	57
2.13. <i>X-Ray crystal structures of di-protonated ligands</i>	64
2.14. <i>Summary of crystal structures</i>	67
2.15. <i>Experimental</i>	70
2.16. <i>Crystal Structure Determinations</i>	89
Chapter 3 Iron(II) and ruthenium(II) complexes of 4'-hydrazone functionalised 2,2':6',2''-terpyridine ligands	93
3.1. <i>General considerations</i>	93
3.2. <i>Synthesis of Iron(II) and Ruthenium(II) complexes</i>	93
3.3. <i>Characterisation of Fe(II) and Ru(II) complexes</i>	94
3.4. <i>Substituent effects</i>	98
3.5. <i>UV-Vis spectroscopy of Fe(II) and Ru(II) complexes</i>	99

3.6.	<i>The effect of deprotonation</i>	100
3.7.	<i>Electrochemistry</i>	103
3.8.	<i>X-ray crystal structures</i>	105
3.9.	<i>Iron(II) and ruthenium(II) complexes of N-Me ligand (20)</i>	119
3.9.1.	<i>Electrochemistry of N-Me derivatives [Fe(20)₂](PF₆)₂ and [Ru(20)₂](PF₆)₂</i>	120
3.9.2.	<i>X-Ray crystal structures</i>	122
3.10.	<i>Hydrazone bridges</i>	126
3.11.	<i>Experimental</i>	132
3.12.	<i>Crystal Data</i>	141
Chapter 4 Building blocks for extended structures: iron(II) and ruthenium(II) bis(terpyridine) complexes with pendant donors		144
4.1.	<i>General considerations</i>	144
4.2.	<i>Preparation of ligands</i>	148
4.3.	<i>Preparation of Fe(II) and Ru(II) complexes</i>	154
4.4.	<i>Preparation of Cu(II) and Pd(II) complexes</i>	159
4.5.	<i>Discussion of X-ray crystal structures</i>	161
4.6.	<i>Summary of crystal structures</i>	192
4.7.	<i>Experimental</i>	192
4.7.1.	<i>Precursors</i>	192
4.7.2.	<i>Ligands</i>	193
4.7.3.	<i>Fe(II) complexes</i>	196
4.7.4.	<i>Ru(II) complexes</i>	199
4.7.5.	<i>Cu(II) complexes</i>	208
4.7.6.	<i>Pd(II) complexes</i>	208
4.7.7.	<i>Ni(II) complex</i>	209
4.7.8.	<i>Crystal structure determinations: general</i>	210
4.7.9.	<i>Crystall data for individual structures</i>	210
Chapter 5 Coordination polymers and networks		216
5.1.	<i>General considerations</i>	216
5.2.	<i>Self-complementary hydrogen-bonded polymers</i>	216
5.3.	<i>One dimensional coordination polymers</i>	222
5.4.	<i>Two-dimensional coordination sheets</i>	233
5.5.	<i>Conclusions</i>	239
5.6.	<i>Experimental</i>	240
Chapter 6 4'-Pyridyl hydrazone functionalised 2,2':6',2''-terpyridine ligands and their Fe(II) and Ru(II) complexes		244
6.1.	<i>General considerations</i>	244
6.2.	<i>Synthesis of ligands</i>	244
6.3.	<i>Synthesis and characterisation of Fe(II) complexes</i>	244

6.4.	<i>Synthesis and characterisation of Ru(II) complexes</i>	248
6.5.	<i>Solution behaviour of Ru(II) complexes: UV-vis</i>	249
6.6.	<i>Crystal structures of complexes of pyridyl derivatives 26 and 27</i>	251
6.7.	<i>Extended structures: A hydrogen bonded polymer and a coordination polymer</i>	258
6.8.	<i>Experimental</i>	262
	Curriculum Vitae	266
	References	269

Acknowledgements

Firstly I'd like to thank my supervisors, Prof Ed Constable and Prof Catherine Housecroft for giving me the fantastic opportunity of working (and living!) in Switzerland! I'm especially grateful for the independence you both gave me with my research, for being permanently optimistic, generous and a great inspiration in research. The Constable/Housecroft group is a truly unique work environment, and I will miss it dearly (and waiting for the tv show).

As reflected by the content of this thesis, a lot of credit is due to the Basel squadron of crystallographers who are responsible for solving the vast majority of the crystal structures: Markus Neuburger and Silvia Schaffner, and more recently, Jennifer Zampese. Thanks so much for creating such marvellous things from such tiny crystals, this work would definitely not have been possible without you. Thanks especially to Jennifer for patiently teaching me how to actually 'do' crystallography!

Dr Daniel Häussinger is particularly acknowledged, not only for being the hardest working guy in the department, but for helping me with every conceivable NMR problem often at irregular times.

Special mention for the other technical staff which have made life so much easier here: Klas Kulicke, Herr Lips, Franz Stelin, Frau Buchmüller of Reisefonds fame and everyone at the Studiensekretariat at Petersplatz. Thanks guys for showing me a truly Swiss experience.

To the members of the Constable/Housecroft group past and present with an honourable mention for the night dwellers: Michael Malarek, Valerie Jullien (thanks for being such a selfless help with everything!), Conor Brennan (lots of amusing, if hazy, memories!), and crazy Valerie Chaurin – it was always fun to have you guys around! My partner in crime, Emma “Mrs Bean” Dunphy, has been an excellent workmate, friend and source of entertainment- thanks for all the unforgettable memories! Ellie Shadlow, deserves mention for being truly one of the strangest people I've ever met (and a tolerant flatmate!), other members of the ‘old lab’: Ana, Kate, Jason, Marc and Paulina: big

thanks for tolerating my invasive mess and for generally being reasonable people. Liselotte is particularly thanked for her help with the autotitrator and with the TGA.

My colleagues at the University of Sydney, especially Prof. Cameron Kepert, are especially thanked for letting me work briefly in their lab and for the productive results and useful input they provided. Dr David Price is acknowledged for solving several very exciting crystal structures.

Dr Tony Keene at the University of Bern is thanked for rapid magnetic measurements and interpretations and for being an all-round decent guy.

I owe the staff and regulars at the Kurds, especially Paulina the Slovak and Yasser, tremendous thanks for providing us with such a friendly and cheap place to will the hours away. Other ‘Kurds’: Andy and his charming girlfriend, Benny Hill, Frank Zappa, Big Red Machine, Bluey, Dave and his grandma, Flaming Fabulous, the Scary Dykes, Funny Face, the crazy Scot, Christians from Africa and other people that I probably shouldn’t recognise in the street.

A lot of credit is due to my wacky family back in Australia, who despite being far away always stay in great contact and are just as amusing from a distance. Thanks for your continuing support, encouragement and eventual acceptance of my relentless pursuit of activities which lead me further and further away from a ‘real job’!

Finally thanks to my wonderful Emma: tack så mycket min lille älskling! Utan dig jag vet inte vad jag ska äta!

Abstract

This thesis concerns the design of ligands for use in the construction of larger supramolecular systems, with emphasis on the application of 4'-substituted 2,2',6',2"-terpyridine ligands and their iron(II) and ruthenium(II) complexes in crystal engineering. The first section considers 4'-hydrazone functionalized 2,2',6',2"-terpyridines and their dynamic behaviour in solution and structural characteristics in the solid state, with respect to protonation. Neutral, mono- and di-protonated ligands are considered. The iron(II) and ruthenium(II) complexes of these ligands are reported and their properties studied by variable temperature NMR, UV-visible spectroscopy and single crystal X-ray crystallography. Subtle changes in substituents were found to have dramatic effects on crystal packing and some common packing arrangements were identified. A range of potential ‘expanded ligands’ (complexes which can themselves act as ligands for additional metal centres), are introduced in the next section. These can be potentially used to bridge metal centres to form both discrete and infinite structures, in particular in the solid state. In a systematic study of single crystal X-ray crystal structures of these complexes many were found to be more flexible than they first appear, and that the crystal packing arrangements were often sensitive to solvent. The next section describes the first crystallographically characterized coordination polymers and networks which include metal bis(terpyridine) units. Self-complementary hydrogen bonding was also found to be a stabilizing motif, with a number of such structures prepared. The final chapter blends the ideas of previous sections: 4'-(x-pyridyl) functionalized 2,2',6',2"-terpyridine ligands are used to form ‘expanded ligands’ with iron(II) and ruthenium(II) centres. These were characterized in solution, with protonation of the distant pendant pyridyl ring found to significantly influence the MLCT absorption of the complexes. These complexes were incorporated into two larger structures and characterised by single crystal X-ray crystallography. A self-complementary hydrogen bonded polymer which possesses nanopores through the crystal lattice is reported. Iron bis(thiocyanate) was also used to form a bridged coordination polymer.

Summary

Chapter 2: Preparation and characterisation of 4'-functionalised-hydrazone-2,2':6',2"-terpyridine ligands

A family of 4'-(hydrazone)-2,2':6',2"-terpyridine ligands are presented and characterised. Their dynamic solution behaviour is examined with respect to protonation. A detailed examination of 14 X-ray crystal structures of neutral, mono- and di-protonated ligands is presented.

Chapter 3: Iron(II) and Ruthenium(II) complexes of 4'-hydrazone functionalised 2,2':6',2"-terpyridine ligands

The Fe(II) and Ru(II) complexes of 4'-hydrazone functionalised ,2':6',2"-terpyridine ligands are synthesised. Solution state behaviour is characterised by ^1H , ^{13}C (and variable temperature) NMR and UV-vis spectroscopy and electrochemical properties are investigated. The X-ray crystal structures of 11 complexes are presented and their packing effects discussed.

Chapter 4: Building blocks for extended structures: iron(II) and ruthenium(II) bis(terpyridine) complexes with pendant donors

A range of prototype metal complexes which may function as components for larger assemblies are prepared and characterised. The X-ray crystal structures of 20 complexes are presented and structural variation is discussed.

Chapter 5: Coordination polymers and networks

Using the complexes introduced in Chapter 4, a collection of hydrogen bonded and coordination networks are presented.

Chapter 6: 4'-Pyridylhydrazone functionalised 2,2':6',2"-terpyridine ligands and their Fe(II) and Ru(II) complexes

Bringing together the concepts introduced in Chapter 2 and 5, this chapter presents Fe(II) and Ru(II) complexes of 4'-pyridylhydrazone functionalised 2,2':6',2"-terpyridines and their use to form coordination polymers and hydrogen bonded polymers.

Parts of the work published in this thesis have been published in the following publications:

Chapter 2:

4'-Hydrazone derivatives of 2, 2':6',2''-terpyridine: protonation and substituent effects

J. E. Beves, E. C. Constable, C. E. Housecroft, M. Neuburger, S. Schaffner, J. A. Zampese, *Eur. J. Org. Chem.*, 2008, 3569.

Chapter 3: None

Chapter 4:

Expanding the 4,4'-bipyridine ligand: structural variation in {M(pytpy)₂}²⁺ complexes (pytpy = 4'-(4-pyridyl)-2,2':6',2''-terpyridine, M = Fe, Ni, Ru) and assembly of the hydrogen-bonded, one-dimensional polymer {[Ru(pytpy)(Hpytpy)]_n}_{3n+}

J. E. Beves, D. J. Bray, J. K. Clegg, E. C. Constable, C. E. Housecroft, K. A. Jolliffe, C. J. Kepert, L. F. Lindoy, M. Neuburger, D. J. Price, S. Schaffner, F. Schaper. *Inorg. Chim. Acta*, 2008, **361**, 2582.

A pyrazolyl-terminated 2,2':6',2''-terpyridine ligand: iron(II), ruthenium(II) and palladium(II) complexes of 4'-(3,5-dimethylpyrazol-1-yl)-2,2':6',2''-terpyridine
J. E. Beves, E. C. Constable, C. E. Housecroft, M. Neuburger, S. Schaffner, *Polyhedron*, 2008, accepted.

Vectorial property dependence in bis{4'-(n-pyridyl)-2,2':6',2''-terpyridine}iron(II) and ruthenium(II) complexes with n = 2, 3 and 4
J. E. Beves, E. L. Dunphy, E. C. Constable, C. E. Housecroft, C. J. Kepert, M. Neuburger, D. J. Price and S. Schaffner. *Dalton Trans.* 2008, 386-396.

A palladium(II) complex of 4'-(4-pyridyl)-2,2':6',2''-terpyridine: Lattice control through an interplay of stacking and hydrogen bonding effects.
J. E. Beves, E. C. Constable, C. E. Housecroft, M. Neuburger, S. Schaffner, *Inorg. Chem. Commun.*, 2007, **10**, 1185-1188.

Chapter 5:

The first example of a coordination polymer from the expanded 4,4'-bipyridine ligand [Ru(pytpy)₂]²⁺ (pytpy = 4'-(4-pyridyl)-2,2':6',2''-terpyridine).
J. E. Beves, E. C. Constable, C. E. Housecroft, C. J. Kepert, D. J. Price, *CrystEngComm*, 2007, **9**, 456-459.

The conjugate acid of bis{4'-(4-pyridyl)-2,2':6',2''-terpyridine}iron(II) as a self-complementary hydrogen-bonded building block
J. E. Beves, E. C. Constable, C. E. Housecroft, C. J. Kepert, M. Neuburger, D. J. Price and S. Schaffner, *CrystEngComm* 2007, **9**, 1073-1077.

A one-dimensional copper(II) coordination polymer containing $[Fe(pytpy)_2]^{2+}$ ($pytpy = 4'-(4\text{-pyridyl})-2,2':6',2''\text{-terpyridine}$) as an expanded 4,4'-bipyridine ligand: a hydrogen-bonded network penetrated by rod-like polymers.

J. E. Beves, E. C. Constable, C. E. Housecroft, M. Neuburger and S. Schaffner, *CrystEngComm*, 2008, **10**, 344.

Homoleptic metal complexes of 4'-(5-pyrimidinyl)-2,2':6',2''-terpyridine: tetrafurcated expanded ligands

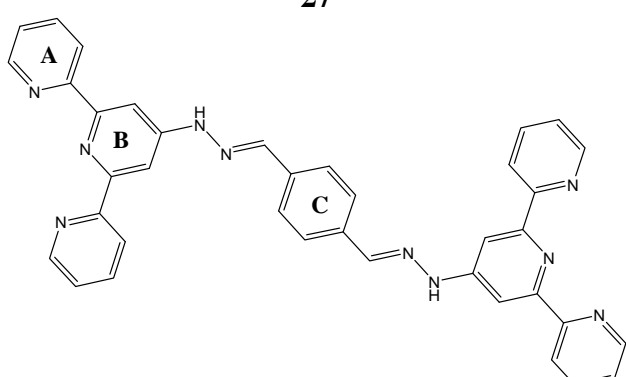
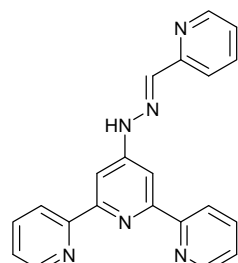
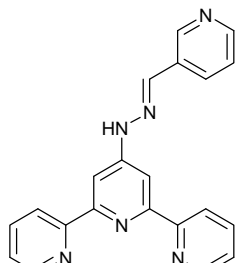
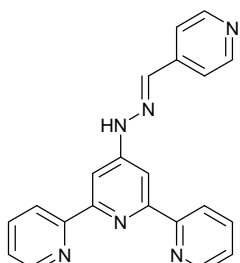
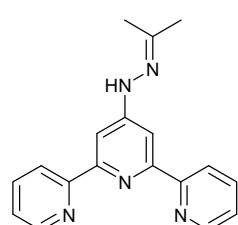
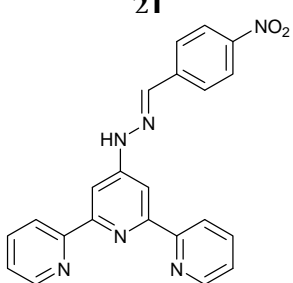
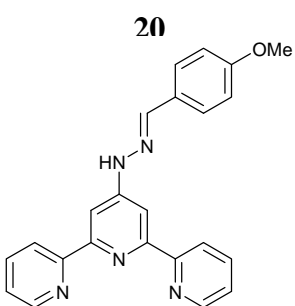
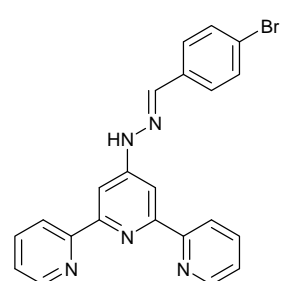
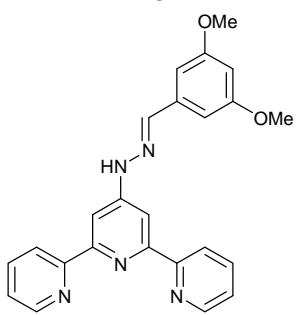
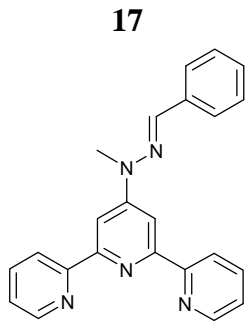
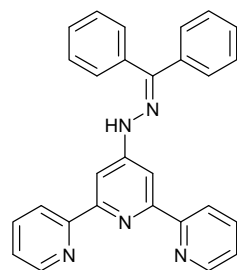
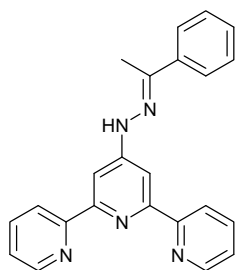
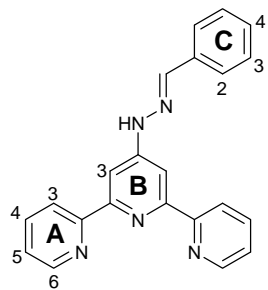
J. E. Beves, E. C. Constable, S. Decurtins, E. L. Dunphy, C. E. Housecroft, T. D. Keene, M. Neuburger, S. Schaffner, *CrystEngComm*, 2008, **10**, 986.

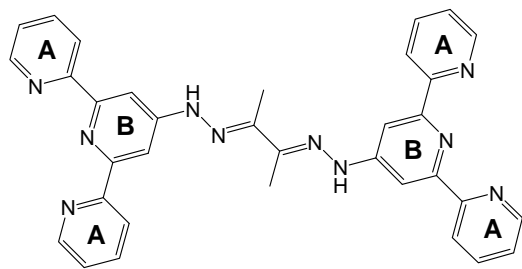
Chapter 6:

Curly-curly, loop-loop: homoleptic metal(II) complexes of pyridinecarbaldehyde 4'-(2,2':6',2''-terpyridyl)hydrazones and their coordination polymers

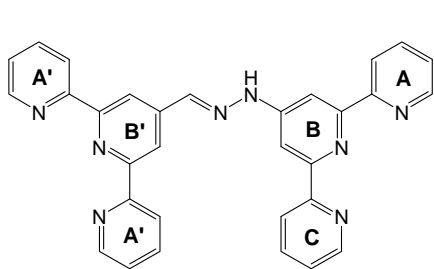
J. E. Beves, E. C. Constable, C. E. Housecroft, C. J. Kepert, M. Neuburger, D. J. Price, S. Schaffner, *Dalton Trans.*, *in press*.

Compound Numbering

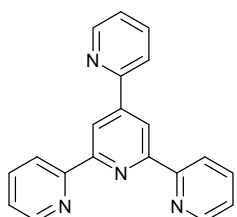




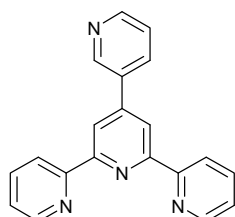
30



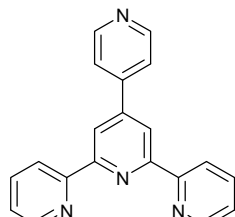
31



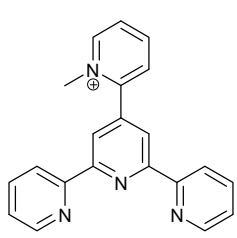
33



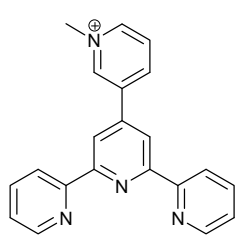
34



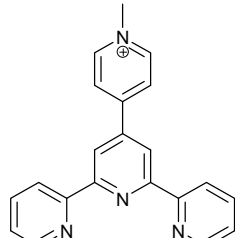
9



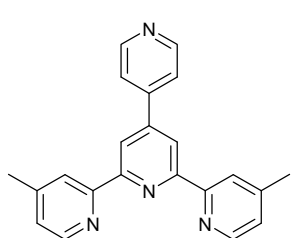
35



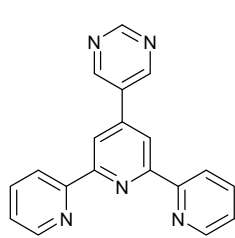
36



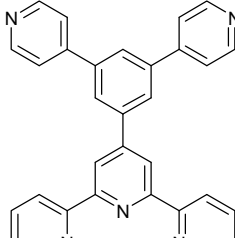
37



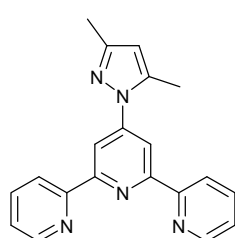
38



39



40



41

Chapter 1 Introduction

1.1. Supramolecular Chemistry

Interest in ‘supramolecular’ chemistry has exploded in the 20 years following the 1987 Nobel Prize awarded to Cram, Lehn and Pedersen (Figure 1-1). Supramolecular chemistry is notoriously difficult to define¹ and is best considered a philosophy to be applied to chemistry. Many different fields of chemistry - ranging from organic host-guest interactions to classical coordination chemistry to crystallography – have been placed under the single title of supramolecular chemistry. What is supramolecular chemistry and why is it so popular?

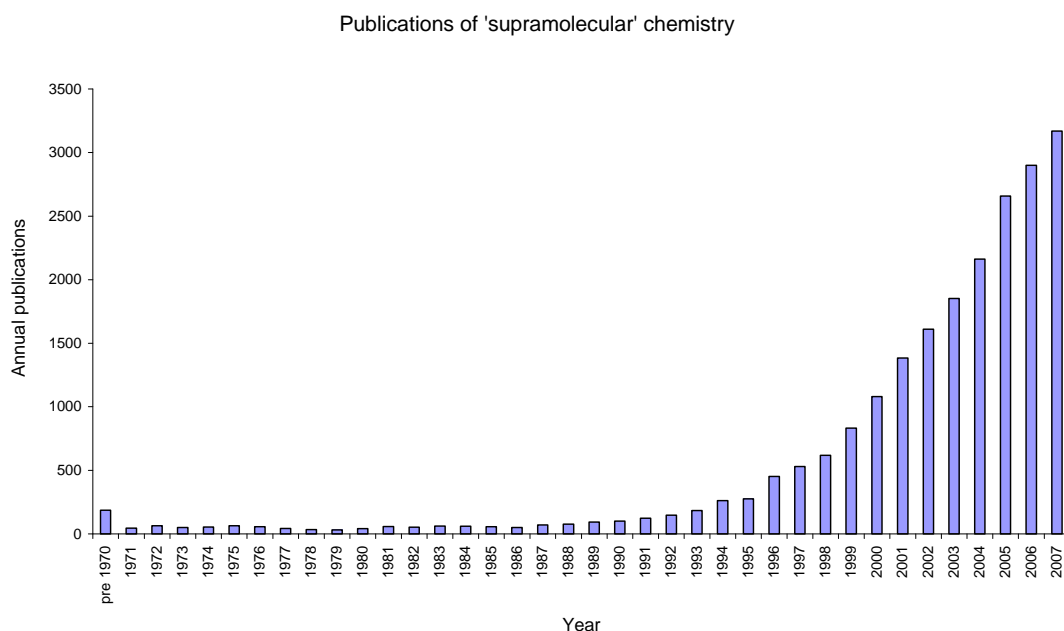


Figure 1-1 Scifinder search for ‘supramolecular’ October 2008, 2008 data excluded.

Traditionally chemists have used irreversible reactions and the formation of strong covalent bonds to prepare new compounds. By contrast, supramolecular chemistry focuses solely on reversible (usually weak) interactions (and studies of combinations of interactions) *between* molecules. Such intermolecular interactions include π - π stacking²⁴ and other π interactions,⁵⁻⁹ hydrogen bonding,¹⁰⁻¹³ hydrophobic interactions, van der

Waals' interactions, dipole-dipole interactions and metal-ligand coordination bonds,¹⁴ the latter of which can be both strong and highly directional.

Nature has provided much inspiration for supramolecular chemistry as reversible weak interactions are used to assemble small building blocks into virtually all larger natural structures ranging from DNA to proteins to entire complex systems such as people! However, just as birds inspired mankind to fly but planes are not direct mimics of birds, most supramolecular chemists do not aim to directly mimic Nature but rather to develop wholly synthetic approaches. Therefore, rather than focusing on naturally occurring systems such as proteins or nucleic acids, supramolecular chemistry primarily makes use of synthetic systems such as crown ethers, calixarenes, cyclodextrins, a range of synthetic hydrogen bond donor-acceptor pairs, and ligands in combination with suitable metal ions.

A central concept in supramolecular chemistry is that of 'self-assembly': the spontaneous assembly of molecules into structured, stable, non-covalently joined aggregates.¹⁵ The simplest concept for the design of ordered structures parallels that which is widely utilised by Nature, namely the use of 'pre-programmed' complementary subunits. Much of supramolecular chemistry depends upon the presence of weak intermolecular interactions and their reversible formation and dissociation. This grants supramolecular systems a major advantage not available to covalent systems – the capacity for 'self-correction'.¹⁶ Additionally, the simultaneous assembly of pre-organised building blocks is normally highly convergent, requiring fewer steps than stepwise covalent bond formation. This results in a potential for quantitative yields with the formation of almost defect-free, thermodynamically favoured structures.¹⁶ Where applicable, the latter represents a major advantage over classical stepwise organic synthesis.¹⁵ It is largely for this reason that rationally designed, self-assembly continues to receive very considerable attention.

The use of metals in supramolecular chemistry (conveniently termed metallosupramolecular¹⁷) play essentially two (often complementary) roles. The first is that of purely structural components. While biological systems rely on many weak (mainly hydrogen bond) interactions (typical energies ranging from 5-25 kJ/mol),¹⁰

metal-ligand bonds are much stronger (typically ~ 200 kJ/mol) and often highly directional, aiding the formation of well-defined rigid geometries. Many metal ions have well defined preferences for specific donors and coordination geometries.¹⁸

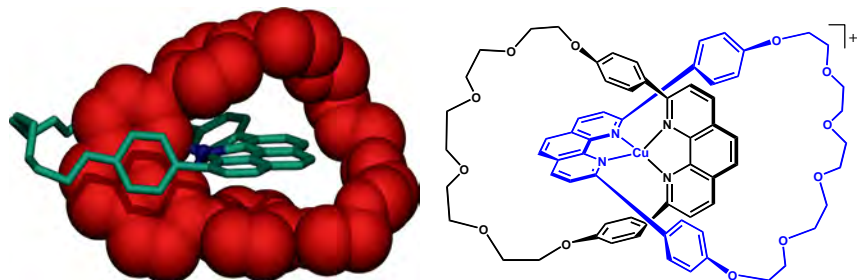


Figure 1-2 The first X-ray crystal structure of a catenane, prepared by Sauvage *et al.*¹⁹

For example, Cu(I) (d^{10}) is known²⁰ to prefer a distorted tetrahedral geometry whereas Cu(II) (d^9) prefers to be octahedral, or 5-coordinate²¹ and Pd(II), being a second row transition metal with a d^8 configuration, almost exclusively adopts a square planar geometry.²² Therefore, in combination with appropriate organic ligands, these preferences can be used to direct the assembly of multi-component structures. Classic examples of the use of metal ions to direct the assembly of discrete structures include catenanes based on Cu(I) introduced by Sauvage (Figure 1-2),²³ helicates based on Cu(I) by Lehn²⁴ and Cd(II) by Constable^{25, 26} (Figure 1-3) and molecular squares using Pd(II) groups by Fujita (see Figure 1-4).^{27, 28}

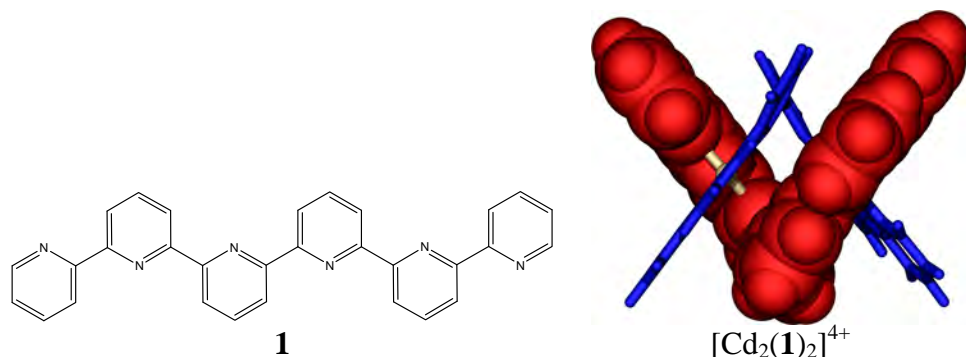


Figure 1-3 The X-ray crystal structure of a [2 x 2] helicate formed with Cd(II) and 2,2':6',2":6",2'':6'',2''':6''',2''''-sexipyridine (**1**).²⁶

Fujita^{27, 28} designed the first molecular square using a square planar metal centre, Pd(II), with two cis-positions occupied by a strongly bound bidentate ligand, 1,2-ethylenediamine (en) and the remaining two positions occupied by weakly bound nitrate

ligands, which could be easily displaced by better ligands, such as pyridine. Simple mixing of $\text{Pd}(\text{en})(\text{NO}_3)_2$ (**2**) with 4,4'-bipyridine (**3**) resulted in the spontaneous and quantitative formation of a molecular square (Figure 1-4). However, the choice of this corner unit was not trivial. A large range of metal ions, blocking groups and bridging ligands attempted before the landmark discovery was made (although this has only recently had been reported).²² This highlights one of the pitfalls of supramolecular chemistry: although simple concepts are very useful in designing new assemblies, systems are (usually) not as simple as they are portrayed.

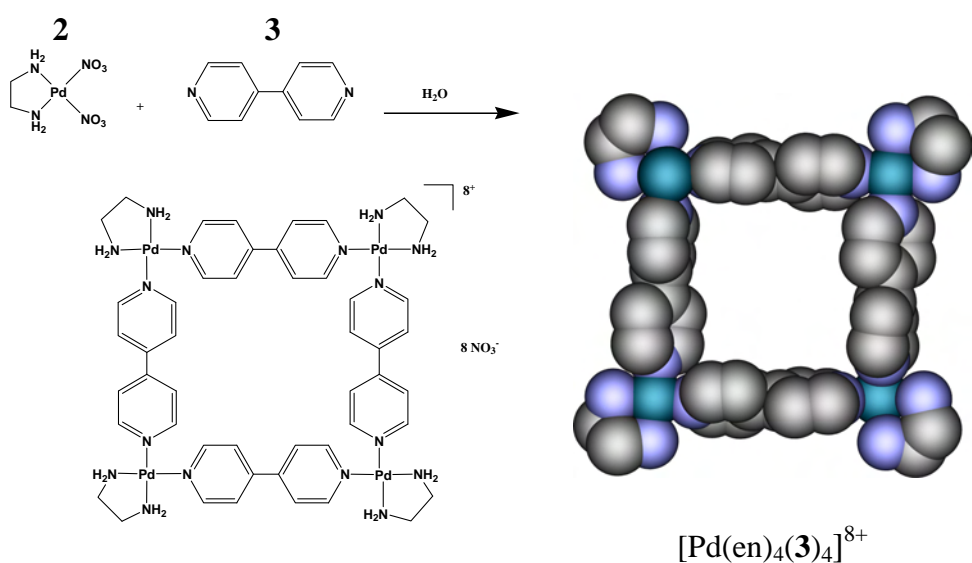


Figure 1-4 The first molecular square, prepared by Fujita^{27, 28} was subsequently characterised by X-ray crystallography.²⁹ en = 1,2-diaminoethane.

However, from these simple starting concepts, considerably more complex architectures have been developed. It is widely accepted that entropy drives systems to form structures from the smallest number of components,³⁰⁻³⁶ although the use of rigid ligands has allowed the formation of much larger structures. For example, Fujita has prepared impressive polyhedra from a large number of individual components.^{28, 37} Recent examples include cages³⁸ (e.g. Figure 1-5), some of which contain ‘hydrocarbon droplets’ which can dissolve dye molecules.³⁹ Other related reports include chiral cages by Raymond⁴⁰ and capsules which exhibit selective anion binding by Lindoy.⁴¹ Catenanes have been extended to contain complex multinuclear systems incorporating multiple bridged porphyrin groups⁴² (Figure 1-6) and helicates have been recently used by Nitschke to form molecular wires.⁴³ Another recent example to take advantage of the

preference^{i,21} of Cu(II) to adopt a 5-coordinate coordination environment is the self-assembly of a M₆L₆ hexamer from a ligand with joined bidentate and tridenate binding motifs (Figure 1-7).⁴⁴

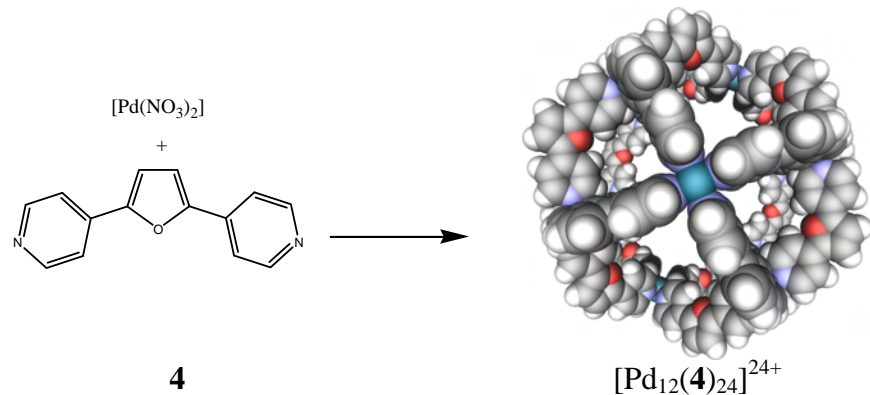


Figure 1-5 The self-assembly of a nano-scale sphere from 36 small components reported by Fujita (X-ray crystal structure shown).³⁸

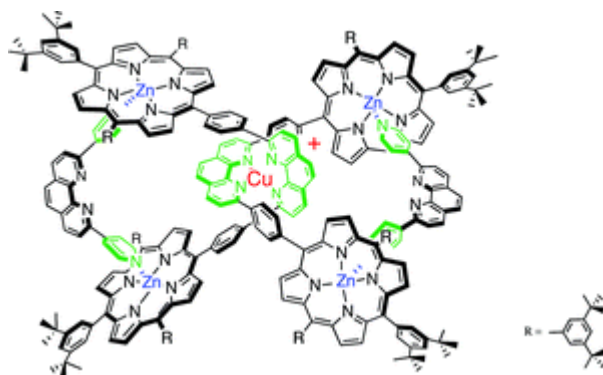


Figure 1-6 Recent examples of catenanes by Sauvage include multinuclear systems containing multiple porphyrin groups.⁴²

The second role of metals in metallosupramolecular chemistry is as a source of properties such as chromophore or redox centres, luminescent or magnetic properties, or sites to conduct reactions, such as for catalysis or guest binding. Luminescent metallosupramolecular structures have been recently the subject of review^{45, 46} and supramolecular catalysis has recently seen an entire book dedicated to the topic.⁴⁷ Photo-driven molecular devices have been recently surveyed,⁴⁸⁻⁵⁰ with Ru(II) complexes

ⁱ It should be noted that although Cu(II) does form 5-coordinate complexes, four- and six-coordinate complexes are both very common, with a favoured coordination number of six although ligand asymmetry and Jahn-Teller distortions often result in one or two weakly bound ligands. 5-coordinate systems are preferred when tpy and bipy/phen ligands are available.

remaining the major focus,⁴⁹ and the development of metallosupramolecular systems with useful magnetic properties has also been reviewed in the past year.⁵¹ A few recent examples will now be given.

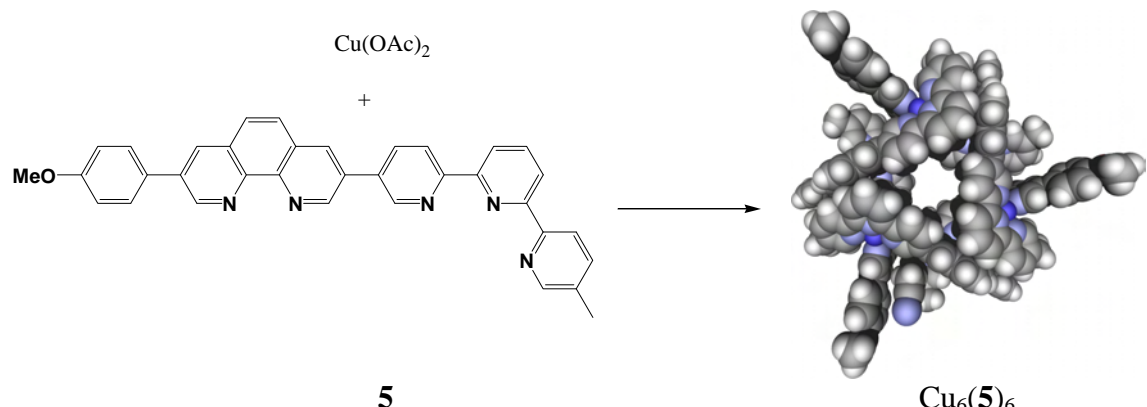


Figure 1-7 Metallosupramolecular hexamer formed from $\text{Cu}(\text{OAc})_2$ reported by Coronado (X-ray crystal structure shown).⁴⁴

Hupp and co-workers have prepared a number of molecular squares which have been used as catalysts.⁵² For example, Figure 1-8 shows a structure which has been suggested to act as an artificial enzyme. The protective cage of the square prolongs the lifetime of the free manganese-porphyrin epoxidation catalyst by 20-fold and the restricted environment also may affect significant substrate size-selectivity in catalytic epoxidation. This type of reactivity within confined spaces has also been reviewed.^{53, 54}

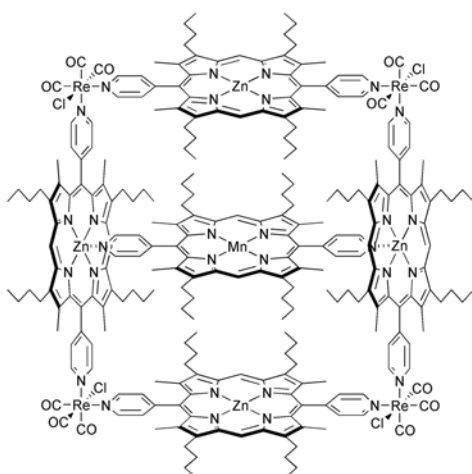


Figure 1-8 An artificial enzyme: a molecular square with an encapsulated Mn(II) porphyrin, prepared by Hupp.⁵²

Stepwise assembly of [2 x 2] grids allowed the preparation of mixed Co(III)/Zn(II) systems by Lehn,⁵⁵ an example of which is shown in Figure 1-9. The use of ionisable

(NH) and non-ionisable (N-Me) groups allowed the redox properties of the metal to be controlled according to the charge in the binding pocket. Related Fe(II)-containing systems could be directed to low spin, high spin or spin crossover depending on the steric effects of the substituents employed.

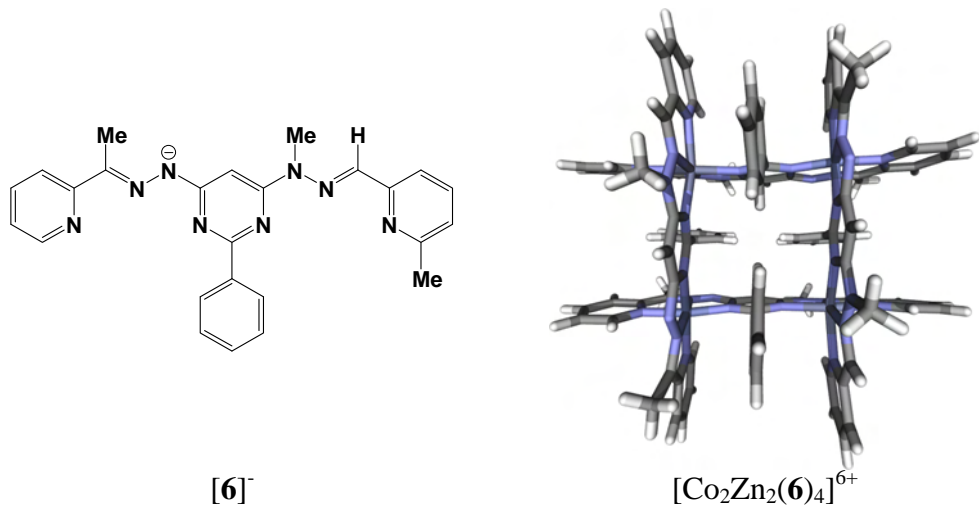
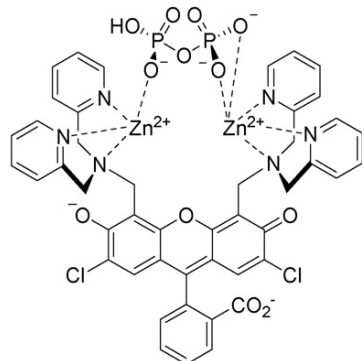


Figure 1-9 The solid-state structure of [2x2] grid array $[\text{Co}^{\text{III}}_2\text{Zn}^{\text{II}}_2(\mathbf{6})_4](\text{PF}_6)_3(\text{BF}_4)_3^{55}$ with addressable redox centres.

Coordination complexes have also received considerable attention as selective anion receptors.^{56, 57} An example of which (Figure 1-10) is a dimetallic Zn(II) complex which acts as a fluorescent sensor for pyrophosphate in water.



7

Figure 1-10 Yoon and coworkers demonstrated that complex **7** acts as a fluorescent sensor for pyrophosphate in water at physiological pH.⁵⁸

A considerably more complex system of a ‘molecular abacus’ has been reported by Balzani and Stoddart.⁵⁹ In this system, visible light is harvested by the metal-containing photosensitiser to drive the movement of an electron donor macrocycle between two electron acceptor sites.

These examples represent only a very small number of the vast number of different metallosupramolecular systems that have been reported,¹⁶ developments have been reviewed annually for the past several years.⁶⁰⁻⁶⁸

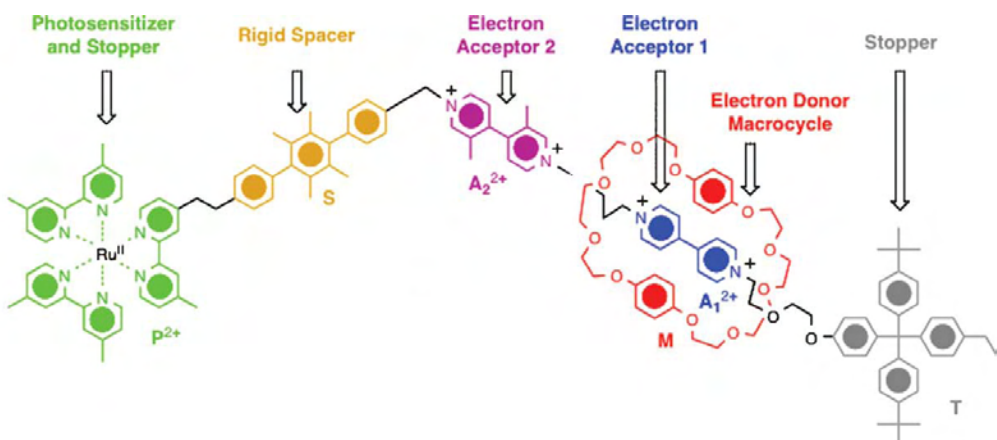
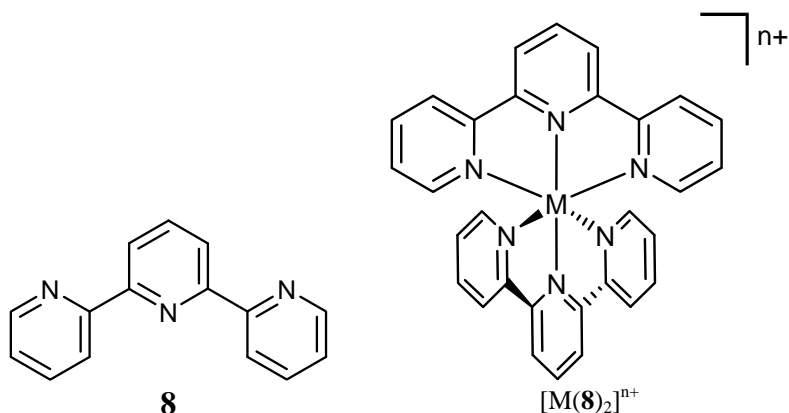


Figure 1-11 A ‘molecular abacus’ reported by Balzani and Stoddart.⁵⁹

1.2. *Terpyridine in supramolecular chemistry*



The tridentate polypyridyl ligand 2,2':6',2''-terpyridine (tpy, **8**) is enjoying enormous and continuing popularity in supramolecular chemistry.⁶⁹ This ligand forms very stable octahedral complexes with a wide range of metal ions (e.g., logK for Fe(tpy)₂ is logK >20)^{70, 71} and has a major advantage over the bidentate analogue 2,2'-bipyridine (bpy): unlike {M(bpy)₃}ⁿ⁺ complexes, {M(tpy)₂}ⁿ⁺ complexes are achiral (provided only symmetrical substitution of the tpy ligands are used) which becomes particularly important when considering multinuclear systems. The origin of this lack of chirality can be seen in Figure 1-12 which compares a {M(bpy)₃} centre with a symmetrically

substituted $M(tpy)_2$ centre. The former has two enantiomers (Λ and Δ) as is the case for ideal octahedral metal complexes. However, in $\{M(tpy)_2\}$, where three of the donor atoms are coplanar, the mirror images are superimposable (the complex possesses an inversion centre at the metal atom), rendering the complex achiral. Where desired, chirality can be introduced into $\{M(tpy)_2\}$ complexes where desired by attachment of chiral groups to the tpy ligand, several examples of which are known.⁷²⁻⁸¹

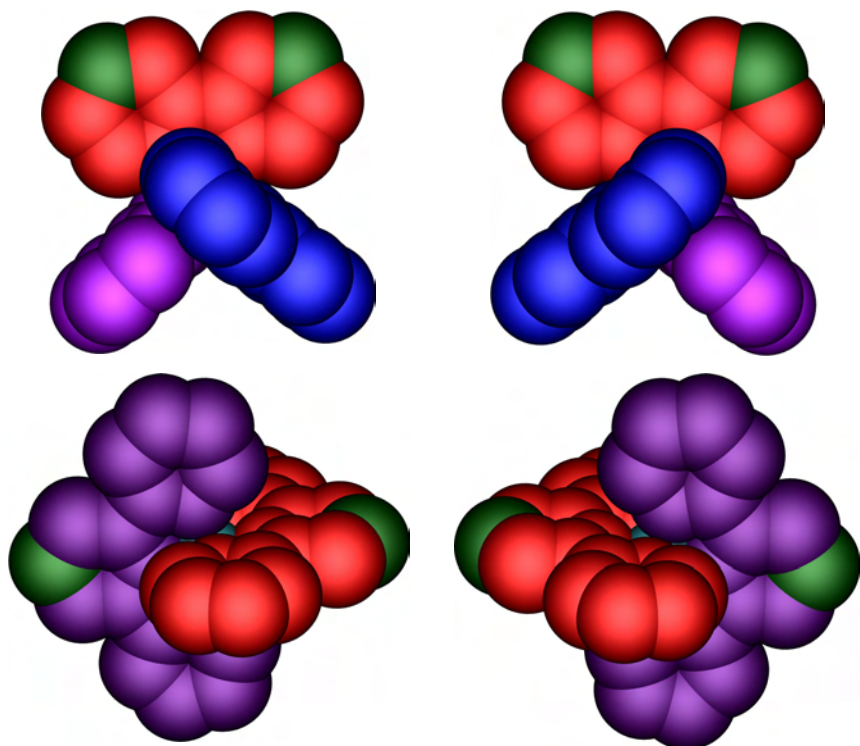


Figure 1-12 Λ and Δ enantiomers of $M(bpy)_3$ (top) and an achiral $M(tpy)_2$ with symmetrical ligands (bottom). Substitution of bpy ligands results in the formation of diastereoisomers, symmetrical substitution of tpy ligands leaves $M(tpy)_2$ complexes achiral.⁶⁹

The photophysical and redox properties of these complexes are strongly influenced by substitution at the 4'-position,⁸² allowing derivatives to be prepared with desired electronic properties. Ruthenium(II) complexes of tpy have long been the focus of intense research interest due to their photophysical properties.⁸³ Their potential in developing useful light-powered molecular machines^{49, 50} has been well established, as is their position as the most efficient dyes for dye sensitised solar cells (Grätzel cells).⁸⁴⁻⁸⁹

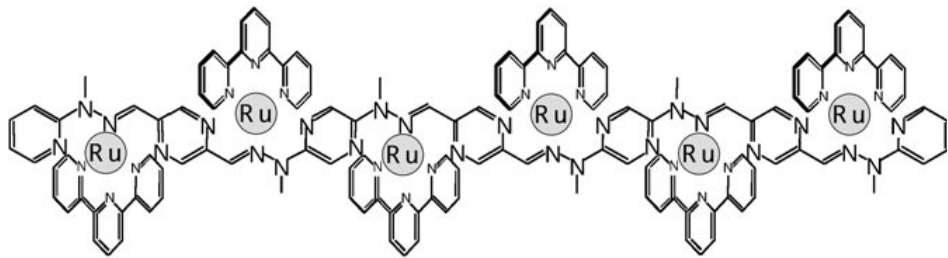


Figure 1-13 A rack-type assembly of Ru(tpy) centres and a poly-hydrazone ligand which show splitting of the multiple Ru(II/III) oxidation potentials.⁹⁰

Recent examples include self-assembled mixed-metal supramolecular porphyrin arrays with {Ru(tpy)₂} cores,⁹¹ luminescent fluoride sensors,⁹² water splitting catalysts,^{93, 94} rack-type multinuclear complexes which show splitting of the metal-based oxidation potentials (Figure 1-13)⁹⁰ and arrays by Newkome (Figure 1-14).⁹⁵

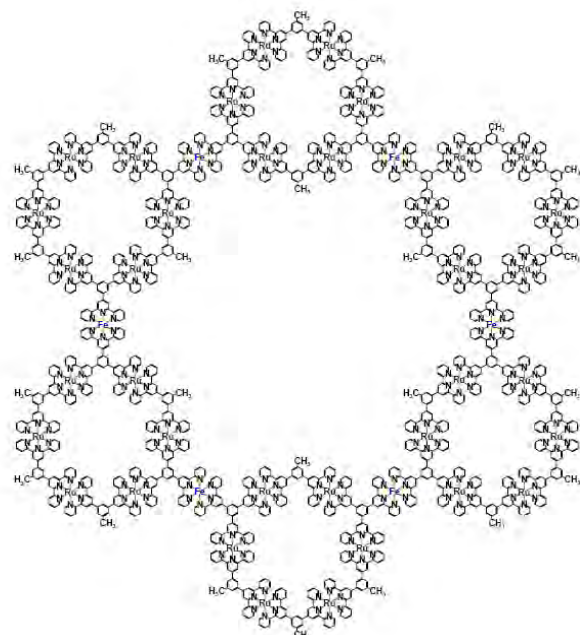


Figure 1-14 Newkome's "Sierpinski hexagonal gasket"⁹⁵ formed with 36 Ru(II) and 6 Fe(II) ions.

1.3. ‘Crystal Engineering’ as Supramolecular Chemistry

Dunitz first described a crystal as a supramolecular entity, stating ‘a crystal is, in a sense, the supramolecule *par excellence*’⁹⁶ as it comprises billions of identical molecules precisely ordered over very long distances by repeating energetically stabilizing interactions. The ability to predict, design, control or direct crystal packing - so called crystal engineering - offers enormous potential for the development of materials by use of specific intermolecular interactions to control bulk properties.

Advances in crystallographic technology, and most importantly computer software, have made analysis of weak interactions in the solid state significantly easier and recurring motifs have been identified and employed in designing new systems. Combined with the ability to search the Cambridge Structural Database (CSD) for known structures this has resulted in the recent establishment of high impact scientific journals wholly devoted to crystal engineering, such as CrystEngComm (1999, 2006 impact factor 3.729) and Crystal Growth & Design (2001, ISI Impact Factor in 2007 4.046, making it #1 in impact factor in crystallography). Furthermore, an increasing number of publications in more general chemistry journals are focusing on crystal engineering. A recent review by Desiraju⁹⁷ covers many of the issues concerning crystal engineering in terms of supramolecular chemistry.

Crystal Engineering with {M(tpy)₂}

Dance⁹⁸⁻¹⁰⁰ identified a common packing arrangement of {M(tpy)₂} complexes in the solid state which was termed a ‘tpy embrace’ as it is attractive, mutual and multi-armed. This cation-cation interaction, shown in Figure 1-15, is a combination of face-to-face (same colours) and edge-to-face (different colours) between the terminal pyridine rings of M(tpy)₂ complexes and results in the formation of two-dimensional sheets. This stabilising interaction, which naively would appear unlikely due to Coulombic repulsion, has been estimated to be ~29 kJ mol⁻¹.¹⁰⁰ Given this strong stability (comparable to the energy of a strong hydrogen bonds, 15-40 kJ/mol),¹⁰ the use of this motif in the assembly of new, larger systems is very appealing.

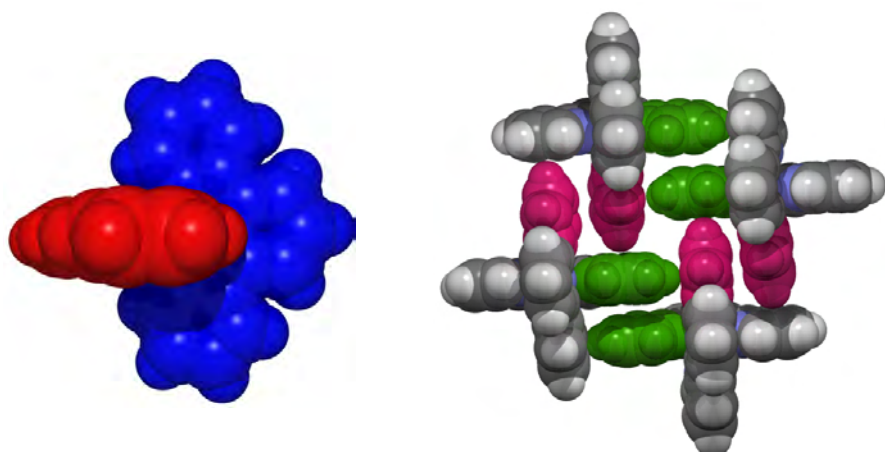


Figure 1-15 The X-ray crystal structure of $[\text{Ru}(8)_2](\text{PF}_6)_2$ ¹⁰¹ and the 2D-sheets formed by cation-cation packing interactions termed ‘tpy embraces’.

Infinite Supramolecular Systems: Coordination Networks

The formation of infinite structures of organic molecules linked by metal ions has been termed ‘coordination networks’, ‘coordination polymers’, molecular materials or frameworks, nanoporous solids and, unfortunately (as it incorrectly implies metal–carbon bonds), ‘metal-organic frameworks’ (MOFs) and remains the topic of immense current research interest (see recent reviews¹⁰²⁻¹³¹). Although the concept of a coordination polymer has been in use since the 1960s¹³² and descriptions of network solids were presented in detail by Wells in the 1970s,¹³³ the use of these concepts to describe coordination networks was only popularised by Robson^{134, 135} in the early 1990s. In the 18 years since these seminal publications, much effort has been made to design new, relatively simple, ligands for the formation of increasing complex materials with properties ranging from catalysis^{117, 120, 136-144} to gas storage^{139, 145-149} and molecular sensing.¹⁵⁰⁻¹⁵⁵ Two classes of examples are particularly worth mentioning. Of the structurally characterised coordination polymers containing M-N bonds, 30% use one of the simplest available bridging ligands, 4,4'-bipy (**3**) – these networks have been recently reviewed.¹¹³

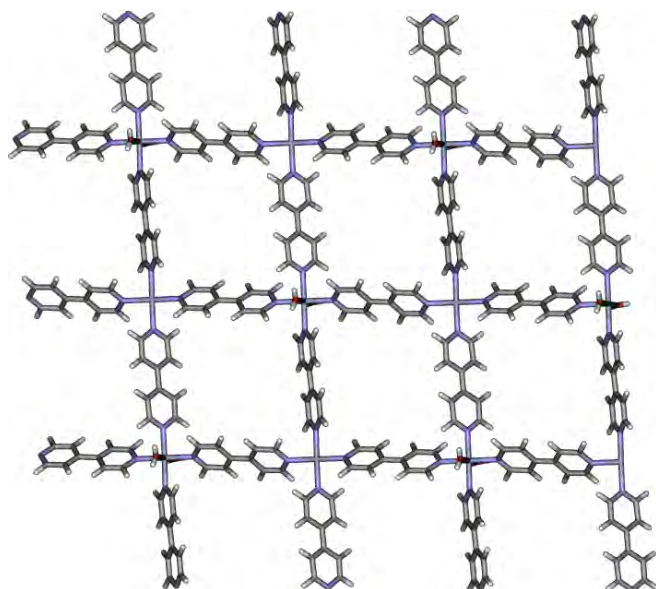


Figure 1-16 The first square grid network, $\{\text{Zn}(\text{bpy})_2(\text{H}_2\text{O})_2\}[\text{SiF}_6]\}_n$, reported by Robson¹⁵⁶

The metal ions employed with 4,4'-bipy include [in order of number of structures] Cu, Co, Zn, Cd, Ni, Mn, Fe and Ag, with geometries ranging from linear polymers to complex interpenetrating cubic networks,¹¹³ often depending strongly on the selection

of anions.¹⁵⁷ An example network, the first square grid network reported,¹⁵⁶ is shown in Figure 1-16. As is the case in many similar structures, due to the size of the grid cavity, the network is doubly interpenetrated (not shown). A packing efficiency of ~68-70% should normally be attained for the formation of favourable structures.¹³³ The presence of large holes is therefore undesirable and this problem is often solved by interpenetration.¹⁵⁸⁻¹⁶⁰ A related example, reported by Fujita,¹⁶¹ is that of the square grid network formed with units which was shown to catalyses the cyanosilylation of imines under heterogeneous conditions.

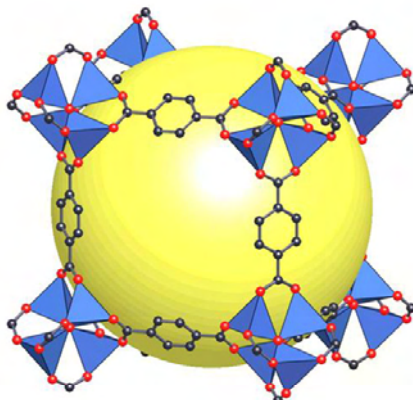


Figure 1-17 MOF-5 OZn₄(O₂C-C₆H₄-CO₂)₃: a highly porous and robust ‘metal-organic-framework’ which is stable when fully desolvated and when heated up to 300 °C.¹⁶²

A class of coordination networks which use Zn(II)-carboxylate bonds was introduced by Yaghi.¹⁶³ These impressive structures have very high porosity (~4,800 m²/g) and the lowest density crystalline materials ever reported. An example is shown in Figure 1-17,¹⁶² which is not interpenetrated and has very large cavities. These types of networks have been demonstrated to remain crystalline even when guest molecules are removed to leave a vacuum in the cavities! This is an ultimate goal of many crystal engineers but is rarely achieved. Reversible filling and emptying of the cavities would, of course, be ideal for the development of applications for these systems. They possess remarkable properties for gas storage and a number have already reached commercial production by BASF.¹⁶⁴

Ligand design: coordination polymers containing terpyridine

In order to prepare extended structures incorporating {M(tpy)₂} groups design of possible building blocks must be considered. Obviously, the ligand should possess a tpy (or bpy) motif which is able to bind strongly to metal ions. Additionally, a pendant

group should be attached which could be potentially used to bind to secondary metal centres, or interact with organic molecules to form extended structures. A convenient method of considering possible candidates is using the ‘expanded ligands’ concept.¹⁶⁵ This idea begins by considering an organic multitopic ligand with any functional groups known to bind metal ions (for forming metal bridged structures) or to interact with other molecules *via* other types of interactions (such as formation of hydrogen bonds or other molecular recognition). Examples of useful functional groups include carboxylic acids, pyridyl nitrogens, catechols, phosphorus donors and a range of hydrogen bond donors, such as amines and amidinium groups. The next step, likely the most complicated, is to ‘insert’ a {M(tpy)₂} group between these function groups to benefit from the combination of the reactivity of the pendant functional groups and the redox, photophysical, magnetic or other properties inherent in the {M(tpy)₂} core.

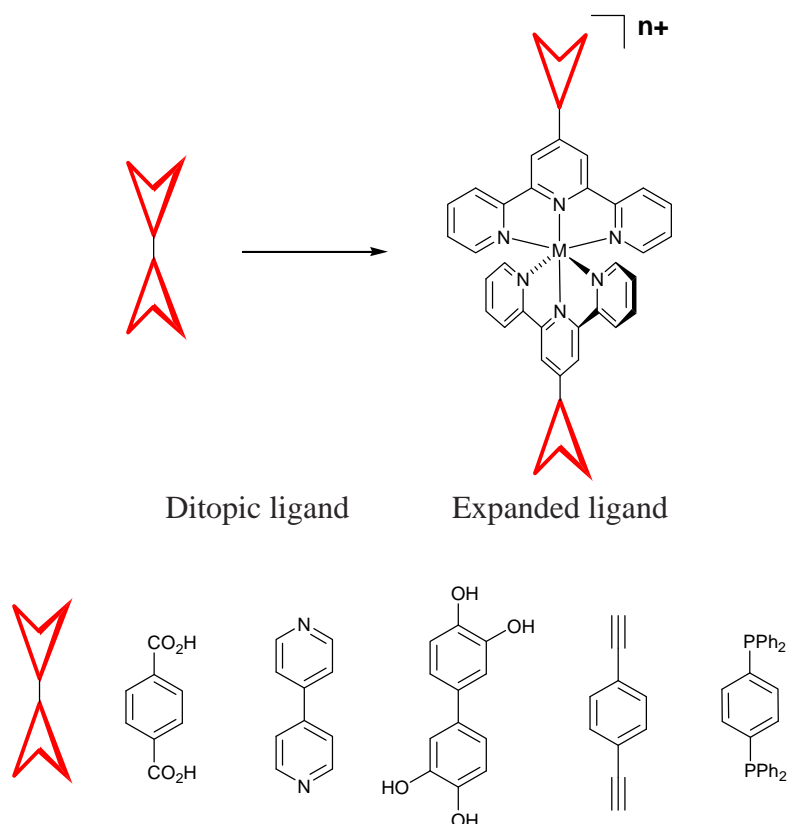
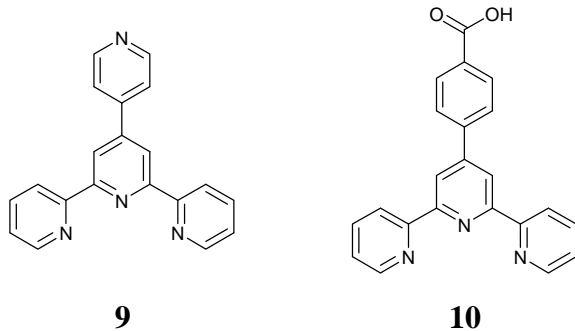


Figure 1-18 The idea of ‘expanded ligands’ with a number of potential examples.

Two obvious choices are 4'-(4-pyridyl)-2,2':6', 2''-terpyridine (**9**)¹⁶⁶ and 4'-(4-carboxyphenyl)-2,2':6', 2''-terpyridine (**10**).¹⁶⁷ Each of these possess groups both

capable of interacting with additional metal centres, or participating in hydrogen bonding interactions. A few examples of coordination polymers containing



4'-(4-pyridyl)-2,2':6',2''-terpyridine (**9**) have been described,¹⁶⁸⁻¹⁷⁰ but these do not contain $[M(\mathbf{9})_2]^{n+}$ motifs - only mono-terpyridine complexes are used (Figure 1-19). In only one,¹⁷⁰ using Co(II), has a structure of type **11** where the metal centre is directly coordinated to an adjacent complex, the others are of type **12** where an infinite structure is formed by other bridging units (often involving additional metal centres).^{168, 169} No coordination polymers or networks had been previously described for this class of complexes.

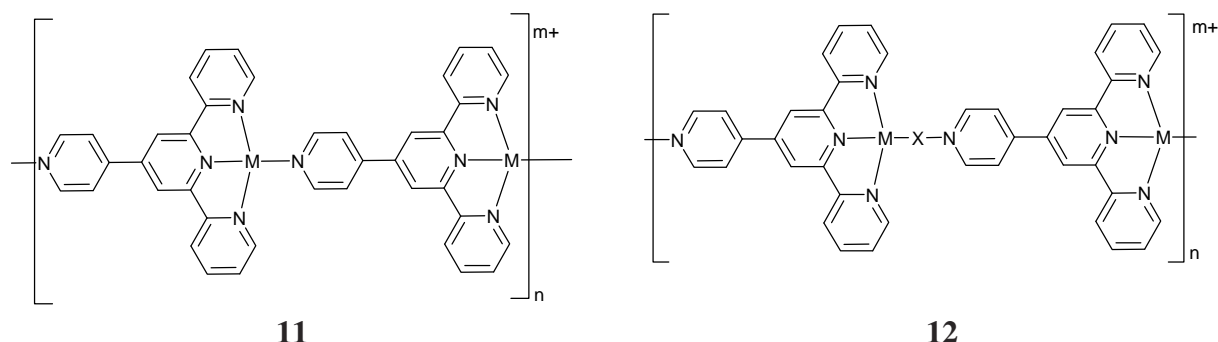
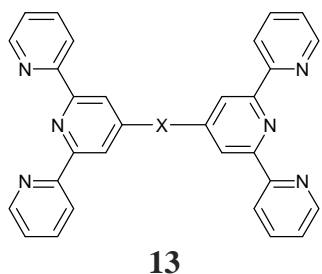


Figure 1-19 Infinite mono-terpyrine complexes have been reported.

Bis-tpy ligands of type **13** ($X = \text{nothing}, C_6H_4, \text{polyethylene glycol and many others}$) are also worth mentioning. These have been used to form a range of coordination polymers and continue to receive much research attention¹⁷¹⁻¹⁸⁵ although no single crystal X-ray diffraction studies of these types of polymers have been reported.



1.4. This thesis

The broad goal of this thesis is to design ligands for assembling larger structures, especially in the solid-state. This was achieved by investigations of the solution and solid state behaviour of a number of tpy ligands and their metal complexes, followed by incorporation of some of these into the first crystallographically characterised coordination polymers to contain {M(tpy)₂} groups.

Chapter 2 Preparation and characterisation of 4'-functionalised-hydrazone-2,2':6',2"-terpyridine ligands

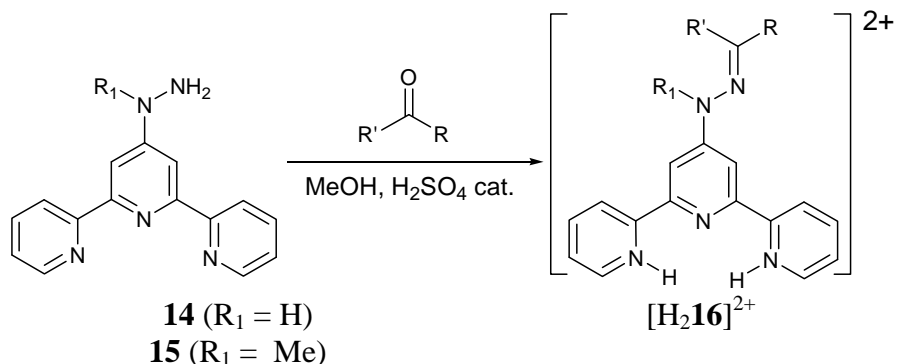
2.1. Introduction

The chemistry of hydrazones and their metal complexes has long been an area of active interest, because of their properties appropriate for application in, for example, sensors, non-linear optical^{186, 187} and polymeric materials and their biological applications.¹⁸⁸ Additionally, it is known that they form intensely coloured compounds, 4-nitro phenylhydrazones in particular display pH-dependent perfect reversibility of colour change¹⁸⁹ with uses as alkaline pH indicators¹⁹⁰ as they change colour yellow to red in the pH range 10-14.¹⁹¹ More recently, pyridyl hydrazones^{192, 193} have found applications in medicine¹⁹⁴⁻¹⁹⁹ although their structural and electronic properties have not been explored. Within supramolecular chemistry, Lehn has incorporated hydrazone units into pyrimidine- and pyridine-containing molecular strands that undergo programmed self-organization into metal-free helical architectures²⁰⁰⁻²⁰² and metal-containing helical wires^{203, 204} or grid-like arrays.^{90, 205-210} Among the latter are $[\text{Co}_4\text{L}_4]^{8+}$ complexes [$\text{L} = 4,6\text{-bis(benzylidenehydrazino)-2-phenylpyrimidine or 2-phenylpyrimidine-4,6-dicarbaldehyde bis(phenylhydrazone)}$] in which the eight hydrazone NH protons can be sequentially and reversibly removed in pH-dependent steps resulting in significant changes in the absorption spectra of the complexes.²⁰⁷ This chapter will introduce a number of hydrazone-functionalised 2,2':6',2"-terpyridine ligands and study their structural properties in solution and the solid state.

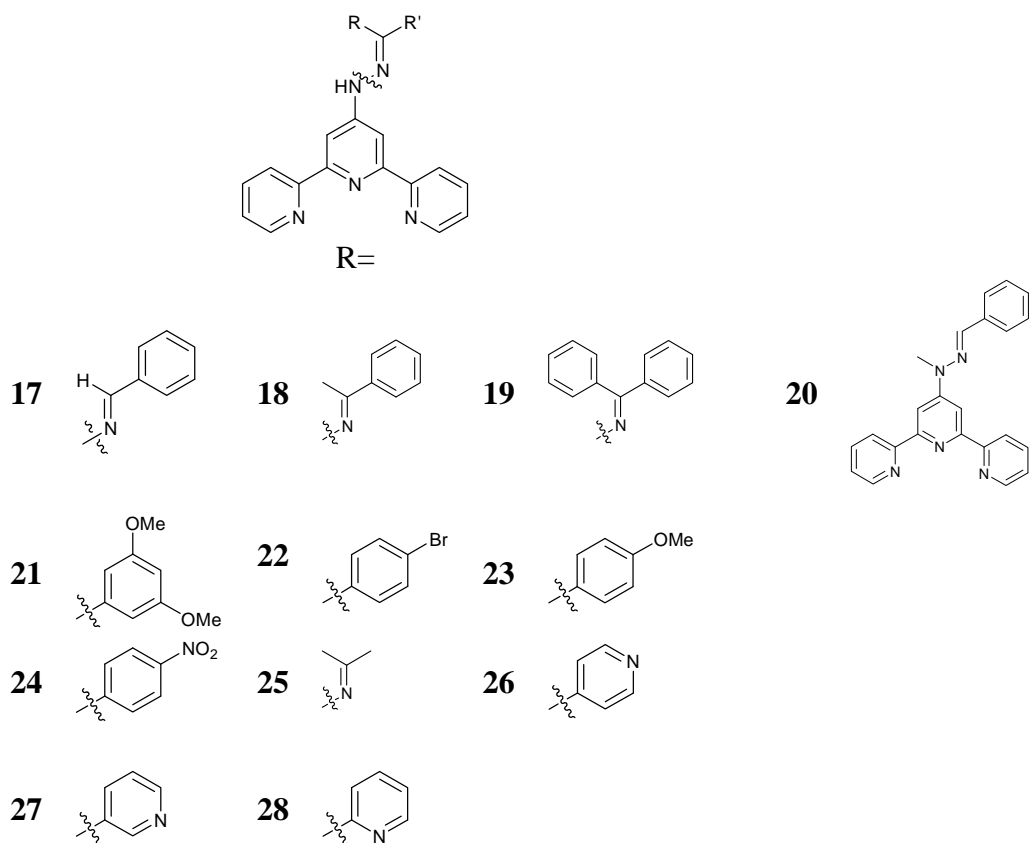
2.2. 4'-Hydrazone functionalised-2,2':6',2"-terpyridine ligands

The synthetic route to hydrazones of type **16** (Scheme 1) was by the well established acid-catalysed condensation of a hydrazine (4'-hydrazino-2,2':6',2"-terpyridine (**14**) or 4'-(1-methylhydrazino)-2,2':6',2"-terpyridine (**15**)) and an aldehyde or ketone. A representative selection of these products are shown below (compounds **17-25**, see Figure 2-1 for the labelling scheme adopted). In the interests of simplicity, the following

discussion will focus on ligands **17**, **18**, **19** and **20** which are the condensation products from the reaction of **14** or **15** with benzaldehyde for **17** and **20**, acetophenone for **18** and benzophenone for **19**.



Scheme 1 Formation of hydrazones of type $[H_2\mathbf{16}]^{2+}$ as the methyl sulfate salt



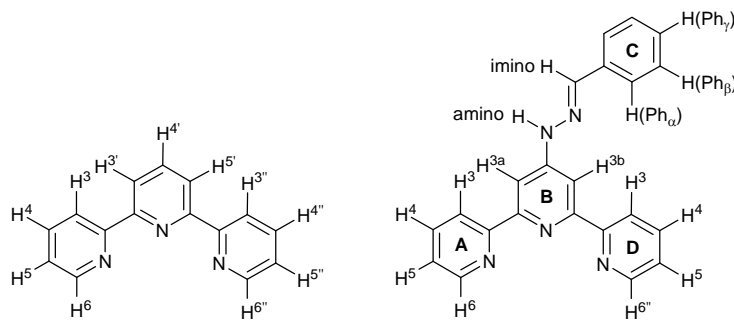


Figure 2-1 The numbering and naming scheme adopted. The numbering scheme on the left is traditional numbering for terpyridine. For the sake of easier discussion, where a symmetric species was observed the equivalent positions are named for one side only. E.g.: H^{A3} refers to H^{A3} and H^{D3} .

The reaction of 4'-hydrazino-2,2':6',2"-terpyridine and benzaldehyde in methanol in the presence of a few drops of concentrated H_2SO_4 resulted in the formation of a bright yellow solid, elemental analysis of which was consistent with the methyl sulfate salt of $[H_2\mathbf{17}]^{2+}$. The electrospray mass spectrum of $[H_2\mathbf{17}][MeOSO_3]_2$ was unhelpful in confirming the protonation state of **17**, showing evidence only for the $[H\mathbf{17}]^+$ ion (m/z 352). The room temperature 1H NMR spectrum in $DMSO-d_6$ showed the presence of methyl protons at δ 3.38 and 3.15 ppm. The latter was assigned to $MeOH^{211}$ and the former to the $[MeOSO_3]^-$ ion.²¹² The combined relative integrals for the methyl proton signals with respect to signals for the tpy protons were consistent with the formulation $[H_2\mathbf{17}][MeOSO_3]_2$. In the ^{13}C NMR spectrum ($DMSO-d_6$), signals at δ 48.6 and 53.0 ppm were assigned to $MeOH^{211}$ and $[MeOSO_3]^-$, respectively. We attribute the presence of the $MeOH$ (always present to some extent in $DMSO-d_6$ solutions of the sample) to hydrolysis of $[MeOSO_3]^-$ by residual water in the solvent.²¹³ The isolation of ethyl or methyl sulfate salts of complexes from media in which esterification of sulfate or sulfuric acid²¹³ has precedent, although examples appear to be rare.²¹⁴⁻²¹⁶ When the reaction of 4'-hydrazino-2,2':6',2"-terpyridine and benzaldehyde was carried out in methanol in the presence of a few drops of concentrated HNO_3 or HCl , a bright yellow solid was isolated in each case. $DMSO-d_6$ solutions of these products exhibited the same 1H NMR spectroscopic signatures for the tpy unit as in $[H_2\mathbf{17}][MeOSO_3]_2$, suggesting the formation of $[H_2\mathbf{17}][NO_3]_2$ and $[H_2\mathbf{17}][Cl]_2$. In each salt, the signals for protons H^{A3} and H^{B3} are either very broad or are not observed at 295 K. We return to a more detailed discussion of the NMR spectra later. The salts $[H_2\mathbf{18}][MeOSO_3]_2$, $[H_2\mathbf{19}][MeOSO_3]_2$ and $[H_2\mathbf{20}][MeOSO_3]_2$ (all bright yellow solids) were made in an analogous manner to $[H_2\mathbf{17}][MeOSO_3]_2$. Although the electrospray mass spectra of

these salts provided evidence only for $[H_2\mathbf{18}]^+$ (m/z 366), $[H_2\mathbf{19}]^+$ (m/z 428) and $[H_2\mathbf{20}]^+$ (m/z 366), respectively, the NMR spectroscopic data were consistent with the formation of $[H_2\mathbf{18}][MeOSO_3]_2$, $[H_2\mathbf{19}][MeOSO_3]_2$ and $[H_2\mathbf{20}][MeOSO_3]_2$. As with $[H_2\mathbf{17}][MeOSO_3]_2$, hydrolysis of the anion by water in the DMSO- d_6 solvent led to the presence of MeOH in addition to $[MeOSO_3]^-$.

Treatment of each of aqueous solutions of $[H_2\mathbf{17}][MeOSO_3]_2$, $[H_2\mathbf{18}][MeOSO_3]_2$, $[H_2\mathbf{19}][MeOSO_3]_2$ and $[H_2\mathbf{20}][MeOSO_3]_2$ salts with excess NaBF₄ led to the formation of pale yellow $[H_2\mathbf{17}][BF_4]$, $[H_2\mathbf{18}][BF_4]$, $[H_2\mathbf{19}][BF_4]$ and $[H_2\mathbf{20}][BF_4]$ respectively. Changes in the NMR spectroscopic data were consistent with the conversion of each diprotonated to monoprotonated tpy species. For example, a comparison of the ¹³C NMR spectra (in DMSO- d_6) revealed that signals for carbons C^{A4} and C^{A5} shifted to lower frequency upon reaction of $[H_2\mathbf{17}][MeOSO_3]_2$ with $[BF_4]^-$; $\Delta\delta = 0.6$ and 0.3 ppm for C^{A4} and C^{A5}, respectively where $\Delta\delta = \delta([MeOSO_3]^- \text{ salt} - [BF_4]^- \text{ salt})$. Similarly, although the signal for C^{A3} is broad, a change in chemical shift to lower frequency is observed. The addition of NH₄PF₆ to an aqueous solution of $[H_2\mathbf{17}][MeOSO_3]_2$ yielded, after purification, a pale yellow solid product, analytical data for which were consistent with $[H_2\mathbf{17}][PF_6]$. The aromatic region of the ¹³C NMR spectrum of a DMSO- d_6 solution of the hexafluorophosphate salt was essentially identical to that of the tetrafluoroborate salt. The change in protonation state was also confirmed by single crystal structure determinations (see later).

The reactions of $[H_2\mathbf{17}][MeOSO_3]_2$, $[H_2\mathbf{18}][MeOSO_3]_2$, $[H_2\mathbf{19}][MeOSO_3]_2$ and $[H_2\mathbf{20}][MeOSO_3]_2$ with K₂CO₃ allowed the neutral compounds **17**, **18**, **19** and **20** to be isolated. All compounds have been fully characterized by electrospray mass spectrometry, elemental analysis, ¹H and ¹³C NMR spectroscopy and single-crystal X-ray crystallography. In the ¹H NMR spectra, the loss of the resonance for the methyl sulfate anion was consistent with the formation of each neutral product.

2.3. *Neutral ligands: solution behaviour*

The assignment of ¹H-NMR (DMSO- d_6) signals for neutral ligands **17**, **18**, **19** and **20** was straightforward (Figure 2-2) and was confirmed in each case using 2D COSY and

NOESY spectra. In solution, each of compounds exists as a single isomer, shown by NOESY experiments to be the (*E*)-isomer. This is the expected isomer for aryl hydrazones.^{192, 217, 218} The resonances assigned to the tpy protons reveal that pyridine rings A and D (Figure 2-1) are equivalent in the NMR timescale, suggesting that there is fast rotation (on the NMR timescale) of the 4'-substituent about the C_{py}–N_{amine} bond. With the exception of proton H^{A6} in compound **19**, the only signal the line shape of which changes along the series is that assigned to H^{B3}, i.e. the proton closest to the 4'-substituent.

The addition of D₂O resulted in the disappearance of the NH peak, confirming its assignment. Importantly, the imino (N=CH) signal was unaffected by D₂O addition, establishing no hydrazone-azo tautomerism occurs for these species in agreement with previous reports for phenylhydrazones.²¹⁹

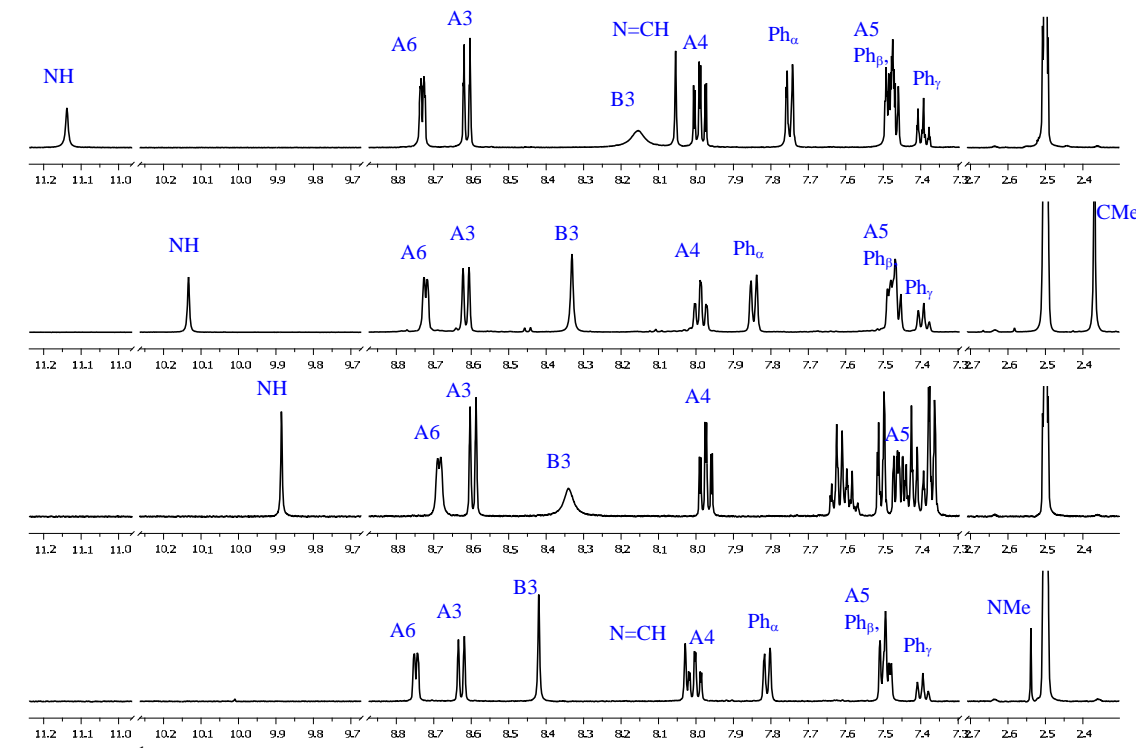


Figure 2-2 ¹H-NMR spectra (500MHz, DMSO-d₆, 295K) of neutral **17** (top), **18**, **19** and **20** (bottom).

2.3.1. Variable temperature NMR

Variable temperature NMR spectroscopy was used to investigate dynamic processes occurring at rates comparable to the NMR timescale. A temperature decrease would result in either a broadening of the signals (suggesting the observed spectrum was an average from multiple species) *or* a sharpening of the signals (suggesting a single species is observed). High temperature measurements were conducted in DMSO-d₆ but due the high melting point of DMSO, low temperature experiments were measured in acetone-d₆. We consider first ligand **17**. At lower temperatures all the tpy signals become split into sets of 1:1 signals (Figure 2-3). The H⁴ and H⁵ signals appear as overlapping pairs of signals whereas the H^{A6}, H^{A3} and H^{B3} each show two well separated signals each, separated by 0.08 ppm, 0.03 ppm and 0.64 ppm respectively (500 MHz).

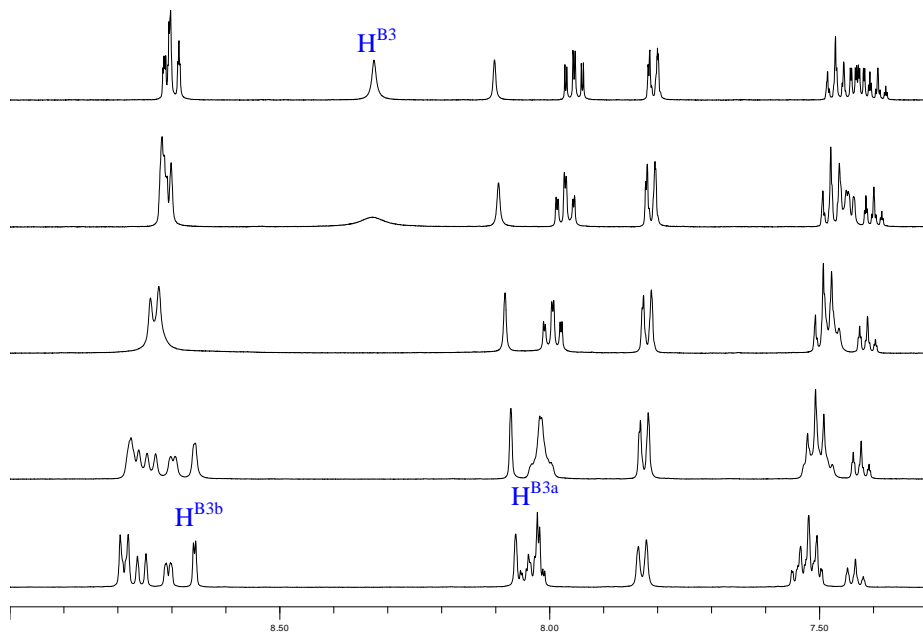


Figure 2-3 ¹H-NMR spectra (500 MHz, acetone-d₆) of neutral **17** at 295 K (top), 275, 245, 220 and 195 K (bottom). The two non-equivalent H^{B3}signals are marked.

The H^{B3} protons appear as a pair of doublets ($J_{HH} = 2.1$ Hz) which was shown to be H^{B3a}-H^{B3b} coupling from a COSY spectrum. This establishes that these signals are from a single species rather than being, for example, a mixture of isomers. A NOESY spectrum at 195K (Figure 2-4) allows absolute assignment of the signals as only the upfield H^{B3} signal (8.01 ppm) exhibits a cross-peak with the NH establishing this signal corresponds to the H^{B3a} (See Figure 2-1 for labelling). Additional NH...CH=N cross-

peaks were also observed (confirming the (*E*)-isomer) although peak overlap prevented absolute assignment of the two sides of the terpy molecule (i.e.: identifying H^{A3} and H^{D3}). H^{B3a}-H^{B3b} cross-peaks were observed indicating chemical exchange between these two non-equivalent sites. The amine and imine signals are both sharp signals at all temperatures studied, indicating a single environment exists for each of these protons in all cases. These peaks, however, shift on cooling from 295 to 195K, the amine becoming sharper and shifting downfield (10.15 to 10.81 ppm) and the imine shifting less significantly upfield (8.10 to 8.06 ppm). The phenyl signals are almost unaffected by the temperature change (Ph_{*a*} 7.81 to 7.83 ppm). For all signals, the peaks at high temperature (315K) represent the average environment of the two environments observed at 195K. These results indicate that the dynamic process is effectively ‘frozen’ at low temperature and the resulting species has an asymmetric tpy environment but a single environment for the 4'-substituent (NH-N=CH-Ph). The structure of this species is discussed later and smashing your dreams.

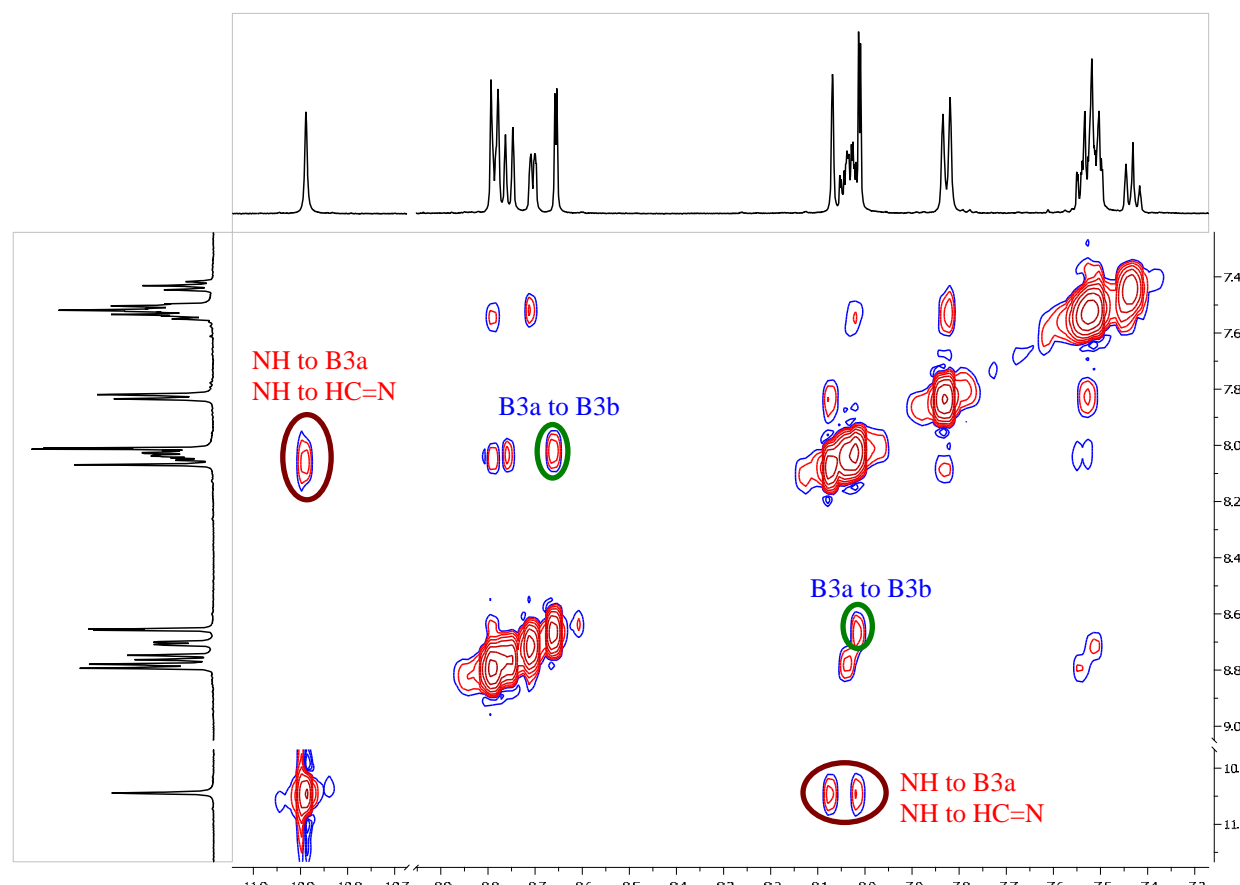


Figure 2-4 NOESY spectrum of neutral **17** (500 MHz, acetone-d₆, 195K)

The variable temperature ^1H NMR spectra of **18**, **19** and **20** broadly parallel that of **17**, spectra at 195K are shown in Figure 2-5. Again, each of the tpy proton signals splits into two signals at 195K, although overlap of signals precludes unambiguous assignments to rings A and D. In the 195K ^1H NMR spectrum of **18** the signals are assigned in a similar manner as for **17**. The $\text{H}^{3''}$ signal at 295K (8.42 ppm) appears as the average of the two environments observed at 195K (8.69, 8.23 ppm) which display the same $\text{H}^{\text{B}3\text{a}}\text{-H}^{\text{B}3\text{b}}$ coupling described earlier. The NOESY spectrum (Figure 2-6) shows a cross peak between NH and one $\text{H}^{\text{B}3}$ environment but not the other, again to the more upfield of the two signals (8.23ppm) confirming that this signal corresponds to $\text{H}^{\text{B}3\text{a}}$, adjacent to the NH (Figure 2-1). In the case of compound **20**, the signal for $\text{H}^{3\text{B}}$ splits, but only broad signals at δ 9.05 and 8.19 ppm are resolved at 195K. The latter have been assigned to H^{3b} and H^{3a} , respectively by analogy with compounds **17**, **18** and **19**.

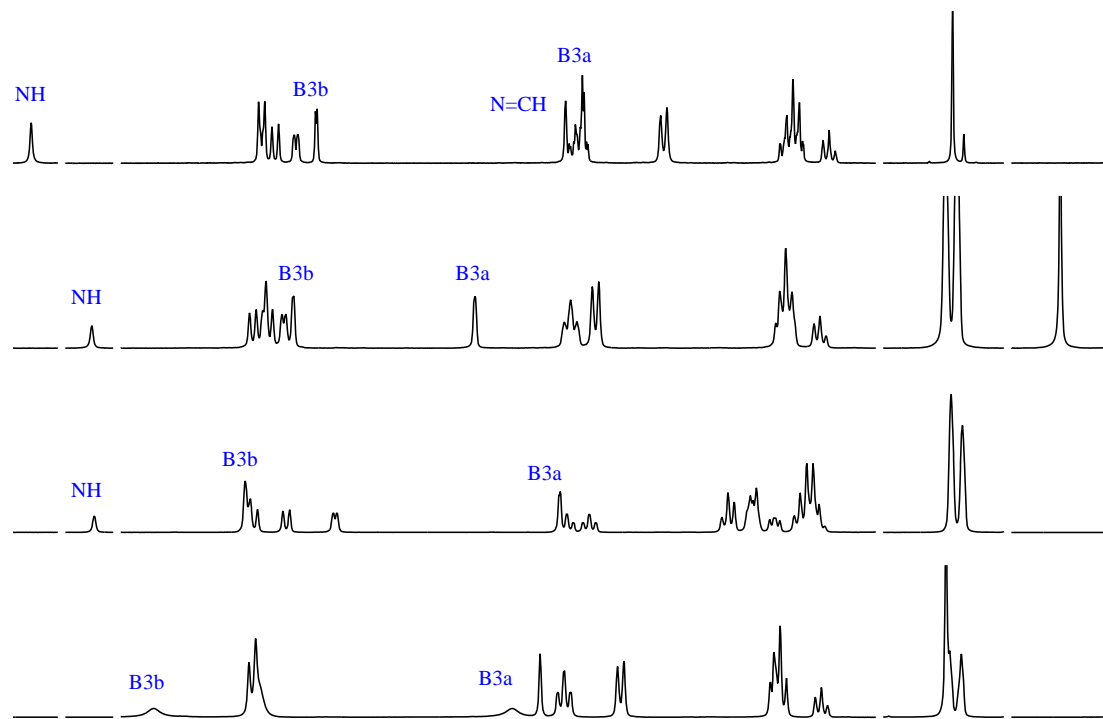


Figure 2-5 ^1H NMR spectra (500 MHz, acetone- d_6 , 195K) of neutral **17** (top), **18**, **19** and **20** (bottom).

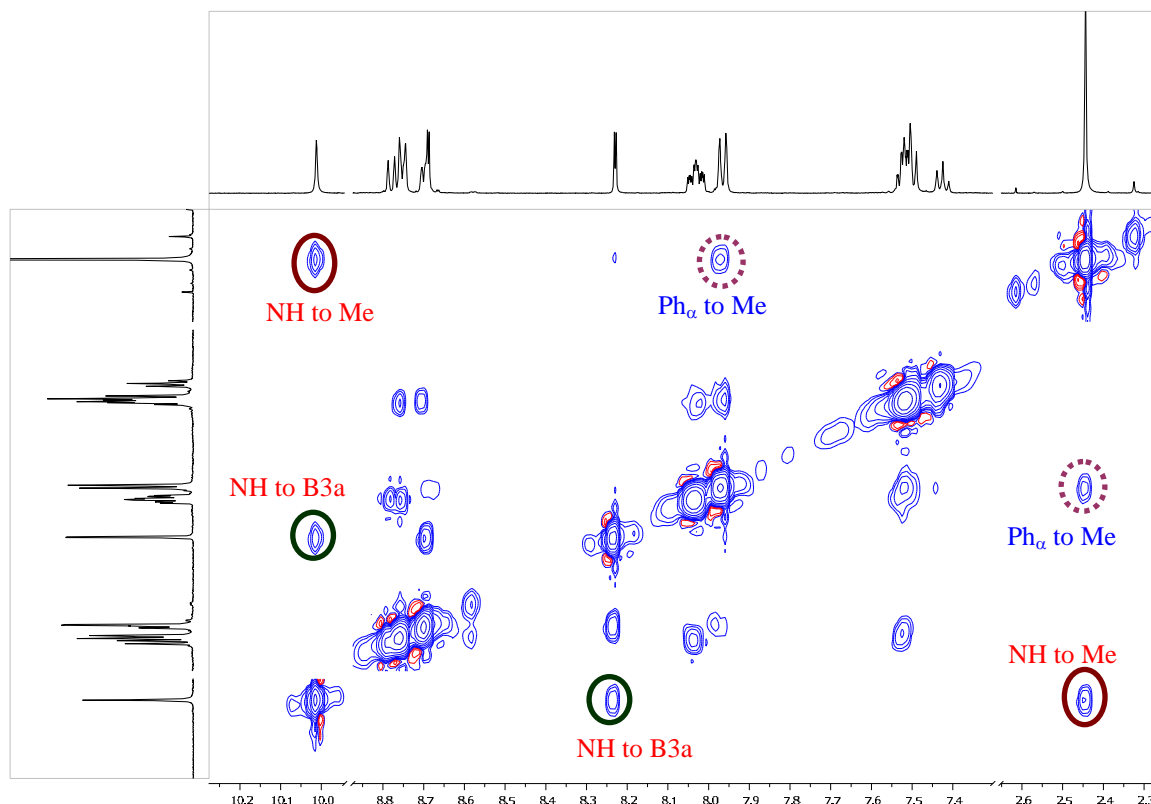
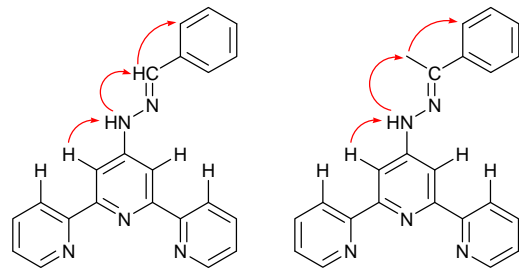


Figure 2-6 NOESY spectrum (500 MHz, acetone- d_6) of **18** at 195K



17 **18**

Figure 2-7 Observed NOESY interactions at 195K (acetone- d_6) from the spectra shown in Figure 2-4 and Figure 2-6.

2.4. Identification of dynamic processes

The process which results in the asymmetry observed at low temperatures could be potentially any of the rotations shown in Figure 2-8. Rotamers resulting from rotation around the N-N single bond (type C) are the least likely due to steric hindrance between the H^{B3} and the imino CH proton. The signal for the imino CH is always sharp, indicating its environment is not significantly affected by the observed rotation, which effectively eliminates rotamer type C. Differentiation between rotamers of types A and

B is more difficult. At low temperature (where the dynamic process is effectively ‘frozen’) an asymmetric tpy environment is observed with a single environment for the 4'-substituent (-NH-N=CH-Ph). This asymmetry could be explained by the single observed species being the *cis-trans* isomer of the pyridyl rings (see Figure 2-9). This could be a plausible explanation for mono protonated ligands (several X-ray structures of mono-protonated terpyridine in *cis-trans* conformations have been reported²²⁰⁻²²² and it has been reported that the energy difference between *cis-cis* and *cis-trans* for mono-protonated tpy is small²²³) although for the neutral ligand there does not appear to be any reason why one C_{py}-C_{py} bond would be significantly more restricted than the other and the usual *trans-trans* isomer would be expected (as predicted by *ab initio* quantum mechanics calculations of neutral tpy ligands).²²³ More significantly, low temperature NOESY spectra (Figure 2-4, Figure 2-6) show cross peaks between only one H^{B3} signal and NH (Figure 2-7).

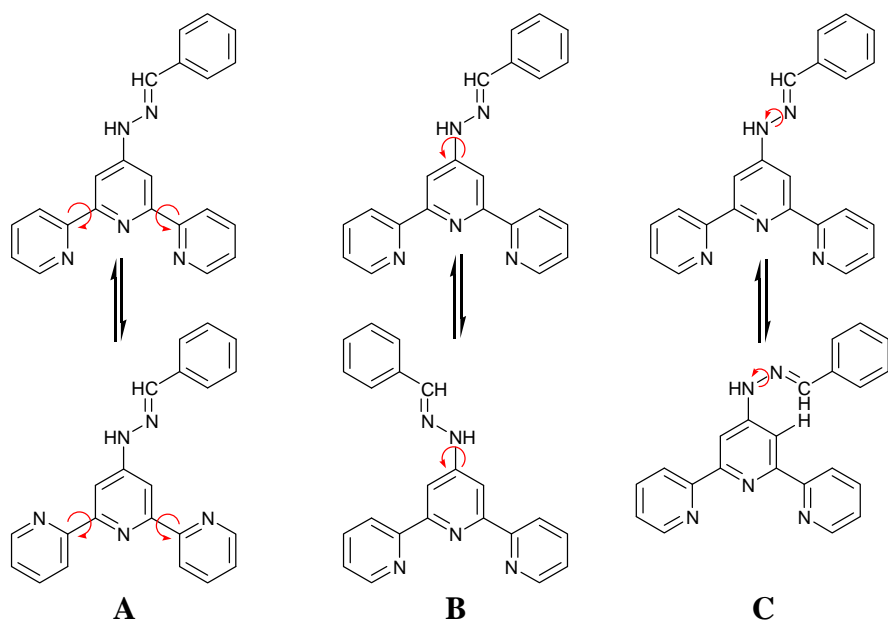


Figure 2-8 Possibly rotamers of **14**.

Combined with the coalescence of non-equivalent signals at higher temperature (i.e.: H^{B3a}+H^{B3b} → 1 H^{B3}) establishes unambiguously that slow rotation occurs about the tpy-NH bond and rotamers of type B as the most likely process responsible for the observed peak broadening. The ¹H, COSY and NOESY NMR spectra are in accord with this assignment, showing single environments for NH and HC≡N but two environments for

each of the tpy signals with the difference between the $\text{H}^{\text{B}3}$ signals being the greatest, as expected.

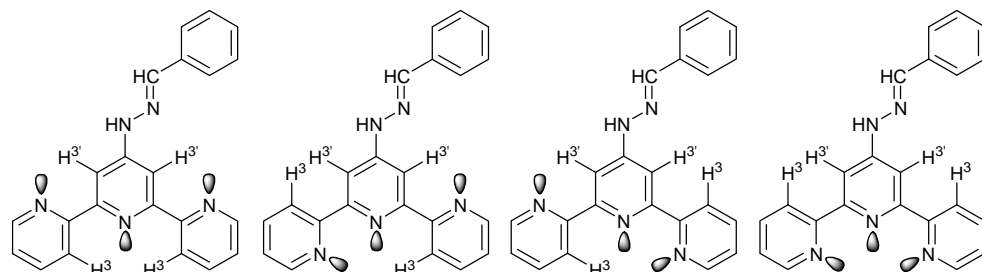


Figure 2-9 Rotational conformers of **17** (left to right): *trans-trans*, *cis-trans*, *trans-cis*, and *cis-cis*.

2.5. Protonated ligands

The effects of protonation on dynamic behaviour was considered with a detailed study of the series **17**, $[\text{H17}]^+$ and $[\text{H}_2\text{17}]^{2+}$. There is a significant change in the chemical shift for the signal assigned to the NH proton and signals in the aromatic region when **17** is protonated. This is exemplified by comparing the ^1H NMR spectra of **17**, $[\text{H17}]^{\text{PF}_6}$ and $[\text{H}_2\text{17}][\text{MeOSO}_3]_2$ (Figure 2-10).

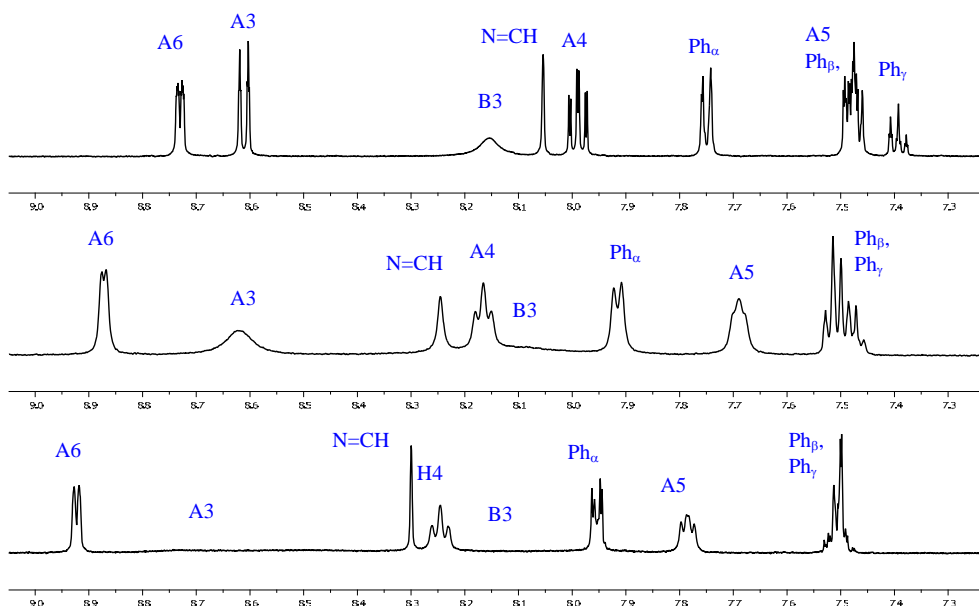


Figure 2-10 ^1H -NMR (500 MHz, DMSO-d_6 , 295K) of **17** (top), $[\text{H17}]^{\text{PF}_6}$ and $[\text{H}_2\text{17}][\text{MeOSO}_3]_2$

The figure also illustrates that in the room temperature spectrum of **17**, the signal for $\text{H}^{\text{B}3}$ is broad while that for $\text{H}^{\text{A}3}$ is a well-resolved doublet. In contrast, both signals are

extremely broad in the spectrum of $[H_2\mathbf{17}][MeOSO_3]_2$. Upon warming to 360 K, the resonances assigned to H^{A3} and H^{B3} sharpen (Figure 2-11), confirming their assignments.

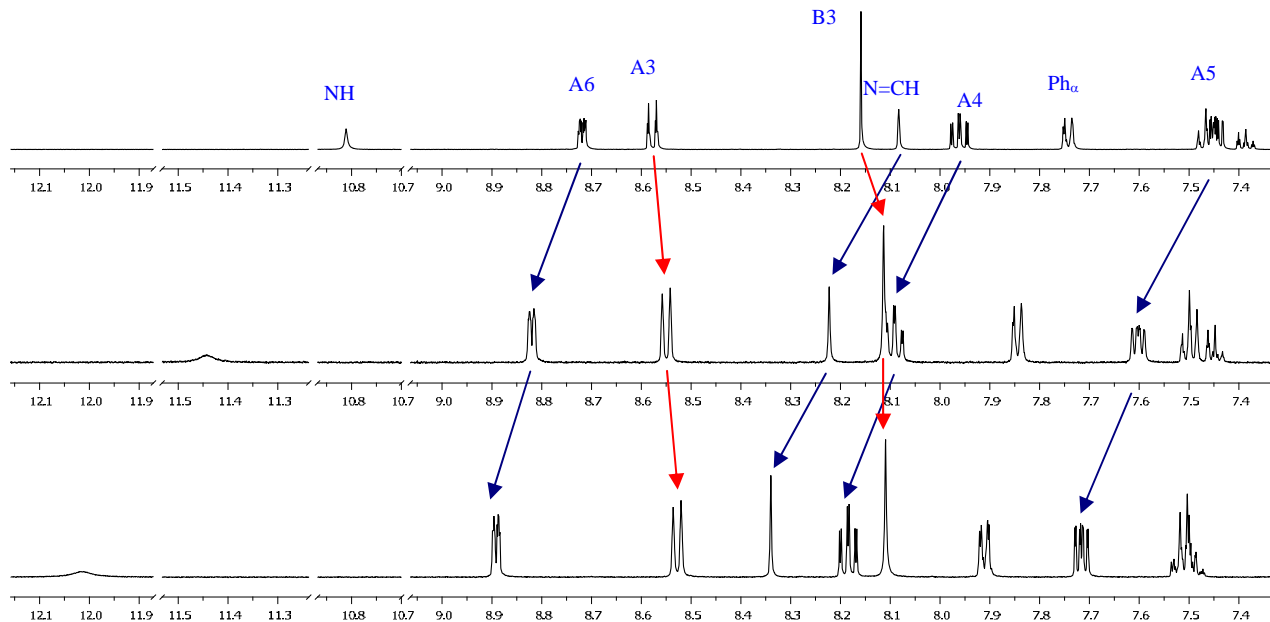


Figure 2-11 1H -NMR (500 MHz, DMSO-d₆, 360K) of **17** (top), $[H\mathbf{17}]PF_6$ and $[H_2\mathbf{17}][MeOSO_3]_2$

Low temperature 1H NMR spectra of $[H_2\mathbf{17}][MeOSO_3]_2$ could not be acquired because the compound was very poorly soluble in common low freezing point solvents such as acetone-d₆ or acetonitrile-d₃. However, salts of $[H\mathbf{17}]^+$ were more amenable to low temperature studies. Cooling an acetone-d₆ solution of $[H\mathbf{17}]PF_6$ (Figure 2-12) to 255 K results in a splitting of the H^{A6} , H^{A4} and H^{A5} signals into overlapping pairs of signals whereas the H^{A3} and H^{B3} show two well separated signals each, separated by 0.36 ppm and 0.68 ppm respectively. The H^{B3} protons appear as a pair of doublets ($J_{HH} = 1.8$ Hz at 220K) which was shown to be H^{B3} - H^{B3} coupling from a COSY spectrum. Pairs of signals for all the pyridine ring protons are resolved by 220K. The assignments shown in the lowest trace in Figure 2-12 were made using NOESY and COSY experiments, similar to those described earlier. Only the upfield H^{B3} signal (7.93 ppm) exhibits a NOESY cross-peak with the NH, establishing this signal corresponds to the H^{B3a} , adjacent to the NH. A NOESY cross peak between this H^{B3a} signal and the more upfield of the two $H^{A3/D3}$ signals (8.44 ppm) allows the assignment of H^{A3} and H^{D3} signals (Figure 2-1 for labelling). Interestingly, the separation between the H^{A3} and H^{D3} signals

is much greater for the protonated ligand than for the neutral compound (0.36 ppm and 0.03 ppm, 500 MHz).

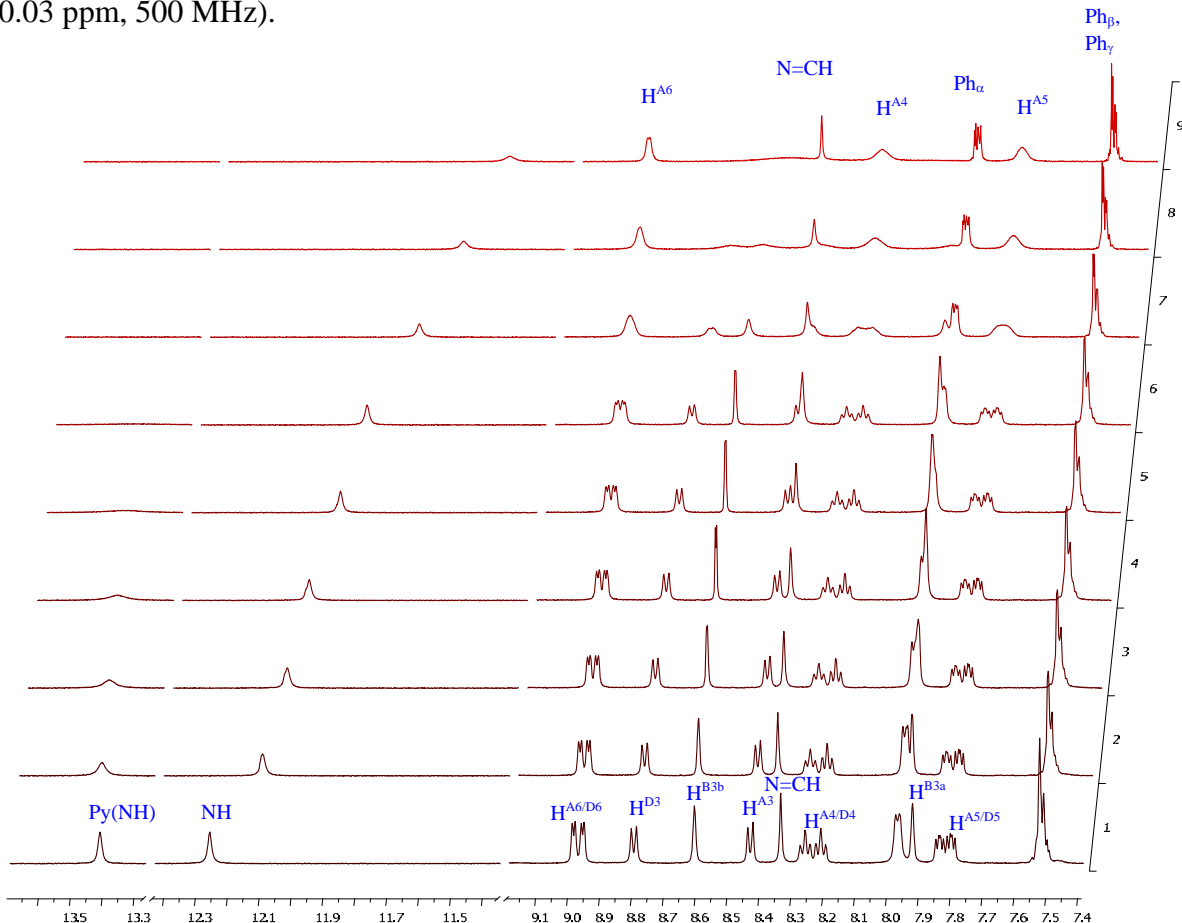


Figure 2-12 Variable temperature ^1H -NMR spectra (500 MHz, acetone- d_6) for $[\text{H}17]\text{PF}_6$. 195K (bottom), 220, 227, 235, 245, 255, 275, 295, 315K (top).

The amine and imine signals are again both sharp signals at all temperatures studied, indicating a single environment exists for each of these protons in all cases. These peaks shift on cooling from 295 to 195K similar to that observed for the neutral ligand (i.e.: the amine becoming sharper and shifting downfield (11.67 to 12.26 ppm) and the imine shifting less significantly upfield (8.44 to 8.34 ppm)). The phenyl signals are unaffected by the temperature change (Ph_α 7.96 at 295K, 7.97 at 195K). Finally, the amine NH signal is sharp (δ 12.3 ppm at 195 K and δ 11.6 ppm at 315 K in acetone- d_6) over the whole 360–195 K temperature range. The sharpness of the amino NH signal is possibly due to hydrogen bonding, which can result in the NH signal being sharp while the H^{A3} and H^{B3} signals are broad. The pyridinium proton is not observed above 255 K (Figure 2-12), however on cooling a broad signal at δ 13.4 ppm becomes visible and is sharp at 195 K. A NOESY spectrum indicated cross-peaks between this proton signal and the

water signal only and thus was unable to confirm the site of protonation. Analogous pyridinium proton peaks were also observed at low temperature for [H17]BF₄ and [H18]BF₄.

2.6. Identification of dynamic processes of protonated ligands

The spectroscopic data illustrated in the figures indicate that the activation barrier to rotation increases upon protonation of **17**. For [H17]PF₆ separate signals are clearly visible at 275 K, whereas as low as 245 K only a broadened average spectrum is observed for neutral **17**. For all the same arguments given above for the neutral ligand regarding relative peak broadening and variable temperature NMR, the dynamic process observed for the protonated ligand is also assigned to rotamers of type B. Furthermore, in the case of protonated ligands more informative low temperature NOESY spectra were obtained (Figure 2-14) which showed H^{A3}-H^{B3} cross-peaks allowing unambiguous assignment of each side of the tpy. However, *all* the peaks of the protonated ligand appear broader than that of the neutral ligand (Figure 2-10). Type A bond rotation (see earlier) perhaps best explains this additional source of broadening due to protonation. If protonation occurred on a pyridyl ring then py-py bond rotation would be slower due to hydrogen bonding between the pyridyl N-H and the free pyridyl nitrogens (see Figure 2-15b).

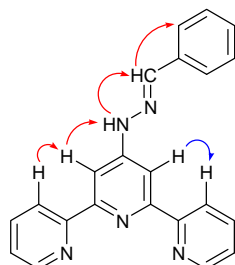


Figure 2-13 Observed NOESY interactions at 195K (acetone-d₆) from the spectrum shown in Figure 2-14.

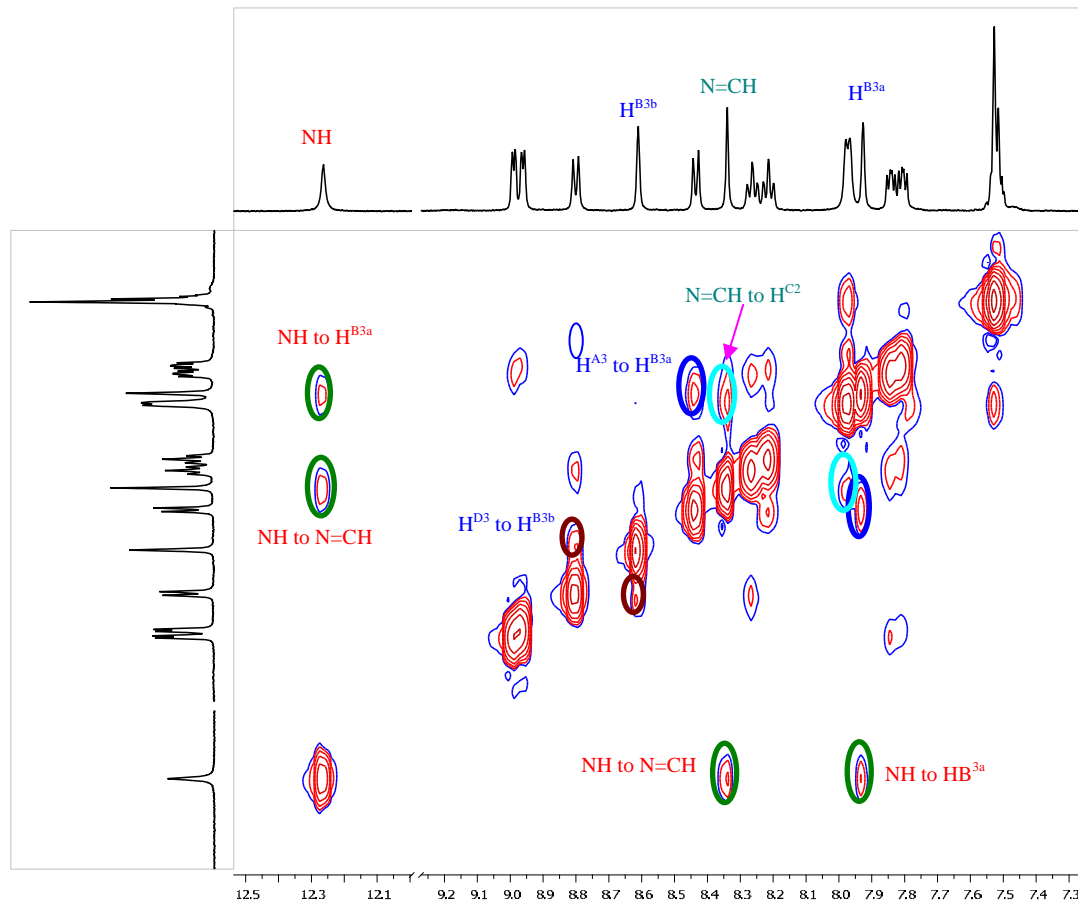


Figure 2-14 NOESY [H^{17}]PF₆ spectrum (500 MHz, acetone-d₆) at 195K showing the amine NH has cross peaks to only one of the two H^{B3} environments.

2.7. Where is the site of protonation and how does this restrict rotation?

There are a number of possible protonation sites with the most likely being the imino nitrogen (Figure 2-15a) or the nitrogens of the terminal or central pyridine rings (Figure 2-15b). It may appear logical that protonation of the imino nitrogen would be the most likely explanation for the slowed rotation. The distance between the imino NH and H^{B3} would be less than 2Å [based on PM3 level Spartan calculations]²²⁴ at the closest-contact rotamer which could be close enough to hinder rotation about the tpy-NH bond and would explain the observed behaviour.

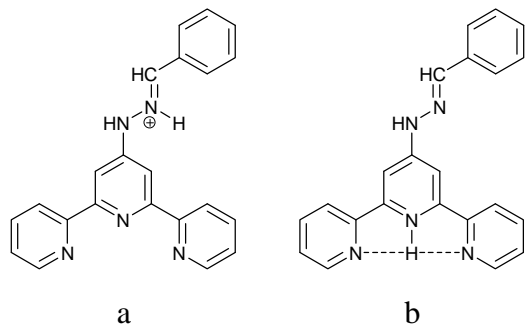
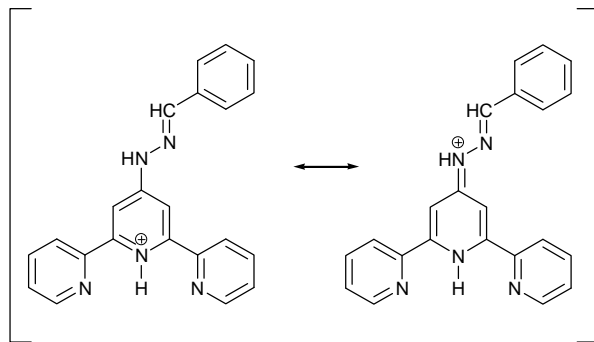


Figure 2-15 Possible protonation sites of **17**

Protonation at one of the pyridyl rings (Figure 2-15b) would adequately explain slowed rotation about the py-py bonds but does not provide any steric reason for hindered tpy-NH rotation. However, if the charge delocalisation occurred involving the resonance form shown in Scheme 2, then partial double-bond character could result in the tpy-NH bond, which would restrict rotation. Such a resonance form would also result in greater positive charge on the amino nitrogen which would promote stronger hydrogen bonding between the amino proton and anions/solvent which would be expected to hinder rotation. Although hydrogen bonding in phenyl hydrazones has aroused interest for a long time,¹⁸⁹ to date pyridyl hydrazones have not been studied.



Scheme 2 Delocalisation of charge

The first substantial evidence for the protonation site being the pyridyl ring(s) is given by Figure 2-11 which compares the $^1\text{H-NMR}$ (DMSO-d_6) spectra of **17** (neutral), $[\text{H17}]^{\text{PF}_6}$ and $[\text{H}_2\text{17}](\text{MeOSO}_3)_2$ at 360K. This high temperature comparison is useful as each spectrum represents an average conformation with sharp, well resolved signals. All the signals are shifted downfield on protonation (as expected since the molecule becomes electron deficient) with the exception of $\text{H}^{\text{A}3}$ and $\text{H}^{\text{B}3}$, which are both shifted slightly upfield. This is consistent with the equilibrium orientation of the pyridyl rings

being shifted towards the *cis-cis* conformation (Figure 2-9) when protonated, where the H^{A3} and H^{B3} protons are not in the deshielding region of the nitrogen lone pairs.

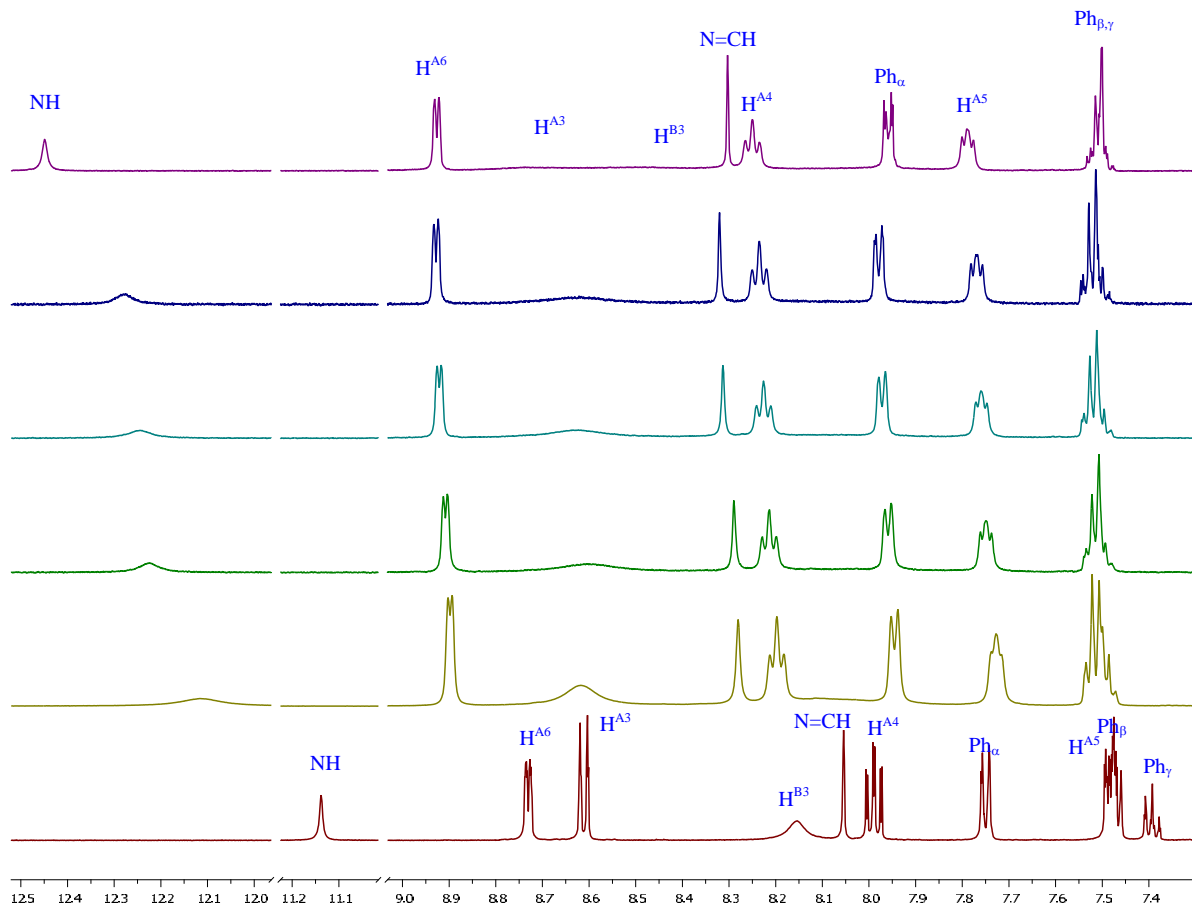


Figure 2-16 ^1H -NMR spectra (500 MHz, DMSO- d_6 , 295 K) of $[\text{H}_2\mathbf{17}](\text{MeOSO}_3)_2$ (top), $[\text{H}_2\mathbf{17}](\text{NO}_3)_2$, $[\text{H}_2\mathbf{17}](\text{PF}_6)_2$, $[\text{H}_2\mathbf{17}]\text{BF}_4$, $[\text{H}_2\mathbf{17}]\text{PF}_6$ and $\mathbf{17}$ (bottom) and showing the influence of protonation state and anions on the $\text{H}^{\text{A}3}$, $\text{H}^{\text{B}3}$ and NH signals.

The influence of solvent and counter-ions were found to be significant. Figure 2-16 show a comparison of the ^1H NMR (DMSO- d_6) spectra for $\mathbf{17}$ as (MeOSO_3)₂, (NO_3)₂, (PF_6)₂, BF_4^- and PF_6^- salts as well as the neutral ligand. Two clear observations can be made. Firstly, the amine signal is shifted significantly downfield when the ligand is protonated [by 0.83 (PF_6^-), 1.09 (BF_4^-), 1.11 (PF_6)₂, 1.14 (NO_3)₂, 1.31 (MeOSO_3)₂ and relative to the free ligand], consistent with it being involved in stronger hydrogen bonding when the ligand is protonated. Secondly, the amine signal chemical shift appears to be dependant both the protonation state and on the anion present. The signal becomes sharper and is shifted downfield as the anion changes from BF_4^- and PF_6^- to NO_3^- and MeOSO_3^- . The imino signal is also shifted downfield, but to a much smaller extent. The $\text{H}^{\text{A}3}$ and $\text{H}^{\text{B}3}$ signals concurrently become broader, as expected when the tpy-NH bond rotation becomes slower. A possible explanation for the observed slowing

of tpy-NH bond rotation is the presence of hydrogen bonding between the amino proton and an anion. This would add significant bulk to the hydrazone moiety and thus hinders rotation (Figure 2-17) in addition to further promoting delocalisation and increasing the double-bond character of the tpy-NH bond. In order to differentiate between the influence of anion and protonation-state effects, the diprotonated $[H_2\mathbf{17}][PF_6]_2$ was prepared. The addition of HPF_6 (60% aqueous) to a solution of **17** in EtOH resulted in the immediate precipitation of a bright yellow solid. Elemental analysis was consistent with the formation of $[H_2\mathbf{17}][PF_6]_2$. A comparison of the room temperature 1H NMR ($DMSO-d_6$) with those of the other protonated species suggested a diprotonated species was formed, although there is evidence that in acetone- d_6 solution, an equilibrium mixture of $[H_2\mathbf{17}][PF_6]_2$ and $[H\mathbf{17}][PF_6]$ exists; the spectrum at 195 K exhibits two sets of signals (one well resolved and the other broadened). Both $[H_2tpy]^{2+}$ and $[Htpy]^+$ are weak acids ($pK_a = 3.57$ and 4.54, respectively, 298 K, in 0.2 m aqueous KCl).²²⁵ The fact that treatment of $[H_2\mathbf{17}][MeOSO_3]_2$ in hot MeOH with $NaBF_4$ or NH_4PF_6 results in the formation of tetrafluoroborate or hexafluorophosphate salts of $[H\mathbf{17}]^+$ indicates that, in the absence of a strong hydrogen-bond acceptor (*viz.* $[MeOSO_3]^-$), $[H_2\mathbf{17}]^{2+}$ will partially deprotonate in solution. Therefore we propose that hydrogen bonding plays a key role in the solution species behaviour which can be significantly influenced by anion and solvent selection in addition to protonation state.

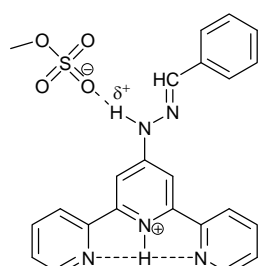


Figure 2-17 Hydrogen bond formation between the amino proton of $[H\mathbf{17}]^+$ and the $MeOSO_3^-$ counter-ion.

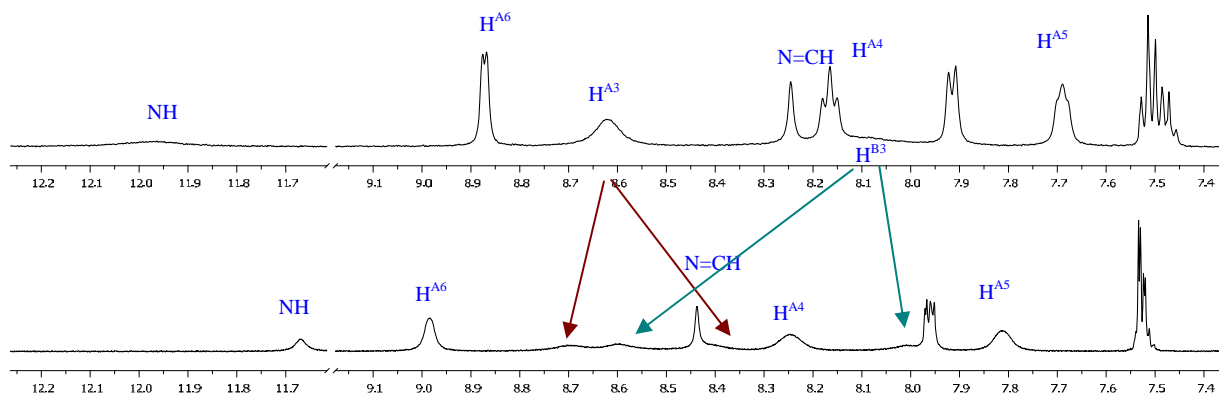


Figure 2-18 ^1H -NMR (500 MHz) spectrum of $[\text{H}17]\text{PF}_6$ in $\text{DMSO}-d_6$ (top) and $\text{acetone}-d_6$ (bottom) both at 295K. Similar observations were obtained for the analogous BF_4 salt.

The solvent dependence of the dynamic behaviour of **17** can also be rationalized in terms of the ability of the NH proton to engage in hydrogen bonding with a suitable acceptor.²²⁶⁻²²⁸ DMSO is expected to be a better hydrogen bond acceptor than acetone,²²⁹ and association between **17** and the solvent will result in steric hindrance that will slow down the rate of rotation about $\text{C}_{\text{py}}-\text{N}_{\text{amine}}$ bond. Consistent with this, the NH signal are shifted downfield (e.g.: for **17**, δ_{NH} DMSO- d_6 11.14 ppm, acetone- d_6 10.15 ppm) and broadens the $\text{H}^{\text{A}3}$ and $\text{H}^{\text{B}3}$ signals as rotation is slowed. Solvent effects for the protonated ligands are more difficult to explain. An example, $[\text{H}17]\text{PF}_6$, is shown in Figure 2-18. In this case, the room temperature spectrum in acetone is below the coalescence temperature whereas the spectrum in DMSO is approximately at coalescence temperature at the same temperature. That is, bond rotation is significantly *slower* in acetone than in DMSO; a similar effect was also observed for the BF_4 salt.

We now consider ligands **17**, **18**, **19** and **20**. It is important to note that the solid-state structural data for these compounds reveal that the $\text{C}_{\text{py}}-\text{N}_{\text{amine}}$ bond lengths are the same (1.38 Å, see later). Hence, differences in the barrier to rotation about the $\text{C}_{\text{py}}-\text{N}_{\text{amine}}$ bond are likely to be steric rather than electronic in origin. Consistent with this, we observe that on going from **18** to **19** in $\text{DMSO}-d_6$, the increased steric demands of the *C*-phenyl vs. *C*-methyl substituent increases the barrier to rotation. At room temperature, the observation that $\text{H}^{\text{B}3}$ appears as a broad signal for **17**, but a sharp singlet for **18**, indicates that introducing the *C*-methyl substituent *lowers* the barrier to rotation about the $\text{C}_{\text{py}}-\text{N}_{\text{amine}}$ bond. Based on steric arguments, this was an unexpected

observation. However, changing the solvent to acetone-*d*₆ results in the expected trend: the H^{3B} signal full-width-at-half-height 4.8, 5.3 and 9.0 Hz for as the bulk of the substituent increases from H, Me to Ph for **17**, **18** and **19** respectively. A comparison with the *N*-methyl derivative **20** now becomes useful. Firstly, to establish the broadening of signals that was observed for the hydrazones of type **16** was unambiguously due to rotation around the C_{py}-NH bond and secondly to investigate the role played by hydrogen bonding as *N*-methylation prevents hydrogen-bond associations in phenyl hydrazones.¹⁸⁹



Slowed rotation due to hydrogen bonding No hydrogen bonding to the amine, less restricted rotation

The presence of well defined ¹H NMR signals (Figure 2-19), even for the protonated species, suggests that the bond rotation must be *faster* for the N-Me derivative than the N-H. Analogous dynamic behaviour is observed for the NHMe substituent in *N*-methylaniline.²³⁰ This observation is also in keeping with hydrogen bonding to anions and solvent (increasing the bulk of the hydrazone moiety) being a significant source of the restricted rotation.

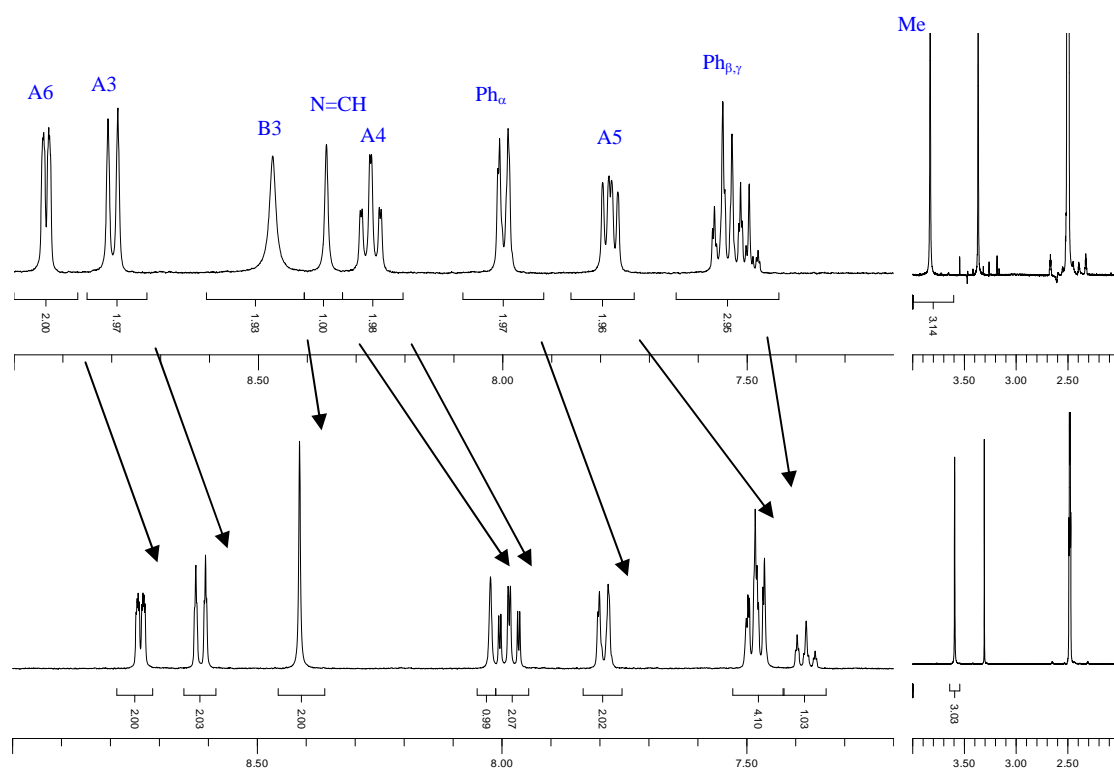


Figure 2-19 ^1H NMR (500 MHz) spectrum for $[\text{H}_2\mathbf{20}][\text{MeOSO}_3]_2$ (top) and **20** (bottom) in DMSO-d_6 (295K).

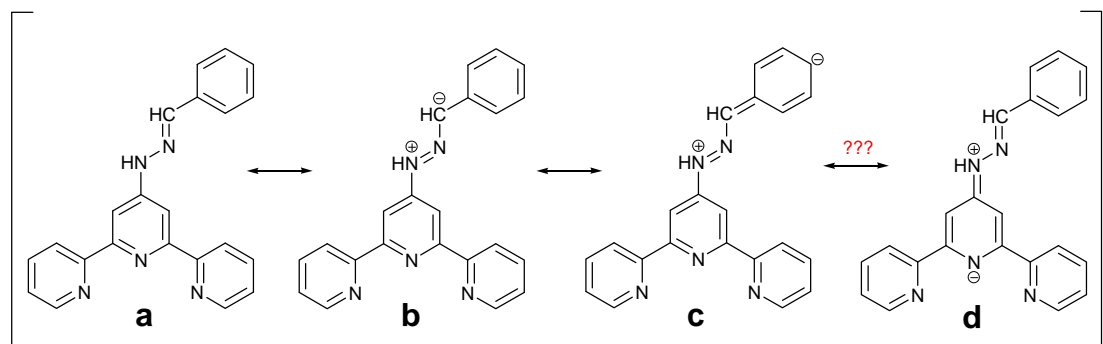
2.8. Substituent Effects

The preparation of ligands **17-25** was analogous to that previously described; the experimental details are contained in the experimental section. In all cases the ligands were isolated as bright yellow solids, consistent with diprotonated MeOSO₃ or EtOSO₃ salts. Anion exchange reactions, and isolation of neutral ligands was often more difficult due to solubility problems or the formation of gum-like pastes on base addition.

2.8.1. ^1H and ^{13}C NMR spectroscopy

The only signals significantly affected by the nature of the substituents on the phenyl ring were those arising from the amine NH and the imino CH. Considering the neutral ligands with -C₆H₄-X substituents [in order of increasing electron withdrawing, in DMSO-d₆, 295K] δ /ppm H^{N=CH} 8.00 for **23** (-OMe), 8.06 for **17** (-H), 8.02 for **22** (-Br), 8.14 for **24** (-NO₂); H^{NH} 10.97 for **23** (-OMe), 11.14 for **17** (-H), 11.21 for **22** (-Br), 11.52 ppm for **24** (-NO₂)].

The ^{13}C NMR spectral data (see experimental for details) also showed a strong consistency for the tpy signals, with a range of signals less than 2 ppm for all signals. Similar to the proton spectrum, the imino signal was the most affected [neutral ligands with $-\text{C}_6\text{H}_4\text{-X}$ substituents, DMSO-d₆, 295K, δ /ppm C^{N=CH} 140.7 for **23** (-OMe), 140.7 for **17** (-H), 139.5 for **22** (-Br), 138.2 ppm for **24** (-NO₂)] and, perhaps surprisingly, the C^{B3} was unaffected [DMSO-d₆, 295K, δ /ppm C^{B3} 103.7 for **23** (-OMe), 103.8 for **17** (-H), 103.8 for **22** (-Br), 103.7 ppm for **24** (-NO₂)]. Much larger ranges (up to 10.5 ppm for C^{C=NH}) were observed for protonated ligands, although these shifts did not follow a simple electron withdrawing order and could not be interpreted meaningfully. Observation of quaternary carbons was usually not possible for protonated ligands due to these being broadened into the baseline.



Scheme 3 Possible resonance contributions of **17**.

Resonance structures, as shown in Scheme 3, may provide a useful explanation for the observed effects. It has been previously reported^{231, 232} that the ^{13}C -NMR signal for the iminyl carbon of hydrazones and phenylhydrazones is dependant on the substituent attached to the iminyl carbon. As the *electron withdrawing* ability of the substituent increased the ^{13}C -NMR chemical shift of the iminyl carbon moved *upfield* as resonance forms of types b and c (Scheme 3) are increasingly stabilised. Additionally, it has been reported²³³ that the ^{15}N -NMR chemical shift of the imino nitrogen is *less sensitive* to substituent effects than the signal of the amino nitrogen. This is also consistent with the resonance structures shown as the amino nitrogen experiences a much greater change in charge distribution and bond order than does the imino nitrogen. Similarly, for phenylhydrazones the *electron density* on NH (or NMe) and N=C *decreases* when the phenyl substituent becomes *more electron-withdrawing* and corresponding ^{15}N -NMR chemical shift are shifted *upfield* (as expected) and the signal of N=C is *more sensitive* to substituents than the NH (or NMe).²³² Also ‘*the charge on the C=N nitrogen is less*

sensitive to substitution than that on the C=N carbon'. The observations reported here are in keeping with these previous findings. However, such trends were much more difficult to analyse for the protonated ligands. For example, both strongly electron-withdrawing $-C_6H_4NO_2$ (**24**) and electron-donating $-C_6H_4OMe$ (**23**) had similar chemical shifts for the imine signals (monoprotonated BF_4^- salts, $DMSO-d_6$, 295K 8.24 and 8.23 ppm respectively). This is likely due to the electronic effects on protonation (see previous discussion) which dominate, minimising any substitution effects.

2.8.2. UV-Vis spectra of select ligands

As mentioned in the introduction, phenylhydrazones have been long known to exhibit strong and reversible colour changes with pH changes¹⁸⁹, even being used as alkaline pH indicators^{190, 191}. All of the ligands presented here are coloured when protonated. Generally they are coloured bright yellow as $MeOSO_3^-$ salts and green as BF_4^- salts. On the addition of a base, such as NaOH, the ligands are deprotonated (to give the neutral ligands) and the colour is progressively reduced, as shown in Figure 2-20.

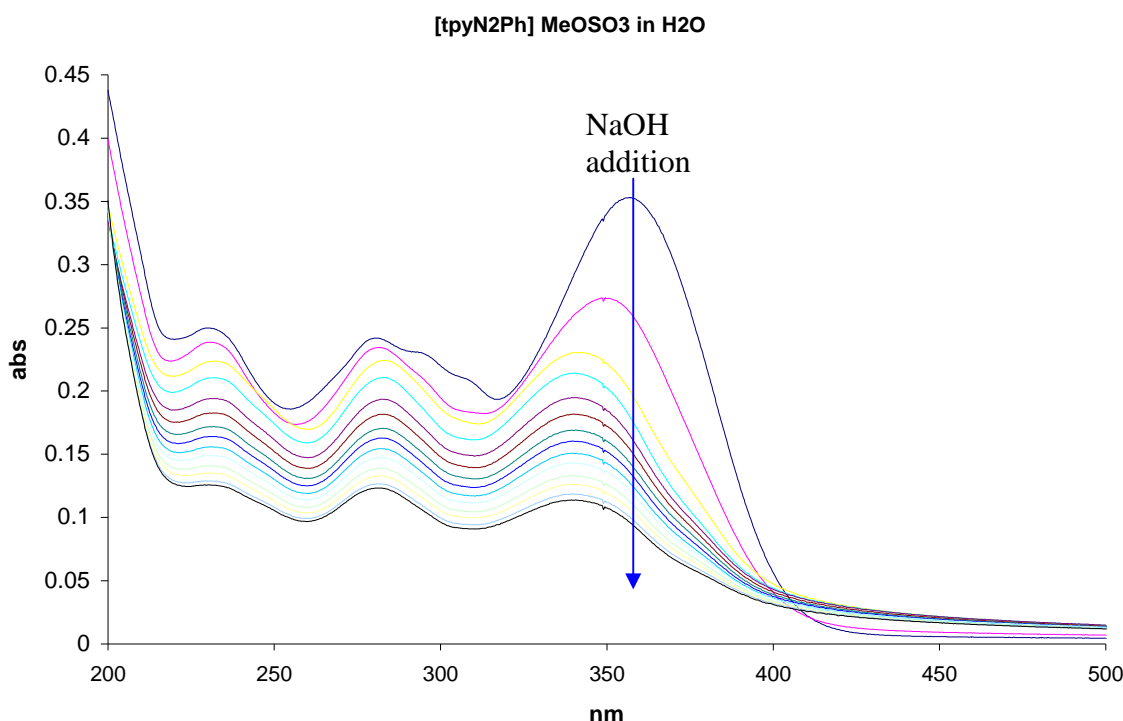


Figure 2-20 UV-Vis spectrum of $[H_217](MeOSO_3)_2$ (1.3×10^{-5} mol/L, H_2O) showing the effect of NaOH addition. λ_{max} is at 356nm

On further addition of base it is possible to remove the amino proton which results in more significant colour changes (the type of which was found for other phenyl hydrazones). Two specific examples are ligands **17** and **24**.

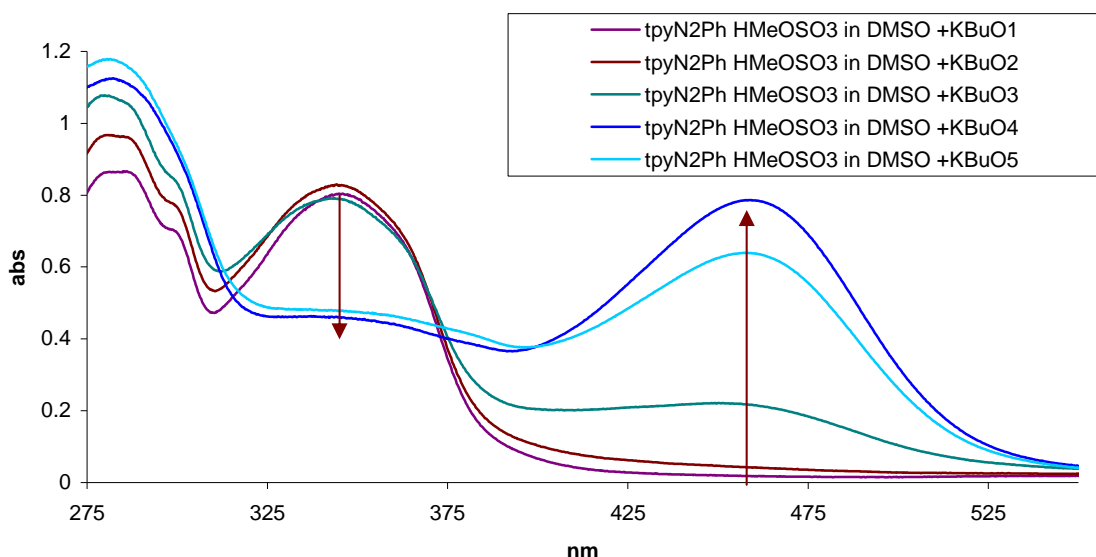


Figure 2-21 UV-Vis spectrum of $[H_2\mathbf{17}](MeOSO_3)_2$ (2.9×10^{-5} mol/L in DMSO) showing the effect of $KOBu^1$ addition. λ_{max} shifts from 344 nm to 459 nm

Deprotonation of ligand **17** results in a significant colour change as a strong absorption appears at 459 nm and an accompanying decrease in the peak at 344nm, as shown in Figure 2-21. This is a result of the conjugation extending throughout the molecule on deprotonation and is a common feature of all the phenyl hydrazones presented here. Ligand **24** is a special case, as a more dramatic colour change is observed where the $-NO_2$ chromophore causes an broad and intense red adsorption centred at 646 nm (Figure 2-23) on deprotonation. This is well understood in terms of the resonance structures in Figure 2-22 and it is for this reason that nitrophenyl hydrazones have been used as dyes.

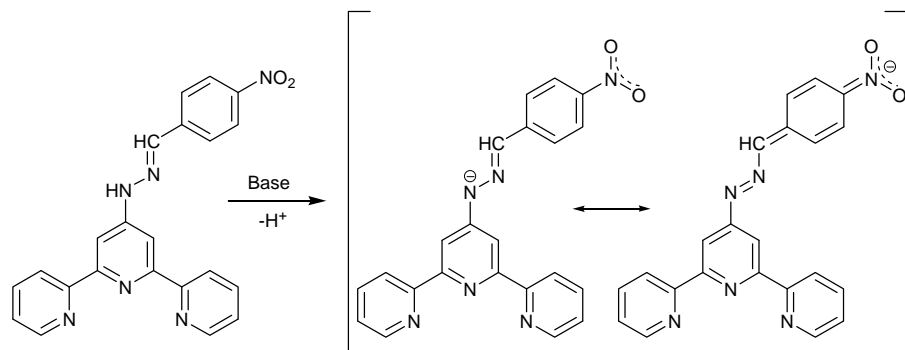


Figure 2-22 Deprotonation of **24** on base addition to give delocalised charge.

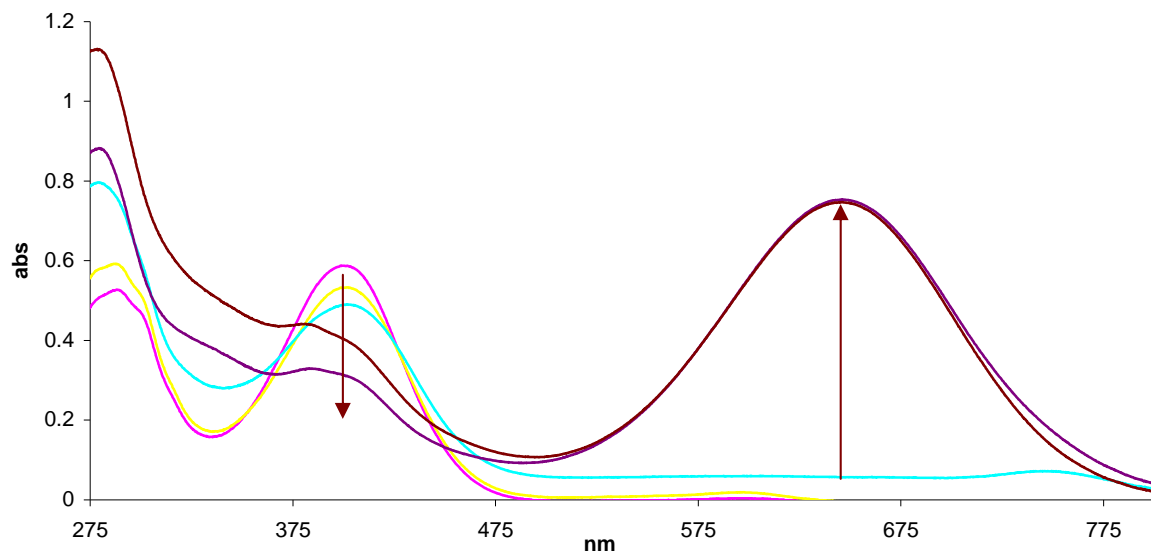


Figure 2-23 UV-Vis spectrum of **24** (2.2×10^{-5} mol/L in DMSO) with KOBu^t addition to give an intense absorption at 646 nm

2.9. Deprotonation

Deprotonation could also be followed by NMR spectroscopy to investigate the structural changes that occur. The simplest example is **25** which bears only methyl substituents allowing the aromatic region to remain easy to interpret. On addition of solid potassium *tert*-butoxide to a DMSO-d₆ solution of **25** (with heating) significant changes in the ¹H-NMR spectrum were observed (Figure 2-24).

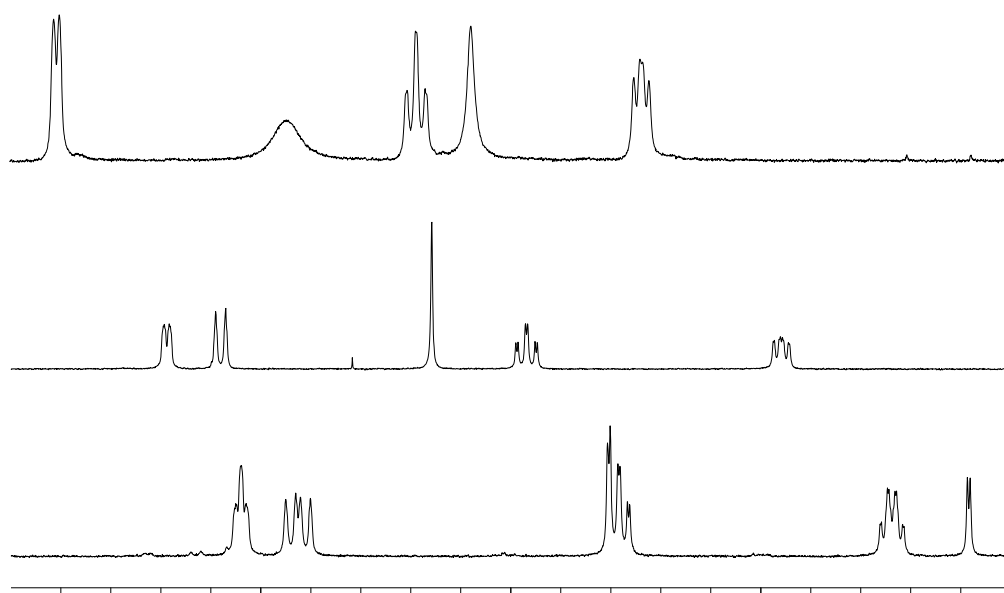
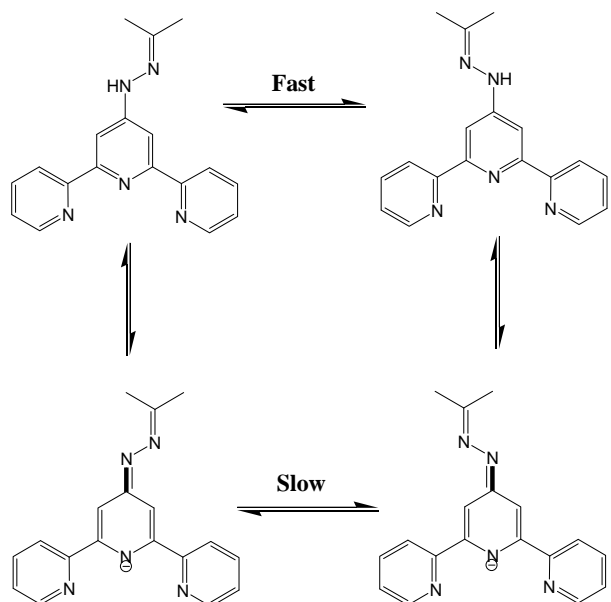


Figure 2-24 ¹H-NMR spectrum (500 MHz, DMSO-d₆, 295K) of $\text{H}_2\mathbf{25}(\text{MeOSO}_3)_2$ (top), neutral **25** and $(\mathbf{25}-\text{H})^-$ (bottom)

The resulting structure was shown to contain an asymmetric tpy environment similar to that observed previously at low temperatures. The observations of base addition to **25** are also in accord the type of restricted rotation discussed previously, although acting via a different mechanism. In this case, on deprotonation of the amino NH the negative charge is delocalised (as shown in Scheme 4) which results in a more double-bond character of the tpy-NH bond. This restricts the rotation about this bond and results in the observed asymmetry of the molecule. Other ligands act similarly, although several, especially **24**, were found to be unstable in solution on base addition, decomposing into other tpy-containing species, likely HOtpy.



Scheme 4 Restricted rotation of **25** on deprotonation of the amino NH

2.10. X-ray structure characterisation

General summary of presented X-ray structures

The X-ray crystal structures were determined for the following ligands:

Neutral

- **17**
- **18**
- **19·CH₂Cl₂**
- **20**
- **26·CHCl₃·H₂O**

- **22** \cdot H₂O
- **24**
- **25**

Monoprotonated

- [H**17**](CF₃CO₂) \cdot EtOH \cdot 0.5H₂O
- [H**17**](PF₆).H₂O
- [H**18**](BF₄)
- [H**21**](BF₄)
- [H**19**](MeOSO₃)

Diprotonated

- [H₂**18**](NO₃)(MeOSO₃) \cdot H₂O
- [H₂**17**]Cl₂ \cdot DMSO

The neutral ligands all adopts the expected²²³ *trans-trans* conformation (Figure 2-9) of the pyridyl rings as is typical of terpyridine ligands to minimise lone-pair interactions. In contrast, all the mono- and di-protonated ligands adopt the *cis-cis* confirmation with intramolecular hydrogen bonding between py(N-H) and py(N). For example, the calculated bond distance for [H**17**][PF₆] from py(N-H) to py(N) is 2.25 and 2.24 Å with bond angles of 107° (both). This provides strong evidence that the protonation site is the central pyridyl ring and the free lone pairs of the non-protonated pyridyl rings are involved in hydrogen bonding which results in the *cis,cis* conformation, as previously predicted by *ab initio* quantum mechanics calculations for tpy²²³. A number of crystal structures of diprotonated terpyridines^{221, 223, 234-240} have been reported which also display *cis,cis* conformations, although all reported monoprotonated structures²²⁰⁻²²² have adopted *cis,trans* conformations. The structures reported here are the only to date which are mono-protonated and adopt *cis,cis* conformation. In all cases, the substituents around the C=N bond adopt an (*E*)-configuration, as observed in solution.

2.11. X-Ray crystal structures of neutral ligands

Colourless plates of **17** were grown by slow evaporation of a CHCl₃ solution of the compound. Figure 2-25 shows the molecular structure of **17**, with the tpy unit in the anticipated *trans,trans*-conformation with typical bond lengths and angles. The aromatic

rings are significantly twisted with respect to one another [angles between the least-squares planes of rings containing N1 and N2, N2 and N3, and N2 and C17: 10.64(7), 20.87(7) and 24.26(8) $^{\circ}$].

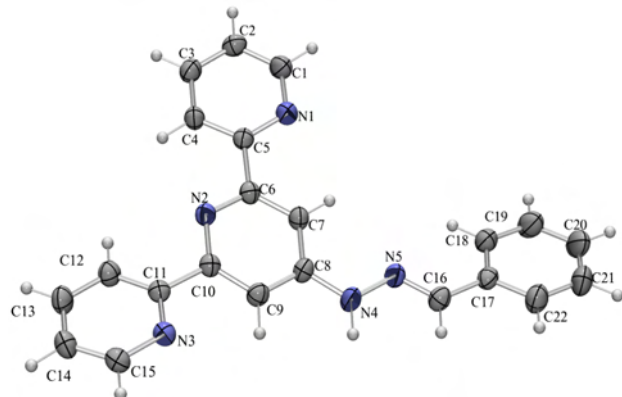


Figure 2-25 An ORTEP plot of neutral **17** with displacement ellipsoids drawn at 50% probability. The numbering scheme adopted is shown.

In the absence of other hydrogen bond acceptors, the amino NH is hydrogen bonded to the pyridyl nitrogen atom N3 ring of an adjacent molecule to form hydrogen bonded pairs which associate as shown in Figure 2-26..

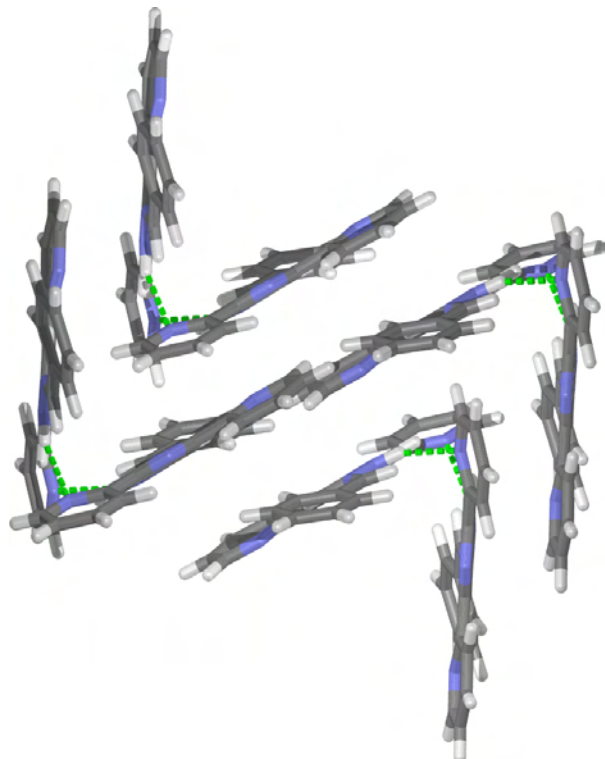


Figure 2-26 X-Ray crystal structure of neutral **17** showing the arrangement of molecules into hydrogen-bonded pairs.

The evolution of the two symmetry related N4–H1…N3i interactions leads to the formation of weaker CH_{imine}…N_{pyridine} interactions as well as a repulsive H91…H91i contact (2.38 Å). The V-shaped dimeric motifs assemble as shown in Figure 2-26 forming interlocking zigzag chains which run parallel to the crystallographic *c*-axis. The observation that molecule is twisted away from planarity and is not involved in the type of π–π stacking which is observed for the protonated ligands (see later) directly implies that the stabilisation gained from this type of hydrogen bonding arrangement must be significant.

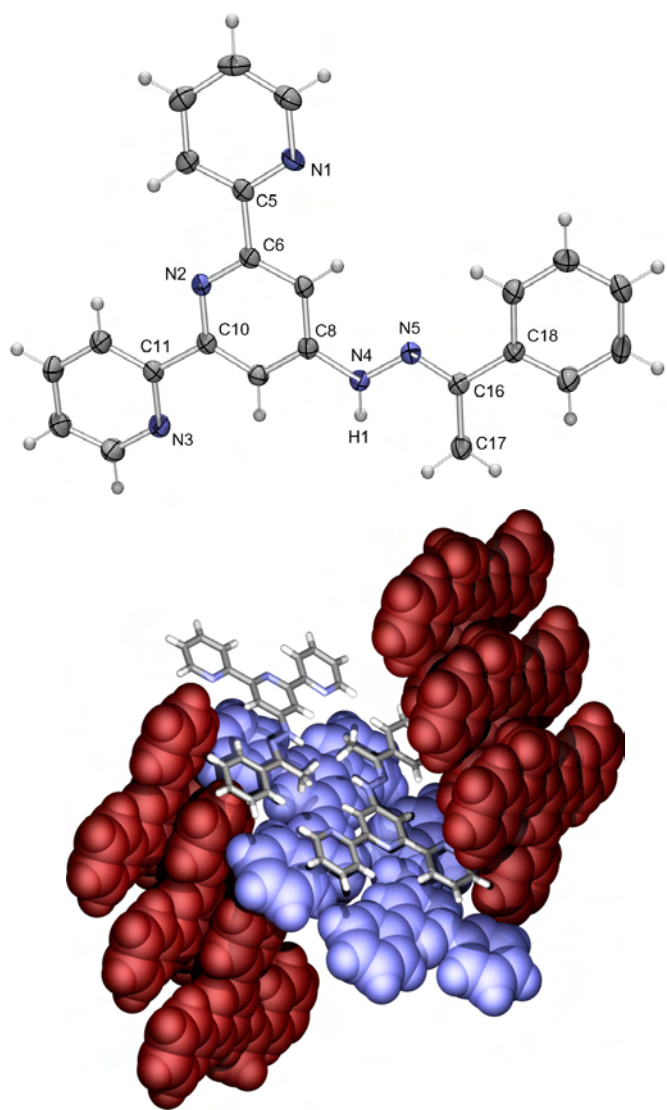


Figure 2-27 (a) X-Ray crystal structure of neutral **18** with thermal ellipsoids plotted at the 50% probability level. Selected bond lengths and angles: N4–C8 1.378(2), N4–N5 1.364(2), N5–C16 1.293(2), C16–C17 1.502(2), C16–C18 1.483(2) Å, N5–N4–C8 120.2(1), N4–N5–C16 118.2(1), N5–C16–C17 124.3(1), N5–C16–C18 115.9(1)°. (b) Packing diagram for **18** showing interlocking π-stacked pairs of molecules. One pair is shown in stick representation, and illustrates the close C_{tpy}H…CH₃ contacts.

X-Ray-quality colourless plates of **18** (Figure 2-27a) were grown by slow evaporation of a CH₂Cl₂ solution of the compound. Bond lengths and angles are unexceptional, the tpy unit has the usual *trans,trans*-conformation.. The angles between the least-squares planes of the rings containing N1 and N2, N2 and N3, and N2 and C17 are 6.06(7), 6.44(7) and 67.5(8)^o, and therefore a molecule of **18** is much closer to being planar than is **1**. This is, presumably, a consequence of the packing which is dominated by π -stacking (Figure 2-27b). Pairs of molecules stack in slightly offset columns with a distance of 3.20 Å between the least-squares planes of the molecules. The columns interlock as shown in Figure 2-27. The packing efficiency of the crystalline lattice is 70.5%,¹⁸¹ and the stabilizing energy gained from the extensive π -stacking must compensate for the repulsive energy of the close C_{tpy}H \cdots CH₃ contacts within each pair of molecules (H91 \cdots H173i = 2.37 Å, symmetry code i = 1 - x, 2 - y, 1 - z). The mode by which efficient packing is achieved by **18** contrasts with that in **17** (packing efficiency of 69.9%¹⁸¹) in which NH_{imine} \cdots N_{pyridine} and CH_{imine} \cdots N_{pyridine} interactions are important (Figure 2). In **18**, the steric requirements of the methyl substituents presumably prevent the evolution of efficient NH_{imine} \cdots N_{pyridine} interactions, with the result that hydrogen bonding interactions are less favourable than in **17**.

Crystals of **19**.CH₂Cl₂ suitable for X-ray diffraction were grown by slow evaporation of a CH₂Cl₂ solution of the compound. Figure 2-28 illustrates that the tpy domain is close to being planar [angles between the least-squares planes of rings containing N1 and N2, and N2 and N3: 2.51(8) and 6.74(8) Å] and adopts the expected *trans,trans*-conformation.

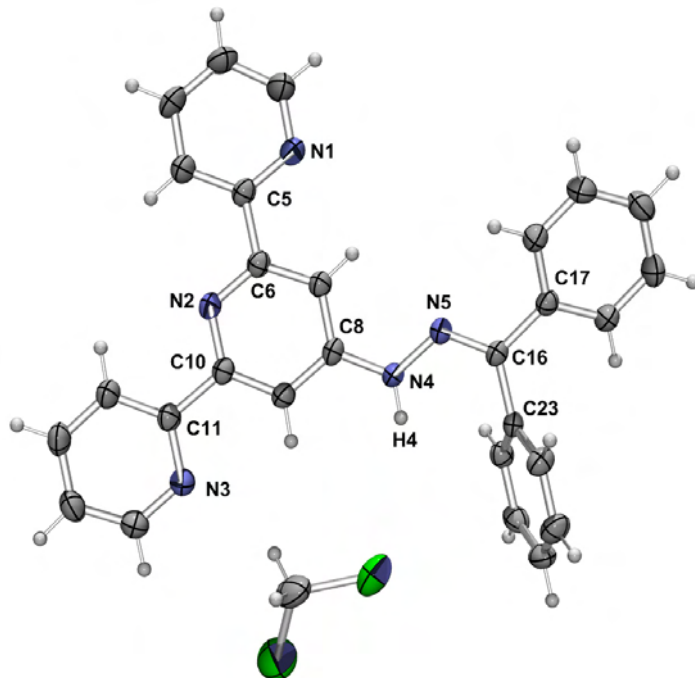


Figure 2-28 The molecular structure of **19** in **19.CH₂Cl₂** with thermal ellipsoids plotted at the 50% probability level. Selected bond lengths and angles: N4–C8 1.378(2), N4–N5 1.361(2), N5–C16 1.288(2), C16–C17 1.479(2), C16–C23 1.495(2) Å; N5–N4–C8 118.5(1), N4–N5–C16 118.6(1), N5–C16–C17 116.2(1), N5–C16–C23 123.9(1)°.

The phenyl substituents are twisted away from the plane of the hydrazone unit [angles between the least squares planes of rings containing N2 and C17, and N2 and C23: 19.15(8) and 75.01(8)°], thus minimising steric interactions. It is worth noting that the imine hydrogen atom H4 is in close contact with the *ipso*-carbon atom C23 (H4…C23 2.42 Å) and the adjacent C28 (H4…C28 2.67 Å), a situation discussed previously by Drew et al.²²⁶ The molecules pack so that pairs of tpy units are π -stacked, with the planes of pyridine rings containing N2 and N3 being 3.58 Å apart. The solvent CH₂Cl₂ molecules reside in cavities (Figure 2-29), hydrogen bonded to pyridine N atoms [C29H292…N3 2.45 Å, C29…N3 3.273(3) Å, C29–H292…N3 143°, C29H291…N2i 2.55 Å, C29…N2i 3.417(3) Å, C29–H292…N2i 153°; symmetry code i = 1 – x, 1 – y, 1 – z] and with additional weak contacts to phenyl rings (C11…H21ii 2.94 Å, symmetry code ii = –1 + x, –1 + y, z; C11…centroid ring containing C23 3.79 Å). Presumably, the proximity of a phenyl substituent to the imine NH group prevents the latter engaging in hydrogen bonded interactions. The closest approach of one CH₂Cl₂ chlorine atom is 3.26 Å (N4H4…Cl1).

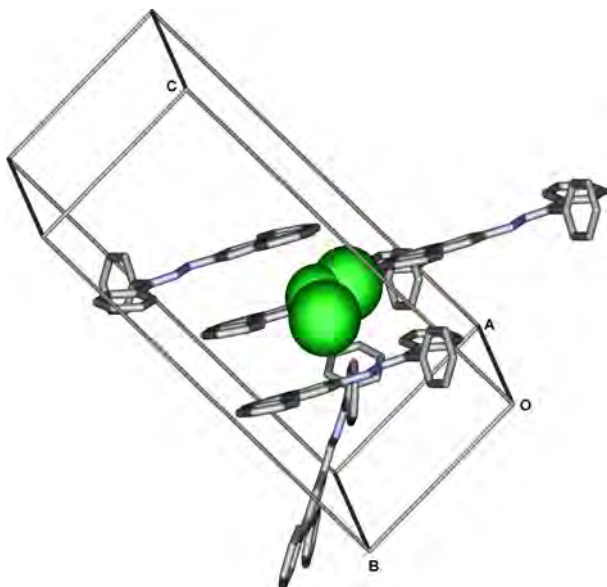


Figure 2-29 The packing of CH_2Cl_2 (in green CPK) in **19**. CH_2Cl_2 in close contacts with four neighbouring molecules of **19**.

In each of compounds **17**, **18** and **19**, the hydrazone unit contains an NH unit which has the potential to engage in hydrogen bonded interactions, although in **19** this appears to be unfavourable on steric grounds (see above). The deviation of the HNN=C framework from the plane of the central pyridine ring of the tpy domain in each compound is small. Each compound exhibits the same $\text{C}_{\text{py}}-\text{N}_{\text{amine}}$ bond length (see Figure captions) and this is shorter than the sum of the covalent radii (1.52 \AA) indicating that the bond contains some π -character.

X-ray-quality crystals of **20** were grown by slow evaporation of a $\text{CH}_2\text{Cl}_2/\text{EtOH}$ solution of the compound, allowing us to investigate the structural consequences of introducing an *N*-methyl substituent. The structure of **20** is shown in Figure 2-30; bond parameters are as expected. The tpy domain has the anticipated *trans,trans*-conformation, and deviates slightly from planarity [angles between the least-squares planes containing N1 and N2, and N2 and N3: $9.45(9)$ and $9.00(9)^\circ$, respectively].

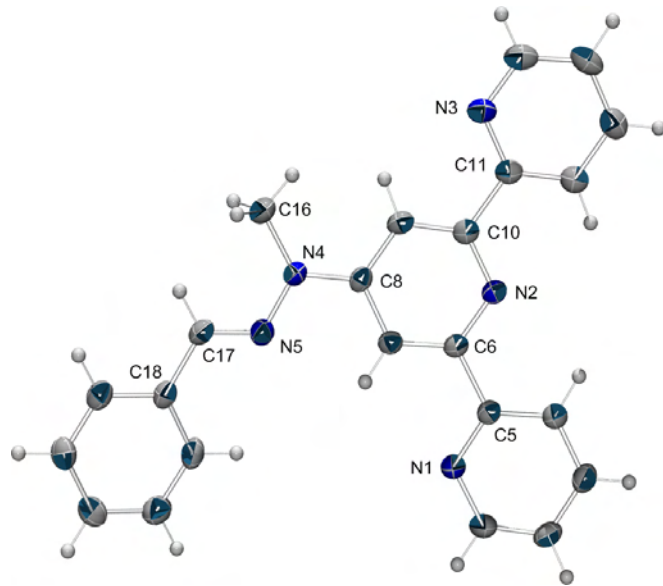


Figure 2-30 X-Ray crystal structure of neutral **20** with thermal ellipsoids plotted at the 50% probability level. Selected bond lengths and angles: N4–C8 1.389(2), N4–N5 1.363(2), N5–C17 1.284(2), N4–C16 1.450(2), C17–C18 1.466(3) Å; N5–N4–C8 115.8(1), N4–N5–C17 119.1(2), N5–C17–C18 120.2(2)°.

The phenyl substituent is twisted out of the plane of the central pyridine ring by 20.42(9)°. The deviation of the N5N4C16 unit from the least-squares plane of the ring containing N2 is only 11.4(2)°, compared to a corresponding angle of 7.4(2)° for compound **17**. This results in repulsive H_{Me}···H_{py} contacts, but this is presumably offset by retention of some π - character in the C8–N4 bond [1.389(2) Å compared to 1.378(2) or 1.379(2) Å in **17**, **18** and **19**]. Other simple *N*-methyl hydrazones also show this preference.^{241–244} Pairs of molecules (related by a crystallographic inversion centre) assemble so that the central pyridine rings (containing N2) are π -stacked (distance between planes of rings: 3.363 Å, Figure 2-31). Atom N2 makes a weak contact to a phenyl CH group in an adjacent pair of molecules (N2···H_{231i}C_{23i} 2.70 Å, symmetry code i = 1/2 + x , 3/2 – y , 1/2 + z).

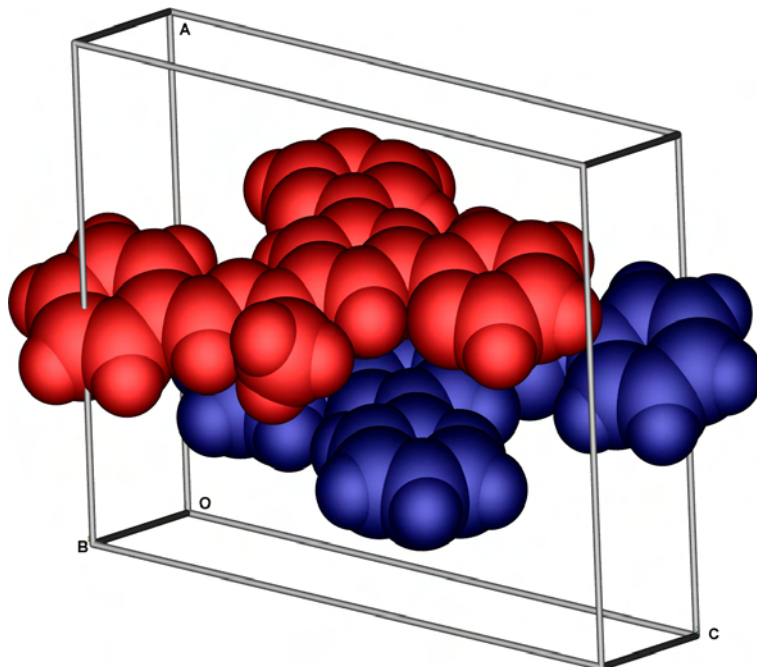


Figure 2-31 X-Ray crystal structure of **20** showing π -stacked pairs related by a crystallographic inversion centre. Distance of centroid to plane of rings containing N2 and N2i (symmetry code $i = 1-x, 1-y, 1-z$) is 3.363 Å.

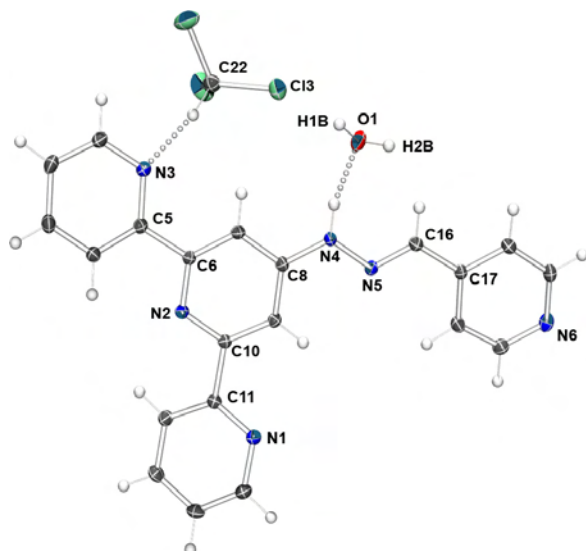


Figure 2-32 Molecular structure of **26** in **26·CHCl₃·H₂O** with ellipsoids plotted at the 50% probability level. Selected bond parameters: N4–C8 = 1.374(3), N4–N5 = 1.357(3), N5–C16 = 1.288(4), C16–C17 = 1.455(4) Å; N5–N4–C8 = 119.1(2), C16–N5–N4 = 116.5(2), N5–C16–C17 = 119.7(2)°. Hydrogen bond contacts: N4H4B...O1 = 2.04 Å; N4...O1 = 2.865(3) Å; N4–H4B...O1 = 155°; Cl3...H7AC7 = 2.94 Å; Cl3...C7 = 3.73(2) Å; Cl3...H7A–C7 = 141°.

Single crystals of **26·CHCl₃·H₂O** were grown from a CHCl₃ solution of **26**, and the structure of the ligand is shown in Figure 2-32. The pyridine rings deviate significantly from being coplanar, with the angles between the least squares planes of the rings containing atoms N1 and N2, N2 and N3, and N2 and N6 being 24.2(1), 16.1(1) and

$9.4(1)^\circ$, respectively. The origin of the twisting of the rings is the presence of a hydrogen bonded network involving three of the pyridine nitrogen atoms (N1, N3 and N6), the imine NH unit and both the water and chloroform molecules (Figure 2-33).

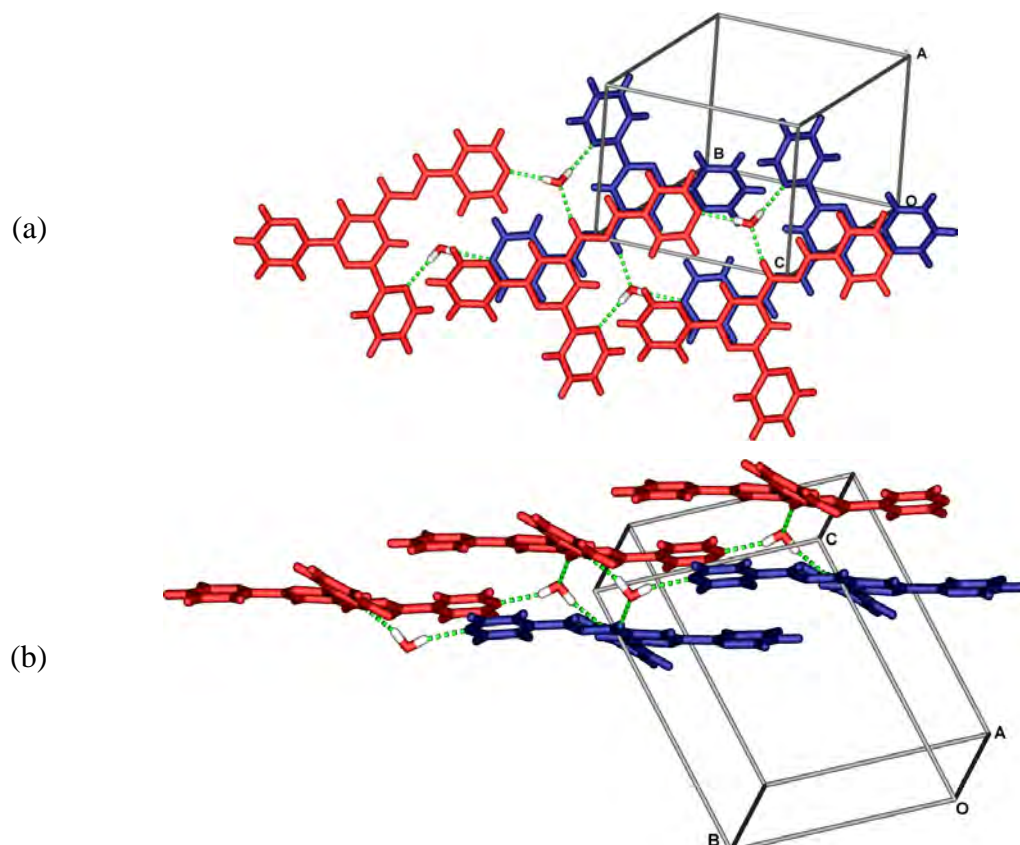


Figure 2-33 Two views of the hydrogen bonding between ligand and water molecules in **26**· $\text{CHCl}_3\cdot\text{H}_2\text{O}$. Symmetry codes: i = $x, 1 + y, z$; ii = $-x, 2 - y, 2 - z$. Additional hydrogen bond contacts: N6...H1BiO1i = 2.06(5) Å, N6...O1i = 2.857(3) Å, N6...H1Bi-O1i = 165(5)°; O1H2B...N1ii = 2.04(4) Å, O1...N1ii = 50 2.902(3) Å, O1-H2B...N1ii = 164(4)°; C22H22A...N3 = 2.24 Å, C22...N3 = 3.216(4) Å, C22-H22A...N3 = 164°.

Large pale yellow blocks of **25** suitable of X-ray analysis were grown by slow evaporation of a CDCl_3 solution, the molecular structure is shown in Figure 2-34. All bond lengths and angles are as expected and one pyridyl ring is twisted much more significantly out of the plane of the central ring than the other [angles between least squares planes of rings containing N1, N2 and N3, N2 are 1.44(4) and 17.92(4)°, respectively].

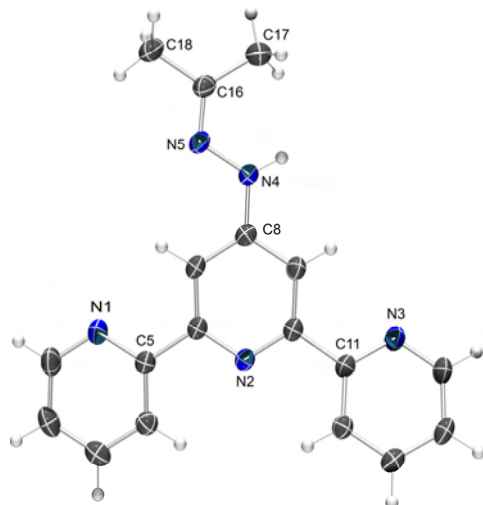
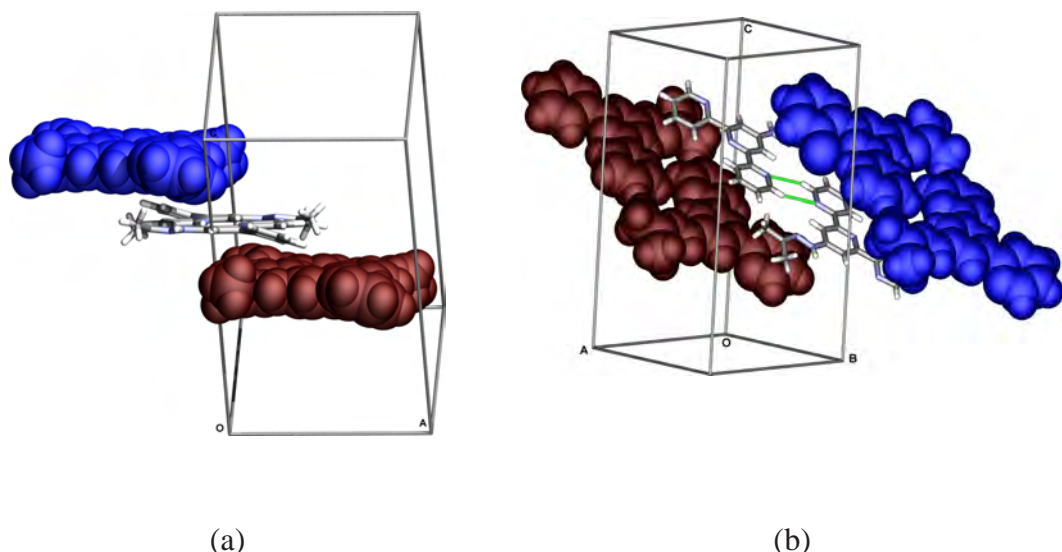


Figure 2-34 Molecular structure of **25**. Displacement ellipsoids drawn at 50% probability level.

Close contacts involving N1 and C1H1 stabilise dimers of the ligand which form π - π stacked chains, as shown Figure 2-35 (a) and (b). The origin of the twisting of the ring containing N3 is a weak hydrogen bonding from the all I hear and see is laughter pyridyl nitrogen to a neighbouring molecule (Figure 2-35c) which is likely the most significant between chains of ligands.



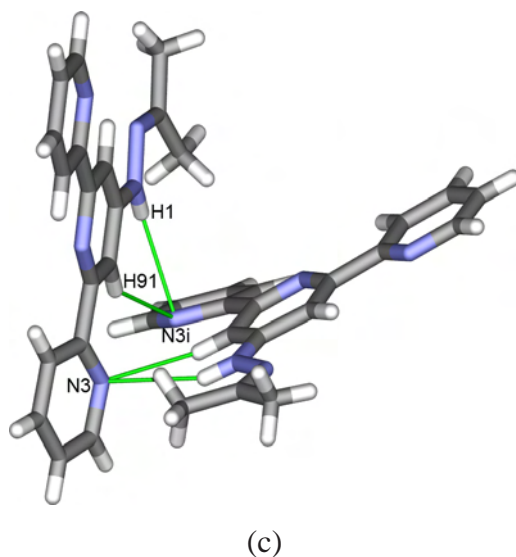


Figure 2-35 Three views of the packing arrangement of **25**. (a) Top view of a π - π stacked chain. (b) Closest contacts are between N1 and C1i-H11i 2.685 Å, shown in green [symmetry operation $i = -x, 1-y, 1-z$]. (c) Weak hydrogen bonding dimers formed between chains [N3 – H91iC9i 2.769, N3-H1iN4i 2.769 Å; N3-H91i-C9 147.6, N3-H1-N4 153.3°; symmetry operation $i = -x, y, 1.5-z$].

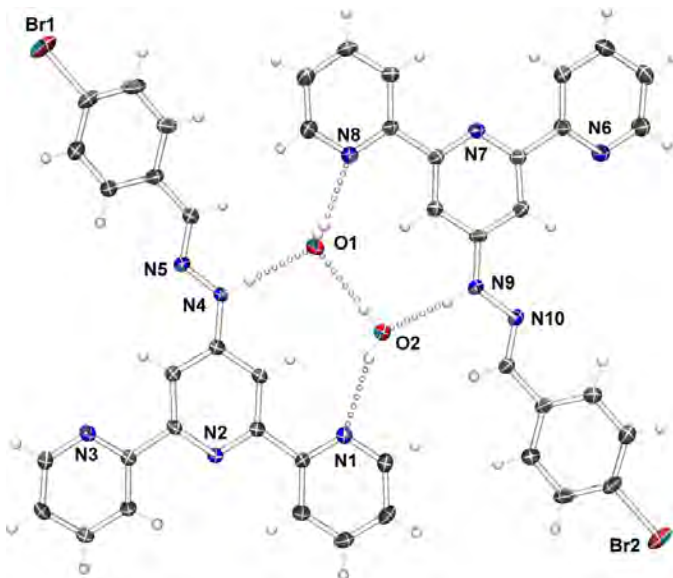


Figure 2-36 The asymmetric unit of $2[22\text{H}_2\text{O}]$. Displacement ellipsoids drawn at 50% probability. Hydrogen bond distances (D-A): O2...N1 2.880(3); N9 ...O2 2.855(3); O2...O1 2.904(3); N4 ...O1 2.930(3); O1...N8 2.923(3); O1...N3i 2.859(3) (not shown). Symmetry operator $i = -x, 1-y, 1-z$. Angles between least squares planes of rings containing N1 and N2, 13.3(1), N3 and N1 21.8(1), N5 and N6 21.1(1), N8 and N7 13.7(1)°.

Single crystals of $2[22\text{H}_2\text{O}]$ were grown by slow evaporation of a CHCl_3 solution of the ligand, the structure is shown in Figure 2-36. The two water molecules are involved in hydrogen bonding to the amino protons ($\text{N}4\text{H}4\text{B}$ and $\text{N}9\text{H}9\text{B}$) and to the terminal pyridyl nitrogens (N1, N3 and N8, see the figure caption for bond lengths) and fill the

space between the ligands and disrupt the pseudo symmetry of the structure. This hydrogen bonding forms tetramers (Figure 2-37).

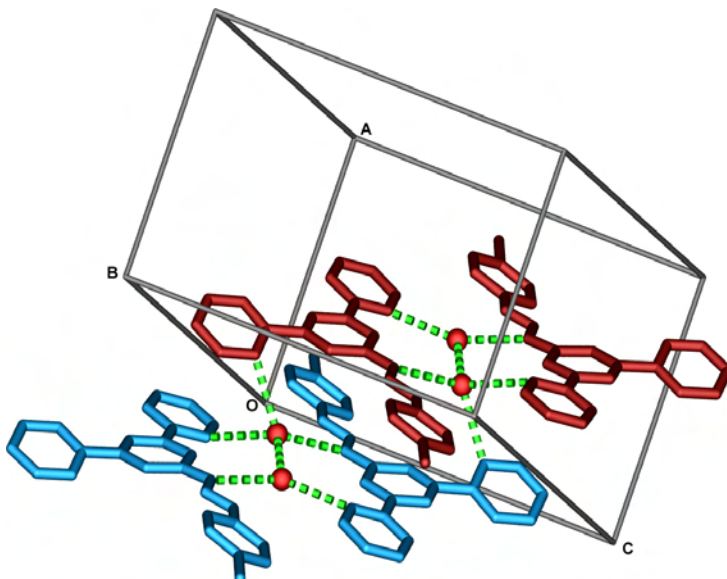


Figure 2-37 A tetramers of $[22\text{H}_2\text{O}]$ in $2[22\text{H}_2\text{O}]$ showing hydrogen bond contacts. Water oxygens in ball representation, hydrogens omitted. Symmetry operations: red is x, y, z ; blue is $-x, 1-y, -z$.

The remaining terminal ring (containing N6) is twisted out of the plane of the central ring by a similar angle (see figure caption) although it is engaged in weak $\text{N}_{\text{py}}\dots\text{HC}$ hydrogen bonding [$\text{N}6\dots\text{H}13\text{AiC}13\text{i}$ 2.710 Å, $\text{N}6\text{-H}13\text{Ai-C}13\text{i}$ 159°, symmetry code i = 1-x, 1-y, 1-z] instead of to a water molecule (as for N1, N3 and N8). Both terminal rings containing N6 and N3 are in close contact with neighbouring bromines [$\text{Br}1\dots\text{N}6\text{i}$ 3.417(3), $\text{Br}2\dots\text{N}3\text{ii}$ 3.341(2) Å, symmetry codes i = -1+x, 1+y, z, ii = 1+x, -1+y, z] which likely contributes to the lack of coplanarity to avoid unfavourable N-Br interactions. These contacts link the tetramers together into chains, shown in Figure 2-38. Adjacent chains are assembled *via* weak $\pi\text{-}\pi$ interactions involving the pyridyl rings containing N6 [centroid to plane distance 3.655 Å] to form two dimensional sheets. The closest points of contact between these sheets are weak $\pi\text{-}\pi$ interactions [$\text{C}10\dots\text{C}38\text{i}$ 3.374(3) and $\text{C}9\dots\text{C}44\text{i}$ 3.308(4) Å, symmetry codes i = 1-x, 1-y, 1-z] although overall overlap is minimal.

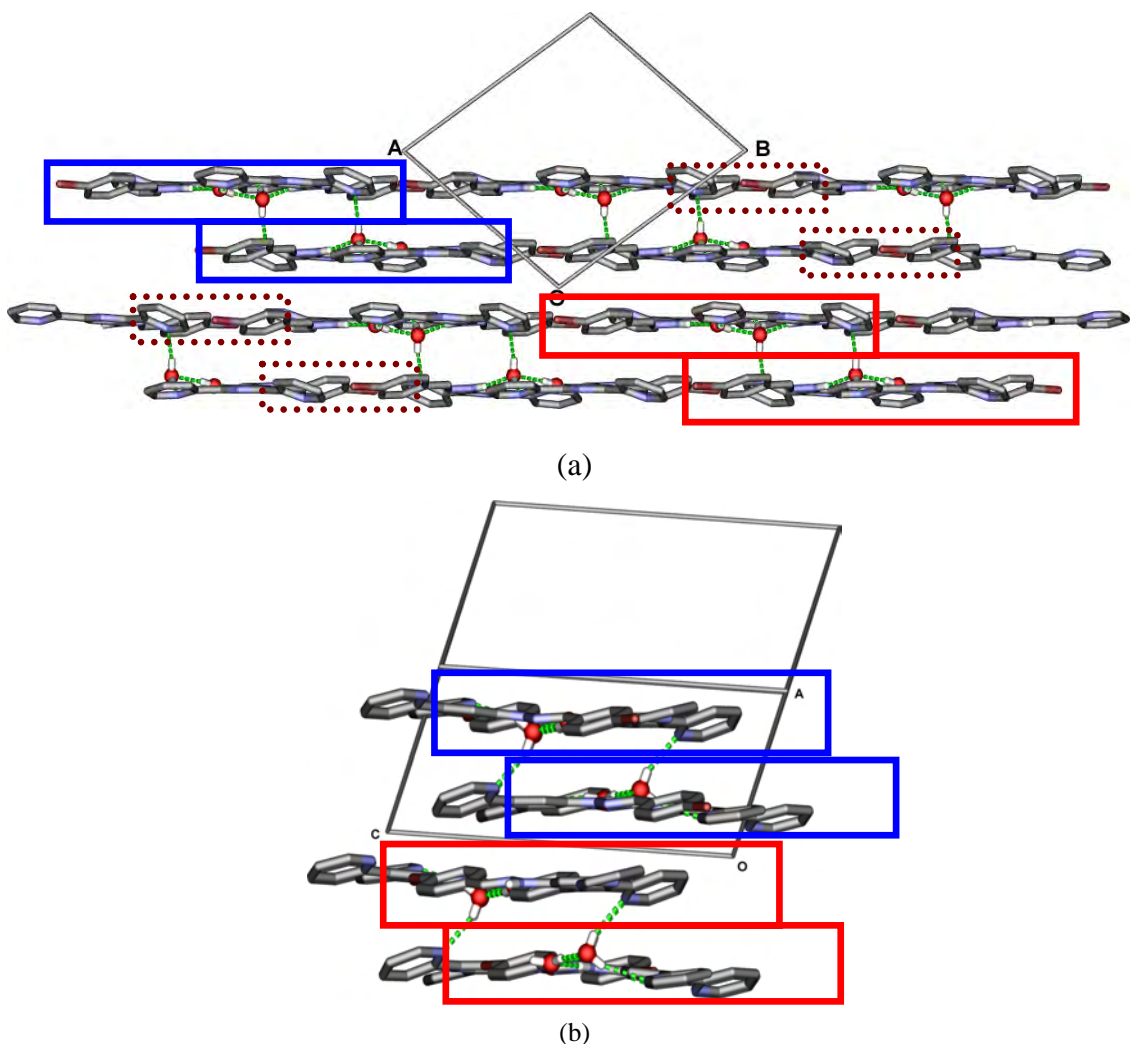


Figure 2-38 Two views of the assembly of $[22\text{H}_2\text{O}]$ tetramers (shown in solid red and blue boxes) into chains via Br-N contacts (in dotted boxes). (a) looking down the ab -plane, (b) looking down the off-set ac -plane.

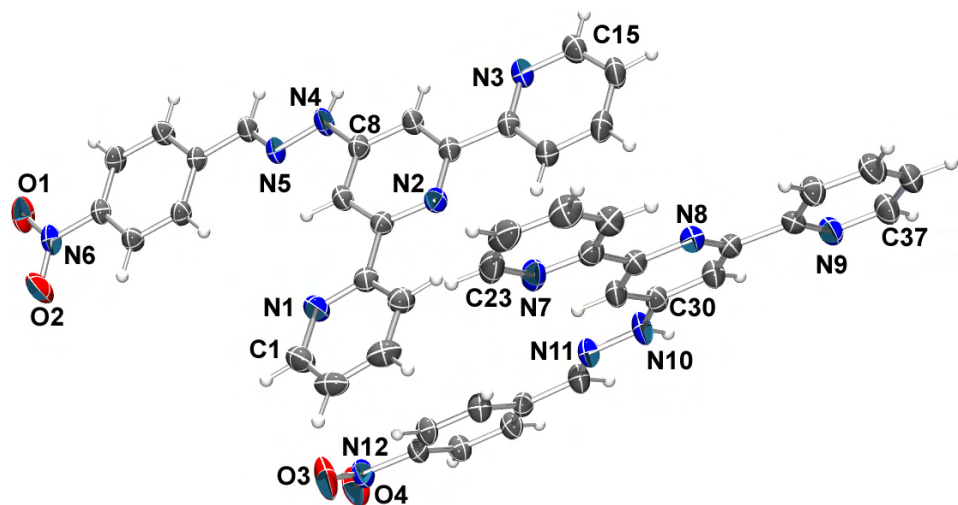


Figure 2-39 The asymmetric unit of $2[24]$. The space group is $\text{P}21/c$. Angles between the least-squares planes of pyridyl rings containing N1 and N2; N3 and N2 are $10.9(1)$ and $3.6(1)^\circ$; N7 and N8; N9 and N8 are $2.06(1)$ and $2.29(1)^\circ$.

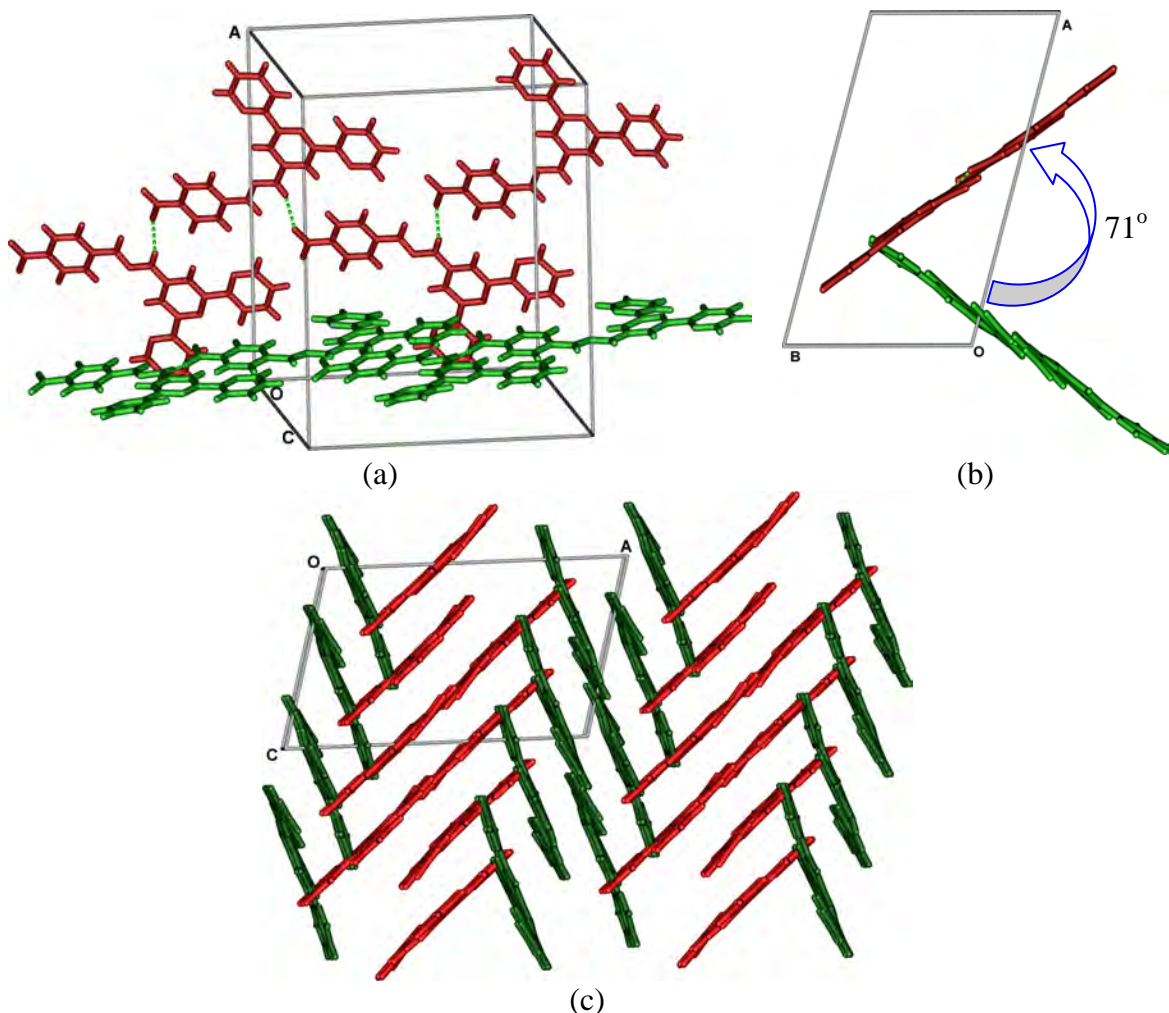


Figure 2-40 Formation of one dimensional chains via amino-nitro hydrogen bonding in the structure of 2[24]. Molecules coloured by symmetry equivalence, those in green are molecule A (containing N1), and those in red are molecule B (containing N7). Hydrogen bond distances (D-A) and angles (D-H-A) involving amino group: N4H4'...O1 3.062(3) Å, N4-H4'-O1i 156(3)°; N10H10'...O4ii 3.050(4) Å, 158(3)°. Hydrogen bond distances (D-A) and angles (D-H-A) of nitro-CH contacts: O2...C14iii 3.271(4) Å, 129°; O3...C36iii 3.219(4) Å, 131°. [Symmetry operators i = -x, $\frac{1}{2} + y$, $-\frac{1}{2} - z$; ii = $1-x$, $\frac{1}{2} + y$, $\frac{1}{2} - z$; iii = x , $-1+y$, z].

Yellow block single crystals of 2[24] were grown by slow evaporation of a CHCl_3 solution. The asymmetric unit contains two structurally similar but crystallographically independent molecules, molecules A (containing N1) and B (containing N7), shown in Figure 2-39. Both molecules are almost perfectly planar and involved in intermolecular hydrogen bonding from the nitro oxygens to the amino proton and a pyridyl CH of adjacent molecules (see figure for bond details). This results in the formation of one dimensional chains of the molecules of molecules A and B (Figure 2-40) which are oriented 70.6° to one another. The crystal packing is completed by extensive π -stacking, the key interactions are shown in Figure 2-41.

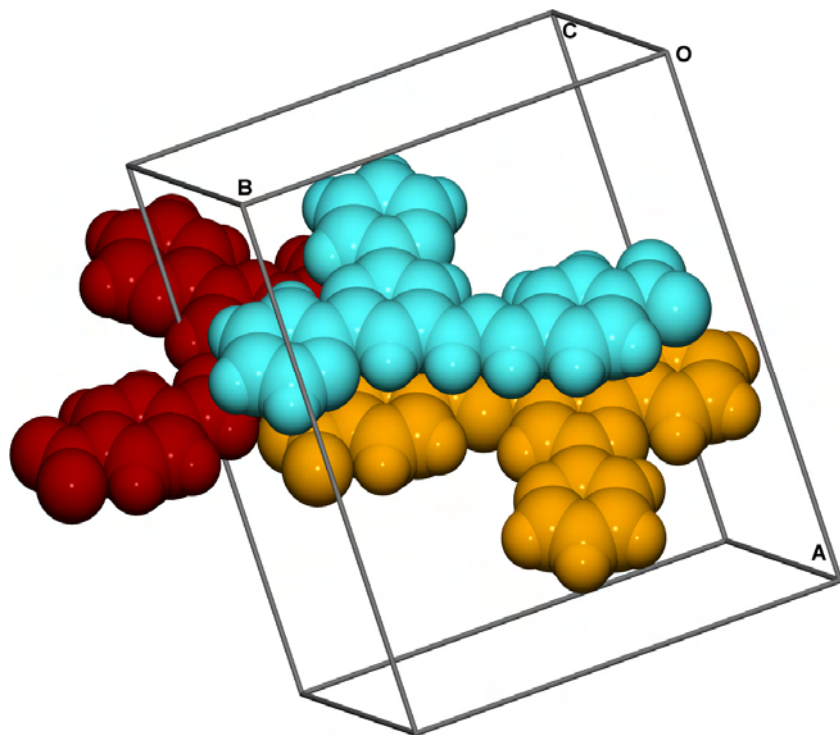


Figure 2-41 CPK representation of π - π stacking between molecules B (containing atom N7) of **24** in the structure of 2[**24**]. Intermolecular contacts C30...C39i 3.392(4); N10...C35ii 3.257(4). [Symmetry operators: light blue (containing N7) = x, y, z ; yellow = $i = -x, 1-y, 1-z$; red = $ii = x, 3/2-y, -1/2+z$.] Related distances in molecule A (containing N1, not shown): C2...C6iii 3.382(4); C17...C21iv 3.369(4) [iii = $x, 1/2-y, 1/2+z$; iv = $-x, -y, -z$].

2.12. X-Ray crystal structures of mono protonated ligands

The mono- and diprotonated states of the 4'-hydrazone derivatives of 2,2':6',2"-terpyridine were confirmed by representative structural studies.

Attempts to grow crystals of yellow $[\text{H}_2\mathbf{19}][\text{MeOSO}_3]_2$ by slow evaporation of an aqueous solution of the salt instead gave rise to X-ray-quality colourless plates of $[\text{H}\mathbf{19}]^+[\text{MeOSO}_3]$. The structure of the $[\text{H}\mathbf{19}]^+$ cation is shown in Figure 2-42. The tpy domain is close to being planar [angles between the least-squares planes of rings containing atoms N1 and N2, and N2 and N3: 2.8(1) and 11.42(9) $^\circ$, respectively]. It adopts a *cis,cis*-conformation, with both of atoms N1 and N3 participating in hydrogen-bonded interactions with the N2H₂ unit [see discussion of $(\mathbf{H}\mathbf{17})^+$ and $(\mathbf{H}\mathbf{18})^+$]. The deviations of atoms N4, N5 and C16 from the least-squares plane of the central pyridine ring are 0.08, 0.11 and 0.41 Å, respectively. Neither phenyl substituent is coplanar with the central pyridine ring [angles between the least-squares planes of the rings containing C17 and N2, and C23 and N2: 23.6(1) and 64.2(1) $^\circ$, respectively].

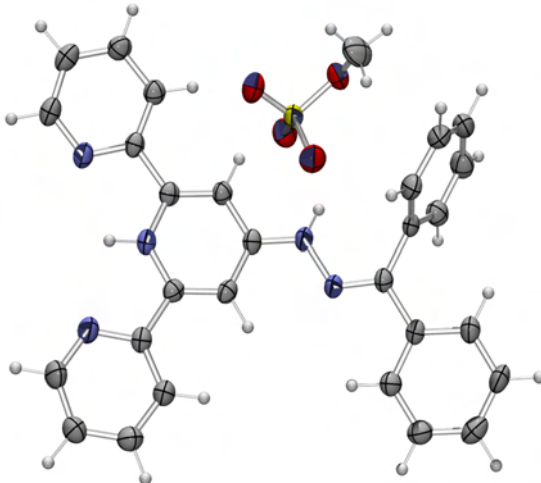


Figure 2-42 The molecular structure of the $[H19]^+$ cation in $[H19][MeOSO_3]$; thermal ellipsoids are plotted at the 50% probability level. Selected bond lengths and angles: N4–N5 1.376(2), N4–C8 1.348(2), N5–C16 1.292(2), N2–H2 0.98, N1…H2 2.20, N3…H2 2.25, N1…N2 2.630(2), N2…N3 2.650(2) Å; N5–N4–C8 118.8(2), N4–N5–C16 117.1(2)°.

In the crystal lattice, cations are arranged in head-to-tail pairs with π -stacking of the central rings of the tpy units (distance between rings containing atoms N2: 3.40 Å), shown in Figure 2-43. This results in unfavourable H11…H251a contacts (2.2 Å, symmetry code $a = -x, 1 - y, 1 - z$). The cation pairs assemble into columns, with adjacent pairs being slightly offset from one another.

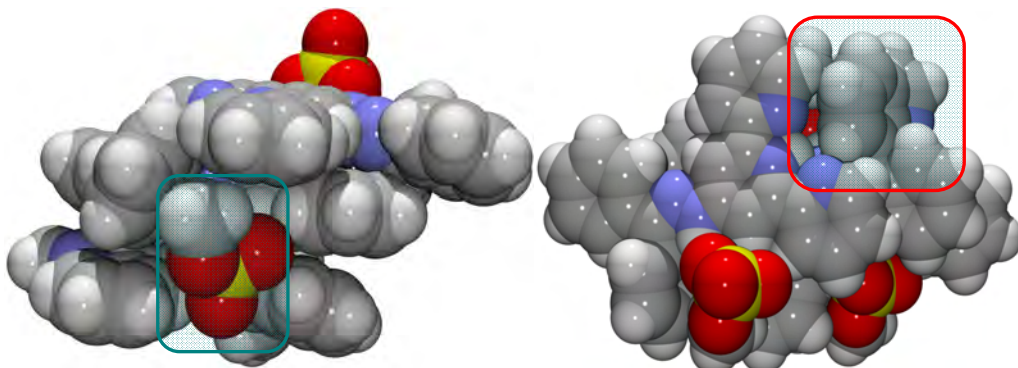


Figure 2-43 Two views of a CPK representation of three molecules of $[H19]MeOSO_3$. The phenyl ring oriented towards the tpy group of adjacent molecule is indicated on the right and the $MeOSO_3^-$ anion fitting neatly into the space between molecules is indicated on the left.

The most twisted phenyl ring is involved in edge-to-face aromatic interactions with a pyridyl ring of the adjacent molecule [distances from C28H281 and C27H271 to the plane containing ring N1i are 2.515(2) and 3.093(2) respectively, symmetry code $1-x, 1-y, 1-z$]. This angle also positions the ring towards the cavity in front of another tpy group and places it in close contact with a $MeOSO_3^-$ anion (C26...H293C29 is 2.885(2)). Importantly, the positioning of the molecules allows the $MeOSO_3^-$ anion to

hydrogen bond effectively with the amino NH [N4H4 \cdots O3 1.89 Å, N4 \cdots O3 2.789(2) Å, N4– H4 \cdots O3 151°] and fit well into the space between two adjacent molecules.

Single crystal structure determinations were also performed for [H18][BF₄] [colourless plates grown by slow evaporation of an aqueous acetone (1:5) solution of the salt] and of [H17][PF₆]·H₂O [colourless plates obtained by slow evaporation of a MeCN/H₂O (5:1) solution of the compound]. Figure 2-44 and Figure 2-45 show the molecular structures of the [H17]⁺ and [H18]⁺ ions present in [H17][PF₆]·H₂O and [H18][BF₄], respectively.

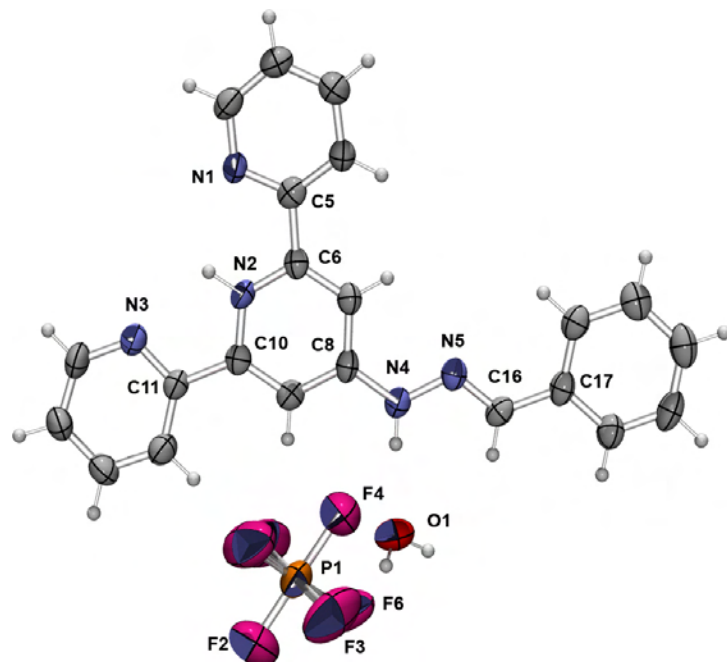


Figure 2-44 An ORTEP plot the asymmetric unit of [H17]PF₆·H₂O with displacement ellipsoids drawn at 50% probability. N4...O1 hydrogen bond distance of 2.806(5) Å.

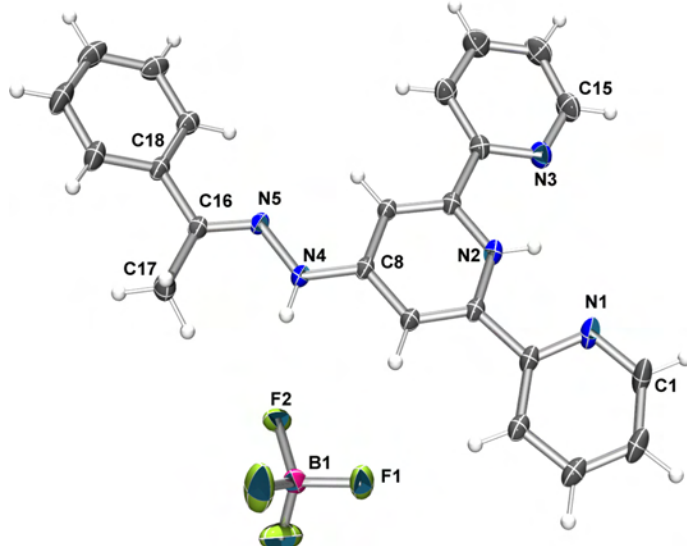


Figure 2-45 An ORTEP plot the asymmetric unit of [H18]BF₄ with displacement ellipsoids drawn at 50% probability. Weak N4...F2 hydrogen bond distance of 2.798(4) Å. Disorder in BF₄⁻ not shown.

In both salts, the tpy unit adopts a *cis,cis*-conformation, as discussed above for [H3][MeOSO₃]. This is in contrast to the *cis,trans*-conformation observed in [Htpy][CF₃SO₃]²²⁰ and [Htpy][ReO₄]²⁴⁵. In these salts, a [CF₃SO₃]⁻ or [ReO₄]⁻ anion resides close to the site of protonation in the cation and participates in a hydrogen bonded interaction which is in addition to the N–H···N interaction responsible for the *cis*-arrangement of two of the pyridine rings. A pertinent difference between [Htpy]⁺ and the family of monoprotonated tpy ligands in this study is the presence of the hydrazone NH group which may also become involved in hydrogen bonding. Similarly to the case of [H19]MeOSO₃, in both [H17][PF₆]·H₂O and [H18][BF₄], the hydrazone NH group participates in hydrogen bonding, to a water and a BF₄⁻ anion respectively. In [H17][PF₆]·H₂O, the hydrazone NH is hydrogen bonded to the solvate water molecule [N4H2···O1 1.93 Å, N4···O1 2.806(5) Å, N4–H2···O1 178°], and the latter forms weak hydrogen bonds to the PF₆⁻ anion. In [H17][BF₄] the BF₄⁻ anion is disordered although its location indicates the same type of hydrogen bonding occurs.

We propose that the [H17]⁺, [H18]⁺ and [H19]⁺ cations adopt *cis,cis*-conformations in order that both of the outer pyridine *N*-atoms may be involved in stabilizing hydrogen-bonded interactions with the NH unit, while the counterions or solvate are preferentially involved in hydrogen bonding with the hydrazone NH. The two outer pyridine rings in each of the [H18]⁺ and [H17]⁺ cations are twisted out of the plane of the central ring with angles between the least-squares planes of the rings containing N1 and N2, and N2 and N3 of 10.8(1) and 6.5(1)^o in [H18][BF₄], and 7.2(2) and 16.3(2)^o in [H17][PF₆]·H₂O. The phenyl ring in [H18][BF₄] is not coplanar with the central pyridine ring [angle between the least-squares planes: 18.4(9)^o]. This results in a reduction in the conjugation along the C8N4N5C16C18 chain, which manifests itself in a longer C_{phenyl}–C_{azomethine} bond [1.483(3) Å] compared to that in [H17][PF₆]·H₂O [1.457(6) Å] in which the phenyl and central pyridine rings are coplanar [angle between least squares planes: 0.7(2)^o]. The difference between the molecular structures of the cations appears to be associated with the crystal packing.

In [H17][PF₆]·H₂O, cations are arranged head-to-tail in rows and π–π stacked (via tpy groups (Figure 2-46) with alternating separations of 3.29 and 3.32 Å. This pattern arises from the interactions of each phenyl ring with an imino nitrogen atom (N5) on one side

and a π -stacked pyridine ring (containing N2) on the other. The overall packing can be described in terms of stacks of cations, between which run columns of hydrogen-bonded water molecules and $[\text{PF}_6]^-$ anions (Figure 2-46a).

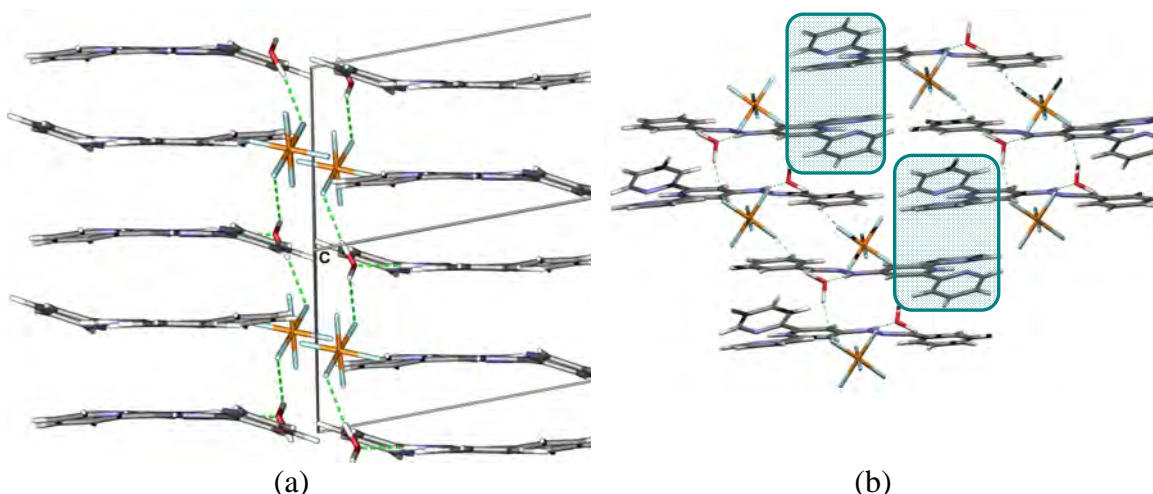


Figure 2-46 The packing arrangement of $[\text{H17}](\text{PF}_6)\cdot\text{H}_2\text{O}$ showing (a) hydrogen-bonded channels of PF_6^- and H_2O molecules and (b) the paired $\pi-\pi$ stacking arrangement.

In $[\text{H17}][\text{BF}_4]$ the deviations from planarity possibly result in an unusual packing arrangement. The molecules are arranged in head-to-tail $\pi-\pi$ stacking pairs but these pairs are related by a C_2 axis (Figure 2-47). There is π -stacking between pairs of pyridine rings containing N3 (distance between planes: 3.35 Å) and N2 (distance between planes: 3.31 Å). The cavity formed by the hydrazone NH and methyl group accommodates a $[\text{BF}_4]^-$ ion with associated hydrogen-bonded interactions [N4 \cdots F2i 2.798(4) Å, N4—H4 \cdots F2i 148°; C4 \cdots F1 3.337(3) Å, C4—H41 \cdots F1i 172°; C7 \cdots F1i 3.359(3) Å, C7—H71 \cdots F1i 171°; C17 \cdots F2i 3.427(4) Å, C17—H173 \cdots F2i 163°; symmetry code i = x , 1 - y , $1/2 + z$]. The packing is then further extended through aromatic CH \cdots F interactions and stacking of dimeric motifs.

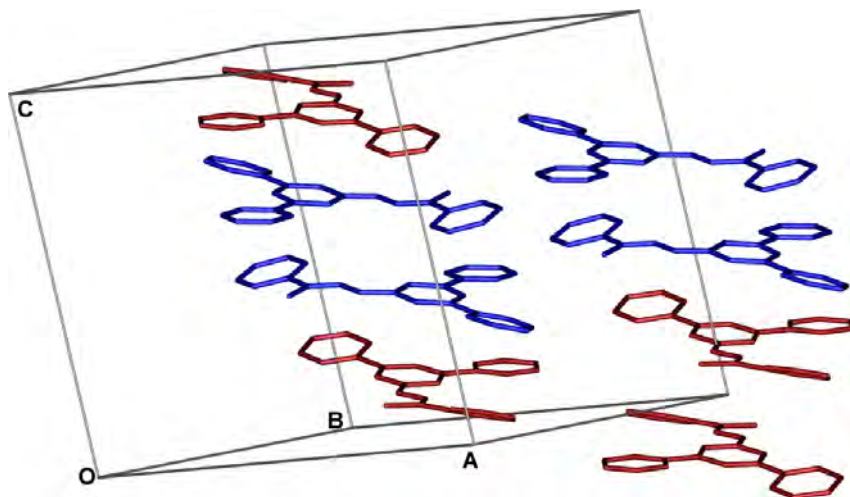


Figure 2-47 The packing arrangement of $[H18]BF_4$ showing alternating $\pi\cdots\pi$ stacking pairs.

Single crystals of $[2[H17](CF_3CO_2)_2(EtOH)\cdot H_2O]$ were obtained from slow evaporation of an ethanol solution of **17** with a drop of TFA added. The asymmetric unit (Figure 2-48) contains two crystallographically independent but structurally similar molecules. Similar to the structures previously discussed, the pyridyl rings adopt a *cis,cis* orientation to allow the terminal pyridyl nitrogens to hydrogen bond to the $N_{py}H$ which confines molecule to be planar [the increase in conjugation is reflected in $C_{phenyl}-C_{azomethine}$ bond [1.461(5)] which is similar to that $[H17][PF_6]\cdot H_2O$ [1.457(6) Å]. The amino NH is involved in hydrogen bonding interactions with counterions (see figure caption).

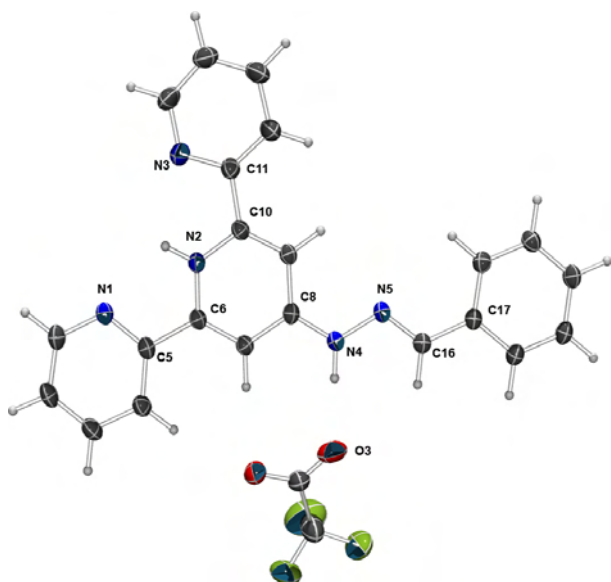


Figure 2-48 An ORTEP plot the one molecule of $[H17](CF_3CO_2)$ in $[2[H17](CF_3CO_2)_2(EtOH)\cdot H_2O]$ with displacement ellipsoids drawn at 50% probability. Hydrogen bond distances of $N9\cdots O2$ 2.738(4), $O3\cdots N4$ 2.705(4) Å. Angles between least squares planes of rings containing $N6$ and $N7$, $N8$ and $N7$, $N1$ and $N2$, $N3$ and $N2$ are 5.4(2), 5.1(2), 3.6(2) and 3.6(2) °. $C8-N4$ 1.339(4), $N9-C38$ 1.337(4) Å.

The packing arrangement is significantly different from those discussed above. The molecules are arranged head-to-tail in a π - π stacking arrangement (Figure 2-49) with the distance between the least squares planes of two adjacent molecules (symmetry operators x, y, z to $1-x, 1-y, 1-z$) being 3.2 Å. The C=NH bond is centred over the terminal ring of one of the adjacent molecules and the phenyl ring is staggered over the central tpy ring of the other adjacent molecule.

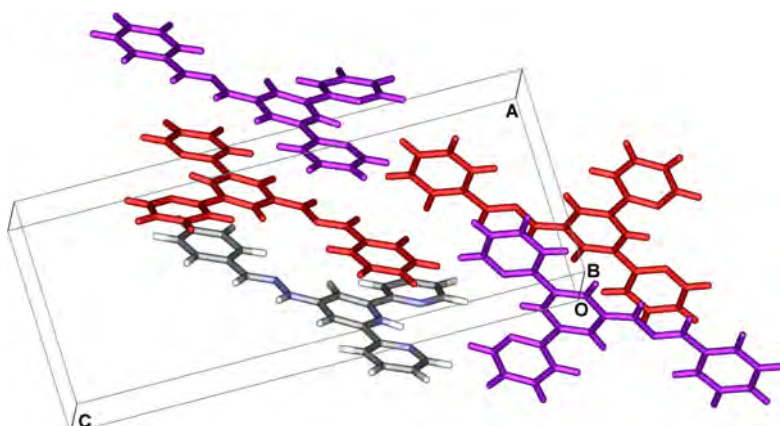


Figure 2-49 The head-to-tail stacking arrangement of $[2\text{H}17](\text{CF}_3\text{CO}_2)_2(\text{EtOH})\cdot\text{H}_2\text{O}$ via a crystallographic inversion centre. Solvent and anions have been removed for clarity. Symmetry operators (x, y, z to $1-x, 1-y, 1-z$)

In the X-ray crystal structure of $[\text{H}12]\text{BF}_4$ (Figure 2-50) the amino NH is hydrogen bonded to a BF_4^- counterion and no solvent molecules are present. The molecule is almost exactly planar and is arranged in π - π stacked columns in a herringbone arrangement (Figure 2-51), similar to that observed for $[\text{H}_2\text{18}](\text{NO}_3)(\text{MeOSO}_3)\cdot\text{H}_2\text{O}$.

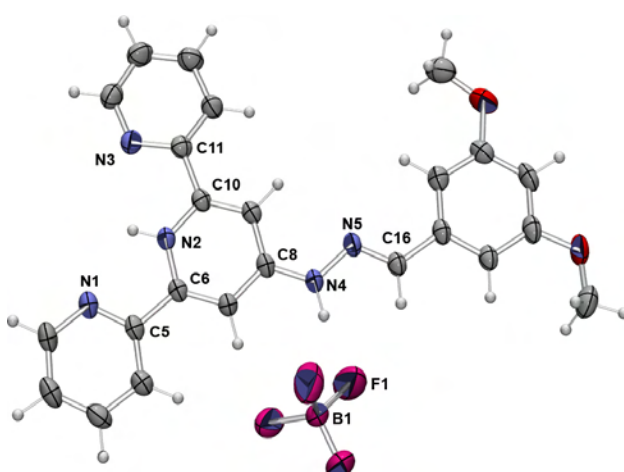


Figure 2-50 An ORTEP plot the asymmetric unit of $[\text{H}21]\text{BF}_4$ with displacement ellipsoids drawn at 50% probability. N4H4...F1 hydrogen bond distance of 2.858(3) Å, N-H..F 169 °. C17-C16 1.461(4), C8-N4 1.346(3) Å. Least squares planes between rings contains N1 and N2, N3 and N2 3.50(11) and 7.11(11) °.

The molecules alternate 3.21 Å and 3.38 Å in separation (least squares planes through each molecule). The BF_4^- anion is also in close contact with seven aromatic CH groups with F...HC distances ranging from 2.26 to 2.63 Å.

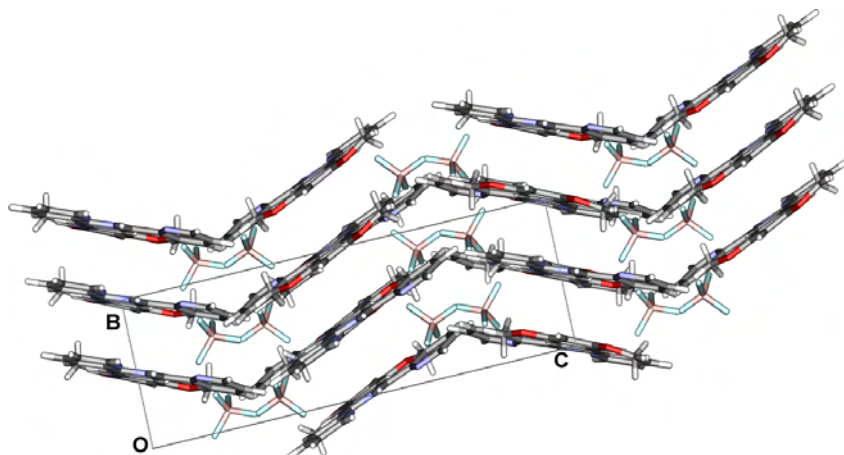


Figure 2-51 Crystal packing of $[\text{H12}]\text{BF}_4$ showing $\pi\text{-}\pi$ stacking looking down the crystallographic *a*-axis. The molecules are arranged in head-to-tail in the stacked columns

2.13. X-Ray crystal structures of di-protonated ligands

X-ray-quality crystals of $[\text{H}_2\mathbf{17}]\text{Cl}_2\cdot\text{DMSO}$ were grown from a DMSO solution of the compound. Figure 7 shows the $[\text{H}_2\mathbf{17}]^{2+}$ cation, hydrogen bonded to the two chloride ions in the asymmetric unit. The tpy domain adopts a *cis,cis*-configuration. In an $[\text{H}_2\text{tpy}]^{2+}$ ion, it is usual for the two outer pyridine rings to carry one proton each and for the latter to be involved in hydrogen bonded interactions with the central pyridine *N*-atom as well as with an acceptor atom.^{223, 234, 236, 239, 240, 246, 247} As Figure 2-52 illustrates, the $[\text{H}_2\mathbf{17}]^{2+}$ ion in $[\text{H}_2\mathbf{17}]\text{Cl}_2\cdot\text{DMSO}$ falls into this structural pattern, with one chloride ion acting as a hydrogen-bond acceptor with respect to the $[\text{H}_2\mathbf{17}]^{2+}$ ion. The imine NH also acts as a hydrogen-bond donor, interacting with the second chloride ion (see Figure caption). The hydrogen-bonded motif locks the tpy unit into a near planar conformation [angles between the least-squares planes of the rings containing N1 and N2, and N2 and N3 are 9.90(7) and 7.72(7)°, respectively].

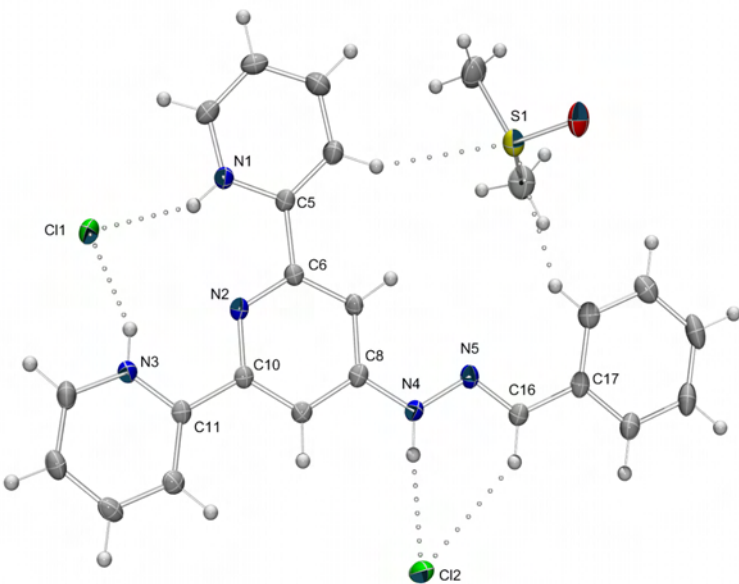


Figure 2-52 The molecular structure of $[H_2\mathbf{17}]Cl_2$ in the asymmetric unit of $[H_2\mathbf{1}]Cl_2 \cdot DMSO$ with thermal ellipsoids plotted at the 50% probability level. Selected bond lengths and angles: N4–C8 1.362(2), N4–N5 1.367(2), N5–C16 1.290(2), C16–C17 1.465(2) Å; N5–N4–C8 119.7(1), N4–N5–C16 115.0(1)°. Hydrogen bond parameters: N1H1…Cl1 2.26 Å, N1…Cl1 3.018(1) Å, N1–H1…Cl1 151°; N3H3…Cl1 2.25 Å, N3…Cl1 3.049(1) Å, N3–H3…Cl1 154°; N1H1…N2 2.26 Å, N1…N 2.619(2) Å, N1–H1…N2 106°; N3H3…N2 2.30 Å, N3…N2 2.638(2) Å, N3–H3…N2 104°; N4H4…Cl2 2.29 Å, N3…N2 3.158(2), N3–H3…N2 173°.

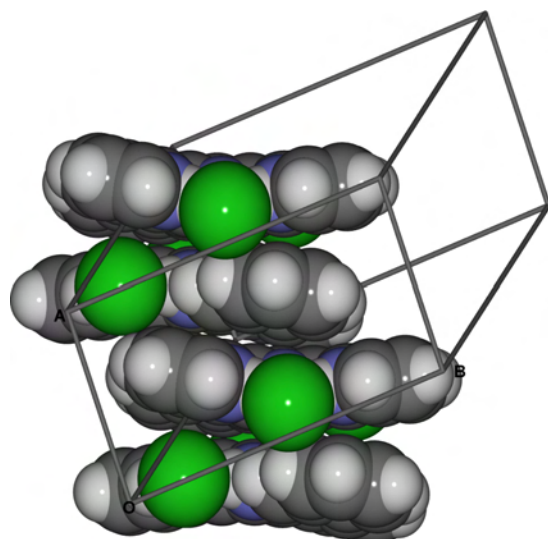


Figure 2-53 The π -stacked columns of $[H_2\mathbf{17}]Cl_2$ units with alternating distances of 3.19 and 3.49 Å between the least-squares planes drawn through adjacent cations.

The phenyl substituent also lies close to this plane [angle between the least-squares planes of rings containing N1 and C17: 8.95(8)°]. The latter is a consequence of the molecular packing; $[H_2\mathbf{17}]^{2+}$ cations assemble into π -stacked columns (Figure 2-53). The packing is completed by extensive hydrogen bonding interactions involving the chloride ions and DMSO solvent molecules.

Yellow plates of $[H_2\mathbf{18}][NO_3][MeOSO_3] \cdot H_2O$ were grown by adding a drop of dilute aqueous HNO_3 to an aqueous solution of $[H_2\mathbf{18}][MeOSO_3]_2$ and allowing the solvent to evaporate slowly. A single-crystal X-ray diffraction study confirmed that **18** is diprotonated (Figure 2-54).

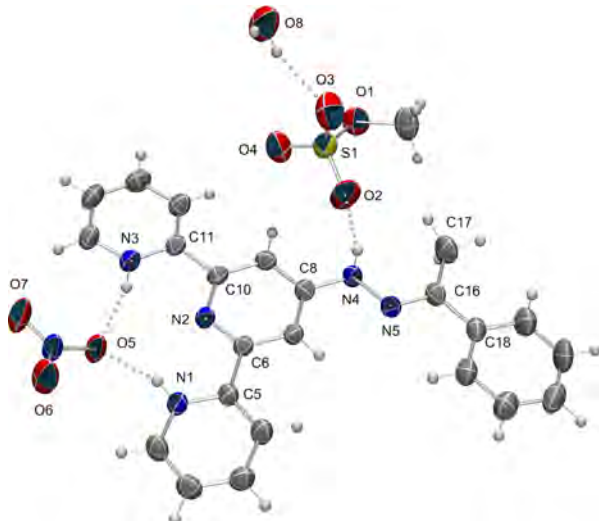


Figure 2-54 The asymmetric unit of $[H_2\mathbf{18}][NO_3][MeOSO_3] \cdot H_2O$; thermal ellipsoids are plotted at the 50% probability level. Selected bond lengths and angles: C8–N4 1.377(4), N4–N5 1.363(3), C16–N5 1.299(4), C16–C17 1.494(4), C16–C18 1.492(4) Å, C8–N4–N5 118.9(2), N4–N5–C16 118.6(2), C18–C16–N5 115.2(3), C17–C16–N5 123.9(3), C17–C16–C18 120.9(3)°. Angles between the least-squares planes of the rings containing N1 and N2, and N2 and N3, C6 and N2: 2.7(1), 4.6(1) and 6.2(2)° respectively. Hydrogen bonding involving NO_3^- : [N1H1…O5 1.92 Å, N1…O5 2.733(3) Å, N1–H1…O5 161°; N3H3…O5 1.95 Å, N3…O5 2.762(3) Å, N3–H3…O5 161°] Interactions involving N2 [N3H3…N2 2.29 Å, N3…N2 2.660(3) Å, N3–H3…N2 107°; N1H1…N2 2.29 Å, N1…N2 2.670(3) Å, N1–H1…N2 107°].

The three pyridine rings adopt a *cis,cis*-configuration, with the nitrate ion acting as a hydrogen-bond acceptor. The diprotonated state of the tpy derivative is further stabilized by hydrogen-bonded interactions to N2 (see Figure 2-54 caption). As in $[H_2\mathbf{17}]^{2+}$, this hydrogen bonding compels the tpy unit in $[H_2\mathbf{18}]^{2+}$ to be essential planar (see caption), in contrast to the mono-protonated example discussed above. The crystal packing (Figure 2-55) combines ‘head-to-tail’ π - π stacking of the ligand molecules with hydrogen-bonded-dimers formed by $MeOSO_3^-$ and H_2O molecules via a crystallographic inversion centre. The amino NH group is also hydrogen-bonded to atom O4 of the $[MeOSO_3]^-$ anion [N4H4…O2 2.04 Å, N4…O2 2.859(4) Å, N4–H4…O2 161°]. The resulting assembly does not result in infinite hydrogen bonded networks; instead each hydrogen-bonded-dimer fits neatly into the space between adjacent ligand molecules. The columns of stacked ligands are then arranged in a herringbone architecture (Figure 2-55b) consisting of alternating layers with separations (calculated

for least square planes through each molecule) of 3.22 and 3.48 Å. The shorter of these separations arises from π -stacking between pyridine rings containing atoms N2 and N3, whereas C_{methyl}...py_{centroid} interactions (C17...centroid of ring containing N1: 3.55 Å) give rise to the larger layer spacing.

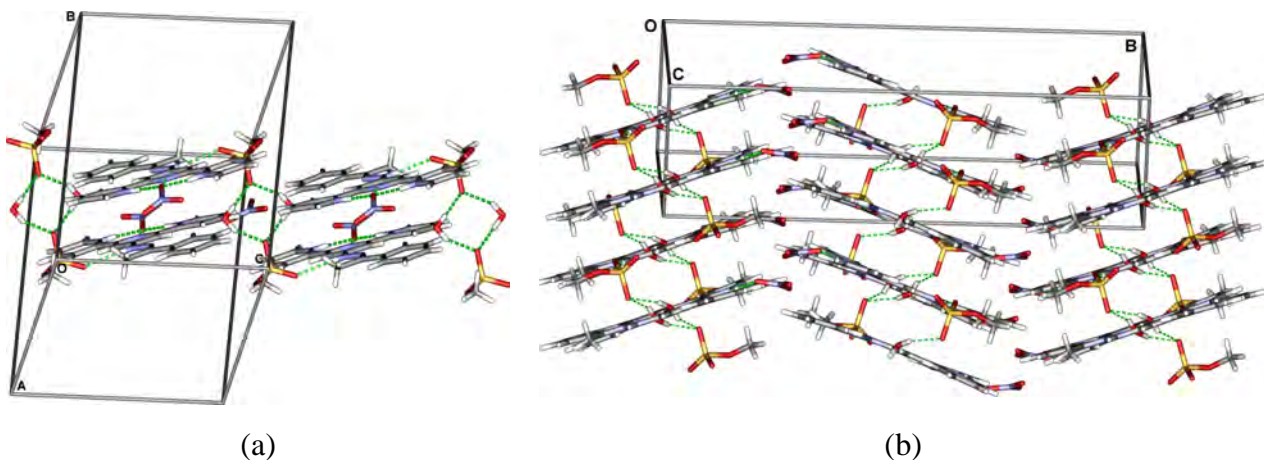


Figure 2-55 X-ray crystal structure of $[H_2\mathbf{18}](NO_3)(MeOSO_3)\cdot H_2O$ showing (a) ‘head-to-tail’ π - π stacking between molecules in addition to H_2O -bridged $MeOSO_3^-$ anions hydrogen-bonded to the amino NH. (b) showing herringbone arrangement.

2.14. Summary of crystal structures

Neutral

- **17**
- **18**
- **19.CH₂Cl₂**
- **20**
- **26.H₂O·CHCl₃**
- **2[22·H₂O]**
- **25**

Monoprotonated

- **[H17](CF₃CO₂)·EtOH·0.5H₂O**
- **[H17](PF₆)·H₂O**
- **[H18](BF₄)**
- **[H21](BF₄)**
- **[H19](MeOSO₃)**

Diprotonated

- **[H₂18](NO₃)(MeOSO₃)·H₂O**
- **[H₂17.Cl₂]·DMSO**

The hydrogen bonding capacity of the imine NH in the structures presented is apparent in its packing in the solid state, and this observation is in line with the results of several studies of phenylhydrazones which conclude that such hydrogen bonding is the predominant factor in determining solid state conformation and solution dynamic behaviour.^{226-228, 248} The bond lengths (Table 1) of the ligands are all similar and very close to the average distances for phenyl hydrazones. The most significant changes are observed on going from neutral to mono-protonated ligands. The average C8-N4H distance shortens by 0.03 Å on protonation and the N4-N5 distances lengthens by 0.01 Å. The C=N bond lengths are longer than typical N=C distance, suggesting a delocalised double bond but not involving C16-C17 (see table).²⁴⁹ The changes in bond lengths are consistent with a delocalisation of the positive charge as shown in Scheme 2, and also with the hydrogen-bonding shown in Figure 2-17 which would also promote further charge delocalisation. Torsion angles (Table 2), show that the molecules, in general, become closer to planar when they are protonated, suggesting extended conjugation throughout the molecule and delocalisation of charge.

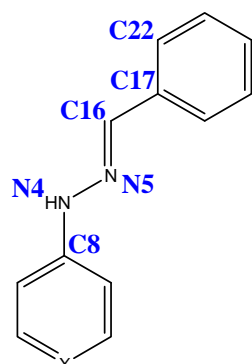


Figure 2-56 The numbering system used in Table 1 and Table 2. X = CH or N for CSD search, X = N for tpy ligands presented in this chapter.

Table 1 Selected bond lengths (Å)

	C8-N4	N4-N5	N5-C16	C16-C17
17	1.379(2)	1.371(2)	1.283(2)	1.458(2)
18	1.378(2)	1.364(2)	1.293(2)	1.483(2)
19.CH₂Cl₂	1.378(2)	1.361(2)	1.288(2)	1.479(2)
20	1.389(2)	1.363(2)	1.284(2)	1.466(3)
26H₂O·CHCl₃	1.374(4)	1.357(3)	1.287(4)	1.455(4)
2[22.H₂O]	1.378(4)	1.362(3)	1.289(4)	1.456(4)
	1.370(3)	1.368(3)	1.282(3)	1.455(4)
2[24]	1.385(3)	1.358(3)	1.289(3)	1.463(3)
	1.380(3)	1.352(3)	1.282(4)	1.455(3)
25	1.367(2)	1.379(2)	1.277(2)	1.494(2)
[H17](CF ₃ CO ₂)·EtOH·0.5H ₂ O	1.339(4)	1.387(4)	1.290(4)	1.461(5)
[H17](PF ₆).H ₂ O	1.347(5)	1.377(5)	1.284(5)	1.457(6)
[H18](BF ₄)	1.354(2)	1.372(2)	1.289(3)	1.483(3)
[H21](BF ₄)	1.346(3)	1.378(3)	1.284(3)	1.461(4)
[H19](MeOSO ₃)	1.348(2)	1.376(2)	1.292(2)	1.487(3)
[H ₂ 18](NO ₃)(MeOSO ₃)·H ₂ O	1.377(4)	1.364(3)	1.299(4)	1.492(5)
[H ₂ 17 .Cl ₂]·DMSO	1.362(3)	1.370(2)	1.287(3)	1.467(3)
Average [†] for phenyl hydrazones (median) [†]	1.376 (1.366)	1.368 (1.370)	1.288 (1.287)	1.470 (1.467)

[†] From CSD search August 2006, 158 structures of Ph-NH-N=CH-PhX

End of passion play, crumbling away, I'm your source of self-destruction, Veins that pump with fear, sucking darkest clear, Leading on your deaths construction, Taste me you will see, More is all you need, You're dedicated to, How I'm killing you, Come crawling faster, Obey your master, Your life burns faster, Obey your master, Master, Master of puppets I'm pulling your strings, Twisting your mind and smashing your dreams, Blinded by me, you cant see a thing, Just call my name, 'cause I'll hear you scream, Master Master, Just call my name, 'cause I'll hear you scream, Master Master. Needlework the way, never you betray, Life of death becoming clearer, Pain monopoly, ritual misery, Chop your breakfast on a mirror, Taste me you will see, More is all you need, You're dedicated to, How I'm killing you, Come crawling faster, Obey your master, Your life burns faster, Obey your master, Master, Master of puppets I'm pulling your strings, Twisting your mind and smashing your dreams, Blinded by me, you cant see a thing, Just call my name, 'cause I'll hear you scream, Master Master, Just call my name, 'cause I'll hear you scream, Master Master. Master, master, wheres the dreams that I've been after? Master, master, you promised only lies, Laughter, laughter, all I hear and see is laughter, Laughter, laughter, laughing at my cries, Hell is worth all that, natural habitat, Just a rhyme without a reason, Neverending maze, drift on numbered days, Now your life is out of season, Taste me you will see, More is all you need,

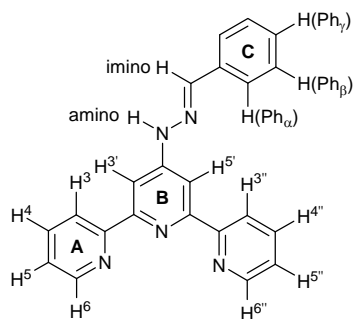
You're dedicated to, How I'm killing you, Come crawling faster, Obey your master,
 Your life burns faster, Obey your master, Master, Master of puppets I'm pulling your
 strings, Twisting your mind and smashing your dreams, Blinded by me, you can't see a
 thing, Just call my name, `cause I'll hear you scream, Master Master, Just call my name,
 `cause I'll hear you scream, Master Master.

Table 2 Relevant torsion angles (degrees, absolute)

	C8-N4- N5=C16	N5=C16- C17-C22	Py-py torsions	
17	13.3 (1)	9.3 (2)	9.5 (1)	20.0 (1)
18	5.1 (1)	1.8 (2)	6.2 (1)	6.0 (1)
19.CH₂Cl₂	2.2 (1)	18.3 (2)	2.7 (1)	5.0 (1)
20	7.9 (2)	7.8 (3)	9.0 (2)	7.6 (2)
26H₂O·CHCl₃	3.8 (2)	1.4 (4)	14.2 (2)	25.2 (2)
2[22.H₂O]	7.0 (3)	7.6 (5)	20.9 (2)	12.2 (3)
24	5.5 (2)	7.3 (4)	10.1 (2)	2.4 (2)
	0.7 (2)	6.3 (4)	2.1 (2)	1.2 (2)
25	4.5 (1)	-	0.6 (1)	16.2 (1)
[H 17](CF ₃ CO ₂)·EtOH·0.5H ₂ O	2.7 (3)	1.2 (3)	8.9 (5)	2.4 (4)
[H 17](PF ₆)·H ₂ O	6.0 (3)	5.9 (6)	5.8 (5)	15.0 (5)
[H 18](BF ₄)	3.3 (2)	14.8 (2)	9.7 (2)	6.0 (2)
[H 21](BF ₄)	2.8 (2)	2.3 (2)	1.2 (3)	6.3 (3)
[H 19](MeOSO ₃)	11.9 (2)	7.7 (3)	8.3 (2)	3.2 (2)
[H ₂ 17 .Cl ₂]·DMSO	5.1 (2)	4.1 (3)	2.9 (3)	5.8 (3)
[H ₂ 18](NO ₃)(MeOSO ₃)·H ₂ O	13.3 (3)	2.6 (4)	1.2 (3)	4.4 (3)
Average for phenyl hydrazones	10.1	20.6	-	-
(median)†	(4.6)	(8.5)	-	-

† From CSD search August 2006, 158 structures of Ph-NH-N=CH-PhX

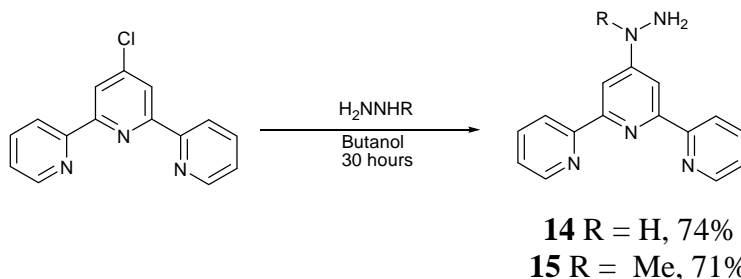
2.15. Experimental



General: ¹H and ¹³C NMR spectra were recorded on a Bruker Avance DRX 500 spectrometer; the numbering scheme for the ligands is shown above. Chemical shifts for ¹H and ¹³C NMR spectra are referenced to residual solvent peaks with respect to TMS = δ 0 ppm. Electrospray mass spectra were recorded using a Finnigan MAT LCQ mass

spectrometer. Melting points were recorded on a Stuart Scientific melting point apparatus SMP3. In the ^1H NMR spectra listed below, data at 360 K are given whenever the spectrum at 295 K contains very broad or unresolved signals.

Synthesis of 4'-hydrazino-2,2':6'.2''-terpyridine (14)



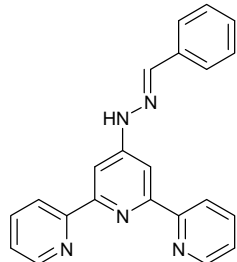
The title compound was prepared by a modification of a known procedure.²⁵⁰ All analytical data was in agreement with the literature.

4'-Chloro-2,2':6',2''-terpyridine²⁵¹ (600 mg, 2.2 mmol) was dissolved in butanol (12 mL). Excess hydrazine hydrate (4 mL) was added. The mixture was then heated to reflux for 30 h. On cooling white crystals precipitated out of solution. These were collected by filtration and washed with a small volume of cold water to yield analytically pure 4'-hydrazino-2,2':6'.2''-terpyridine (439 mg, 74%). NMR (DMSO- d_6): ^1H δ (ppm) 8.66 (ddd, J 4.7, 1.8, 0.9 Hz, 2H, H^{A6}), 8.56 (td, J 8.0, 1.1 Hz, 2H, H^{A3}), 7.94 (ddd, J 7.9, 7.5, 1.8 Hz, 2H, H^{A4}), 7.83 (s, 2H, H^{B3}), 7.92 (br s, 1H, H^{NH}), 7.43 (ddd, J 7.5, 4.7, 1.2 Hz, 2H, H^{A5}), 4.40 (br s, 2H, NH_2). $^{13}\text{C}\{^1\text{H}\}$ δ (ppm) 148.8 (C^{A6}), 123.8 (C^{A5}), 137.0 (C^{A4}), 120.6 (C^{A3}), 102.8 (C^{B3}). CHN: Found: C 68.50, H 4.91, N 26.76 %. $\text{C}_{15}\text{H}_{13}\text{N}_5$ requires C 68.43, H 4.98, N 26.60 %

Synthesis of 4'-N-methylhydrazino-2,2':6',2''-terpyridine (15)

The title compound was prepared by a modification of a known procedure.²⁵⁰ All analytical data was in agreement with the literature. 4'-Chloro-2,2':6',2''-terpyridine (200 mg, 0.75 mmol) was dissolved in butanol (10 mL). Excess Methyl hydrazine (1.5 mL) was added. The mixture was then heated to reflux for 48 h. No precipitate formed on cooling, the solvent was removed and the oily residue was recrystallised from methanol with cooling in the freezer to give fine white needles (yield: 146mg, 71%). NMR (DMSO- d_6) ^1H δ (ppm) 8.68 (ddd, J 4.7, 1.8, 0.9 Hz, 2H, H^{A6}), 8.58 (dt, J 8.0, 1.1 Hz, 2H, H^{A3}), 7.97 (s, 2H, $\text{H}^{B3'}$), 7.95 (ddd, J 7.9, 1.5, 1.8 Hz, 2H, H^{A4}), 7.44 (ddd, J

7.4, 4.7, 1.2 Hz, 2H, H^{A5}), 4.84 (br s, 2H, NH₂), 3.26 (s, 3H, Me). Found C 69.25, H 5.47, N 25.63 % ; C₁₆H₁₅N₅ requires C 69.29, H 5.45, N 25.25 % m.p. 214-214 °C (lit.²⁵⁰ 217-219 °C).



Synthesis of 17

[H₂**17**][MeOSO₃]₂: 4'-Hydrazino-2,2':6',2"-terpyridine (0.20 g, 0.76 mmol) was dissolved in hot methanol (15 cm³), and excess benzaldehyde (0.10 g, 0.94 mmol) was added giving a colourless solution. A few drops of concentrated H₂SO₄ were added, and a yellow precipitate formed almost immediately. The suspension was heated at reflux for 3 h and then cooled to room temperature. The bright yellow solid product was collected by filtration and washed with EtOH. [H₂**17**][MeOSO₃]₂ was isolated as a yellow powder (0.42 g, 0.73 mmol, 96%). ¹H NMR (500 MHz, DMSO-d₆, 360 K) δ / ppm 12.02 (br, H^{NH}), 8.89 (ddd, J 4.8, 1.7, 0.9 Hz, 2H, H^{A6}), 8.53 (d, J 8.0 Hz, 2H, H^{A3}), 8.34 (s, 1H, HHC=N), 8.19 (td, J 7.7, 1.7 Hz, 2H, H^{A4}), 8.11 (s, 2H, H^{B3}), 7.91 (dd, J 7.9, 1.5 Hz, 2H, H^{C2}), 7.72 (ddd, J 7.6, 4.8, 1.0 Hz, 2H, H^{A5}), 7.5 (m, 3H, H^{C3+C4}), 3.39 (s, HOMe, see text). ¹H NMR (500 MHz, DMSO-d₆, 295 K) δ / ppm 12.45 (s, NH), 8.93 (d, J 4.4 Hz, 2H, H^{A6}), 8.7 (v br, H^{A3}), 8.5 (v br, H^{B3}), 8.30 (s, 1H, HHC=N), 8.25 (t, J 7.6 Hz, 2H, H^{A4}), 7.96 (dd, J 7.5, 2.0 Hz, 2H, H^{C2}), 7.79 (dd, J 6.8, 5.3 Hz, 2H, H^{A5}), 7.50 (m, 3H, H^{C3+C4}), 3.38 (s, HOMe, see text). ¹³C NMR (125 MHz, DMSO-d₆, 295 K) δ / ppm 156.0 (C^{B4}), 149.2 (C^{A6}), 147.8 (C^{C=N}), 146.8 (C^{A2+B2}), 139.8 (C^{A4}), 133.7 (C^{C1}), 130.7 (C^{C4}), 129.0 (C^{C3}), 127.8 (C^{C2}), 127.1 (C^{A5}), 122.8 (broad, C^{A3}), 105 (broad, C^{B3}), 53.0 (C^{Me}). ES-MS m/z 352 [H₂**17**]⁺. Found, C 48.77, H 4.21, N 11.97; C₂₄H₂₇N₅O₉S₂ requires C 48.56, H 4.58, N 11.80 %.

[H₂**17**][NO₃]₂: The method and scale were as for [H₂**17**][MeOSO₃]₂, replacing concentrated H₂SO₄ by HNO₃ (*caution!*). [H₂**17**][NO₃]₂ was isolated as a bright yellow powder (0.24 g, 0.50 mmol, 70%). ¹H NMR (500 MHz, DMSO-d₆, 360 K) δ / ppm

11.80 (s, NH), 8.87 (ddd, J 4.9, 1.7, 0.9 Hz, 2H, H^{A6}), 8.53 (d, J 7.9 Hz, 2H, H^{A3}), 8.29 (s, 1H, H^{HC=N}), 8.15 (td, J 7.8, 1.7 Hz, 2H, H^{A4}), 8.08 (s, 2H, H^{B3}), 7.89 (dd, J 8.0, 1.4 Hz, 2H, H^{C2}), 7.68 (ddd, J 7.6, 4.8, 1.0 Hz, 2H, H^{A5}), 7.50 (m, 3H, H^{C3+C4}). ¹H NMR (500 MHz, DMSO-d₆, 295 K) δ / ppm 12.28 (br, NH), 8.93 (d, J 4.7 Hz, 2H, H^{A6}), 8.6 (v br, H^{A3}), 8.32 (s, 1H, H^{HC=N}), 8.24 (t, J 7.3 Hz, 2H, H^{A4}), 7.98 (dd, J 7.8, 1.5 Hz 2H, H^{C2}), 7.77 (dd, J 7.5, 5.0 Hz, 2H, H^{A5}), 7.50 (m, 3H, H^{C3+C4}); signal for H^{B3} not observed at 295 K. ¹³C NMR (125 MHz, DMSO-d₆, 295 K) δ / ppm 149.1 (C^{A6}), 147.0 (C^{C=N}), 139.4 (C^{A4}), 133.8 (C^{C1}), 130.5 (C^{C4}), 128.9 (C^{C3}), 127.6 (C^{C2}), 126.8 (C^{A5}), 122.4 (broad, C^{A3}), C^{A2, B2, B3, B4} not observed. ES-MS m/z 352 [H¹⁷]⁺. Found, C 54.93, H 3.93, N 20.11; C₂₂H₁₉N₇O₆ .0.25H₂O requires C 54.83, H 4.08, N 20.34 %.

[H₂¹⁷]Cl₂: The method and scale were as for [H₂¹⁷][MeOSO₃]₂, replacing concentrated H₂SO₄ by HCl. [H₂¹⁷]Cl₂ was isolated as a bright yellow powder (0.17 g, 0.40 mmol, 53 %). ¹H NMR (500 MHz, DMSO-d₆, 360 K) 12.71 (s, NH), 8.90 (d, J 4.7 Hz, 2H, H^{A6}), 8.52 (d, J 8.0, 2H, H^{A3}), 8.44 (s, 1H, H^{HC=N}), 8.20 (t, J 7.8 Hz, 2H, H^{A4}), 8.17 (s, 2H, H^{B3}), 7.90 (d, J 6.6 Hz, 2H, H^{C2}), 7.73 (dd, J 7.5, 4.8 Hz, 2H, H^{A5}), 7.50 (m, 3H, H^{C3+C4}). ¹H NMR (500 MHz, DMSO-d₆, 295 K) δ / ppm 12.66 (s, H^{NH}), 8.93 (d, J 4.3 Hz, 2H, H^{A6}), 8.62 (br, H^{A3}), 8.37 (s, 1H, H^{HC=N}), 8.24 (t, J 7.6 Hz, 2H, H^{A4}), 7.97 (d, J 7.0 Hz 2H, H^{C2}), 7.77 (dd, J 6.5, 4.9 Hz, 2H, H^{A5}), 7.51 (m, 3H, H^{C3+4}), signal for H^{B3} not observed at 295 K. ¹³C{¹H} NMR (125 MHz, DMSO-d₆, 295 K) δ / ppm 155.6 (C^{A2+B2}), 149.1 (C^{A6}), 147.9 (C^{C=N}), 139.4 (C^{A4}), 133.8 (C^{C1}), 130.4 (C^{C4}), 128.9 (C^{C3}), 127.5 (C^{C2}), 126.7 (C^{C5}), 122.4 (C^{A3}), 104 (br, C^{B3}), C^{B4} not observed. ES-MS m/z 352 [H¹⁷]⁺. Found, C 54.02, H 5.02, N 14.40; C₂₂H₁₉Cl₂N₅ .3.5H₂O requires C 54.22, H 5.38, N 14.37 %.

[H¹⁷][BF₄]: [H₂¹⁷][MeOSO₃]₂ (0.10 g, 0.17 mmol) was dissolved in a minimum volume of hot water and excess NaBF₄ was added. The yellow-green precipitate that formed was collected by filtration and washed with water and cold EtOH. [H¹⁷][BF₄] was isolated as a pale yellow solid (0.070 g, 0.16 mmol, 92%). ¹H NMR (500 MHz, DMSO-d₆, 360 K) δ / ppm 11.42 (br, H^{NH}), 8.82 (d, J 4.8 Hz, 2H, H^{A6}), 8.55 (d, J 8.0 Hz, H^{A3}), 8.22 (s, 1H, H^{HC=N}), 8.11 (s, 2H, H^{B3}), 8.09 (t, J 7.4 Hz, 2H, H^{A4}), 7.96 (d, J 6.4 Hz, 2H, H^{C2}), 7.75 (ddd, J 7.7, 4.9, 0.8 Hz, 2H, H^{A5}), 7.5 (m, 3H, H^{C3+C4}). ¹H NMR (500 MHz, DMSO-d₆, 295 K) δ / ppm 12.23 (br, H^{NH}), 8.91 (d, J 4.3 Hz, 2H, H^{A6}), 8.6

(v br, H^{A3,B3}), 8.29 (s, 1H, H^{HC=N}), 8.21 (t, *J* 7.4 Hz, 2H, H^{A4}), 7.96 (d, *J* 6.4 Hz, 2H, H^{C2}), 7.75 (t, *J* 7.7 Hz, 2H, H^{A5}), 7.5 (m, 3H, H^{C3+4}). ¹³C{¹H} NMR (125 MHz, DMSO-d₆, 295 K) δ / ppm 155.6 (C^{B4}), 149.3 (C^{A6}), 148.0 (C^{A2+B2}), 146.8 (C^{C=N}), 139.2 (C^{A4}), 133.8 (C^{C1}), 130.5 (C^{C4}), 128.9 (C^{C3}), 127.6 (C^{C2}), 126.8 (C^{A5}), 122.4 (br, C^{A3}), 104.1 (br, C^{B3}). ESI-MS m/z 352 [H17]⁺. Found, C 57.02, H 4.37, N 15.07; C₂₂H₁₈BF₄N₅ · 1.5H₂O requires C 56.67, H 4.54, N 15.02 %.

[H17][PF₆]: An excess of NH₄PF₆ was added to a solution of [H₂17][MeOSO₃]₂ (0.10 g, 0.17 mmol) dissolved in a minimum volume of hot water. A pale yellow precipitate formed and was collected by filtration, washed with water and cold EtOH. [H17][PF₆] was isolated as a pale yellow solid (0.042 g, 0.084 mmol, 49 %). Slow evaporation of a solution of [H17][PF₆] in acetone–water (5 : 1) gave X-ray quality crystals of [H17][PF₆].H₂O. ¹H NMR (500 MHz, DMSO-d₆, 360 K) δ / ppm 11.45 (br, H^{NH}), 8.82 (d, *J* 4.7 Hz, 2H, H^{A6}), 8.55 (d, *J* 8.0 Hz, H^{A3}), 8.22 (s, 1H, H^{HC=N}), 8.11 (s, 2H, H^{B3}), 8.09 (dt, *J* 7.8, 1.7 Hz, 2H, H^{A4}), 7.84 (d, *J* 7.0 Hz, 2H, H^{C2}), 7.75 (dd, *J* 7.5, 4.7 Hz, 2H, H^{A5}), 7.50 (m, 3H, H^{C3+4}). ¹H NMR (500 MHz, DMSO-d₆, 295 K) δ / ppm 11.97 (s, H^{NH}), 8.68 (d, *J* 4.0 Hz, 2H, H^{A6}), 8.62 (br, H^{A3}), 8.25 (s, 1H, H^{HC=N}), 8.16 (t, *J* 7.4 Hz, 2H, H^{A4}), 8.1 (v br, H^{B3}), 7.92 (d, *J* 7.1 Hz, 2H, H^{C2}), 7.69 (t, *J* 5.2 Hz, 2H, H^{A5}), 7.50 (m, 3H, H^{C3+4}). ¹³C{¹H} NMR (125 MHz, DMSO-d₆, 295 K) δ / ppm 55.4 (C^{B4}), 149.4 (C^{A6}), 148.5 (C^{A2+B2}), 146.6 (C^{C=N}), 139.1 (C^{A4}), 133.9 (C^{C1}), 130.4 (C^{C4}), 128.9 (C^{C3}), 127.5 (C^{C2}), 126.6 (C^{A5}), 122.4 (br, C^{A3}), 104.2 (br, C^{B3}). ES-MS m/z 352 [H17]⁺. Found, C 51.71, H 3.86, N 13.63; C₂₂H₁₈N₅PF₆ · 0.75H₂O requires C 51.72, H 3.85, N 13.71 %.

[H₂17][PF₆]₂: HPF₆ (60% in water, 2 cm³) was added to a solution of **17** (0.10 g, 0.28 mmol) in EtOH (30 cm³). A bright yellow precipitate which formed was collected by filtration and washed with EtOH (10 cm³). The solid was dissolved in acetone, HPF₆ (1 cm³) was added and the solution was filtered to remove a small amount of solid material. Et₂O was added and the resulting yellow precipitate was collected.

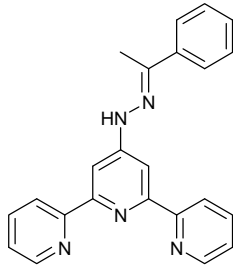
[H₂17][PF₆]₂ (0.036 g, 0.056 mmol, 20%). ¹H NMR (500 MHz, DMSO-d₆, 360 K) δ / ppm 11.74 (s, H^{NH}), 8.86 (d, *J* 4.7 Hz, 2H, H^{A6}), 8.54 (d, *J* 7.9 Hz, H^{A3}), 8.28 (s, 1H, H^{HC=N}), 8.15 (dt, *J* 7.9, 1.6 Hz, 2H, H^{A4}), 8.10 (s, 2H, H^{B3}), 7.89 (d, *J* 6.9 Hz, 2H, H^{C2}), 7.67 (dd, *J* 7.1, 5.2 Hz, 2H, H^{A5}), 7.49 (m, 3H, H^{C3+4}). ¹H NMR (500 MHz, DMSO-d₆,

295 K) 12.25 (s, H^{NH}), 8.92 (d, *J* 4.4 Hz, 2H, H^{A6}), 8.62 (br, H^{A3}), 8.31 (s, 1H, H^{HC=N}), 8.23 (t, *J* 7.7 Hz, 2H, H^{A4}), 8.10 (v br, H^{B3}), 7.97 (d, *J* 6.9 Hz, 2H, H^{C2}), 7.76 (dd, *J* 6.8, 5.1 Hz, 2H, H^{A5}), 7.52 (m, 3H, H^{C3+4}). ¹³C{¹H} NMR (125 MHz, DMSO-d₆, 295 K) δ / ppm 155.8 (C^{A2+B2}), 149.2 (C^{A6}), 147.3 (C^{C=N}), 139.5 (C^{A4}), 133.7 (C^{C1}), 130.6 (C^{C4}), 128.9 (C^{C3}), 127.7 (C^{C2}), 126.9 (C^{A5}), C^{A3,B3,B4} not observed. ESI-MS m/z 352 [H17]⁺. Found: C 39.69, H 3.26, N 10.14; C₂₂H₁₈F₁₂N₅P₂ .1.5H₂O requires C 39.42, H 3.31, N 10.45 %.

17: [H₂17][MeOSO₃]₂ (0.50 g, 0.87 mmol) was dissolved in water (100 cm³) to give a yellow solution. Solid K₂CO₃ was added until a colourless solution was obtained. The solution was extracted into CH₂Cl₂ (3 × 50 cm³) and the solution was dried over Na₂SO₄. Solvent was removed to give neutral **17** which was purified by chromatography using a short column (alumina, CH₂Cl₂ with 1% MeOH). **17** was isolated as a white solid (0.25 g, 0.71 mmol, 82%). m.p. 210-212 °C. ¹H NMR (500 MHz, DMSO-d₆, 360 K) δ / ppm 10.81 (s, 1H, H^{NH}), 8.72 (ddd, *J* 4.7, 1.9, 0.9 Hz, 2H, H^{A6}), 8.58 (dt, *J* 7.9, 1.1 Hz, 2H, H^{A3}), 8.16 (s, 2H, H^{B3}), 8.08 (s, 1H, H^{HC=N}), 7.96 (ddd, *J* 7.9, 7.5, 1.8 Hz, 2H, H^{A4}), 7.74 (m, 2H, H^{C2}), 7.45 (m, 2H, H^{C3}), 7.44 (ddd, *J* 7.4, 4.7, 1.2 Hz, 2H, H^{A5}), 7.39 (m, 1H, H^{C3}). ¹H NMR (500 MHz, DMSO-d₆, 295 K) δ / ppm 11.14 (H^{NH}), 8.74 (ddd, *J* 4.7, 1.7, 0.8 Hz, 2H, H^{A6}), 8.62 (td, *J* 8.0, 1.0 Hz, 2H, H^{A3}), 8.16 (br, H^{B3}), 8.06 (s, 1H, H^{HC=N}), 7.99 (td, *J* 7.6, 1.8 Hz, 2H, H^{A4}), 7.76 (dd, *J* 7.2, 1.3 Hz, 2H, H^{C2}), 7.48 (m, 4H, H^{A5+C3}), 7.39 (tt, *J* 7.3, 1.3 Hz, 1H, H^{C4}). ¹³C{¹H} NMR (125 MHz, DMSO-d₆, 295 K) δ / ppm 155.5, (C^{A2/B2}), 155.4 (C^{A2/B2}), 152.7 (C^{B4}), 149.2 (C^{A6}), 140.7 (C^{C=N}), 137.2 (C^{A4}), 134.8 (C^{C1}), 129.1 (C^{C4}), 128.9 (C^{C3}), 126.3 (C^{C2}), 124.2 (C^{A5}), 120.8 (C^{A3}), 103.8 (br, C^{B3}). ES-MS m/z 352 [H17]⁺. Found: C 71.62, H 4.97, N 18.88; C₂₂H₁₇N₅ .H₂O requires C 71.53, H 5.18, N 18.96 %. Slow evaporation of a CDCl₃ solution of **17** gave X-ray quality needles.

[H17](CF₃CO₂)

A drop of TFA was added to a solution of **17** in CHCl₃/EtOH resulting in the solution becoming bright yellow. Slow evaporation afforded large X-ray quality bright yellow needles of [H17]₄[CF₃CO₂]₄H₂O. Found: C 61.85, H 3.90, 14.93. C₂₂H₁₇N₅.HCF₃CO₂ requires C 61.94, H 3.90, N 15.05 %



Synthesis of **18**

[H₂**18**][MeOSO₃]₂: 4'-Hydrazino-2,2':6',2''-terpyridine (0.20 g, 0.76 mmol) was dissolved in hot methanol (15 cm³), and excess acetophenone (0.10 g, 0.83 mmol) was added giving a colourless solution. A few drops of concentrated H₂SO₄ were added, and a bright yellow precipitate formed after heating the mixture for a few minutes. The suspension was heated at reflux for 3 h and then cooled to room temperature. The bright yellow solid was collected by filtration and washed well with MeOH.

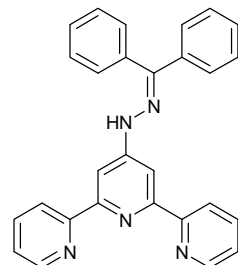
[H₂**18**][MeOSO₃]₂ was isolated as a yellow powder (0.45 g, 0.76 mmol, 100%). ¹H NMR (500 MHz, DMSO-d₆, 360 K) δ / ppm 11.28 (s, H^{NH}), 8.93 (d, J 4.4 Hz, 2H, H^{A6}), 8.57 (br, H^{A3}), 8.28 (s, 2H, H^{B3}), 8.25 (t, J 7.7 Hz, 2H, H^{A4}), 8.04 (dd, J 7.7, 1.4 Hz, 2H, H^{C2}), 7.78 (dd, J 6.8, 5.2 Hz, 2H, H^{A5}), 7.50 (m, 3H, H^{C3+4}), 3.38 (s, H^{OMe}, see text), 2.50 (H^{CMe}, overlaps with solvent peak). ¹³C{¹H} NMR (125 MHz, DMSO-d₆, 295 K) δ / ppm 149.2 (C^{A6}), 139.5 (C^{A4}), 128.5(C^{C3,C4}), 126.8 (C^{A5}), 126.5 (C^{C2}), 14.4 (C^{MeC}), C^{A2,A3,B2,B3,B4,C1,C=N} not observed. ESI-MS m/z 366 [H₂**18**]⁺. Found, C 49.72, H 4.61, N 11.41; C₂₅H₂₇N₅O₈S₂·0.75H₂O requires C 49.78, H 4.76, N 11.61 %.

[H₂**18**][BF₄]: [H₂**18**][MeOSO₃]₂ (0.10 g, 0.17 mmol) was dissolved in a minimum volume of hot water and an excess of NaBF₄ was added. The mixture was heated to 50°C and was maintained at this temperature with stirring for 1 h, after which time a yellow-green solid had formed. The precipitate was collected by filtration and was washed well with water and cold EtOH. [H₂**18**][BF₄] was isolated as a yellow-green solid (0.062 g, 0.13 mmol, 80 %). ¹H NMR (500 MHz, DMSO-d₆, 360 K) δ / ppm 10.67 (br, H^{NH}), 8.81 (ddd, J 4.3, 1.7, 0.9 Hz, 2H, H^{A6}), 8.46 (dt, J 8.0, 1.0 Hz, 2H, H^{A3}), 8.22 (s, 2H, H^{B3}), 8.09 (dt, J 8.0, 1.7 Hz, 2H, H^{A4}), 7.91 (dd, J 8.3, 1.4 Hz, 2H, H^{C2}), 7.61 (ddd, J 7.6, 4.8, 1.1 Hz, 2H, H^{A5}), 7.44 (m, 3H, H^{C3+4}), 2.47 (C^{Me}). ¹³C{¹H} NMR (125 MHz, DMSO-d₆, 295 K) δ / ppm 149.3 (C^{A6}), 139.2 (C^{A4}), 137.6 (C^{C1}), 129.6 (C^{C4}), 128.6 (C^{C3}), 126.6 (C^{C2}), 126.4 (C^{A5}), 122.3 (C^{A3}), 104.5 (broad, C^{B3}), 14.3 (C^{Me}), C^{B4,A2,B2,C=N} not observed. ESI-MS m/z 366 [H₂**18**]⁺. Found: C 59.93, H 4.41, N 15.17;

$C_{23}H_{20}BF_4N_5 \cdot 0.5H_2O$ requires C 59.76, H 4.58, N 15.15 %. Slow evaporation of an acetone/water mixture (5:1) gave X-ray quality crystals of [18.HBF₄].

18: [H₂**18**][MeOSO₃]₂ (0.30 g, 0.51 mmol) was dissolved in warm H₂O (10 cm³) and the mixture was filtered through fluted filter paper to remove a small amount of solid impurities. Solid K₂CO₃ was added to the cream precipitate that formed was extracted into CH₂Cl₂ (3 × 100 cm³) and dried over Na₂SO₄. Removal of the solvent gave **18** which was purified by chromatography using a short column (alumina, CH₂Cl₂ with 1% MeOH). **18** was isolated as an off-white solid (0.11 g, 0.30 mmol, 58%). m.p. 192–193 °C. ¹H NMR (500 MHz, DMSO-d₆, 295 K) δ / ppm 10.13 (s, H^{NH}), 8.72 (d, *J* 4.1 Hz, 2H, H^{A6}), 8.61 (d, *J* 7.9 Hz, 2H, H^{A3}), 8.33 (s, 2H, H^{B3}), 7.99 (t, *J* 7.6 Hz, 2H, H^{A4}), 7.85 (d, *J* 7.3 Hz, 2H, H^{C2}), 7.47 (m, 4H, H^{C3+A5}), 7.39 (m, 1H, H^{C4}), 2.37 (s, 3H, H^{Me}). ¹³C{¹H} NMR (125 MHz, DMSO-d₆, 295 K) δ / ppm 155.7, (C^{A2+B2}), 153.5 (C^{B4}), 149.1 (C^{A6}), 145.1 (C^{C=N}), 138.8 (C^{C1}), 137.2 (C^{A4}), 128.5 (C^{C3}), 128.4 (C^{C4}), 125.7 (C^{C2}), 124.1 (C^{A5}), 120.7 (C^{A3}), 104.3 (br, C^{B3}), 13.6 (C^{Me}). ESI-MS m/z 366 [H**18**]⁺. Found: C 74.58, H 5.37, N 18.72; $C_{23}H_{19}N_5 \cdot 0.33H_2O$ requires C 74.38, H 5.34, N 18.86 %. Slow evaporation of a CH₂Cl₂ solution of **18** gave X-ray quality crystals.

[**18.HMeOSO₃.HNO₃**]: [**18.HMeOSO₃**] was dissolved in water and a drop of dilute HNO₃ was added to the solution. Slow evaporation yielded X-ray quality crystals of [**18.HMeOSO₃.HNO₃**].H₂O.



Synthesis of **19**

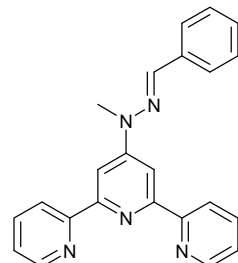
[H₂**19**][MeOSO₃]₂: Excess benzophenone (0.16 g, 0.87 mmol) and 4'- hydrazino-2,2':6',2''-terpyridine (0.20 g, 0.76 mmol) were dissolved in hot MeOH (20 cm³). A few drops of concentrated H₂SO₄ were added to the solution and a white precipitate formed which redissolved on heating. The solution was heated at reflux for 3 h to ensure that the reaction had reached completion. On cooling the reaction mixture to room

temperature, only a small amount of solid precipitated. Et₂O was added to afford [H₂**19**][MeOSO₃]₂ as a bright yellow powder which was collected and washed with MeOH (0.42 g, 0.64 mmol, 85%). ¹H NMR (500 MHz, DMSO-d₆, 295K) δ / ppm 10.74 (s, 1H, H^{NH}), 8.92 (d, *J* 3.8 Hz, 2H, H^{A6}), 8.6 (v br, 2H, H^{A3}), 8.33 (br, 2H, H^{B3}), 8.24 (br dd, *J* 7.8, 4.6 Hz, 2H, H^{A4}), 7.77 (br dd, *J* 5.7, 4.0 Hz, 2H, H^{A5}), 7.67 (m, 5H, H^{C/E}), 7.46 (m, 5H, H^{C/E}), 3.37 (s, 6H, H^{Me}). ¹H (DMSO-d₆, 360K) δ / ppm 10.20 (s, H^{NH}), 8.84 (d, *J* 4.7 Hz, 2H, H^{A6}), 8.48 (d, *J* 7.9 Hz, 2H, H^{A3}), 8.30 (s, 2H, H^{B3}), 8.13 (td, *J* 7.8, 1.6 Hz, 2H, H^{A4}), 7.66 (m, 7 H, H^{A5+C/E}), 7.45 (m, 3H, H^{C/E}), 7.42 (dd, 7.8, 1.5 Hz, 2H, H^{C/E}). ¹³C{¹H} (DMSO-d₆, 295K) δ / ppm 149.1 (C^{A6}), 139.1 (C^{A4}), 132.3 (C^{C/E1}), 137.1 (C^{C/E1}), 130.0 (C^{C/E}), 129.6 (C^{C/E}), 129.0 (C^{C/E}), 128.6 (C^{C/E}), 127.7 (C^{C/E}), 126.7 (C^{A5}), 52.8 (C^{Me}), C^{A2,A3,B2,B3,B4,C=N} not observed. ESI-MS m/z 428 [H**19**]⁺. Found C 52.28, H 4.67, N 10.22; C₃₀H₂₉N₅O₈S₂.2H₂O requires C 52.39, H 4.84, N 10.18 %. Slow evaporation of a aqueous solution of [H₂**19**](MeOSO₃)₂ afforded X-ray quality crystals of [H**19**](MeOSO₃).

[H**19**][BF₄]: [H₂**19**][MeOSO₃]₂ (0.20 g, 0.31 mmol) was dissolved in hot water (10 cm³) and excess NaBF₄ was added. After stirring at room temperature for 1 h, the resulting solid was collected and washed well with water and cold EtOH. [H**19**][BF₄] was isolated as a green-yellow powder (0.06 g, 0.12 mmol, 37%). ¹H NMR (DMSO-d₆, 295K) δ/ppm 10.53 (s, 1H, H^{NH}), 8.86 (br d, *J* 3.3 Hz, 2H, H^{A6}), 8.53 (br s, 2H, H^{A3}), 8.33 (br s, 2H, H^{B3}), 8.17 (t, *J* 7.1 Hz, 2H, H^{A4}), 7.66 (m, 7H, H^{A5+C/E}), 7.46 (dq, *J* 4.9, 1.7 Hz, 3H, H^{C/E}), 7.45 (d, *J* 3.3 Hz, 2H, H^{C2}). ¹³C{¹H} (DMSO-d₆, 295K) δ / ppm 149.2 (C^{A6}), 138.8 (C^{A4}), 137.4 (C^{C1/E1}), 132.4 (C^{C1/E1}), 129.8 (C^{C4/E4}), 129.7 (C^{C4/E4}), 129.5 (C^{C/E2/3}), 129.0 (C^{C/E2/3}), 128.6 (C^{C/E2/3}), 127.4 (C^{C/E2/3}), 126.1 (C^{A5}), 122.0 (H^{A3}), 105.4 (H^{B3}), C^{A2,B2,B4,C=N} not observed. ESI-MS m/z 428 [H**19**]⁺. Found: C 62.86, H 4.16, N 12.93; C₂₈H₂₂BF₄N₅.H₂O requires C 63.06, H 4.54, N 13.13%.

19: [H₂**19**][MeOSO₃]₂ (0.25 g, 0.38 mmol) was dissolved in H₂O (10 cm³), and solid K₂CO₃ (5 g) was added. CH₂Cl₂ (50 cm³) was added and the biphasic mixture was sonicated for 1 h. The two phases were separated and the aqueous layer extracted with CH₂Cl₂ (3 × 300 cm³). The combined organic fractions were dried over Na₂SO₄ and the solvent was removed to give **19** as a pale orange microcrystalline solid which was recrystallised from EtOH/CH₂Cl₂ to give **19** as an off-white solid (0.065 g, 0.15 mmol,

40%). m.p. 212-214 °C. ^1H NMR (DMSO-d₆, 295K) δ / ppm: 9.89 (s, H^{NH}), 8.69 (d, *J* 3.9 Hz, H^{A6}), 8.60 (d, *J* 7.9 Hz, H^{A3}), 8.34 (s, H^{B3}), 7.97 (td, *J* 7.7, 1.7 Hz, HA4), 7.61 (m, 3H, H^{C/E3+4}), 7.51 (dd, *J* 8.3, 1.4 Hz, 2H, H^{C2/E2}), 7.46 (ddd, *J* 7.4, 4.7, 1.1 Hz, H^{A5}), 7.41 (m, 3H, H^{C/E3+4}), 7.37 (dd, *J* 8.0, 1.5 Hz, 2H, H^{C2/E2}). $^{13}\text{C}\{\text{H}\}$ (DMSO-d₆, 295K) δ / ppm 155.7 (C^{A2/B2}), 155.3 (C^{A2/B2}), 153.1 (C^{B4}), 149.1 (C^{A6}), 147.3 (C^{C=N}), 138.3 (C^{C1/E1}), 137.1 (C^{A4}), 133.0 (C^{C1/E1}), 129.4 (C^{C3/E3}), 129.2 (C^{C4/E4}), 129.1 (C^{C3/E3}), 128.6 (C^{C4/E4}), 128.5 (C^{C3/E3}), 126.6 (C^{C2/E2}), 124.1 (C^{A5}), 120.7 (C^{A3}), 105.0 (C^{B3}). ESI-MS m/z 428 [H¹⁹]⁺. Found: C, 76.75; H, 4.97, N, 16.05 %. C₂₈H₂₁N₅ 0.5H₂O requires C, 77.04, H, 5.08, N, 16.04 %. Slow evaporation of a CH₂Cl₂ solution of **19** gave X-ray quality crystals.

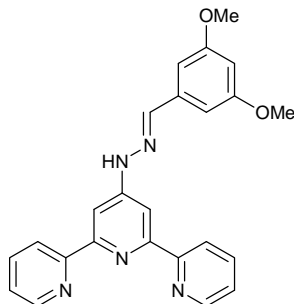


*Preparation of **20***

[H₂**20**][MeOSO₃]₂: Excess benzaldehyde (0.10g, 0.94 mmol) was added to a solution of 4'-(1-methylhydrazino)-2,2':6',2"-terpyridine (0.20 g, 0.72 mmol) in hot methanol (15 cm³). Upon the addition of a few drops of concentrated H₂SO₄ followed by stirring for a few minutes, the cloudy reaction mixture converted into a pale yellow solution. This was heated under reflux for 12 h, after which time it was cooled to room temperature. Et₂O was added until a cream precipitate began to form. The reaction mixture was left in the freezer overnight and was then filtered. The solid residue was washed well with Et₂O, and [H₂**20**][MeOSO₃]₂ was isolated as a pale yellow microcrystalline solid (0.33 g, 0.56 mmol, 78%). ^1H NMR (500 MHz, DMSO-d₆, 295 K) δ / ppm 8.94 (d, *J* 4.6 Hz, 2H, H^{A6}), 8.81 (d, *J* 8.0 Hz, 2H, H^{A3}), 8.46 (s, 2H, H^{B3}), 8.37 (s, 1H, H^{HC=N}), 8.24 (t, *J* 7.5 Hz, 2H, H^{A4}), 8.00 (d, *J* 7.2 Hz, 2H, H^{C2}), 7.80 (dd, *J* 7.2, 5.2 Hz, 2H, H^{A5}), 7.54 (m, 2H, H^{C3,C4}), 3.83 (s, 3H, H^{Me}), 3.37 (s, H^{OMe}, see text). $^{13}\text{C}\{\text{H}\}$ NMR (125 MHz, DMSO-d₆, 295 K) δ / ppm 157.1 (C^{B4}), 147.7 (C^{A2,B2}), 149.0 (C^{A6}), 144.1 (C^{C=N}), 139.3 (C^{A4}), 134.5 (C^{C1}), 130.3 (C^{C4}), 129.0 (C^{C3}), 126.9 (C^{C2}), 126.4 (C^{A5}), 122.5 (C^{A3}), 105.8 (C^{B3}), 52.8 (C^{OMe}), 33.3 (C^{Me}). ESI-MS m/z 366 [H²⁰]⁺. Found: C 49.37, H 4.55, N 11.66; C₂₅H₂₇N₅O₈S₂ .H₂O requires C 49.41, H, 4.81, N 11.53 %.

[H²⁰][BF₄]: [H₂**20**][MeOSO₃]₂ (0.15 g, 0.26 mmol) was dissolved in a hot 1 : 4 MeOH:H₂O (50 cm³) mixture and excess aqueous solution of NaBF₄ was added to give a pale yellow precipitate which was collected and washed well with water and a little MeOH (0.096 g, 0.21 mmol, 83 %). ¹H NMR (500 MHz, DMSO-d₆, 295 K) δ / ppm 8.90 (d, *J* 4.4 Hz, 2H, H^{A6}), 8.76 (d, *J* 8.2 Hz, 2H, H^{A3}), 8.45 (s, 2H, H^{B3}), 8.30 (s, 1H, H^{HC=N}), 8.21 (t, *J* 7.4 Hz, 2H, H^{A4}), 7.96 (d, *J* 7.3 Hz, 2H, H^{C2}), 7.72 (dd, *J* 7.0, 5.0 Hz, 2H, H^{A5}), 7.54 (t, *J* 7.4 Hz, 2H, H^{C3}), 7.48 (t, *J* 7.3 Hz, H^{C4}), 3.78 (s, 3H, H^{Me}). ¹³C{¹H} NMR (125 MHz, DMSO-d₆, 295 K) δ / ppm 149.1 (C^{A6}), 145.5 (C^{C=N}), 138.9 (C^{A4}), 130.0 (C^{C4}), 129.0 (C^{C3}), 127.5 (C^{C2}), 126.2 (C^{A5}), 122.3 (C^{A3}), 105.7 (C^{B3}), 39.5 (C^{Me}), C^{A2,B2,B4,C1} not observed. ESI-MS m/z 366 [H²⁰]⁺, 388 [20 + Na]⁺, 753 [2(20) + Na]⁺. Found: C 59.27, H 4.33, N 14.92; C₂₃H₂₀BF₄N₅ · 0.75H₂O requires C 59.18, H 4.64, N 15.00 %.

20: [H₂**20**][MeOSO₃]₂ (0.10 g, 0.17 mmol) was dissolved in H₂O (10 cm³) and solid K₂CO₃ was added until a precipitate formed. The cream solid was extracted into CH₂Cl₂ (3 × 30 cm³), the combined extracts were dried over MgSO₄ and the solvent was removed. The residue was recrystallised from CH₂Cl₂/EtOH (with added solid K₂CO₃ to ensure complete deprotonation). **20** was isolated as a cream microcrystalline solid (0.015 g, 0.041 mmol, 24%). m.p. 211–212 °C. ¹H NMR (500 MHz, DMSO-d₆, 295 K) δ / ppm 8.75 (ddd, *J* 4.8, 1.6, 0.8 Hz, 2H, H^{A6}), 8.63 (d, *J* 7.9 Hz, 2H, H^{A3}), 8.42 (s, 2H, H^{B3}), 8.03 (s, 1H, H^{HC=N}), 8.00 (td, *J* 7.8, 1.8 Hz, 2H, H^{A4}), 7.81 (d, *J* 7.3 Hz, 2H, H^{C2}), 7.49 (m, 4H, H^{C3+C5}), 7.40 (t, *J* 7.3 Hz, 1H, H^{C4}), 3.60 (s, 3H, H^{Me}). ¹³C{¹H} NMR (125 MHz, DMSO-d₆, 295 K) δ / ppm 155.7 (C^{A2/B2}), 155.6 (C^{A2/B2}), 154.6 (C^{B4}), 149.3 (C^{A6}), 139.4 (C^{A4}), 137.4 (C^{C=N}), 135.8 (C^{C1}), 129.0 (C^{C3+C4}), 126.6 (C^{C2}), 124.4 (C^{A5}), 121.1 (C^{A3}), 105.4 (C^{B3}), 32.8 (C^{Me}). ESI-MS m/z 366 [H²⁰]⁺. Found, C 72.00, H 5.25, N 18.07; C₂₃H₁₉N₅ H₂O requires C 72.04, H 5.52, N 18.26 %.

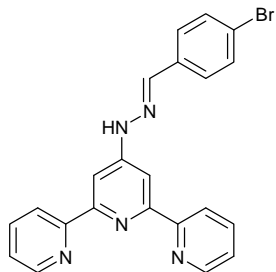


Synthesis of 21

[H₂**21**](MeOSO₃)₂: Excess 3,5-dimethoxybenzaldehyde (0.15g, 0.90 mmol) was added to **14** (0.20g, 0.76 mmol) in hot methanol. A few drops of H₂SO₄ were added to the clear solution and a bright yellow precipitate formed after a few seconds. The suspension was refluxed for 3 hours to ensure it had reached completion and cooled to room temperature. The bright yellow powder was collected and washed with ethanol. [H₂**21**](MeOSO₃)₂: 0.30g, 0.47 mmol, 62 %.

[H₂**21**]BF₄ : [H₂**21**](MeOSO₃)₂ was dissolved in a minimum amount of hot water and NaBF₄ was added. After stirring at room temperature for an hour a yellow-green solid formed which was collected and washed well with water and cold ethanol. [H₂**21**]BF₄: ESI-MS: 412.1, 411.2, 845.0 *m/z* [21H⁺] requires; 434.4, [21Na⁺] requires 434.2, [(21)₂Na⁺] requires 845.3 *m/z*. Found: C 52.44, H 4.20, N 12.60. [H₂**21**]BF₄·3H₂O requires C 52.19, H 4.93, N 12.68 %. Slow evaporation of a methanol/water (10:1) solution gave X-ray quality crystals of [H₂**21**]BF₄.

21: [H₂**21**](MeOSO₃)₂ (0.20g, 31 mmol) was partially dissolved in water (50mL) and solid K₂CO₃ (5g) was added. CH₂Cl₂ (100mL) was added and the mixture was treated in a sonicator bath for 1 h. The phases were separated and the organic fraction was washed with water (x 100 mL) and dried over MgSO₄. The solvent was removed to give **21** as a cream powder (0.11g, 0.27 mmol, 86%). ¹H NMR (DMSO-d₆ 295K), 11.15 (s, 1H, H^{NH}), 8.73 (d, *J* 4.1 Hz, 2H, H^{A6}), 8.60 (d, *J* 7.9 Hz, 2H, H^{A3}), 8.15 (br s, 2H, H^{B3}), 7.98 (t, *J* 7.7 Hz, 2H, H^{A4}), 7.97 (s, 1H, H^{N=CH}), 7.47 (dd, *J* 6.6, 5.4 Hz, 2H, H^{A5}), 6.91 (s, 2H, H^{C2}), 6.56 (s, 1H, H^{C4}), 3.82 (s, 6H, OMe). ¹³C{¹H} : 160.8 (C^{C2}), 155.5 (C^{A2+B2}), 152.6 (C^{B4}), 149.2 (C^{A6}), 140.5 (C^{C=NH}), 137.2 (C^{A4}), 136.9 (C^{C1}), 124.2 (C^{A5}), 120.7 (C^{A3}), 104.4 (C^{A2}), 103.8 (C^{B3}), 100.7 (C^{C4}), 55.3 (OMe). Found C 68.56, H 5.40, N 16.06 %. C₂₄H₂₁N₅O₂ 0.5MeOH requires C 68.83, H 5.42, N 16.38 %. ESI-MS: 412.2, [21H⁺] requires 412.2 *m/z*.



Synthesis of 22

[H₂**22**](MeOSO₃)₂: Excess 4-bromobenzaldehyde (0.15g, 0.81 mmol) was added to **14** (0.20g, 0.76 mmol) in hot methanol. A few drops of H₂SO₄ were added to the clear solution and a bright orange precipitate formed immediately. The suspension was refluxed for 3 hours to ensure it had reached completion and cooled to room temperature. The bright yellow powder was collected and washed with ethanol.

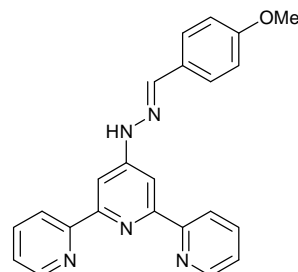
[H₂**22**](MeOSO₃)₂: Yield: 0.36g, 0.55 mmol, 55%.

[H₂**22**]BF₄: [H₂**22**](MeOSO₃)₂ was dissolved in a minimum amount of hot water and NaBF₄ was added and a yellow-green precipitate formed immediately. Elemental analysis: Found: C 47.18, H 3.78, N 12.53 %. C₂₂H₁₇N₅BrBF₄·2.5H₂O requires C 46.92, H 3.94, N 12.44 %. ESI: Found 432.0, [22H⁺] requires 431.3 m/z.

22: [H₂**22**](MeOSO₃)₂ (0.20g, 0.31 mmol) was dissolved in H₂O (10mL) and saturated KHCO₃ (20mL) was added. The resulting pale yellow suspension was extracted into DCM (3 x 50mL) and the clear yellow solution was dried over MgSO₄. Removal of the solvent gave crude **22** as a sticky yellow solid which was purified by a short column (AlOx, DCM/MeOH 99:1) to give **22** as yellow needles. (0.051 g, 0.12 mmol, 39 %).

¹H-NMR (CDCl₃, 295K): 8.71 (d, *J* 4.1 Hz, 2H, H^{A6}), 8.61 (d, *J* 7.9 Hz, 2H, H^{A3}), 8.21 (s, 1H, H^{NH}), 8.15 (s, 2H, H^{B3}), 7.85 (t, *J* 7.7 Hz, 2H, H^{A4}), 7.64 (s, 1H, H^{N=CH}), 7.58 (d, *J* 7.4 Hz, 2H, H^{C2}), 7.50 (d, *J* 7.4 Hz, 2H, H^{C3}), 7.33 (t, *J* 5.5 Hz, 2H, H^{A5}). ¹³C{¹H} 156.6 (C^{A2}), 152.3 (C^{B2}), 149.1 (C^{A6}), 139.0 (C^{N=CH}), 137.0 (C^{A4}), 133.6 (C^{C1}), 131.9 (C^{C3}), 128.3 (C^{C2}), 123.9 (C^{A5}), 123.3 (C^{C4}), 121.6 (C^{A3}), 105.0 (C^{B3}). ¹H-NMR (DMSO-d₆, 295K) 11.21 (s, 1H, H^{NH}), 8.73 (d, *J* 4.6 Hz, 2H, H^{A6}), 8.61 (d, *J* 7.9 Hz, 2H, H^{A3}), 8.15 (br s, 2H, H^{B3}), 8.02 (s, 1H, H^{CH=N}), 7.99 (td, *J* 7.8, 1.7 Hz, 2H, H^{A4}), 7.70 (d, 8.7 Hz, 2H, H^{C2}), 7.67 (d, *J* 8.7 Hz, 2H, H^{C3}), 7.48 (ddd, *J* 7.4, 4.9, 0.9, 2H, H^{A5}). ¹³C{¹H} 155.6 (C^{C2/B2}) 155.5 (C^{A2/B2}), 152.5 (C^{B4}), 149.2 (C^{A6}), 139.5 (C^{C=NH}), 137.2 (C^{A4}), 134.2 (C^{C1}), 131.8 (C^{C3}), 128.1 (C^{C2}), 124.2 (C^{A5}), 122.0 (C^{C4}), 120.7

(C^{A3}), 103.8 (C^{B3}). ESI: Found 432.0, [22H⁺] requires 432.1 m/z, [. Found: C 60.77, H 3.86, N 15.61 %. C₂₂H₁₆N₅Br0.33H₂O requires C 60.57, H 3.85, N 16.05 %



Synthesis of 23

[H₂**23**](MeOSO₃)₂: Excess 4-methoxybenzaldehyde (0.11g, 0.81 mmol) was added to **14** (0.20g, 0.76 mmol) in hot methanol. A few drops of H₂SO₄ were added to the clear solution and a bright orange precipitate formed immediately. The suspension was refluxed for 3 hours to ensure it had reached completion and cooled to room temperature. The bright orange powder was collected and washed with ethanol.

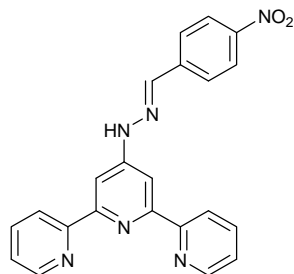
[H₂**23**](MeOSO₃)₂: Yield: 0.46g, 0.75 mmol, 99%.

[H₂**23**]BF₄: [H₂**23**](MeOSO₃)₂ was dissolved in a minimum amount of hot water and NaBF₄ was added and a yellow precipitate formed immediately. ESI-MS: 382.1, [H₂**23**]⁺ requires 382.2 m/z. Found: C 57.33, H 4.32, N 14.51%. C₂₃H₂₀N₅OBF₄.(H₂O)_{0.75} requires C 57.22, H 4.49, N 14.51 %.

23:

[H₂**23**](MeOSO₃)₂ (0.20g, 0.33 mmol) was dissolved in 20ml hot water and solid K₂CO₃ (5g) was added to give a milky suspension. CH₂Cl₂ (100mL) was added and the biphasic mixture was treated in a sonicator bath for 1 h. The aqueous layer was extracted with CH₂Cl₂ (2 x 100ml) and the combined organic phases were washed with water (2 x 100mL) and dried over NaSO₄. The solvent was removed and the remaining residue was purified by short column chromatography (alumina, CH₂Cl₂ : MeOH, 99:1) to give **23** as a pale yellow solid (0.093 g, 0.24 mmol, 74%). ¹H NMR (DMSO-d₆ 295K): 10.97 (s, 1H, H^{NH}), 8.72 (d, J 4.4 Hz, 2H, H^{A6}), 8.60 (d, J 7.9 Hz, 2H, H^{A3}), 8.12 (s, 2H, H^{B3}), 8.00 (s, 1H, H^{N=CH}), 7.98 (t, J 7.5 Hz, 2H, H^{A4}), 7.69 (d, J 8.5 Hz, 2H, H^{C2}), 7.48 (dd, J 6.9, 5.4, 2H, H^{A5}), 7.05 (d, J 8.8, 2H, H^{C3}), 3.81 (s, 3H, Me). ¹³C{¹H}: 160.1 (C^{C4}), 156.6 C^{A2}), 156.4 (C^{B2}), 152.7 (C^{B4}), 149.1 (C^{A6}), 140.7 (C^{N=CH}), 137.2

(C^{A4}), 127.8 (C^{C2}), 127.5 (C^{C1}), 124.1 (C^{A5}), 120.7 (C^{A3}), 114.4 (C^{C3}), 103.7 (C^{B3}), 55.3 (C^{OMe}). Found C 71.60, H 5.19, N 17.84 %. C₂₃H₁₉N₅O·0.25H₂O requires C 71.58, H 5.09, N 18.15 % ESI-MS: 382.2 *m/z*, [H²³]⁺ requires 382.2 *m/z*.



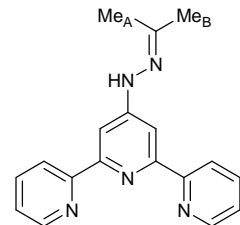
Synthesis of 24

[H₂**24**](EtOSO₃)₂: Excess 4-nitrobenzaldehyde (0.15g, 0.99 mmol) was added to **14** (0.21g, 0.80 mmol) in hot ethanol. A few drops of H₂SO₄ were added to the clear solution and a bright yellow-orange precipitate formed after a few seconds. The suspension was refluxed for 3 hours to ensure it had reached completion and cooled to room temperature. The bright yellow powder was collected and washed well with ethanol to give [H₂**24**](EtOSO₃)₂ (0.43g, 0.66 mmol, 87%). Elemental analysis: C 46.97, H 4.12, N 12.61 %. C₂₆H₂₆N₆O₁₀S₂H₂O requires 46.98, 4.25, 12.64 %.

[H₂**24**]HBF₄ : [H₂**24**](EtOSO₃)₂ (0.20g, 0.31 mmol) was dissolved in a minimum amount of hot water and NaBF₄ was added to give a yellow-green solid which was collected and washed well with water and cold ethanol. [H₂**24**]HBF₄ (0.081g, 0.17 mmol, 54%). ESI: Found 397.1, [24H⁺] requires 397.2 *m/z*.

24: [H₂**24**](EtOSO₃)₂ (0.20g, 0.31 mmol), was dissolved in H₂O (50mL) and solid K₂CO₃ (5g) was added. The resulting suspension was extracted into CH₂Cl₂ (3 x 150mL), washed with water (2 x 250mL), dried over MgSO₄ and the solvent removed to give an orange powder. Recrystallisation from EtOH/CH₂Cl₂ (twice) gave bright orange needles (0.052g, 0.13 mmol, 41%). ¹H NMR (DMSO-d₆ 295K) 11.52 (s, ¹H, H^{NH}), 8.74 (d, *J* 3.8 Hz, 2H, H^{A6}), 8.62 (d, *J* 7.9 Hz, 2H, H^{A3}), 8.33 (d, *J* 8.8 Hz, 2H, H^{C2}), 8.20 (br s, 2H, H^{B3}), 8.14 (s, 1H, H^{C=NH}), 8.00 (m, 4H, H^{A4+C3}), 7.50 (ddd, *J* 7.6, 4.9, 1.1 Hz, 2H, H^{A5}). ¹³C{¹H} 155.7 (C^{A2/B2}), 155.4 (C^{A2/B2}), 152.2 (C^{B4}), 149.2 (C^{A6}), 147.0 (C^{C4}), 141.4 (C^{C1}), 138.2 (C^{CH=N}), 137.3 (C^{A4}), 127.0 (C^{C2}), 124.3 (C^{A5/C3}), 124.2

(C^{A5/C3}), 120.8 (C^{A3}), 103.7 (C^{B3}). ESI: Found 397.1, [24H⁺] requires 397.4 m/z Found C 66.51, H 4.10, N 21.00 % C₂₂H₁₆N₆O₂ requires: C 66.66, H 4.07, N 21.20 %



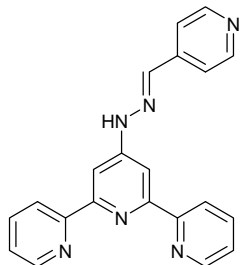
Synthesis of 25

[H₂**25**](MeOSO₃)₂: Excess acetone (~0.5mL, ~7 mmol) was added to **14** (0.20g, 0.76 mmol) in hot methanol. A few drops of H₂SO₄ were added to the clear solution and a yellow precipitate formed which dissolved within a few minutes. The solution was refluxed for 3 hours to ensure it had reached completion and cooled to room temperature. On cooling only a small amount of solid was present; diethyl ether was added to afford a bright yellow solid. The sticky, hygroscopic solid was collected and washed with EtOH/Et₂O. [H₂**25**](MeOSO₃)₂: Yield: 0.30g, 0.57 mmol, 75%.

[H₂**25**]BF₄: [H₂**25**](MeOSO₃)₂ was dissolved in a minimum amount of hot water and NaBF₄ was added. After stirring at room temperature for an hour a yellow-green solid formed which was collected and washed well with water and cold ethanol. ESI-MS: Found: 304.1, 326.1, 629.0 m/z. [25H⁺] requires 304.4, , [25Na⁺] requires 326.1, , [(25)₂Na⁺] requires 629.3 m/z.

25: [H₂**25**](MeOSO₃)₂: (0.20 g, 0.38 mmol) was dissolved in water (30mL) and saturated KHCO_{3(aq)} was added to give a clear, colourless solution. The solution was extracted with CHCl₃ (4 x 100mL), dried over MgSO₄ and the residue was recrystallised from MeOH/CHCl₃ to give **25** as an off-white solid. (0.092 g, 0.30 mmol, 79%). ¹H-NMR (CDCl₃, 295K): 8.69 (d, *J* 3.2 Hz, 2H, H^{A6}), 8.61 (d, *J* 7.9 Hz, 2H, H^{A3}), 8.10 (s, 2H, H^{B3}), 7.83 (t, *J* 7.7 Hz, 2H, H^{A4}), 7.48 (s, 1H, H^{NH}), 7.31 (dd, *J* 5.2, 5.8 Hz, 2H, H^{A5}), 2.09 (s, 3H, C^BH₃), 1.88 (s, 3H, C^AH₃). ¹³C{¹H} 156.7 (C^{A2/B2}), 156.2 (C^{A2/B2}), 153.32 (C^{B4}), 149.0 (C^{A6}), 146.5 (C^{C(Me)}), 136.8 (C^{A4}), 123.6 (C^{A5}), 121.4 (C^{A3}), 104.9 (C^{B3}), 25.3 (C^BH₃), 14.2 (C^AH₃). ¹H-NMR (DMSO-d₆, 295K): 9.62 (s, 1H, NH), 8.68 (ddd, *J* 4.6, 1.3, 0.6 Hz, 2H, H^{A6}), 8.58 (d, *J* 7.8 Hz, 2H, H^{A3}), 8.16 (s, 2H,

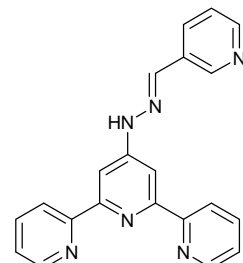
$\text{H}^{\text{B}3}$), 7.96 (td, J 7.7, 1.7 Hz, $\text{H}^{\text{A}4}$), 7.45 (ddd, J 7.5, 4.8, 1.1 Hz, 2H, $\text{H}^{\text{A}5}$), 2.03 (s, 3H, H^{MeB}), 1.96 (s, 3H, H^{MeA}). $^{13}\text{C}\{\text{H}\}$ 155.8 ($\text{C}^{\text{A}2}$), 155.1 ($\text{C}^{\text{B}2}$), 153.7 ($\text{C}^{\text{B}4}$), 149.0 ($\text{C}^{\text{A}6}$), 147.6 (C^{CMe}), 137.1 ($\text{C}^{\text{A}4}$), 124.0 ($\text{C}^{\text{A}5}$), 120.6 ($\text{C}^{\text{A}3}$), 104.1 ($\text{C}^{\text{B}3}$), 25.1 (C^{MeB}), 17.0 (C^{MeA}). ESI: Found 304.1, [25H⁺] requires 304.4. Found C 69.95, H 5.66, N 21.81 %. $\text{C}_{18}\text{H}_{17}\text{N}_5$ 0.33MeOH requires C 69.57, 6.00, 21.93 %



Synthesis of 26

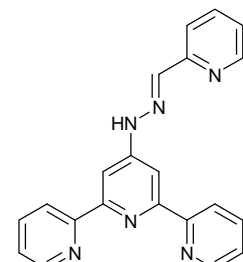
4'-Hydrazino-2,2':6',2"-terpyridine (0.40 g, 1.45 mmol), and 4-pyridinecarbaldehyde (0.18 g, 1.68 mmol) were dissolved in EtOH (40 mL). A few drops of concentrated H_2SO_4 were added, resulting in the precipitation of a bright yellow solid. The suspension was heated at reflux for 3 h, during which time a thick yellow precipitate formed. After cooling to room temperature, the yellow solid was collected by filtration and washed with EtOH (2 × 10 mL). The solid was dissolved in dilute H_2SO_4 (1.0 M, 150 mL). Excess aqueous K_2CO_3 was added to the yellow solution and the resulting suspension was treated in a sonicator bath for 30 min and extracted into CH_2Cl_2 (3 × 100 mL). The orange solution was dried over MgSO_4 and the solvent removed. The residue was purified by a short column (alumina, CH_2Cl_2 , 1% MeOH) to give **26** as a pale yellow microcrystalline solid (0.21 g, 0.59 mmol, 39%). m.p. 243–5 °C. ^1H NMR (500 MHz, DMSO-d₆) δ / ppm 12.14 (s, 1H, NH), 8.85 (d, J 6.6 Hz, 2H, $\text{H}^{\text{C}2}$), 8.78 (d, J 4.6 Hz, 2H, $\text{H}^{\text{A}6}$), 8.66 (d, J 7.9 Hz, 2H, $\text{H}^{\text{A}3}$), 8.27 (br s, 2H, $\text{H}^{\text{B}3}$), 8.21 (d, J 6.6 Hz, $\text{H}^{\text{C}3}$), 8.17 (s, 1H, $\text{H}^{\text{N=CH}}$), 8.08 (td, J 7.8, 1.6, 2H, $\text{H}^{\text{A}4}$), 7.58 (ddd, J 7.2, 4.8, 0.6 Hz, 2H, $\text{H}^{\text{A}5}$). ^1H NMR (500 MHz, CDCl₃) δ / ppm 8.72 (ddd, J 4.8, 1.6, 0.8 Hz, 2H, $\text{H}^{\text{A}6}$), 8.64 (dd, J 4.6, 1.4 Hz, 2H, $\text{H}^{\text{C}2}$), 8.63 (d, J 7.6 Hz, 2H, $\text{H}^{\text{A}3}$), 8.29 (s, 1H, H^{NH}), 8.20 (s, 1H, $\text{H}^{\text{B}3}$), 7.87 (td, J 7.7, 1.6 Hz, 2H, $\text{H}^{\text{A}4}$), 7.68 (s, 1H, $\text{H}^{\text{N=CH}}$), 7.60 (dd, J 4.7, 1.4 Hz, 2H, $\text{H}^{\text{C}3}$), 7.35 (ddd, J 7.4, 4.8, 1.0 Hz, 2H, $\text{H}^{\text{A}5}$). $^{13}\text{C}\{\text{H}\}$ NMR (125 MHz, CDCl₃) δ / ppm 156.6 ($\text{C}^{\text{A}2/\text{B}2}$), 156.2 ($\text{C}^{\text{A}2/\text{B}2}$), 150.3 ($\text{C}^{\text{C}2}$), 149.2 ($\text{C}^{\text{A}6}$), 141.5 ($\text{C}^{\text{C}4}$), 65 137.3 ($\text{C}^{\text{C=NH}}$), 136.9 ($\text{C}^{\text{A}4}$), 123.9 ($\text{C}^{\text{A}5}$), 121.4 ($\text{C}^{\text{A}3}$), 120.7 ($\text{C}^{\text{C}3}$), 105.3 ($\text{C}^{\text{B}3}$). ESI-MS m/z 353.2 MH⁺ requires 353.15 m/z. Found C 68.19, H 4.92, N 22.39. $\text{C}_{21}\text{H}_{16}\text{N}_6 \cdot \text{H}_2\text{O}$

requires C 68.09, H 4.90, N 22.69 %. Slow evaporation of a CHCl₃ solution of **26** gave X-ray quality crystals of **26**·CHCl₃·H₂O.



Synthesis of 27

Compound **27** was prepared in an analogous manner to **26**, starting with 4'-hydrazino-2,2':6',2"-terpyridine (0.40 g, 1.45 mmol) and 3-pyridinecarbaldehyde (0.18 g, 1.68 mmol). After extraction into CH₂Cl₂, the yellow solution was dried over MgSO₄ and the solvent removed. The residue was purified by a short column (alumina, CH₂Cl₂, 1% MeOH) to give **27** as an off-white microcrystalline solid (0.27 g, 0.76 mmol, 50%). m.p. 235-8 °C. ¹H NMR (500 MHz, CDCl₃) δ / ppm 8.79 (s, 1H, H^{C2}), 8.71 (d, *J* 4.0 Hz, 2H, H^{A6}), 8.61 (d, *J* 7.7 Hz, 2H, H^{A3}), 8.56 (d, *J* 3.6 Hz, 1H, H^{C6}), 8.43 (s, 1H, H^{NH}), 8.17 (s, 7H, 2H, H^{B3}), 8.16 (partly obscured d, 1H, H^{C4}), 7.85 (td, *J* 7.6 Hz, 1.0, 2H, H^{A4}), 7.72 (s, 1H, H^{CH=N}), 7.33 (m, 3H, H^{A5+C5}). ¹³C{¹H} (125 MHz, CDCl₃) δ / ppm 156.6 (C^{A2/B2}), 156.5 (C^{A2/B2}), 152.2 (C^{B4}), 150.1 (C^{C6}), 149.2 (C^{A6}), 148.8 (C^{C2}), 137.0 (C^{A4}), 136.7 (C^{C=NH}), 133.2 (C^{C4}), 130.7 (C^{C3}), 123.9 (C^{A5}), 123.8 (C^{C5}), 121.5 (C^{A3}), 105.1 (C^{B3}). ESI-MS *m/z* 353, [27 + H]⁺. Found C 71.27, H 4.68, N 23.75 %. C₂₁H₁₆N₆ requires C 71.58, H 4.58, N 23.85 %.



Synthesis of 28

Compound **28** was prepared in an analogous manner to **26** and **27**, starting with 4'-hydrazino-2,2':6',2"-terpyridine (0.40 g, 1.45 mmol) and 2-pyridinecarbaldehyde (0.18 g, 1.68 mmol). The colour changes were as for the preparation of **27**. Compound **28** was isolated as an off-white microcrystalline solid (0.34 g, 0.96 mmol, 64%). m.p. 235-6 °C.

NMR ^1H (500 MHz, CDCl_3) δ / ppm 8.72 (d, J 4.4 Hz, 2H, $\text{H}^{\text{A}6}$), 8.63 (d, J 7.9 Hz, 2H, $\text{H}^{\text{A}3}$), 8.58 (d, J 4.4 Hz, 1H, $\text{H}^{\text{C}6}$), 8.26 (s, 1H, H^{NH}), 8.21 (s, 2H, $\text{H}^{\text{B}3}$), 8.21 (overlapping d, J 7.3 Hz, 1H, $\text{H}^{\text{C}3}$), 7.90 (s, 1H, $\text{H}^{\text{N=CH}}$), 7.86 (td, J 7.6, 1.7 Hz, 2H, $\text{H}^{\text{A}4}$), 7.76 (t, J 7.7 Hz, 1H, $\text{H}^{\text{C}4}$), 7.34 (dd, J 6.9, 5.4 Hz, 2H, $\text{H}^{\text{A}5}$), 7.24 (m, 1H, $\text{H}^{\text{C}5}$). $^{13}\text{C}\{\text{H}\}$ NMR (125 MHz, CDCl_3) δ / ppm 156.7 ($\text{C}^{\text{A}2/\text{B}2}$), 156.5 ($\text{C}^{\text{A}2/\text{B}2}$), 153.9 ($\text{C}^{\text{C}2}$), 152.1 ($\text{C}^{\text{B}4}$), 149.4 ($\text{C}^{\text{C}6}$), 149.2 ($\text{C}^{\text{A}6}$), 140.9 ($\text{C}^{\text{C=NH}}$), 136.8 ($\text{C}^{\text{A}4}$), 136.4 ($\text{C}^{\text{C}4}$), 123.9 ($\text{C}^{\text{A}5}$), 123.5 ($\text{C}^{\text{C}5}$), 121.5 ($\text{C}^{\text{A}3}$), 120.6 ($\text{C}^{\text{C}3}$), 105.2 ($\text{C}^{\text{B}3}$). ESI-MS m/z 353.3 [**28** + H] $^+$. Found C 71.20, H 4.50, N 23.60 %. $\text{C}_{21}\text{H}_{16}\text{N}_6$ requires C 71.58, H 4.58, N 23.85 %.

2.16. Crystal Structure Determinations

General: Data were collected on a Bruker–Nonius Kappa or Stoe IPDS CCD instrument; data reduction, solution and refinement used the programs COLLECT²⁵² and SIR92²⁵³ or XRED²⁵⁴ and SHELXS86,²⁵⁵ DENZO/SCALEPACK²⁵⁶ and CRYSTALS²⁵⁷; or using the programs XPREP,⁷ solved by direct methods using SHELXS and were refined using SHELX-97.^{7,258} Structures have been analysed using Mercury v. 1.4.2,²² and searches for related structures carried out in the Cambridge Structural Database (v. 5.28)¹⁹⁴ using Conquest v. 1.9.²²

Crystal Data for 17: $C_{22}H_{17}N_5$, $M = 351.41$, monoclinic, space group $C2/c$, $a = 14.0879(8)$, $b = 12.5006(6)$, $c = 20.1787(9)$ Å, $\beta = 94.112(3)^\circ$, $V = 3544.5(3)$ Å³, $Z = 8$, $D_c = 1.317$ Mgm⁻³, $\mu(\text{Mo}-K_\alpha) = 0.082$ mm⁻¹, $T = 173$ K, 4058 reflections collected. Refinement of 2306 reflections (244 parameters) with $I > 2.0\sigma$ (I) converged at final $R1 = 0.0394$ [$R1$ (all data) = 0.0845], $wR2 = 0.0428$ [$wR2$ (all data) = 0.0782], $gof = 0.919$.

Crystal Data for [H17][PF₆]·H₂O: $C_{22}H_{20}F_6N_5O_1P_1$, $M = 515.40$, triclinic, space group $P-1$, $a = 8.5007(7)$, $b = 11.4295(7)$, $c = 12.079(1)$ Å, $\alpha = 75.730(5)$, $\beta = 89.492(4)$, $\gamma = 85.558(5)^\circ$, $V = 1133.9(2)$ Å³, $Z = 2$, $D_c = 1.509$ Mgm⁻³, $\mu(\text{Mo}-K_\alpha) = 0.197$ mm⁻¹, $T = 173$ K, 5171 reflections collected. Refinement of 2616 reflections (316 parameters) with $I > 1.0\sigma$ (I) converged at final $R1 = 0.0955$ ($R1$ (all data) = 0.1851), $wR2 = 0.0898$ [$wR2$ (all data) = 0.1395], $gof = 1.020$.

Crystal Data for ([H17][CF₃CO₂]₄(EtOH)₂(H₂O)):

$C_{100}H_{84}F_{12}N_{20}O_{11}$, $M = 1969.87$, triclinic, space group $P-1$, $a = 8.6685(2)$ $b = 11.9459(3)$, $c = 23.6684(5)$ Å, $\alpha = 75.9214(15)$, $\beta = 84.1592(13)$, $\gamma = 80.0292(15)^\circ$, $V = 2336.84(10)$ Å³, $Z = 1$, $D_c = 1.400$ Mgm⁻³, $\mu(\text{Mo}-K_\alpha) = 0.082$ mm⁻¹, $T = 173$ K, 19619 reflections collected. Refinement of 5938 reflections (713 parameters) with $I > 2.0 \sigma$ (I) converged at final $R1 = 0.0810$ [$R1$ (all data) = 0.1329], $wR2 = 0.0975$ [$wR2$ (all data) = 0.1387], $gof = 1.124$.

Crystal Data for [H₂17]Cl₂·DMSO: C₂₄H₂₅Cl₂N₅O₁S₁, $M = 502.47$, triclinic, space group $P-1$, $a = 7.228(1)$, $b = 13.115(3)$, $c = 13.320(3)$ Å, $\alpha = 77.47(3)$, $\beta = 74.47(3)$, $\gamma = 86.72(3)$ °, $V = 1187.7(5)$ Å³, $Z = 2$, $D_c = 1.405$ Mgm⁻³, $\mu(\text{Mo-}K_{\alpha}) = 0.389$ mm⁻¹, $T = 173$ K, 10344 reflections collected. Refinement of 6375 reflections (298 parameters) with $I > 2.0\sigma$ (I) converged at final $R1 = 0.0528$ [$R1$ (all data) = 0.0826], $wR2 = 0.0491$ [$wR2$ (all data) = 0.0618], $gof = 1.079$.

Crystal Data for [H18][BF₄]: C₂₃H₂₀BF₄N₅, $M = 453.25$, monoclinic, space group $C2/c$, $a = 21.8489(2)$, $b = 13.7414(1)$, $c = 14.6131(2)$ Å, $\beta = 98.8945(5)$ °, $V = 4334.60(8)$ Å³, $Z = 8$, $D_c = 1.389$ Mgm⁻³, $\mu(\text{Mo-}K_{\alpha}) = 0.108$ mm⁻¹, $T = 173$ K, 6359 reflections collected. Refinement of 3549 reflections (335 parameters) with $I > 3.0\sigma$ (I) converged at final $R1 = 0.0530$ [$R1$ (all data) = 0.0821], $wR2 = 0.0511$ [$wR2$ (all data) = 0.0630], $gof = 1.297$.

Crystal Data for [H18][NO₃][MeOSO₃]·H₂O: C₂₄H₂₆N₆O₈S₁, $M = 588.57$, monoclinic, space group $P2_1/c$, $a = 8.3471(4)$, $b = 27.284(1)$, $c = 11.7194(4)$ Å, $\beta = 106.504(3)$ °, $V = 2559.0(2)$ Å³, $Z = 4$, $D_c = 1.450$ Mgm⁻³, $\mu(\text{Mo-}K_{\alpha}) = 0.188$ mm⁻¹, $T = 173$ K, 5797 reflections collected. Refinement of 3348 reflections (352 parameters) with $I > 1.0\sigma$ (I) converged at final $R1 = 0.0690$ [$R1$ (all data) = 0.1279], $wR2 = 0.0671$ [$wR2$ (all data) = 0.0944], $gof = 1.125$.

Crystal Data for 18: C₂₃H₁₉N₅, $M = 365.44$, monoclinic, space group $P2_1/n$, $a = 16.547(1)$, $b = 5.4934(4)$, $c = 20.324(1)$ Å, $\beta = 99.378(3)$ °, $V = 1822.8(2)$ Å³, $Z = 4$, $D_c = 1.332$ Mgm⁻³, $\mu(\text{Mo-}K_{\alpha}) = 0.082$ mm⁻¹, $T = 173$ K, 3887 reflections collected. Refinement of 2614 reflections (253 parameters) with $I > 1.0\sigma$ (I) converged at final $R1 = 0.0447$ [$R1$ (all data) = 0.0752], $wR2 = 0.0523$ [$wR2$ (all data) = 0.0714], $gof = 1.139$.

Crystal Data for [H19][MeOSO₃]: C₂₉H₂₅N₅O₄S₁, $M = 539.61$, monoclinic, space group $P2_1/c$, $a = 8.9734(3)$, $b = 23.860(1)$, $c = 12.3514(3)$ Å, $\beta = 105.356(2)$ °, $V = 2550.1(2)$ Å³, $Z = 4$, $D_c = 1.405$ Mgm⁻³, $\mu(\text{Mo-}K_{\alpha}) = 0.174$ mm⁻¹, $T = 173$ K, 5813 reflections collected. Refinement of 3582 reflections (352 parameters) with $I > 1.7\sigma$ (I) converged at final $R1 = 0.0495$ [$R1$ (all data) = 0.0873], $wR2 = 0.0543$ [$wR2$ (all data) = 0.0684], $gof = 1.150$.

Crystal Data for 19·CH₂Cl₂: C₂₉H₂₃Cl₂N₅, $M = 512.44$, monoclinic, space group $P2_1/c$, $a = 10.8031(4)$, $b = 9.6855(4)$, $c = 24.417(1)$ Å, $\beta = 99.785(2)^\circ$, $V = 2517(2)$ Å³, $Z = 4$, $D_c = 1.352$ Mg m⁻³, $\mu(\text{Mo-} K_{\alpha}) = 0.286$ mm⁻¹, $T = 173$ K, 4905 reflections collected. Refinement of 3632 reflections (325 parameters) with $I > 3.0\sigma$ (I) converged at final $R1 = 0.0379$ [$R1$ (all data) = 0.0507], $wR2 = 0.0441$ [$wR2$ (all data) = 0.0554], $gof = 1.111$.

Crystal Data for 20: C₂₃H₁₉N₅, $M = 365.44$, monoclinic, space group $P2_1/n$, $a = 13.7297(8)$, $b = 8.5408(5)$, $c = 15.9176(9)$ Å, $\beta = 102.628(4)^\circ$, $V = 1821.4(2)$ Å³, $Z = 4$, $D_c = 1.333$ Mg m⁻³, $\mu(\text{Mo-} K_{\alpha}) = 0.082$ mm⁻¹, $T = 173$ K, 4369 reflections collected. Refinement of 2626 reflections (253 parameters) with $I > 1.5\sigma$ (I) converged at final $R1 = 0.0454$ [$R1$ (all data) = 0.0851], $wR2 = 0.0562$ [$wR2$ (all data) = 0.0760], $gof = 1.110$.

Crystal Data for [H21][BF₄]: C₂₄H₂₂N₅O₂·BF₄, $M = 499.28$, monoclinic, space group $C2/c$, $a = 32.0072(8)$, $b = 7.0994(2)$, $c = 25.6676(6)$ Å, $\beta = 122.9852(13)^\circ$, $U = 4892.4(2)$ Å³, $Z = 8$, $D_c = 1.356$ Mg m⁻³, $\mu(\text{Mo-} K_{\alpha}) = 0.108$ mm⁻¹, $T = 173$ K, 10876 reflections collected. Refinement of 3282 reflections (326 parameters) with $I > 2.0\sigma$ (I) converged at final $R1 = 0.0564$ [$R1$ (all data) = 0.0996], $wR2 = 0.0654$ [$wR2$ (all data) = 0.0916], $gof = 1.1042$.

Crystal Data for 22:

C₂₂H₁₈Br₁N₅O₁, $M = 448.31$, Triclinic, space group $P-1$, $a = 11.147(2)$, $b = 12.328(3)$, $c = 15.273(3)$ Å, $\alpha = 95.93(3)$, $\beta = 102.46(3)$, $\gamma = 104.38(3)^\circ$, $V = 1957.7(8)$ Å³, $Z = 4$, $D_c = 1.521$ Mg m⁻³, $\mu(\text{Mo-} K_{\alpha}) = 2.124$ mm⁻¹, $T = 200$ K, 40694 reflections collected. Refinement of 9413 reflections (535 parameters) with $I > 2.0\sigma$ (I) converged at final $R1 = 0.0527$ [$R1$ (all data) = 0.0669], $wR2 = 0.1144$ [$wR2$ (all data) = 0.1207], $gof = 1.185$.

Crystal Data for 24:

C₂₂H₁₆N₆O₂, $M = 396.41$, monoclinic, space group $P2_1/c$, $a = 19.617(4)$, $b = 17.698(3)$, $c = 11.301(2)$ Å, $\beta = 105.66(3)^\circ$, $V = 3777.9(12)$ Å³, $Z = 8$, $D_c = 1.394$ Mg m⁻³, $\mu(\text{Mo-} K_{\alpha}) = 0.094$ mm⁻¹, $T = 223$ K, 47531 reflections collected. Refinement of 6671 reflections (557 parameters) with $I > 2.0\sigma$ (I) converged at final $R1 = 0.0635$ [$R1$ (all data) = 0.0851], $wR2 = 0.1193$ [$wR2$ (all data) = 0.1268], $gof = 1.237$.

Crystal Data for 25: C₁₈H₁₇N₅, $M = 303.37$, monoclinic, space group $C2/c$, $a = 12.200(2)$, $b = 12.502(3)$, $c = 20.658(4)\text{\AA}$, $\beta = 91.56(3)^\circ$, $V = 3149.7(11)\text{ \AA}^3$, $Z = 8$, $D_c = 1.279\text{ Mgm}^{-3}$, $\mu(\text{Mo- } K_\alpha) = 0.082\text{ mm}^{-1}$, $T = 173\text{ K}$, 12128 reflections collected. Refinement of 2695 reflections (214 parameters) with $I > 2.0\sigma(I)$ converged at final $R1 = 0.0404$ [$R1$ (all data) = 0.0431], $wR2 = 0.1025$ [$wR2$ (all data) = 0.1003], $gof = 1.124$.

Chapter 3 Iron(II) and ruthenium(II) complexes of 4'-hydrazone functionalised 2,2':6',2"-terpyridine ligands

3.1. General considerations

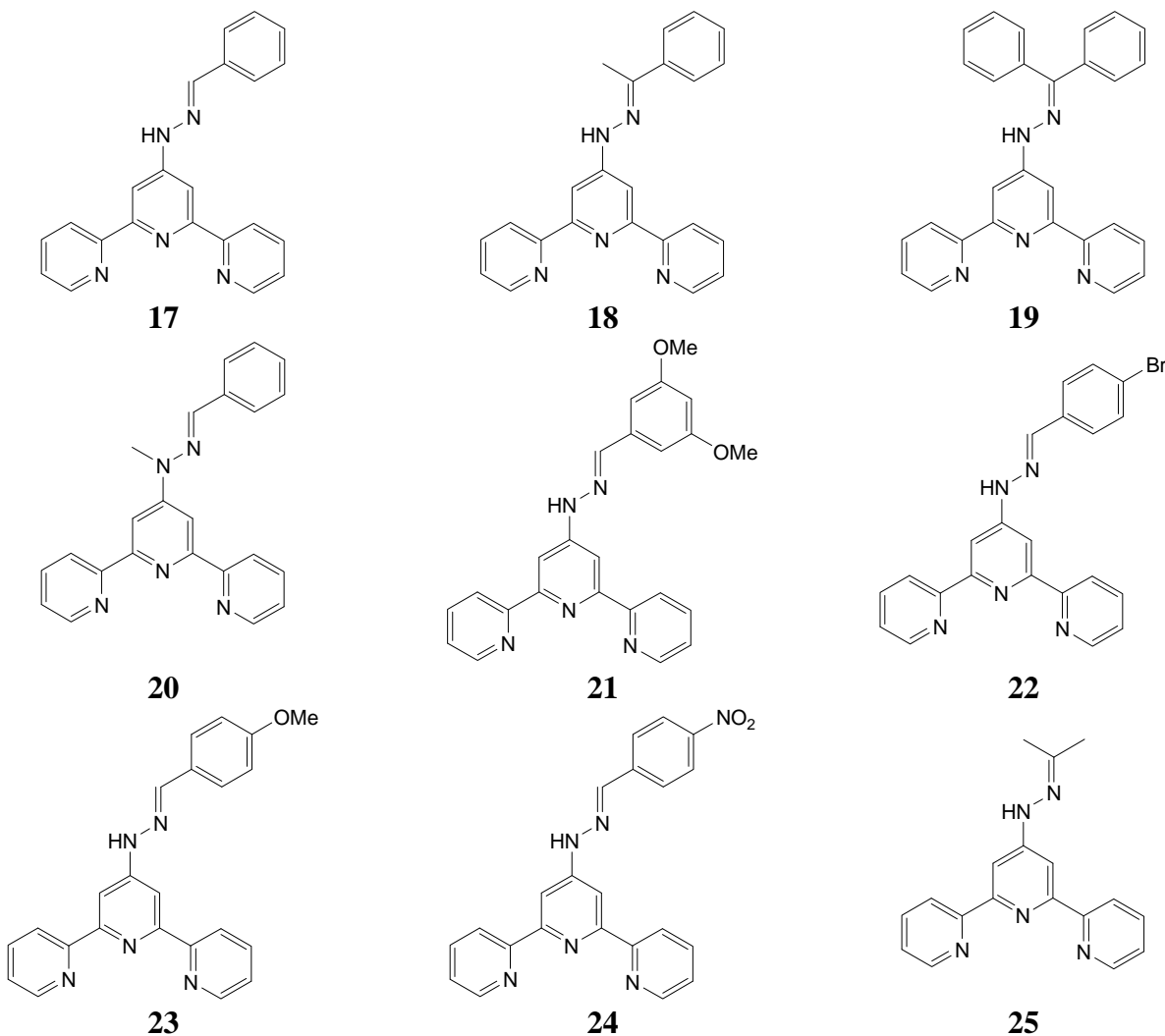
This chapter describes the iron(II) and ruthenium(II) complexes of nine 4'-hydrazone-functionalised 2,2':6',2"-terpyridine ligands. The ligands were selected to give a range of both steric constraints and electron withdrawing/donating effects to investigate possible impacts of these on the structural and electronic properties of the complexes. All complexes were characterised by ^1H and ^{13}C NMR spectroscopy (all signals assigned), electrospray mass spectrometry, UV-visible spectroscopy and elemental analysis. Dynamic solution-state processes and substitution effects were examined by variable temperature NMR and UV-visible spectroscopy was used to investigate the pH dependence of the electronic properties of the complexes. Finally, ten complexes were characterised in the solid state using single crystal X-ray crystallography and their crystal packing interactions were examined.

3.2. Synthesis of Iron(II) and Ruthenium(II) complexes

Homoleptic iron(II) complexes of ligands **17-25** were prepared by reacting $\text{FeCl}_2 \cdot 4\text{H}_2\text{O}$ with two equivalents of the corresponding ligand in MeOH and were isolated as purple hexafluorophosphate salts in yields that varied from 40% to 90%.ⁱⁱ The use of protonated ligand salts (e.g.: $[\text{H}_2\text{L}](\text{MeOSO}_3)_2$) as starting materials did not pose any problems and reflects the very high stability of $[\text{Fe}(\text{tpy})_2]$ complexes ($\log K > 20$)^{70, 71} and the relative acidity of tpy nitrogens ($\text{pK}_{\text{a}1}$ 4.66, $\text{pK}_{\text{a}2}$ 3.28, measured with a ionic strength 0.01)²⁵⁹. Homoleptic ruthenium(II) complexes were prepared by reacting $\text{Ru}(\text{DMSO})\text{Cl}_2$ with two equivalents of ligand in refluxing MeOH, or in ethylene glycol under microwave conditions. The ruthenium(II) complexes were isolated as red hexafluorophosphate salts and purified by column chromatography (silica, $\text{MeCN:H}_2\text{O:saturated KNO}_3_{(\text{aq})}$ 7:2:2) and recrystallised from acetonitrile-water to give isolated yields of 40-90%. The more inert nature of Ru(II) compared with Fe(II) results

ⁱⁱ The use of salts with varying solvent/water content resulted in unreliable yield calculations.

in the stoichiometry of the reactants being considerably more important when preparing Ru(II) complexes. The use of protonated ligand salts (with varying anion and water compositions) resulted in poor yields and difficulties with reproducibility. Therefore, all Ru(II) complexes were prepared using neutral ligands as starting materials.



3.3. Characterisation of Fe(II) and Ru(II) complexes

The complexes were more straightforward to characterise than the free ligands due to the lack of protonation-state ambiguity or py-py bond rotation. In each case the ^1H -NMR (acetonitrile-d₃) signals were generally sharp and well defined, presumably due to the poor hydrogen-bond-acceptor-capability of PF₆⁻ and acetonitrile limiting hydrogen bonding with the amino NH. However, in acetone-d₆ the signals of the H^{A3} and H^{B3} are broadened (Figure 3-1). The greater hydrogen-bond acceptor ability of acetone over

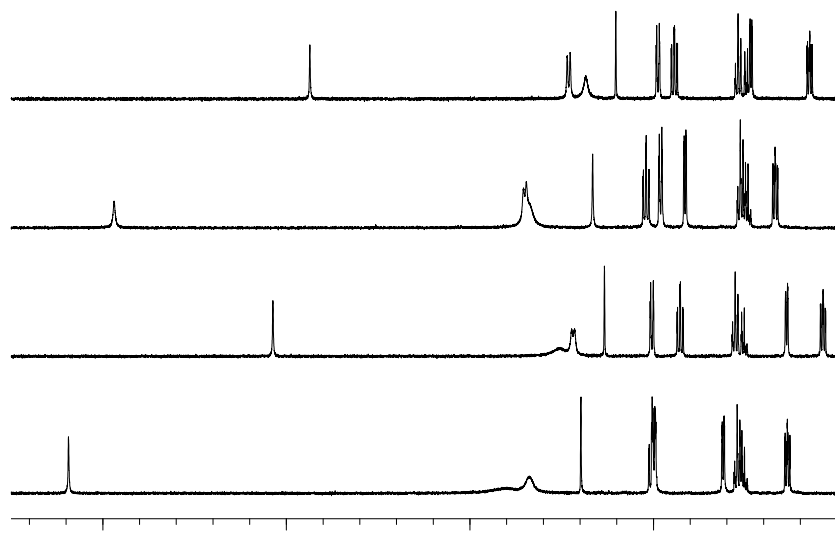


Figure 3-1 ^1H -NMR spectrum of $[\text{Fe}(\mathbf{17})_2](\text{PF}_6)_2$ at 295K in acetonitrile- d_3 (top), acetone- d_6 ; $[\text{Ru}(\mathbf{17})_2](\text{PF}_6)_2$ at 295K in acetonitrile- d_3 and acetone- d_6 (bottom).

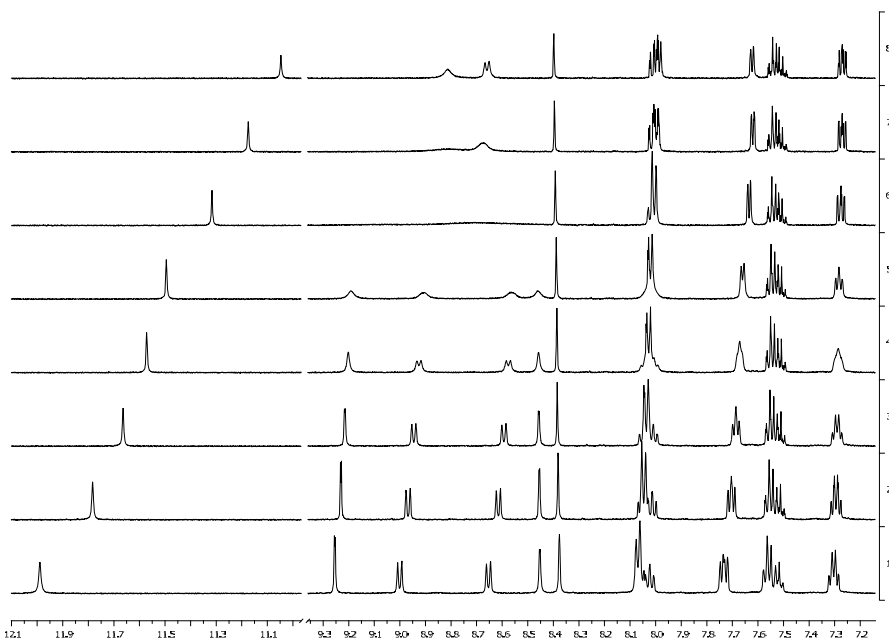
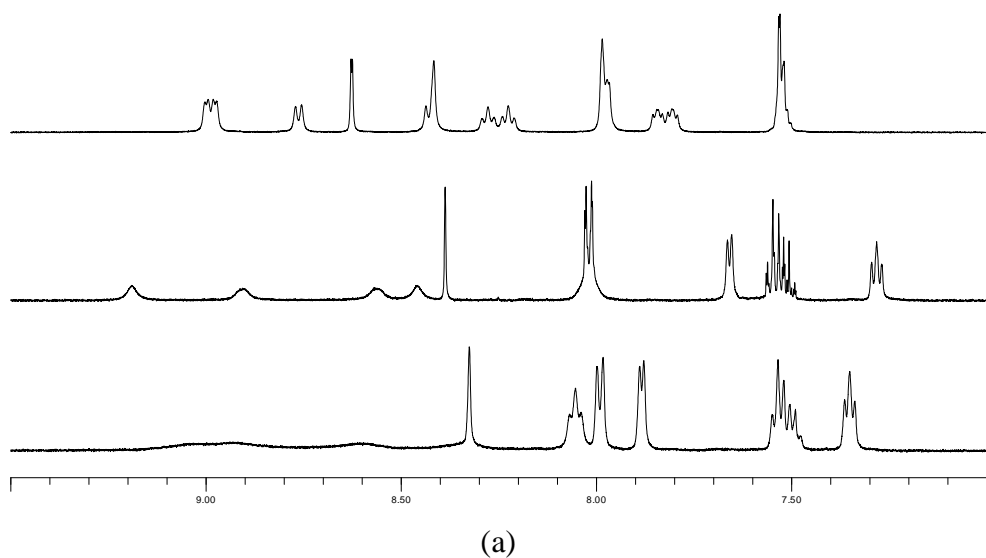


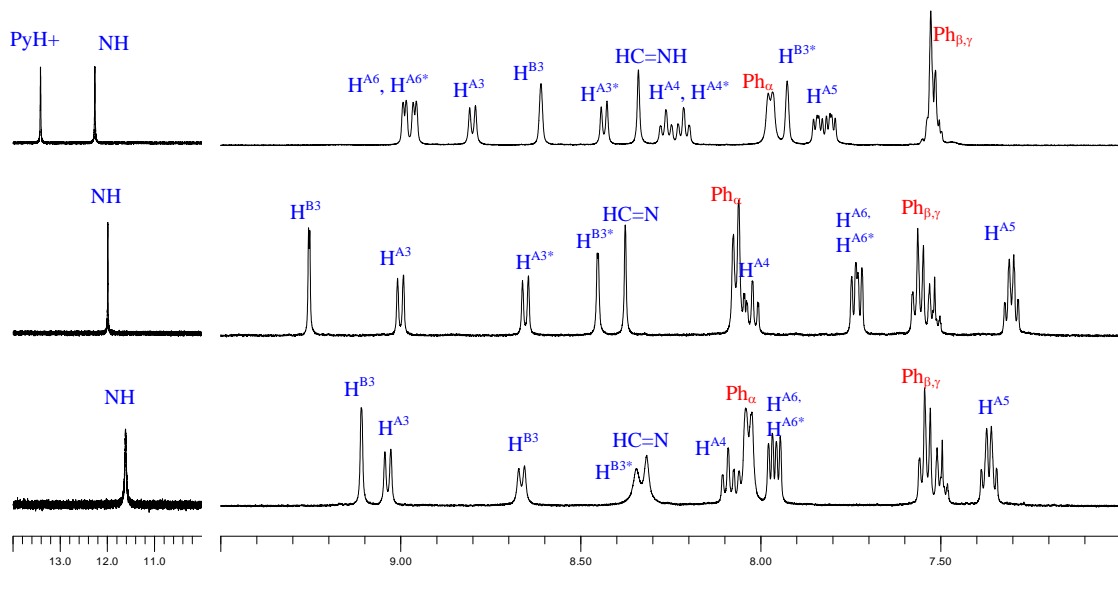
Figure 3-2 Variable temperature ^1H -NMR (acetone- d_6) for $[\text{Fe}(\mathbf{17})_2](\text{PF}_6)_2$. Top to bottom: 8: 315, 7: 295, 6: 275, 5: 255, 4: 245, 3: 235, 2: 220 and 1: 195 K.

acetonitrile is likely responsible for this broadening. This is in accord with the previous assignment of N-tpy bond rotation as the process responsible for the broadening of $\text{H}^{\text{A}3}$ and $\text{H}^{\text{B}3}$ as no py-py bond rotation is possible for the complexes without breaking strong metal-ligand bonds. Variable temperature NMR was also used to investigate bond rotations occurring at rates similar to the NMR timescale. Low temperature measurements (acetone- d_6) allowed the observation of an asymmetric tpy environment, shown in Figure 3-2 for $[\text{Fe}(\mathbf{17})_2](\text{PF}_6)_2$. Interestingly in this case, at 255K the separate

signals could be observed, indicating that N-tpy bond rotation occurs at a rate intermediate between neutral **17** and [H**17**]PF₆. The ruthenium(II) complexes behaved similarly, although the coalescence temperature is lower as asymmetric tpy signals could only be observed at 245K (compared to above 255K for [Fe(**17**)₂](PF₆)₂, see Figure 3-3 for a comparison). This indicates that tpy-NH bond rotation is *faster* for the Ru(II) complex than for the corresponding Fe(II) complex. Additionally, one set of H^{A3} and H^{B3} signals (those adjacent to the NH) appear broader than the other, a phenomenon not seen for the free ligand, the protonated ligand or for the Fe(II) complex.



(a)



(b)

Figure 3-3 Comparison of ¹H-NMR (acetone-d₆) of [H**17**]PF₆ (top), [Fe(**17**)₂](PF₆)₂ and [Ru(**17**)₂](PF₆)₂ (bottom) at (a) 255 K and (b) 195 K.

A comparison of chemical shifts between the Fe(II) and Ru(II) complexes of ligand **17** is given in Table 3. Concentration and water content did not appear to significantly affect the ^1H -NMR spectra. From 195K to 295K the $\text{H}^{\text{A}3}$ signals for both complexes are virtually identical and those of the $\text{H}^{\text{B}3}$ are shifted upfield by 0.12-0.14 ppm from Fe(II) to Ru(II). This is as expected for normal Fe(II) and Ru(II) tpy complexes [e.g., 4'-tolyl-2,2':6',2"-terpyridine complexes: ^1H NMR $\text{H}^{\text{B}3}$ δ : Fe(II) 9.16 ppm, ^{165}Ru (II) 8.99 ppm¹⁷²]. At 195K the separation between the pairs of non-equivalent $\text{H}^{\text{A}3}$ and $\text{H}^{\text{B}3}$ signals were also similar indicating the 4'-substituent adopts a similar conformation in both complexes. The effect on the amino and imino signals from Fe(II) to Ru(II) was more significant, displaying shifts upfield of 0.39 and 0.33 ppm respectively, reflecting the electronic influence of the metal on the hydrazone group.

Table 3 Comparison of ^1H -NMR (acetone- d_6) chemical shifts for $[\text{Fe}(\mathbf{17})_2](\text{PF}_6)_2$ and $[\text{Ru}(\mathbf{17})_2](\text{PF}_6)_2$ with **17** and $[\text{H}17]\text{PF}_6$ at 195K.

	17	$[\text{H}17]\text{PF}_6$	$\text{Fe}(\mathbf{17})_2$	$\text{Ru}(\mathbf{17})_2$	$\text{Ru}(\mathbf{17})_2 - \text{Fe}(\mathbf{17})_2$ difference
NH	10.81	12.26	11.99	11.60	-0.39
$\text{H}^{\text{B}3}$	8.66	8.61	9.25	9.12	-0.13
$\text{H}^{\text{A}3}$	8.77	8.80	9.00	9.04	0.04
$\text{H}^{\text{B}3*}$	8.02	7.93	8.45	8.33	-0.12
$\text{H}^{\text{A}3*}$	8.74	8.44	8.65	8.67	0.02
N=CH	8.06	8.34	8.38	8.05	-0.33
$\text{H}^{\text{B}3}-\text{H}^{\text{B}3*}$ difference	0.64	0.68	0.80	0.79	0.01
$\text{H}^{\text{A}3}-\text{H}^{\text{A}3*}$ difference	0.03	0.36	0.35	0.37	0.02

The observation that the rate of tpy-NH bond rotation is in the order:



possibly reflects the influence of metal back-bonding in the complexes. That is, Ru(II) is able to back-donate more electron density which both reduces the double bond character of the tpy-NH bond and also reduces the positive charge on the amino NH making it a poorer hydrogen bond donor (i.e.: stabilising the charge distribution shown in Figure 3-4). Both of these effects would lower the barrier to bond rotation. Fe(II) is a poorer electron back-donor and (obviously) H^+ is unable to offer any additional stability via back bonding. This dependence of the rate of bond rotation on the metal ion could be useful not only for the complexes presented here, but also as a means to measure the distribution of charge in other tpy complexes. For example, the ^1H -NMR ($\text{DMSO}-d_6$

spectrum of $[\text{Pd}(\mathbf{17})\text{Cl}]\text{Cl}$ (Figure 3-5) shows well-separated pairs of peaks for $\text{H}^{\text{A}3}$ and $\text{H}^{\text{B}3}$ indicating that tpy-NH bond rotation is much slower in this case than those discussed previously.ⁱⁱⁱ

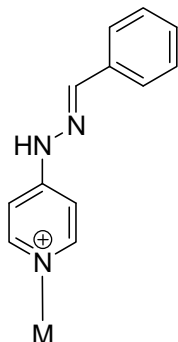


Figure 3-4 Classical representation of charge distribution.

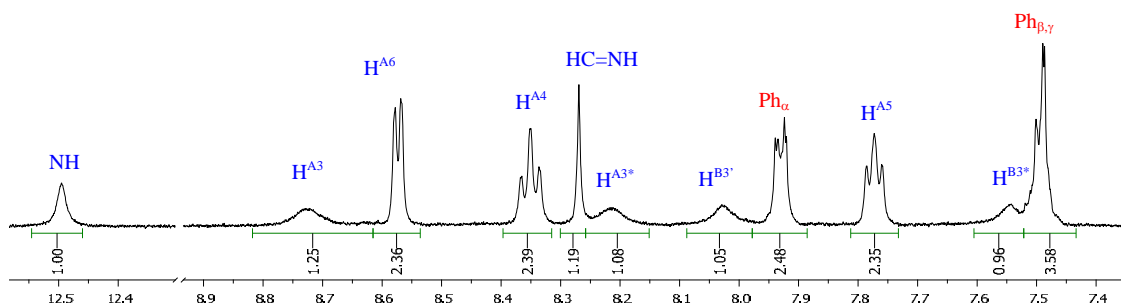


Figure 3-5 $[\text{Pd}(\mathbf{17})\text{Cl}]\text{Cl}$ in $\text{DMSO}-d_6$ (295K). Tpy-NH bond rotation is slow on the NMR timescale.

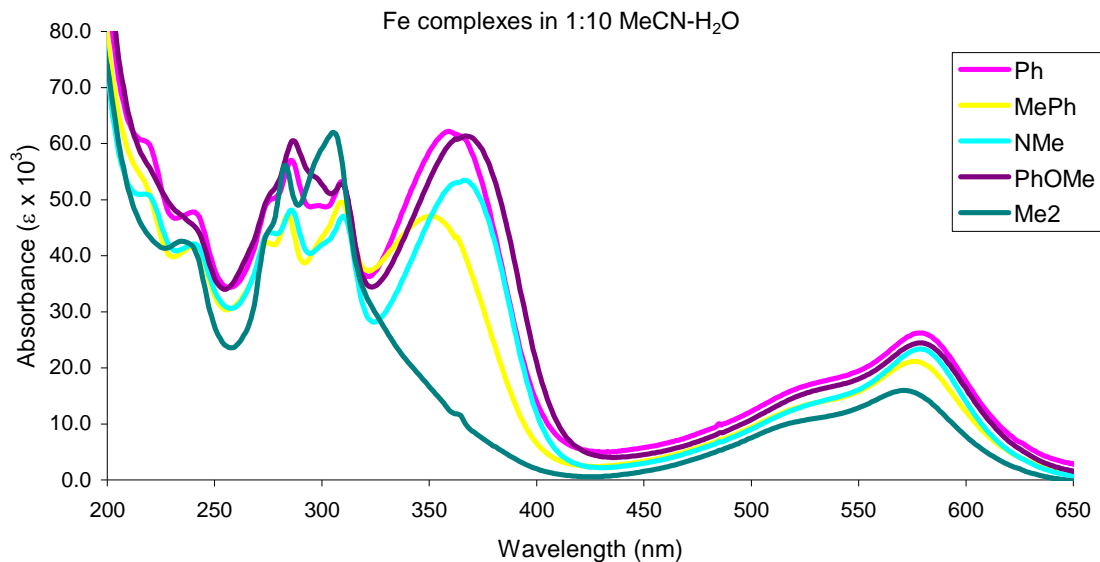
3.4. Substituent effects

Substitution of the hydrazone group does not affect the tpy ^1H -NMR signals, with the exception of the $\text{H}^{\text{B}3}$ signal which was too broad to make meaningful comparisons. The signals for the amine (H^{NH}) varied with substitution, shifting downfield as the substituent became more electron withdrawing [in order of increasing electron withdrawing $\text{C}_6\text{H}_4\text{-X}$ substituent ^1H NMR δ H^{NH} 10.01 for **23** ($\text{X} = \text{-OMe}$), 10.07 for **17** (-H), 10.11 for **22** (-Br), 10.36 for **24** (-NO_2)]. The imine signal ($\text{H}^{\text{N=CH}}$) was less significantly affected [δ ^1H $\text{H}^{\text{N=CH}}$ 8.21 for **23** (-OMe), 8.27 for **17** (-H), 8.22 for **22** (-Br), 8.34 ppm for **24** (-NO_2)]. The ^{13}C NMR also showed generally similar trends, although the effects were much less pronounced [δ ^{13}C $\text{C}^{\text{N=CH}}$ 145.4 for **23** (-OMe), 145.4 for **17** (-H), 144.1 for **22** (-Br), 142.7 for **24** (-NO_2); $\text{C}^{\text{B}3}$ 107.9 for **23** (-OMe), 108.1 for **17** (-H), 108.2 for **22** (-Br), 108.6 ppm for **24** (-NO_2)].

ⁱⁱⁱ It should be noted, however, that the solvent is much more polar (ie: $\text{DMSO}-d_6$ vs CD_3CN) and so a direct comparison between metal ions should not be made here.

3.5. UV-Vis spectroscopy of Fe(II) and Ru(II) complexes

The electronic absorption spectra of acetonitrile (or acetonitrile-water) solutions of $[\text{Fe}(\mathbf{L})_2](\text{PF}_6)_2$ ($\mathbf{L} = \mathbf{17-25}$) and selected Ru(II) complexes were investigated and the spectra are shown in Figure 3-6 and Figure 3-7 respectively. All Fe(II) and Ru(II) complexes exhibit MLCT bands (around 580 nm and 510 nm respectively) which are shifted around 30 nm to longer wavelength compared to the parent $\text{Fe}(\text{tpy})_2$ and $\text{Ru}(\text{tpy})_2$ complexes (551 nm and 475 nm respectively)¹⁷ resulting from a lowering of the ligand π^* orbitals on introduction of the hydrazone substituent.

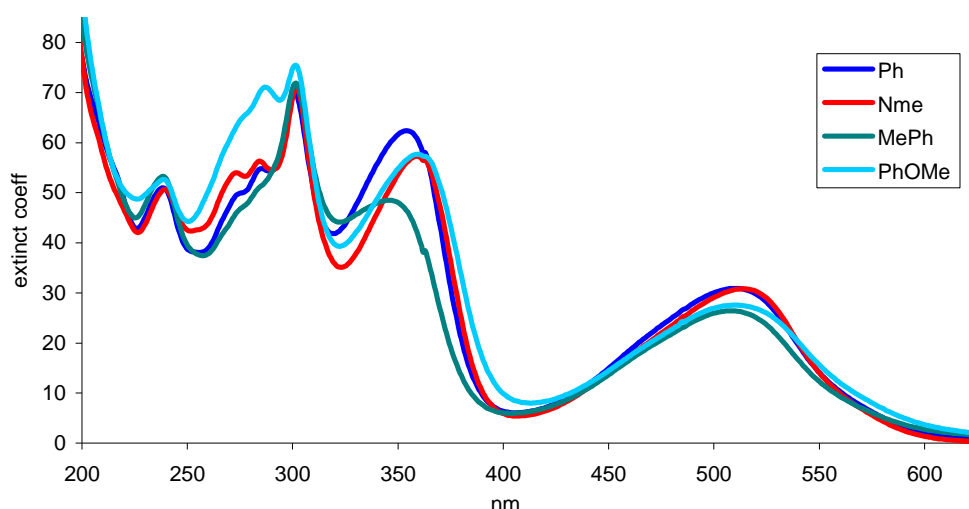


Absorption λ_{max} / nm ($\epsilon / 10^3 \text{ dm}^3 \text{ mol}^{-1} \text{ cm}^{-1}$):

$[\text{Fe}(\mathbf{17})_2](\text{PF}_6)_2$	240 (47.8)	277 (50.1)	286 (57.0)	309 (53.2)	359 (62.2)	520 (sh, 16.1)	579 (26.2)
$[\text{Fe}(\mathbf{18})_2](\text{PF}_6)_2$	240 (41.8)	275 (42.3)	284 (47.2)	309 (49.6)	350 (47.0)	520 (sh, 12.8)	576 (21.2)
$[\text{Fe}(\mathbf{19})_2](\text{PF}_6)_2$	239 (52.7)	276 (49.0)	285 (53.9), 299 (46.7)	309 (51.1)	360 (58.5)	520 (sh, 14.9)	579 (27.0)
$[\text{Fe}(\mathbf{20})_2](\text{PF}_6)_2$	240 (42.0)	276 (44.2)	286 (48.2)	310 (47.0)	366 (53.4)	520 (sh, 12.6)	579 (23.4)
$[\text{Fe}(\mathbf{21})_2](\text{PF}_6)_2$	238 (sh, 51.7)	275 (47.3)	287 (53.2)	310 (53.2)	359 (61.4)	520 (sh, 14.3)	578 (24.7)
$[\text{Fe}(\mathbf{22})_2](\text{PF}_6)_2$	238 (sh, 42.5)	276 (sh, 46.1)	286 (52.5)	309 (47.9)	363 (58.2)	520 (sh, 13.9)	578 (23.8)
$[\text{Fe}(\mathbf{23})_2](\text{PF}_6)_2$	238 (sh, 46.0)	276 (sh, 51.1)	287 (60.4)	309 (52.8)	367 (61.3)	520 (sh, 14.7)	578 (24.4)
$[\text{Fe}(\mathbf{24})_2](\text{PF}_6)_2$	239 (39.5)	276 (44.1)	286 (48.2)	309 (48.4)	354 (54.8)	520 (sh, 13.3)	576 (23.1)
$[\text{Fe}(\mathbf{25})_2](\text{PF}_6)_2$	235 (42.6)	-	283 (56.1)	305 (62.0)	-	520 (sh 10.3)	571 (16.0)

Figure 3-6 UV-Vis absorption data (MeCN:H₂O 1:10) of $(\text{Fe}(\mathbf{L})_2)(\text{PF}_6)_2$, selected spectra shown. The addition of water did not significantly alter the spectra. Concentrations: range 4.1×10^{-6} to 1.4×10^{-5} mol.L⁻¹.

However, neither the intensity nor the wavelength of the MLCT showed any significant dependence on hydrazone substitution. The Fe(II) and Ru(II) complexes also show shoulders around 520 nm and 470 nm, although much more pronounced in the case of Fe(II). The electronic spectra also exhibit a series of higher energy absorptions arising from ligand-centred $\pi^* \leftarrow \pi$ and $\pi^* \leftarrow n$ transitions. The most significant of these occurs around 360 nm in both Fe(II) and Ru(II) complexes, except for the complexes of ligand **18** (MePh) where this band is both shifted to higher energy [Fe(II): 350 nm and Ru(II): 346 nm] and significantly decreased in intensity (by over 20% relative to the complexes of **17**). The source of this difference is not obvious as **19** (Ph₂) was remarkably similar to that of **17** (Ph), indicating that the presence of an imino CH is not the cause. This absorption is also observed for the protonated free ligand, decreasing dramatically as the ligand is neutralised (see previous chapter).



$\lambda_{\text{max}}/\text{nm} (\varepsilon_{\text{max}}/10^3 \text{dm}^3 \text{mol}^{-1} \text{cm}^{-1})$:

[Ru(17) ₂](PF ₆) ₂	238 (50.6)	285 (54.2)	301 (69.0)	354 (61.8)	510 (30.6)
[Ru(18) ₂](PF ₆) ₂	239 (53.2)	285 (51.4 (sh))	302 (71.8)	346 (48.5)	508 (26.4)
[Ru(20) ₂](PF ₆) ₂	239 (50.6)	273 (54.0)	302 (70.9)	359 (57.3)	514 (30.8)
[Ru(23) ₂](PF ₆) ₂	239 (52.6)	287 (71.1)	300 (74.7)	359 (57.7)	510 (27.6)

Figure 3-7 UV-Visible spectra of Ru(**17**)₂(PF₆)₂, Ru(**18**)₂(PF₆)₂, Ru(**20**)₂(PF₆)₂ and Ru(**23**)₂(PF₆)₂ in MeCN. The addition of water did not significantly alter the spectra. Concentrations range 5.5×10^{-6} to $2.1 \times 10^{-5} \text{ mol.L}^{-1}$.

3.6. The effect of deprotonation

The removal of the amino proton on base addition results in significant changes to the absorption spectra of the complexes. The MLCT band is shifted to lower energy [by 80

nm in both Fe(II) and Ru(II) complexes] and a ligand-centred transition is also strongly affected [Fe(II): 359 nm, Ru(II) 354 nm shifted to 430nm and 414 nm respectively]. For example, the addition of $\text{NaOH}_{(\text{aq})}$ to an acetonitrile (or acetonitrile-water) solution of $[\text{Fe}(\mathbf{17})_2](\text{PF}_6)_2$ resulted in a shift of the MLCT peak to 659 nm (shoulder at 600nm) and of a ligand-centred transition to 430 nm, as shown in Figure 3-8. The addition of more concentrated NaOH resulted in more complex behaviour (Figure 3-9) suggesting the presence of more than two species in solution. One possibility is that the lability of the iron(II) complex results in partial decomplexation of the metal caused by hydroxide ions. Supporting this is the observation that similar addition of $\text{NaOH}_{(\text{aq})}$ to a solution of the more inert $[\text{Ru}(\mathbf{17})_2](\text{PF}_6)_2$ (Figure 3-10) leaves the 200-370 nm region virtually unaffected and clean isosbestic points were observed.

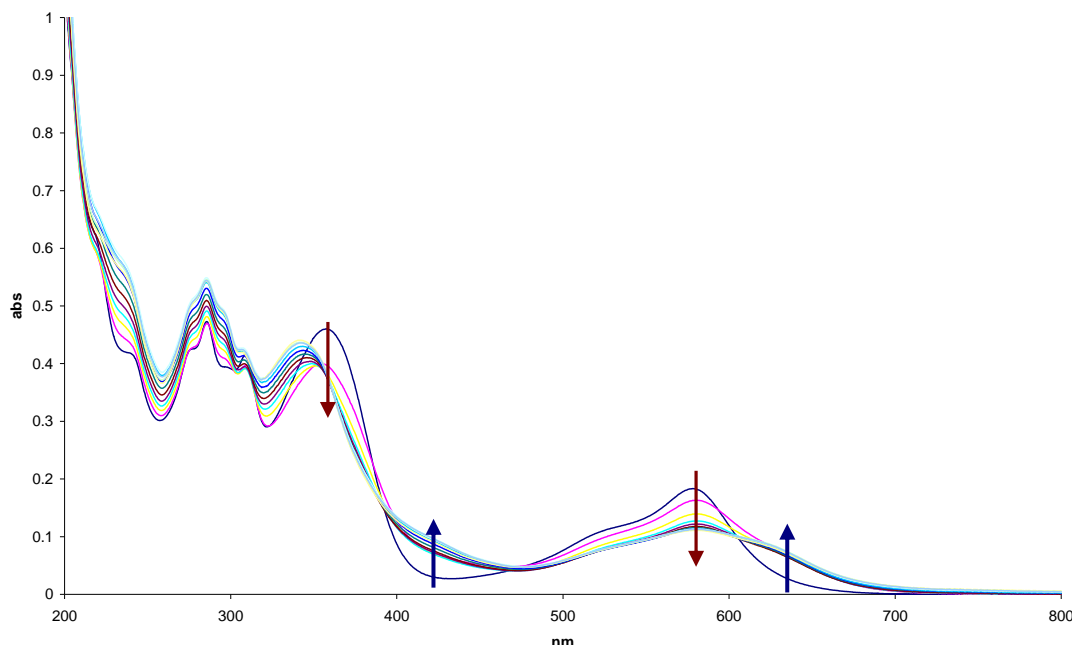


Figure 3-8 The effect of adding dilute NaOH to a solution of $[\text{Fe}(\mathbf{17})_2](\text{PF}_6)_2$. Additions (10 μl) of $\text{NaOH}_{(\text{aq})}$ (2.0×10^{-4} mol/L) to $[\text{Fe}(\mathbf{17})_2](\text{PF}_6)_2$ (MeCN, 3mL of 1.1×10^{-5} mol/L).

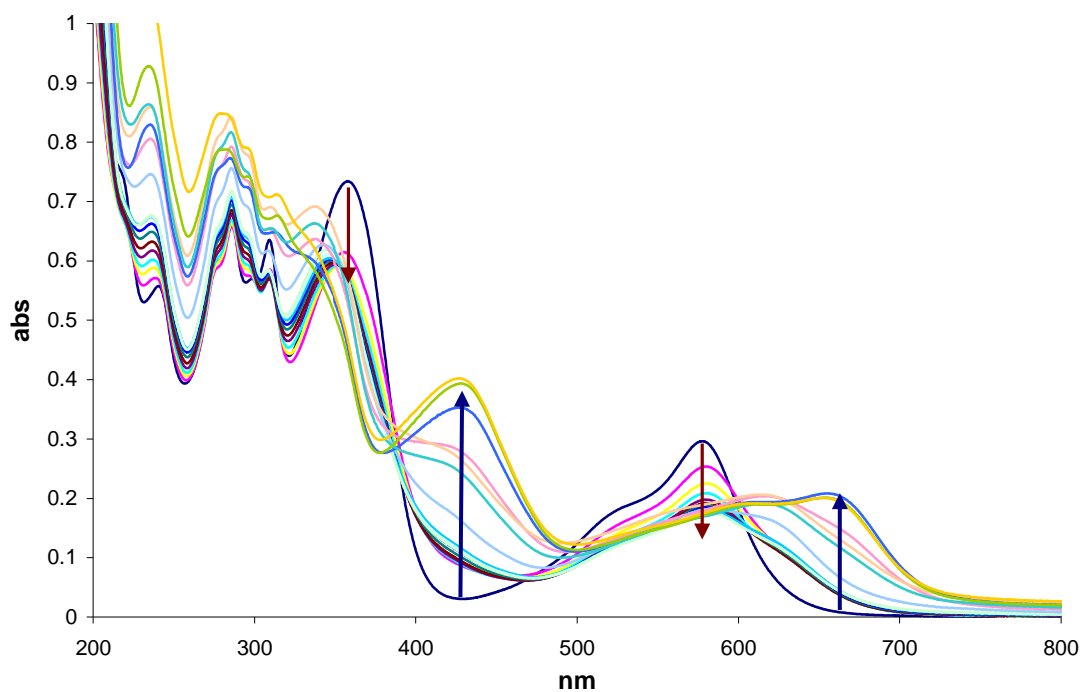


Figure 3-9 The effect of adding concentrated NaOH to a solution of $[\text{Fe(17)}_2](\text{PF}_6)_2$. $10\mu\text{l}$ additions of $\text{NaOH}_{(\text{aq})}$ (1.2×10^{-2} mol/L) to $[\text{Fe(17)}_2](\text{PF}_6)$ (MeCN, 3mL of 1.1×10^{-5} mol/L). After final additions λ_{\max}/nm ($\varepsilon_{\max}/10^3 \text{dm}^3 \text{mol}^{-1} \text{cm}^{-1}$) 427 (36), 652 (18).

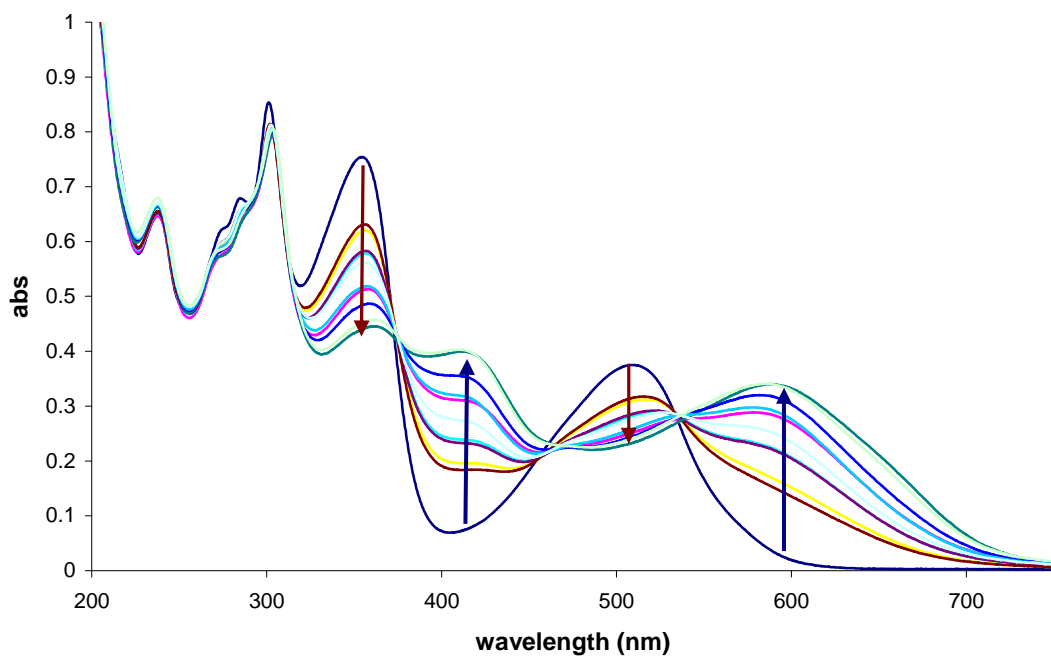


Figure 3-10 UV-Vis (MeCN) of $[\text{Ru(17)}_2](\text{PF}_6)_2$ showing the affect of $\text{NaOH}_{(\text{aq})}$ addition. Additions of $\text{NaOH}_{(\text{aq})}$ ($10\mu\text{l}$ additions, 1.2×10^{-2} mol/L) to $[\text{Ru(17)}_2](\text{PF}_6)_2$ (3mL of 1.2×10^{-5} mol/L). After final additions λ_{\max}/nm ($\varepsilon_{\max}/10^3 \text{dm}^3 \text{mol}^{-1} \text{cm}^{-1}$) 358 (37), 409 (35), 585 (28). Isosbestic points were observed at 374, 464 and 537nm.

3.7. *Electrochemistry*

Routine cyclic voltammetry (CV) was attempted for the complexes presented in this chapter. The CV and DPV of $[\text{Ru(17)}_2](\text{PF}_6)$ are shown in Figure 3-11 and Figure 3-12 and are typical of the complexes presented here. A series of irreversible ligand oxidation processes occur at 0.48, 0.65 and 0.76 V (vs. Fc/Fc^+) and the $\text{Ru}^{\text{II/III}}$ couple occurs at 0.98 V although the latter is also only quasi-reversible. These oxidation processes are more clearly seen in the DPV (Figure 3-12). Collecting consecutive scans at 100 mV.s^{-1} provided some information about chemical changes occurring in the system. First of all, the ligand-based processes around 0.5 V begin to disappear after the first scans and the $\text{Ru}^{\text{II/III}}$ process (0.98 V) shifts slightly in potential but also becomes significantly less reversible. The probable explanation is the first (irreversible) ligand oxidation results in the deprotonation of the amino proton , lowering the overall charge on the complex and giving rise to multiple $\text{Ru}^{\text{II/III}}$ oxidations from different molecular species. Spectroelectrochemistry was used to investigate this possibility for $[\text{Ru(17)}_2](\text{PF}_6)_2$ and it was found that peaks corresponding to the deprotonated complex were observed, providing some evidence for this hypothesis. Furthermore, as previously mentioned for the free ligands, some complexes were found to decompose on base addition possibly by hydroxide attack at the tpy 4'-position; ligand **24** (PhNO_2) was found to be particularly sensitive. Similarly it appears that the complexes are not stable to oxidation due to the operation of a similar mechanism which attacks the deprotonated complexes. Due to the obviously complicated nature of these electrochemical reactions, the electrochemistry of these complexes was not explored further.

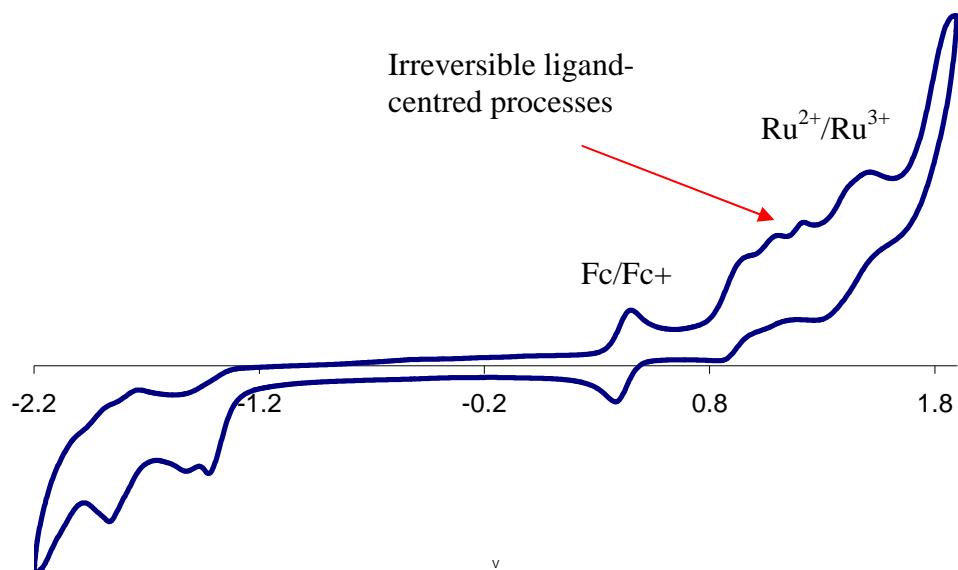


Figure 3-11 A typical cyclic voltammogram of $[\text{Ru}(\mathbf{17})_2](\text{PF}_6)_2$ (with added Fc) showing complicated and irreversible oxidation processes which occur. Experiment conducted in MeCN with a glassy carbon working electrode, TBAPF₆ as supporting electrolyte, silver wire as the reference electrode and a scan rate of 200mV/s, the third scan is shown.

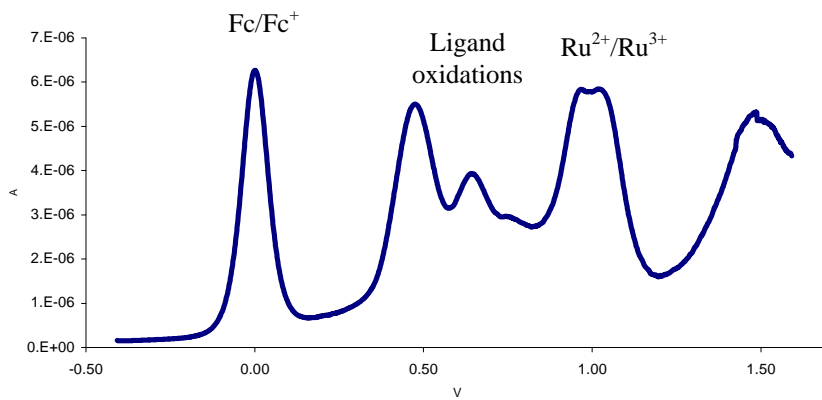


Figure 3-12 Differential pulse voltammogram of $[\text{Ru}(\mathbf{17})_2](\text{PF}_6)_2$. Experiment conducted in MeCN with a glassy carbon electrode, TBAPF₆ as supporting electrolyte, silver wire as the reference electrode and a scan rate of 200mV/s.

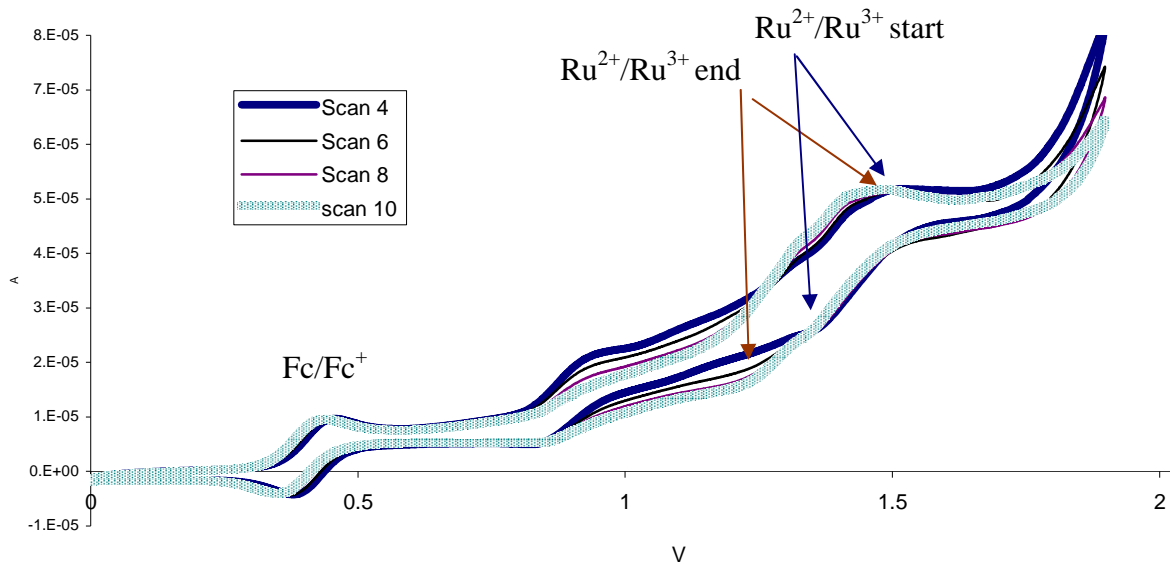


Figure 3-13 Repeated CV scans of $[\text{Ru}(\mathbf{17})_2](\text{PF}_6)_2$ (same conditions as above figures) from 0 to 1.8 V at 100ms. Redox [vs. Fc/Fc^+ (separation)] Scan 4: L_{ox} 0.49 V, (170 mV), $\text{Ru}^{\text{II/III}}$ 1.00 (198 mV). Scan 10: L_{ox} 0.51 V (138 mV), Ru 0.99 (207 mV).

3.8. X-ray crystal structures

Single crystals suitable for X-ray crystallography were grown from slow evaporation of aqueous-acetonitrile solutions of the complexes. The following crystal structures of N-H derivatives were solved:

- $[\text{Fe}(\mathbf{17})_2](\text{PF}_6)_2 \cdot 1.5\text{MeCN} \cdot 1.5\text{H}_2\text{O}$ and $[\text{Ru}(\mathbf{17})_2](\text{PF}_6)_2 \cdot 1.5\text{MeCN} \cdot 1.5\text{H}_2\text{O}$
- $[\text{Fe}(\mathbf{18})_2](\text{PF}_6)_2 \cdot 0.33\text{MeCN} \cdot 0.33\text{H}_2\text{O}$ and $[\text{Ru}(\mathbf{18})_2](\text{PF}_6)_2 \cdot 0.33\text{MeCN} \cdot 0.33\text{H}_2\text{O}$
- $2([\text{Fe}(\mathbf{21})_2](\text{PF}_6)_2) \cdot 0.75\text{MeCN} \cdot 0.33\text{H}_2\text{O}$
- $[\text{Fe}(\mathbf{23})_2](\text{PF}_6)_2$ and $[\text{Ru}(\mathbf{23})_2](\text{PF}_6)_2 \cdot 2.75\text{MeCN}$

Structures of complexes of the N-Me derivative ligand **20** will be discussed later.

The structures of $[\text{Fe}(\mathbf{17})_2](\text{PF}_6)_2 \cdot 1.5\text{MeCN} \cdot 1.5\text{H}_2\text{O}$ and $[\text{Ru}(\mathbf{17})_2](\text{PF}_6)_2 \cdot 1.5\text{MeCN} \cdot 1.5\text{H}_2\text{O}$ are not isostructural, although they only differ significantly by the positions of the anions and solvent. The molecular structure of the Ru(II) complex is shown in Figure 3-14. One of the tpy ligands is significantly more distorted than the other [angles between least-squares-planes of the rings containing N1

and N3 with N2 are 10.73(12) and 12.12(12) $^{\circ}$; N6 and N8 with N7 are 2.68(13), 3.18(12) $^{\circ}$.

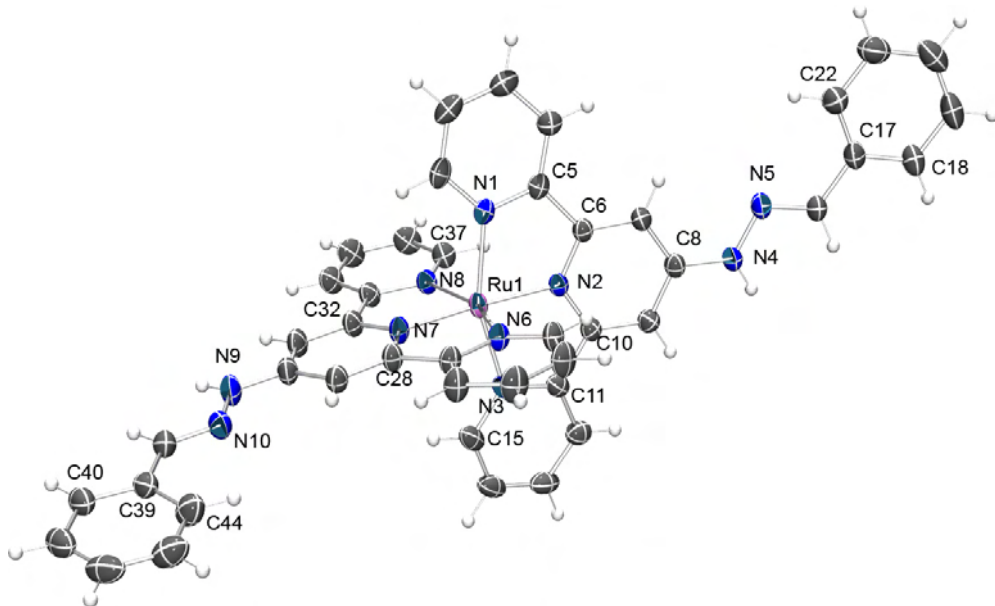


Figure 3-14 The molecular structure of the $[\text{Ru}(17)_2]^{2+}$ ion in the X-ray crystal structure of $[\text{Ru}(17)_2](\text{PF}_6)_2 \cdot 1.5\text{MeCN} \cdot 1.5\text{H}_2\text{O}$. Ellipsoids drawn at 50% probability. Space group P-1. Selected bond lengths and angles : Ru1-N1 2.073(2); Ru1-N2 1.986(2); Ru1-N3 2.070(2); Ru1-N6 2.0739(19); Ru1-N7 1.985(2); Ru1-N8 2.076(2); N4-C8 1.361(3); N4-N5 1.369(3); N9-C30 1.363(3); N9-N10 1.370(3) Å. N1-Ru1-N2 78.51(8); N1-Ru1-N3 157.09(8), N2-Ru1-N3 78.81(8); N6-Ru1-N7 78.93(8), N6-Ru1-N8 157.24(8); N7-Ru1-N8 78.38(8) $^{\circ}$. Hydrogen bonds D-A (not shown) and angles D-H-A: N4H4...O1 2.934(3) Å, 158 $^{\circ}$; N9H9...O2 3.007(8) Å, 170 $^{\circ}$.

Although the more planar ligand does engage in π - π stacking interactions (distance from the phenyl ring containing C39 to the centroid of the ring containing N6i is 3.212 Å), the overlap is not ideal, As shown in Figure 3-15a. Close edge-to-face interactions between the rings containing N1 and N8, shown in Figure 3-15b ($\text{C}4\dots\text{H}361\text{i}-\text{C}36\text{i} = 2.868$ Å, $\text{C}1\dots\text{H}351\text{i}-\text{C}35\text{i} = 2.796$ Å, $\text{I} = -1+x, y, z$) are not complemented by close face-to-face embraces (distance from the centroid of the ring containing N6 to least squares plane of the ring containing N8i is 3.746 Å, $i = -1 + x, y, z$). This is perhaps surprising as the observed intermolecular interactions do not appear to preclude the formation of ideal π - π embraces and also suggests that the tpy framework is considerably more flexible than expected. Similar to the free ligands, the amino protons participate in hydrogen bond interactions, however in the absence of a good hydrogen-bond-acceptor, water molecules are preferred over counter-ions (PF_6^-) or solvent (MeCN). In the Ru(II) complex (Figure 3-14) two crystallographically independent water molecules are involved [hydrogen bond distances N4...O1 2.934(3) Å, N4-H4-O1 158 $^{\circ}$, N9...O2 3.007(8) Å, N9-H9-O2 170 $^{\circ}$]. One water molecule acts as a bridge

between adjacent complexes via the imino nitrogen ($O_1 \dots N_{5i}$ 2.983 Å, $O_1-H_1-N_{5i}$ 164° , $i = 1-x, 1-y, -z$) and close contacts with PF_6^- counterions are also present.

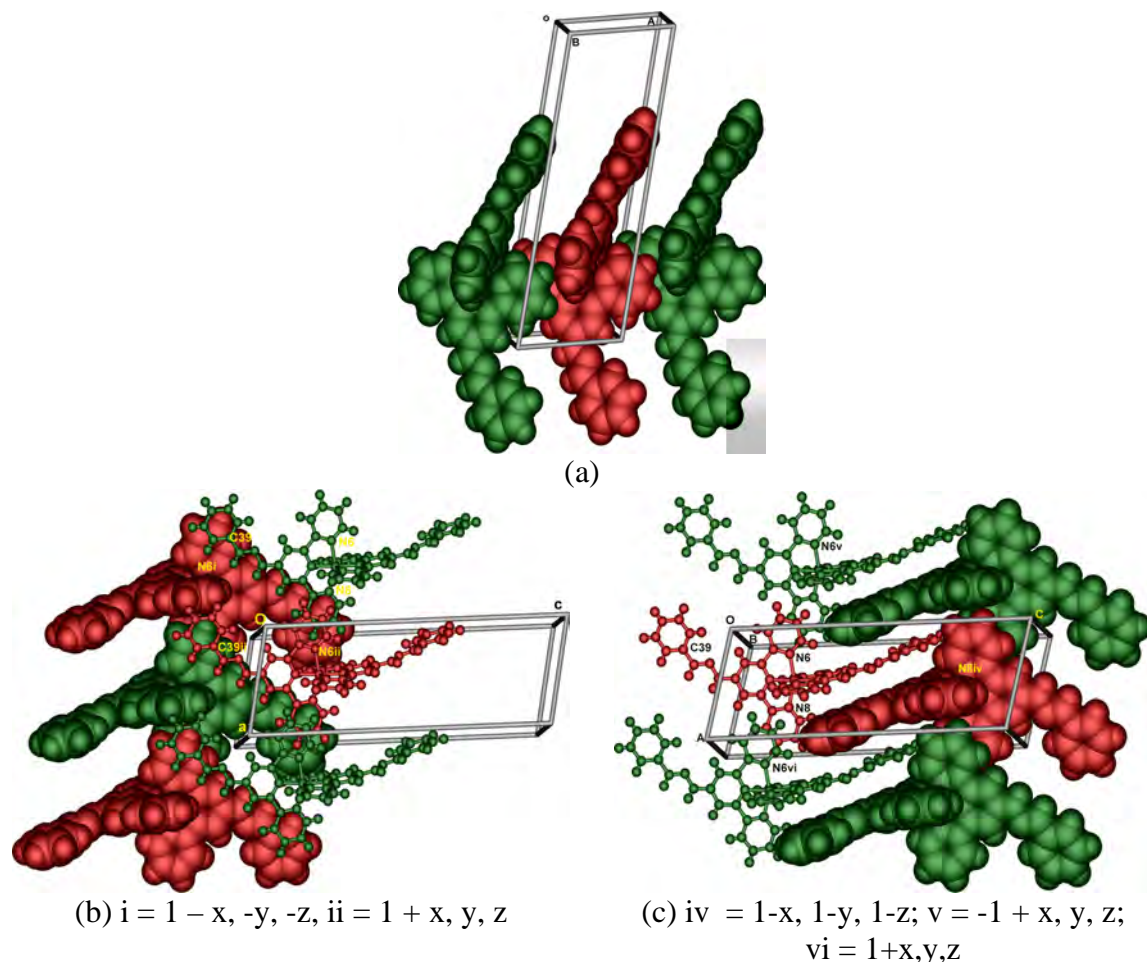


Figure 3-15 X-Ray crystal structure of $[Ru(17)_2](PF_6)_2 \cdot 1.5\text{MeCN} \cdot 1.5\text{H}_2\text{O}$ showing two views of the crystal packing (solvent and anions removed for clarity). (a) Typical tpy-tpy embraces along the a -axis. (b) Complementary overlap of hydrazone groups along the a -axis. (c) Interdigitating ‘bent’ hydrazone moieties along the a -axis. All complexes are crystallographically equivalent.

The interactions of the anions and solvent in the structure of the Fe(II) analogue $[Fe(17)_2](PF_6)_2 \cdot 1.5\text{MeCN} \cdot 1.5\text{H}_2\text{O}$ is shown in Figure 3-16. These differ from those of the Ru(II) complex although the molecular complex adopts a similar conformation [for example, least squares planes between rings contain N1 and N3 with N2 are $8.7(3)$ and $9.7(3)^\circ$, between N6 and N9 with N7 are $2.8(3)$ and $2.9(3)^\circ$]. The amino NH protons are each hydrogen-bonded to a water molecule (see figure caption) which are also in close contact with PF_6^- counter ions.

The molecular structure of $[Fe(21)_2]^{2+}$ in $[Fe(21)_2](PF_6)_2 \cdot 0.75\text{MeCN} \cdot 0.33\text{H}_2\text{O}$ and is shown in Figure 3-17. The tpy ligands are almost orthogonal [angle between least

squares planes of rings containing N1, N2, N3 with N6, N7, N8 is 87.02(4) $^{\circ}$] and the py rings of the tpy ligands are also close to coplanar [angle between least squares planes of rings containing N1 and N3 is 5.0(1) $^{\circ}$; rings containing N6 and N8 is 0.8(1) $^{\circ}$]. The pendant phenyl rings are both twisted slightly out of the plane of the tpy rings [angles between least squares planes of ring with O3/O4 substituents to tpy containing N6, N7, N8 is 11.75 $^{\circ}$; ring with O1/O2 substituents to tpy containing N1, N2, N3 is 23.65 $^{\circ}$].

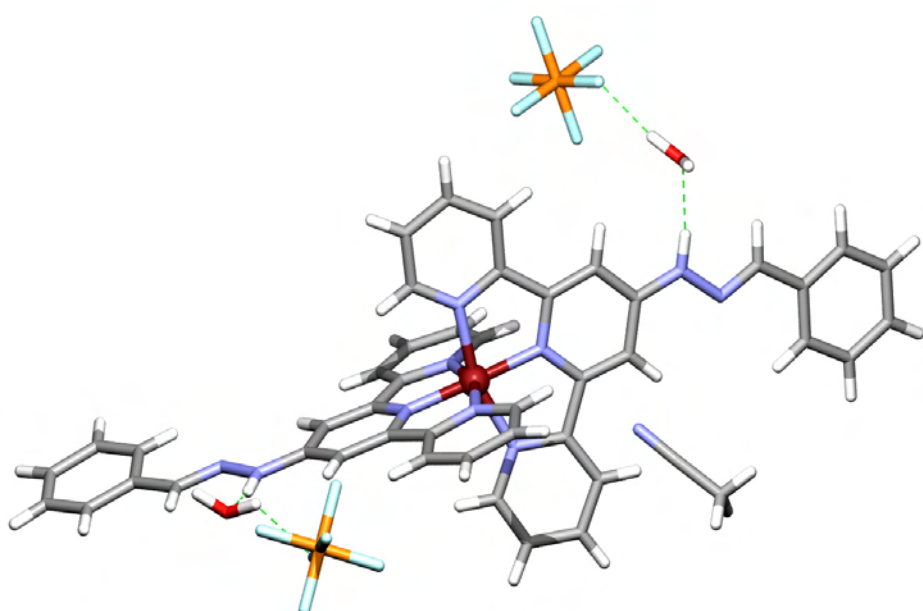


Figure 3-16 X-Ray crystal structure of $[\text{Fe}(17)_2](\text{PF}_6)_2 \cdot 1.5\text{MeCN} \cdot 1.5\text{H}_2\text{O}$ (disorder of PF_6^- anions and water molecules not shown). Space group P-1. Selected bond lengths and angles: Fe1-N1 1.970(5); Fe1-N2 1.884(4); Fe1-N3 1.980(5); Fe1-N6 1.985(5); Fe1-N7 1.878(4); Fe1-N8 1.969(5); N4-C8 1.365(7); N4-N5 1.369(8); N9-C30 1.369(7); N9-N10 1.375(7) Å. N1-Fe1-N2 80.71(19); N1-Fe1-N3 161.05(19); N2-Fe1-N3 80.5(2), N6-Fe1-N7 80.2(2); N6-Fe1-N8 161.38(19) $^{\circ}$. Hydrogen bond distances (D-A): N4-H4...O2 2.869(8) Å, N4-H4-O2 169 $^{\circ}$; N9-H9...O16i 2.911(17) Å, N9-H9-O16 167 $^{\circ}$; O2-H1...N5ii 3.188(8) Å O2-H1-N5ii 128 $^{\circ}$. To PF_6^- : O2H2...F6 2.896(8), O2-H2-F6 169 $^{\circ}$. Symmetry codes: i = 1 + x, y, z, ii = 1-x, 1-y, 1-z.

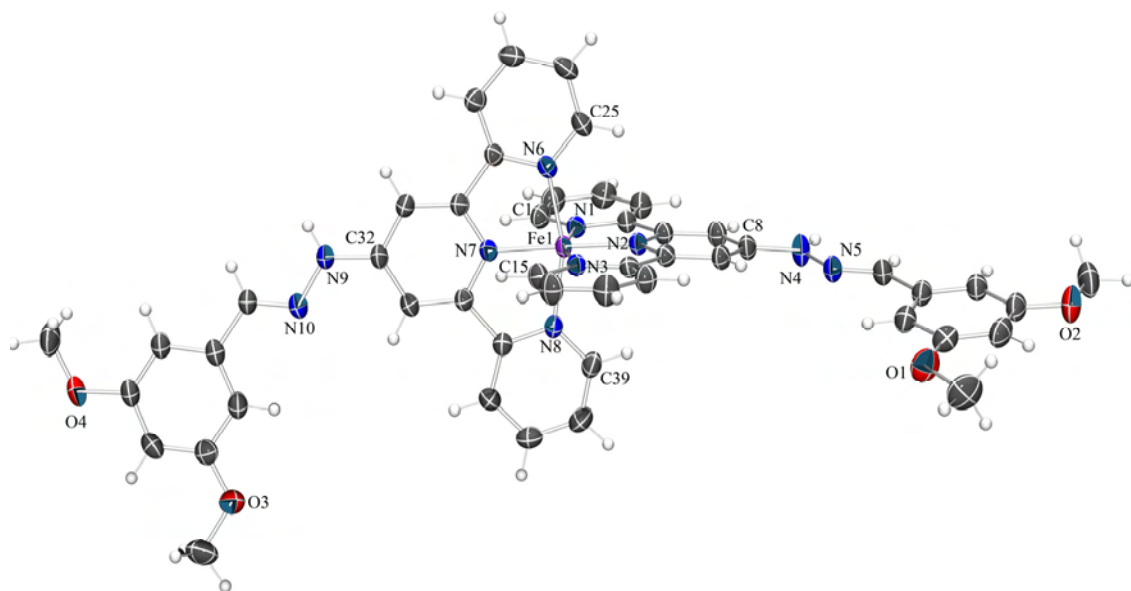


Figure 3-17 Molecular structure of $[\text{Fe}(\mathbf{21})_2]^{2+}$ in $[\text{Fe}(\mathbf{21})_2](\text{PF}_6)_2 \cdot 0.75\text{MeCN} \cdot 0.33\text{H}_2\text{O}$. Displacement ellipsoids are drawn at 50%. Space group P-1. Selected bond lengths and angles: $\text{Fe1-N1 } 1.972(2)$; $\text{Fe1-N2 } 1.887(2)$; $\text{Fe1-N3 } 1.968(2)$; $\text{Fe1-N6 } 1.979(2)$; $\text{Fe1-N7 } 1.894(2)$; $\text{Fe1-N8 } 1.978(2)$; $\text{N4-C8 } 1.361(4)$; $\text{N9-C32 } 1.362(4)$; $\text{N4-N5 } 1.367(3)$; $\text{N9-N10 } 1.366(3)$ Å. $\text{N1-Fe1-N2 } 80.51(9)$; $\text{N1-Fe1-N3 } 161.02(9)$; $\text{N2-Fe1-N3 } 80.52(9)$; $\text{N6-Fe1-N7 } 80.83(10)$; $\text{N6-Fe1-N8 } 160.89(9)$; $\text{N7-Fe1-N8 } 80.07(9)$ °. Hydrogen bond distances (D-A) and angles from amino NH to PF_6^- anions (not shown): $\text{N4-H4B...F24 } 2.96(1)$, 158° ; $\text{N9-H9B...F14i } 2.933(4)$, 174° . Symmetry code i = x, -1 + y, z.

The packing of the complexes is shown in Figure 3-18 and reveals that $\pi-\pi$ stacking between hydrazone moieties on adjacent complexes dominates in the assemble of the cations [distance between the least squares planes of ligands containing $[\text{N6-N7-N8}]$ and $[\text{N6i-N7i-N8i}]$ is 3.32 Å, symmetry operator $i = 1-x, -y, -z$]. Notably, no tpy-tpy embraces occur with tpy groups well separated in the structure. However, face-to-face stacking occurs between terminal pyridyl rings and phenyl groups [between rings containing N1 and bearing O1; containing N6 and bearing O3] and weaker face-to-edge interactions are also observed [between rings containing N3 and N8 with rings bearing O3 and O1 respectively]. The overall stacking is therefore not ideal, as clearly shown in the view depicted in Figure 3-18b. The methoxy substituents are partly responsible by preventing closer approaches of the aromatic groups. The sheets are orientated perpendicular to the bc-plane (Figure 3-18c). Finally, the amino NH protons engage in hydrogen bonding to PF_6^- anions [$\text{F14...H9Bi } 2.07$, $\text{F23-H4B } 2.62$, $\text{F24-HB4 } 2.14$ Å; $\text{N9-H9B-F14 } 174^\circ$, $\text{N4-H4B-F24 } 158^\circ$] and also in other close contacts with CH protons [$\text{F13...H28Ai } 2.61$, $\text{F13...H31Ai } 2.39$, $\text{F10...H47Bii } 2.41$, $\text{F10...H14Aiii } 2.57$ Å]. Symmetry operators $i = x, 1+y, z$, $ii = -x, 1-y, -z$, $iii = 1-x, 1-y, -z$].

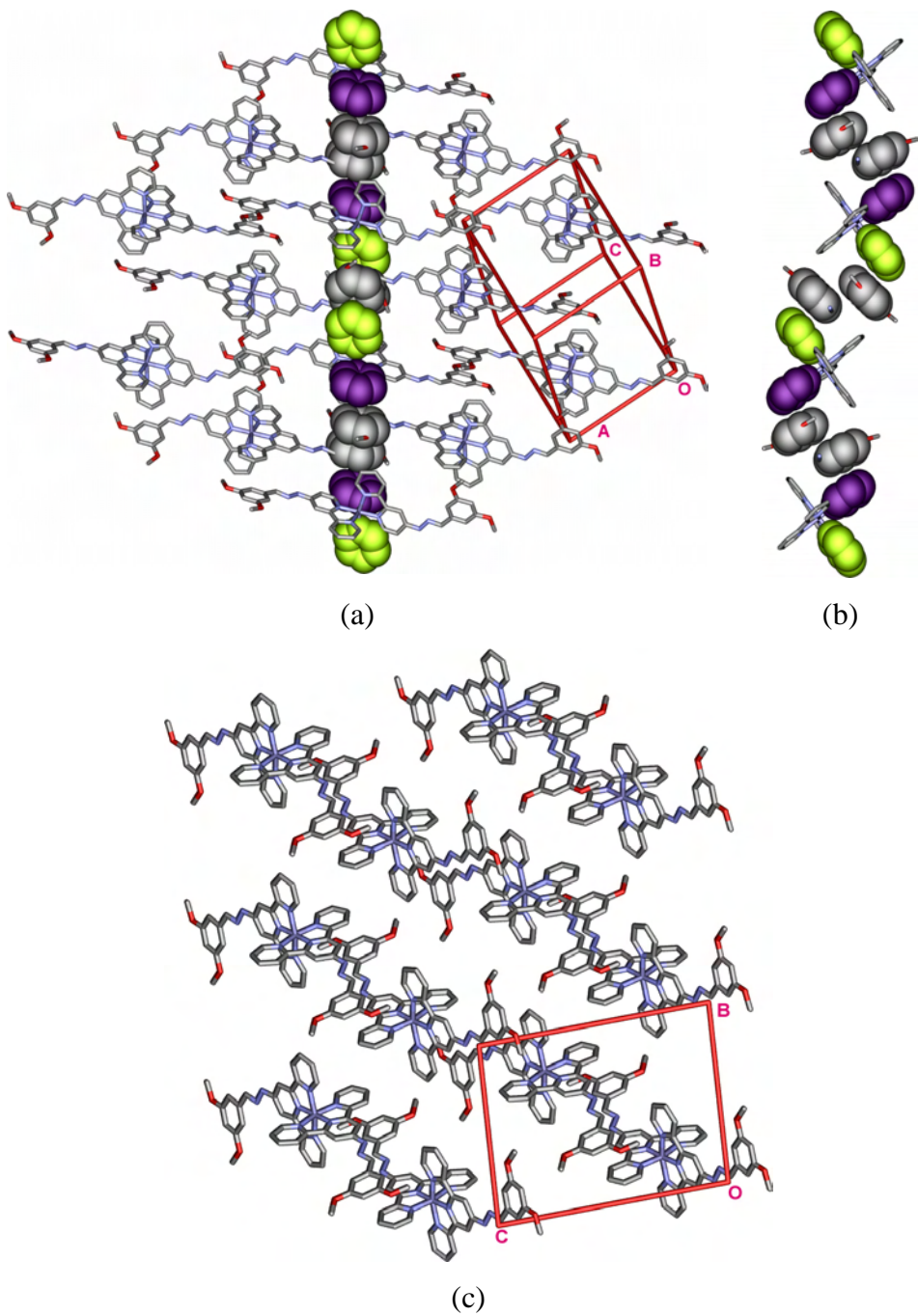


Figure 3-18 The packing arrangement of 2D sheets of $[\text{Fe}(\mathbf{21})_2]^{2+}$ in $[\text{Fe}(\mathbf{21})_2](\text{PF}_6)_2 \cdot 0.75\text{MeCN} \cdot 0.33\text{H}_2\text{O}$. Hydrogen atoms, counter ions and solvent omitted for clarity. (a) A single sheet of $[\text{Fe}(\mathbf{21})_2]^{2+}$ complexes, rings coloured green contain N6, coloured purple contain N1. (b) A side view of a single sheet looking approximately down the a -axis. (c) A view down the a -axis, showing the spacing between adjacent sheets. Phenyl-pyridyl distances: from the centroid of the phenyl ring with O3/O4 substituents to least squares plane of ring containing N6i is 3.236 Å; from centroid of ring containing O1/O2 to least squares plane of ring containing N1ii is 3.317 Å, (symmetry operators i = 1-x, -y, -z, ii = 2-x, 1-y, 1-z). Additional contacts involving O3 and C43 and CH protons of a neighbouring complex [O3...H13Ai-C13i is 2.61 Å; C43...H14Ai-C14i 2.77 Å, symmetry operator i = -1 + x, y, z].

The molecular structure of $[\text{Fe}(\mathbf{23})_2](\text{PF}_6)_2$ is shown in Figure 3-19. The quality of structural data for $[\text{Fe}(\mathbf{23})_2](\text{PF}_6)_2$ was less than ideal, however some comments about the packing arrangement can still be justified. Similar to that observed for $2([\text{Fe}(\mathbf{21})_2](\text{PF}_6)_2) \cdot 5\text{MeCN} \cdot 0.66\text{H}_2\text{O}$, hydrazone-hydrazone π - π stacking occurs in preference to tpy-tpy embraces. Figure 3-20 shows the key features, head-to-tail overlap of the hydrazone moieties and the poor overlap of the pyridyl groups, shown in red boxes.

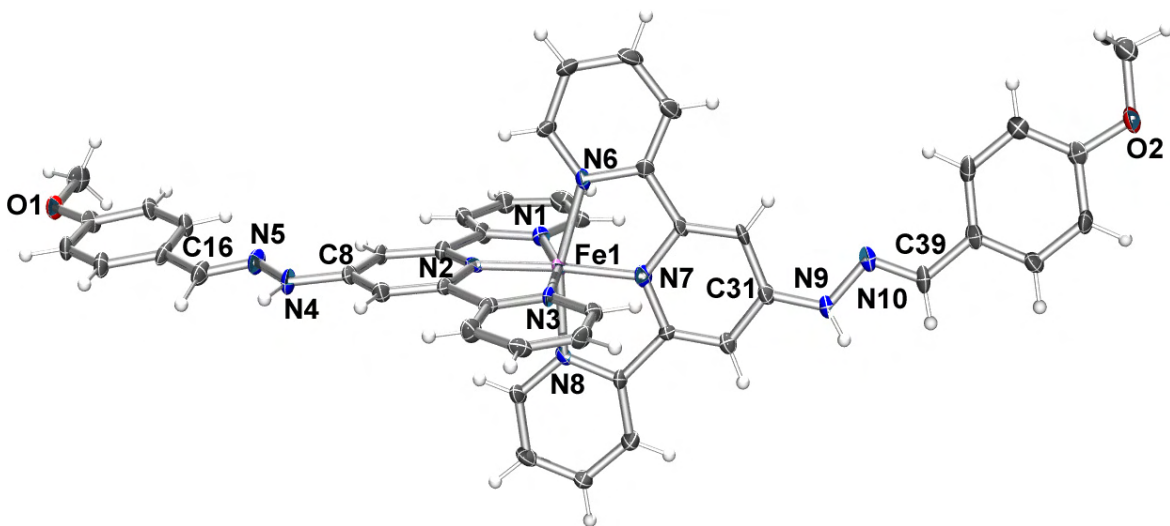


Figure 3-19 Molecular structure of $[\text{Fe}(\mathbf{23})_2]^{2+}$ in $[\text{Fe}(\mathbf{23})_2](\text{PF}_6)_2$. Space group $P\bar{2}_1/c$. Displacement ellipsoids are drawn at 30%. Analogous data for Fe complex: Fe1-N1 1.968(8); Fe1-N2 1.890(7); Fe1-N3 1.976(8); Fe1-N6 1.990(8); Fe1-N7 1.890(9); Fe1-N8 1.988(8); N4-C8 1.369(13); N4-N5 1.381(13); N9-C31 1.363(13); N9-N10 1.384(12) Å. N1-Fe1-N2 81.2(4); N1-Fe1-N3 161.4(3); N2-Fe1-N3 80.2(3); N6-Fe1-N7 80.7(3); N6-Fe1-N8 161.3(3); N7-Fe1-N8 80.6(4)°.

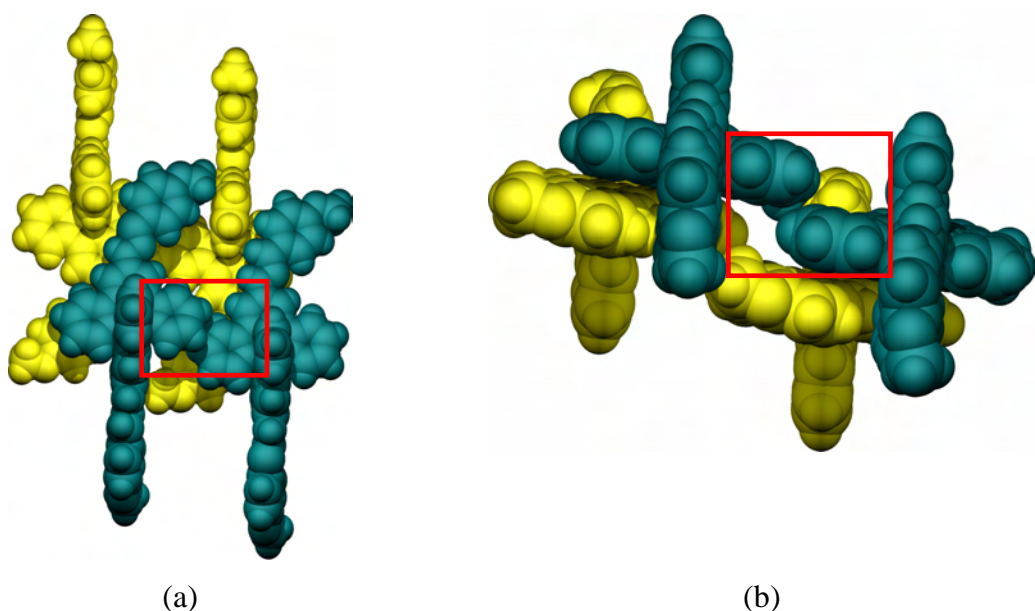


Figure 3-20 Molecular packing arrangement of $[\text{Fe}(\mathbf{23})_2]^{2+}$ in $[\text{Fe}(\mathbf{23})_2](\text{PF}_6)_2$. The poor py-py overlap is shown in red boxes.

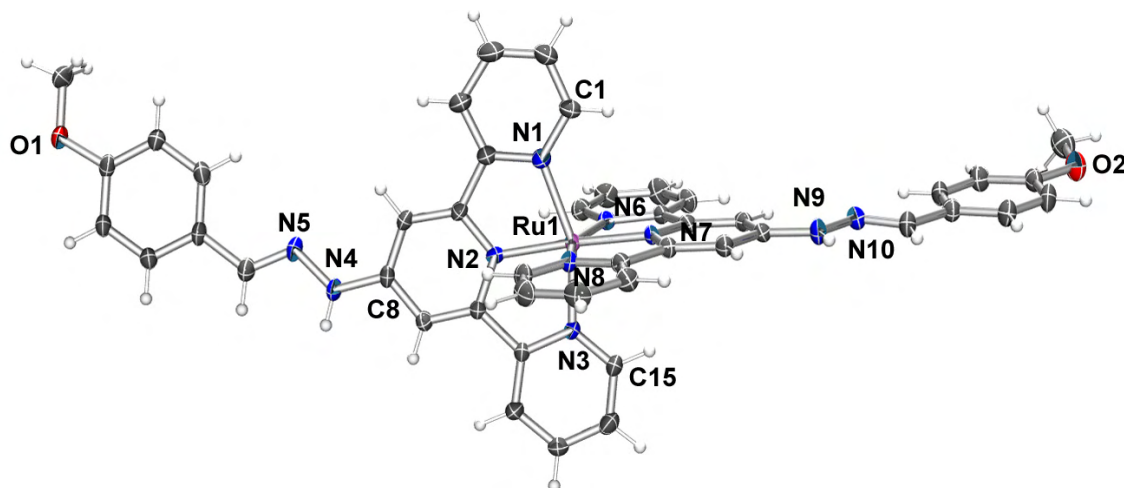


Figure 3-21 Molecular structure of $[\text{Ru}(23)_2]^{2+}$ in $[\text{Ru}(23)_2](\text{PF}_6)_2 \cdot 1.75\text{MeCN}$. Space group P 2₁/c. Displacement ellipsoids are drawn at 30%. Selected bond lengths and angles: Ru1-N1 2.079(4), Ru1-N2 1.985(5), Ru1-N3 2.070(4), Ru1-N6 2.060(5), Ru1-N7 2.004(4), Ru1-N8 2.068(5) Å.. N1-Ru1-N7 104.90(18), N1-Ru1-N8 95.90(19), N2-Ru1-N3 78.44(18), N2-Ru1-N6 103.69(19), N2-Ru1-N7 175.50(18), N2-Ru1-N8 98.80(19), N3-Ru1-N6 93.94(18), N3-Ru1-N7 97.95(18), N3-Ru1-N8 89.62(18), N6-Ru1-N7 79.11(18), N6-Ru1-N8 157.49(19), N7-Ru1-N8 78.38(19)°.

The structure of the Ru(II) analogue, $[\text{Ru}(23)_2](\text{PF}_6)_2 \cdot 1.75\text{MeCN}$, is of much better quality, and the molecular structure is shown Figure 3-21. Although the molecular structure appears similar in both cases (and both structures solve in the same space group, P2₁/c), the volume of the unit cell is found to significantly increase from 5102 Å³ to 5421 Å³ although a similar packing arrangement is observed. In this case, two types of π-stacking can be identified (Figure 3-22). The closer of the two types involves stacking between the hydrazone moieties of adjacent complexes (Figure 3-22a, yellow and green) which position the phenyl ring over the central ring of the adjacent complex to form chains of close packed complexes. This stacking is also stabilised by intermolecular O...HC hydrogen bonding (see figure caption for details). The second type of π-interaction (Figure 3-22b, yellow and blue), which also benefits from excellent offset π-stacking between hydrazone groups and aromatic rings, interconnects the chains formed by the first type of interaction (Figure 3-22c) to form two dimensional sheets which are separated by disordered PF_6^- anions and acetonitrile molecules (Figure 3-23).

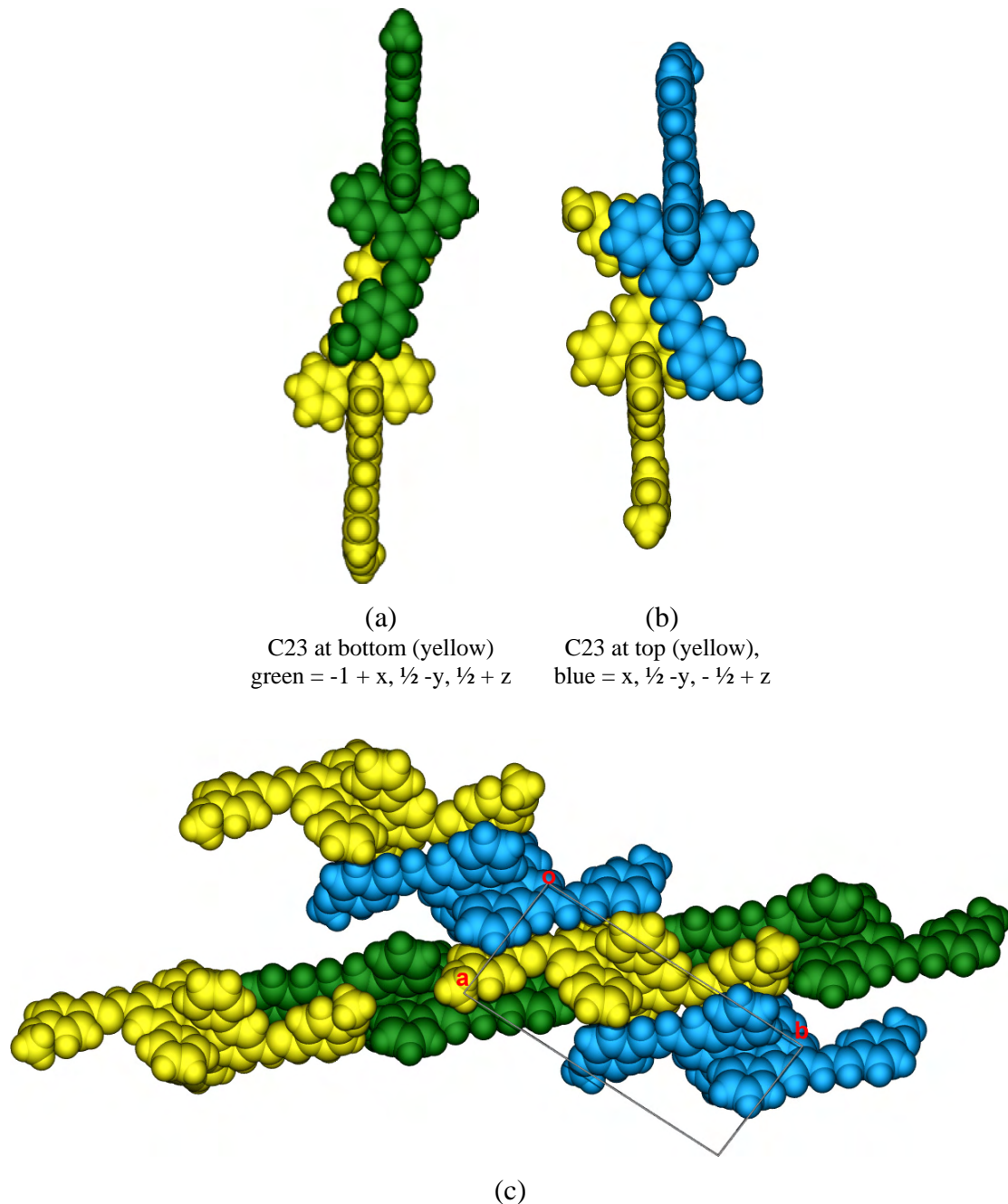


Figure 3-22 The packing of $[\text{Ru}(23)_2]^{2+}$ in $[\text{Ru}(23)_2](\text{PF}_6)_2 \cdot 1.75\text{MeCN}$ showing the intersection of the two main π -stacking interactions which form 2D sheets. (a) The ring with the O1 substituent is positioned over the central ring containing N7. Intermolecular distances: Ph-py: C19...C30i 3.347(9) Å, C42...C7ii 3.474(10) Å; Hydrazone-Ph: C16...C45i 3.383(10), C39...C22ii 3.437(10). Hydrogen bonds: O1...C15i 3.128(8) Å, O1-H15i-C15i = 144°; O2...C38ii 3.139(8) Å, O2-H38ii-C38ii 142°. (b) The phenyl ring with the O2 substituent is positioned over the terminal ring containing N3. Intermolecular distances: Ph-Py: C40...C12iii 3.469(9), C17...C35iv 3.389(10), C19...C37iv 3.488(10) Å; hydrazone-Ph interactions: N4...C32iv 3.365(9), N9...C9iii 3.385(9) Å [Symmetry operations: i = $1 + x, \frac{1}{2} - y, -\frac{1}{2} + z$; ii = $-1 + x, \frac{1}{2} - y, \frac{1}{2} + z$; iii = $x, \frac{1}{2} - y, \frac{1}{2} + z$; iv = $x, \frac{1}{2} - y, -\frac{1}{2} + z$].

Two other features are notable, namely a short methyl-methyl contact [C23...C23i 3.383(12) Å, i = $2 - x, -y, -z$], likely a consequence of crystal packing, and hydrogen

bonding between both amino protons and PF_6^- counter ions (see Figure 3-23 caption for details).

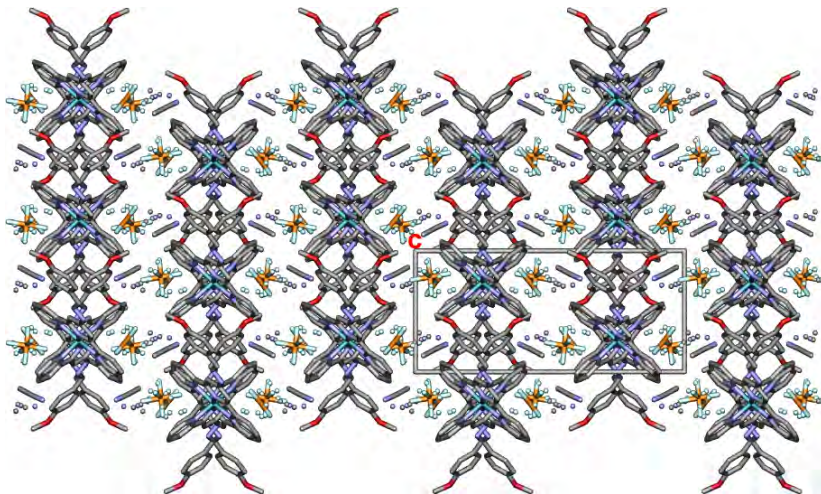


Figure 3-23 The separation of 2D sheets of complexes by solvent and anion molecules in $[\text{Ru}(23)_2](\text{PF}_6)_2 \cdot 1.75\text{MeCN}$, looking down the crystallographic c -axis. Amino NH... PF_6^- hydrogen bond details: [H-A, D-A, D-H-A: N9--H9'...F22 2.16(7) Å, 3.017(9) Å, 168(6)°; N4--H(4')...F11 2.14(7) Å, 2.950(9) Å, 162(7)°; i = x, ½ -y, ½ +z].

X-Ray quality crystals of $[\text{Ru}(\mathbf{18})_2](\text{PF}_6)_2 \cdot 0.33\text{MeCN} \cdot 0.33\text{H}_2\text{O}$ and $[\text{Fe}(\mathbf{18})_2](\text{PF}_6)_2 \cdot 0.33\text{MeCN} \cdot 0.33\text{H}_2\text{O}$ were both grown by slow evaporation of acetonitrile-water solutions of the complexes. The structures are isomorphous and have surprisingly high symmetry (space group R-3) and beautiful crystal morphology (Figure 3-24).

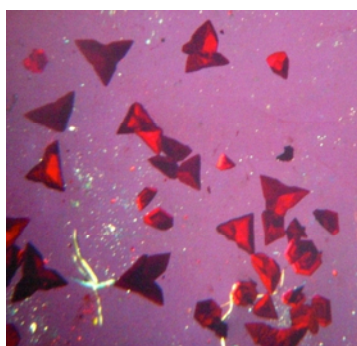


Figure 3-24 Crystals of $[\text{Ru}(\mathbf{18})_2](\text{PF}_6)_2 \cdot 0.33\text{MeCN} \cdot 0.33\text{H}_2\text{O}$

The molecular structure of $[\text{Ru}(\mathbf{18})_2]^{2+}$ is shown in Figure 3-25. The tpy components of the ligands are essentially planar and almost perfectly orthogonal [angle between least squares planes of tpy rings of the ligands is $89.3(1)^\circ$]. Both phenyl rings are twisted out of the plane of the tpy pyridyl rings, although one is twisted by a much greater degree than the other [angle between least-squares planes of the ring containing C20 and the

tpy rings containing N1-N2-N3 is $12.5(3)^\circ$; between the ring containing C42 and tpy rings containing N6-N7-N8 is $35.1(3)^\circ$. This is a consequence of an interesting packing arrangement formed by extensive π - π stacking. The principle interactions can be divided into several parts. In the following series of diagrams, the molecule with general symmetry operator (x, y, z) is always coloured purple for clarity. The most important interactions (in terms of the overall arrangement) are shown in Figure 3-26 and are reminiscent of more common tpy-tpy embraces as they are comprised of both face-to-face and edge-to-face interactions, although the 90° rotation of one complex appears unusual. Adjacent complexes are packed together with phenyl embraces between the rings containing N1, N8 and N6 (see figure for symmetry codes) to give an angle between the least-squares planes of tpy ligands [N1-N2-N3]-[N6i-N7i-N8i] of 69.52° ($i = x-y, x, 2-z$). These interactions result in the formation of hexamer units with a PF_6^- anion in the centre (on a special position with six-fold symmetry).

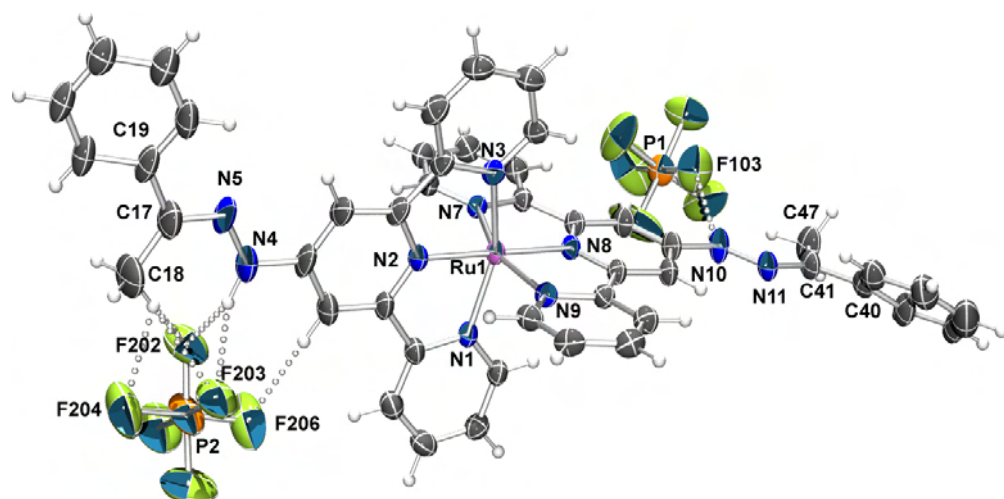


Figure 3-25 The molecular structure of $[\text{Ru}(18)_2](\text{PF}_6)_2$ in $[\text{Ru}(18)_2](\text{PF}_6)_2 \cdot 0.33\text{MeCN} \cdot 0.33\text{H}_2\text{O}$. Displacement ellipsoids drawn at 30% probability. Space group R-3. Selected bond lengths: $\text{Ru}(1) - \text{N}(1)$ 2.077(5), $\text{Ru}(1)-\text{N}(2)$ 1.980(5), $\text{Ru}(1)-\text{N}(3)$ 2.087(5), $\text{Ru}(1)-\text{N}(6)$ 2.084(5), $\text{Ru}(1)-\text{N}(7)$ 1.985(5), $\text{Ru}(1)-\text{N}(8)$ 2.063(6), $\text{N}(4)-\text{C}(8)$ 1.400(12), $\text{N}(9)-\text{C}(32)$ 1.376(8), $\text{N}(4)-\text{N}(5)$ 1.374(10), $\text{N}(9)-\text{N}(10)$ 1.370(10) Å. Hydrogen bond distances from amino protons to PF_6^- anions (D-A) and angles: $\text{N}4-\text{H}4' \dots \text{F}202$ 2.87(1) Å, $148(11)^\circ$; $\text{N}4-\text{H}4' \dots \text{F}203$ 2.95(1) Å, $145(11)^\circ$; $\text{N}10-\text{H}10' \dots \text{F}(103)$ 3.12(1), $152(7)^\circ$.

Face-to-face π - π stacking between pyridyl rings containing N8 and phenyl rings containing C19i ($i = x-y, x, 3-z$) (Figure 3-27) assemble the hexamer units into columns along the crystallographic *c*-axis. A stack of three hexamers is shown in Figure 3-28, showing the central channel formed. Finally, the columns are packed together with short $\text{CH}_3-\text{C}_{\text{Py}}$ contacts and longer $\text{C}_{\text{Ph}}-\text{C}_{\text{Py}}$ contacts. There is not any significant π - π stacking

between these groups - the distance between the least squares planes of the hydrazone moieties is over 4 Å.

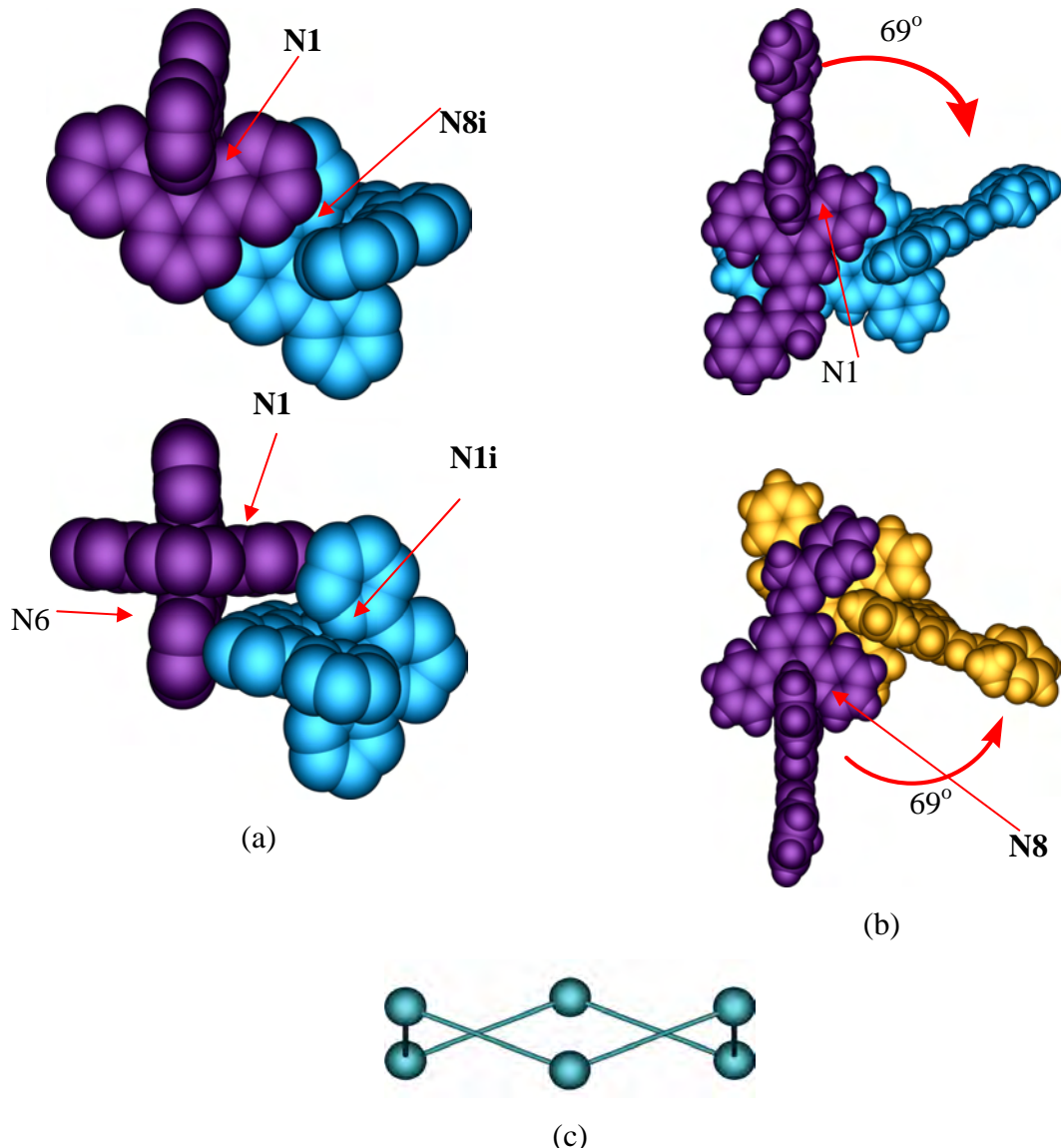


Figure 3-26 Views of the key packing features which form hexamers in the structure of $[\text{Ru}(18)_2](\text{PF}_6)_2 \cdot 0.33\text{MeCN} \cdot 0.33\text{H}_2\text{O}$. (a) The key phenyl embraces comprised of face-to-face interactions between rings containing N1 and N8i [$\text{C}1 \dots \text{C}37i$ distance is 3.335 Å] and face-to-edge interactions between rings containing N7 and N8i [$\text{C}25 \dots \text{H}36i\text{-C}36i$ distance is 2.78 Å]. Only tpy moieties shown, hydrogen atoms are omitted. (b) Illustration of the resulting angle of 69° between adjacent complexes. (c) The resulting cyclohexane-like connectivity of the Ru(II) atoms. The Ru-Ru distance is 8.6 Å, inter-Ru angles and torsions are 110, 58° respectively. [Symmetry codes: purple is x, y, z ; blue = $i = x-y, x, 2-z$; orange is $y, -x+y, 2-z$].

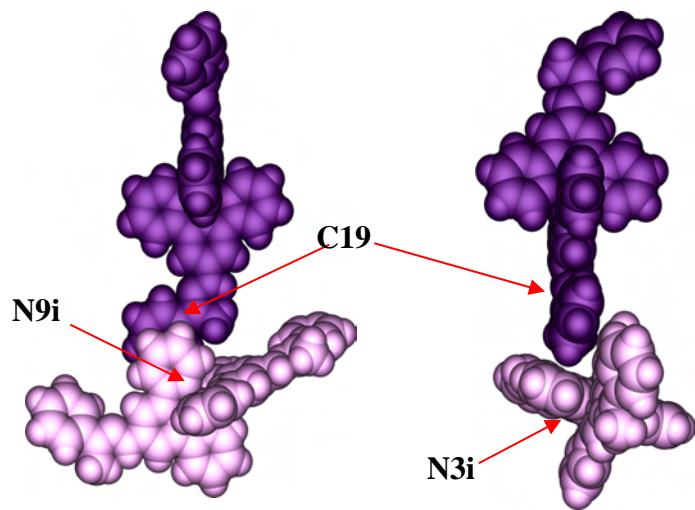


Figure 3-27 Two views of the face-to-face interaction responsible for assembling the hexamers into columns. The distance from the centroid [of the phenyl ring containing C19] to the least-squares-plane [of the pyridyl ring containing N8i] is 3.314 Å. Distances from the least squares plane of the ring containing N3i to H24C24 and H23C23 are 3.048 and 2.866 Å. Symmetry codes: purple is x, y, z; pink = i = x-y, x, 3-z.

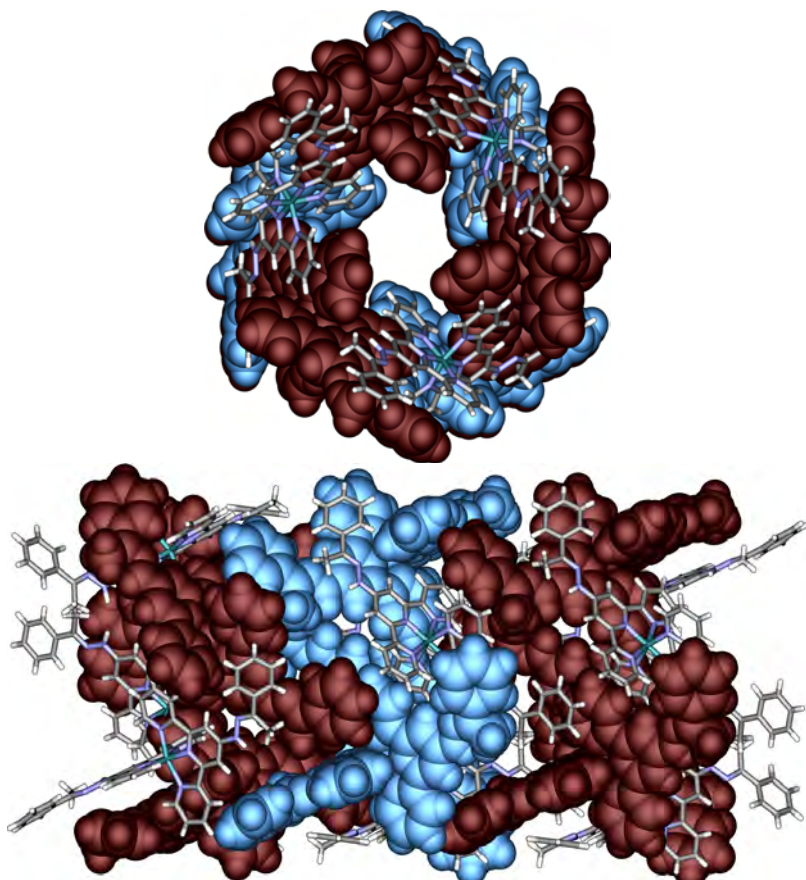


Figure 3-28 A stack of three hexamers viewed along the crystallographic *c*-axis (left) and *a*-axis (right). Within a hexamer, the molecules are represented in alternating CPK and stick forms. Anions and solvent molecules have been omitted.

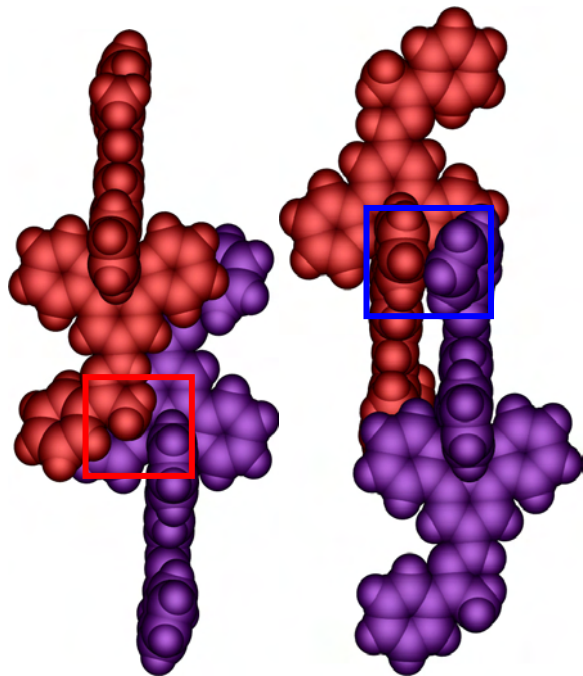


Figure 3-29 Connections between adjacent columns. $C_{Py}-CH_3$ contacts [$C15 \dots H(41C)iC41i = 3.00 \text{ \AA}$, $C41 \dots C15i = 3.485 \text{ \AA}$, and vice versa, i.e.: $C15 \dots C41i$] are indicated with the red box. Weaker $C_{Ph}-C_{Py}$ contacts [$C47-C27i = 3.471 \text{ \AA}$] are indicated with the blue box. Symmetry operators: purple is x, y, z ; red = $i = 1/3 - x, 2/3 - y, 5/3 - z$.

The large unit cell of the overall structure is shown in Figure 3-30. Each column is homochiral (considering the twist of the hexamers), but the overall structure is achiral due to the presence of inversion centres. There is relatively little solvent in the lattice, 0.33 MeCN and two partial occupancy water positions (one of which lies on a special position) to give a total of 0.33 water molecules per complex. The two PF_6^- anions not on special positions are hydrogen bonded to the amino protons, as shown in the Ortep representation in Figure 3-25. As such, these do not appear to play a major role in directing the overall packing arrangement. Interestingly, the PF_6^- ion which lies on the special position (containing atom P3) is not involved in any close contacts, although the presence of isolated, non-hydrogen bonded water molecules (with partial occupancy) hints that the central channels are likely occupied by highly disordered water molecules which could not be located in the difference map.

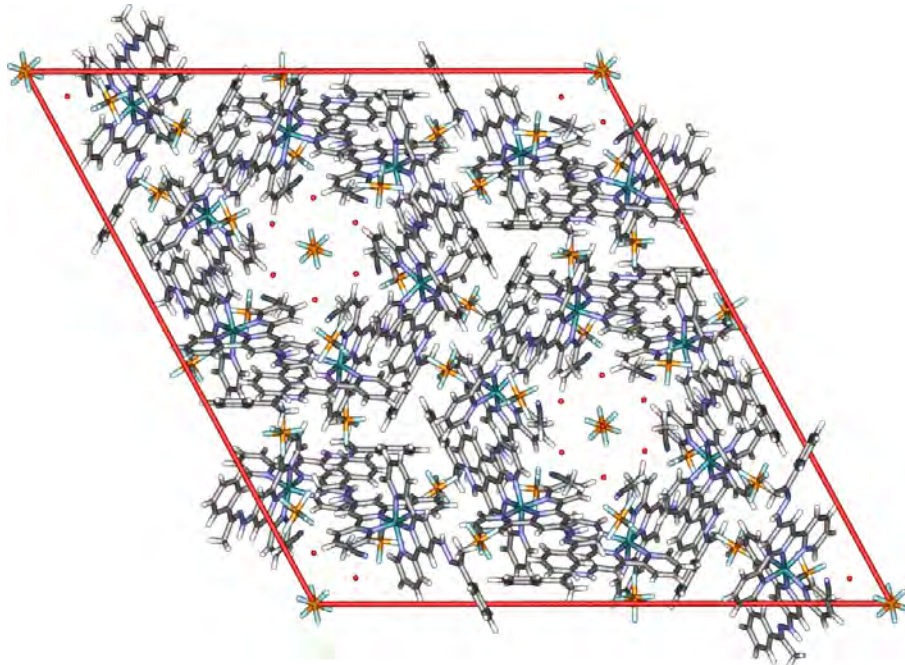


Figure 3-30 The unit cell of $[\text{Ru}(18)_2](\text{PF}_6)_2 \cdot 0.33\text{MeCN} \cdot 0.33\text{H}_2\text{O}$ looking down the c -axis showing channels running through the structure with PF_6^- anions on special positions with 6-fold symmetry.

3.9. Iron(II) and ruthenium(II) complexes of N-Me ligand (20)

Homoleptic iron(II) and ruthenium(II) complexes were prepared using analogous procedures to those discussed earlier for the N-H compounds. As described above for the protonated ligand $[\text{H}_2\mathbf{20}][\text{MeOSO}_3]_2$, the iron(II) and ruthenium(II) complexes exhibit faster tpy-N bond rotation than the analogous N-H derivatives. An example is shown in Figure 3-31 which compares the $^1\text{H-NMR}$ spectrum of the Ru(II) complexes of the N-H and N-Me derivatives **17** and **20** respectively. As can be clearly seen, the H^{A3} and particularly the H^{B3} signals are much sharper for the N-Me derivative at room temperature. Most of the other signals are unaffected by the methylation. These results are consistent with the broadening of the H^{A3} and H^{B3} signals being associated with hydrogen-bond dependent tpy-N bond rotation.

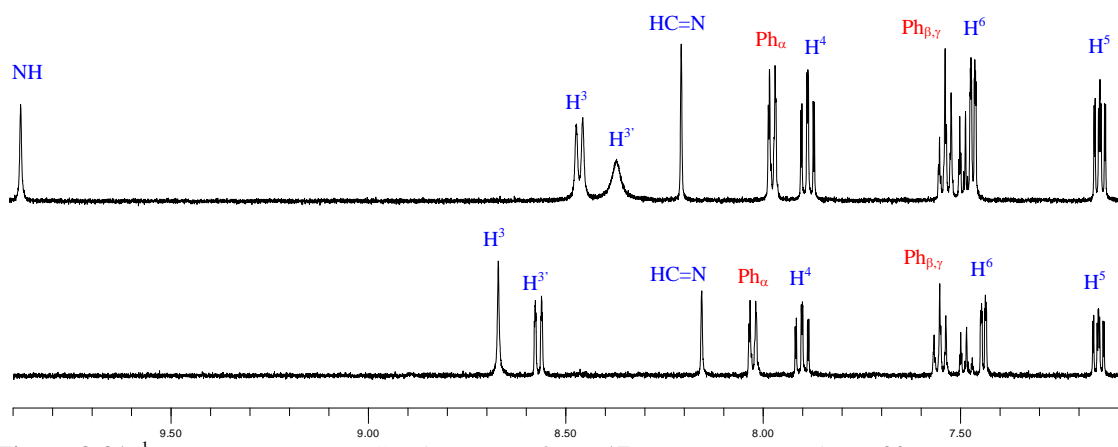


Figure 3-31 ^1H NMR spectra (MeCN-d_3 , 295K) of $[\text{Ru}(17)_2](\text{PF}_6)_2$ (top) and $[\text{Ru}(20)_2](\text{PF}_6)_2$.

The electronic absorption spectrum of $[\text{Ru}(20)_2](\text{PF}_6)_2$ (Figure 3-32) was found to be unaffected by base addition, in agreement with the observed spectral changes for the N-H analogue (see earlier) resulting from deprotonation of one of the amine sites.

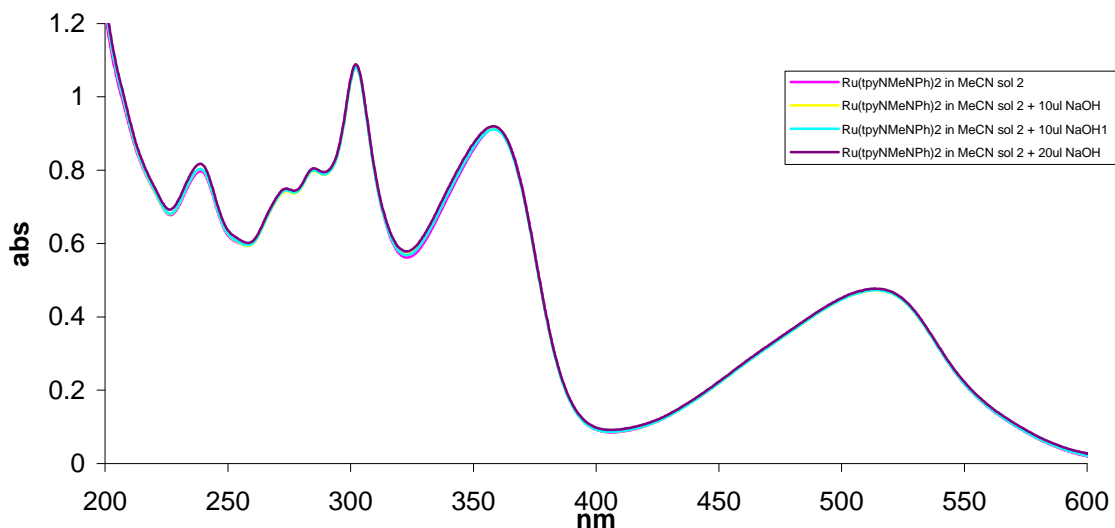


Figure 3-32 The UV-vis (MeCN , $1.53 \times 10^{-5}\text{ mol/L}$, 3mL) spectrum of $[\text{Ru}(20)_2](\text{PF}_6)_2$ with NaOH (0.1 mol/L) addition.

3.9.1. *Electrochemistry of N-Me derivatives $[\text{Fe}(20)_2](\text{PF}_6)_2$ and $[\text{Ru}(20)_2](\text{PF}_6)_2$*

In contrast the N-H derivatives discussed previously, both the $[\text{Fe}(20)_2](\text{PF}_6)_2$ and $[\text{Ru}(20)_2](\text{PF}_6)_2$ presented no problems with electrochemical measurements. This is also good evidence that the acidity of the N-H proton in previous cases was the source of electrochemical difficulties. The cyclic voltammetry (CV) and differential pulse

voltammetry (DPV) plots of $[\text{Fe(20)}_2](\text{PF}_6)_2$ are shown in Figure 3-46 and Figure 3-33 respectively [those of $[\text{Ru(20)}_2](\text{PF}_6)_2$ are found in experimental section]. Each show four ligand reductions and two ligand oxidations in addition to the $\text{M}^{\text{II}/\text{III}}$ couple. The metal $\text{M}^{\text{II}/\text{III}}$ oxidations ($\text{Fe}^{\text{II}/\text{III}} 0.42 \text{ V}$, $\text{Ru}^{\text{II}/\text{III}}: +0.51 \text{ V}$) are considerably shifted to lower potential compared to the parent $\text{M}(\text{tpy})_2$ complexes ($\text{Fe} +0.74 \text{ V}^{17}$; $\text{Ru} +0.88 \text{ V}^{260}$), although closer to the related complexes of 4'-dimethyl-amino-2,2':6',2"-terpyridine ($\text{Fe}^{\text{II}/\text{III}} +0.28 \text{ V}^{261}$; $\text{Ru}^{\text{II}/\text{III}} +0.42 \text{ V}^{82}$).

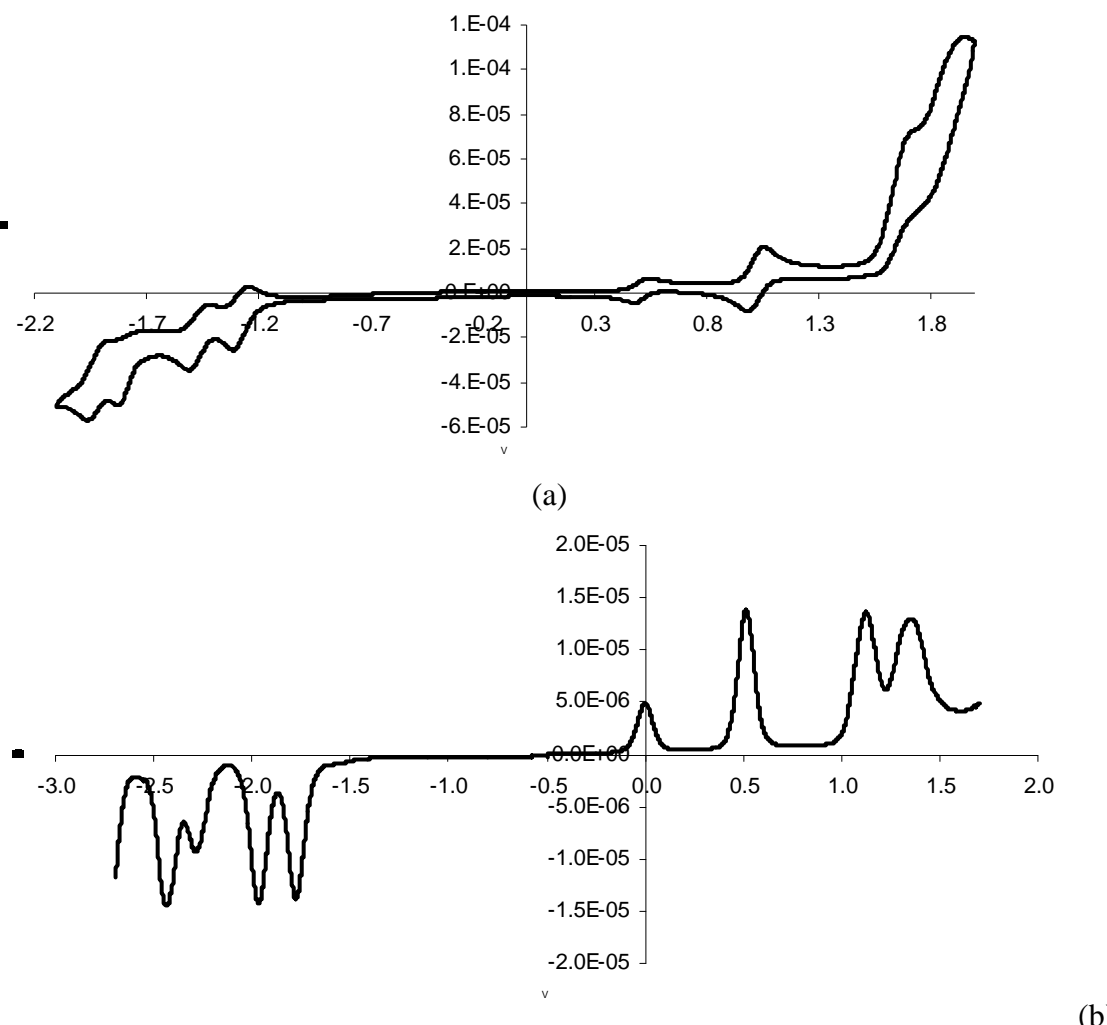


Figure 3-33 Electrochemical measurements of $[\text{Ru(20)}_2](\text{PF}_6)_2$ in MeCN with a glassy carbon electrode, a silver reference wire and TBAPF₆ as the supporting electrolyte. (a) CV; (b) DPV. Ru(II/III): 0.51 (rev), ligand oxidations: 1.12 (irrev), 1.36 (q rev), ligand reductions: -1.79 (rev), -1.99 (rev), -2.28 (irrev), -2.44 (irrev).

3.9.2. X-Ray crystal structures

Slow evaporation of a MeCN-H₂O-KNO_{3(aq)} solution of [Ru(**20**)₂](PF₆)₂ gave large, block-like crystals of [Ru(**20**)₂](NO₃)₂.MeCN.8H₂O and the asymmetric unit is shown in Figure 3-34. The ligands are almost planar and orthogonal [angle between least squares planes of rings contains N1, N2, N3 with N4, N5, N6 is 88.13(4) °]. The most significant feature of the packing arrangement is the absence of tpy-tpy embraces. The complexes are arranged in pairs (Figure 3-35) with the closest π-π interactions between hydrazone C=N-N-Me moieties on adjacent molecules with distances from [N7-C401i, 3.564(4), C32-N9i 3.435(4), C37-C25i 3.495(5), C38-C23i 3.434(4), C38-C24i 3.449(5), i = ½ + x, 1½ – y, ½ + z]. These are shown in Figure 3-35 between complexes of different colours. Further π-π stacking between phenyl rings and terminal pyridyl rings (shown in the figure in boxes) complete the packing [distance from centroid of the ring containing N4 and the least-squares planes of the ring containing C33i is 3.329 Å, i = - 1/2 + x, 1.5 – y, - ½ + z]. These pairs of π-π stacked complexes are surrounded by a hydrogen-bonded network of anions and water molecules, preventing π-π interactions in the orthogonal direction

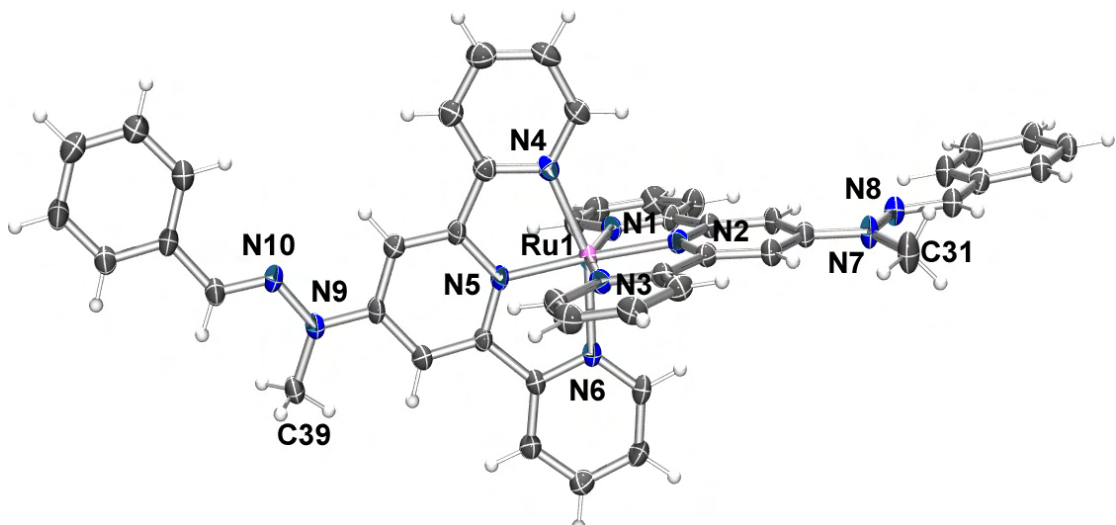


Figure 3-34 An ORTEP representation of [Ru(**20**)₂](NO₃)₂.MeCN.8H₂O. Ellipsoids drawn at 50% probability. Space group P21/n. Selected bond lengths and angles: Ru1-N1 2.072(2); Ru1-N2 1.994(2); Ru1-N3 2.064(2); Ru1-N4 2.077(2); Ru1-N5 1.978(2); Ru1-N6 2.071(2); N7-C8 1.391(4); N7-C31 1.458(5); N7-N8 1.372(4); N9-C23 1.377(4); N9-C39 1.463(4); N9-N10 1.369(3) Å. N1-Ru1-N2 78.53(9); N1-Ru1-N3 157.73(9); N2-Ru1-N3 79.20(9); N4-Ru1-N5 78.36(9); N4-Ru1-N6 157.66(9); N5-Ru1-N6 79.30(9)°.

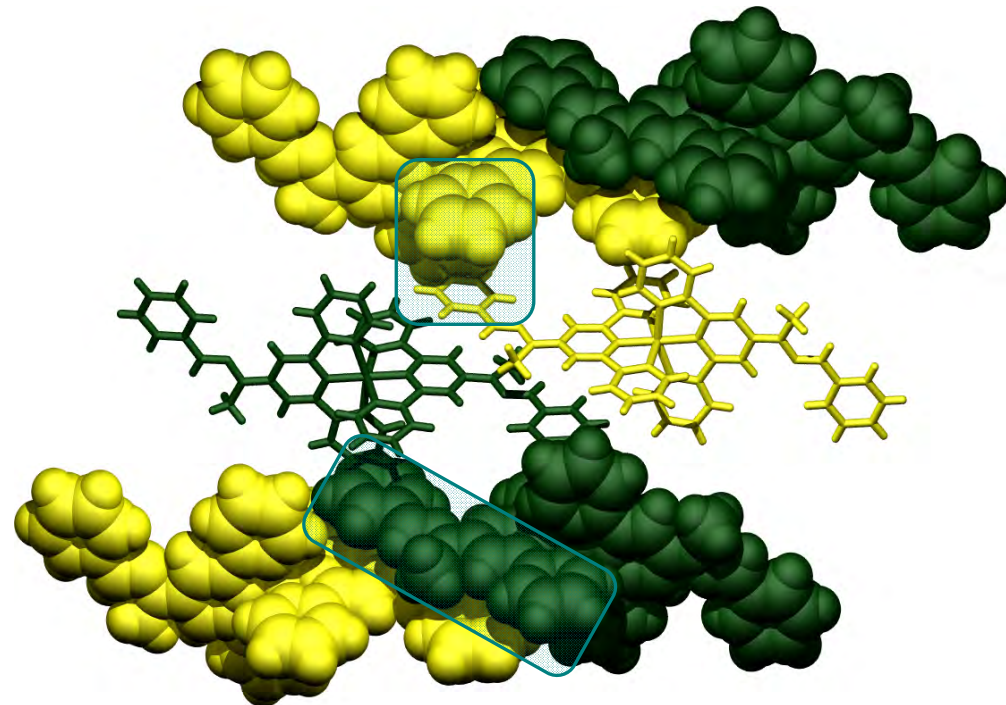


Figure 3-35 X-Ray crystal structure of $[\text{Ru}(20)_2](\text{NO}_3)_2 \cdot \text{MeCN} \cdot 8\text{H}_2\text{O}$, solvent and anions omitted. Regions of π - π stacking are marked with boxes.

Slow evaporation of a MeCN-H₂O solution of $[\text{Ru}(20)_2](\text{PF}_6)_2$ gave single crystals of $[\text{Ru}(20)_2](\text{PF}_6)_2 \cdot 2\text{MeCN}$ suitable for X-ray crystal structure determination (Figure 3-36a). Interestingly, it crystallised in the same space group at the nitrate salt ($P2_1/n$), despite a different packing arrangement..

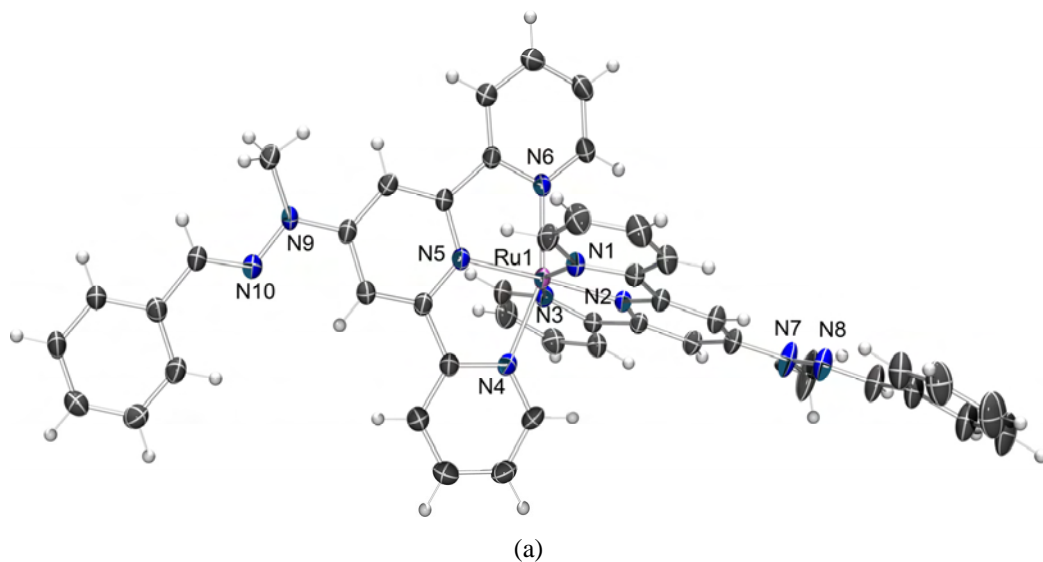


Figure 3-36 (a) The molecular structure of $[\text{Ru}(20)_2]^{2+}$ in $[\text{Ru}(20)_2](\text{PF}_6)_2 \cdot 2\text{MeCN}$ (anions and solvent omitted). Ellipsoids drawn at 50% probability. Space group $P2_1/n$. Selected bond lengths and angles: $\text{Ru1-N1 } 2.079(2)$; $\text{Ru1-N2 } 1.983(2)$; $\text{Ru1-N3 } 2.069(2)$; $\text{Ru1-N4 } 2.087(2)$; $\text{Ru1-N5 } 1.982(2)$; $\text{Ru1-N6 } 2.074(2)$; $\text{N7-C8 } 1.383(4)$; $\text{N7-N8 } 1.370(4)$; $\text{N7-C31 } 1.455(5)$; $\text{N9-C23 } 1.382(4)$; $\text{N9-N10 } 1.370(4)$; $\text{N9-C39 } 1.451(4)$. $\text{N1-Ru1-N2 } 78.71(9)$; $\text{N1-Ru1-N3 } 157.02(9)$; $\text{N2-Ru1-N3 } 78.46(8)$; $\text{N4-Ru1-N5 } 78.50(10)$; $\text{N4-Ru1-N6 } 156.60(9)$; $\text{N5-Ru1-N6 } 78.44(10)$; $\text{C8-N7-C31 } 123.2(3)$; $\text{C23-N9-C39 } 123.0(2)^\circ$.

A comparison of this structure with that of the NH analogue ($[\text{Ru(17)}_2](\text{PF}_6)_4 \cdot 3\text{MeCN} \cdot 3\text{H}_2\text{O}$) is useful. Firstly, in the absence of an hydrogen bond donor (i.e.: NH), no water molecules were included in the crystal lattice, again suggesting the importance of hydrogen bonding in the previous structures where hydrogen bond acceptors are almost always present. Also notable is the significant deviation from ideal orthogonal orientation of the tpy ligands [77.7(1) $^\circ$ between least squares planes] compared to both the nitrate salt discussed above (88.1(1) $^\circ$) and the analogous NH complex $[\text{Ru(17)}_2](\text{PF}_6)_2$ which are both nearly ideal [88.5(1) $^\circ$]. Additional distortions within the tpy moieties [angles between least-squares planes of terminal pyridyl rings containing N1 and N3, N6 and N4 are 9.50(15) $^\circ$ and 11.14(14) $^\circ$ respectively]. Both methyl groups are twisted out of the plane of the central pyridyl ring to avoid unfavourable Me-CH interactions (torsion angles C9-C8-N7-C31 5.69 $^\circ$, C24-C23-N9-C39 is -15.97 $^\circ$). This collection of distortions results in an unusual packing arrangement, shown in Figure 3-37. Similar to the nitrate salt discussed above, the complexes are arranged with close π - π stacking between hydrazone moieties, shown in red boxes in the figure. However, unlike in the previous structures, close edge-to-face phenyl contacts between the pendant phenyl rings (C36-H361... C46i = 2.83 Å, C36-H361...C45i = 2.95 Å, i = - $\frac{1}{2}$ + x, $\frac{1}{2}$ - y, - $\frac{1}{2}$ + z) play a major role in crystal packing, dominating over traditional tpy-tpy embraces or face-to-face stacking. Chains of complexes with very poor π - π stacking between the tpy regions are formed (shown in the figure in blue dotted boxes). For example, the angle between the least-squares planes of rings containing N1 and N3i is 43.2 $^\circ$ (i = - $\frac{1}{2}$ + x, $\frac{1}{2}$ - y, - $\frac{1}{2}$ + z), compared to the equivalent angle in the NH derivative of 5.70 $^\circ$ ($[\text{Ru(17)}_2](\text{PF}_6)_4 \cdot 3\text{MeCN} \cdot 3\text{H}_2\text{O}$, angle between least-squares planes of rings containing N6 and N8i (i = -1+x, y, z)].

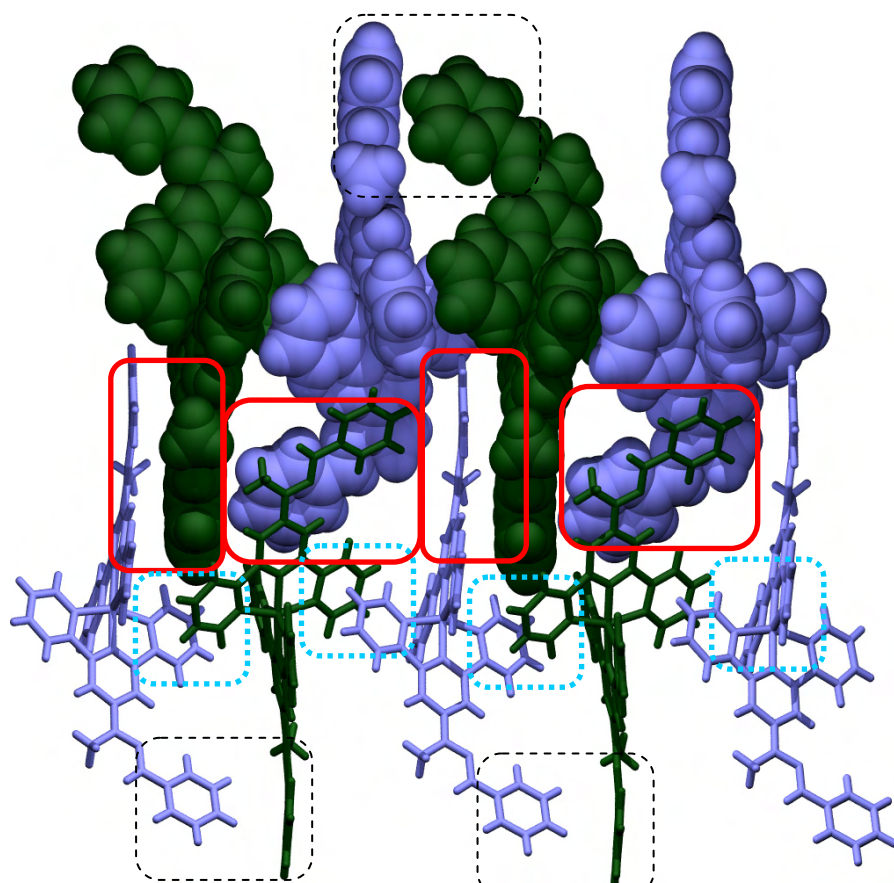


Figure 3-37 Packing arrangement of $[\text{Ru}(20)_2]^{2+}$ in $[\text{Ru}(20)_2](\text{PF}_6)_2 \cdot 2\text{MeCN}$ (anions and solvent omitted). Major π - π stacking between hydrazone moieties are shown in red boxes. Edge-to-face interactions involving the pendant phenyl rings are shown with black hashed boxes. Region of poor π - π stacking between tpy ligands is shown in blue dotted boxes.

Conclusions from complex crystal structures

The first observation from the structures presented here is the tpy-tpy planes are almost perfectly orthogonal ($87^\circ - 88^\circ$) in all cases, except for the *N*-methyl derivate $[\text{Ru}(20)_2](\text{PF}_6)_2$. However, the ligands are perhaps more flexible than first expected; the angles between the terminal pyridyl rings on one tpy ligand were found to often deviate from co-planarity. All other bond angles and lengths are as expected.

Structure	Angles between least squares planes of terminal rings within each tpy ligand (°)
[Ru(17) ₂](PF ₆) ₂ ·1.5MeCN·1.5H ₂ O	14.0, 5.7
[[Fe(17) ₂](PF ₆) ₂ ·1.5MeCN·1.5H ₂ O	11.7, 5.5
[Fe(21) ₂](PF ₆) ₂ ·0.75MeCN·0.33H ₂ O	5.0, 0.8
[Fe(23) ₂](PF ₆) ₂	3.7, 3.4
[Fe(18) ₂](PF ₆) ₂ ·0.33MeCN·0.33H ₂ O	8.0, 8.3
[Ru(18) ₂](PF ₆) ₂ ·0.33MeCN·0.33H ₂ O	8.5, 8.5
[Ru(20) ₂](PF ₆) ₂ ·2MeCN	9.5, 11.1
Ru(20) ₂ (NO ₃) ₂ ·MeCN·8H ₂ O	4.9, 4.8

In terms of crystal packing, a range of different packing arrangements were observed, with no significant preference for one type of packing over another. Although π - π stacking plays a very significant role in all of the structures, ‘tpy embraces’ are frequently not observed. This leads to the conclusion that while the ‘tpy embrace’ is often a common feature of simple tpy complexes, it does not dominate in structures where larger ligands must be accommodated. Furthermore, it is shown here that given the opportunity to participate in tpy embraces, the complexes often adopted alternative aryl-aryl interactions (which potentially lack the additional stability of the common tpy-tpy embraces). Therefore, it appears likely that interactions with anions and solvent, which appear weak and poorly directional in all cases, may play very significant roles in terming crystal packing.

3.10. Hydrazone bridges

The ditopic ligands **29** and **30** were prepared by reaction of two equivalents of 4'-hydrazino-2,2':6',2"-terpyridine with terephthalaldehyde and 2,2-butandione respectively, in the presence of an acid catalyst, as described in Chapter 2. In the case of **29** the resulting solid has very poor solubility in all common organic solvents, including DMSO. ¹H-NMR (Figure 3-41) and elemental analysis confirmed the tetraprotonation state of the ligand, [H₄**29**][EtOSO₃]₄. The ¹H NMR signals for the H^{A3} and H^{B3} are characteristically broad (almost completely into the baseline at 295K), although at high temperature (360K) the signals become sharp and their assignment straightforward.

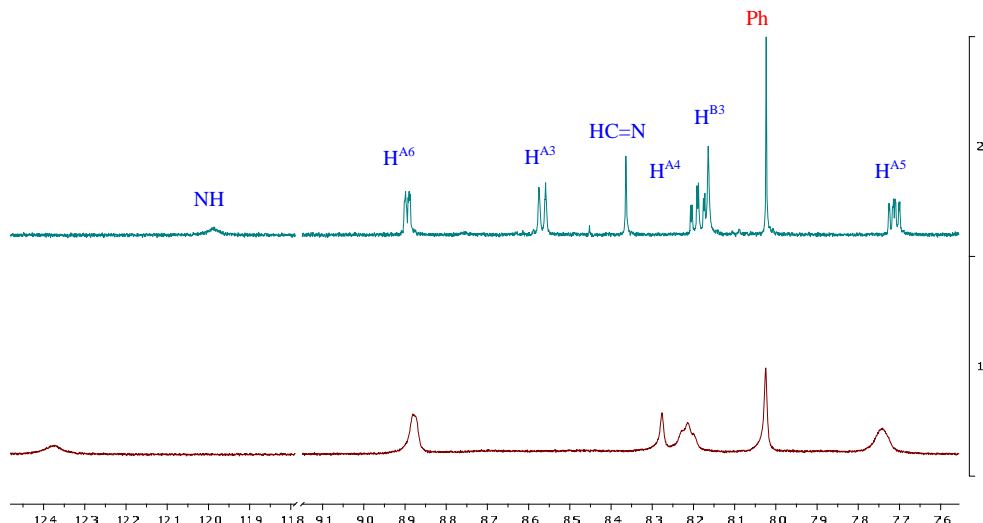
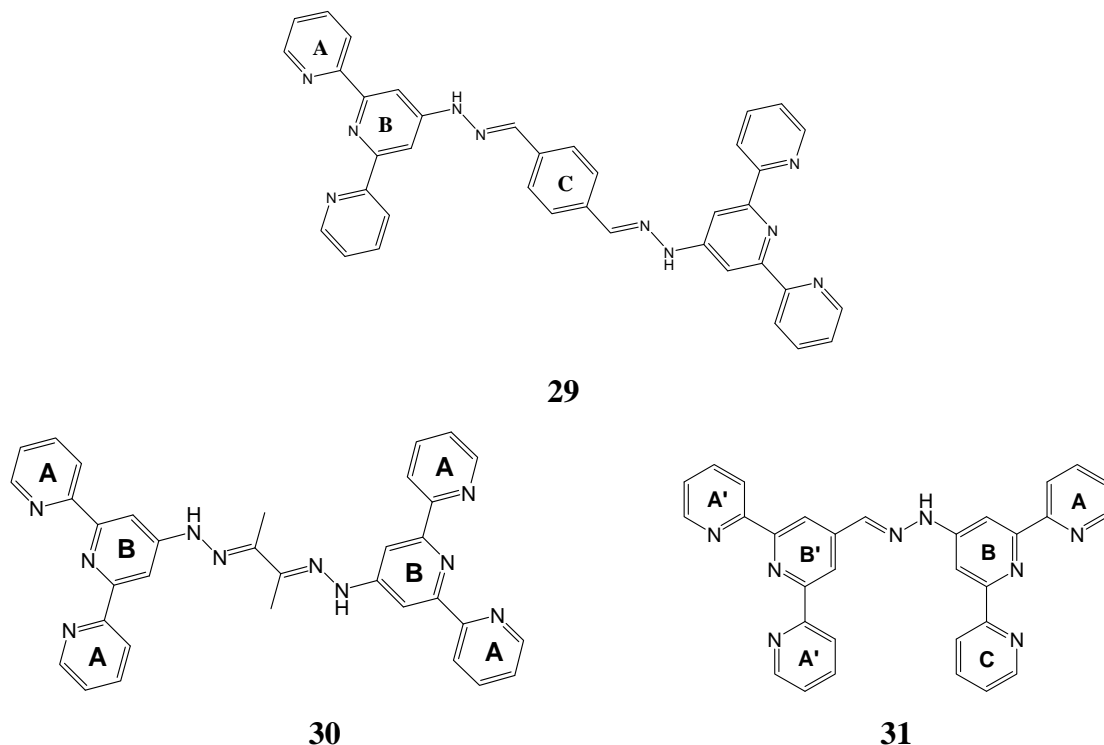


Figure 3-38 ^1H NMR spectrum ($\text{DMSO}-d_6$) of $[\text{H}_4\mathbf{29}](\text{EtOSO}_3)_4$ at 295K (bottom) and 360K (top).

Compound **30** was considerably more soluble, and isolation of the neutral ligand was possible by dissolving in H_2O , treating with $\text{KCO}_{3(\text{aq})}$, extracting into DCM and removal of the solvent. The ^1H NMR assignments were straightforward (Figure 3-39).

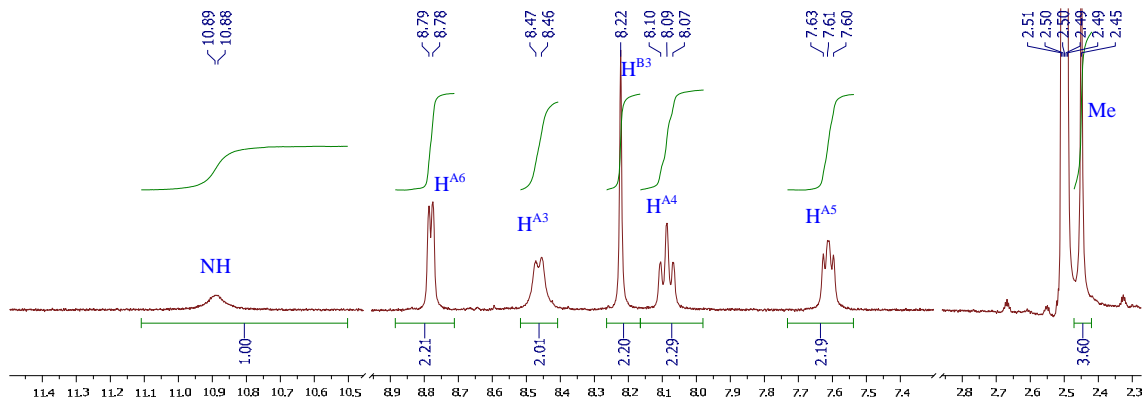


Figure 3-39 ^1H -NMR spectrum (500 MHz, $\text{DMSO}-d_6$, 295K) of neutral ligand **30**.

Ligand **31** was prepared by reaction of 4'-hydrazino-2,2':6',2"-terpyridine with 4'-formyl-2,2':6',2"-terpyridine²⁶² in the presence of an acid catalyst. This ligand was isolated as a neutral compound by treatment of the resulting solid with aqueous K_2CO_3 , extraction into DCM and column chromatography. The ^1H NMR spectrum (Figure 3-40) shows a 1:1 ratio of tpy signals, with pairs of signals for H^{A6} , H^{A5} , H^{A4} , H^{A3} and the only major difference being the H^{B3} signals. A sharp H^{B3} signal was observed for the tpy without the 4'-NH and a characteristically broad signal for H^{B3} for the tpy with the hydrazone substituent.

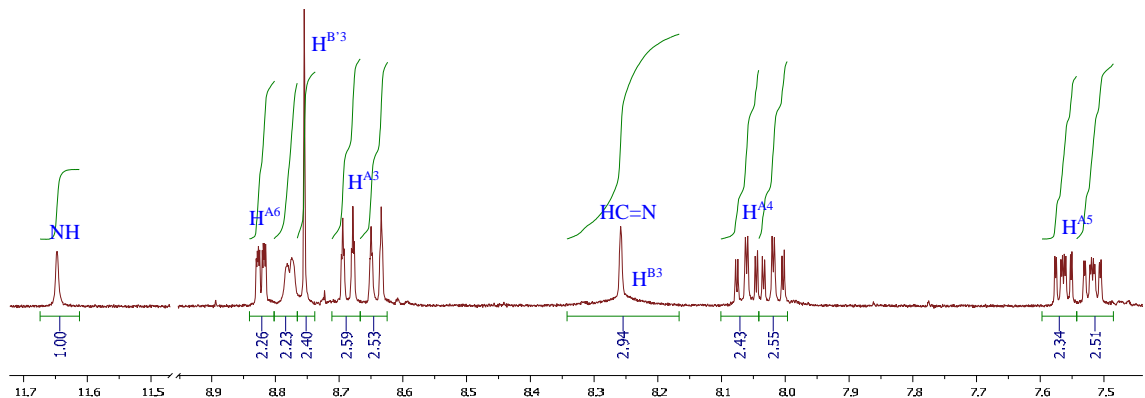
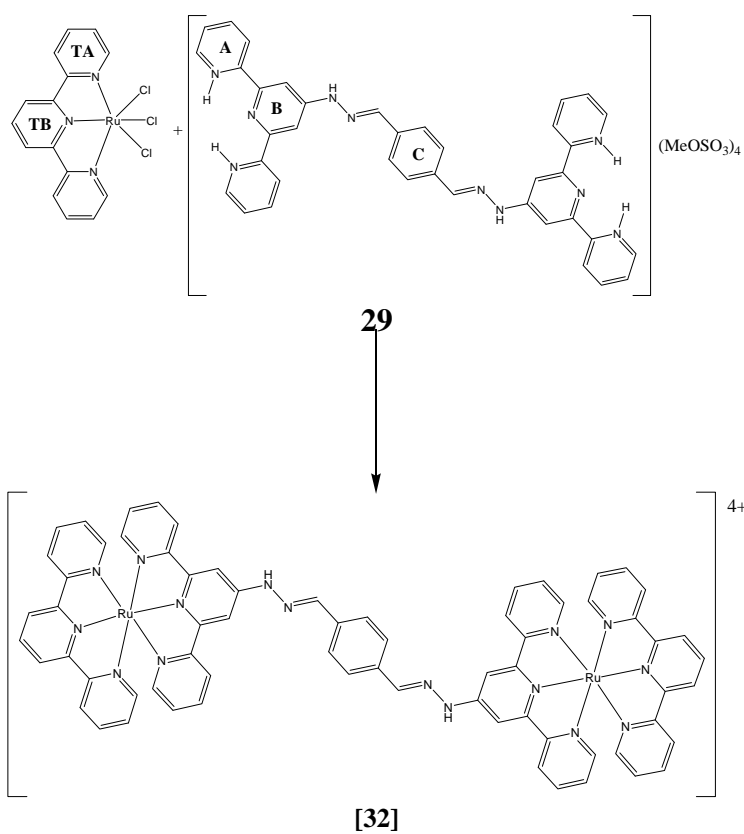


Figure 3-40 ^1H -NMR spectrum (500 MHz, $\text{DMSO}-d_6$, 295K) of neutral ligand **31**.

Combining compound **31** with $\text{FeCl}_2 \cdot 4\text{H}_2\text{O}$ resulted in the formation of intensively blue solution which after anion exchange with NH_4PF_6 and reducing the solvent volume gave a dark blue-purple solid which was soluble in ethanol and acetonitrile. ^1H -NMR showed only very weak and poorly resolved signals, suggesting the formation of a polymer in solution. Compound **30** behaved similarly, although the resulting products were less soluble. These were not investigated further.



Scheme 5 Synthesis of $[32](\text{PF}_6)_4$

Combining $[\text{H}_4\mathbf{29}][\text{EtOSO}_3]_4$ with one equivalent of $\text{FeCl}_2 \cdot 4\text{H}_2\text{O}$ resulted in the formation of very dark green-blue insoluble (likely polymeric) material. However, reaction of two equivalents of $\text{Ru}(\text{tpy})\text{Cl}_3$ with ligand $[\text{H}_4\mathbf{29}][\text{EtOSO}_3]_4$ in the presence of *N*-ethylmorpholine as a reducing agent, followed by anion exchange with NH_4PF_6 results in the formation of the complex $[\mathbf{32}](\text{PF}_6)_4$. The crude product was purified by column chromatography to give $[\mathbf{32}](\text{PF}_6)_4$ in a yield of 87%. $^1\text{H-NMR}$ spectroscopy (Figure 3-41) confirms the structure of a symmetrical dinuclear complex with a single, sharp singlet for the central phenyl ring at 8.11 ppm. As described for the complexes previously, the $\text{H}^{\text{A}3}$ and $\text{H}^{\text{B}3}$ are broad due to slow tpy-NH rotation (again, notably faster than for the protonated ligand alone) although all other signals are sharp and well resolved.

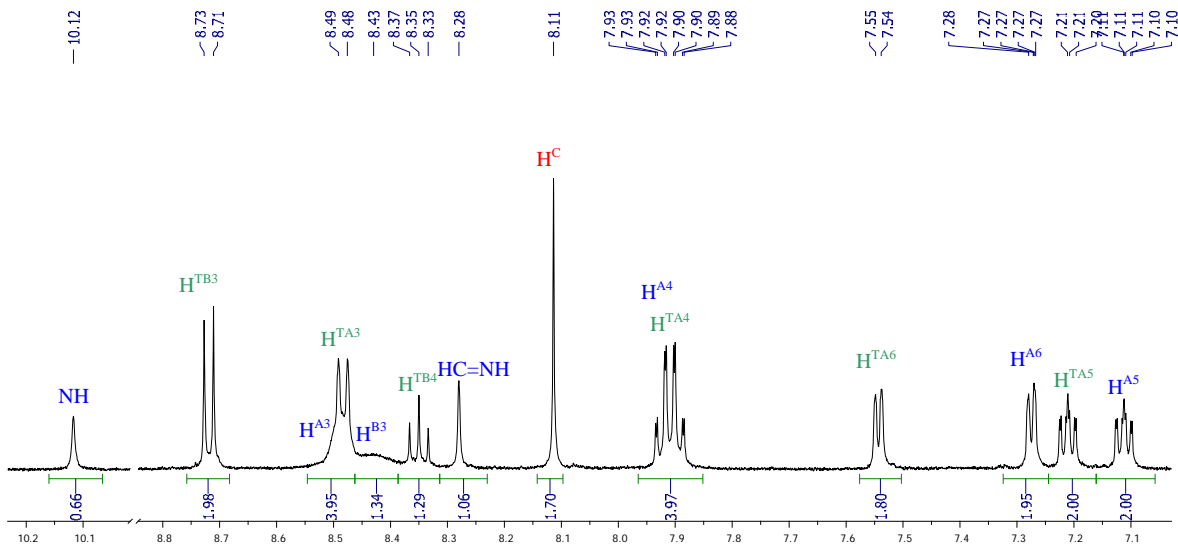


Figure 3-41 ^1H NMR spectrum (CD_3CN) of $[\mathbf{32}](\text{PF}_6)_4$

The UV-visible absorption spectrum of $[\mathbf{32}](\text{PF}_6)_4$ (Figure 3-42) exhibits an MLCT band centred at 501 nm, slightly blue shifted from the mono-nuclear $[\text{Ru}(\mathbf{17})_2](\text{PF}_6)_2$ (510 nm). The intensity of the absorption, corrected for the number of metal centres, is essentially unchanged from $[\text{Ru}(\mathbf{17})_2](\text{PF}_6)_2$ ($\varepsilon / 1000 = 28.0$ and 30.6 respectively). Interestingly, a new band at 391 nm is observed, somewhat reminiscent of the band observed at 409 nm for $[\text{Ru}(\mathbf{17})_2](\text{PF}_6)_2$ on deprotonation.

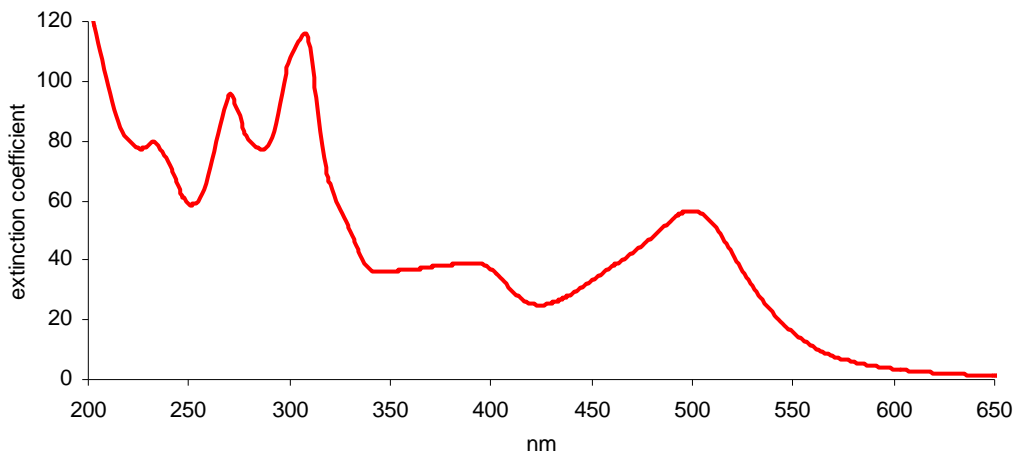


Figure 3-42 UV-visible spectrum of $[\mathbf{32}](\text{PF}_6)_4$ in MeCN. $\lambda_{\text{max}} / \text{nm}$ ($\varepsilon / 10^3 \text{dm}^3 \text{mol}^{-1} \text{cm}^{-1}$) 232 (78), 271 (95.3), 307 (115.0), 391 (38.8), 501 (55.9).

Slow evaporation of an MeCN solution of the complex gave X-ray quality crystals of $[\mathbf{32}](\text{PF}_6)_4 \cdot 8\text{MeCN}$, the molecular structure is shown in Figure 3-43. The structure has high symmetry with ordered solvent molecules and anions to give an asymmetric unit of half a cation of **32**.

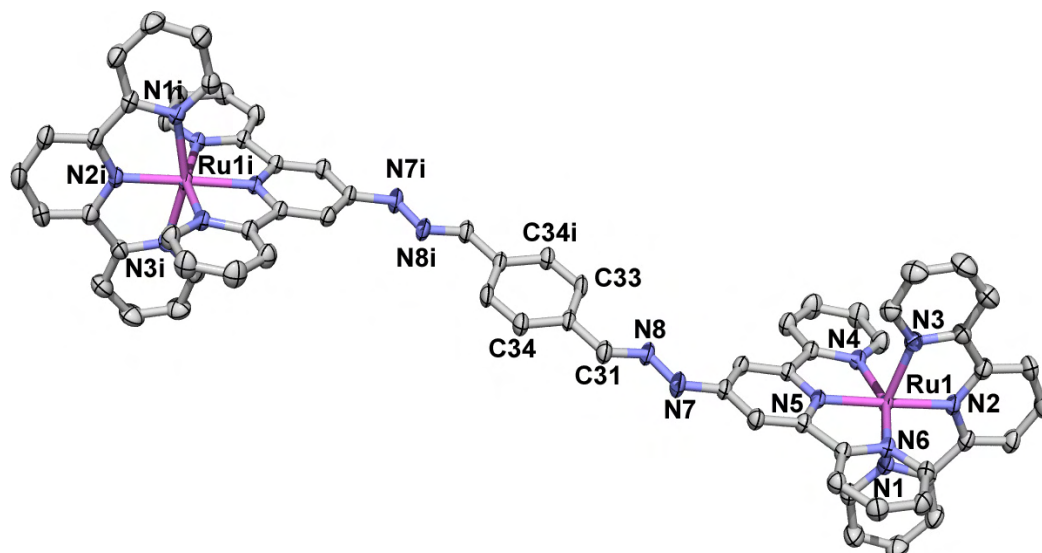


Figure 3-43 X-ray crystal structure of the cation $[32](\text{PF}_6)_4 \cdot 8\text{MeCN}$. Solvent and anions are omitted for clarity. Space group P-1. Selected bond lengths and angles: Ru1-N1 2.061(2); Ru1-N2 1.970(2); Ru1-N3 2.062(2); Ru1-N4 2.061(2); Ru1-N5 1.982(2); Ru1-N6 2.071(2); N7-N8 1.363(3); N7-C23 1.367(3). N1-Ru1-N2 78.99(8); N1-Ru1-N3 158.16(8); N2-Ru1-N3 79.23(8); N4-Ru1-N5 78.63(7); N4-Ru1-N6 157.53(7); N5-Ru1-N6 78.93(7) $^\circ$. Symmetry code: i = -x, -y, 1-z

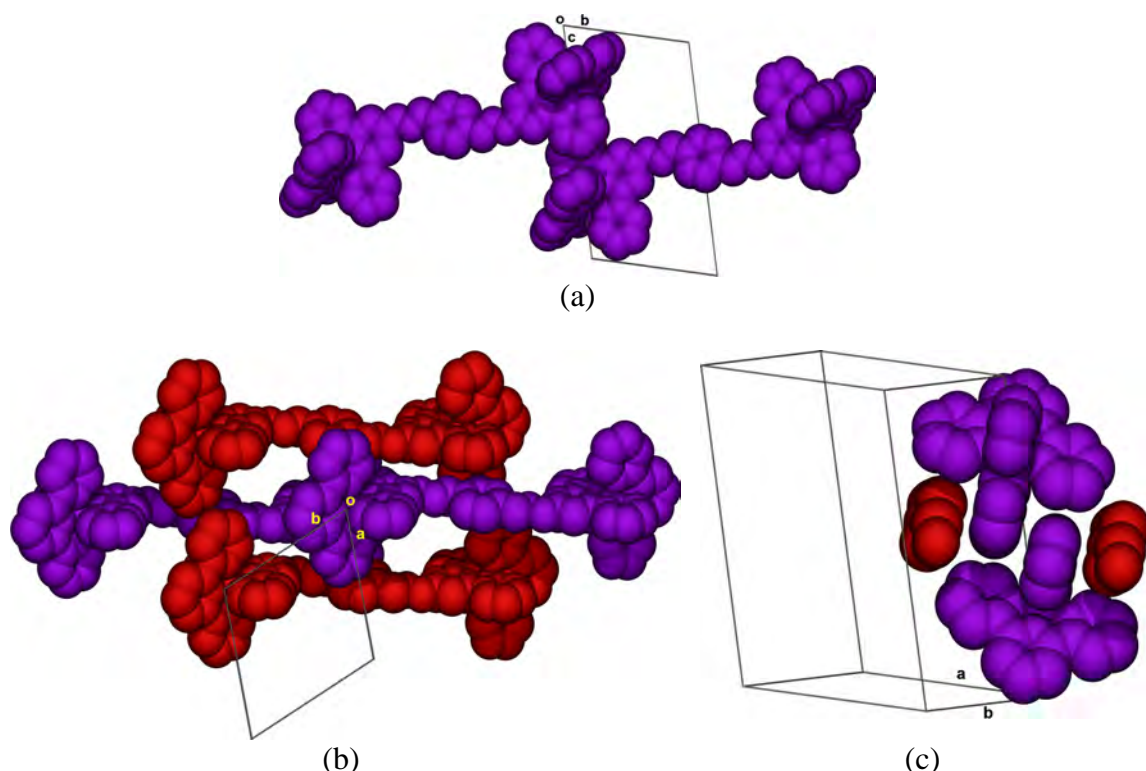


Figure 3-44 Crystal packing of $[32](\text{PF}_6)_4 \cdot 8\text{MeCN}$, solvent, anions and hydrogens omitted. (a) A tpy-embrace pair, looking down the crystallographic *a*-axis. Face-to-face stacking of ring containing N6-N6i distance between least squares planes 3.604 Å; edge-to-face contacts C1...H281iC28i 2.793, C2...H281iC28i 2.892 Å. (b) Looking down the *c*-axis showing weak overlap between rings containing N1-N3ii (red-red), C3-C13ii 3.431 Å. (c) Additional phenyl-pyridyl interactions (red-purple). Phenyl-pyridyl contacts: C34-C28iii 3.515 Å. Phenyl-imine contacts: C27-C31iii 3.515 Å, pyridyl-imine: C24-N7iii 3.575 Å. Symmetry codes: i = -x, 2-y, 1-z; ii = 1+x, y, z; iii = -x, 1-y, 1-z.

The packing of $[32]^{4+}$ in $[32](\text{PF}_6)_4 \cdot 8\text{MeCN}$ is shown in Figure 3-44. The complexes pack together with tpy embraces with rings containing N6/N6i π -stacked (separation of least squares planes is 3.604 Å, Figure 3-44a, $i = -x, 2-y, 1-z$), with weak interactions between rings containing N1 and N3 [distance from the centroid of ring containing N1 to the plane containing N3ii is 2.590 Å although the overlap is poor, as shown Figure 3-44b, ($ii = 1+x, y, z$)]. Additional π -interactions involving the central phenyl ring (Figure 3-44c) complete the packing to form two dimensional sheets (Figure 3-45) separated by MeCN molecules and PF_6^- anions.

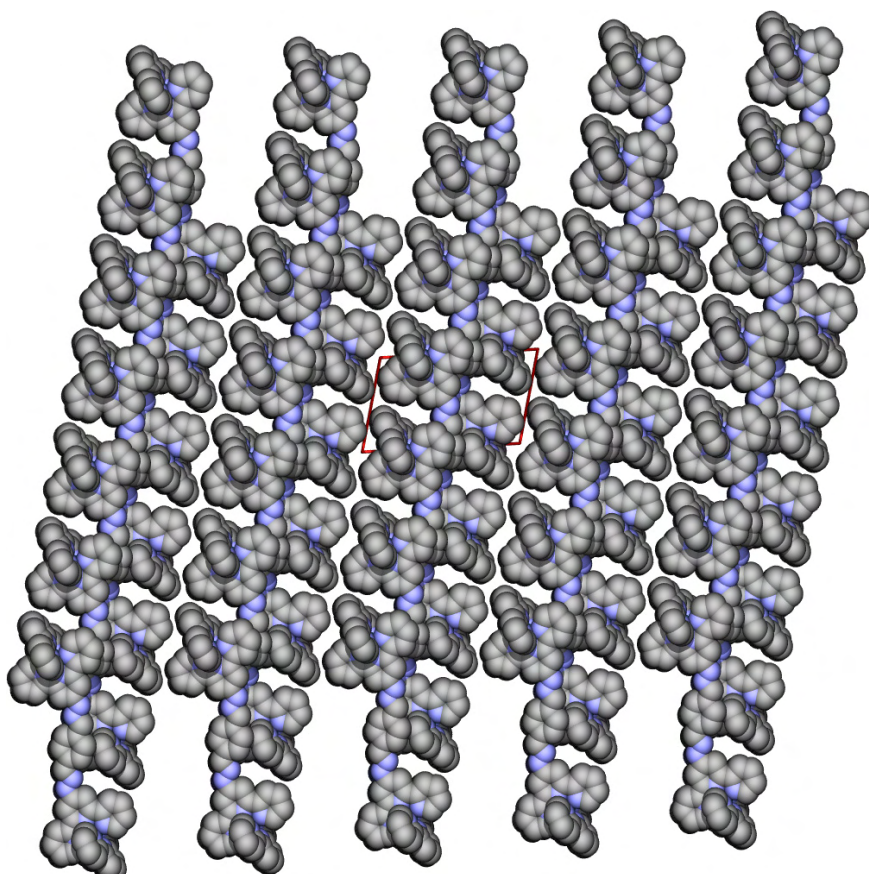


Figure 3-45 Sheets of complexes of $[32]^{4+}$ in $[32](\text{PF}_6)_4 \cdot 8\text{MeCN}$ viewed down the a -axis. Solvent, anions and hydrogens omitted.

3.11. Experimental

Synthesis of Iron(II) complexes

Iron(II) complexes were prepared using standard methods.²⁶³ One equivalents of $\text{FeCl}_2 \cdot 4\text{H}_2\text{O}$ was added to two equivalents of L, $[\text{HL}] \text{BF}_4^-$ or $[\text{H}_2\text{L}] (\text{MeOSO}_3)_2$ in methanol or ethanol. A deep purple colour resulted instantly in most cases, depending

on the solubility of L. The solution was stirred at room temperature for 1 hour and excess aqueous NH_4PF_6 was added to precipitate the desired product as $[\text{Fe}(\text{L}_2)](\text{PF}_6)_2$. This was collected on Celite and washed well with water, ethanol and ether. The residue was redissolved in acetonitrile/water and the acetonitrile was removed under reduced pressure. The resulting precipitate was collected and washed with water, ethanol and ether. If required, the complexes were further purified using a short Al_2O_3 column ($\text{MeCN:H}_2\text{O:saturated KNO}_3\text{(aq)}$ 7:7:2). All reactions were performed using the same volumes and concentrations as the typical procedure outlined below.

Representative procedure:

$[\text{H}_2\textbf{17}](\text{MeOSO}_3)_2$ (0.50g, 0.87 mmol) and $\text{FeCl}_2 \cdot 4\text{H}_2\text{O}$ (0.085g, 0.43 mmol) were dissolved in MeOH (50 mL) and stirred at room temperature for 1 hr. Excess aqueous NH_4PF_6 was added to the deep purple solution to form a microcrystalline precipitate which was collected on Celite and washed well with water (100mL), EtOH (20mL) and diethyl ether (10mL). The residue was re-dissolved in MeCN (100mL) and water (20mL) was added to the solution. The volume was reduced to ~20mL and the solution cooled to form fine purple crystals which were collected. $[\text{Fe}(\textbf{17})_2](\text{PF}_6)_2$ (0.35g, 0.33 mmol, 77%).

Synthesis of Ruthenium(II) complexes

Ruthenium(II) complexes were prepared by several methods:

- i) “ $\text{RuCl}_3 \cdot 3\text{H}_2\text{O}$ ” was reacted with one equivalent of L and refluxed for 2 hours. The resulting brown solid (RuLCl_3) was collected, washed with methanol and used in the next step without further analysis. One equivalent of L was added to a suspension of RuLCl_3 in methanol with a few drops of *N*-ethylmorpholine. The mixture was refluxed for 3 hours and filtered (hot) through Celite. Excess aqueous NH_4PF_6 was added to the deep red filtrate to give $[\text{RuL}_2](\text{PF}_6)_2$ as a red microcrystalline solid which was collected, washed with water, ethanol and ether. If required, the product was purified by column chromatography (silica, $\text{MeCN:H}_2\text{O:saturated KNO}_3\text{(aq)}$ 7:7:2).
- ii) One equivalent of “ $\text{RuCl}_3 \cdot 3\text{H}_2\text{O}$ ” and two of L were added to a small volume (~10mL) of ethylene glycol. The suspension was irradiated in a domestic microwave oven (600W) for 3-5 minutes. The deep red solution was added to excess aqueous NH_4PF_6 (volume of water at least 5 times greater than the volume of ethylene glycol

used) to give a red precipitate which was collected and washed well with water, ethanol and ether.

iii) $\text{Ru}(\text{DMSO})_4\text{Cl}_2$ ²⁶⁴ and two equivalents of L were refluxed in methanol for 4 hours to give a deep red solution. After filtering through Celite, excess NH_4PF_6 was added to give $[\text{Ru}(\text{L})_2](\text{PF}_6)_2$. Column chromatography was generally not required. Alternatively, this procedure could be conducted more quickly in a domestic microwave (see below)

Representative procedure:

Ligand **17** (0.050g, 0.14 mmol) and $\text{Ru}(\text{DMSO})_4\text{Cl}_2$ (0.019g, 0.071 mmol) were suspended in ethylene glycol (10mL) and heated in a domestic microwave (800W, 8 min) to give a deep red solution. The solution was cooled to room temperature and poured into excess aqueous NH_4PF_6 (150mL) to give an immediate orange-red precipitate which was collected on Celite and washed well with water (200mL), followed by ethanol (10mL) and ether (10mL). The residue was redissolved in MeCN and water (10mL) was added. The volume was reduced until a precipitate began to form, then the solution was cooled in the fridge to give a red microcrystalline solid which was collected and washed with a little water, ethanol and ether. $[\text{Ru}(\text{17})_2](\text{PF}_6)_2$ (0.063g, 0.058 mmol, 81%). The crude product (over 95% pure) was purified by column chromatography (SiO_2 , MeCN:H₂O:saturated KNO_3 _(aq) 7:7:2) and the main red band was collected. Excess aqueous NH_4PF_6 was added and the volume reduced until a deep red precipitate formed which was collected on Celite and washed well with water (to remove salt), followed by a little ethanol and ether. The residue was redissolved in MeCN (40mL) and water was added (10mL). The volume was reduced until a precipitate began to form and then the solution was cooled in the fridge to give a pure microcrystalline solid (0.037g, 0.034 mmol, 48%).

*Synthesis of ditopic ligand **29***

4'-Hydrazino-2,2':6",2'-terpyridine (0.20 g, 0.75 mmol) and terephthalaldehyde (0.051g, 0.38 mmol) were dissolved in EtOH and 2 drops of concentrated H_2SO_4 were added. The mixture was heated to reflux for an hour and cooled to room temperature. The solid was collected and washed well with ethanol, chloroform and ether to give $[\text{H}_4\text{29}](\text{EtOSO}_3)_4$ as a bright orange powder (0.31 g, 0.27 mmol, 72 %). ¹H-NMR (DMSO-d₆, 360K): 11.99 (br s, 2H, NH), 8.89 (ddd, *J* 4.8, 1.7, 0.8, 4H, H^{A6}), 8.57 (d, *J*

8.2 Hz, 4H, H^{A3}), 8.36 (s, 1H, HC=N), 8.19 (td, *J* = 7.8, 1.8 Hz, 4H, H^{A4}), 8.16 (s, 4H, H^{B3}), 8.02 (s, 4H, H^{C2}), 7.71 (ddd, *J* 7.6, 4.8, 1.0 Hz, 4H, H^{A5}), 3.48 (q, *J* 7.0 Hz, 8H, CH₃CH₂OSO₃), 1.09 (t, *J* 7.0 Hz, 12H, CH₃CH₂OSO₃). Found C 42.83, H 4.33, N 12.03 %. C₄₂H₄₄N₁₀O₁₆S₄·6H₂O requires C 42.71, H 4.78, N 11.86 %

Synthesis of ditopic ligand 30

4'-Hydrazino-2,2':6",2'-terpyridine (0.20 g, 0.75 mmol) and 2,3-butanedione (0.033g, 0.38 mmol) were dissolved in MeOH and 2 drops of concentrated H₂SO₄ were added. The mixture was heated to reflux for an hour and cooled to room temperature. The solid was collected and washed well with ethanol, chloroform and ether to give [H₄29](MeOSO₃)₄ as a pale orange powder (0.23 g, 0.22 mmol, 58%). This solid was dissolved in water and aqueous K₂CO₃ was added to give a milky precipitate which was extracted in DCM and dried over MgSO₄. Removal of the solvent gave **30** as an off-white solid. (0.062g, 0.11 mmol, 14%). ¹H NMR (500 MHz, DMSO-d₆): 10.89 (s, 2H, NH), 8.78 (d, 4H, *J* 4.5 Hz, H^{A6}), 8.46 (d, *J* 6.6 Hz, 4H, H^{A3}), 8.22 (s, 2H, CH=N), 8.09 (t, *J* 7.4 Hz, 4H, H^{A4}), 7.61 (dd, *J* 7.0, 5.1 Hz, 4H, H^{A5}), 2.45 (s, 6H, Me).

Synthesis of ditopic ligand 31

Formyl-2,2':6",2"-terpyridine was prepared from 4'-methyl-2,2':6",2"-terpyridine as described by.²⁶² 4'-methyl-2,2':6",2"-terpyridine was prepared from 4'-methylthiol-2,2':6",2"-terpyridine which was prepared as described in the literature.²⁶⁵ 4'-Hydrazino-2,2':6",2'-terpyridine (0.20 g, 0.75 mmol) and formyl-2,2':6",2"-terpyridine (0.20 g, 0.75 mmol) were dissolved in MeOH and 2 drops of concentrated H₂SO₄ were added. The mixture was heated to reflux for an hour and cooled to room temperature. The solid was collected and washed well with ethanol, chloroform and ether to give [H₄29](MeOSO₃)₄ as a bright yellow-orange powder (0.45 g, 0.53 mmol, 71%). This solid was dissolved in water and aqueous K₂CO₃ was added to give a milky precipitate which was extracted in DCM and dried over MgSO₄. Removal of the solvent gave **31** as an off-white solid. (0.095g, 0.24 mmol, 32%). ¹H-NMR (500 MHz, DMSO-d₆): 11.65 (s, 1H, NH), 8.82 (ddd, *J* 4.7, 1.8, 0.9 Hz, 2H, H^{A'6}), 8.78 (br d, 2H, H^{A6}), 8.75 (s, 2H, H^{B'3}), 8.69 (2H, dt, *J* 8.0, 1.1 Hz, H^{A'3}), 8.64 (2H, dt, *J* 7.9, 0.9 Hz, H^{A3}), 8.26 (s, 1H, N=CH), 8.24 (v. br, 2H, H^{B3}), 8.06 (2H, td, *J* 7.6, 1.9 Hz, 2H, H^{A'4}), 8.02 (td, *J* 7.7, 1.7

Hz, 2H, H^{A4}), 7.56 (ddd, *J* 7.4, 4.7, 1.2 Hz, 2H, H^{A'5}), 7.52 (ddd, *J* 7.6, 4.8, 1.2 Hz, 2H, H^{A5}).

Synthesis of complex [32](PF₆)₄·4H₂O

Ligand [H₂**29**][MeOSO₃]₂ (0.10g, 0.093 mmol) and Ru(tpy)Cl₃ (0.12g, 0.27 mol, excess) were suspended in MeOH (10mL) and one drop of *N*-ethylmorpholine was added as a reducing agent. The mixture was refluxed for 20 hours and cooled to room temperature. The bright red solution was filtered through Celite to remove any remaining Ru(tpy)Cl₃. Excess aqueous NH₄PF₆ was added to give a red precipitate which was collected on Celite and washed well with water, EtOH and Et₂O. The residue was dissolved in MeCN and purified by column chromatography (SiO₂, MeCN:H₂O: saturated KNO₃(aq) 7:7:2). The main red band was collected, excess NH₄PF₆ was added and the volume reduced to give a microcrystalline solid which was collected and washed well with water. [32](PF₆)₄·0.15g, 0.081 mmol, 87%). See tables for characterisation.

Table 4 Elemental Analysis and ESI-MS

Complex	Yield (%) [†]	Required			Found			Found	ESI-MS	
		C %	H %	N %	C %	H %	N %		[Fe(L) ₂] ²⁺	[[Fe(L) ₂]-H] ⁺
<i>Iron(II)</i>										
[Fe(17) ₂](PF ₆) ₂ ·3H ₂ O	77%	47.93	3.66	12.70	48.07	3.44	12.74	379.5 757.4	379.6	757.2
[Fe(18) ₂](PF ₆) ₂ ·3H ₂ O	83 %	48.87	3.92	12.38	48.81	3.84	12.00	393.5 785.3	393.6	785.3
[Fe(19) ₂](PF ₆) ₂ ·4H ₂ O	65 %	52.84	3.96	11.00	52.80	3.74	11.04	455.5 909.3	455.7	909.3
[Fe(20) ₂](PF ₆) ₂	87 %	51.32	3.56	13.01	51.41	3.55	12.81	393.1 930.9 ^a	393.6	-
[Fe(21) ₂](PF ₆) ₂ ·2H ₂ O	96%	47.50	3.90	11.54	47.37	3.61	11.33	439.5 877.2	439.6	877.3
[Fe(22) ₂](PF ₆) ₂ ·4H ₂ O	48%	41.34	3.16	10.96	41.01	3.13	10.71	458.0 915.0	458.5	915.0
[Fe(23) ₂](PF ₆) ₂ ·2H ₂ O	28%	48.27	3.70	12.23	48.03	3.41	11.92	409.3 817.2	409.6	817.2
[Fe(24) ₂](PF ₆) ₂ ·2H ₂ O	34%	44.99	3.09	14.41	44.87	3.26	14.35	424.4 847.2	424.6	847.2
[Fe(25) ₂](PF ₆) ₂ ·2H ₂ O	33%	43.74	3.87	14.17	43.57	3.65	14.24	331.4 661.2	331.6	661.2
<i>Ruthenium(II):</i>										
[Ru(17) ₂] (PF ₆) ₂ ·3.5H ₂ O	48%	45.68	3.57	12.11	45.86	3.47	11.82	402.0 803.1	402.6	803.2
[Ru(18) ₂](PF ₆) ₂ ·4.5H ₂ O	91%	45.93	3.94	11.64	45.64	3.63	11.51	416.1 831.1 977.0 ^a	416.6	831.2
[Ru(20) ₂](PF ₆) ₂	34%	49.25	3.41	12.49	49.02	3.51	12.79	416.0 977.0 ^a	416.6	-
[Ru(23) ₂](PF ₆) ₂	53%	47.88	3.32	12.14	47.75	3.25	12.15	432.0 863.1	432.6	863.2
[32](PF ₆) ₄ ·4H ₂ O	87%	41.99	3.01	11.52	42.16	3.03	11.36	431.0 646.6	431.8 ^b	646.6 ^c

[†] yield calculations were unreliable as protonated salts of the corresponding ligands were used

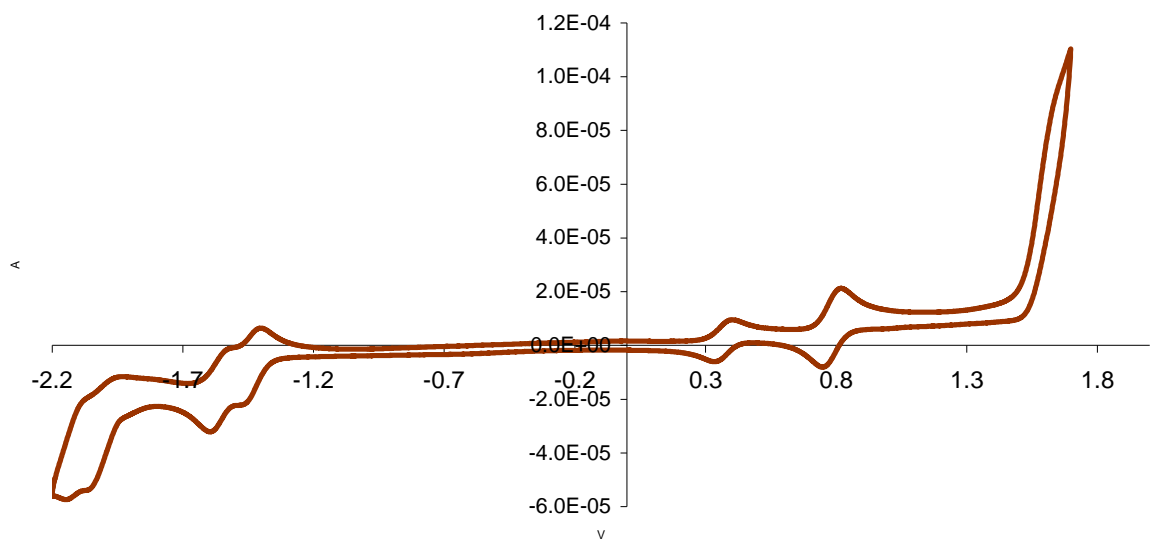
^a [M(L)₂(PF₆)₂]⁺, ^b [M - H]³⁺, ^c [M-2H]²⁺

Table 5 ^1H -NMR of $[\text{Fe}(\text{L}_2)](\text{PF}_6)_2$ in acetonitrile-d₃ (except where noted). o/l = overlap.

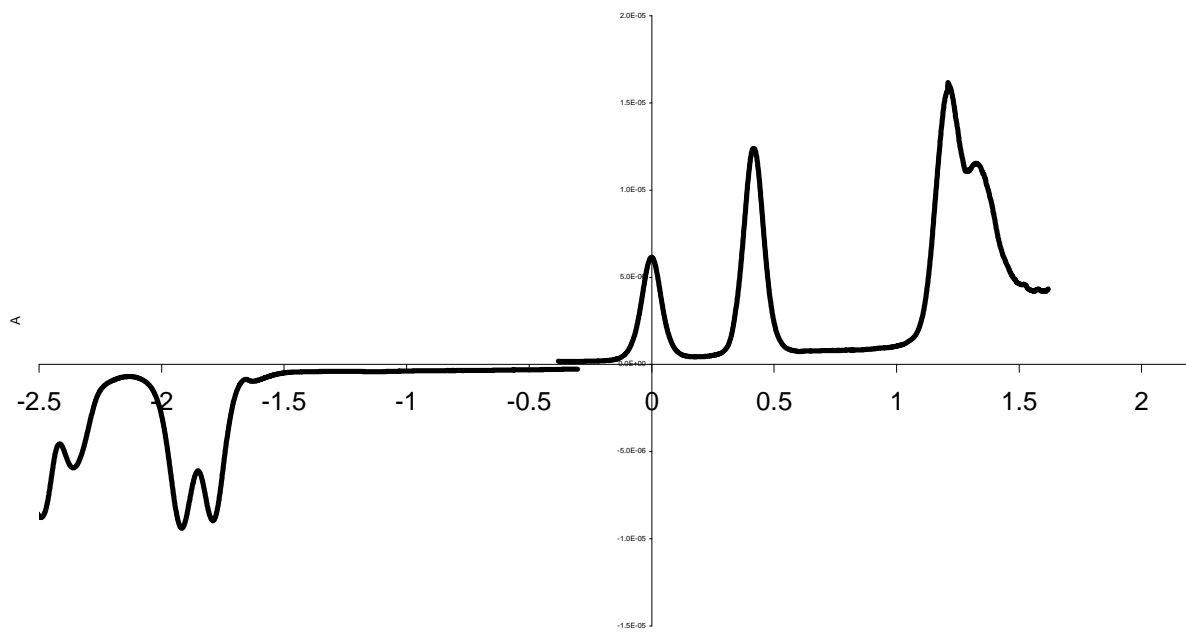
$[\text{Fe}(\text{L}_2)](\text{PF}_6)_2$ $\text{L} =$	NH	N=CH	A6	J (Hz)	A5	J (Hz)	A4	J (Hz)	A3	J (Hz)	B3	Ph _a	J (Hz)	Ph _b	J (Hz)	Ph _y	J (Hz)	Other
1	7.52	-	7.23 (d)	5.2	7.04 (ddd)	6.9, 5.6, 1.1	7.80 (td)	7.9, 1.4	8.29 (d)	8.1	8.27	-	-	-	-	-	-	4.41 (s, NH ₂)
17	10.07	8.27	7.27 (d)	5	7.07 (ddd)	7.3, 5.6, 1.3	7.85 (td)	7.8, 1.4	8.44 (d)	8.1	8.50 (br)	8	7.14	7.55 (m)	-	7.50 (m)	-	
17 (acetone-d ₆ , 295K)	11.26	8.39	7.64 (d)	5.7	7.28 (ddd)	7.5, 5.6, 1.2	8.02 (td, o/l Ph _a)	-	8.68 (v br)	-	9.12 (v br)	8 (d, o/l HA4)	6.8	7.53 (m)	-	7.53 (m)	-	
18	9.60	-	7.28 (ddd)	5.6, 1.4, 0.7	7.07 (ddd)	7.4, 5.6, 1.3	7.85 (td)	7.6, 1.5	8.40 (br d)	5.9	8.65 (br)	8.11 (dd)	8.4, 1.4	7.54 (m)	-	7.49 (m)	-	2.57 (s, Me)
19	9.25	-	7.23 (ddd)	5.6, 1.3, 0.6	7.06 (ddd)	7.5, 5.6, 1.2	7.85 (o/l)	-	8.36 (br)	-	8.60 (v br)	7.54 (m), 7.50 (o/l m)	-	7.78 (m), 7.83 (o/l m)	-	7.50 (o/l m)	-	
20	-	8.23	7.24 (d)	5.5	7.07 (ddd)	7.1, 5.8, 1.0	7.87 (td)	7.9, 1.3	8.54 (d)	7.9	8.82	8.06 (d)	7.3	7.60 (t)	7.5	7.50 (t)	7.3	3.94 (s, Me)
21	10.09	8.17	7.27 (ddd)	5.6, 1.4, 0.7	7.07 (t)	6.6	7.85 (td)	7.7, 1.3	8.42 (d)	7.6	8.50 (br)	7.14 (d)	2.2	-	-	6.63 (t)	2.2	3.90 (s, OMe)
22	10.11	8.22	7.26 (ddd)	5.7, 1.4, 0.7	7.07 (ddd)	7.5, 5.6, 1.3	7.85 (td)	7.6, 1.4	8.44 (br d)	7.7	8.51 (br)	7.93 (d)	8.4	7.72 (d)	8.5	-	-	
23	10.01	8.21	7.27 (d)	5.1	7.06 (td o/l)	6.4, 1.1	7.84 (td)	7.9, 1.2	8.42 (d)	6.8	8.48 (br)	7.94 (d)	8.8	7.09 (d)	8.7	-	-	
24	10.36	8.34	7.26 (d)	5.6	7.08 (ddd)	7.5, 5.6, 1.3	7.88 (td)	1.8, 1.4	8.46 (d)	7.6	8.55 (br)	8.21 (d)	9.0	8.37 (d)	9.0	-	-	
25	9.13	-	7.25 (d)	5.2	7.05 (td)	7.2, 5.6, 1.2	7.82 (td)	7.8, 1.4	8.31 (d)	7.9	8.49	-	-	-	-	-	-	2.23 (Me1), 2.15 (Me2), adjacent to NH
$[\text{Ru}(\text{L}_2)](\text{PF}_6)_2$ $\text{L} =$																		
17	9.87	8.20	7.47 (ddd)	5.6, 1.4, 0.7	7.15 (ddd)	7.6, 5.6, 1.3	7.89 (ddd)	8.2, 7.6, 1.5	8.46 (d)	8.0	8.37	7.97 (d)	7.1	7.54 (m)	-	7.49 (m)	-	
18	9.32	-	7.47 (d) o/l	5.7	7.15 (ddd)	7.4, 5.4, 1.0	7.89 (td)	7.9, 13	8.42 (d)	8.0	8.49	8.08 (d)	7.3	7.53 (m)	-	7.48 (o/l m)	-	2.52 (Me)
20	8.16		7.45 (ddd)	5.6, 1.5, 0.7	7.15 (ddd)	7.4, 5.5, 1.3	7.90 (ddd)	8.0, 7.6, 1.5	8.57 (d)	7.7	8.67	8.03 (d)	7.3	7.55 (t)	7.5	7.49 (ddd)	7.3, 3.8, 1.3	3.87 (NMe)
23	9.74	8.14	7.48 (ddd)	5.6, 1.5, 0.7	7.15 (ddd)	7.5, 5.6, 1.3	7.88 (td)	7.9, 1.5	8.44 (d)	8.0	8.33 (br)	7.91 (d)	8.8	7.07 (d)	9.0	-	-	3.88 (OMe)
[32](\text{PF}_6)_4	10.12	8.28	7.27 (ddd)	5.6, 1.4, 0.6	7.11 (ddd)	7.4, 5.6, 1.3	7.92 (td)	7.9, 1.5	8.49 (br o/l)	-	8.43 (br)	8.11 (s)	-	-	-	-	-	
	Tpy	-	7.54 (ddd)	5.6, 1.4, 0.7	7.21 (ddd)	7.5, 5.7, 1.3	7.90 (td)	7.9, 1.6	8.48 (d)	7.9	8.72 (d) 8.2	-	-	-	-	-	-	8.35 (t) 8.1 T4'

Table 6 ^{13}C -NMR of $[\text{Fe}(\text{L}_2)](\text{PF}_6)_2$ in acetonitrile-d₃

$[\text{Fe}(\text{L}_2)](\text{PF}_6)_2$ $\text{L} =$	N=CH	A6	A5	A4	A3	B3	Ph _a or py2	Ph _b or py3	Ph _g or py4	B4	A2	B2	Ph _i
1	-	154.4	127.7	138.9	123.6	107.2	-	-	-	159.9	159.7	160.1	-
17	145.4	154.4	127.9	139.1	124.1	108.1	128.2	130.1	131.1	154.0	159.5	160.6	135.4
18	150.2	154.4	127.9	139.1 (o/l)	124.0	108.7	127.5	129.6	130.4	154.7	159.5	160.5	139.1 (o/l) 14.3 (Me)
19	152.5	154.4	127.9	139.1	124.0	108.8	130.0	131.0	131.1	154.0	159.5	160.5	133.3
							129.6*	128.5	130.7				138.4
20	141.5	154.3	127.9	139.1	124.2	109.8	128.4	130.0	130.9	156.0	159.7	160.5	136.1 33.8 (NMe)
21	145.3	154.4	127.9	139.1	124.2	108.2	106.2	162.3	102.8	153.9	159.4	160.6	137.4 56.3 (Me)
22	144.1	154.4	127.9	139.1	124.2	108.2	129.8	133.0	124.6	153.9	159.4	160.7	134.7
23	145.4	154.4	127.8	139.1	124.0	107.9	129.8	115.4	162.4	154.0	159.5	160.5	128.0 56.2 (Me)
24	142.7	154.4	128.0	139.2	124.3	108.6	128.8	125.1	149.3	153.7	159.4	160.8	141.7
25	153.2	154.4	127.8	139.0	123.8	108.1	-	-	-	154.9	159.6	160.3	- 25.5 (Me1), 17.4 (Me2)
$[\text{Ru}(\text{L}_2)](\text{PF}_6)_2$ $\text{L} =$													
17	144.9	153.5	128.1	138.4	125.0	107.7	128.1	130.0	131.0	152.3	159.7	156.5	135.5
18	149.6	153.5	128.1	138.5	124.9	108.3	127.4	129.5	130.3	152.9	159.8	156.4	139.2 14.1 (CMe)
20	140.9	153.4	128.1	138.5	125.1	104.5	128.33	130.0	130.7	154.3	159.9	156.3	136.2 33.7 (NMe)
23	144.8	153.5	128.1	138.4	124.9	107.5	129.7	115.3	162.3	152.3	159.8	156.4	128.1 56.2 (OMe)
32 - hydrazone	144.4	153.6	128.1	138.8	125.1	109.2	128.6	-	-	152.8	159.3	155.8	136.8
32 -tpy	-	153.3	128.4	138.8	125.2	124.5	-	-	-	135.8	159.3	157.1	-



(a)



(b)

Figure 3-46 Electrochemical measurements of $\text{Fe(17)}_2(\text{PF}_6)_2$ in MeCN with a glassy carbon electrode, a silver reference wire and TBAPF₆ as the supporting electrolyte. (a) CV; (b) DPV. Fe(II/III): 0.42 V (rev), ligand oxidations: 1.20 (q rev), 1.33 (q rev), ligand reductions -1.43 (rev), -1.56 (rev) -2.01 (irrev), -2.48 (irrev).

3.12. Crystal Data

	Structure number	jb346	jb133-1-red	jb747
Structure		$2\{[\text{Ru}(\mathbf{17})_2](\text{PF}_6)_2\}_2 \cdot 3\text{MeCN}\cdot 3\text{H}_2\text{O}$	$2\{[\text{Fe}(\mathbf{17})_2](\text{PF}_6)_2\}\cdot 3\text{MeCN}\cdot 3\text{H}_2\text{O}$	$2\{[\text{Fe}(\mathbf{21})_2](\text{PF}_6)_2\}\cdot 5\text{MeCN}\cdot 0.66\text{H}_2\text{O}$
Formula		$2(\text{C}_{44}\text{H}_{34}\text{N}_{10}\text{Ru})(\text{PF}_6)_2 \cdot 3(\text{C}_2\text{H}_3\text{N})\cdot 3(\text{H}_2\text{O})$	$2(\text{C}_{44}\text{H}_{34}\text{FeN}_{10})(\text{PF}_6)_4 \cdot 3\text{C}_2\text{H}_3\text{N}\cdot 3\text{H}_2\text{O}$	$2(\text{C}_{48}\text{H}_{42}\text{FeN}_{10}\text{O}_4)(\text{PF}_6)_2 \cdot 5(\text{C}_2\text{H}_3\text{N})\cdot 0.66(\text{H}_2\text{O})$
Empirical formula		$\text{C}_{94}\text{H}_{83}\text{F}_{24}\text{N}_{23}\text{O}_3\text{P}_4\text{Ru}_2$	$\text{C}_{94}\text{H}_{83}\text{F}_{24}\text{Fe}_2\text{N}_{23}\text{O}_3\text{P}_4$	$\text{C}_{106}\text{H}_{99}\text{F}_{24}\text{Fe}_2\text{N}_{25}\text{O}_{8.66}\text{P}_4$
Formula weight		2364.83	2274.37	2553.24
T (K)		173	173	223(2)
λ (Å)		0.71073	0.71073	0.71073
Crystal system		Triclinic	Triclinic	Triclinic
Space group		P-1	P-1	P-1
a (Å)		8.8609(2)	8.8383(3)	11.880(2)
b (Å)		11.5244(2)	11.4962(4)	13.566(3)
c (Å)		24.9307(5)	24.9761(11)	18.611(4)
α (°)		97.6672(11)	95.588(2)	93.20(3)
β (°)		100.2701(8)	98.9488(19)	93.68(3)
γ (°)		100.4029(11)	101.524(3)	94.46(3)
V (Å ³)		2427.53(9)	2434.59(16)	2978.5(10)
Z		1	1	1
D_c (Mg.m ⁻³)		1.618	1.551	1.423
Absorption coefficient (mm ⁻¹)		0.488	0.474	0.400
Reflections collected		21322	19811	54235
Unique reflections		11474	10974	10485
R (int)		0.028	0.024	0.1081
Data / restraints / parameters		8552 / 1136 / 757	6142 / 1172 / 757	10485 / 0 / 842
Goodness-of-fit on F^2		1.1248	1.1921	1.098
Final R indices [$I > 2\sigma(I)$]		R1 = 0.0407, wR2 = 0.0443	R1 = 0.0933, wR2 = 0.0758	R1 = 0.0559, wR2 = 0.1513
R indices (all data)		R1 = 0.0601, wR2 = 0.0500	R1 = 0.1531, wR2 = 0.1004	R1 = 0.0629, wR2 = 0.1580

	jb847	jb405	jb303	jb406
Structure number				
Structure	[Ru(23) ₂](PF ₆) ₂ ·1.75MeCN	[Fe(23) ₂](PF ₆) ₂	[Ru(18) ₂](PF ₆) ₂ ·0.33MeCN·0.33H ₂ O	[Fe(18) ₂](PF ₆) ₂ ·0.33MeCN·0.33H ₂ O
Formula				
Empirical formula	C49.50 H43.25 F12 N11.75 O2 P2 Ru	C46 H37 F12 Fe N10 O2 P2	C46H38N10Ru, 2(F6 P), 0.33(C2 H3 N), 0.2(O)	H36.50 F12 Fe N10.50 O0.83 P2
Formula weight	1225.72	1107.65	1139.05	1107.49
T (K)	223(2)	223(2)	223(2)	173(2)
λ (Å)	0.71073	0.71073	0.71073	0.71073
Crystal system	Monoclinic	Monoclinic	Orthorhombic	Orthorhombic
Space group	P2 ₁ /c	P2 ₁ /c	R-3	R-3
a (Å)	10.6435(2)	11.115(2)	42.281(6)	41.6777(7)
b (Å)	21.8808(2)	20.354(4)	42.281(6)	41.6777(7)
c (Å)	23.6182(2)	22.483(5)	15.227(3)	15.0442(6)
α (°)	90	90	90	90
β (°)	98.252(3)	99.79(3)	90	90
γ (°)	90	90	120	120
V(Å ³)	5443.5	5012.1(17)	23574(7)	22631.2(11)
Z	4	4	18	18
D _c (Mg.m ⁻³)	1.502	1.468	1.444	1.463
Absorption coefficient (mm ⁻¹)	0.439	0.458	0.447	0.455
Reflections collected	37570	88594	77091	119397
Unique reflections	9696	8857	9496	9893
R(int)	0.0885	0.4039	0.0798	0.0595
Data / restraints / parameters	9696 / 44 / 814	8857 / 0 / 707	9274 / 0 / 694	9893 / 24 / 709
Goodness-of-fit on <i>F</i> ²	1.149	1.139	1.125	1.117
Final R indices [I>2σ(I)]	R1 = 0.0697, wR2 = 0.1253	R1 = 0.1421, wR2 = 0.3044	R1 = 0.0732, wR2 = 0.1793	R1 = 0.0860, wR2 = 0.2516
R indices (all data)	R1 = 0.1100, wR2 = 0.1387	R1 = 0.1971, wR2 = 0.3426	R1 = 0.0926, wR2 = 0.1949	R1 = 0.1458, wR2 = 0.3365

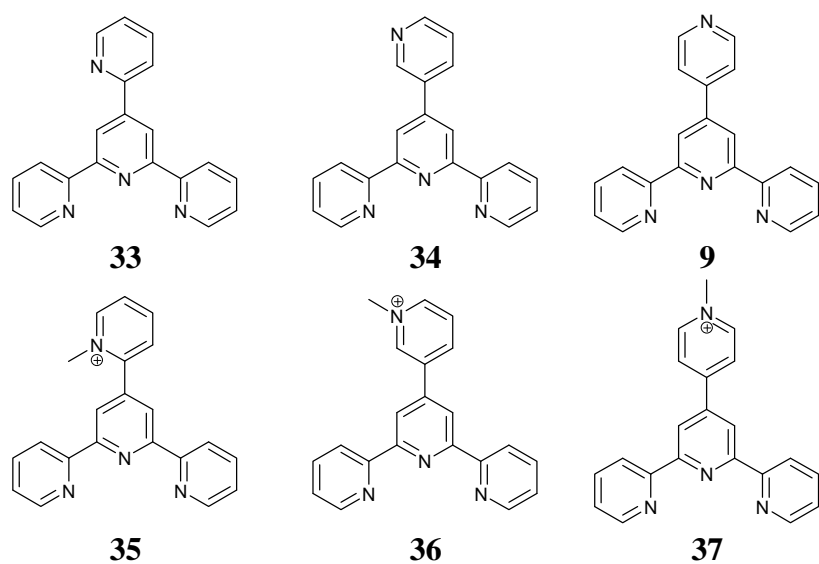
	Jb434	JB951	JB719
Structure number			
Structure	[Ru(20) ₂](NO ₃) ₂ ·MeCN·8H ₂ O	Ru(20) ₂](PF ₆) ₂ ·2MeCN	[32](PF ₆) ₄ ·8MeCN
Formula			
Empirical formula	C48 H53 N13 O14 Ru1	C50 H44 F12 N12 P2 Ru1	C84 H74 F24 N24 P4 Ru2
Formula weight	1137.1	1203.97	2201.66
T (K)	173	173	173
λ (Å)	0.71073	0.71073	0.71073
Crystal system	Monoclinic	Monoclinic	Triclinic
Space group	P2 ₁ /n	P2 ₁ /n	P-1
a (Å)	10.5463(2)	13.3358(2)	11.3747(2)
b (Å)	19.6544(3)	29.0471(4)	11.7421(2)
c (Å)	25.9818(4)	13.8633(2)	19.2614(4)
α (°)	90	90	73.3048(11)
β (°)	96.0901	105.1524(6)	81.4097(10)
γ (°)	90	90	68.2302(11)
V (Å ³)	5355.14(15)	5183.48(13)	2285.77(8)
Z	4	4	1
D _c (Mg.m ⁻³)	1.41	1.543	1.599
Absorption coefficient (mm ⁻¹)	0.369	0.457	0.509
Reflections collected	46695	41321	21439
Unique reflections	12683	12387	10881
R(int)	0.046	0.042	0.022
Data / restraints / parameters	7920 / 72 / 730	7231 / 32 / 694	8172 / 0 / 622
Goodness-of-fit on F ²	1.1136	1.1279	1.0884
Final R indices [I>2σ(I)]	R1 = 0.0466, wR2 = 0.0450	R1 = 0.0343, wR2 = 0.0388	R1 = 0.0326, wR2 = 0.0370
R indices (all data)	R1 = 0.0788, wR2 = 0.0516	R1 = 0.0616, wR2 = 0.0611	R1 = 0.0476, wR2 = 0.0501

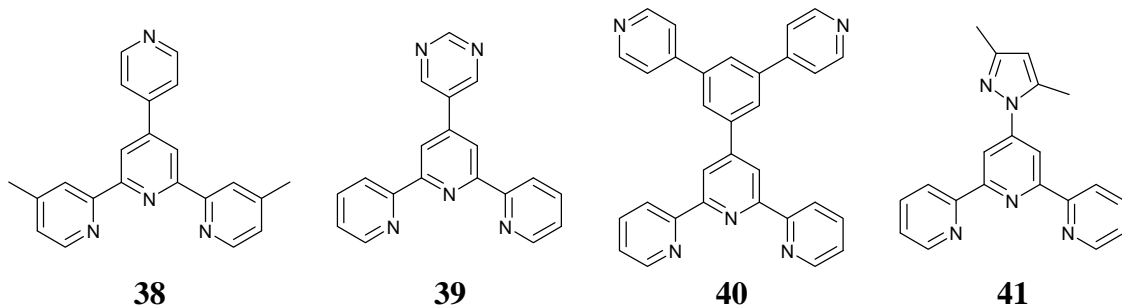
Chapter 4 Building blocks for extended structures: iron(II) and ruthenium(II) bis(terpyridine) complexes with pendant donors

4.1. General considerations

Metallosupramolecular chemistry is built upon the use of appropriate metal ion–ligand interactions,¹⁷ and is a valuable concept for the construction of functional materials and devices.^{54, 266–268} A natural extension of these principles is to the use of metal complexes as scaffolds bearing additional functionality.

The incorporation of metal bis(terpyridine) units into extended structures is a very attractive proposition as the potential of building their rich redox and photophysical properties into molecular frameworks could allow the development of a range of electrical and photo-addressable materials. Possible applications range from molecular switches and sensors to small molecule storage, solid state catalysts and designed ‘nano-flasks’ in which to perform reactions. As a first step towards realising this goal, this chapter presents a systematic study of complexes which might function as potential building blocks for the assembly of larger structures. Ligands discussed in this chapter are shown below:





'Expanded Ligands'

'Expanded ligands'¹⁶⁵ are metal-binding domains linked through metal-containing scaffolds. Typical scaffolds are $[M(bpy)_3]^{n+}$ ^{17, 269-275} and $[M(tpy)_2]^{n+}$ ^{69, 218, 276} moieties ($bpy = 2,2'$ -bipyridine, $tpy = 2,2':6',2''$ -terpyridine) which possess different topological and topographical properties as well as potentially different numbers of attached metal-binding domains.^{277, 278} The strategy is illustrated in comparison with 4,4'-bipyridine (**3**) and the expanded ligand $[Ru(\mathbf{9})_2]^{2+}$ (**9** = 4'-(4-pyridyl)-2,2':6',2"-terpyridine, Figure 4-1). The origin of the term 'expanded ligands' is also seen in Figure 4-1 which presents the idealised N...N distances in the two species; the incorporation of the $[Ru(tpy)_2]^{2+}$ scaffold increases the N...N distance from ~7 to ~18 Å

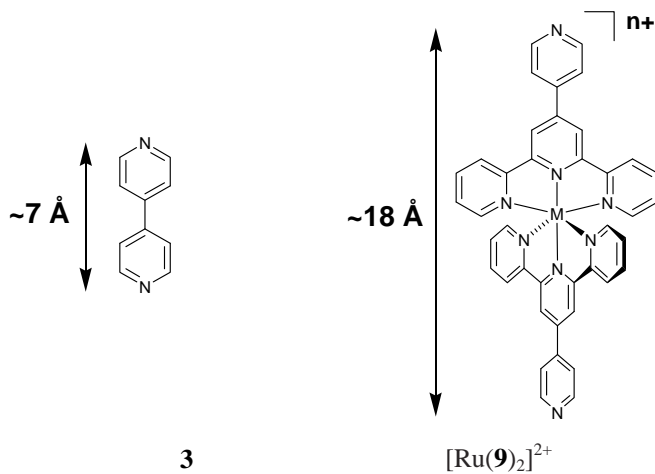


Figure 4-1 The concept of an expanded ligand exemplified by the comparison of 4,4'-bipyridine and the complex cation bis(4'-(4-pyridyl)-2,2':6',2"-terpyridine)ruthenium(II). The N...N distance between the pendant pyridine nitrogen donors is increased from ~7 Å to ~18 Å upon inserting the $[Ru(tpy)_2]^{2+}$ moiety.

It has been shown that the reactivity of the pendant pyridine rings in $[Ru(\mathbf{9})_2]^{2+}$ parallels that in **3** and that this may be used as an assembly strategy for novel metallosupramolecular structures.^{17, 166, 272, 273, 279, 280} Naturally, the presence of the double positive charge associated with the ruthenium(II) centre in $[Ru(\mathbf{9})_2]^{2+}$ plays a

role in modifying the reactivity of the expanded ligand in comparison to the parent species **3**, and it might be anticipated that $[M(\mathbf{9})_2]^{2+}$ is a poorer ligand than **3**.

Pyridyl terpyridine complexes

Complexes of the type $[M(\mathbf{9})_2]^{n+}$ have been previously reported ($n = 2$, $M = \text{Fe}$,^{271, 280} Ru ,^{17, 275} Os ,¹⁷ Ir ,²⁸¹ $n = 3$, $M = \text{Rh}$ ²⁸²). It has been demonstrated that the pendant 4-pyridyl group in $[M(\mathbf{9})_2]^{n+}$ retains its characteristic reactivity and reacts with protons,^{17, 271, 279, 280} and alkylating agents.^{17, 271-273, 280} The effects of protonation of the pendant 4-pyridyl units in $[M(\mathbf{9})_2]^{2+}$ ($M = \text{Fe}, \text{Ru}, \text{Os}$) on their electrochemical and photophysical properties have been previously reported.^{17, 271, 279} Studies of the mono- and diprotonation of $[\text{Ru}(\mathbf{9})_2]^{2+}$ and $[\text{Os}(\mathbf{9})_2]^{2+}$ lead to the conclusion that protonation of the pendant 4-pyridyl group lowers the energy of the lowest lying π^* molecular orbitals, thereby increasing the electron accepting ability of the complexes. The absorption and luminescence bands of both complexes are red-shifted to lower energy upon protonation, and protonation acts as a luminescent switch. For $[\text{Ru}(\mathbf{9})_2]^{2+}$, the luminescence intensity is increased by protonation, whereas the reverse is observed when $[\text{Os}(\mathbf{9})_2]^{2+}$ is protonated.²⁷⁹

Interest in complexes of 4'-(X-pyridyl)-2,2':6',2"-terpyridine ligands ($X = 2, 3$ or 4) has not been limited to the work presented in this chapter; an increasing number of recent publications use $\{M(\mathbf{9})_2\}$ complexes in a range of applications, including the construction of molecular squares,^{283, 284} metal-linked porphyrins⁹¹ the formation of polyelectrolyte films via *N*-alkylation of **9**^{94, 169} and other related polymeric materials,^{285, 286} supramolecular assemblies of rotaxanes^{287, 288} and metallostars.²⁸⁹ The complexes $[M(\mathbf{33})_2]^{n+}$ and $[M(\mathbf{34})_2]^{n+}$ have received little attention with only $[\text{Ir}(\mathbf{33})_2][\text{PF}_6]_3$ ²⁸¹, $[\text{Ni}(\mathbf{33})_2][\text{PF}_6]_2$ ²⁹⁰, $[\text{Ru}(\mathbf{34})_2][\text{PF}_6]_2$,^{274, 291} and $[\text{Ir}(\mathbf{34})_2][\text{PF}_6]_3$ ²⁸¹ being reported to date. The luminescent properties of the iridium(III) complexes $[\text{Ir}(\mathbf{L})_2]$ ($\mathbf{L} = \mathbf{33-9}$) have been investigated in terms of alkylation²⁹² and protonation^{281, 293} effects. Additionally, mono-terpyridyl complexes of **33** and **9** have also been recently explored.^{168, 290, 294-298} Co(II) and Co(III) containing systems with emphasis on their magnetic properties include one-dimensional chains of $[\text{Co}(\mathbf{9})\text{Cl}_2]$ ¹⁷⁰ and polymers of $[\text{Co}(\mathbf{9})(\text{NCS})_2]$ ²⁹⁴ and $[\text{Co}(\mathbf{9})(\text{SO}_4)]$ ²⁹⁴ in addition to bis-terpyridyl examples such as $[\text{Co}(\mathbf{9})_2][\text{NO}_3]_2$ ²⁹⁹. Other related examples include mono-terpyridyl complexes such as

[Cr(**33**)L]X₃²⁹⁵, and [Ni(**33**)X]²⁹⁰, dimers formed with {Pb(**9**)}²⁹⁶ and chiral self- catenated networks formed by {Zn(**9**)}³⁰⁰ units. Cu(II) has been used to assemble rectangular grid-type coordination polymers¹⁶⁸ as well as a range of more simple structures²⁹⁷ using ligands **33** and **9**. Among the products obtained from hydrothermal reactions of **33** with CuI and KI is the mixed oxidation state compound [Cu₂(**33**)₂I₂]₂[Cu₂(μ-I)₂I₂] containing a discrete mixed oxidation state cation comprising a [Cu^{II}(**33**)₂] moiety in which one of the 2-pyridyl substituents is coordinated to a [Cu^{II}₂] unit.²⁹⁸ Of the reported compounds, several have been characterized by X-ray crystallography:

bis-terpyridyl	complexes	[Ru(34) ₂][PF ₆] ₂ ²⁷⁴
{[Ru(9) ₂](PF ₆)(NO ₃)}DMSO, ²⁷⁵	{[Fe(9 N=O) ₂][BF ₄] ₂ }·1.5H ₂ O, ¹⁶⁹	{[Fe(9) ₂][NO ₃] ₂ }3H ₂ O·MeCN, ²⁸⁰
{[Cu(9)][PF ₆] ₂ }·MeOH·0.5CH ₂ Cl ₂ , ¹⁶⁹		{[Rh(9) ₂][PF ₆] ₃ }·8EtOH, ²⁸²
[Co(9) ₂][NO ₃] ₂ ·MeCN·4H ₂ O, ²⁹⁹	[Co(9) ₂][ClO ₄] ₂ ²⁹⁹	[Co(H9) ₂][ClO ₄] ₅ ·2.5H ₂ O, ²⁹⁹
[Co(9) ₂][NO ₃] ₂ ·MeCN·4H ₂ O, ²⁹⁹	and a series of Cu(II) bridged mono- terpyridyl complexes	Cu(II) complexes ¹⁶⁸ such as [Cu ₂ (9)(μ-1,1-SCN)(μ- Cl)Cl] _n , [Cu ₂ (9)(μ-I) ₂ Cl] _n , [Cu ₂ (9)(μ-Br) ₂ Br] _n and [Cu ₂ (9)(μ-1,3-SCN) ₂ (SCN)] _n .

X-Ray crystal structures of M(tpy)₂ complexes

Despite widespread interest in bis-terpyridine metal complexes in supramolecular chemistry,⁶⁹ there are surprisingly few X-ray crystal structures, and very few systematic studies of these.³⁰¹ A search of the Cambridge Structural Database (using Conquest,²² October 2008) for compounds incorporating a {M(tpy)₂} core shown in Figure 4-2, reveals:

- 332 structures of complexes (including multiple fragments of same crystal structure)
- 129 are unsubstituted M(tpy)₂ only
- 64(7) are Ru, Fe 39(5), Cu 28(6) (tpy only)
- 2 are coordination polymers or networks (see next chapter)

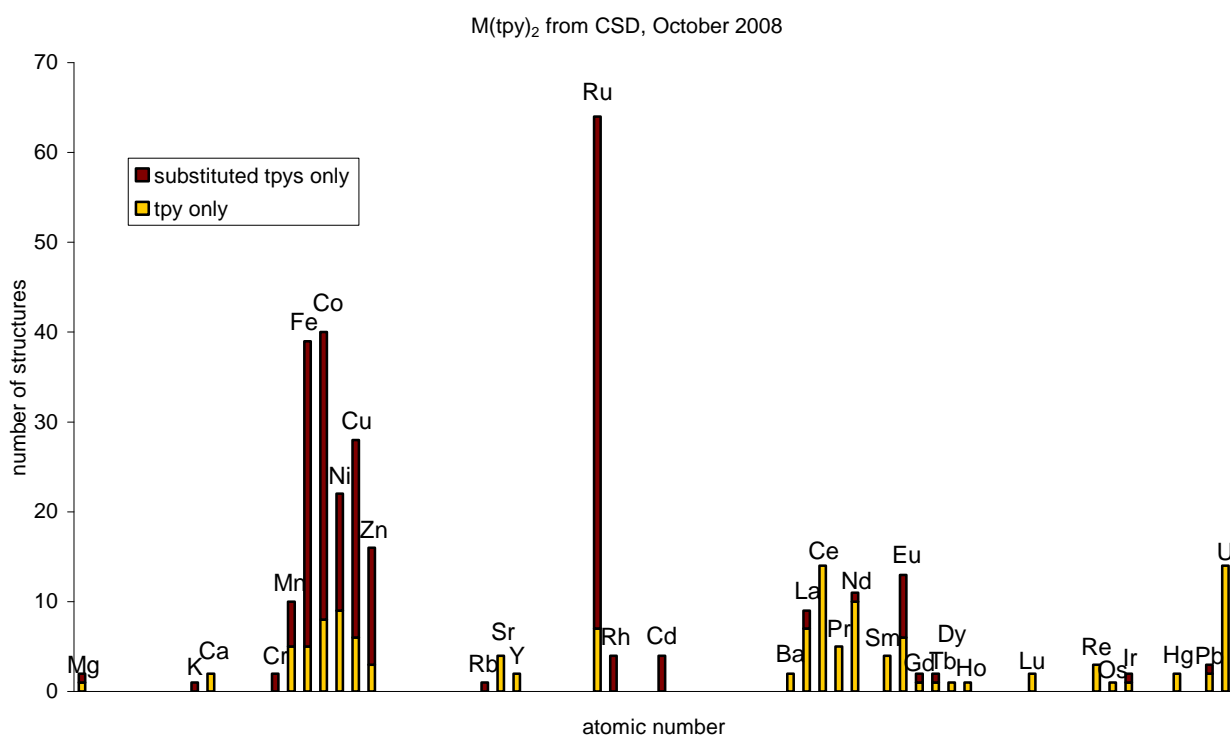


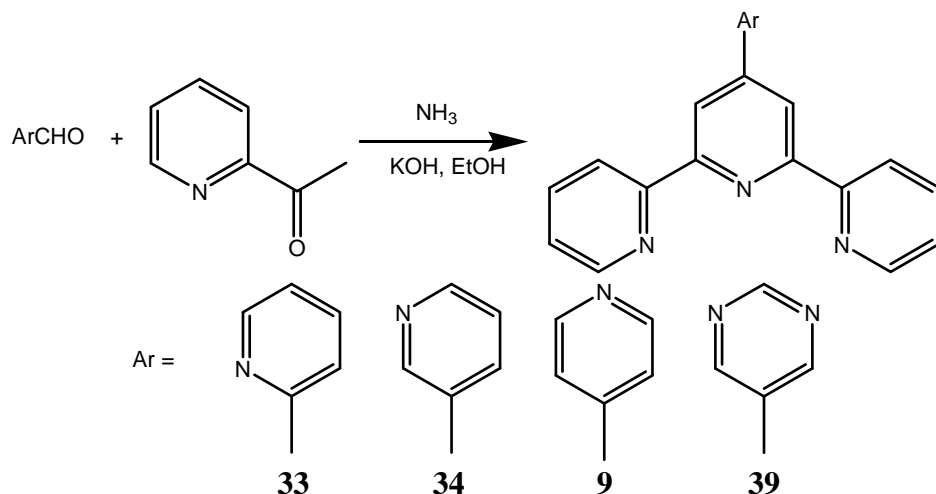
Figure 4-2 Results from a search of the Cambridge Structural Database using Conquest,²² (October 2008) of [M(tpy)₂]ⁿ⁺ complexes.

With such a limited number of crystal structures available, an solid-state investigation of a number of [M(tpy)₂] complexes which could function as expanded ligands appears timely. This chapter presents the preparation, characterisation and systematic study of the solution and solid state structures of the homoleptic iron(II) bis-terpyridine complexes of ligands **33-39** and ruthenium(II) complexes of ligands **33-9, 41-39**, all as hexafluorophosphate salts. All of these complexes possess 4'-pendant rings with nitrogen donors available for coordination to additional metal centres and therefore represent potential building blocks for extended structures. Of the complexes presented in this chapter, [Ru(**34**)₂](PF₆)₂,²⁷⁴ and [Ru(**9**)₂](PF₆)₂¹⁷ have been previously reported, but the latter has not been previous characterised by X-ray crystallography.

4.2. Preparation of ligands

The ligands **35, 36, 38** and **41** are previously unreported and have been characterised by ¹H and ¹³C-NMR, ESI-MS and elemental analysis. Ligands **33-9** and **39** were prepared using the excellent one pot method introduced by Hanan³⁰² for the synthesis of **9** (Scheme 6) in yields of 38, 44, 42³⁰² and 34% respectively. This method reacts two

equivalents of 2-acetyl pyridine with one equivalent of an appropriate aryl aldehyde in EtOH in the presence of excess base (KOH) and a large excess of aqueous NH₃. Characterisation of these ligands was straightforward; details are given in the experimental section.



Scheme 6 The Hanan method³⁰² of 4'-aryl substituted 2,2':6',2''-terpyridines

The major benefit of this method of preparing 4'-aryl substituted 2,2':6',2''-terpyridines is the ligands are easily isolated as analytically pure compounds requiring no further work-up other than, perhaps, a simple recrystallisation. This, combined with the commercial availability (and relative low cost) of the starting materials, establishes this ‘feel good’ reaction as the simplest and most effective method for preparing these type of ligands. As a comparison, there has been little consensus in the literature concerning the ideal synthesis of 4'-tolyl-2,2':6',2''-terpyridine^{172, 184, 303-313} and this has involved the use of low freezing point solvents (acetamide),³¹³ multi-step reactions and cumbersome purification procedures¹⁷² resulting in poor yields (e.g.: 30%,³¹³ 23%¹⁷²) in contrast to the Hanan method which delivers a yield of 49% within 2 hours.³⁰²

Ligand **39** has previously been reported.³¹⁴ The synthesis gave a modest yield (20%), and required several steps with long reaction times and the use of toxic stannylated intermediates. No coordination chemistry of **39** has been described. Using the versatile one-pot method of Hanan,³⁰² ligand **39** was prepared in 34% yield in 4 h.

Ligands **35-37** were not isolated as free ligands but as Ru(II) complexes prepared by reactions on the parent (non-methylated) complexes (discussed later). Ligand **40** was also not prepared as a free ligand but by reaction of the Ru(II) complex of 4'-(3,5-dibromophenyl)-2,2':6",2"-terpyridine (see later).

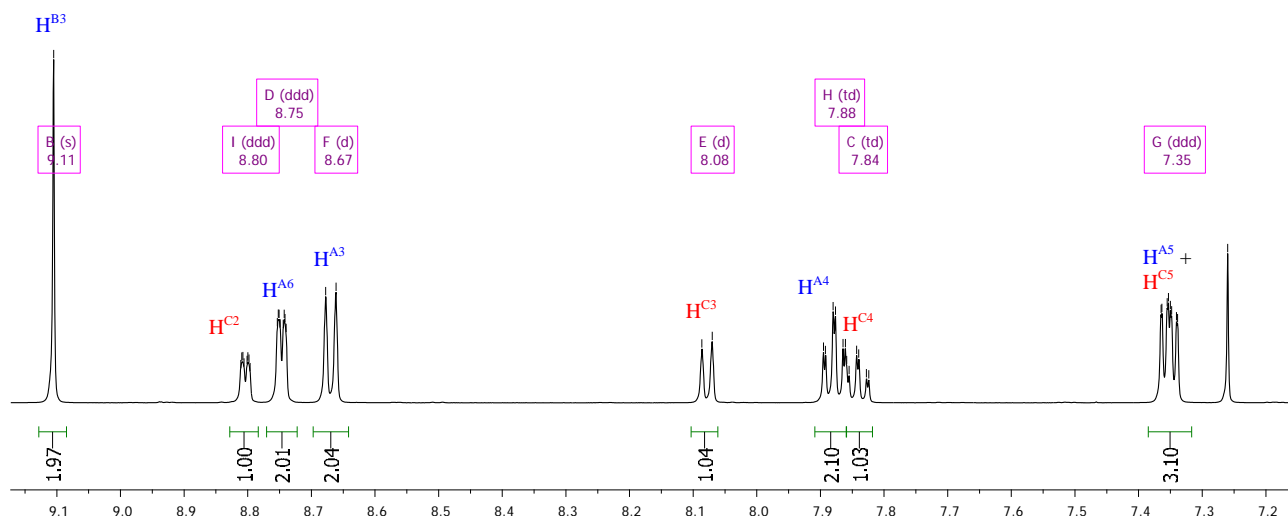
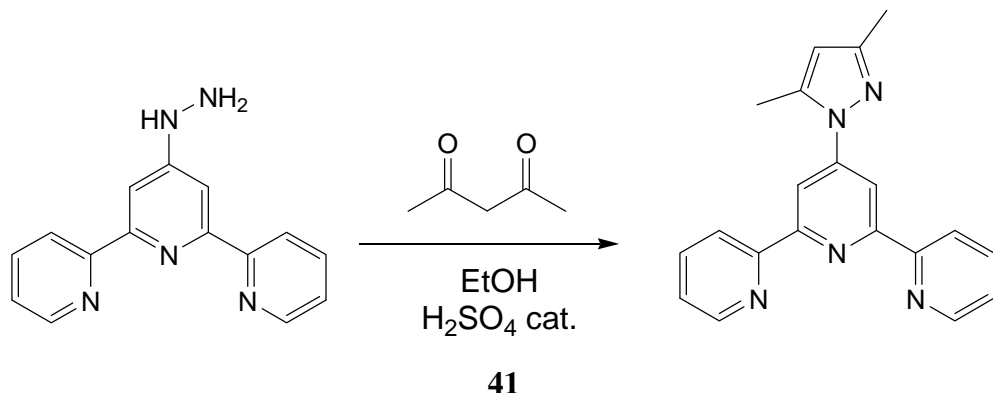


Figure 4-3 ^1H NMR spectrum (500 MHz, CDCl_3) of ligand **33**.

The strategy for the preparation of ligand **41** was the cyclization reaction of pentane-2,4-dione with 4'-hydrazino-2,2':6',2"-terpyridine.²⁵⁰ Such cyclizations are well documented for the syntheses of a range of pyrazoles, both in solution and over heterogeneous catalysts.³¹⁵⁻³¹⁷ The conditions shown in Scheme 7 are similar to those reported recently for the synthesis of 1,3,5-trisubstituted pyrazoles.³¹⁸ Treatment of 4'-hydrazino-2,2':6',2"-terpyridine with pentane-2,4-dione in methanol in the presence of concentrated H_2SO_4 , followed by cooling, resulted in the formation of an off-white crystalline solid. An analogous reaction in ethanol proceeded in a similar manner also to give a white solid. Both products proved to be poorly soluble in common organic solvents, and their solution ^1H NMR spectra were not well resolved. Elemental analysis indicated that methyl or ethyl sulfate salts of the diprotonated ligand $[\text{H}_2\textbf{41}]^{2+}$ had been formed, and this was confirmed by a single crystal X-ray diffraction study. X-ray quality crystals of $[\text{H}_2\textbf{41}][\text{EtOSO}_3]_2 \cdot \text{H}_2\text{O}$ were grown by slow evaporation of an ethanol/water (1:1) solution of $[\text{H}_2\textbf{41}][\text{EtOSO}_3]_2$.



Scheme 7 Synthetic route to ligand **41**: (i) MeOH or EtOH at reflux, conc. H_2SO_4 catalyst.

The diprotonated state of the ligand was consistent with the presence of two ethyl sulfate ions in the asymmetric unit, and is also consistent with the observation of a *cis,cis*-conformation for the tpy unit (see chapter 1). In $[\text{H}_2\mathbf{41}][\text{EtOSO}_3]_2 \cdot \text{H}_2\text{O}$, the $[\text{H}_2\mathbf{41}]^{2+}$ ion is hydrogen-bonded to atom O4 of one ethyl sulfate ion as illustrated in Figure 4-4 ($\text{N}1 \dots \text{O}1 = 2.757(2)$ Å, $\text{N}1-\text{H}1 \dots \text{O}1 = 159^\circ$, $\text{N}1 \dots \text{N}2 = 2.630(2)$ Å, $\text{N}1-\text{H}1 \dots \text{N}2 = 101^\circ$, $\text{N}3 \dots \text{O}1 = 2.752(2)$ Å, $\text{N}3-\text{H}1 \dots \text{O}1 = 156^\circ$, $\text{N}3 \dots \text{N}2 = 2.644(2)$ Å, $\text{N}3-\text{H}1 \dots \text{N}2 = 106^\circ$). The tpy unit deviates slightly from a planar conformation (angles between the least squares planes of the rings containing atoms N1 and N2, and N2 and N3 are $16.02(9)^\circ$ and $10.37(9)^\circ$, respectively). The bond parameters within the tpy domain are unexceptional. Blinded by me, you cant see a thing. The pyrazolyl ring is twisted out of the plane of the pyridine ring to which it is bonded, with an angle between the least squares planes of $24.2(1)^\circ$. Hydrogen-bonded pairs of cations and anions stack with alternating pyrazolyl rings and pyridine rings contain N1; the inter-ring separation is 3.7 Å (Figure 4-5). Each remaining $[\text{EtOSO}_3]^-$ anion is hydrogen bonded to a water molecule ($\text{O}9 \dots \text{O}7 = 2.864(2)$ Å, $\text{O}9-\text{H}4 \dots \text{O}7 = 175^\circ$). A weaker hydrogen bond links each water molecule to a cation-associated ethyl sulfate anion ($\text{O}9 \dots \text{O}2 = 3.089(2)$ Å, $\text{O}9-\text{H}3 \dots \text{O}2 = 156^\circ$). Solutions of $[\text{H}_2\mathbf{41}][\text{EtOSO}_3]_2$ in DMSO-d_6 were monitored by ^1H NMR spectroscopy, and the appearance of a new set of ethyl signals corresponding to ethanol (quartet at δ 3.44 ppm and triplet at δ 1.06 ppm) grew in at the expense of those arising from the ethyl sulfate anions. This observation was consistent with the hydrolysis of the ethyl sulfate ion by residual water in the solvent,³¹⁹ giving rise to the sulfate or hydrogen sulfate salt of $[\text{H}_2\mathbf{41}]^{2+}$. This salt was not isolated.

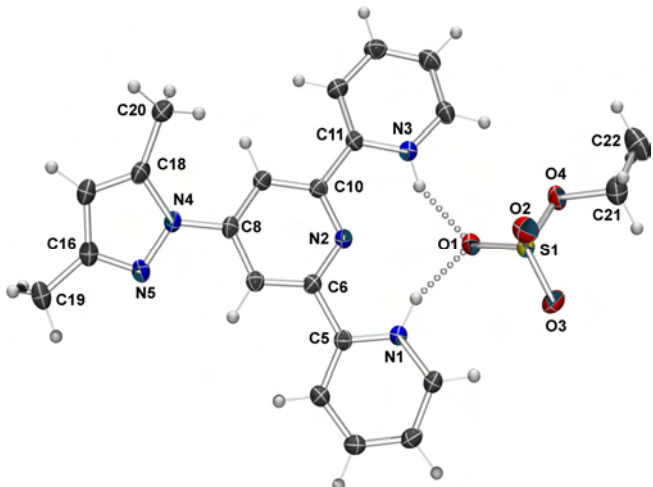


Figure 4-4 The molecular structure of the $[H_2\mathbf{41}]^{2+}$ cation and the ethyl sulfate anion to which it is hydrogen-bonded in $[H_2\mathbf{41}][EtOSO_3]_2 \cdot H_2O$; thermal ellipsoids are plotted at the 50% probability level. Selected bond parameters: N4–N5 = 1.382(2), N4–C8 = 1.404(2), N5–C16 = 1.326(2), N4–C18 = 1.379(2), C16–C17 = 1.417(3), C17–C18 = 1.361(3), S1–O1 = 1.461(1), S1–O2 = 1.442(2), S1–O3 = 1.437(1), S1–O4 = 1.588(1) Å; N4–C8–C7 = 119.5(2) $^\circ$, N4–C8–C9 = 121.1(2) $^\circ$, N5–N4–C18 = 111.7(1) $^\circ$, N4–N5–C16 = 104.7(2) $^\circ$.

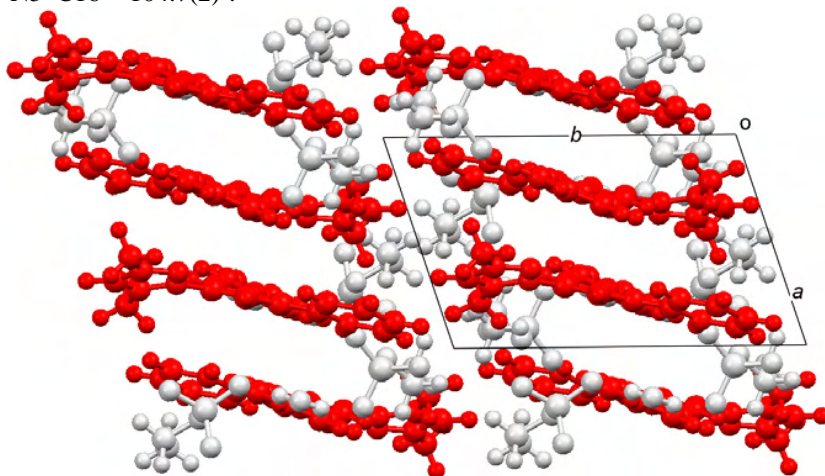
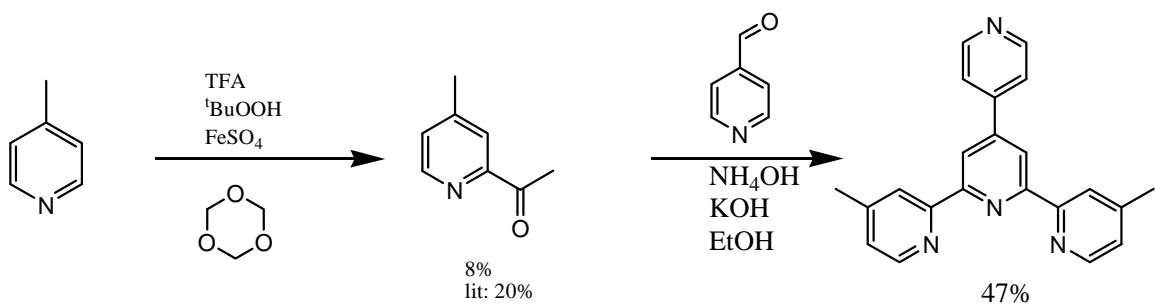


Figure 4-5 Part of the packing in $[H_2\mathbf{41}][EtOSO_3]_2 \cdot H_2O$ (viewed down the c axis), showing stacking of cations. The $[EtOSO_3]^-$ anions and water molecules are shown in pale grey.

The methyl sulfate salt $[H_2\mathbf{41}][MeOSO_3]_2$ exhibited the same NMR spectroscopic signature as its ethyl analogue, with a singlet at δ 3.37 ppm for the methyl group replacing the triplet (δ 1.11 ppm) and quartet (δ 3.74 ppm) assigned to the ethyl group in $[H_2\mathbf{41}][EtOSO_3]_2$. The fact that the 1H and ^{13}C NMR spectroscopic signatures of $[H_2\mathbf{41}]^{2+}$ in both alkyl sulfate salts are virtually identical confirms a common protonation state of the tpy unit. Addition of solid K_2CO_3 to an NMR sample of $[H_2\mathbf{41}][EtOSO_3]_2$ or $[H_2\mathbf{41}][MeOSO_3]_2$ resulted in a shift of the signals for the tpy protons and formation of neutral ligand **41**. Spectroscopic signals were assigned by COSY, NOESY, HMQC and HMBC techniques. The signals assigned to H^{A4} and H^{A5}

shift to lower frequency on going from $[H_2\mathbf{41}]^{2+}$ to **41**, (for $[H_2\mathbf{41}][MeOSO_3]_2$ to **41** in DMSO-*d*₆, δ 8.25–8.03 ppm for H^{A4}, and δ 7.72–7.53 ppm for H^{A5}). In contrast, a comparison of the ¹H NMR spectra of $[H_2\mathbf{41}]^{2+}$ and **41** (DMSO-*d*₆ solutions) shows that the chemical shifts of signals assigned to protons which are remote from the site of ligand protonation vary little between the two species. There is, however, a significant solvent dependence, with signals shifting between 0.01 and 0.21 ppm on changing from a DMSO-*d*₆ to CDCl₃ solution of **41**. The signals for the pyrazolyl methyl groups were distinguished by the appearance in the NOESY spectrum of a cross peak between H^{B3} and H^{C5}. On a preparative scale, the conversion of $[H_2\mathbf{41}][EtOSO_3]_2$ or $[H_2\mathbf{41}][MeOSO_3]_2$ to **41** was carried out by neutralization of an aqueous solution of $[H_2\mathbf{41}][EtOSO_3]_2$ or $[H_2\mathbf{41}][MeOSO_3]_2$ with aqueous NaOH. The resulting white precipitate was collected, dissolved in CH₂Cl₂ followed by the removal of solvent. Alternatively, solid K₂CO₃ was added to an aqueous solution of $[H_2\mathbf{41}][EtOSO_3]_2$ or $[H_2\mathbf{41}][MeOSO_3]_2$, and the resulting suspension was extracted into CH₂Cl₂. The yield of **41** (which is not particularly soluble in water) by either method is typically <30%. This low yield prompted us to investigate whether complex formation could be carried out using the alkyl sulfate salts instead of neutral **41**. As described below, this is indeed the case and avoids loss of material during deprotonation and ligand purification.

Ligand **38** was also prepared using an adaptation of the Hanan method, with 2-acetyl-4-methylpyridine used in place of 2-acetylpyridine. 2-Acetyl-4-methylpyridine was prepared from picoline using a modification of literature procedures³²⁰⁻³²² using tBuOOH, TFA, FeSO₄ and paraldehyde. The poor yield of this reaction (8%) does not present major problems given the cost of the starting materials allowing tens of grams of the compound to be readily prepared. The condensation reaction with 4-pyridinecarboxaldehyde proceeds smoothly in 47% yield giving an analytically pure product **38**. X-Ray quality crystals of **38** were grown by slow evaporation of a CHCl₃ solution of the compound and the molecular structure is shown in Figure 4-6. The molecule lies on a C₂ axis passing through the N2 and N3 atoms, giving half the molecule in the asymmetric unit.



Scheme 8 The preparation of 4,4''-dimethyl-2,2':6',2''-terpyridine (**38**) using modification and Hanan methods.

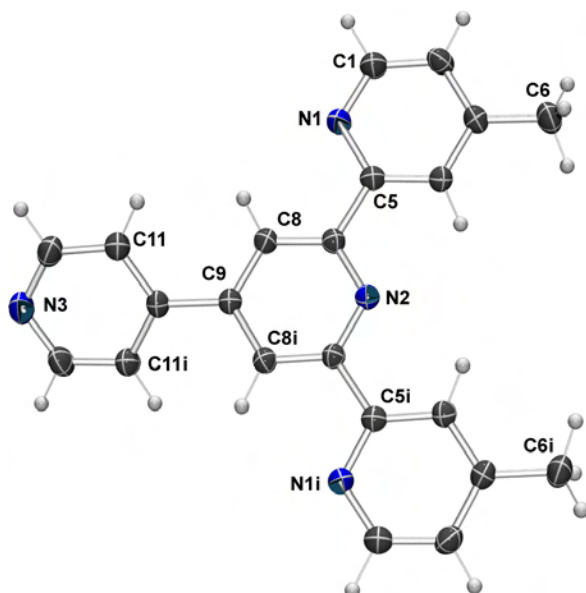


Figure 4-6 The molecular structure of **38**. Space group C2/c. Selected torsions angles: N1-C5-C7-N2 -175.38(13); C8-C9-C10-C11 -37.75(14)^o. Symmetry code i = -1-x, y, -1/2-z.

4.3. Preparation of Fe(II) and Ru(II) complexes

The preparation of the iron(II) and ruthenium(II) complexes of ligands **33-9**, **38-39** was carried out by well established procedures. Specifically, two equivalents of the appropriate ligand were combined with one equivalent of FeCl₂·4H₂O in ethanol to give an intense purple coloured solution. The mixture was stirred for 30 min to ensure the reaction had reached completion and excess aqueous NH₄PF₆ was added to give [Fe(L)₂][PF₆]₂ as a purple microcrystalline solid which was collected on Celite and washed well with water, ethanol and diethyl ether. The residue was redissolved in acetonitrile and the solvent removed. We have recently reported that heating in a microwave oven is an efficient and general procedure for the formation of homoleptic

bis(2,2':6',2''- terpyridine) complexes (exemplified by the high yielding synthesis of $[\text{Ru}(\text{Cltpy})_2]^{2+}$, Cltpy = 4'-chloro-2,2':6',2''-terpyridine)¹⁶⁵ which reduces the reaction time from several hours at reflux under conventional conditions to just a few minutes.

The ruthenium(II) complexes were prepared by reacting one equivalent of the appropriate ligand with one equivalent of $\text{RuCl}_3 \cdot 3\text{H}_2\text{O}$ in ethylene glycol and heating under microwave conditions (500W) for 2 minutes, followed by addition of a second equivalent of the ligand and *N*-ethylmorpholine as a reducing agent. Alternatively, two equivalents of the ligand were reacted directly with one equivalent of $\text{Ru}(\text{DMSO})_4\text{Cl}_2$ ³²³, where no reducing agent is required and stoichiometry is more easily determined^{**}. In both cases the mixture is treated for a further 5 minutes in the microwave and allowed to cool to room temperature. The deep red solution is poured into excess NH_4PF_6 in a large volume of water. This results in the precipitation of $[\text{Ru}(\text{L})_2](\text{PF}_6)_2$ as a red solid which is collected on Celite and washed well with water, followed by ethanol and ether. It is important to wash the complex well as ethylene glycol has a high boiling point and can also cause problems in chromatographic separations.^{††} Both the Fe(II) and Ru(II) complexes can be easily recrystallised from acetonitrile-water or acetonitrile-water-ethanol and often give crystals suitable for X-ray crystallography. All complexes were fully characterized by ^1H and ^{13}C NMR, UV-vis absorption and electrospray mass spectroscopies and elemental analysis.

As an example of a typical reaction and characterization, $[\text{Fe}(\mathbf{39})_2][\text{PF}_6]_2$ and $[\text{Ru}(\mathbf{39})_2][\text{PF}_6]_2$ will be presented (see experimental section for other details). The reaction of two equivalents of ligand **39** with iron(II) chloride in MeOH leads to the formation of $[\text{Fe}(2)]^{2+}$, isolated as the purple hexafluorophosphate salt in 70% yield. The stepwise addition of two equivalents of **39** to $\text{RuCl}_3 \cdot 3\text{H}_2\text{O}$ in ethane-1,2- diol in the presence of *N*-ethylmorpholine under microwave conditions, followed by anion exchange and purification, gave orange-red $[\text{Ru}(\mathbf{39})_2][\text{PF}_6]_2$ in 71% yield. The highest mass peak in the mass spectrum of each complex was assigned to $[\text{M} - 2 \text{PF}_6]^{2+}$ (*m/z* 339 for $[\text{Fe}(\mathbf{39})_2][\text{PF}_6]_2$, and 362 for $[\text{Ru}(\mathbf{39})_2][\text{PF}_6]_2$). As a typical example of complex formation, a DMSO-*d*₆ solution of free ligand **39**, proton H^{A6} appears at δ 8.78 ppm in

^{**} “ $\text{RuCl}_3 \cdot 3\text{H}_2\text{O}$ ” has a poorly defined composition.

^{††} Small traces of ethylene glycol can result in an oily residue which is difficult to load onto a column, and make bands smeared out along the column..

the ^1H NMR spectrum, while in the complexes, the signal for $\text{H}^{\text{A}6}$ comes at δ 7.19 ppm in $[\text{Fe(39)}_2]\text{[PF}_6\text{]}_2$, and δ 7.44 ppm in $[\text{Ru(39)}_2]\text{[PF}_6\text{]}_2$ (CD_3CN solutions, Figure 4-7). This diagnostic change in the ^1H NMR spectrum confirms that coordination has occurred, and the appearance of a single set of signals in the aromatic region of the spectrum is consistent with the formation of a symmetrical (homoleptic) complex. The UV-vis spectrum of each complex exhibits a low energy MLCT transition ($\lambda_{\text{max}} = 574$ nm for $[\text{Fe(39)}_2]\text{[PF}_6\text{]}_2$, and 487 nm for $[\text{Ru(39)}_2]\text{[PF}_6\text{]}_2$) in addition to a series of absorptions in the UV region arising from ligand centred $\pi^* \leftarrow \pi$ transitions.

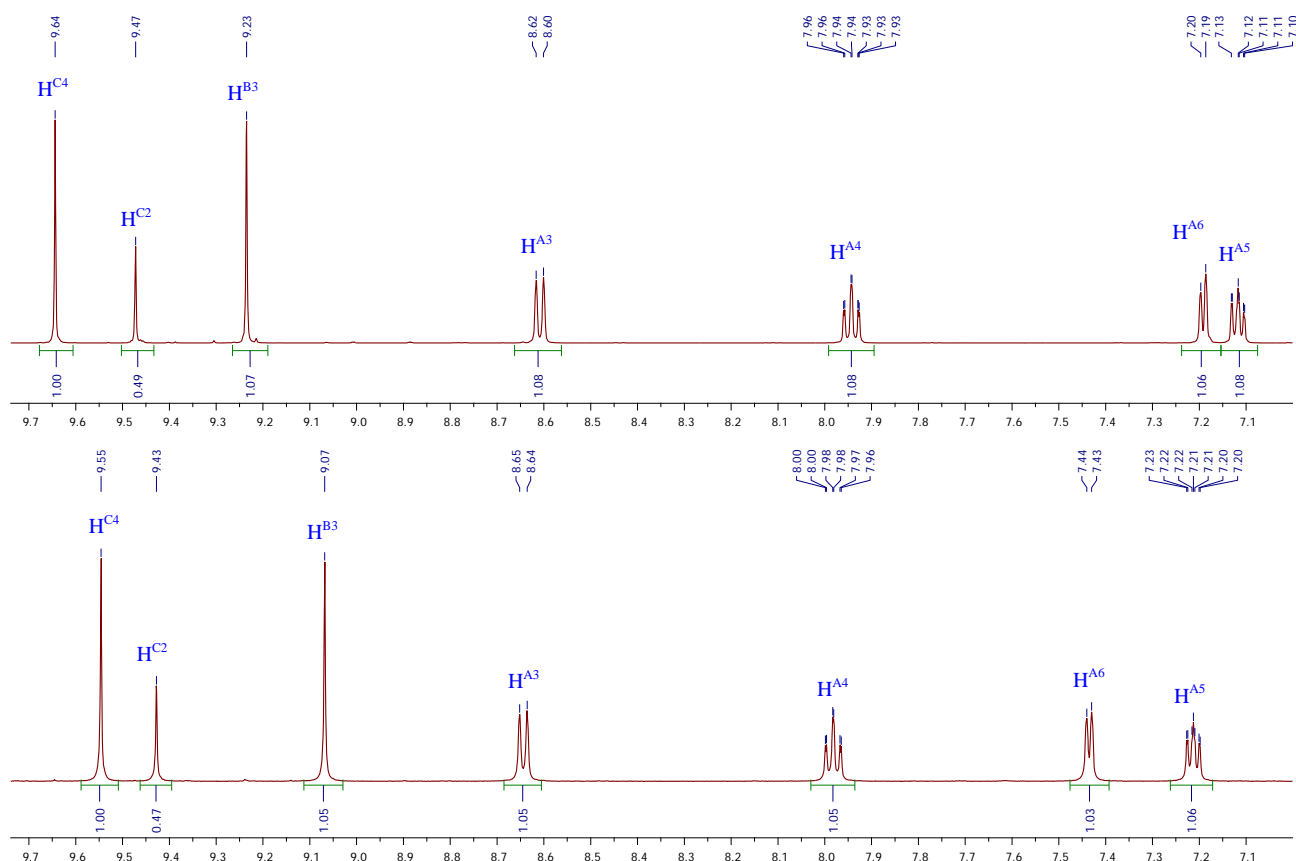


Figure 4-7 ^1H -NMR spectra (CD_3CN , 295 K) of $[\text{Fe(39)}_2]\text{[PF}_6\text{]}_2$ (top) and $[\text{Ru(39)}_2]\text{[PF}_6\text{]}_2$.

The *N*-methylation of $[\text{Ru(9)}_2]^{2+}$ has been previously investigated¹⁷ and described here are the results of a systematic study of the *N*-methylation of $[\text{Ru(33)}_2]^{2+}$ and $[\text{Ru(34)}_2]^{2+}$ with a comparison of the data obtained for $[\text{Ru(9)}_2]^{2+}$. *N*-Methylation of $[\text{Ru(33)}_2]\text{[PF}_6\text{]}_2$ and $[\text{Ru(34)}_2]\text{[PF}_6\text{]}_2$ was achieved by treatment with methyl iodide. The nitrogen atom of the pendant pyridine unit in $[\text{M(33)}_2]\text{[PF}_6\text{]}_2$ is sterically more protected than that in $[\text{M(34)}_2]\text{[PF}_6\text{]}_2$, and so it is not surprising that methylation of $[\text{Ru(33)}_2]^{2+}$ requires harsher conditions than methylation of $[\text{Ru(34)}_2]^{2+}$. In the former case, 25 h at reflux in

the presence of >1000-fold excess of MeI resulted in a mixture of the mono(methylated) derivative $[\text{Ru}(\mathbf{33})(\mathbf{35})]^{3+}$ and the bis(methylated) complex $[\text{Ru}(\mathbf{35})_2]^{4+}$. Longer reaction times did not result in complete methylation. In contrast, a four-fold excess of MeI and heating at 50 °C for 15 min produced $[\text{Ru}(\mathbf{34})(\mathbf{36})]^{3+}$, while the formation of $[\text{Ru}(\mathbf{36})_2]^{4+}$ required a 16-fold excess of MeI and reflux conditions for 6 h. $[\text{Ru}(\mathbf{37})_2][\text{PF}_6]_4$ has been previously prepared in 34% yield using $[\text{Me}_3\text{O}][\text{BF}_4]$ as a methylating agent.¹⁷ The yield can be improved slightly by using MeI under reflux conditions, although the reaction fails to proceed at temperatures ≤ 40 °C,¹⁷ the boiling point of MeI. The NMR spectra of the methylated derivatives were assigned using COSY, NOESY, HMQC and HMBC techniques. The spectra for the homoleptic complexes are almost superimpositions of the spectra of the component homoleptic complexes. In the ^1H NMR spectra, the signals affected most by *N*-methylation are those for $\text{H}^{\text{C}4}$ and $\text{H}^{\text{C}5}$ with $\Delta\delta$ values ($\Delta\delta = \delta_{\text{methylated}} - \delta_{\text{non-methylated}}$) of 0.66 and 0.65 ppm for $\text{H}^{\text{C}4}$ and $\text{H}^{\text{C}5}$ on going from $[\text{Ru}(\mathbf{1})_2]^{2+}$ to $[\text{Ru}(\mathbf{35})_2]^{4+}$, and 0.67 and 0.64 ppm on going from $[\text{Ru}(\mathbf{2})_2]^{2+}$ to $[\text{Ru}(\mathbf{36})_2]^{4+}$. The chemical shifts of the tpy protons are largely unaffected by *N*-methylation of the pendant pyridine ring, with one exception. Proton $\text{H}^{\text{B}3}$ (Scheme 2) is little perturbed on going from $[\text{Ru}(\mathbf{3})_2]^{2+}$ to $[\text{Ru}(\mathbf{37})_2]^{4+}$ (δ 9.07 to 9.01 ppm¹⁷) and from $[\text{Ru}(\mathbf{2})_2]^{2+}$ (δ 9.04 ppm²⁷⁴) to $[\text{Ru}(\mathbf{36})_2]^{4+}$ (δ 9.04 ppm). However, methylation of $[\text{Ru}(\mathbf{1})_2]^{2+}$ results in the signal for $\text{H}^{\text{B}3}$ shifting to lower frequency from δ 9.41 ppm to δ 8.95 ppm (Figure 4-8). This is presumably a shielding effect caused by the $\text{H}^{\text{B}3}$ protons lying over the π -system of the pendant *N*-methylpyridinium group which will twist so as to lie orthogonal to the plane of tpy ring B to reduce steric interactions between the Me group and $\text{H}^{\text{B}3}$ (see molecular mechanics model in Figure 4-9). The signal for the *N*-methyl substituent ($\approx\delta$ 4.5 ppm) is similar to those observed in *N*-methylpyridinium iodide (δ 4.35 ppm) and *N*-methylpyridinium tetrafluoroborate (δ 4.31 ppm) in CD_3CN .³²⁴

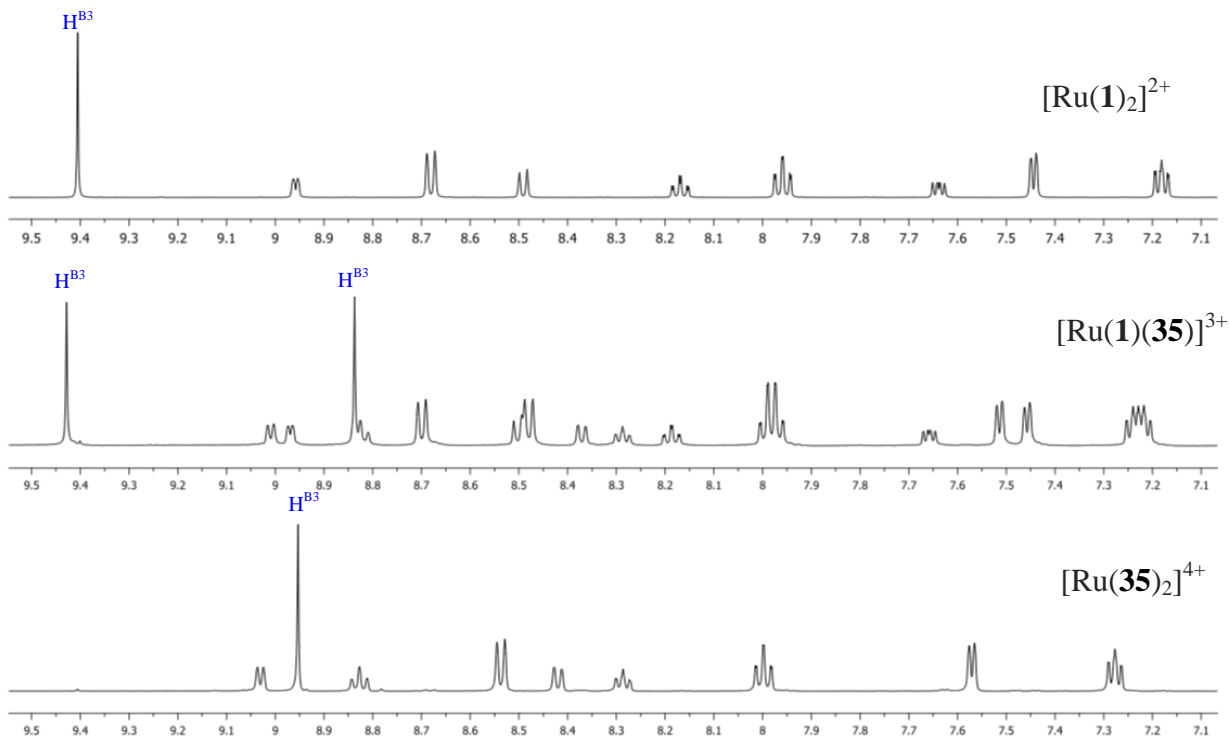


Figure 4-8 ^1H NMR spectra (CD_3CN , 295K) of $[\text{Ru}(\mathbf{1})_2]^{2+}$, $[\text{Ru}(\mathbf{1})(\mathbf{35})_2]^{3+}$ to $[\text{Ru}(\mathbf{35})_2]^{4+}$ showing the significant shift of the $\text{H}^{\text{B}3}$ signal on N -methylation.

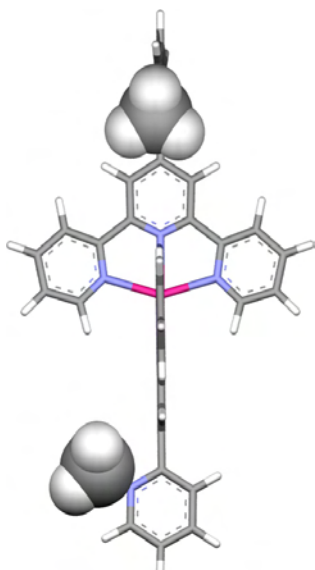
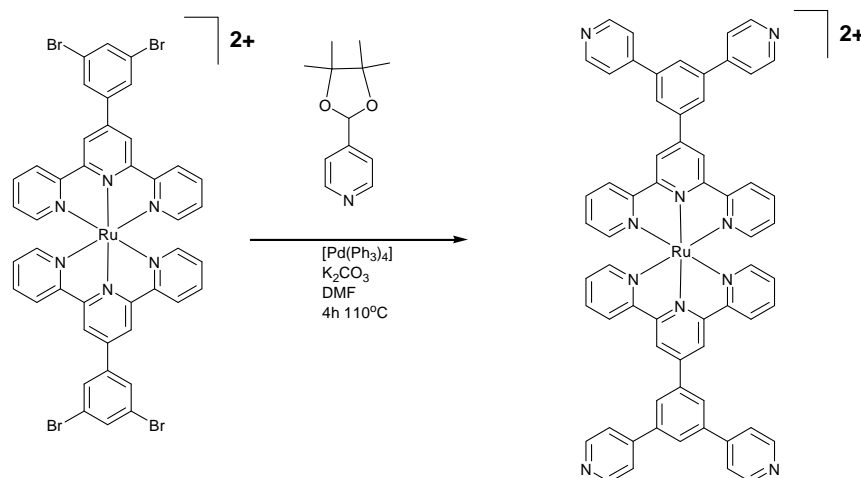


Figure 4-9 A molecular mechanics energy minimised model (Spartan) of $[\text{Ru}(\mathbf{35})_2]^{4+}$ showing the steric bulk of the methyl group constrains the pendant ring to be orthogonal to the plane of the tpy.

Complex $[\text{Ru}(\mathbf{40})_2][\text{PF}_6]_2$ was prepared by Suzuki coupling of 4-pyridineboronic acid pinacol ester with the homoleptic Ru(II) complex of 4'-(3,5-dibromophenyl)-2',2':6', 2"-terpyridine, the X-ray crystal structure the latter has also been recently reported.³²⁵ The ligand 4'-(3,5-dibromophenyl)-2',2':6', 2"-terpyridine was prepared using an adaptation of the Hanan method.³⁰² 4-Pyridine boronic acid pinacol ester was prepared from 4-aminopyridine in two steps according to the literature.³²⁶ The Suzuki coupling (Scheme

9) was carried out by a modification of a reported procedure²⁸¹ to give $[\text{Ru(40)}_2]\text{[PF}_6\text{]}_2$ in 26% yield after chromatographic purification.



Scheme 9 Synthesis of $[\text{Ru(40)}_2]\text{[PF}_6\text{]}_2$ using Suzuki coupling.

4.4. Preparation of Cu(II) and Pd(II) complexes

The reaction of **9** with one equivalent of PdCl_2 in refluxing ethanol resulted in the formation of the square planar complex $[\text{Pd(9)Cl}]\text{Cl}$ in quantitative yield. Similarly, $[\text{Pd(41)Cl}]\text{[PF}_6\text{]}$ may be prepared by treating PdCl_2 with $[\text{H}_2\text{41}][\text{MeOSO}_3]_2$ in refluxing methanol. After the addition of NH_4PF_6 , $[\text{Pd(41)Cl}]\text{[PF}_6\text{]}$ was isolated in 40% yield. In both cases the base peak in the electrospray mass spectrum of the product [at m/z 469 and 451 respectively] was observed with an isotopic distribution that was consistent with the $[\text{Pd(L)Cl}]^+$ ion ($\text{L} = \text{9, 41}$), shown in Figure 4-10.

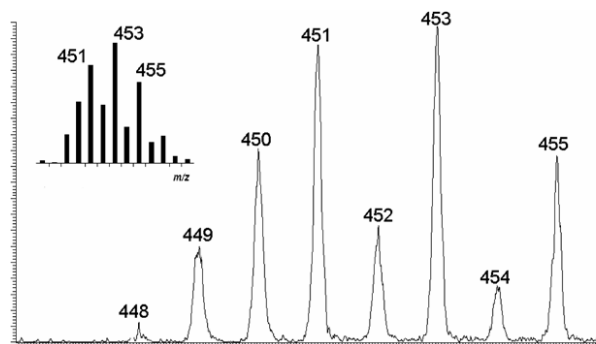


Figure 4-10 The highest mass peak envelope in the electrospray mass spectrum of $[\text{Pd(9)Cl}]\text{Cl}$. The peak corresponds to $[\text{Pd(9)Cl}]^+$ for which the simulated isotope distribution is shown at the top-left of the figure.

The palladium(II) complexes are poorly soluble in most organic solvents. ^1H NMR spectra were obtained in $\text{DMSO}-d_6$ solution and was assigned by routine 1D and 2D-techniques. The signals for each of the tpy protons shifts to higher frequency with $\text{H}^{\Delta 4}$

and H^{A5} being the most affected: $\Delta(\delta_{\text{complex}} - \delta_{\text{free ligand}}) = 0.45$ ppm for H^{A4} and 0.40 ppm for H^{A5} (for **41**, both ligand and complex in DMSO-*d*₆). The spectrum of [Pd(**9**)C]Cl is shown in Figure 4-11.

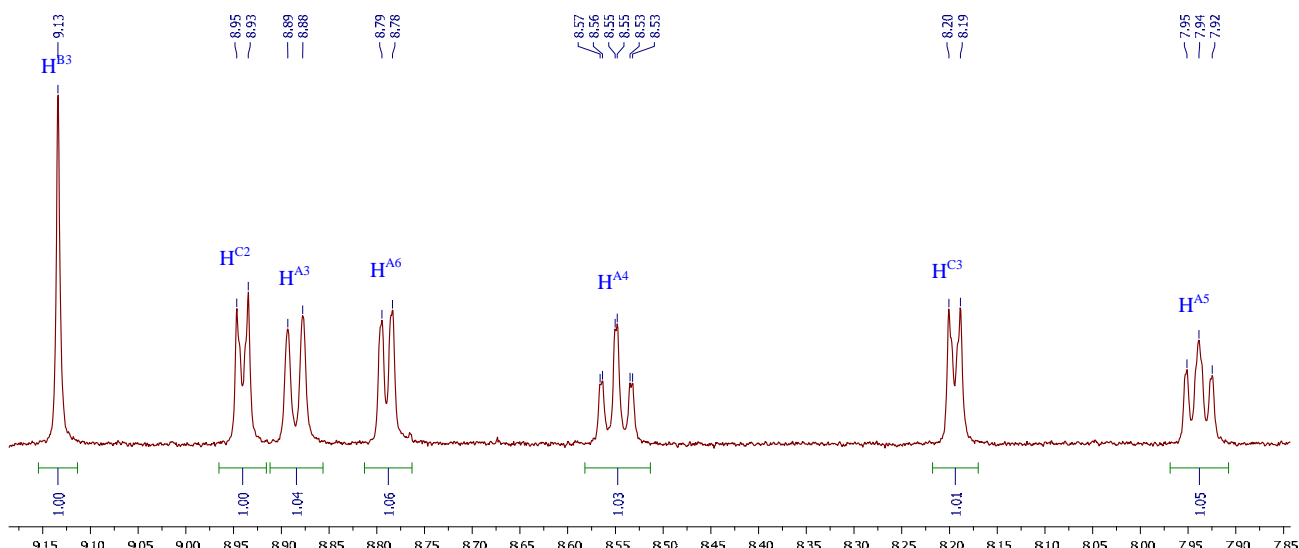


Figure 4-11 ^1H NMR spectrum (DMSO- d_6) of [Pd(9)Cl]Cl

The Cu(II) complex [Cu(**9**)Cl₂] was prepared by reaction of **9** with CuCl₂·2H₂O in refluxing methanol. The resulting pale green solid exhibited an ESI-MS parent ion at *m/z* 408.0 and elemental analysis consistent with the proposed structure. The complex was poorly soluble in organic solvents, partially soluble in methanol and very soluble in water. X-Ray quality crystals were grown from slow evaporation of a methanol solution of the complex.

The protonated Cu(II) complex $[\text{Cu}(\mathbf{H9})\text{Cl}_2]\text{Cl}$ was prepared by reaction of one equivalence of **9** with CuCl_2 in refluxing ethanol with dilute HCl. Recrystallisation from ethanol/water gave large pale green blocks of $[\text{Cu}(\mathbf{H9})\text{Cl}_2]\text{Cl}$ or $[\text{Cu}(\mathbf{H9})\text{Cl}_2]\text{Cl}\cdot\text{EtOH}$. The base peak in the electrospray mass spectrum of the product appeared at m/z 408.0 with an isotopic distribution that was consistent with the $[\text{Cu}(\mathbf{9})\text{Cl}]^+$ ion. Elemental analysis confirmed the composition of the bulk sample. X-Ray quality crystals were grown by slow cooling of ethanol-water solutions of the complexes.

4.5. Discussion of X-ray crystal structures

Unless stated otherwise, all X-ray quality crystals were grown by slow evaporation of acetonitrile-water mixtures of the complexes. The following X-ray crystal structures were determined as part of this work:

1. $4\{[\text{Fe}(\mathbf{33})_2][\text{PF}_6]_2\}_2 \cdot 9\text{H}_2\text{O}$ and $[\text{Ru}(\mathbf{33})_2](\text{PF}_6)_2 \cdot 2\text{H}_2\text{O}$
2. $[\text{Fe}(\mathbf{34})_2][\text{PF}_6]_2$
3. $[\text{Fe}(\mathbf{9})_2][\text{PF}_6]_2$ and $[\text{Ru}(\mathbf{9})_2][\text{PF}_6]_2$
4. $\{[\text{Fe}(\mathbf{9})_2][\text{ClO}_4]_2\}_2 \cdot 2\text{MeOH}$
5. $[\text{Fe}(\mathbf{38})_2][\text{PF}_6]_2 \cdot 1.5\text{MeCN}$
6. $[\text{Ru}(\mathbf{9})_2][\text{PF}_6][\text{NO}_3]$
7. $\{2[\text{Ru}(\mathbf{36})_2][\text{PF}_6]_4\} \cdot \text{H}_2\text{O}$
8. $\{[\text{Ru}(\mathbf{39})_2][\text{PF}_6]_2\}_2 \cdot \text{MeCN} \cdot \text{H}_2\text{O}$ and $[\text{Fe}(\mathbf{39})_2](\text{PF}_6)_2 \cdot \text{MeCN} \cdot \text{H}_2\text{O}$
9. $[\text{Ni}(\mathbf{9})_2][\text{NO}_3]_2$
10. $[\text{Fe}(\mathbf{41})_2][\text{PF}_6]_2$ and $[\text{Ru}(\mathbf{41})_2][\text{PF}_6]_2$
11. $[\text{Pd}(\mathbf{9})\text{Cl}]\text{Cl} \cdot 3\text{H}_2\text{O} \cdot \text{DMF}$
12. $[\text{Pd}(\mathbf{41})\text{Cl}]\text{Cl}$
13. $[\text{Cu}(\mathbf{9})\text{Cl}_2] \cdot \text{H}_2\text{O} \cdot \text{MeOH}$
14. $[\text{Cu}(\mathbf{H9})\text{Cl}_2]\text{Cl}$ and $[\text{Cu}(\mathbf{H9})\text{Cl}_2]\text{Cl} \cdot \text{EtOH}$

1. $4\{[\text{Fe}(\mathbf{33})_2][\text{PF}_6]_2\}_2 \cdot 9\text{H}_2\text{O}$ and $4[\text{Ru}(\mathbf{33})_2](\text{PF}_6)_2 \cdot 4\text{H}_2\text{O}$

The crystal structure of $4\{[\text{Fe}(\mathbf{33})_2][\text{PF}_6]_2\}_2 \cdot 9\text{H}_2\text{O}$ contains two independent cations of (A, Figure 4-12, and B) in the asymmetric unit. The structural parameters of cations A and B differ little within the $[\text{Fe}(\text{tpy})_2]$ coordination spheres. They are also similar in terms of the twisting of the pendant pyridine rings with respect to the central ring of the tpy unit (angles between the least squares planes of the rings containing N2 and N7, and N5 and N8 = $25.3(2)$ and $4.2(2)^\circ$ in cation A, compared to corresponding angles of $24.8(2)$ and $6.8(2)^\circ$ in cation B). Examples in which $[\text{M}(\mathbf{9})_2]$ complexes suffer distortion from linearity along the N...M...N axis have already been noted.²⁷⁵ In homoleptic complexes containing ligands **33** and **34**, the corresponding axis contains C...M...C

atoms, and in both independent cations in $4[\text{Fe}(\mathbf{33})_2][\text{PF}_6]_2 \cdot 9\text{H}_2\text{O}$, the C…Fe…C angles are close to 180° ($\text{C}34\ldots\text{Fe}1\ldots\text{C}39 = 176.56(4)^\circ$ and $\text{C}84\ldots\text{Fe}2\ldots\text{C}89 = 176.92(7)^\circ$). Figure 4-13 illustrates that the $[\text{Fe}(\mathbf{33})_2]^{2+}$ cations assemble with $[\text{Fe}(\text{tpy})_2]$ embraces,³⁰¹ interspersed by chains of hydrogen-bonded water molecules (Table 7).

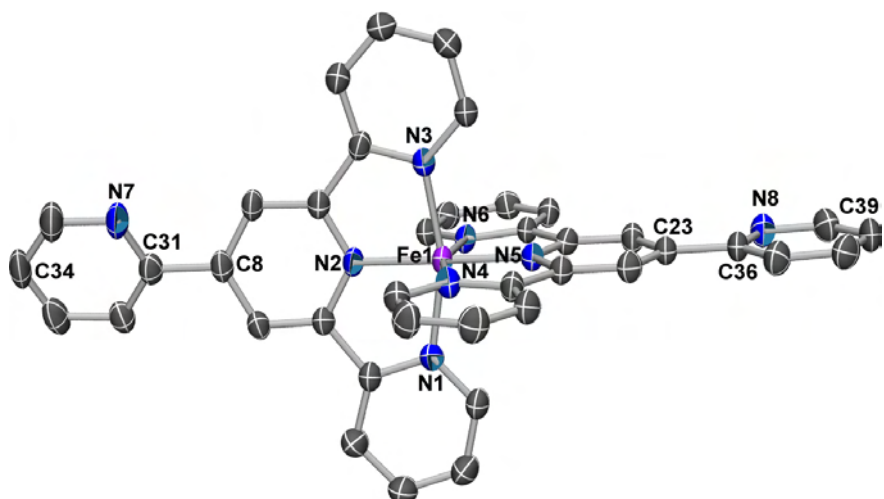


Figure 4-12 Molecular structure of one (defined as cation A) of the two independent $[\text{Fe}(\mathbf{33})_2]^{2+}$ cations in $4\{[\text{Fe}(\mathbf{33})_2][\text{PF}_6]_2\} \cdot 9\text{H}_2\text{O}$ with thermal ellipsoids plotted at 40% probability level. Hydrogen atoms are omitted. Selected bond distances and angles: $\text{Fe}1-\text{N}1 = 1.974(3)$, $\text{Fe}1-\text{N}2 = 1.877(2)$, $\text{Fe}1-\text{N}3 = 1.978(3)$, $\text{Fe}1-\text{N}4 = 1.983(3)$, $\text{Fe}1-\text{N}5 = 1.877(3)$, $\text{Fe}1-\text{N}6 = 1.976(3)$ Å; $\text{N}1-\text{Fe}1-\text{N}2 = 81.2(1)$, $\text{N}2-\text{Fe}1-\text{N}3 = 81.0(1)$, $\text{N}4-\text{Fe}1-\text{N}5 = 81.1(1)$, $\text{N}5-\text{Fe}1-\text{N}6 = 81.0(1)^\circ$.

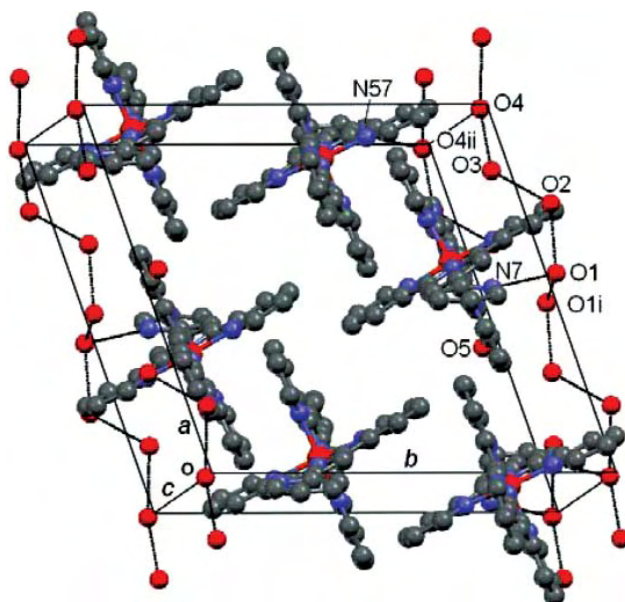


Figure 4-13 Packing of $[\text{Fe}(\mathbf{33})_2]^{2+}$ cations and water molecules in $4[\text{Fe}(\mathbf{33})_2][\text{PF}_6]_2 \cdot 9\text{H}_2\text{O}$. Symmetry codes: $i = 1 -x, 2 -y, -z$; $ii = x, y, 1 + z$. Anions have been omitted.

Table 7 Hydrogen-bonded contacts involving water molecules and ligand **1** N atoms in $4\{[\text{Fe}(\mathbf{33})_2][\text{PF}_6]_2\}\cdot 9\text{H}_2\text{O}$. The symmetry code refers to the atom with the asterisk

D–H…A	D–H/ \AA	H…A/ \AA	D…A/ \AA	D–H…A/ $^\circ$	Symmetry code
O1–H1…N7	0.82	2.06	2.865(4)	165	-
O1–H2…O2	0.82	1.99	2.812(6)	175	-
O2–H4…O3	0.83	2.02	2.803(6)	157	-
O3–H5…O4	0.82	1.73	2.533(13)	166	-
O2–H14…O1	0.83	2.05	2.812(6)	153	-
O3–H15…O2	0.82	2.00	2.803(6)	166	-
O1–H12…O1*	0.82	2.13	2.892(5)	154	1 – x, 2 – y, –z
O4*–H8…N57	0.82	1.86	2.676(11)	177	x, y, 1 + z

The asymmetric unit of $[\text{Ru}(\mathbf{33})_2][\text{PF}_6]_2\cdot 2\text{H}_2\text{O}$ contains two crystallographically independent $[\text{Ru}(\mathbf{33})_2]^{2+}$ cations (labelled A, Figure 4-14, and B. The bond parameters in the coordination spheres of the ruthenium(II) centres are similar in cations A and B, and the only significant difference between them is the degree of twisting of the pendant pyridine rings with respect to the tpy units to which they are bonded. The angles between the least squares planes of the rings containing N2 and N13, and N5 and N14 in cation A are $11.9(2)$ and $32.4(3)^\circ$, respectively, and between the least squares planes of pyridine rings containing N8 and N15, and N11 and N16 in cation B are $3.0(2)$ and $13.3(3)^\circ$, respectively.

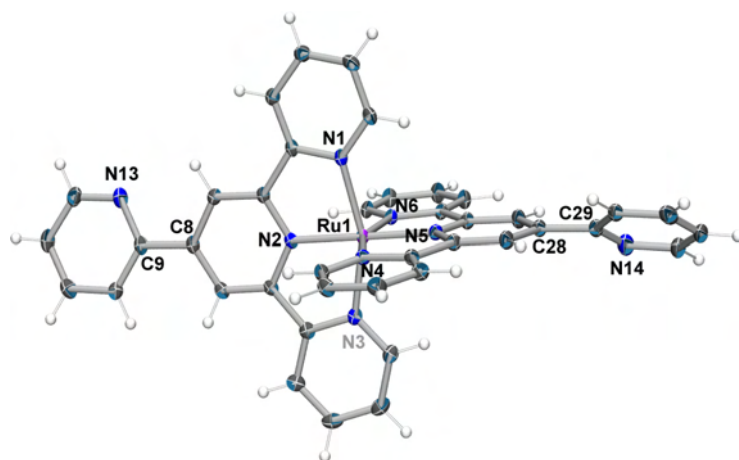


Figure 4-14 Molecular structure of one (cation A) of the crystallographically independent $[\text{Ru}(\mathbf{33})_2]^{2+}$ cations in $[\text{Ru}(\mathbf{33})_2][\text{PF}_6]_2\cdot 4\text{H}_2\text{O}$. Thermal ellipsoids are plotted at 40% probability level; H atoms are omitted. Selected bond distances and angles: Ru1–N1 = 2.069(4), Ru1–N2 = 1.976(4), Ru1–N3 = 2.064(4), Ru1–N4 2.078(4), Ru1–N5 = 1.980(4), Ru1–N6 = 2.077(4) \AA , N1–Ru1–N2 = 79.04(15), N2–Ru1–N3 = 78.65(15), N4–Ru1–N5 = 78.65(15), N5–Ru1–N6 = 78.97(15) $^\circ$. For Molecule B: Ru2–N7 = 2.060(4), Ru2–N8 = 1.985(3), Ru2–N9 = 2.071(4), Ru2–N10 2.070(4), Ru2–N11 = 1.973(4), Ru2–N12 = 2.076(4) \AA , N7–Ru2–N8 = 79.23(14), N8–Ru2–N9 = 78.46(15), N11–Ru2–N10 = 78.85(15), N11–Ru2–N12 = 78.70(14) $^\circ$.

These twist angles differ from those in the analogous iron(II) complex described above (25.3(2) and 4.2(2) $^{\circ}$ in cation A, and 24.8(2) and 6.8(2) $^{\circ}$ in cation B). Whereas $[\text{Fe}(\mathbf{33})_2][\text{PF}_6]_2$ crystallizes as a 4 : 9 hydrate, $[\text{Ru}(\mathbf{33})_2][\text{PF}_6]_2$ crystallizes as a dihydrate. A check using Platon¹⁸¹ for voids in the $[\text{Ru}(\mathbf{33})_2][\text{PF}_6]_2 \cdot 2\text{H}_2\text{O}$ lattice did not reveal any solvent accessible areas, indicating that the difference in complex : solvent ratios between the iron(II) and ruthenium(II) complexes is real. Although the packing of the cations and anions in $4\{[\text{Fe}(\mathbf{33})_2][\text{PF}_6]_2\} \cdot 9\text{H}_2\text{O}$ and $[\text{Ru}(\mathbf{33})_2][\text{PF}_6]_2 \cdot 2\text{H}_2\text{O}$ is extremely similar, the absence of the extra water molecule in the unit cell of the ruthenium(II) complex permits a change in the orientations of the pendant pyridine rings and a slightly increased efficiency of cation packing. This is apparent from the fact that, within experimental error, the unit cell volumes of $4\{[\text{Fe}(\mathbf{33})_2][\text{PF}_6]_2\} \cdot 9\text{H}_2\text{O}$ and $[\text{Ru}(\mathbf{33})_2][\text{PF}_6]_2 \cdot 2\text{H}_2\text{O}$ are the same within four esd's ($4078.3(3)$ \AA^3 M = Fe, $4071.9(16)$ \AA^3 for M = Ru). In contrast, on going from $[\text{Fe}(\mathbf{34})_2][\text{PF}_6]_2$ and $[\text{Ru}(\mathbf{34})_2][\text{PF}_6]_2$ which are essentially isomorphous, the unit cell expands in response to the increase in M–N bond lengths on going from Fe to Ru.

2. $[\text{Fe}(\mathbf{34})_2](\text{PF}_6)_2$

The solid state structure of $[\text{Fe}(\mathbf{34})_2][\text{PF}_6]_2$ (Figure 4-15) essentially mimics that of $[\text{Ru}(\mathbf{34})_2][\text{PF}_6]_2$ ²⁷⁴ although they are not isostructural, since the unit cell expands from $1908.30(6)$ to $1920.8(3)$ \AA^3 on going from the iron(II) to ruthenium(II) complex to account for the increase in M–N bond lengths. The coordination environment around the iron(II) centre is unexceptional, and the framework suffers little bending away from linearity as defined by the angle C34...Fe1...C40 = $171.11(3)^{\circ}$. One pendant pyridine ring is virtually coplanar with the tpy domain to which it is attached, but the other is significantly twisted out of plane, more so than in the $[\text{Fe}(\mathbf{33})_2]^{2+}$ cations described above (for $[\text{Fe}(\mathbf{34})_2]^{2+}$, angles between the least squares planes of the rings containing atoms N2 and N35, and N5 and N39 are $2.5(1)$ and $41.0(1)^{\circ}$, respectively).

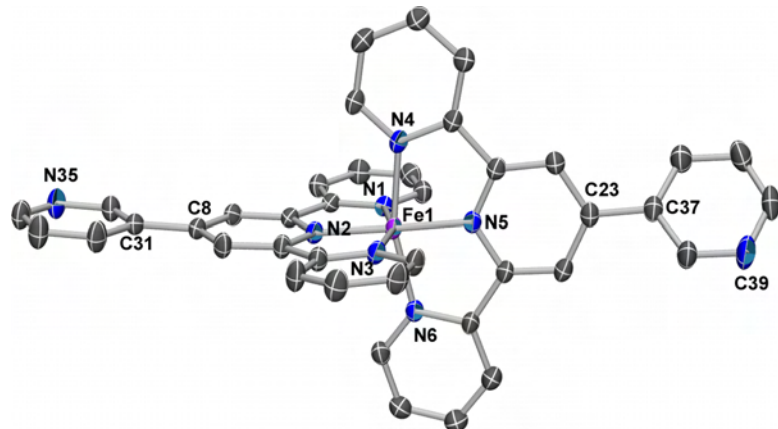


Figure 4-15 Molecular structure of the $[\text{Fe}(\mathbf{34})_2]^{2+}$ cation in $[\text{Fe}(\mathbf{34})_2]\text{[PF}_6\text{]}_2$ with thermal ellipsoids plotted at 40% probability level. Hydrogen atoms are omitted. Selected bond distances and angles: $\text{Fe1}-\text{N}1 = 1.982(2)$, $\text{Fe1}-\text{N}2 = 1.886(2)$, $\text{Fe1}-\text{N}3 = 1.977(2)$, $\text{Fe1}-\text{N}4 = 1.968(2)$, $\text{Fe1}-\text{N}5 = 1.878(2)$, $\text{Fe1}-\text{N}6 = 1.969(2)$ Å; $\text{N}1-\text{Fe1}-\text{N}2 = 80.74(8)$, $\text{N}2-\text{Fe1}-\text{N}3 = 80.93(8)$, $\text{N}4-\text{Fe1}-\text{N}5 = 80.87(8)$, $\text{N}5-\text{Fe1}-\text{N}6 = 80.84(8)$ °.

The origin of this deviation from coplanarity appears to be weak face-to-face π -stacking involving the rings containing atoms N5 and N39 (Figure 4-16). The separation between the planes of these rings is 3.99 Å. At the other end of the cation, the approximately coplanar 4'-(3-pyridyl)-tpy ligand lies over, but offset from, another such ligand in an adjacent cation of the chain.

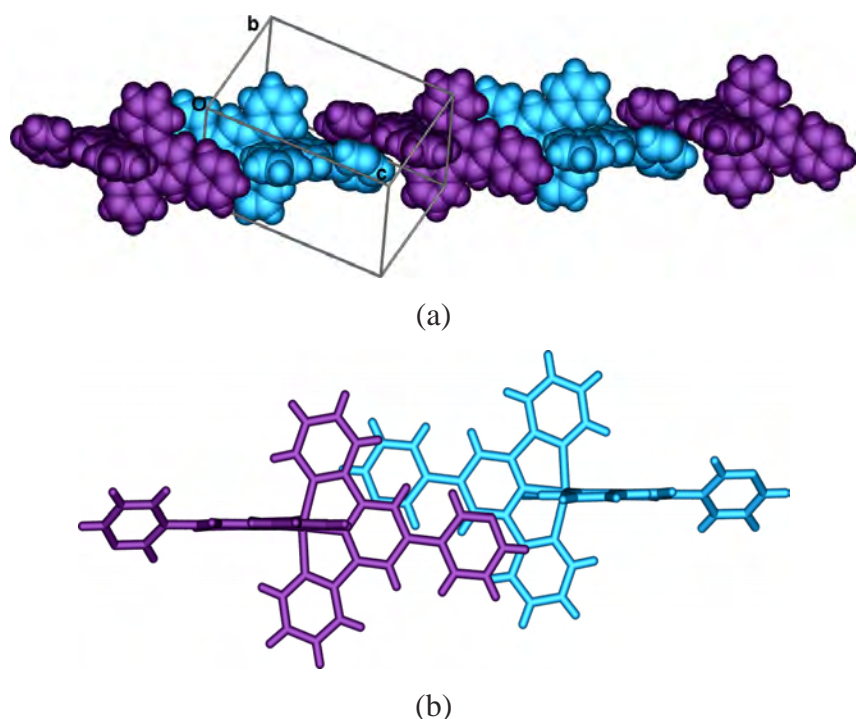


Figure 4-16 (a) Cations in $[\text{Fe}(\mathbf{34})_2]\text{[PF}_6\text{]}_2$ assemble into chains with weak π -stacking interactions between alternating pairs of pendant pyridine rings. Two such interactions are shown. (b) Offset π -stacking between pairs of approximately planar 4'-(3-pyridyl)-tpy ligands.

The distance between the least squares planes of the 24 C and N atoms per ligand is 3.70 Å, indicating the presence of weak π -stacking. The chains lie parallel to one another and engage in rather loose {Fe(tpy)₂} embraces,³⁰¹ with the [PF₆][−] ions residing in the cavities between the chains.

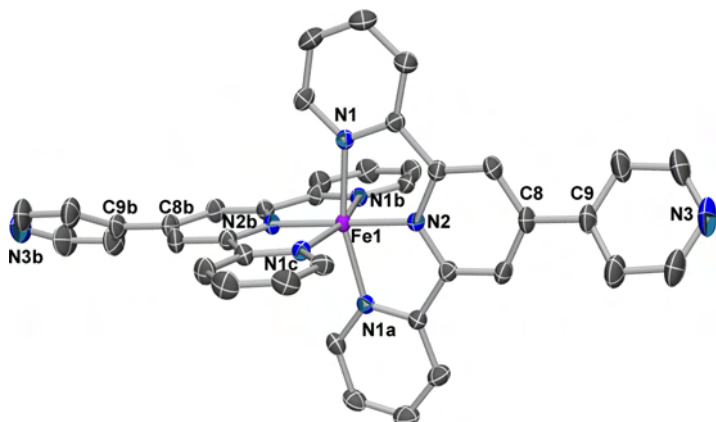


Figure 4-17 Molecular structure of the [Fe(9)₂]²⁺ cation in [Fe(9)₂][PF₆]₂·2MeCN with thermal ellipsoids plotted at 40% probability level, and hydrogen atoms omitted. Selected bond distances and angles: Fe1–N1 = 1.983(2) Å, Fe1–N2 = 1.882(2) Å, N1–Fe1–N2 = 80.67(4)^o. Symmetry codes: a = −x, −y + 1/2, −z + 1/4; b = −x + 1/4, y + 3/4, −z + 1/4; c = x + 1/4, −y + 1/4, −z + 1/4.

3. [Fe(9)₂](PF₆)₂

The iron atom in the [Fe(9)₂]²⁺ cation (Figure 4-17) of [Fe(9)₂][PF₆]₂·2MeCN lies on the special position 4-bar inversion axis (Wyckoff letter b) of the I41/a space group (origin choice 2), and the N3...Fe1...N3b vector is constrained to being linear. The twisting of each pendant pyridine ring with respect to the central ring of the tpy unit is 32.9(2)^o. Packing of the cations in the crystal is controlled by two factors: π -stacking between pendant pyridine rings and face-to-face and edge-to-face π -interactions involving the tpy domains. Figure 4-18a shows part of infinite chains of π -stacked interactions (shown in different colours, interring separation = 3.63 Å). The pendant pyridine rings on the extremities of each chain engage in a second set of π -stacking (Figure 4-18a) with the result that the chains are interlocked into a three-dimensional network. Figure 4-18b shows a view down the crystallographic *c* axis, illustrating {Fe(tpy)₂} embraces³⁰¹ (face-to-face separation 3.45 Å and CH...centroid of ring containing N1 = 3.25 Å).

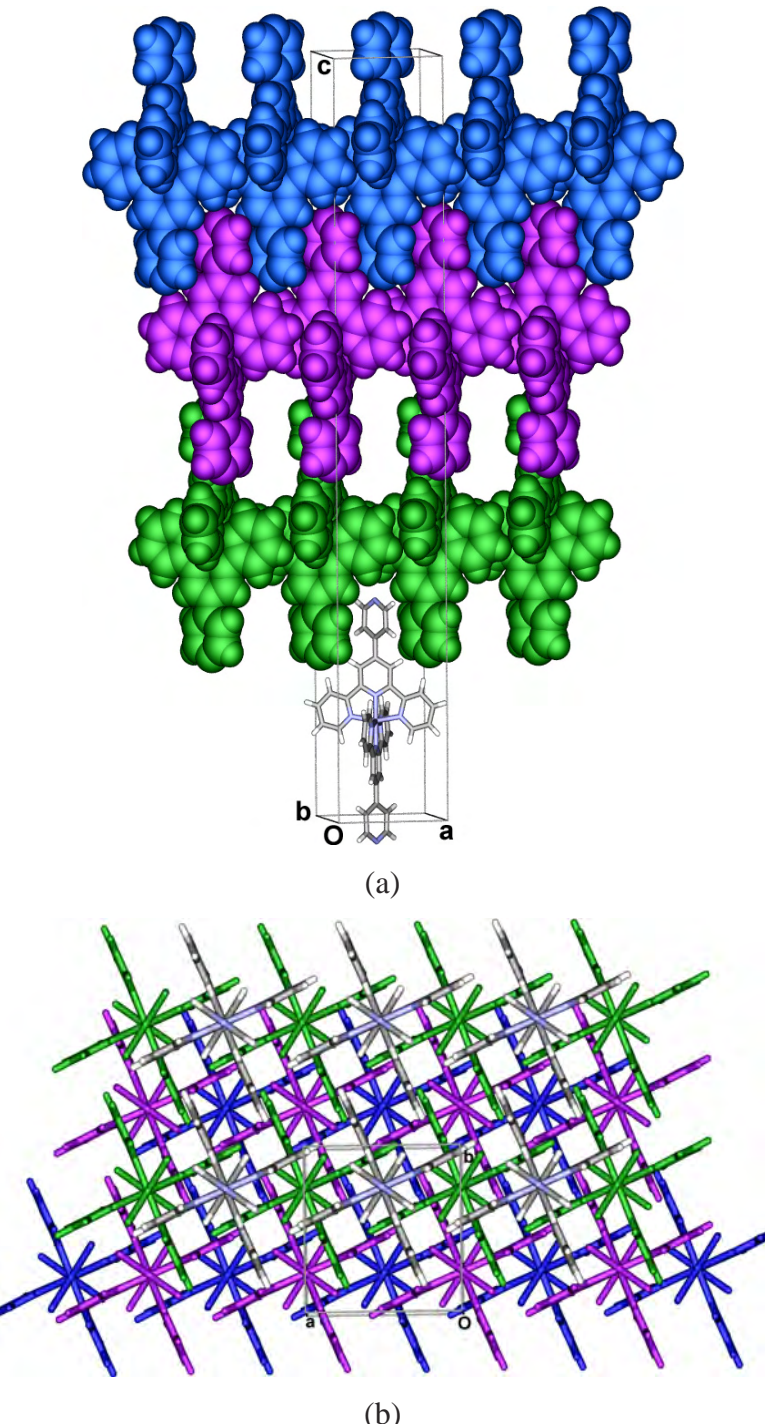


Figure 4-18 (a) interlocking of chains of $[\text{Fe}(\mathbf{9})_2]^{2+}$ cations in $[\text{Fe}(\mathbf{9})_2][\text{PF}_6]_2\text{2MeCN}$ assembled via π -stacking between pendant pyridine rings. (b) A view down the c axis showing $\{\text{Fe}(\text{tpy})_2\}$ embraces. Solvent molecules and anions have been omitted.

The $[\text{PF}_6]^-$ ions and acetonitrile solvent molecules are disordered, and each has been modelled over two sites of equal occupancies. Both reside in cavities between pendant pyridine rings of adjacent molecules; three of these cavities are visible in Figure 4-18b. The high symmetry of the $[\text{Fe}(\mathbf{9})_2]^{2+}$ cation in $[\text{Fe}(\mathbf{9})_2][\text{PF}_6]_2\text{2MeCN}$ makes it difficult

to give a meaningful comparison between the structures of the cation in this salt and in $[\text{Fe}(\mathbf{9})_2][\text{NO}_3]_2 \cdot 3\text{H}_2\text{O} \cdot \text{MeCN}$.²⁸⁰ The latter crystallizes in the P-1 space group and therefore lacks the symmetry constraints imposed on the $[\text{Fe}(\mathbf{9})_2]^{2+}$ cation in $[\text{Fe}(\mathbf{9})_2][\text{PF}_6]_2 \cdot 2\text{MeCN}$.

4. $\{[\text{Fe}(\mathbf{9})_2](\text{ClO}_4)_2\}_2 \cdot 2\text{MeOH}$

X-ray quality crystals of $[\text{Fe}(\mathbf{9})_2][\text{ClO}_4]_2 \cdot 2\text{MeOH}$ were grown serendipitously during attempts to produce coordination polymers by combining the preformed building block $[\text{Fe}(\mathbf{9})_2]^{2+}$ with $\text{Fe}(\text{ClO}_4)_2$ in the presence of NH_4SCN (see discussion in next chapter). There are two independent cations (labelled A and B) in the asymmetric unit of $[\text{Fe}(\mathbf{9})_2][\text{ClO}_4]_2 \cdot 2\text{MeOH}$ and the structure of cation A is depicted in Figure 4-19. The bond distances and angles for cations A and B are similar, and those for the iron(II) coordination sphere are given in the figure caption. Each pendant pyridine ring is twisted with respect to the tpy domain to which it is attached. For cation A, the angles between the least squares planes of the rings containing atoms N2 and N4, and N6 and N8 are $11.2(3)$ and $25.6(3)^\circ$, respectively. For cation B, the angles between the least squares planes of the rings with atoms N10 and N12, and N14 and N16 are $16.6(3)$ and $44.6(3)^\circ$, respectively. The difference in twist angles observed for the independent cations is associated with the molecular packing (see below). The deviation from linearity of the $\text{N}_{\text{py}} \dots \text{Fe} \dots \text{N}_{\text{py}}$ ($\text{N}_{\text{py}} = \text{N}$ atom of a pendant pyridine ring) vector is noteworthy. For the two independent cations, the angles $\text{N}8 \dots \text{Fe}1 \dots \text{N}4$ and $\text{N}12 \dots \text{Fe}2 \dots$ are $170.83(6)^\circ$ and $170.26(6)^\circ$, respectively, and these values are similar to that observed for the $\text{N}_{\text{py}} \dots \text{Ru} \dots \text{N}_{\text{py}}$ angle in $[\text{Ru}(\mathbf{9})_2][\text{PF}_6][\text{NO}_3] \cdot \text{DMSO}$.²⁷⁵

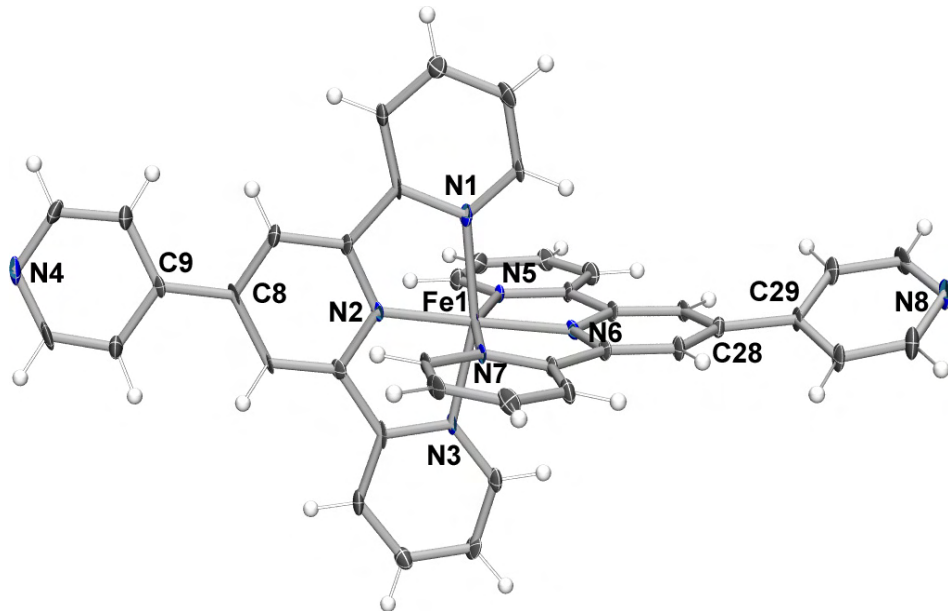


Figure 4-19 Molecular structure of one of the crystallographically independent $[\text{Fe}(\mathbf{9})_2]^{2+}$ cations (labelled cation A) in $[\text{Fe}(\mathbf{9})_2][\text{ClO}_4]_2 \cdot 2\text{MeOH}$ with thermal ellipsoids plotted at the 30% probability level. Hydrogen atoms are omitted. Selected bond parameters in cation A: $\text{Fe1}-\text{N}1 = 1.981(6)$, $\text{Fe1}-\text{N}2 = 1.866(5)$, $\text{Fe1}-\text{N}3 = 1.969(5)$, $\text{Fe1}-\text{N}5 = 1.972(5)$, $\text{Fe1}-\text{N}6 = 1.869(5)$, $\text{Fe1}-\text{N}7 = 1.957(5)$ Å, $\text{N}1-\text{Fe1}-\text{N}2 = 81.6(2)$, $\text{N}2-\text{Fe1}-\text{N}3 = 80.8(2)$, $\text{N}5-\text{Fe1}-\text{N}6 = 81.0(2)$, $\text{N}6-\text{Fe1}-\text{N}7 = 81.4(2)^\circ$; in cation B: $\text{Fe2}-\text{N}9 = 1.971(5)$, $\text{Fe2}-\text{N}10 = 1.873(5)$, $\text{Fe2}-\text{N}11 = 1.968(6)$, $\text{Fe2}-\text{N}13 = 1.982(5)$, $\text{Fe2}-\text{N}14 = 1.877(5)$, $\text{Fe2}-\text{N}15 = 1.966(5)$ Å, $\text{N}9-\text{Fe2}-\text{N}10 = 81.4(2)$, $\text{N}10-\text{Fe2}-\text{N}11 = 80.7(2)$, $\text{N}13-\text{Fe2}-\text{N}14 = 80.8(2)$, $\text{N}14-\text{Fe2}-\text{N}15 = 81.6(2)^\circ$.

One factor that may contribute towards this deformation is the fact that one pendant pyridine ring of each cation is hydrogen bonded to a methanol solvent molecule giving rise to hydrogen-bonded dimers comprising AA and BB cation pairs. The pairs of cations A and B in $[\text{Fe}(\mathbf{9})_2][\text{ClO}_4]_2 \cdot 2\text{MeOH}$ are shown in Figure 4-20a and b, respectively, and hydrogen bonded metric parameters are given in the figure caption; (the H atoms of the MeOH molecules could not be localized in the structure determination). There are slight differences between the positions of methanol molecules with respect to the cations in the two crystallographically independent dimers, and also in the relative orientations of the pairs of pendant pyridine rings containing N8 in cations A, or N12 in cations B. In the BB dimers, pairs of pendant rings containing N12 stack with the classical offset orientation and inter-ring separation of 3.39 Å (distance between least squares planes). However, in AA dimers, symmetry related pairs of pyridine rings containing N8 share no common region of overlap and, although the distance between the least squares planes of the rings is 3.29 Å, no effective π -stacking operates. The reasons for these differences are not clear cut. However, we note that the perchlorate ions, which are accommodated in the cavities between the AA and BB dimers, are engaged in extensive C–H_{aromatic}...O_{anion} close

contacts and that these, along with the hydrogen bonding to the methanol molecules, contribute to the observed conformations of four crystallographically independent pendant pyridine rings.

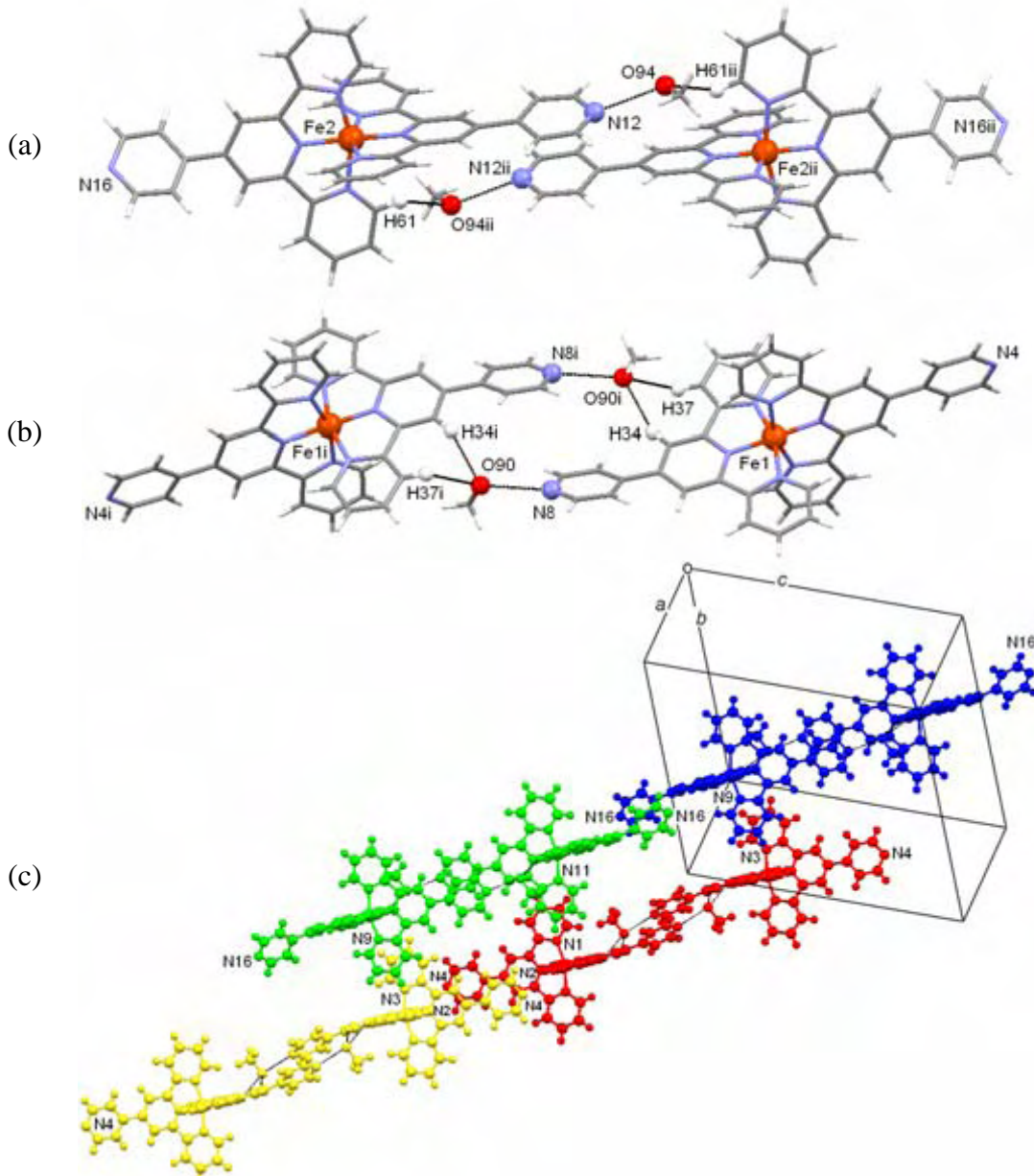


Figure 4-20 (a) Pairs of cations A and MeOH solvent molecules form hydrogen-bonded dimers in $[\text{Fe}(\mathbf{9})_2][\text{ClO}_4]_2 \cdot 2\text{MeOH}$; symmetry code i = 3-x, 2 - y, - z. $\text{N}8 \dots \text{O}90 = 2.770(8)$ Å, $\text{C}34\text{H}34 \dots \text{O}90i = 2.40$ Å, $\text{C}34 \dots \text{O}90i = 3.228(8)$ Å, $\text{C}34 - \text{H}34 \dots \text{O}90i = 146^\circ$; $\text{C}37\text{H}37 \dots \text{O}90i = 2.41$ Å, $\text{C}37 \dots \text{O}90i = 3.177(8)$ Å, $\text{C}37 - \text{H}37 \dots \text{O}90i = 138^\circ$. (b) Hydrogen-bonded dimers also form between pairs of cations B and MeOH solvent molecules; symmetry code ii = 1-x, 1 - y, 1 - z. $\text{N}12 \dots \text{O}94 = 2.7756(8)$ Å, $\text{C}61\text{H}61 \dots \text{O}94ii = 2.32$ Å, $\text{C}61 \dots \text{O}94ii = 3.059(9)$ Å, $\text{C}61 - \text{H}61 \dots \text{O}94ii = 135^\circ$. (c) Chains of dimers (the lower cations are of type A, the upper cations are of type B) assemble through aromatic ring π-stacking.

The $\{[\text{Fe}(\mathbf{9})_2]^{2+} \cdot \text{MeOH}\}_2$ dimers assemble into chains, each chain comprising either cations A or B (Figure 4-20c). π-Stacking between pendant pyridine rings with atoms

N16 (distance between rings = 3.45 Å) support each chain of cations A. In contrast, cations B overlap more extensively with weak π -stacking involving the pendant pyridine rings containing N4 and the central tpy ring containing N2 (distance between planes = 3.67 Å). The chains run parallel to one another and overlap with face-to-face tpy ring interactions (Figure 4-20b, distance between the rings containing N3 and N9 = 3.58 Å, and between the rings containing N1 and N11 = 3.56 Å). The perchlorate ions occupy the cavities between the chains, and there are extensive CH_{aromatic}...O_{perchlorate} non-classical hydrogen-bonded interactions throughout the lattice. We conclude that the organization of the [Fe(9)₂]²⁺ cations in [Fe(9)₂][ClO₄]₂·2MeOH is a result of a subtle balance of three effects: hydrogen bonding involving the pendant pyridine N-donor and methanol molecules, C–H...O interactions involving the [ClO₄][−] counterions, and π -stacking interactions.

5. [Fe(38)₂](PF₆)₂ · 1.5MeCN

The molecular structure of the [Fe(38)₂]²⁺ cation in [Fe(38)₂][PF₆]₂·1.5MeCN is shown in Figure 4-21.

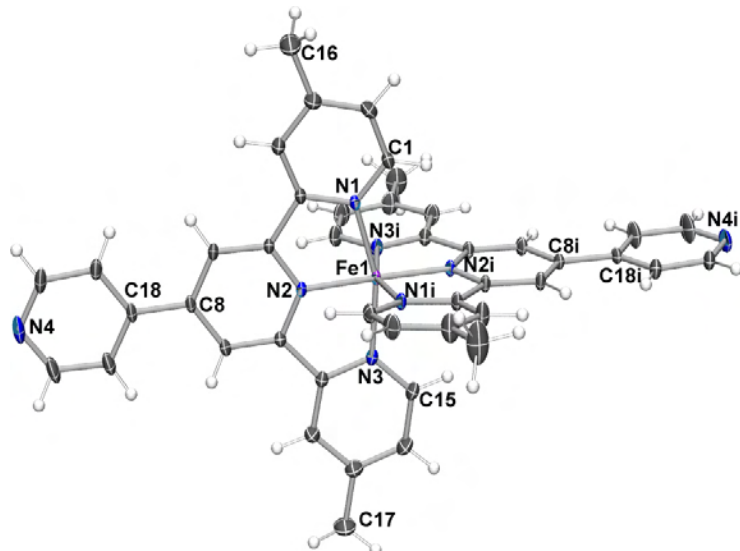


Figure 4-21 The molecular structure of [Fe(38)₂]²⁺ in [Fe(38)₂][PF₆]₂·1.5MeCN. Thermal ellipsoids drawn at 50% probability level. Space group: C2/c. Selected bond lengths and angles Fe1-N1 = 1.979(2), Fe1-N2 = 1.883(1) Å, Fe1-N3 = 1.968(2) Å; N1-Fe1-N2 = 80.38(7), N1-Fe1-N3 = 160.9(1)°. Angle between least squares planes of tpy moieties 87.94°. Symmetry code: i = 1 - x, y, 3/2 - z.

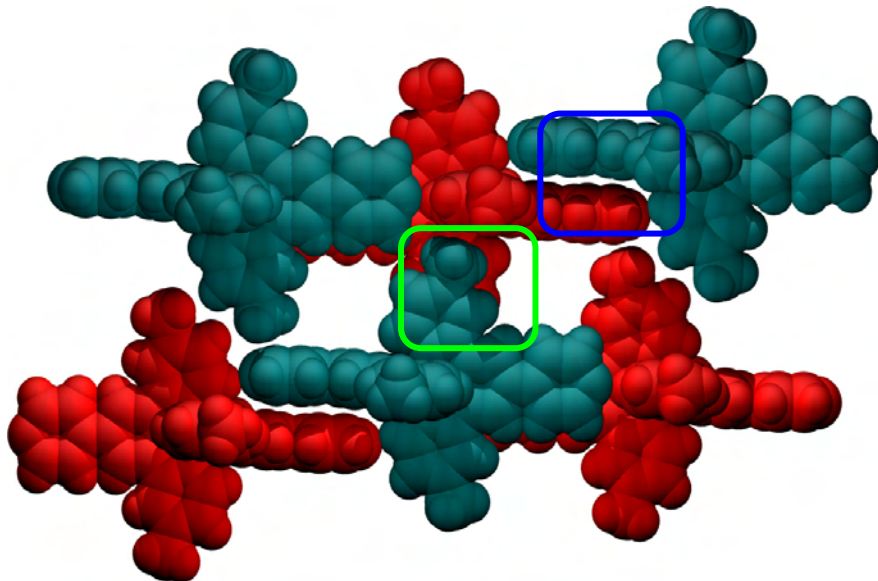


Figure 4-22 Key packing arrangement of $[\text{Fe}(38)_2]^{2+}$ in $[\text{Fe}(38)_2][\text{PF}_6]_2 \cdot 1.5\text{MeCN}$. π -stacking involving the pendant ring is shown in a blue box ,and involving the terminal ring containing N1 is shown in a green box.

Although the spatial demands of the methyl groups prevent the formation of tpy embraces as observed for $[\text{M}(9)_2][\text{PF}_6]_2$, π -stacking still dominates the packing in the crystal structure. The pendant ring is coplanar with the tpy [angle between least-squares planes 5.17 °] and is ideally positioned for face-to-face π -interactions between adjacent complexes [separation between least-squares planes of pendant rings is 3.381 Å] to form chains as shown in Figure 4-22. The terminal rings containing N1 are also involved in face-to-face interactions [separated by 3.579 Å] although the ring containing N3 is not. Instead this ring is positioned to engage in close methyl-aromatic contacts [C17-C21 i 3.328(4) Å, $i = \frac{1}{2} - x, \frac{1}{2} + y, \frac{1}{2} - z$] and non-classical N_{py}...HC interactions to an adjacent pendant pyridyl nitrogen (H15A...N4ii = 2.32 Å, C15...N4ii = 3.210(3) Å, ii = $\frac{1}{2} + x, \frac{1}{2} - y, \frac{1}{2} + z$). The PF₆⁻ anions are also involved in many close contacts with CH atoms [F15...H9A 2.46; F15....H12A 2.46; F15...H22A 2.50; F14...H1Ai 2.47 Å, i = $-\frac{1}{2} + x, \frac{1}{2} + y, z$].

6. $[\text{Ru}(9)_2](\text{PF}_6)_2$ and $[\text{Ru}(9)_2][\text{PF}_6][\text{NO}_3]$

The solid-state structure of $[\text{Ru}(9)_2][\text{PF}_6][\text{NO}_3] \cdot \text{DMSO}$ was recently reported²⁷⁵ and significant bowing away from linearity of the N_{py}...Ru...N_{py} (N_{py} = N in the pendant pyridine ring) vector was observed. Although there are numerous short contacts involving cations, anions and DMSO molecules, a direct relationship between these interactions and the distortion of the $[\text{Ru}(9)_2]^{2+}$ unit was not located. Further insight can

now be obtained by comparing the structure of $[\text{Ru}(\mathbf{9})_2][\text{PF}_6][\text{NO}_3]\cdot\text{DMSO}$ (monoclinic, $P2_1/c$) with those of $[\text{Ru}(\mathbf{9})_2][\text{PF}_6][\text{NO}_3]$ (triclinic, $P-1$) and $[\text{Ru}(\mathbf{9})_2][\text{PF}_6]_2$ (tetragonal, $I4_1/a$). The structures of the $[\text{Ru}(\mathbf{9})_2]^{2+}$ cation in $[\text{Ru}(\mathbf{9})_2][\text{PF}_6][\text{NO}_3]$ and $[\text{Ru}(\mathbf{9})_2][\text{PF}_6]_2$ are shown in Figure 4-23 and Figure 4-24, respectively, and important bond parameters are listed in the figure captions.

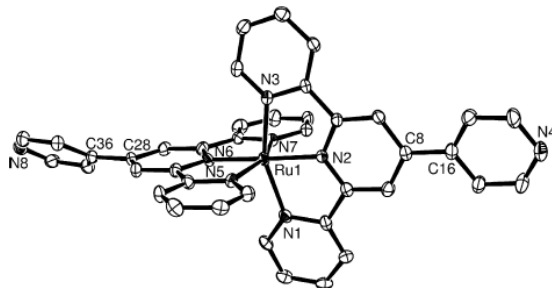


Figure 4-23 Molecular structure of the $[\text{Ru}(\mathbf{9})_2]^{2+}$ cation in $[\text{Ru}(\mathbf{9})_2][\text{PF}_6][\text{NO}_3]$ with thermal ellipsoids plotted at the 30% probability level. Hydrogen atoms are omitted. Selected bond parameters: $\text{Ru1}-\text{N1} = 2.059(6)$, $\text{Ru1}-\text{N2} = 1.971(5)$, $\text{Ru1}-\text{N3} = 2.065(6)$, $\text{Ru1}-\text{N5} = 2.059(6)$, $\text{Ru1}-\text{N6} = 1.953(5)$, $\text{Ru1}-\text{N7} = 2.040(6)$ Å, $\text{N1}-\text{Ru1}-\text{N2} = 78.6(2)$, $\text{N2}-\text{Ru1}-\text{N3} = 78.9(2)$, $\text{N5}-\text{Ru1}-\text{N6} = 78.7(2)$, $\text{N6}-\text{Ru1}-\text{N7} = 79.1(2)$ °.

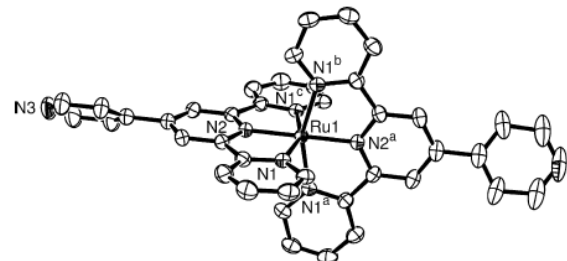


Figure 4-24 Molecular structure of the $[\text{Ru}(\mathbf{9})_2]^{2+}$ cation in $[\text{Ru}(\mathbf{9})_2][\text{PF}_6]_2$ with thermal ellipsoids plotted at the 30% probability level. Hydrogen atoms are omitted. Selected bond parameters: $\text{Ru1}-\text{N1} = 2.082(2)$, $\text{Ru1}-\text{N2} = 1.982(3)$ Å, $\text{N1}-\text{Ru1}-\text{N2} = 78.48(7)$ °. Symmetry codes: $a = -x + 1/4, y + 3/4, -z + 1/4$; $b = x + 1/4, -y + 1/4, -z + 1/4$; $c = -x, -y + 1/2, z$.

The $[\text{Ru}(\text{tpy})_2]$ coordination environments in the two complexes are similar and unexceptional. However, on going from $[\text{Ru}(\mathbf{9})_2][\text{PF}_6][\text{NO}_3]\cdot\text{DMSO}$ ²⁷⁵ to $[\text{Ru}(\mathbf{9})_2][\text{PF}_6][\text{NO}_3]$, the extent of bowing of the backbone of the cation decreases. Using the atom numbering scheme in Figure 4-23, the $\text{N4}\dots\text{Ru1}\dots\text{N8}$ angle is $169.11(4)$ ° in $[\text{Ru}(\mathbf{9})_2][\text{PF}_6][\text{NO}_3]\cdot\text{DMSO}$ and $176.03(7)$ ° in $[\text{Ru}(\mathbf{9})_2][\text{PF}_6][\text{NO}_3]$. In contrast, the $[\text{Ru}(\mathbf{9})_2]^{2+}$ cation in $[\text{Ru}(\mathbf{9})_2][\text{PF}_6]_2$ has crystallographically imposed symmetry. $[\text{Ru}(\mathbf{9})_2][\text{PF}_6]_2$ crystallises in the $I4_1/a$ space group and the ruthenium atom lies on the special position 4-bar inversion axis (Wyckoff letter *b*) of the $I4_1/a$ space group (origin choice 2). The $\text{N3}\dots\text{Ru1}\dots\text{N3a}$ angle is therefore constrained to 180 °. In $[\text{Ru}(\mathbf{9})_2][\text{PF}_6][\text{NO}_3]\cdot\text{DMSO}$, the nitrate ions are involved in extensive C–H_{aromatic}...O_{nitrate} interactions, and the hexafluorophosphate anions and DMSO molecules occupy cavities between columns of cations which run parallel to the *a*-axis.²⁷⁵ As a consequence, the cations are prevented from participating in face-to-face π-stacking. Removal of the DMSO solvent allows the cations in $[\text{Ru}(\mathbf{9})_2][\text{PF}_6][\text{NO}_3]$ to

approach more closely than in $[\text{Ru(9)}_2][\text{PF}_6][\text{NO}_3]\cdot\text{DMSO}$, giving rise to centrosymmetric pairs of π -stacked dimers (Figure 4-25).

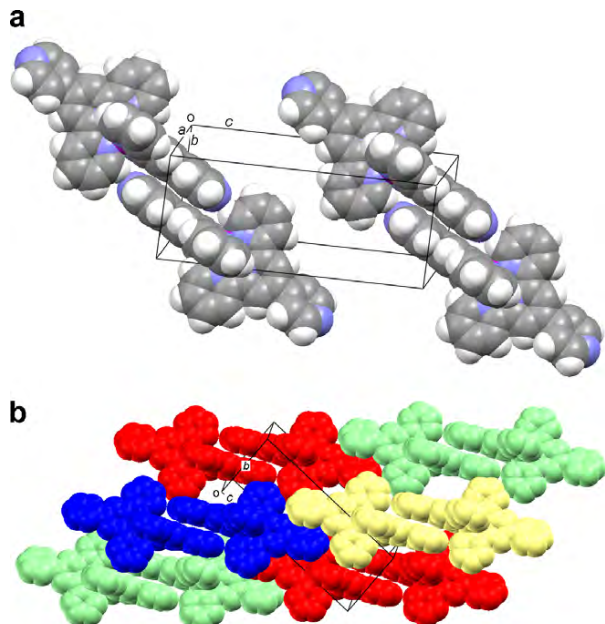


Figure 4-25 (a) Pairs of cations in $[\text{Ru(9)}_2][\text{PF}_6][\text{NO}_3]$ form π -stacked dimers. (b) Assembly of the dimers into loosely held chains (H atoms omitted).

The two cations are arranged in a head-to-head arrangement so that there is π -stacking between pairs of rings comprising a pendant pyridine ring containing N4 of one cation and the central tpy ring containing atom N2 of the second cation (distance between the least squares planes of rings = 3.6\AA). Since the plane of the pendant pyridine ring (with N4) is twisted $8.6(4)^\circ$ out of the plane of the central tpy ring (with N2), the effectiveness of the π -stacking is somewhat reduced. At the other end of the cation in each dimer, each pendant pyridine ring containing N8 is twisted $37.0(4)^\circ$ out of the plane of the central tpy ring to which it is bonded, and the rings containing N8 are involved in weak π -stacking interactions with equivalent rings of adjacent dimers. The distance between the least squares planes of a pair of rings with atoms N8 is 3.51\AA , but the rings are significantly offset and only loosely held chains result. The parallel packing of the chains is illustrated in Figure 4-25b. No $\{\text{M(tpy)}_2\}$ embraces³⁰¹ are present. The nitrate ions are disordered, and the fractional site occupancies preclude detailed discussion of the C–H_{aromatic}...O_{nitrate} short contacts. Both $[\text{Ru(9)}_2][\text{PF}_6][\text{NO}_3]\cdot\text{DMSO}$ and $[\text{Ru(9)}_2][\text{PF}_6][\text{NO}_3]$ exhibit extensive C–H_{aromatic}...O_{nitrate} non-classical hydrogen bonds, and it was therefore of interest to examine the effect of exchanging the $[\text{NO}_3]^-$ for $[\text{PF}_6]^-$ ions. $[\text{Ru(9)}_2][\text{PF}_6]_2$ crystallises in the tetragonal space group $I4_1/a$, and the location of

the ruthenium atoms on a special position 4-bar inversion axis imparts high symmetry to the cation. Each pendant pyridine ring is twisted by $35.3(3)^\circ$ with respect to the central ring of the tpy unit, and the two pendant pyridine rings are constrained by symmetry to being orthogonal.

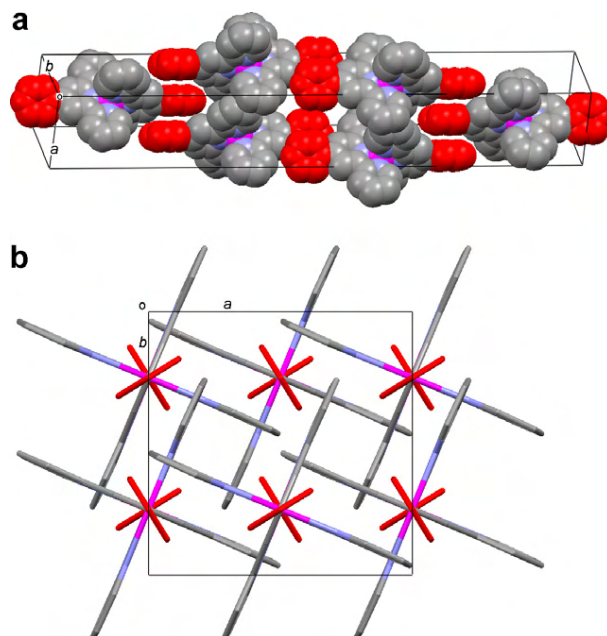


Figure 4-26 (a) π -Stacking between pendant pyridine rings of the $[\text{Ru}(9)_2]^{2+}$ cations in $[\text{Ru}(9)_2]\text{[PF}_6\text{]}_2$. (b) Packing of cations illustrated with a view down the crystallographic c -axis.

Figure 4-26a illustrates the efficient manner in which $[\text{Ru}(9)_2]^{2+}$ cations pack, with pendant pyridine rings forming π -stacks, alternate stacks being orthogonal to one another. The distance between the least squares planes containing pairs of adjacent pendant pyridines is 3.74 Å. Between these stacked domains lie the $[\text{Ru}(\text{tpy})_2]$ units and these engage in the $[\text{M}(\text{tpy})_2]$ embraces that are typical of $[\text{M}(\text{tpy})_2]^{n+}$ complexes³⁰¹. While the face-to-face interactions between pairs of pyridine rings containing atoms N1 are efficient (distance between rings = 3.45 Å), the edge-to-face interactions are forced slightly away from an ideal orientation (pyridine ring centroid...H21C21 = 140°, centroid...H21 = 2.96 Å). This implies that the π -stacking of the pendant pyridine rings has a greater control over the packing than the edge-to-face π -interactions. The hexafluorophosphate ions (which are disordered, two sites with site occupancy factors of 0.2 and 0.3, respectively, plus symmetry generated positions) are accommodated in the cavities between stacked cations. The series of compounds $[\text{Ru}(9)_2]\text{[PF}_6\text{]}_2\text{[NO}_3\text{]}_{\text{DMSO}}$, $[\text{Ru}(9)_2]\text{[PF}_6\text{]}_2\text{[NO}_3\text{]}$ and $[\text{Ru}(9)_2]\text{[PF}_6\text{]}_2$ illustrates the effects on the packing of the $[\text{Ru}(9)_2]^{2+}$ cations of a relatively sterically demanding

solvent and of the presence of a counter ion (viz. nitrate) that can participate in non-classical hydrogen bonding. In $[\text{Ru}(\mathbf{9})_2][\text{PF}_6]_2$, the most favourable situation is reached in which π -stacking involving both the pendant pyridine groups and the $[\text{Ru}(\mathbf{9})_2]^{2+}$ cations is achieved in a tetragonal space group with the ruthenium atoms occupying sites of high (4-bar inversion axis) symmetry.

7. $\{2[\text{Ru}(\mathbf{36})_2](\text{PF}_6)_4\} \cdot \text{H}_2\text{O}$

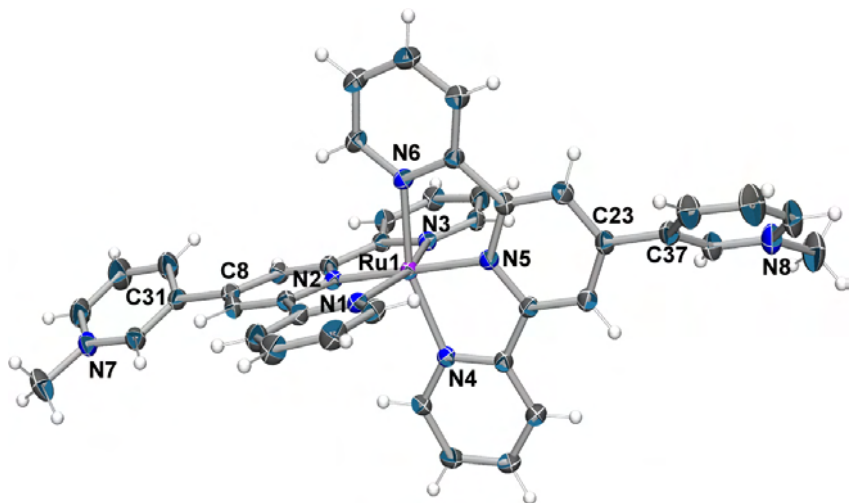


Figure 4-27 Molecular structure of the $[\text{Ru}(\mathbf{36})_2]^{4+}$ cation in $2\{[\text{Ru}(\mathbf{36})_2][\text{PF}_6]_4\} \cdot \text{H}_2\text{O}$ with thermal ellipsoids plotted at 50% probability level. Hydrogen atoms are omitted. Selected bond distances and angles: $\text{Ru1}-\text{N}1 = 2.075(2)$, $\text{Ru1}-\text{N}2 = 1.975(2)$, $\text{Ru1}-\text{N}3 = 2.076(2)$, $\text{Ru1}-\text{N}4 = 2.083(2)$, $\text{Ru1}-\text{N}5 = 1.986(2)$, $\text{Ru1}-\text{N}6 = 2.076(2)$, $\text{N}7-\text{C}36 = 1.481(4)$, $\text{N}8-\text{C}42 = 1.482(4)$ Å ; $\text{N}1-\text{Ru1}-\text{N}2 = 78.44(9)$, $\text{N}2-\text{Ru1}-\text{N}3 = 79.10(9)$, $\text{N}4-\text{Ru1}-\text{N}5 = 78.74(9)$, $\text{N}5-\text{Ru1}-\text{N}6 = 78.66(9)$ °.

The molecular structure of $[\text{Ru}(\mathbf{36})_2]^{4+}$ in $2\{[\text{Ru}(\mathbf{36})_2][\text{PF}_6]_4\} \cdot \text{H}_2\text{O}$ is shown in Figure 4-27. The two ligands are crystallographically independent and each pendant *N*-methylpyridinium ring is twisted out of the plane of the tpy unit to which it is bonded. The angles between the least squares planes of the rings containing atoms N2 and N7, and N5 and N8 are 24.3(1) and 52.2(2)°, respectively, compared with angles of 40.0 and 2.1° for $[\text{Ru}(\mathbf{34})_2]^{2+}$.²⁷⁴ These differences do not arise directly from the presence of *N*-methyl substituents, but rather from differences in packing which are forced by the need to accommodate an increased number of $[\text{PF}_6]^-$ ions. The two $[\text{Ru}(\mathbf{36})_2]^{4+}$ cations in the unit cell area related by the inversion centre of the *P*-1 space group. All cations in Figure 4-28a are structurally identical, but the interactions between them can be separated into two types. Adjacent blue and red cations in Figure 4-28a engage in face-to-face and edge-to-face π -interactions that are typical of $\{\text{M}(\text{tpy})_2\}$ embraces,³⁰¹ *i.e.* these involve the outer pyridine rings of the tpy domains of ligands **36**. In contrast,

adjacent cations coloured red in Figure 4-28a (and similarly, pairs of blue cations) stack so that the tpy pyridine ring containing atom N3 lies over, but offset from, the pendant *N*-methylpyridinium ring of the adjacent cation (Figure 4-28b). Although the distance from the centroid of one ring to the plane containing the other is $\approx 3.6 \text{ \AA}$, the angle between the planes containing the rings is $\approx 18^\circ$, indicating that any π -interactions are weak. Figure 4-28b also shows the close proximity of the water solvent molecules to the $[\text{Ru(36)}_2]^{4+}$ cations. Short contacts exist between each O1 atom and three C–H groups ($\text{C}24\text{H}24\ldots\text{O}1$ with $\text{C}\dots\text{O} = 3.21(1) \text{ \AA}$, $\text{C–H}\dots\text{O} = 173^\circ$, $\text{C}27\text{H}27\ldots\text{O}1$ with $\text{C}\dots\text{O} = 3.53(1) \text{ \AA}$, $\text{C–H}\dots\text{O} = 171^\circ$, and $\text{C}3\text{H}31\ldots\text{O}1i$ with $\text{C}\dots\text{O} = 3.47(1) \text{ \AA}$, $\text{C–H}\cdots\text{O} = 169^\circ$, symmetry code $i = 1 - x, 1 - y, -z$).

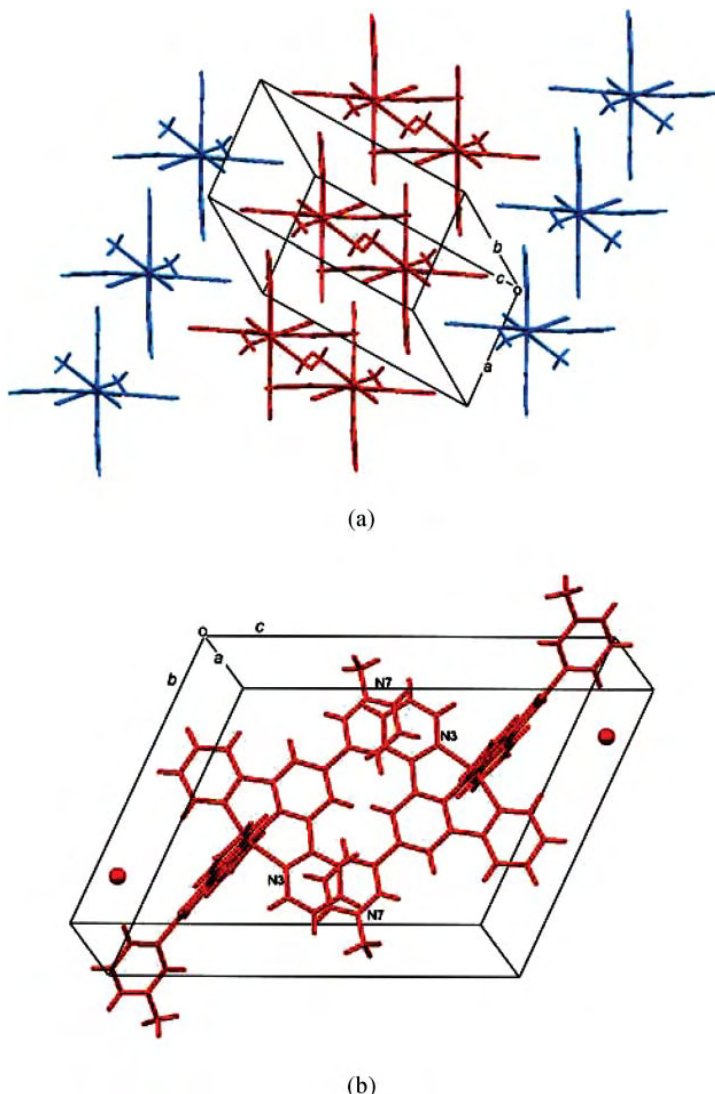


Figure 4-28 Packing of $[\text{Ru(36)}_2]^{4+}$ cations in $2\{[\text{Ru(36)}_2]\text{[PF}_6\text{]}_4\}\cdot\text{H}_2\text{O}$ showing (a) face-to-face and edge-to-face π -interactions between cations coloured red and blue, and (b) a separate set of face-to-face interactions between pairs of cations (red) related by an inversion centre. $[\text{PF}_6]^-$ anions are omitted for clarity.

8. $\{[\text{Ru(39)}_2](\text{PF}_6)_2\}_2 \cdot \text{MeCN} \cdot \text{H}_2\text{O}$ and $[\text{Fe(39)}_2](\text{PF}_6)_2 \cdot \text{MeCN} \cdot \text{H}_2\text{O}$

The asymmetric unit of $\{2[\text{Ru(39)}_2](\text{PF}_6)_2\} \cdot \text{MeCN} \cdot \text{H}_2\text{O}$ contains two crystallographically independent cations; the only significant differences between them are the twist angles of the pendant pyrimidinyl rings (Figure 4-29). The cations assemble through tpy embraces³⁰¹ which are also commonly present in $\{\text{M(tpy)}_2\}$ structures presented above. However, in $\{2[\text{Ru(39)}_2](\text{PF}_6)_2\} \cdot \text{MeCN} \cdot \text{H}_2\text{O}$, the $\pi-\pi$ interactions, appear to be weaker than in salts of $[\text{M(9)}_2]^{2+}$, with longer edge-to-face and face-to-face interactions (Figure 4-30 and Table 8). More important is the close (3.397 Å) and ideally offset π -stacking shown in Figure 4-31b. The one pendant ring is twisted significantly more from the plane of the tpy than the other (ring N9, N10: 26.4°; ring N7, N8: 4.20°) and this may be partially the result of non-classical N...HC hydrogen bonding shown in Figure 4-31a.

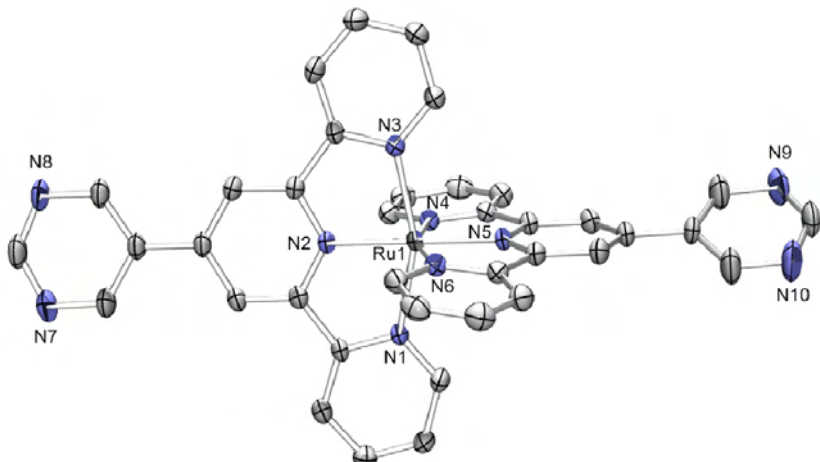


Figure 4-29 Molecular structure of one of two crystallographically independent $[\text{Ru(39)}_2]^{2+}$ cations in $\{2[\text{Ru(39)}_2](\text{PF}_6)_2\} \cdot \text{MeCN} \cdot \text{H}_2\text{O}$; ellipsoids plotted at 30% probability level. Anions, solvent molecules and H atoms are omitted. Selected bond parameters: $\text{Ru1}-\text{N}1 = 2.057(2)$, $\text{Ru1}-\text{N}2 = 1.972(2)$, $\text{Ru1}-\text{N}3 = 2.065(2)$, $\text{Ru1}-\text{N}4 = 2.060(3)$, $\text{Ru1}-\text{N}5 = 1.973(2)$, $\text{Ru1}-\text{N}6 = 2.071(3)$ Å; $\text{N}1-\text{Ru1}-\text{N}2 = 79.35(9)$, $\text{N}2-\text{Ru1}-\text{N}3 = 78.80(9)$, $\text{N}4-\text{Ru1}-\text{N}5 = \text{N}5-\text{Ru1}-\text{N}6 = 79.1(1)$ °; parameters for the second cation are similar. Angles between the least squares planes of rings containing N2 and N7/N8, and N5 and N9/N10 = 4.1(2) and 26.3(2)°; corresponding angles in the second cation = 12.0(2) and 36.8(2)°.

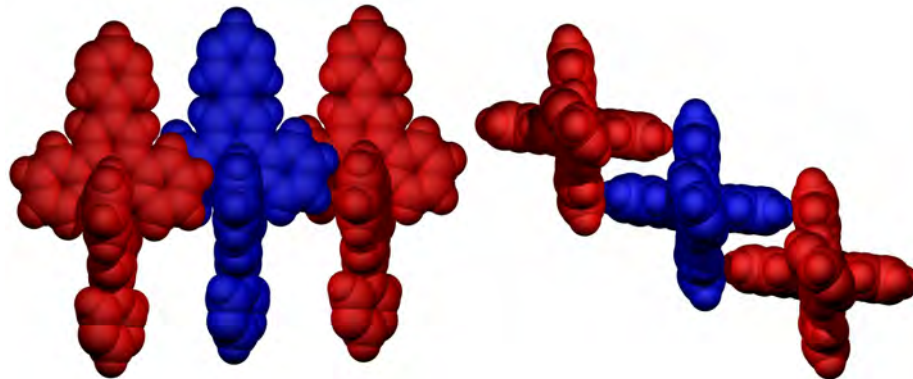
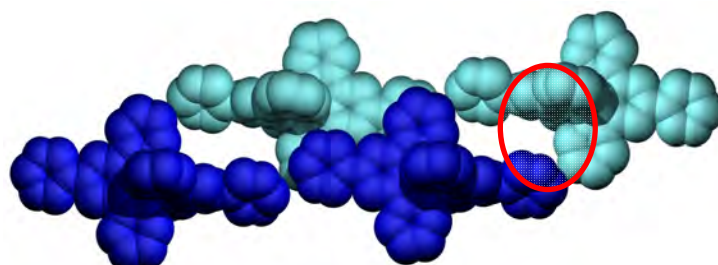


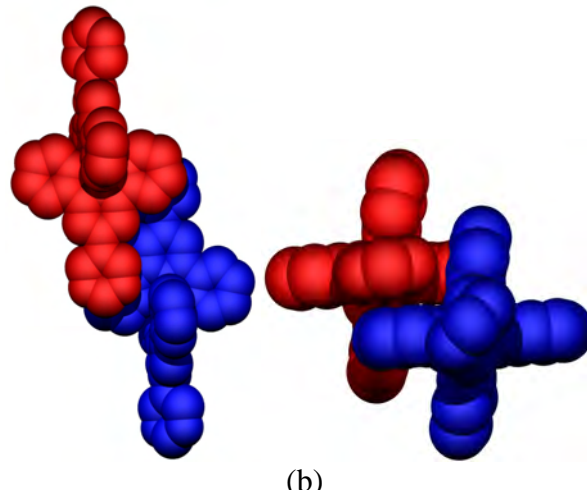
Figure 4-30 π - π embraces of $[\text{Ru}(39)_2](\text{PF}_6)_2$. Complexes coloured by symmetry equivalence, both complex A and B have very similar packing arrangements.

Table 8 (a) Face-to-face distances. Analogous distance for $[\text{Ru}(9)_2](\text{PF}_6)_2$ is 3.445 Å.¹⁶⁵ (b) Edge- to-face distances. Analogous distance for $[\text{Ru}(9)_2](\text{PF}_6)_2$ is: 3.777 Å.¹⁶⁵

(a)			(b)		
From centroid of ring containing atom	To plane containing atom	Distance (Å)	From atom	To centroid of ring containing atom	Distance (Å)
N53	N1	3.720	C52	N6	3.935
N1	N53	3.663	C14	N56	3.952
N51	N3	3.840	C2	N1	3.786
N3	N51	3.949	C64	N6	3.853



(a)



(b)

Figure 4-31 (a) Close N...CH contacts of $[\text{Ru}(39)_2](\text{PF}_6)_2$. Complexes all equivalent (containing Ru2), both complex A and B have very similar packing arrangements. Unconventional hydrogen bond distances (CH...N): C83-H832...N60i = 2.938; C29-H291...N57ii = 2.54; C18-H181...N59iii = 2.55, C87-H871...N58iv = 2.62, C15-H151...N10v = 2.77; C68-H681...N9vi = 2.54 Å. (b) The most extensive π - π overlap between $[\text{Ru}(39)_2](\text{PF}_6)_2$ complexes. Distance from centroid of ring containing N57 and N58 to plane of ring containing N51 is 3.397 Å. All equivalent complexes (containing Ru2).

9. $[\text{Ni}(\mathbf{9})_2](\text{NO}_3)_2 \cdot 2\text{MeOH} \cdot 2\text{H}_2\text{O}$

We next consider the solid-state structure of $[\text{Ni}(\mathbf{9})_2](\text{NO}_3)_2 \cdot 2\text{MeOH} \cdot 2\text{H}_2\text{O}$. Similar to $[\text{Fe}(\mathbf{9})_2](\text{ClO}_4)_2 \cdot 2\text{MeOH} \cdot 0.5\text{H}_2\text{O}$, this structure contains $[\text{M}(\mathbf{9})_2]^{2+}$ motifs with counterions which have the potential to be involved in C–H_{aromatic}...O_{anion} interactions, as well as solvent molecules capable of hydrogen bonding. Figure 4-32 shows the structure of the $[\text{Ni}(\mathbf{9})_2]^{2+}$ cation in $[\text{Ni}(\mathbf{9})_2](\text{NO}_3)_2 \cdot 2\text{MeOH} \cdot 2\text{H}_2\text{O}$.

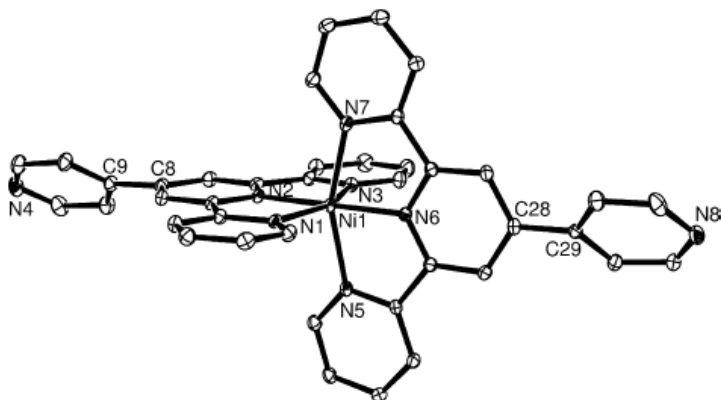


Figure 4-32 Molecular structure of the $[\text{Ni}(\mathbf{9})_2]^{2+}$ cation in $[\text{Ni}(\mathbf{9})_2](\text{NO}_3)_2 \cdot 2\text{MeOH} \cdot 2\text{H}_2\text{O}$ with thermal ellipsoids plotted at the 30% probability level. Hydrogen atoms are omitted. Selected bond parameters: Ni1–N1 = 2.099(3), Ni1–N2 = 1.987(2), Ni1–N3 = 2.120(3), Ni1–N5 = 2.109(3), Ni1–N6 = 1.990(2), Ni1–N7 = 2.108(3) Å, N1–Ni1–N2 = 78.55(10), N2–Ni1–N3 = 77.79(10), N5–Ni1–N6 = 78.03(10), N6–Ni1–N7 = 78.18(10)°.

The octahedral NiN_6 -unit is as expected and the Ni–N bond distances are similar to those reported for other complexes containing the $[\text{Ni}(\text{tpy})_2]^{2+}$ motif.^{301, 327-336} $[\text{Ni}(\mathbf{9})_2](\text{NO}_3)_2 \cdot 2\text{MeOH} \cdot 2\text{H}_2\text{O}$ crystallises in space group *P*-1 and so there are no symmetry constraints on the N4...Ni1...N8 vector. It is noteworthy, therefore, that in contrast to the structures described above, the vector is close to linear (angle N4...Ni1...N8 = 178.02(3)°). Both the pendant pyridine rings are twisted by approximately the same amount out of the plane of the tpy unit (angles between the least squares planes of the rings containing N2 and N4, and N6 and N8 are 39.7(2)° and 40.5(2)°, respectively). When viewed down the N4...Ni1...N8 axis, the two pendant pyridines exhibit an approximately eclipsed conformation, in contrast to the staggered conformation observed in the three complexes described above and in $[\text{Ru}(\mathbf{9})_2](\text{PF}_6)_2[\text{NO}_3]\cdot\text{DMSO}$ ²⁷⁵, $[\text{Rh}(\mathbf{9})_2](\text{PF}_6)_3 \cdot 2\text{EtOH}$ ²⁸² and $[\text{Cu}(\mathbf{9})_2](\text{PF}_6)_2 \cdot \text{MeOH} \cdot 0.5\text{CH}_2\text{Cl}_2$ ¹⁶⁹. Close to eclipsed conformations occur in $[\text{Fe}(\mathbf{9})_2](\text{NO}_3)_2 \cdot 3\text{H}_2\text{O} \cdot \text{MeCN}$ ²⁸⁰ and $[\text{Co}(\mathbf{9})_2](\text{ClO}_4)_2 \cdot \text{MeCN} \cdot 4\text{H}_2\text{O}$ ²⁹⁹. The most notable

feature of the solid-state structure of $[\text{Ni}(\mathbf{9})_2][\text{NO}_3]_2 \cdot 2\text{MeOH} \cdot 2\text{H}_2\text{O}$ is that all the cations, anions and solvent molecules are involved in the basic structural building block. This is the dimeric unit shown in Figure 4-33a. In addition to the hydrogen bonds shown in the figure, C–H_{aromatic}...O_{nitrate} close contacts hold the terminal nitrate ions of the hydrogen-bonded chain in an S-shaped configuration. Figure 4-33b illustrates how the dimeric motifs assemble in the crystal lattice. Extensive CH...O_{nitrate} interactions operate between dimers, in addition to π -stacking between pairs of pendant pyridine rings containing atoms N8 (distance between least squares planes of rings = 3.50 Å) and between significantly offset pairs of tpy rings containing atoms N1 (separation = 3.36 Å). We conclude that the assembly of the three-dimensional structure in $[\text{Ni}(\mathbf{9})_2][\text{NO}_3]_2 \cdot 2\text{MeOH} \cdot 2\text{H}_2\text{O}$ is controlled by hydrogen bonding, and not by cation–cation $\{\text{M}(\text{tpy})_2\}$ face-to-face and edge-to-face interactions which are so common among this family of compounds³⁰¹.

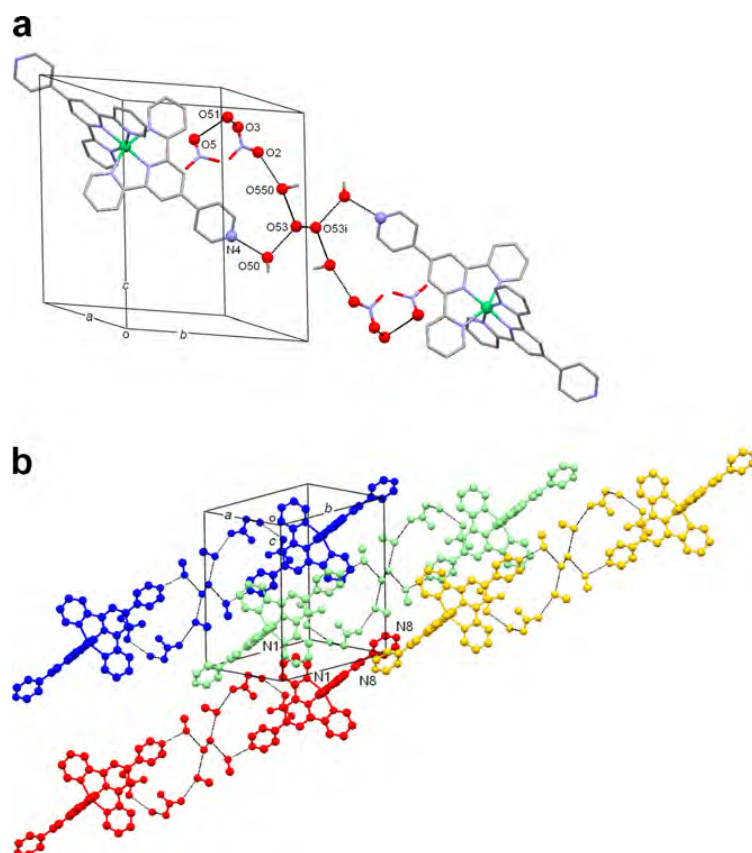


Figure 4-33 (a) The centrosymmetric, dimeric unit that is the structural motif in $[\text{Ni}(\mathbf{9})_2][\text{NO}_3]_2 \cdot 2\text{MeOH} \cdot 2\text{H}_2\text{O}$; hydrogen atoms are omitted. Symmetry code $i = -x, 2-y, 1-z$. Distances: N4...O50 = 2.741(5), O50...O53 = 2.749(6), O53...O53i = 2.77(1), O53...O550 = 2.46(1), O550...O2 = 2.841(8), O3...O51 = 2.977(4), O5...O51 = 2.866(4) Å. (b) Packing of dimeric units; π -stacking occurs between aromatic rings containing N8, and between rings containing N1.

10. $[\text{Fe}(\mathbf{41})_2](\text{PF}_6)_2$ and $[\text{Ru}(\mathbf{41})_2](\text{PF}_6)_2$

The structure of the $[\text{Ru}(\mathbf{41})_2]^{2+}$ cation in $[\text{Ru}(\mathbf{41})_2]\text{[PF}_6\text{]}_2$ is shown in Figure 4-34. The coordination environment around the ruthenium(II) centre is as expected. Each pyrazolyl ring is twisted with respect to the pyridine ring to which it is bonded (angles between the least squares planes for the rings containing N2 and N7, and N5 and N9 are $20.0(3)^\circ$ and $36.2(3)^\circ$, respectively). The packing of cations in the solid state is supported by weak C–H_(methyl)... π _(pyridine) interactions. Each pyrazolyl methyl group containing atom C36 sits directly over a tpy pyridine ring containing atom N1 of the adjacent cation (Figure 4-35), the distance from C36 to the centroid of the pyridine ring is 3.35 Å, which is relatively short for this type of intermolecular contact.³³⁷ These interactions lead to the formation of loosely held chains which run parallel to the crystallographic *b* axis.

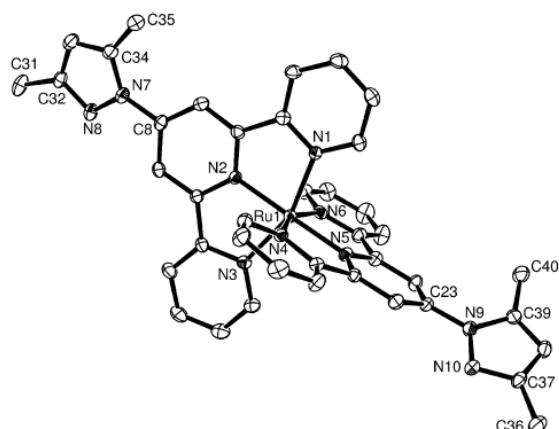


Figure 4-34 Molecular structure of the $[\text{Ru}(\mathbf{41})_2]^{2+}$ cation in $[\text{Ru}(\mathbf{41})_2]\text{[PF}_6\text{]}_2$ with thermal ellipsoids plotted at the 30% probability level; hydrogen atoms are omitted. Selected bond distances and angles: Ru1–N1 = 2.058(4), Ru1–N2 = 1.979(4), Ru1–N3 = 2.058(5), Ru1–N4 = 2.060(4), Ru1–N5 = 1.976(4), Ru1–N6 = 2.070(5), N7–N8 = 1.384(7), N9–N10 = 1.376(7), N7–C8 = 1.417(7), N9–C23 = 1.416(6), N7–C34 = 1.392(8), N9–C39 = 1.389(7) Å; N1–Ru1–N2 = 79.4(2), N2–Ru1–N3 = 78.8(2), N4–Ru1–N5 = 79.3(2), N5–Ru1–N6 = 78.7(2), N8–N7–C34 = 111.4(4), N10–N9–C39 = 111.9(4)°.

Extensive interactions between aromatic C–H hydrogen atoms and the F atoms of the $[\text{PF}_6]^-$ ions also contribute towards the solid state packing. The $\{\text{Ru(tpy)}_2\}$ units are held significantly away from one another, preventing them from engaging in face-to-face or edge-to-face π -interaction. Crystalline $[\text{Fe}(\mathbf{41})_2]\text{[PF}_6\text{]}_2$ is isostructural with $[\text{Ru}(\mathbf{41})_2]\text{[PF}_6\text{]}_2$.

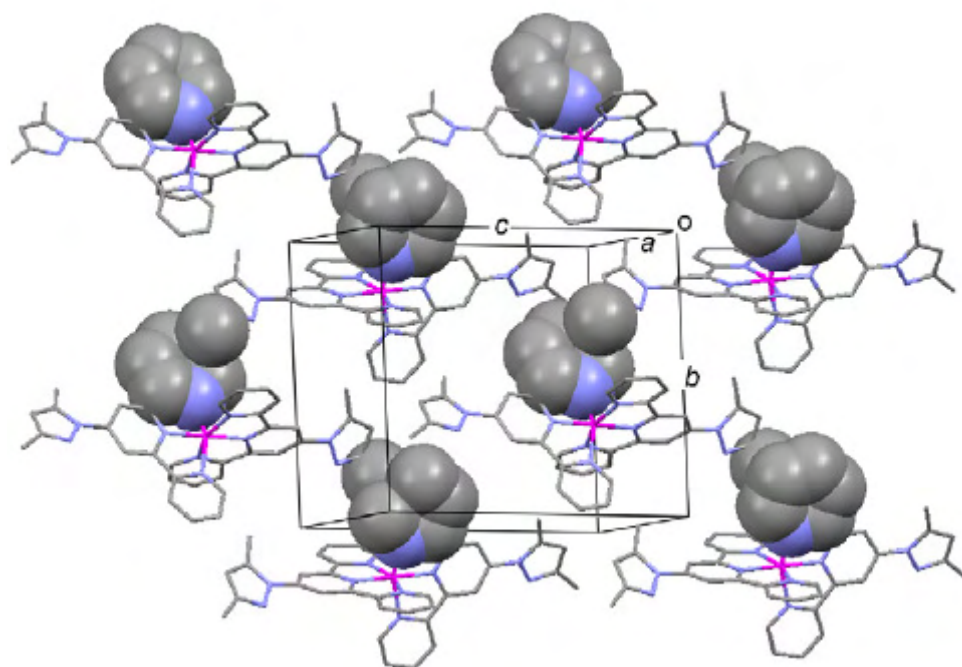


Figure 4-35 Close contacts between pyridine π -systems and pyrazolyl Me substituents (shown in space filling representation) in the solid state structure of $[\text{Ru}(41)_2][\text{PF}_6]_2$. Anions and hydrogen atoms are omitted from the figure.

11. $[\text{Pd}(\mathbf{9})\text{Cl}]\text{Cl}\cdot 3\text{H}_2\text{O}\cdot \text{DMF}$

Single crystals (yellow plates) of $[\text{Pd}(\mathbf{9})\text{Cl}]\text{Cl}\cdot 3\text{H}_2\text{O}\cdot \text{DMF}$ were grown by slow evaporation of the filtrate collected after filtration of the reaction mixture (see experimental section for details). The structure of the $[\text{Pd}(\mathbf{9})\text{Cl}]^+$ cation is shown in Figure 4-36 and bond parameters for the coordination sphere are given in the caption. The four pyridine rings in ligand 1 deviate only slightly from coplanarity; the angles between the least squares planes of the rings containing N1 and N2, N2 and N3, and N2 and N4 are 1.4(4), 2.3(4) and 6.7(5) $^\circ$, respectively. Cations pack in columns (Figure 4-37) supported by short Pd...Pd contacts ($\text{Pd}1\ldots\text{Pd}1\text{i} = 3.367(1)$, $\text{Pd}1\ldots\text{Pd}1\text{ii} = 3.440(1)$ Å; symmetry codes: $\text{i} = -x, 1-y, 1-z$, $\text{ii}=1-x, 1-y, 1-z$). Such stacking has been observed in a number of complexes containing $[\text{Pd}(\text{tpy})]$ or $[\text{Pt}(\text{tpy})]$ units³³⁸⁻³⁴⁷, while in other cases close contacts occur only between pairs of metal centres.^{181, 336, 346}

348-352

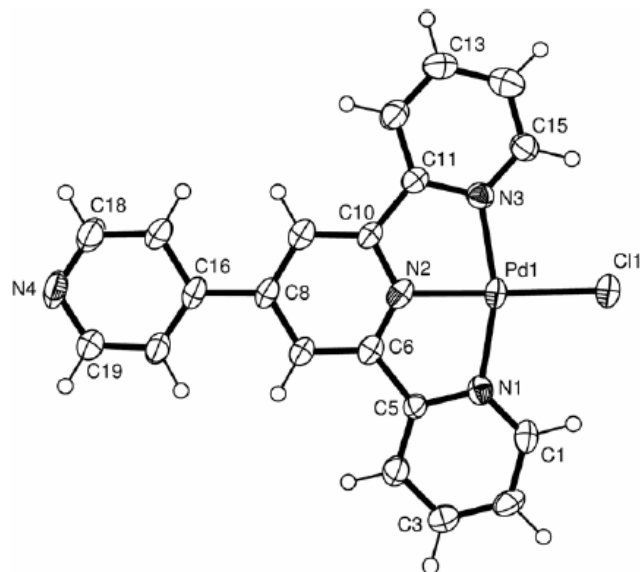


Figure 4-36 Molecular structure of the cation $[\text{Pd}(\mathbf{9})\text{Cl}]^+$ in $[\text{Pd}(\mathbf{9})\text{Cl}]\text{Cl}\cdot 3\text{H}_2\text{O}\cdot \text{DMF}$ with thermal ellipsoids plotted at 50% probability level. Selected bond lengths and angles: $\text{Pd1-Cl1} = 2.293(1)$, $\text{Pd1-N1} = 2.020(6)$, $\text{Pd1-N2} = 1.949(5)$, $\text{Pd1-N3} = 2.031(5)$ Å; $\text{N3-Pd1-N2} = 81.3(2)$, $\text{N1-Pd1-N2} = 80.6(2)$, $\text{N3-Pd1-Cl1} = 97.8(2)$, $\text{N1-Pd1-Cl1} = 100.2(2)$ °.

The $\text{Pd}\dots\text{Pd}$ distances observed between the $[\text{Pd}(\mathbf{9})\text{Cl}]^+$ units in $[\text{Pd}(\mathbf{9})\text{Cl}]\text{Cl}\cdot 3\text{H}_2\text{O}\cdot \text{DMF}$ are typical of those observed in other systems. Since the $\text{Pd}\dots\text{Pd}$ distances of ca. 3.4 Å coincide with the separation required for π -stacking interactions, it is not surprising that the latter are observed between the ring containing N1 in one cation and that containing N3 in the next cation. Figure 4-37 illustrates that stacks of cations are aligned in rows, between which reside water molecules and chloride ions, assembled into a 4.8^2 net.¹³³

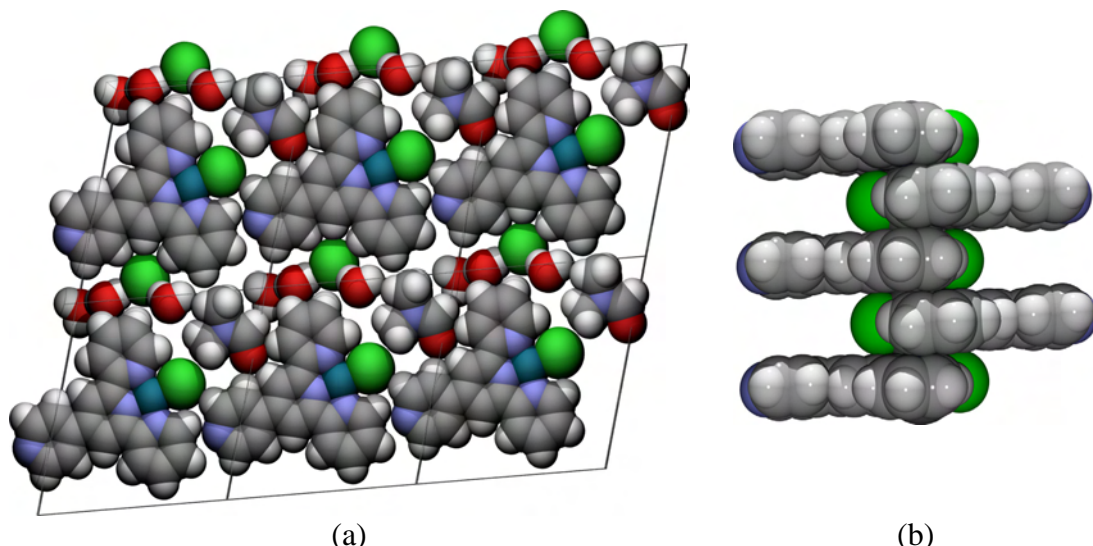


Figure 4-37 (a) Six units cells of $[\text{Pd}(\mathbf{9})\text{Cl}]\text{Cl}\cdot 3\text{H}_2\text{O}\cdot \text{DMF}$ viewed down the crystallographic a -axis. Stacks of $[\text{Pd}(\mathbf{9})\text{Cl}]^+$ cations assemble in rows which are separated by sheets of hydrogen-bonded water molecules and chloride ions surrounding DMF molecules. (b) a single stack of complexes looking down the b -axis.

Part of one net is shown in Figure 4-38. Among the complexes in the CSD¹⁹⁴ that contain {Pd(tpy)} or [Pt(tpy)] units, the phase-separated structure observed for [Pd(**9**)Cl]Cl·3H₂O·DMF is unique. In contrast, an analysis of the structure of [Pt(tpy)Cl]Cl·2H₂O³⁴⁹ reveals that it exhibits ribbons of hydrogen-bonded H₂O molecules and chloride ions with pentagonal motifs.

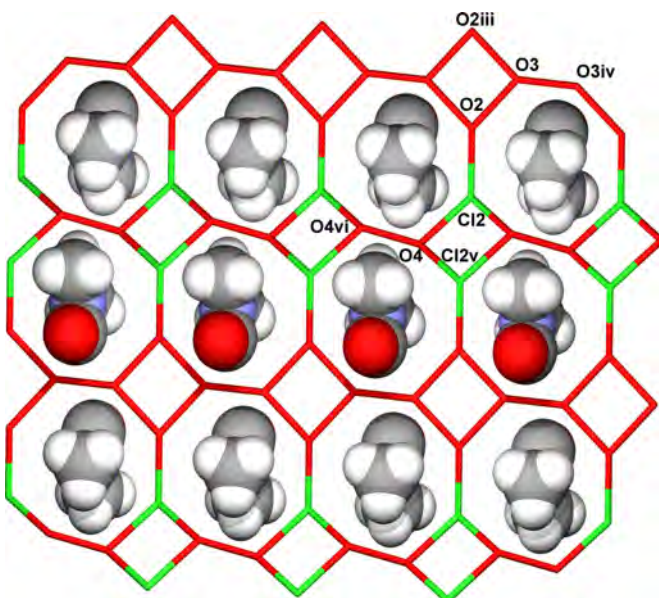


Figure 4-38 Part of the 4.8² net formed by the Cl⁻ ions and water O atoms in with encapsulated DMF molecules in CPK representation in [Pd(**9**)Cl]Cl·3H₂O·DMF. Pertinent distances are O2...Cl2 = 3.033(9), O2...O3 = 2.86(1), O3...O2iii = 2.91(1), O3...O3iv = 2.849(9), O4...Cl2 = 3.07(1), O4...Cl2v = 3.11(1), O4...O4vi = 2.83(1) Å. Symmetry codes: iii = 1 - x, -y, -z; iv = 2 - x, -y, -z; v = 1 - x, 1 - y, -z; vi = -x, 1 - y, -z.

12. [Pd(**41**)Cl]PF6

X-ray quality crystals of [Pd(**41**)Cl][PF₆] grew from a solution of [Fe(**41**)₂][PF₆]₂ and PdCl₂ (in an NMR tube (see synthesis of Pd(II) complexes for details). The structure of the [Pd(**41**)Cl]⁺ cation is depicted in Figure 4-39. The palladium(II) centre is in a square planar environment, and bond parameters for the coordination sphere are as expected. Compared to the free protonated ligand [H₂**41**]²⁺ in [H₂**41**][EtOSO₃]₂ · H₂O, and the coordinated ligands in [Fe(**41**)₂]²⁺ and [Ru(**41**)₂]²⁺, the structure of the metal-bound ligand in [Pd(**41**)Cl]⁺ is noteworthy for the coplanarity of the central pyridine and the pendant pyrazolyl rings. The angle between the least squares planes of these rings is 1.0(2)^o. The origin of this feature can be traced to the stacking of cations in the solid state.

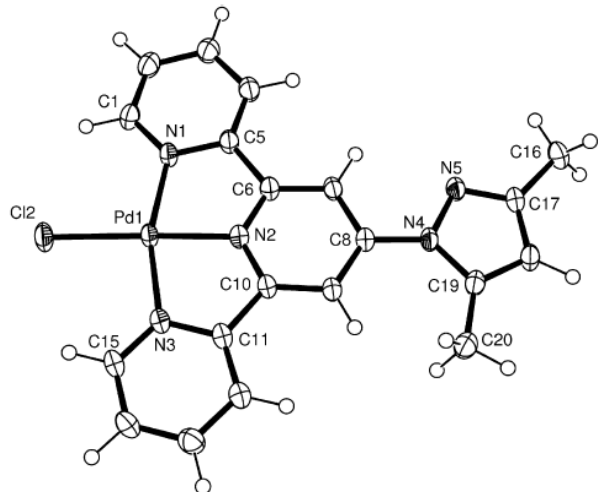


Figure 4-39 Molecular structure of the $[\text{Pd}(\mathbf{41})\text{Cl}]^+$ cation in $[\text{Pd}(\mathbf{41})\text{Cl}][\text{PF}_6]$ with thermal ellipsoids plotted at the 50% probability level. Selected bond parameters: $\text{Pd1}-\text{Cl}2 = 2.2932(6)$, $\text{Pd1}-\text{N}1 = 2.030(2)$, $\text{Pd1}-\text{N}2 = 1.941(2)$, $\text{Pd1}-\text{N}3 = 2.021(2)$, $\text{N}4-\text{C}8 = 1.388(3)$, $\text{N}4-\text{N}5 = 1.381(3)$ Å; $\text{Cl}2-\text{Pd1}-\text{N}1 = 100.13(6)$, $\text{Cl}2-\text{Pd1}-\text{N}3 = 98.17(6)$, $\text{N}1-\text{Pd1}-\text{N}2 = 80.73(8)$, $\text{N}2-\text{Pd1}-\text{N}3 = 80.93(8)$ °.

Figure 4-40a illustrates that cations pair up by virtue of a short $\text{Pd}\dots\text{Pd}$ contact of $3.3218(4)$ Å, and then these dimers assemble into step-like stacks, supported by aromatic π -interactions.

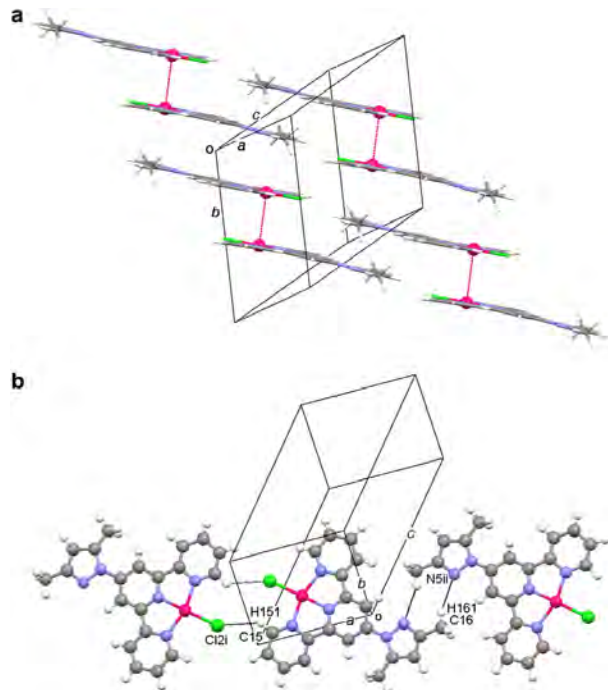


Figure 4-40 (a) The assembly of step-like stacks of $[\text{Pd}(\mathbf{41})\text{Cl}]^+$ cations in $[\text{Pd}(\mathbf{41})\text{Cl}][\text{PF}_6]$. (b) Hydrogen-bonded interactions between stacks (symmetry codes: $i = 2 - x, 1 - y, -z$; $ii = -1 - x, -y, -z$).

The latter occur between sets of three heterocycles, *viz.* a pyridine ring containing N1 in sandwiched between a pyrazolyl ring and a pyridine ring containing N3, with inter-ring

separations of ~ 3.4 Å. Additional hydrogen bond operate between the stacks, in the self-complementary pairs of interactions shown in Figure 4-40b ($C15H151\dots Cl2i = 2.78$ Å, $C15\dots Cl2i = 3.562(3)$ Å, $C15H151\dots Cl2i = 135^\circ$; $C16H161\dots N5ii = 2.61$ Å, $C16\dots N5ii = 3.566(3)$ Å, $C16H161\dots N5ii = 160^\circ$).

13. $[Cu(9)Cl_2]\cdot H_2O\cdot MeOH$

X-Ray quality crystals of $[Cu(9)Cl_2]\cdot H_2O\cdot MeOH$ were grown by slow evaporation of a MeOH solution of the complex. The molecular structure is shown in Figure 4-41.

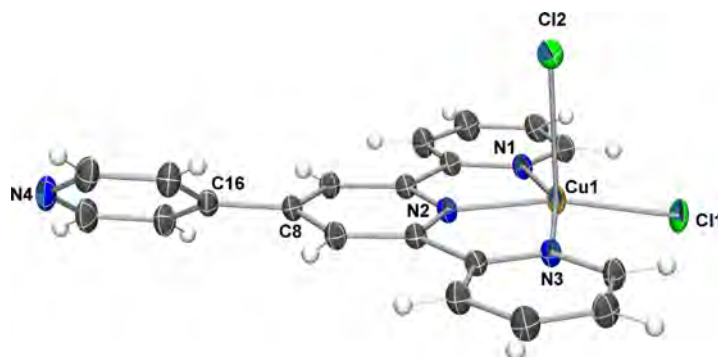


Figure 4-41 The molecular structure of $[Cu(9)Cl_2]$ in $[Cu(9)Cl_2]\cdot H_2O\cdot MeOH$. Displacement ellipsoids drawn at 30% probability level. Selected bond lengths and angles: $Cu1-Cl1$ 2.2248(6), $Cu1-Cl2$ 2.5792(7), $Cu1-N1$ 2.039(2), $Cu1-N2$ 1.941(2), $Cu1-N3$ 2.039(2), Å.. $N(1)-Cu(1)-N(2)$ 79.66(8), $N(2)-Cu(1)-N(3)$ 79.56(8), $N(3)-Cu(1)-N(1)$ 158.32(8), $N(2)-Cu(1)-Cl(1)$ 167.16(6), $N(3)-Cu(1)-Cl(1)$ 99.47(6), $N(1)-Cu(1)-Cl(1)$ 99.41(6), $N(2)-Cu(1)-Cl(2)$ 89.68(6), $N(3)-Cu(1)-Cl(2)$ 90.20(6), $N(1)-Cu(1)-Cl(2)$ 95.78(6), $Cl(1)-Cu(1)-Cl(2)$ 103.14(2)°. Angle between the least-squares planes of the ring containing N4 from the least squares plane of rings containing N1, N2 and N3 is 37.05(11)°.

The Cu(II) centre adopts a distorted square-based pyramidal geometry with the Cu(II) atom lifted slightly above of the plane of the ligand and chlorine Cl1 tilted slightly below [0.174(1) Å above and Cl(1) 0.127(1) Å below the least squares plane of the ligand respectively]. As expected for a Cu(II) complex, the axial chlorine-copper bond length [$Cu1-Cl2$ 2.5792(7) Å] is significantly longer than that of the in-plane chlorine [$Cu1-Cl1$ 2.2248(6) Å]. The pendant ring is significantly twisted out of the plane of the tpy by 37.05(11)° (see figure caption for details). The complexes are packed together via inefficient π -stacking interactions, although the closest C-C contact is 3.367 Å ($C1-C15i$, $i = -x, 1-y, 1-z$) the overlap between the complexes is minimal (Figure 4-42b). Intermolecular Cu-Cl contacts ($Cu1-Cl1i$ 3.344 Å, $i = x, 1-y, 1-z$) are too long to be considered bonds but may play a significant stabilising role (Figure 4-42a).

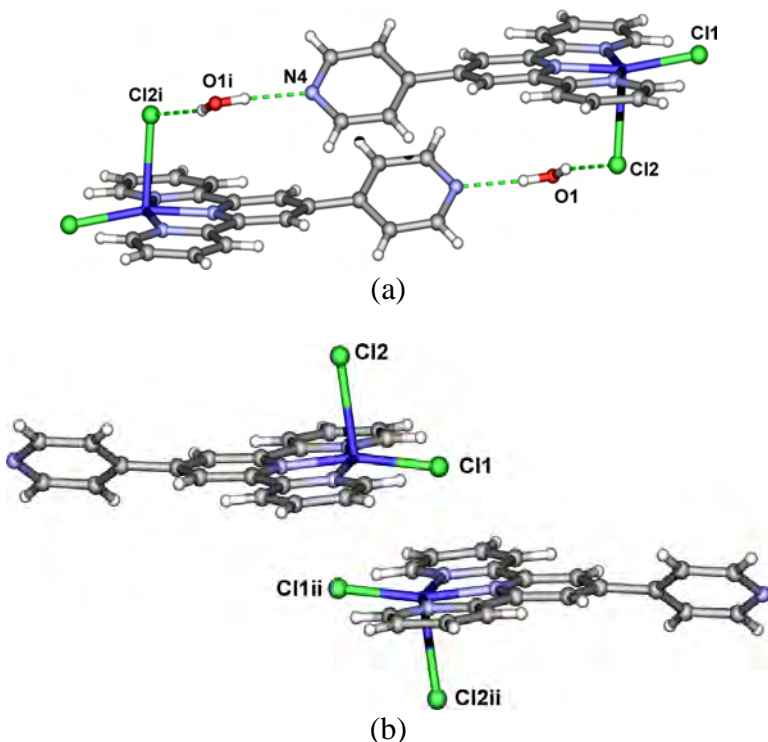


Figure 4-42 Key interactions in the crystal packing of in $[\text{Cu}(\mathbf{9})\text{Cl}_2]\text{H}_2\text{O}\cdot\text{MeOH}$. (a) Water bridged hydrogen-bonded dimers. (b) Weak Cu-Cl interactions and poor π -stacking.

The pendant pyridyl nitrogen is hydrogen-bonded to a water molecule ($\text{N}4 \dots \text{O}1i$ 2.896 Å, $i = -1-x, -y, -z$) which is in turn hydrogen bonded to Cl2 of an adjacent complex ($\text{O}1 \dots \text{Cl}2 = 3.184$ Å) to form hydrogen-bonded dimers (Figure 4-42a). This arrangement appears ideally positioned for the pendant rings to π -stack, although the complexes do not approach each other (distance from least squares plane of ring containing N4 to centroid of ring containing N4i 3.725 Å, $i = 1-x, -y, -z$) indicating that the stability from the hydrogen-bond pairing must outweigh any potential stability gain from π -stacking. Similarly, the terminal rings of the complexes are not involved in π -stacking between these dimers, with no π -overlap at all being present.

14. $[\text{Cu}(\mathbf{H9})\text{Cl}_2]\text{Cl}\cdot 3\text{H}_2\text{O}$ and $[\text{Cu}(\mathbf{H9})\text{Cl}_2]\text{Cl}\cdot \text{EtOH}$

X-Ray quality crystals of $[\text{Cu}(\mathbf{H9})\text{Cl}_2]\text{Cl}\cdot 3\text{H}_2\text{O}$ were grown by cooling of a water-ethanol solution of $[\text{Cu}(\mathbf{H9})\text{Cl}_2]\text{Cl}$, the molecular structure is shown in Figure 4-43. The ligand is almost perfectly planar and the Cu(II) centre adopts a distorted square-based pyramidal geometry very similar to that of the non-protonated complex discussed above.

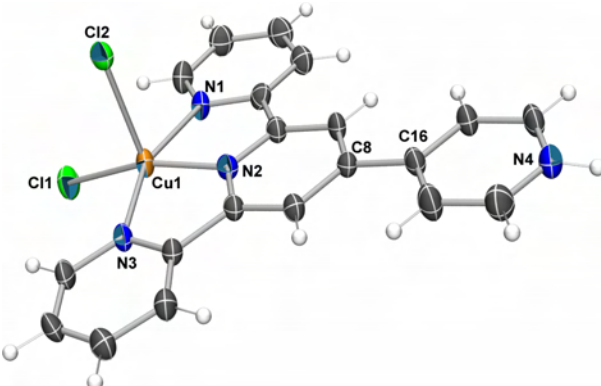
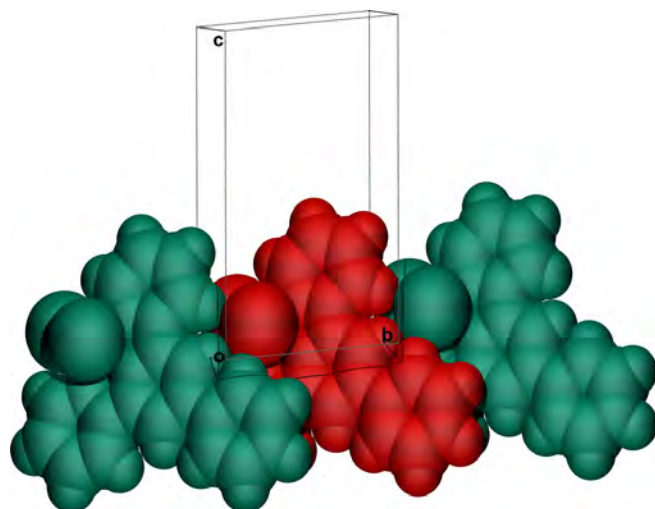


Figure 4-43 The molecular structure of $[\text{Cu}(\text{H9})\text{Cl}_2]$ in $[\text{Cu}(\text{H9})\text{Cl}_2]\text{Cl}\cdot 3\text{H}_2\text{O}$. Displacement ellipsoids drawn at 30% probability level. Selected bond lengths and angles: Cu1-C11 2.218(1), Cu1-Cl2 2.570(1), Cu1-N1 2.051(4), Cu1-N2 1.942(3), Cu1-N3 2.045(4) Å; Cl1-Cu1-Cl2 102.4(1), Cl1-Cu1-N1 99.7(1), Cl1-Cu1-N2 163.5(1), Cl1-Cu1-N3 98.8(1), Cl2-Cu1-N1 92.1(1), Cl2-Cu1-N2 94.2(1), Cl2-Cu1-N3 97.6(1), N1-Cu1-N2 79.6(1), N1-Cu1-N3 157.3(1), N2-Cu1-N3 79.3(1)°. The Cu1 is lifted above the least-squares plane of the ligand by 0.195(1) Å and Cl1 is tilted slightly below by 0.262(1) Å..

Unlike the non-protonated complex, the crystal packing features extensive π -stacking; the key interactions are shown in Figure 4-44. The complexes are assembled in pairs via a crystallographic inversion centre (distance between least squares planes of tpy ligands is 3.408 Å), although the long Cu-Cu distance (3.946 Å) indicates there are no metal-metal interactions. The pendant pyridyl ring is also π -stacked with the terminal rings of an adjacent complex, with more effective overlap to the ring containing N3i than to the ring containing N1ii, ($i = -1 + x, y, z$; $ii = 2-x, 1-y, -z$; see figure caption for details). The overall result is the formation of close-packed two dimensional sheets of the complexes. Coordinated and non-coordinated chloride anions and water molecules form two dimensional sheets (Figure 4-45) which separate the sheets of complexes, reminiscent of the structure of $[\text{Pd}(\text{9})\text{Cl}]\text{Cl}\cdot 3\text{H}_2\text{O}\cdot \text{DMF}$.



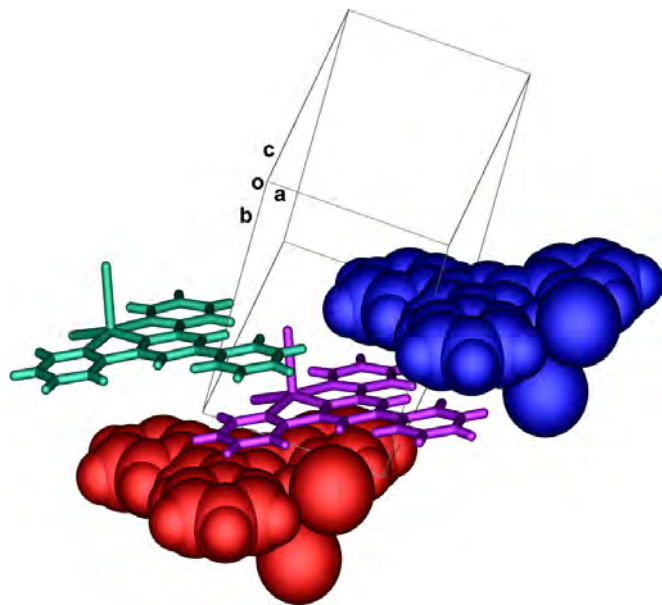


Figure 4-44 (a) A row of three complexes of $[\text{Cu}(\text{H9})\text{Cl}_2]$ in $[\text{Cu}(\text{H9})\text{Cl}_2]\text{Cl}\cdot 3\text{H}_2\text{O}$ along the b -axis, showing π -overlap between ring containing pyridyl rings containing N4 and N3i (red = x, y, z; left = -1+x, y, z; right = i = 1+x, y, z). (b) Key π -stacking interactions in $[\text{Cu}(\text{H9})\text{Cl}_2]\text{Cl}\cdot 3\text{H}_2\text{O}$. Intermolecular distances: between pairs of complexes [least-squares planes of the ligands, i] = 3.408 Å. Involving pendant pyridyl ring: C11-C20ii = 3.399 Å, from centroid (ring N4) to plane (ring N3ii) = 3.400 Å; C19-C5iii 3.320 Å, from centroid (ring N4) to plane (ring N1iii) = 3.354 Å. Symmetry codes: purple = x, y, z; red = i = 1-x, 2-y, -z; -z; green = ii = -1 + x, y, z, blue = iii = 2-x, 1-y, -z. Uncoordinated chlorides and solvent omitted.

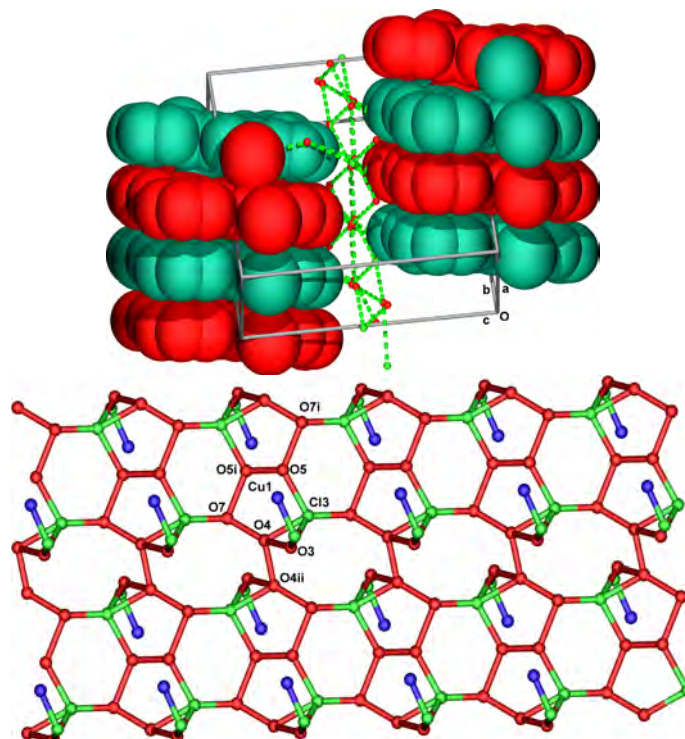


Figure 4-45 A portion of the two dimensional hydrogen-bonded sheet of coordinated and uncoordinated chloride anions and water molecules. Only highest occupancy positions shown. Symmetry operators: i = 1-x, 2-y, 1-z; ii = 3-x, 1-y, 1-z.

[Cu(H9)Cl₂] was also crystallised as [Cu(H9)Cl₂]·3H₂O·EtOH and the molecular structure of the complex (Figure 4-46) is essentially identical to that in [Cu(H9)Cl₂]·3H₂O.

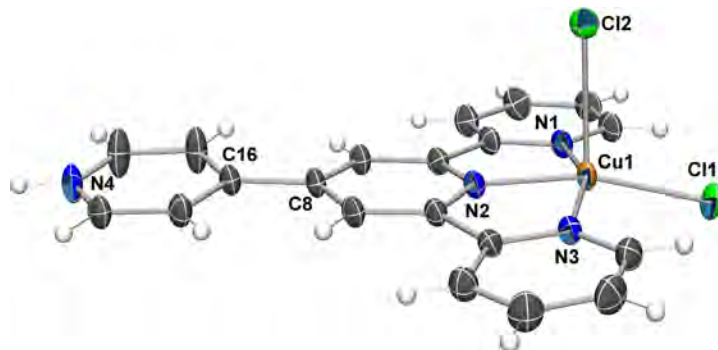


Figure 4-46 Cu1-Cl1 2.208(2), Cu1-Cl2 2.600(2), Cu1-N1 2.052(2), Cu1-N2 1.940(2), Cu1-N3 2.053(2)
Å. Cl1-Cu1-Cl2 103.43(2), Cl1-Cu1-N1 98.78(5), Cl1-Cu1-N2 164.17(5), Cl1-Cu1-N3 99.08(5), Cl2-
Cu1-N1 96.92(5), Cl2-Cu1-N2 92.40(5), Cl2-Cu1-N3 91.47(5), N1-Cu1-N2 79.59(7), N1-Cu1-N3
157.91(6), N2-Cu1-N3 79.67(7)°

4.6. Summary of crystal structures

The range of crystal structures presented in this chapter allows one to reach several worthwhile conclusions. Firstly, π -stacking interactions dominate the assemblies in all cases, and recurring packing motifs are often observed. Secondly, and perhaps somewhat surprisingly, is that considerably more flexibility was observed within the tpy ligands than expected. Despite the coordination sphere of the metal being virtually identical in all cases, significant deviations from coplanarity of the pyridyl rings were observed and also distortions from orthogonality of the two ligands. More noticeable are deviations from coplanarity of the pendant ring, ranging from coplanar [in $[\text{Pd(II)(9)Cl}\cdot\text{DMF}]$ and $[\text{Cu(H9Cl}_2]\text{Cl}\cdot3\text{H}_2\text{O}]$] to twisted by 35.5° [in $\text{Ru(9)}_2(\text{PF}_6)_2$]. Significant distortions along the [pendant ring]-M-[pendant ring] vector, ranging from a perfect 180° [for in $\text{Ru(9)}_2(\text{PF}_6)_2$] to 171° [for $\text{Fe(9)}_2(\text{ClO}_4)_2\cdot2\text{MeOH}$]. As only weak interactions could be identified as responsible for these variations, the logical conclusion is that the packing stability of the complexes is perhaps less directing than previously thought and also that weak solvent and anion interactions play more vital roles in determining the solid state structures of M(tpy)_2 complexes than have been previously supposed.

4.7. Experimental

4.7.1. Precursors

4'-Hydrazino-2,2':6',2"-terpyridine²⁵⁰ was prepared as described in the literature²⁵⁰ from 4'-chloro-2,2':6'2"-terpyridine and excess hydrazine (see chapter 2). Pyrimidine-5-carbaldehyde was prepared from commercially available 5-bromopyrimidine as previously reported.³⁵³ 2-Acetyl-4-picoline was prepared from picoline using a modification of literature procedures.³²⁰⁻³²² 4-Pyridylboronic acid pinacol ester was prepared from 4-iodopyridine as reported.³²⁶

4.7.2. Ligands

Ligand 33

Ligand **33** was prepared by modifying the procedure reported for **9** by Hanan.³⁰² 2-Acetylpyridine (4.84 g, 40.0 mmol) was added to a solution of pyridine-2-carbaldehyde (2.18 g, 20.4 mmol) in EtOH (100 cm³). KOH pellets (2.7 g, 50 mmol) and aqueous NH₃ (60 cm³, 25%, 0.85 mol) were added to the solution which was then stirred at room temperature for 4 h. An off-white solid formed which was collected by filtration and washed with H₂O (3 × 15 cm³) and EtOH (3 × 15 cm³). Recrystallization from CHCl₃-MeOH gave **33** as a white crystalline solid (2.36 g, 7.60 mmol, 38.0%). Spectroscopic and mass spectrometric data were consistent with the literature. Found: C, 77.08; H, 4.68; N, 18.18. C₂₀H₁₄N₄ requires C, 77.40; H, 4.55; N, 18.05.

Ligand 34

Ligand **34** was prepared by the procedure of Hanan reported³⁰² for **9**. 2-Acetylpyridine (4.84 g, 40.0 mmol) was added to a solution of pyridine-3-carbaldehyde (2.18 g, 20.4 mmol) in EtOH (100 cm³). KOH pellets (2.7 g, 50 mmol) and aqueous NH₃ (60 cm³, 25%, 0.85 mol) were added to the solution. This was stirred at room temperature for 4 h, and the off-white solid that formed was collected by filtration and washed with H₂O (3 × 15 cm³) and EtOH (3 × 15 cm³). Ligand **34** was isolated as a white crystalline solid after recrystallization from CHCl₃-MeOH (2.72 g, 8.76 mmol, 43.8%). Spectroscopic and mass spectrometric data were as previously reported.³⁵⁴ Found: C, 77.15; H, 4.62; N, 18.24. C₂₀H₁₄N₄ requires C, 77.40; H, 4.55; N, 18.05.

Ligand 9

Prepared according to the literature.³⁰²

Ligand 38

2-Acetyl-4-picoline (0.50g, 3.7 mmol) in EtOH (5mL) was added to a solution of pyridine-4-carbaldehyde (0.20g, 1.8 mmol) in EtOH (10mL). KOH pellets (0.23 g, 4.1 mmol) and aqueous NH₃ (5mL, 25%, 5 mmol) were added to the solution, which was then stirred at room temperature for 16 h. The resulting off-white solid was collected and washed with EtOH (10mL) to give pure **38** (0.37g, 1.1 mmol, 29%). ¹H-NMR

(CDCl₃): 8.76 (d, *J* 5.7 Hz, 2H, H^{A6}), 8.74 (s, 2H, H^{B3}), 8.59 (d, *J* 4.7 Hz, H^{C2}), 8.48 (s, 2H, H^{A3}), 7.79 (d, *J* 5.7, 2H, H^{A5}), 7.21 (d, *J* 4.7 Hz, 2H, H^{C3}), 2.53 (s, 3H, Me).

¹³C{¹H}: 156.8 (C^{A2/B2}), 155.7 (C^{A2/B2}), 150.7 (C^{C2}), 149.2 (C^{A6}), 148.3 (C^{C4}), 146.2 (C^{B4}), 125.3 (C^{A5}), 122.3 (C^{A3}), 121.9 (C^{C3}), 119.0 (C^{B3}), 21.6 (Me). ESI-MS *m/z* found 339.6, LH⁺ requires 339.2. Found: C 69.93, H 5.70, N 21.77 %. C₂₂H₂₈N₄·0.33MeOH requires C 69.57, H 6.00, N 21.93 %.

Ligand 39

2-Acetylpyridine (7.3 g, 60 mmol) was added to a solution of pyrimidine-5-carbaldehyde³⁵³ (3.2 g, 30 mmol) in EtOH (100 cm³). KOH pellets (3.4 g, 61 mmol) and aqueous NH₃ (75 cm³, 25%, 76 mmol) were added to the solution, which was then stirred at room temperature for 4 h. The off-white solid was collected by filtration and washed with EtOH (4 x 15 cm³). Recrystallisation from CHCl₃-MeOH afforded 2 as a white crystalline solid (3.2 g, 10.2 mmol, 34 %). ¹H NMR spectroscopic data in CDCl₃ were consistent with those published.³¹⁴ ¹H NMR (500 MHz, DMSO-d₆) δ/ppm 9.37 (s, 2 H, H^{C4}), 9.34 (s, 1 H, H^{C2}), 8.78 (ddd, *J* 5.6, 4.8, 1.1 Hz, 2 H, H^{A6}), 8.77 (s, 2 H, H^{B3}), 8.69 (d, *J* 7.9 Hz, 2 H, H^{A3}), 8.06 (td, *J* 7.6, 1.6 Hz, 2 H, H^{A4}), 7.56 (ddd, *J* 7.5, 4.8, 0.9 Hz, 2 H, H^{A5}). ¹³C{¹H} (125 MHz, DMSO-d₆) δ/ppm 158.8 (C^{C5}), 156.0 (C^{B2}), 155.4 (C^{C2}), 154.7 (C^{A2}), 149.4 (C^{A6}), 144.1 (C^{C4}), 137.6 (C^{A6}), 131.5 (C^{B4}), 124.8 (C^{A5}), 121.1 (C^{A3}), 118.5 (C^{B3}). ESI-MS: *m/z* 312 [MH]⁺. Found: C, 72.03; H, 4.18; N, 21.78 %. C₁₉H₁₃N₅·0.25 H₂O requires C, 72.25; H, 4.31; N, 22.17.

Ligand 41

[H₂**41**][EtOSO₃]₂

Pentane-2,4-dione (0.10 g, 1.0 mmol) was added to a solution of 4'-hydrazino-2,2':6'-2"-terpyridine (0.11 g, 0.42 mmol) in EtOH (15 cm³) and the mixture heated. Two drops of concentrated H₂SO₄ were added to the colourless solution causing the immediate formation of a milky, pale yellow suspension which dissolved on heating. The mixture was heated at reflux for 3 h and then cooled to room temperature. Et₂O was added carefully until the first sign of the formation of a precipitate was observed. The solution was then left to stand at -18 °C. The fine white needles of [H₂**41**][EtOSO₃]₂ which formed were collected by filtration and washed with chilled EtOH and Et₂O.

[H₂**41**][EtOSO₃]₂: 0.22 g, 0.38 mmol, 92 %. ¹H NMR (500 MHz, DMSO-d₆) δ / ppm

8.88 (m, 4H, H^{A6,A3}), 8.71 (s, 2H, H^{B3}), 8.32 (t, *J* 7.3 Hz, 2H, H^{A4}), 7.78 (dd, *J* 6.0, 5.5 Hz, 2H, H^{A5}), 6.29 (s, 1H, H^{C4}), 3.74 (q, *J* 8.0 Hz, 4H, CH₂^{anion}), 2.62 (s, 3H, Me^{C5}, 2.27 (s, 3H, Me^{C3}), 1.11 (t, *J* 8.0 Hz, 6H, CH₃^{anion}). ¹³C{¹H} NMR (125 MHz, DMSO-d₆) δ / ppm 154.0 (C^{B2}), 151.8 (C^{A2}), 150.5 (C^{C3}), 148.9 (C^{B4}), 147.5 (C^{A6}), 141.0 (C^{A4}), 140.8 (C^{C5}), 126.0 (C^{A5}), 122.7 (C^{A3}), 114.1 (C^{B3}), 110.2 (C^{C4}), 13.4 (C^{Me(C5)}), 13.3 (C^{Me(C3)}). ESI MS m/z 328 [H₂**41**]⁺. Found: C, 48.94, H 5.18, N 12.27; [H₂**41**][EtOSO₃]₂ · 0.3H₂O requires C 49.23, H 5.11, N, 11.96 %.

[H₂**41**][MeOSO₃]₂

Pentane-2,4-dione (0.090 g, 0.90 mmol) was added to a solution of 4'-hydrazino-2,2':6',2"-terpyridine (0.20 g, 0.76 mmol) in hot MeOH. Two drops of concentrated H₂SO₄ were added to the colourless solution causing the immediate formation of a milky, pale yellow suspension. The reaction mixture was heated at reflux for 2 h, after which time the precipitate had completely dissolved. After a further 3 h at reflux, the solution was cooled to room temperature and Et₂O was added carefully until the first sign of a precipitate was observed. The solution was left standing overnight at -18 °C. [H₂**41**][MeOSO₃]₂ precipitated as an off-white microcrystalline solid which was collected by filtration and washed with cold EtOH. [H₂**41**][MeOSO₃]₂ (0.20 g, 0.36 mmol, 47 %): ¹H NMR (500 MHz, DMSO-d₆) δ / ppm 8.85 (d, 2H, *J* 5.0 Hz, H^{A6}), 8.83 (d, *J* 8.1 Hz, 2H, H^{A3}), 8.71 (s, 2H, H^{B3}), 8.25 (td, *J* 8.0, 1.3 Hz, 2H, H^{A4}), 7.72 (dd, *J* 6.7, 5.6 Hz, 2H, H^{A5}), 6.29 (s, 1H, H^{C4}), 3.37 (s, 3H, CH₃^{anion}), 2.62 (s, 3H, H^{C5}), 2.27 (s, 3H, H^{C3}). ¹³C{¹H} NMR (125 MHz, DMSO-d₆) δ / ppm 154.6 (C^{B2}), 152.5 (C^{A2}), 150.4 (C^{C3}), 148.7 (C^{B4}), 148.0 (C^{A6}), 140.8 (C^{C5}), 139.9 (C^{A4}), 125.7 (C^{A5}), 122.2 (C^{A3}), 113.6 (C^{B3}), 110.2 (C^{C4}), 13.4 (C^{Me(C5,C3)}). ESI MS m/z 328 [H₂**41**]⁺, 677 [2(**41**) + Na]⁺. Found: C, 42.89, H 4.02, N 11.62; [H₂**41**][MeOSO₃]₂ requires C 42.92, H 4.09, N, 11.37 %.

4'-(3,5-Dimethylpyrazol-1-yl)-2,2':6',2"-terpyridine (**41**)

[H₂**41**][EtOSO₃]₂ (100 mg, 0.17 mmol) was dissolved in H₂O (10 cm³) and an aqueous solution of NaOH (0.5 M) was added dropwise until a white precipitate resulted. Collection of the sticky solid was difficult. It was extracted into CH₂Cl₂ and the solvent removed to give neutral **41** (15 mg, 0.046 mmol, 27%). ¹H NMR (400 MHz, CDCl₃) δ / ppm 8.69 (ddd, *J* 4.8, 1.8, 1.0 Hz, 2H, H^{A6}), 8.66 (s, 2H, H^{B3}), 8.63 (dt, *J* 8.0, 1.0 Hz,

2H, H^{A3}), 7.84 (dt, *J* 7.6, 1.5 Hz, 2H, H^{A4}), 7.32 (ddd, *J* 7.6, 4.8, 1.6 Hz, 2H, H^{A5}), 6.06 (s, 1H, H^{C4}), 2.63 (s, 3H, Me^{C5}), 2.32 (s, 3H, Me^{C3}). ¹³C{¹H} NMR (125 MHz, CDCl₃) δ / ppm 157.0 (C^{B2}), 155.7 (C^{A2}) 150.5 (C^{C3}), 149.3 (C^{A6}), 149.0 (C^{B4}), 140.2 (C^{C5}), 136.9 (C^{A4}), 124.1 (C^{A5}), 121.3 (C^{A3}), 114.5 (C^{B3}), 109.1 (C^{C4}), 13.7 (C^{Me(C3)}), 13.5 (C^{Me(C5)}). ¹H NMR (500 MHz, DMSO-d₆) δ / ppm 8.75 (ddd, *J* 4.6, 1.4, 0.8 Hz, 2H, H^{A6}), 8.67 (s, 2H, H^{B3}), 8.66 (d, *J* 7.1, Hz, 2H, H^{A3}), 8.03 (td, *J* 7.8, 1.8 Hz, 2H, H^{A4}), 7.53 (ddd, *J* 7.4, 4.8, 0.9 Hz, 2H, H^{A5}), 6.24 (s, 1H, H^{C4}), 2.59 (s, 3H, Me^{C5}), 2.26 (s, 3H, Me^{C3}). ¹³C{¹H} NMR (125 MHz, DMSO-d₆) δ / ppm 156.4 (C^{B2}), 154.5 (C^{A2}), 150.0 (C^{C3}), 148.4 (C^{B4}), 149.4 (C^{A6}), 140.5 (C^{C5}), 137.5 (C^{A4}), 124.8 (C^{A5}), 121.0 (C^{A3}), 112.3 (C^{B3}), 110.0 (C^{C4}), 13.5 (C^{Me(C5)}), 13.4 (C^{Me(C3)}). ESI-MS *m/z* 328 [41 + H]⁺. Found: C, 73.34, H, 5.29, N, 21.30; C₂₀H₁₇N₅ requires C, 73.37, H, 5.23, N, 21.39 %.

4.7.3. Fe(II) complexes

[Fe(33)₂][PF₆]₂

Ligand **33** (0.20 g, 0.64 mmol) and FeCl₂·4H₂O(0.064 g, 0.32 mmol) were dissolved in MeOH (30 cm³) and stirred at room temperature for 30 min. Excess aqueous NH₄PF₆ was added and the resulting purple precipitate was collected on Celite, washed with H₂O, EtOH and Et₂O, and redissolved in MeCN. Solvent was removed to give [Fe(33)₂][PF₆]₂ as a purple microcrystalline solid (0.18 g, 0.19 mmol, 59%). ¹H NMR (CD₃CN, 500 MHz) δ/ ppm 9.57 (s, 4H, H^{B3}), 9.01 (d, *J* 4.2 Hz, 2H, H^{C6}), 8.65 (d, *J* 8.0 Hz, 4H, H^{A3}), 8.60 (d, *J* 8.0 Hz, 2H, H^{C3}), 8.22 (dt, *J* 7.8, 1.7 Hz, 2H, HC4), 7.92 (dt, *J* 8.0, 1.3 Hz, 4H, H^{A4}), 7.69 (dd, *J* 7.2, 5.0, 2H, H^{C5}), 7.20 (d, *J* 5.5 Hz, 4H, H^{A6}), 7.09 (t, *J* 6.6 Hz, 4H, H^{A5}). ¹³C{¹H} NMR (CD₃CN, 125 MHz) δ/ ppm 161.5 (C^{B2}), 158.9 (C^{A2}), 154.1 (C^{A6}), 153.7 (C^{C2}), 151.7 (C^{C6}), 149.8 (C^{B4}), 139.8 (C^{A4}), 139.2 (C^{C4}), 128.4 (C^{A5}), 126.5 (C^{C5}), 125.0 (C^{A3}), 123.1 (C^{C3}), 121.8 (C^{B3}). ES-MS: *m/z* 822 [M – PF₆]⁺, 339 [M–2PF₆]²⁺. UV/VIS λ_{max}/nm (1.87×10⁻⁵ mol dm⁻³, MeCN) 571 (ε /dm³ mol⁻¹ cm⁻¹ 27 700), 324 (48 700), 285 (76 800), 277 (63 600), 241 (34 800). Found: C, 48.57; H, 3.00; N, 11.40. C₄₀H₂₈F₁₂FeN₈P₂·1.5H₂O requires C, 48.36; H, 3.15; N, 11.28.

[Fe(**34**)₂][PF₆]₂

The preparation of [Fe(**34**)₂][PF₆]₂ was as for [Fe(**33**)₂][PF₆]₂, starting with **34** (0.20 g, 0.64 mmol) and FeCl₂·4H₂O (0.064 g, 0.32 mmol). [Fe(**34**)₂][PF₆]₂ was isolated as a purple solid (0.20 g, 0.21 mmol, 64%). ¹H NMR (CD₃CN, 500 MHz) *d*/ppm 9.50 (d, *J* 1.6 Hz, 2H, H^{C2}), 9.21 (s, 4H, H^{B3}), 8.91 (d, *J* 4.8 Hz, 2H, H^{C6}), 8.64 (d, *J* 8.4 Hz, 2H, H^{C4}), 8.61 (d, *J* 8.0 Hz, 4H, H^{A3}), 7.93 (t, *J* 7.8 Hz, 4H, H^{A4}), 7.79 (dd, *J* 7.8, 4.9 Hz, 2H, H^{C5}), 7.19 (d, *J* 5.6 Hz, 4H, H^{A6}), 7.10 (t, *J* 6.6 Hz, 4H, H^{A5}). ¹³C{¹H} NMR (CD₃CN, 125 MHz) *δ*/ppm 161.5 (C^{B2}), 158.9 (C^{A2}), 154.1 (C^{A6}), 152.6 (C^{C6}), 149.9 (C^{C2}), 148.6 (C^{B4}), 139.9 (C^{A4}), 136.3 (C^{C4}), 133.6 (C^{C3}), 128.4 (C^{A5}), 125.4 (C^{C5}), 124.9 (C^{A3}), 122.8 (C^{B3}). ES-MS: *m/z* 822 [M – PF₆]⁺, 339 [M–2PF₆]²⁺. UV/VIS $\lambda_{\text{max}}/\text{nm}$ (1.87×10⁻⁵ mol dm⁻³, MeCN) 567 (ε /dm³ mol⁻¹ cm⁻¹ 26 600), 322 (52 500), 284 (92 000), 277 (78 400), 244 (40 700). Found: C, 49.41; H, 2.98; N, 11.75. C₄₀H₂₈F₁₂FeN₈P₂ requires C, 49.71; H, 2.92; N, 11.59.

[Fe(**9**)₂][PF₆]₂

The preparation of [Fe(**9**)₂][PF₆]₂ was as for [Fe(**33**)₂][PF₆]₂, starting with **2** (0.20 g, 0.64 mmol) and FeCl₂·4H₂O (0.065 g, 0.33 mmol). [Fe(**9**)₂][PF₆]₂ was isolated as a purple solid (0.24 g, 0.25 mmol, 77%). Spectroscopic data differ slightly from those of the tetrafluoroborate salt previously reported. ¹H NMR (CD₃CN, 500 MHz) *δ*/ppm 9.23 (s, 4H, H^{B3}), 9.02 (d, *J* 6.0 Hz, 4H, H^{C2}), 8.63 (d, *J* 8.0 Hz, 4H, H^{A3}), 8.23 (d, *J* 6.0 Hz, 4H, H^{C3}), 7.93 (t, *J* 7.2 Hz, 4H, H^{A4}), 7.18 (d, *J* 5.3 Hz, 4H, H^{A6}), 7.10 (t, *J* 6.6 Hz, 4H, H^{A5}). ¹³C{¹H} NMR (CD₃CN, 125 MHz) *δ*/ppm 161.7 (C^{B2}), 158.7 (C^{A2}), 154.1 (C^{A6}), 152.3 (C^{C2}), 148.7 (C^{C4}), 145.0 (C^{B4}), 140.0 (C^{A4}), 128.5 (C^{A5}), 125.1 (C^{A3}), 123.0 (C^{C3}), 122.7 (C^{B3}). ESMS: *m/z* 822 [M – PF₆]⁺, 339 [M – 2PF₆]²⁺. UV/VIS $\lambda_{\text{max}}/\text{nm}$ (1.87×10⁻⁵ mol·dm⁻³, MeCN) 569 (ε /dm³ mol⁻¹ cm⁻¹ 25 000), 324 (45 100), 284 (81 700), 276 (74 100), 245 (48 200). Found: C, 48.96; H, 3.20; N, 12.39. C₄₀H₂₈F₁₂FeN₈P₂·0.75MeCN·0.75H₂O requires C, 49.31; H, 3.17; N, 12.13.

[Fe(**9**)₂][ClO₄]₂·2MeOH·0.5H₂O

Dark purple, X-ray quality crystals of [Fe(**9**)₂][ClO₄]₂ 2MeOH 0.5H₂O were grown in an H-tube by slow diffusion of a MeOH/H₂O solution of Fe(ClO₄)₂·9H₂O and NH₄SCN (1:2) into an MeCN/H₂O solution of [Fe(**9**)₂][PF₆]₂ over a period of 2 months. Inadequate sample was isolated for elemental analysis.

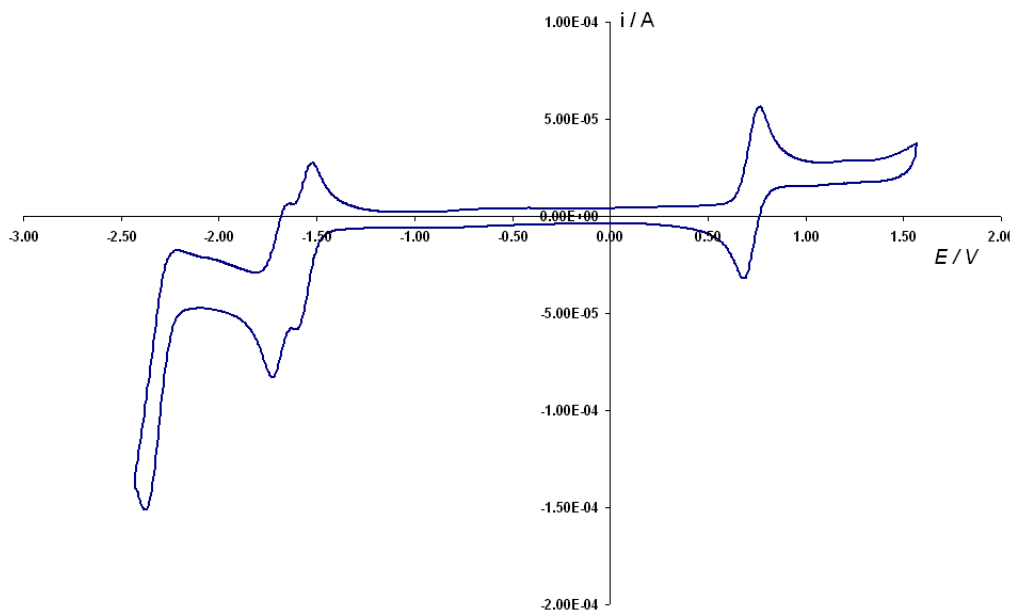
[Fe(39)₂][PF₆]₂

FeCl₂·4H₂O (0.035 g, 0.18 mmol) and **39** (0.11 g, 0.35 mmol) were dissolved in MeOH (20 cm³), and the reaction mixture was stirred at room temperature for 30 min. Excess aqueous NH₄PF₆ was added to precipitate the complex as a purple solid. This was collected on Celite and washed well with H₂O, EtOH and Et₂O. The product was redissolved in MeCN and the solvent removed. Recrystallisation from MeCN/H₂O gave [Fe(39)₂][PF₆]₂ as purple, plate-like crystals (0.12 g, 0.12 mmol, 70%). ¹H NMR (500 MHz, CD₃CN) δ/ppm 9.64 (s, 4 H, H^{C4}), 9.47 (s, 2 H, H^{C2}), 9.24 (s, 4 H, H^{B3}), 8.61 (d, *J* 8.0 Hz, 4 H, H^{A3}), 7.94 (td, *J* 7.9, 1.3 Hz, 4 H, H^{A4}), 7.19 (d, *J* 5.3 Hz, 4 H, H^{A6}), 7.12 (ddd, *J* 7.1, 5.6, 1.0 Hz, 4H, H^{A5}). ¹³C{¹H} (125 MHz, CD₃CN) δ/ppm 161.7 (C^{B2}), 160.6 (C^{C2}), 158.6 (C^{A2}), 157.0 (C^{C5}), 154.1 (C^{A6}), 145.4 (C^{B4}), 140.0 (C^{A4}), 131.8 (C^{C4}), 128.6 (C^{A5}), 125.0 (C^{A3}), 122.6 (C^{B3}). ESI-MS *m/z* 339 [M – 2 PF₆]²⁺. E° vs. Fc⁺/Fc/V: +0.79 (rev), -1.47 (rev), -1.60 (rev), -2.15 (quasi-rev), -2.28 (quasi-rev). UV-vis (MeCN, 1.87 x 10⁻⁵ mol·dm⁻³) λ_{max}/nm (ε_{max}/10³ dm³mol⁻¹cm⁻¹) 574 (24.3), 323 (46.1), 284 (78.9), 278 (64.2), 243 (35.3). Found: C, 46.12; H, 3.05; N, 14.33; C₃₈H₂₆F₁₂N₁₀P₂Fe.1.25 H₂O requires C, 46.06; H, 2.90; N, 14.13 %.

[Fe(41)₂](PF₆)₂

[H₂**41**][EtOSO₃]₂ (19 mg, 0.033 mmol) and FeCl₂·4H₂O (4.0 mg, 0.020 mmol) were dissolved in MeOH (10 mL) and stirred at room temperature for 2 h. Excess aqueous NH₄PF₆ was added to precipitate the purple complex which was collected on Celite, washed with H₂O, EtOH and Et₂O, and redissolved in MeCN. Removal of the solvent gave [Fe(41)₂][PF₆]₂ as a purple solid (15 mg, 0.015 mmol, 78%). ¹H NMR (500 MHz, CD₃CN) δ/ppm 9.04 (s, 4H, H^{B3}), 8.53 (d, *J* 8.0 Hz, 4H, H^{A3}), 7.90 (td, *J* 7.9, 1.4 Hz, 4H, H^{A4}), 7.25 (d, *J* 5.5 Hz, 4H, H^{A6}), 7.10 (ddd, *J* 7.0, 5.7, 1.2 Hz, 4H, H^{A5}), 6.43 (s, 2H, H^{C4}), 2.90 (s, 6H, Me^{C5}), 2.44 (s, 6H, Me^{C3}). ¹³C{¹H} NMR (125 MHz, CD₃CN) δ/ppm 161.7 (C^{B2}), 158.6 (C^{A2}), 154.4 (C^{A6}), 153.3 (C^{C3}), 149.6 (C^{B4}), 142.9 (C^{C5}), 139.7 (C^{A4}), 128.5 (C^{A5}), 125.1 (C^{A3}), 117.3 (C^{B3}), 112.0 (C^{C4}), 13.9 (C^{Me(C3)}), 13.8 (C^{Me(C5)}). ES-MS *m/z* 855 [M -PF₆]⁺, 355 [M-2PF₆]²⁺. UV-vis (MeCN, 8.80 x 10⁻⁶ mol·dm⁻³) λ/nm 565 (e/dm³·mol⁻¹cm⁻¹ 14600), 502 (sh, 5900), 317 (39000), 307 (38000), 284 (46200), 241 (23700). Anal. Calc. for C₄₀H₃₄F₁₂FeN₁₀P₂·1.5CH₃OH·H₂O

requires: C, 46.73; H, 3.97; N, 13.11. Found: C, 47.09; H, 3.61; N, 12.79%. E°/V versus Fc/Fc⁺: +0.75, -1.44 and -1.66 V (all reversible).



Cyclic voltammogram of $[\text{Fe}(\mathbf{41})_2]\text{[PF}_6\text{]}_2$ (MeCN, $[\text{Bu}_4\text{N}]\text{[PF}_6\text{]}$ as supporting electrolyte, referenced to internal Fc/Fc⁺; scan rate 200 mV s⁻¹).

4.7.4. Ru(II) complexes

$[\text{Ru}(\mathbf{33})_2]\text{[PF}_6\text{]}_2$

Ligand **33** (0.30 g, 0.97 mmol) and $\text{RuCl}_3 \cdot 3\text{H}_2\text{O}$ (0.24 g, 0.92 mmol) were suspended in ethane-1,2-diol (15 cm³) and the mixture was heated in a domestic microwave oven (800 W) for 4 min. Another equivalent of **33** (0.30 g, 0.97 mmol) and 3 drops of *N*-ethylmorpholine were added, and the solution was heated in the microwave oven (800 W) for 5 min. The deep red solution was poured into aqueous NH_4PF_6 (150 cm³). A red precipitate formed and was collected on Celite, washed with H_2O , EtOH and Et_2O , and redissolved in MeCN. The product was purified by chromatography (SiO₂, MeCN : H_2O :saturated aqueous KNO_3 7 : 2 : 2). Addition of aqueous NH_4PF_6 and removal of MeCN gave a red precipitate which was collected on Celite, washed with H_2O , EtOH and Et_2O and redissolved in MeCN. Removal of the solvent gave $[\text{Ru}(\mathbf{33})_2]\text{[PF}_6\text{]}_2$ as a red solid (0.34 g, 0.34 mmol, 37%). ¹H NMR (CD_3CN , 500 MHz) δ/ppm 9.41 (s, 4H, $\text{H}^{\text{B}3}$), 8.96 (d, J 4.0 Hz, 2H, $\text{H}^{\text{C}6}$), 8.68 (d, J 8.0 Hz, 4H, $\text{H}^{\text{A}3}$), 8.49 (d, J 8.0 Hz, 2H, $\text{H}^{\text{C}3}$), 8.17 (dt, J 7.8, 1.7 Hz, 2H, $\text{H}^{\text{C}4}$), 7.96 (dt, J 8.0, 1.4 Hz, 4H, $\text{H}^{\text{A}4}$), 7.64 (dd, J 6.9, 4.8

Hz, 2H, H^{C5}), 7.44 (d, *J* 5.1 Hz, 4H, H^{A6}), 7.18 (ddd, *J* 7.2, 5.7, 1.1 Hz, 4H, H^{A5}). ¹³C{¹H} NMR (CD₃CN, 125 MHz) δ/ppm 159.1 (C^{A2}), 156.6 (C^{B2}), 153.7 (C^{C2}), 153.5 (C^{A6}), 151.6 (C^{C6}), 147.6 (C^{B4}), 139.2 (C^{C4}), 139.0 (C^{A4}), 128.5 (C^{A5}), 126.2 (C^{C5}), 125.6 (C^{A3}), 122.9 (C^{C3}), 122.0 (C^{B3}). ES-MS: *m/z* 867 [M – PF₆]⁺, 361 [M – 2PF₆]²⁺; UV/VIS λ_{max}/nm (8.90 × 10⁻⁶ mol dm⁻³, MeCN) 492 (ε/dm³ mol⁻¹ cm⁻¹ 27 200), 316 (56 000), 286 (58 700), 277 (57 800). Found: C, 46.28; H, 2.88; N, 10.95.
C₄₀H₂₈F₁₂N₈P₂Ru·1.5H₂O requires C, 46.25; H, 3.01; N, 10.79.

[Ru(34)₂](PF₆)₂

[Ru(34)₂](PF₆)₂ was prepared as previously described. Mass spectrometric data were consistent with those published; in the ¹H NMR spectrum, a NOESY cross peak between the signal for H^{B3} and H^{C4} allowed assignments of H^{C4} at *d* 8.53 ppm and H^{C6} at *d* 8.86 ppm, reassigned from our previous publication; ¹³C NMR signals for C^{C4} (δ 135.2 ppm) and C^{C5} (δ 124.3 ppm) are also reassigned.²⁷⁴ UV/VIS λ_{max}/nm (8.90 × 10⁻⁶ mol dm⁻³, MeCN) 489 (ε/dm³ mol⁻¹ cm⁻¹ 30 800), 313 (70 700), 278 (78 800).

[Ru(9)₂](PF₆)₂

Prepared using modification of literature procedure.¹⁷ Ligand **9** (0.30 g, 0.97 mmol) and RuCl₃·3H₂O (0.24 g, 0.92 mmol) were suspended in ethane-1,2-diol (30 cm³) and the mixture was heated in a domestic microwave oven (800 W) for 4 min. Another equivalent of **9** (0.30 g, 0.97 mmol) and 3 drops of *N*-ethylmorpholine were added, and the solution was heated in the microwave oven (800 W) for 5 min. The deep red solution was poured into aqueous NH₄PF₆ (150 cm³). A red precipitate formed and was collected on Celite, washed with H₂O, EtOH and Et₂O, and redissolved in MeCN. The product was purified by chromatography (SiO₂, MeCN : H₂O :saturated aqueous KNO₃ 7 : 2 : 2). Addition of aqueous NH₄PF₆ and removal of MeCN gave a red precipitate which was collected on Celite, washed with H₂O, EtOH and Et₂O and redissolved in MeCN. Removal of the solvent gave [Ru(9)₂](PF₆)₂ as a red solid (0.34 g, 0.34 mmol, 37%). The ¹H NMR spectrum in agreement with that previously reported.¹⁷ ¹H NMR (CD₃CN with NEt₃ added to ensure deprotonated): δ/ppm 9.06 (s, 2H, H^{B3}), 8.97 (d, *J* 5.9 Hz, 2H H^{C2}), 8.66, d, *J* 8.1 Hz, 2H, H^{A3}), 8.13 (d, *J* 5.9 Hz, 2H, H^{C3}), 7.87 (t, *J* 7.9 Hz, 2H, H^{A4}), 7.42 (d, *J* 5.4 Hz, 2H, H^{A6}), 7.20 (t, *J* 6.6 Hz, 2H, H^{A5}). ¹³C{¹H}: 158.9

(C^{A2}), 156.7 (C^{B2}), 153.5 (C^{C2}), 151.1 (C^{A6}), 146.5 (C^{C4}), 145.0 (C^{B4}), 139.2 (C^{A4}), 128.6 (C^{A5}), 125.7 (C^{A3}), 122.9 (C^{B3}), 122.8 (C^{C3}).

[Ru(9)₂][PF₆]₂[NO₃]

A warm solution of [Ru(9)₂][PF₆]₂ (2.0 mg, 2.0 µmol) in a mixture of acetone and water (2:1, 3 cm³) was added to a hot solution of [Co(NO₃)₂] · 6H₂O (4.0 mg, 14 µmol) in acetone water (2:1, 3 cm³). The mixture was left to slowly evaporate at room temperature, and X-ray quality crystals of [Ru(9)₂][PF₆]₂[NO₃] grew within 2 days. IR (KBr disc, cm⁻¹) 3047 w, 1598 m, 1384 vs, 1246 w, 1161 w, 1029 w, 845 vs, 789 s, 757 m, 557 s, 410 m. Inadequate sample was isolated for elemental analysis.

[Ru(4)₂][PF₆]₄ and [Ru(33)(35)][PF₆]₃

Iodomethane (5.0 cm³, 80 mmol) was added to a solution of [Ru(33)₂][PF₆]₂ (0.20 g, 0.20 mmol) in MeCN (20 cm³). NH₄PF₆ (0.1 g, 0.6 mmol) was added to prevent the precipitation of the iodide salt. The mixture was heated at reflux and was monitored by thin layer chromatography (SiO₂, MeCN : H₂O : saturated aqueous KNO₃ 7 : 2 : 2). This showed the formation of a yellow product with high *Rf* value (assumed to be an organic derivative, but remaining unidentified) in addition to the desired red products. A further 5 cm³ of MeI was added after 24 h, and the solution was heated to reflux for a further 24 h until chromatography indicated that the formation of the yellow product was becoming increasingly dominant. Solvent was removed from the reaction mixture, and the residue was dissolved in a minimum amount of MeCN and purified by chromatography (SiO₂, MeCN : H₂O : saturated aqueous KNO₃ 7 : 2 : 2). Three, well-separated red bands were collected. The first was [Ru(33)₂][PF₆]₂. The second (major) fraction was [Ru(33)(35)][PF₆]₃; the final fraction was [Ru(4)₂][PF₆]₄. Each was collected and excess aqueous NH₄PF₆ added. Removal of MeCN under reduced pressure gave a red precipitate which was collected on Celite, washed well with H₂O, EtOH and Et₂O and then redissolved in MeCN. Removal of the solvent gave [Ru(1)(35)][PF₆]₃ (81 mg, 0.069 mmol, 35%) and [Ru(35)₂][PF₆]₄ (22 mg, 0.017 mmol, 8.5%) as red powders. [Ru(1)(35)][PF₆]₃: ¹H NMR (CD₃CN, 500 MHz) δ/ppm 9.43 (s, 2H, H^{33B3}), 9.01 (d, *J* 6.2 Hz, 1H, H^{33/35C6}), 8.97 (d, *J* 4.2 Hz, 1H, H^{33/35C6}), 8.84 (s, 2H, H^{35B3}), 8.83 (t, *J* 7.9 Hz, 2H, H^{35C4}), 8.70 (d, *J* 8.0 Hz, 2H, H^{33A3}), 8.50 (d, *J* 8.3 Hz, 1H, H^{33C3}), 8.48 (d, *J* 8.2 Hz, 2H, H^{35A3}), 8.37 (d, *J* 7.3 Hz, 2H, H^{35C3}), 8.29 (ddd, *J* 1.2, 7.5,

6.5 Hz, 2H, H^{35C5}), 8.18 (td, *J* 7.8, 1.7 Hz, 1H, H^{33C4}), 7.66 (dd, *J* 4.9, 7.2 Hz, 1H, H^{33C5}), 7.51 (d, *J* 5.4 Hz, 2H, H^{35A6}), 7.46 (d, *J* 5.4 Hz, 2H, H^{33A6}), 7.24 (ddd, *J* 1.0, 7.1, 6.2 Hz, 2H, H^{35A5}), 7.22 (ddd, *J* 1.0, 7.1, 6.1 Hz, 2H, H^{33A5}), 4.51 (s, 3H, Me). ¹³C{¹H} NMR (CD₃CN, 125 MHz) δ/ppm 159.1 (C^{33A2}), 158.1, (C^{35A2}), 157.0 (C^{33,4B2}), 153.8 (C^{33,35A6}), 153.7 (C^{33C2}), 152.8 (C^{35C2}), 152.0 (C^{33C6}), 148.5 (C^{35C6}), 148.3 (C^{33B4}), 147.8 (C^{4C4}), 139.4 (C^{33C4}), 139.3 (C^{4A4}), 139.1 (C^{33A4}), 138.0 (C^{4B4}), 131.6 (C^{4C3}), 129.6 (C^{35C5}), 129.0 (C^{35A5}), 128.6 (C^{33A5}), 126.6 (C^{33C5}), 125.8 (C^{33A3}), 125.0 (C^{35A3}), 124.5 (C^{35B3}), 123.0 (C^{33C3}), 122.1 (C^{33B3}), 48.9 (C^{Me}). ES-MS: *m/z* 1027 [M–PF₆]⁺. UV-vis λ_{max}/nm (1.22 × 10⁻⁵ mol dm⁻³, MeCN) 490 (ε/dm³ mol⁻¹ cm⁻¹ 23 000), 328 (38 500), 313 (52 500), 278 (57 500). Found: C, 40.15; H, 2.89; N, 9.16.

C₄₁H₃₁F₁₈N₈P₃Ru·2.5H₂O requires C, 40.47; H, 2.98; N, 9.21. *E*^o/V vs. Fc/Fc+: +1.02 (reversible), –1.32 (irreversible), –1.93 (irreversible).

[Ru(35)₂][PF₆]₄

¹H NMR (CD₃CN, 500 MHz): δ/ppm 9.03 (d, *J* 6.1 Hz, 2H, H^{C6}), 8.95 (s, 4H, H^{B3}), 8.83 (t, *J* 7.6 Hz, 2H, H^{C4}), 8.54 (d, *J* 8.1 Hz, 4H, H^{A3}), 8.42 (d, *J* 7.2 Hz, 2H, H^{C3}), 8.29 (t, *J* 7.0 Hz, 2H, H^{C5}), 8.00 (t, *J* 7.3 Hz, 4H, H^{A4}), 7.57 (d, *J* 5.3 Hz, 4H, H^{A6}), 7.28 (t, *J* 6.6 Hz, 4H, H^{A5}), 4.55 (s, 6H, Me). ¹³C{¹H} NMR (CD₃CN, 125 MHz) δ/ppm 158.1 (C^{A2}), 156.7 (C^{B2}), 154.0 (C^{A6}), 152.9 (C^{C2}), 148.4 (C^{C6}), 147.5 (C^{C4}), 139.6 (C^{A4}), 138.9 (C^{B4}), 131.6 (C^{C3}), 129.7 (C^{C5}), 129.1 (C^{A5}), 126.1 (C^{A3}), 124.6 (C^{B3}), 49.3 (C^{Me}). ES-MS: *m/z* 1187 [M – PF₆]⁺. UV/VIS λ_{max}/nm (3.49 × 10⁻⁵ mol dm⁻³, MeCN) 487 (ε/dm³ mol⁻¹ cm⁻¹ 22 900), 331 (18 300), 311 (24 400), 277 (31 400). Found: C 37.13, H 3.00, N 9.09; C₄₂H₃₄F₂₄N₈P₄Ru·2H₂O·0.75CH₃CN requires C 37.30, H 3.04, N 8.75%.

[Ru(34)(36)][PF₆]₃

Iodomethane (0.50 cm³, 8.0 mmol) was added to a solution of [Ru(34)₂](PF₆)₂ (0.22 g, 0.22 mmol) in MeCN (15 cm³). NH₄PF₆ (0.05 g, 0.3 mmol) was then added to prevent the precipitation of the iodide salt. The mixture was heated to 50 °C and monitored by thin layer chromatography (SiO₂, MeCN:H₂O: saturated aqueous KNO₃ 7 : 2 : 2). After 15 min, the mono-methylated species was the major product. Solvent was removed and the residue dissolved in a minimum amount of MeCN and purified by chromatography (SiO₂, MeCN : H₂O: saturated aqueous KNO₃ 7 : 2 : 2). The central portion of the major

(middle) red band was collected and excess aqueous NH_4PF_6 added. Removal of the MeCN under reduced pressure gave a red precipitate which was collected on Celite and washed well with H_2O , EtOH and Et_2O . The solid was redissolved in MeCN, and removal of the solvent gave $[\text{Ru(2)(5)}][\text{PF}_6]_3$ as a red powder (0.020 g, 0.017 mmol, 7.7%). ^1H NMR (CD_3CN , 500 MHz) δ/ppm 9.49 (s, 1H, $\text{H}^{36\text{C}2}$), 9.41 (d, J 2.0 Hz, 1H, $\text{H}^{34\text{C}2}$), 9.22 (d, J 8.2 Hz, 1H, $\text{H}^{36\text{C}4}$), 9.08 (s, 2H, $\text{H}^{36\text{B}3}$), 9.06 (s, 2H, $\text{H}^{34\text{B}3}$), 8.89 (d, J 6.1 Hz, 1H, $\text{H}^{36\text{C}6}$), 8.87 (dd, J 4.7, 1.3 Hz, 1H, $\text{H}^{34\text{C}6}$), 8.66 (d, J 8.1 Hz, 4H, $\text{H}^{34, 36\text{A}3}$), 8.56 (ddd, J 7.9, 1.6, 2.2 Hz, 1H, $\text{H}^{34\text{C}4}$), 8.37 (dd, J 7.9, 6.3 Hz, 1H, $\text{H}^{36\text{C}5}$), 8.00 (td, J 7.7, 1.4 Hz, 2H, $\text{H}^{36\text{A}4}$), 7.97 (td, J 8.0, 1.4 Hz, 2H, $\text{H}^{34\text{A}4}$), 7.75 (dd, J 7.8, 5.0 Hz, 1H, $\text{H}^{34\text{C}5}$), 7.49 (d, J 5.5 Hz, 2H, $\text{H}^{36\text{A}6}$), 7.42 (d, J 5.4 Hz, 2H, $\text{H}^{34\text{A}6}$), 7.24 (ddd, J 7.1, 6.3, 1.0 Hz, 2H, $\text{H}^{36\text{A}5}$), 7.20 (ddd, J 7.2, 6.3, 1.0 Hz, 2H, $\text{H}^{34\text{A}5}$), 4.58 (s, 3H, H^{Me}). $^{13}\text{C}\{^1\text{H}\}$ NMR (CD_3CN , 125 MHz) δ/ppm 158.8 ($\text{C}^{34\text{A}2}$), 158.6 ($\text{C}5\text{A}2$), 157.2 ($\text{C}^{34\text{B}2}$), 156.4 ($\text{C}^{36\text{B}2}$), 153.6 ($\text{C}^{34, 36\text{A}6}$), 152.1 ($\text{C}^{34\text{C}6}$), 149.7 ($\text{C}^{34\text{C}2}$), 146.8 ($\text{C}^{36\text{C}6}$), 146.7 ($\text{C}^{34\text{B}4}$), 145.6 ($\text{C}^{36\text{C}2}$), 144.8 ($\text{C}^{36\text{C}4}$), 141.1 ($\text{C}^{36\text{B}4}$), 139.3 ($\text{C}^{34, 36\text{A}4}$), 138.4 ($\text{C}^{36\text{C}3}$), 136.3 ($\text{C}^{34\text{C}4}$), 133.7 ($\text{C}^{34\text{C}3}$), 129.7 ($\text{C}^{36\text{C}5}$), 128.8 ($\text{C}^{36\text{A}5}$), 128.6 ($\text{C}^{34\text{A}5}$), 125.7 ($\text{C}^{34, 36\text{A}3}$), 125.3 ($\text{C}^{34\text{C}5}$), 122.9 ($\text{C}^{34, 36\text{B}3}$), 49.9 (C^{Me}). UV/VIS $\lambda_{\text{max}}/\text{nm}$ (4.01×10^{-5} mol dm^{-3} , MeCN) 491 ($\varepsilon/\text{dm}^3 \text{ mol}^{-1} \text{ cm}^{-1}$ 27 000), 314 (60 200), 278 (64 400). Found: C, 39.75; H, 3.01; N, 9.05. $\text{C}_{41}\text{H}_{31}\text{F}_{18}\text{N}_8\text{P}_3\text{Ru}\cdot 4\text{H}_2\text{O}$ requires C, 39.59; H, 3.16; N, 9.01. ESMS: m/z 1027 [$\text{M} - \text{PF}_6$]⁻.

[Ru(36)₂][PF₆]₄

Iodomethane (1.0 cm³, 16 mmol) was added to a solution of $[\text{Ru(34)}_2](\text{PF}_6)_2$ (0.10 g, 0.10 mmol) in MeCN (10 cm³). NH_4PF_6 (0.05 g, 0.3 mmol) was added to prevent the precipitation of the iodide salt. The mixture was heated at reflux and monitored by thin layer chromatography (SiO_2 , MeCN : H_2O : saturated aqueous KNO_3 7 : 2 : 2). After 6 h, no further reaction was observed (the reaction does not go to completion, even on addition of more MeI). Solvent was removed and the residue dissolved in a minimum amount of MeCN and purified by chromatography (SiO_2 , MeCN : H_2O : saturated aqueous KNO_3 7 : 2 : 2). The main (lowest R_f) red band was collected and excess aqueous NH_4PF_6 added. Removal of MeCN gave a red precipitate which was collected on Celite, washed with H_2O , EtOH and Et_2O , and redissolved in MeCN. Removal of the solvent gave $[\text{Ru(36)}_2][\text{PF}_6]_4$ as a red powder (0.068 g, 0.051 mmol, 52%). ^1H NMR (CD_3CN , 500 MHz) δ/ppm 9.40 (s, 2H, $\text{H}^{\text{C}2}$), 9.20 (d, J 8.2 Hz, 2H, $\text{H}^{\text{C}4}$), 9.04 (s, 4H,

$\text{H}^{\text{B}3}$), 8.89 (d, J 6.1 Hz, 2H, $\text{H}^{\text{C}6}$), 8.63 (d, J 8.1 Hz, 4H, $\text{H}^{\text{A}3}$), 8.38 (dd, J 8.0, 6.3 Hz, 2H, $\text{H}^{\text{C}5}$), 8.02 (td, J 8.0, 1.3 Hz, 4H, $\text{H}^{\text{A}4}$), 7.45 (d, J 5.2 Hz, 4H, $\text{H}^{\text{A}6}$), 7.24 (ddd, J 7.2, 5.6, 1.1 Hz, 4H, $\text{H}^{\text{A}5}$), 4.57 (s, 6H, Me). $^{13}\text{C}\{\text{H}\}$ NMR (CD_3CN , 125 MHz) δ /ppm 158.5 ($\text{C}^{\text{A}2}$), 157.0 ($\text{C}^{\text{B}2}$), 153.7 ($\text{C}^{\text{A}6}$), 146.9 ($\text{C}^{\text{C}6}$), 145.5 ($\text{C}^{\text{C}2}$), 144.9 ($\text{C}^{\text{C}4}$), 141.5 ($\text{C}^{\text{B}4}$), 139.5 ($\text{C}^{\text{A}4}$), 138.3 ($\text{C}^{\text{C}3}$), 129.8 ($\text{C}^{\text{C}5}$), 129.0 ($\text{C}^{\text{A}5}$), 125.8 ($\text{C}^{\text{A}3}$), 123.0 ($\text{C}^{\text{B}3}$), 50.0 (C^{Me}). ESI-MS: 299 [$\text{M} - 3\text{PF}_6$] $^{3+}$, 521 [$\text{M} - 2\text{PF}_6$] $^{2+}$, 1187 [$\text{M} - \text{PF}_6$] $^+$. UV/VIS λ_{max} /nm (8.90×10^{-6} mol dm $^{-3}$, MeCN) 494 ($\varepsilon/\text{dm}^3 \text{ mol}^{-1} \text{ cm}^{-1}$ 24 500), 315 (39 000), 277 (58 600), 238 (31 300). Found: C 37.34, H 2.69, N 8.45; $\text{C}_{42}\text{H}_{34}\text{F}_{24}\text{N}_8\text{P}_4\text{Ru} \cdot 1.5\text{H}_2\text{O}$ requires C 37.13, H 2.74, N 8.25%.

[Ru(9)(37)][PF₆]₃

Iodomethane (0.25 cm 3 , 4.0 mmol) was added to a solution of [Ru(9)₂][PF₆]₂ (0.10 g, 0.099 mmol) in MeCN (25 cm 3). NH₄PF₆ (0.1 g, 0.6 mmol in 5 mL H₂O) was added to prevent precipitation of the iodide salt of [Ru(9)₂] $^{2+}$. The mixture was heated at reflux and monitored by thin layer chromatography (SiO₂, MeCN:H₂O: saturated aqueous KNO₃ 7 : 2 : 2). After 20 min, [Ru(9)(6)][PF₆]₃ was the major species present. Solvent was removed and the residue dissolved in a minimum amount of MeCN and purified by column chromatography (SiO₂, MeCN : H₂O : saturated aqueous KNO₃ 7 : 2 : 2). The main (middle) red band was collected and excess aqueous NH₄PF₆ was added. Removal of MeCN gave a red precipitate which was collected on Celite, washed with H₂O, EtOH and Et₂O, and redissolved in MeCN. Removal of solvent gave [Ru(9)(37)₂][PF₆]₃ as a red powder (0.047 g, 0.040 mmol, 41%). The lowest R_f fraction from the chromatography column was also collected and yielded [Ru(6)₂][PF₆]₄ as a red powder (0.020 g, 0.015 mmol, 15%, see below). ^1H NMR and UV/VIS spectroscopic and electrochemical data were consistent with the literature data. $^{17}\text{C}\{\text{H}\}$ NMR (125 MHz, CD₃CN) δ /ppm 158.7 ($\text{C}^{\text{37A}2}$), 158.5 ($\text{C}^{\text{9A}2}$), 157.3 ($\text{C}^{\text{37B}2}$), 156.4 ($\text{C}^{\text{9B}2}$), 153.6 ($\text{C}^{\text{9,37A}6}$), 153.6 ($\text{C}^{\text{37C}4}$), 152.1 ($\text{C}^{\text{9C}2}$), 147.4 ($\text{C}^{\text{9C}4}$), 147.3 ($\text{C}^{\text{37C}2}$), 144.9 ($\text{C}^{\text{9B}4}$), 141.4 ($\text{C}^{\text{37B}4}$), 139.4 ($\text{C}^{\text{9,37A}4}$), 129.0 ($\text{C}^{\text{37A}5}$), 128.7 ($\text{C}^{\text{9A}5}$), 127.0 ($\text{C}^{\text{37C}3}$), 125.9 ($\text{C}^{\text{9,37A}3}$), 123.1 ($\text{C}^{\text{9C}3}$), 123.0 ($\text{C}^{\text{37B}3}$), 122.9 ($\text{C}^{\text{9B}3}$), 49.2 (C^{Me}). Found C 40.82, H 3.00, N 10.11; $\text{C}_{41}\text{H}_{31}\text{F}_{18}\text{N}_8\text{P}_3\text{Ru} \cdot 2.5\text{H}_2\text{O} \cdot 0.75\text{CH}_3\text{CN}$ requires C 40.92, H 3.09, N 9.82%.

[Ru(37)₂][PF₆]₄

$[\text{Ru(37)}_2][\text{PF}_6]_4$ has previously been prepared in 34% yield using $[\text{Me}_3\text{O}][\text{BF}_4]$ as methylating agent.¹⁷ Iodomethane (0.25 cm^3 , 4.0 mmol) was added to a solution of $[\text{Ru(9)}_2](\text{PF}_6)_2$ (0.048 g, 0.047 mmol) in MeCN (5 cm^3). The mixture was heated at reflux and monitored by thin layer chromatography (SiO_2 , MeCN: H_2O : saturated aqueous KNO_3 7 : 2 : 2). After 8 h, a red precipitate had formed (assumed to be the iodide salt) and NH_4PF_6 (0.02 g, 0.1 mmol) was added to give a soluble hexafluorophosphate salt. After 10 h, no further reaction was observed; the reaction does not go to completion, even on adding more MeI. Solvent was removed and the residue was dissolved in a minimum amount of MeCN and purified by column chromatography (SiO_2 , MeCN : H_2O : saturated aqueous KNO_3 7:2:2). The main (lowest R_f) red band was collected and excess aqueous NH_4PF_6 was added. Removal of MeCN gave a red precipitate which was collected on Celite, washed with H_2O , EtOH and Et_2O , and redissolved in MeCN. Removal of solvent gave $[\text{Ru(37)}_2][\text{PF}_6]_4$ as a red powder (0.025 g, 0.019 mmol, 40%). ^1H NMR and UV/VIS spectroscopic and electrochemical data matched the literature data¹⁷ $^{13}\text{C}\{\text{H}\}$ NMR (CD_3CN , 125 MHz) δ/ppm 158.4 ($\text{C}^{\text{A}2}$), 157.0 ($\text{C}^{\text{B}2}$), 153.7 ($\text{C}^{\text{A}6}$), 153.3 ($\text{C}^{\text{C}4}$), 147.3 ($\text{C}^{\text{C}2}$), 142.0 ($\text{C}^{\text{B}4}$), 139.6 ($\text{C}^{\text{A}4}$), 129.0 ($\text{C}^{\text{A}5}$), 127.1 ($\text{C}^{\text{C}3}$), 126.0 ($\text{C}^{\text{A}3}$), 123.3 ($\text{C}^{\text{B}3}$), 49.3 (C^{Me}). ES-MS: m/z 1187 [$\text{M} - \text{PF}_6$] $-$. Found: C 36.67, H 2.80, N 8.61; $\text{C}_{42}\text{H}_{34}\text{F}_{24}\text{N}_8\text{P}_4\text{Ru}\cdot 3\text{H}_2\text{O}\cdot 0.5\text{CH}_3\text{CN}$ requires C 36.73, H 2.97, N 8.47%.

[Ru(39)₂][PF₆]₂

$\text{RuCl}_3\cdot 3\text{H}_2\text{O}$ (0.047 g, 0.18 mmol) and **39** (0.058 g, 0.19 mmol) were added to ethane-1,2-diol (10 cm^3) and the solution was heated for 2 min in a microwave oven (800 W). A second equivalent of **39** (0.058 g, 0.19 mmol) and 2 drops of N-ethylmorpholine were added and the reaction mixture was heated in the microwave oven for a further 3 min. The resulting dark red solution was poured into water (200 cm^3) containing an excess of NH_4PF_6 to give a red precipitate which was collected on Celite and washed well with water, EtOH and Et_2O . The solid was redissolved in MeCN and purified by column chromatography (SiO_2 , MeCN : H_2O : saturated aqueous KNO_3 7 : 2 : 2). The centre of the main red band was collected, excess aqueous NH_4PF_6 was added to the fractions, and the volume reduced under reduced pressure to give a red precipitate which was collected on Celite and washed well with H_2O , EtOH and Et_2O . The solid was redissolved in MeCN and the solvent removed to give $[\text{Ru(39)}_2][\text{PF}_6]_2$ as a red powder

(0.13 g, 0.13 mmol, 71%). ^1H NMR (500 MHz, CD_3CN) δ /ppm 9.55 (s, 4 H, H^{C^4}), 9.43 (s, 2 H, H^{C^2}), 9.07 (s, 4 H, H^{B^3}), 8.64 (d, J 8.0 Hz, 4H, H^{A^3}), 7.98 (td, J 8.0, 1.3 Hz, H^{A^4}), 7.44 (d, J 5.1 Hz, 4 H, H^{A^6}), 7.21 (ddd, J 7.1, 5.7, 1.1 Hz, 4 H, H^{A^5}). $^{13}\text{C}\{\text{H}\}$ (125 MHz, CD_3CN) δ /ppm 160.4 (C^{C^2}), 158.8 (C^{A^2}), 156.8 ($\text{C}^{\text{C}^2 + \text{B}^2}$), 153.6 (C^{A^6}), 143.2 (C^{B^4}), 139.3 (C^{A^4}), 131.8 (C^{C^4}), 128.7 (C^{A^5}), 125.7 (C^{A^3}), 122.7 (C^{B^3}). ESI-MS m/z 362 [$\text{M} - 2\text{PF}_6$] $^{2+}$. E° vs. $\text{Fc}^+/\text{Fc}/\text{V}$: +0.91 (rev), -1.56 (rev), -1.81 (rev), -2.22 (quasi-rev), -2.53 (rev). UV-vis 8.9×10^{-5} in MeCN, $\lambda_{\text{max}}/\text{nm}$ ($\epsilon_{\text{max}}/10^3 \text{ dm}^3 \text{ mol}^{-1} \text{ cm}^{-1}$) 487 (21.2), 311 (47.4), 274 (58.4). Found: C 46.47; H 2.91; N 15.18; $\text{C}_{38}\text{H}_{26}\text{F}_{12}\text{N}_{10}\text{P}_2\text{Ru}$.2.25 MeCN requires C 46.15; H 2.98; N 15.51 %.

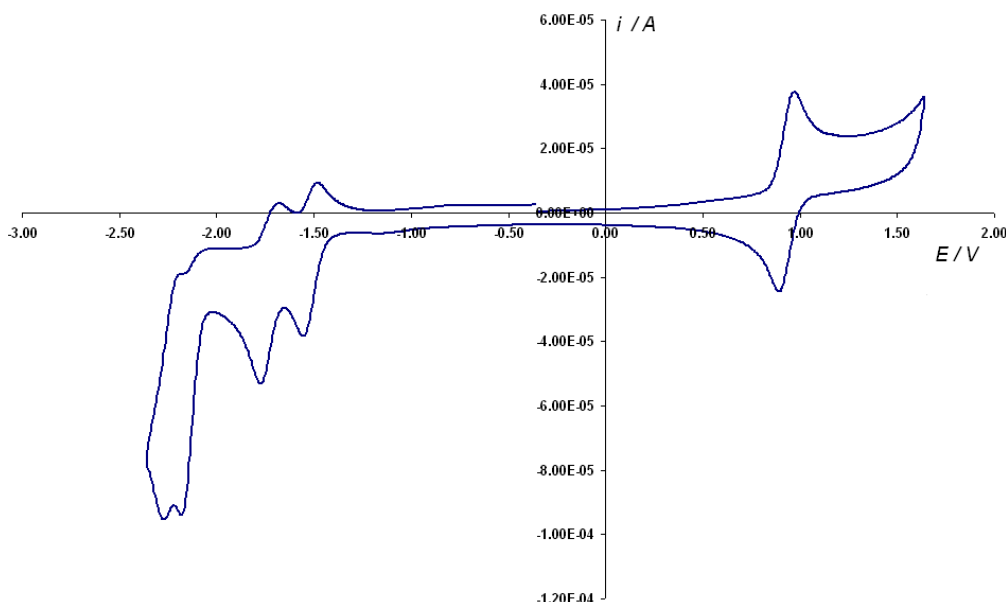
[Ru(40)₂][PF₆]₂

[Ru(4'-(3,5-dibromophenyl)-2,2',6',2"-terpyridine))₂][PF₆]₂ (0.078g, 0.59 mmol) and 4-pyridylboronic acid pinacol ester³²⁶ (0.34g, 1.6 mmol) were dissolved in degassed DMF (15mL) and Pd(PPh₃)₄ (0.10g, 0.09 mmol, 40%) and K₂CO₃ (0.33g, 2.4 mmol) were added. The mixture was heated at 110 °C for 4 hours and cooled to room temperature. The deep red solution was poured into a solution of excess NH₄PF₆ (80mL, deareated water). The resulting red precipitate was collected on Celite and washed with water and EtOH. The residue was dissolved in MeCN and the solvent reduced to ~ 5mL and purified by column chromatography (SiO₂, MeCN : H₂O: saturated KNO_{3(aq)} 7:7:2). The lowest R_f red fraction was collected, and excess NH₄PF_{6(aq)} was added. The volume was reduced until the product began to precipitate and was collected on Celite and washed well with water and redissolved in MeCN. Removal of the solvent gave [Ru(40)₂][PF₆]₂ as a red powder (0.012g, 0.0091 mmol, 15%). ^1H NMR (CD_3CN , 295K) δ /ppm: 9.19 (s, 2H, H^{B^3}), 8.84 (d, 5.8 Hz, 4H, H^{D^2}), 8.73 (d, 7.8 Hz, 2H, H^{A^3}), 8.65 (d, 1.6 Hz, 2H, H^{C^3}), 8.39 (t, 1.6 Hz, 1H, H^{C^4}), 8.08 (d, 6.3 Hz, 4H, H^{C^3}), 7.99 (td, 7.9, 1.5 Hz, 2H, H^{A^4}), 7.47 (d, 5.6 Hz, 2H, H^{A^6}), 7.23 (ddd, 7.4, 5.6, 1.3 Hz, 2H, H^{A^5}). ES-MS m/z 1173.23 [M-PF_6] $^+$, 514.6 [M-2PF_6] $^{2+}$.

[Ru(41)₂][PF₆]₂

RuCl₃·3H₂O (9.0 mg, 0.035 mmol), and [H₂**41**][EtOSO₃]₂ (20 mg, 0.035 mmol) were suspended in ethane-1,2-diol (2 mL) and the reaction mixture was heated in a microwave oven (800 W, 2 min). A second equivalent of [H₂**41**][EtOSO₃]₂ (20 mg, 0.035 mmol) was added with one drop of N-ethylmorpholine and the solution was again

heated in the microwave oven (800 W, 2 min) to give a deep red solution which was cooled to room temperature. It was then poured into water (50 mL) containing an excess of NH_4PF_6 to precipitate the hexafluoridophosphate salt of the product. The resulting red-orange precipitate was collected on Celite and washed well with H_2O , EtOH and Et_2O . The solid was dissolved in MeCN and the solvent removed to give the crude product (35 mg, 0.033 mmol, 96%, approximately 95% pure by ^1H NMR spectroscopy). This was purified by column chromatography (SiO_2 , MeCN: H_2O :saturated aqueous KNO_3 7:2:2). The central portion of the main red fraction was collected, excess NH_4PF_6 was added and the volume reduced leading to the precipitation of the pure product as a dark red microcrystalline solid (26 mg, 0.025 mmol, 72%). ^1H NMR (500 MHz, CD_3CN) δ/ppm 8.86 (s, 4H, $\text{H}^{\text{B}3}$), 8.55 (dt, J 8.0, 1.0 Hz, 4H, $\text{H}^{\text{A}3}$), 7.94 (td, J 8.0, 1.3 Hz, 4H, $\text{H}^{\text{A}4}$), 7.49 (dt, J 5.6, 1.0 Hz, 4H, $\text{H}^{\text{A}6}$), 7.20 (ddd, J 7.0, 5.6, 1.3 Hz, 4H, $\text{H}^{\text{A}5}$), 6.37 (s, 2H, $\text{H}^{\text{C}4}$), 2.81 (s, 6H, $\text{Me}^{\text{C}5}$), 2.42 (s, 6H, $\text{Me}^{\text{C}3}$). $^{13}\text{C}\{^1\text{H}\}$ NMR (125 MHz, CD_3CN) δ/ppm 158.8 ($\text{C}^{\text{A}2}$), 156.7 ($\text{C}^{\text{B}2}$), 153.7 ($\text{C}^{\text{A}6}$), 153.0 ($\text{C}^{\text{C}3}$), 147.6 ($\text{C}^{\text{B}4}$), 142.5 ($\text{C}^{\text{C}5}$), 139.1 ($\text{C}^{\text{A}4}$), 128.7 ($\text{C}^{\text{A}5}$), 125.7 ($\text{C}^{\text{A}3}$), 117.7 ($\text{C}^{\text{B}3}$), 111.4 ($\text{C}^{\text{C}4}$), 13.8 ($\text{C}^{\text{Me}(\text{C}3)}$), 13.5 ($\text{C}^{\text{Me}(\text{C}5)}$). ES-MS m/z 901 [M-PF_6] $^+$, 378 [M-2PF_6] $^{2+}$. UV-Vis (MeCN, 1.51×10^{-5} mol dm $^{-3}$) λ/nm 489 ($\epsilon/\text{dm}^3\text{mol}^{-1}\text{cm}^{-1}$) (23200), 307 (65100), 284 (59400), 241 (28000). Anal. Calc. for $\text{C}_{40}\text{H}_{34}\text{F}_{12}\text{N}_{10}\text{P}_2\text{Ru}$ requires: C, 45.94; H, 3.28; N, 13.39. Found: C, 45.80; H, 3.26; N, 13.40%. E°/V versus Fc/Fc^+ : +0.93, -1.52 and -1.73 V (all reversible).



Cyclic voltammogram of $[\text{Ru}(\mathbf{41})_2][\text{PF}_6]_2$ (MeCN, $[\text{Bu}_4\text{N}][\text{PF}_6]$ as supporting electrolyte, referenced to internal Fc/Fc^+ ; scan rate 200 mV s⁻¹).

4.7.5. Cu(II) complexes

[Cu(**9**)Cl₂]

$\text{CuCl}_2 \cdot 2\text{H}_2\text{O}$ (0.22g, 1.3 mmol) in MeOH (10mL) was added to a solution of **9** (0.40g, 1.3 mmol) in EtOH (100mL). The mixture was heated to reflux for 18 hours and cooled to room temperature. The resulting pale green precipitate was collected, washed with EtOH (20mL) and ether (20mL). [Cu(**9**)Cl₂] (0.41g, 1.0 mmol, 78%). ESI, UV-Vis Found: C 50.11, H 3.55, N 11.73% $\text{C}_{20}\text{H}_{14}\text{N}_4\text{CuCl}_2 \cdot 2\text{H}_2\text{O}$ requires: C 49.96, H 3.77, N 11.65 %.

[Cu(H**9**)Cl₂]Cl

$\text{CuCl}_2 \cdot 2\text{H}_2\text{O}$ (0.082g, 0.49 mmol) in water (10mL) was added to **9** in MeOH (100mL) with an excess of $\text{HCl}_{(\text{aq})}$ (1.0M, 4mL). The solution was refluxed for 16 hours and cooled to room temperature. The resulting green precipitate was collected and washed with EtOH (10mL) and recrystallised from MeOH-H₂O to give pale green plates of [Cu(H**9**)Cl₂]Cl^xH₂O (0.091g, 0.17 mmol, 35%). An additional 110 mg (0.21 mmol, 42%) was recovered from the filtrate. Found: C 47.40, H 3.30, N 11.01 %. $\text{C}_{20}\text{H}_{15}\text{Cl}_3\text{CuN}_4 \cdot 1.5\text{H}_2\text{O}$ requires C 47.26, H 3.57, N 11.02 %.

4.7.6. Pd(II) complexes

[Pd(**9**)Cl]Cl: PdCl_2 (0.060 g, 0.35 mmol) was added to **9** (0.11 g, 0.35 mmol) in DMF (40 cm³) at 100 °C and the mixture was stirred for 12 h. The off-white powder that precipitated was collected by filtration and was washed with H₂O, EtOH and Et₂O.

[Pd(**9**)Cl]Cl was isolated as a off-white solid (0.062 g, 0.13 mmol, 37%). [Pd(**9**)Cl]Cl: ES-MS: 451 *m/z*, $[\text{Pd}(\mathbf{9})\text{Cl}]^+$. ¹H NMR (500 MHz, DMSO-*d*₆) δ/ppm 9.13 (s, 2H, H^{B3}), 8.94 (d, *J* 6.0 Hz, 2H, H^{C2}), 8.89 (d, *J* 7.87 Hz, 2H, H^{A3}), 8.79 (d, *J* 5.6 Hz, 2H, H^{A6}), 8.55 (td, *J* 7.9, 1.4 Hz, 2H, H^{A4}), 8.19 (d, *J* 6.0 Hz, 2H, H^{C3}), 7.94 (t, *J* 6.3 Hz, 2H, H^{A5}). ¹³C{¹H} NMR (125 MHz, DMSO-*d*₆) δ/ppm 121.8 (C^{C2}), 122.0 (C^{B3}), 125.7 (C^{A3}),

129.1 (C^{A5}), 141.8 (C^{B4,C4}), 142.6 (C^{A4}), 151.0 (C^{C3}), 152.2 (C^{A6}), 155.2 (C^{B2}), 157.9 (C^{A2}).

[Pd(**41**)Cl][PF₆]: method 1

[H₂**41**][MeOSO₃]₂ (0.035 g, 0.063 mmol) and PdCl₂ (0.012 g, 0.068 mmol) were dissolved in MeOH (10 mL) and the solution was heated at reflux for 18 h, during which time a cream precipitate formed. The reaction mixture was cooled to room temperature, filtered and the solid product washed with EtOH, CHCl₃ and Et₂O. The solid was dissolved in hot water and excess solid NH₄PF₆ was added to precipitate the hexafluoridophosphate salt which was collected and recrystallised from MeCN/H₂O. [Pd(**41**)Cl][PF₆] was isolated as a pale yellow solid (0.017 g, 0.027 mmol, 40%). ¹H NMR (500 MHz, DMSO-*d*₆) δ/ppm 8.82 (d, *J* 7.8 Hz, 2H, H^{A3}), 8.79 (dd, *J* 5.6, 1.0 Hz, 2H, H^{A6}), 8.69 (s, 2H, H^{B3}), 8.48 (td, *J* 7.9, 1.3 Hz, 2H, H^{A4}), 7.93 (ddd, *J* 6.9, 5.6, 0.9 Hz, 2H, H^{A5}), 6.41 (s, 1H, H^{C4}), 2.66 (s, 3H, Me^{C5}), 2.30 (s, 3H, Me^{C3}). Low solubility prevented ¹³C NMR spectroscopic data from being recorded. ES MS *m/z* 469 [M-PF₆]⁺. Anal. Calc. for C₂₀H₁₇ClF₆N₅PPd · 0.5H₂O requires: C, 38.59; H, 2.92; N, 11.26. Found: C, 38.59; H, 3.11; N, 10.90%.

[Pd(**41**)Cl][PF₆]: method 2 (see text)

[Fe(**41**)₂][PF₆]₂ (0.070 g, 0.068 mmol), PdCl₂ (0.012 g, 0.068 mmol) and K₂CO₃ (0.10 g, 0.73 mmol) were dissolved in MeCN (30 mL). The solution was stirred overnight at room temperature and filtered to remove a small amount of pale yellow precipitate, assumed to be PdCl₂. Aqueous NH₄PF₆ was added and the resulting precipitate was collected and washed with H₂O, EtOH and Et₂O. The ¹H NMR spectrum of a CD₃CN solution of the precipitate indicated the presence of [Fe(**41**)₂][PF₆]₂ and [Pd(**41**)Cl][PF₆]. Slow evaporation of the CD₃CN solution gave X-ray quality crystals of [Pd(**41**)Cl][PF₆].

4.7.7. Ni(II) complex

[Ni(**9**)₂][NO₃]₂

An aqueous solution (5 cm³) of Ni(NO₃)₂·6H₂O (62 mg, 0.21 mmol) was added to a solution of ligand **9** (130 mg, 0.42 mmol) in MeOH (40 cm³). The mixture was heated at

reflux for 6 h and then cooled to room temperature. Cold EtOH was added to precipitate the product as a pale orange solid. This was separated by filtration and washed with cold EtOH followed by CHCl₃ and Et₂O. After recrystallisation from a 1:1 mixture of MeOH and CHCl₃, [Ni(**9**)₂][NO₃]₂ was isolated as orange, block-like crystals (0.13 g, 0.16 mmol, 76%). Anal. Calc. for C₄₀H₂₈N₁₀NiO₆·2MeOH·3H₂O: C, 54.74; H, 4.59; N, 15.20. Found: C, 54.46; H, 4.20; N, 15.41%. ES-MS: *m/z* 340 [M-2PF₆]²⁺. UV-vis (H₂O) λ_{max} /nm 244 ($\epsilon/\text{dm}^3 \text{mol}^{-1} \text{cm}^{-1}$ 49500), 279 (66200), 328 (22 500), 341 (20 600). An X-ray quality crystal of constitution [Ni(**9**)₂][NO₃]₂ ·2MeOH·2H₂O was chosen from the bulk sample.

4.7.8. Crystal structure determinations: general

Data for [Ru(**9**)₂][PF₆]₂ were collected on an Enraf Nonius Kappa CCD instrument; data reduction, solution and refinement used the programs COLLECT,²⁵² SIR92²⁵³ DENZO/SCALEPACK²⁵⁶ and CRYSTALS.²⁵⁷ Data for [Ru(**9**)₂][PF₆][NO₃] were collected on Bruker-Nonius APEX-X8-FR591 diffractometer, and data reduction used the programs SAINT and XPREP,⁷ the structure was solved by direct methods using SIR97,²⁵³ and were refined and extended using SHELX-97.^{7, 258} Data for [Fe(**9**)₂][ClO₄]₂·2MeOH·0.5H₂O, [Ni(**9**)₂][NO₃]₂·2MeOH·2H₂O were collected on a Bruker SMART 1000 CCD diffractometer; data reduction, solution (by Patterson map) and refinement used the programs SAINT⁷, SHELXS-97 and SHELXL-97.^{7, 258} Structures have been analysed using Mercury v. 1.4.2.²² Data for 4{[Fe(**1**)₂][PF₆]₂}·9H₂O, [Fe(**2**)₂][PF₆]₂, [Fe(**3**)₂][PF₆]₂·2MeCN and 2{[Ru(**5**)₂][PF₆]₄}·H₂O were collected on an Enraf Nonius Kappa CCD instrument; data reduction, solution and refinement used the programs COLLECT,²⁵² SIR92,²⁵³ DENZO/SCALEPACK²⁵⁶ and CRYSTALS.²⁵⁷ Data for [Ru(**1**)₂][PF₆]₂·4H₂O were collected on a Bruker SMART 1000 CCD diffractometer; data reduction, solution (by Patterson map) and refinement used the programs SAINT,⁷ SHELXS-97 and SHELXL-97.^{7, 258}

4.7.9. Crystal data for individual structures

1. Crystal data for 4{[Fe(1**)₂][PF₆]₂}·9H₂O**

$\text{C}_{160}\text{H}_{130}\text{F}_{48}\text{Fe}_4\text{N}_{32}\text{O}_9\text{P}_8$, M= 4028.08, Triclinic, space group $P-1$, $a = 15.7521(6)$, $b = 16.1814(6)$, $c = 17.3664(6)$ Å, $\alpha = 94.145(2)$, $\beta = 99.444(2)^\circ$, $\gamma = 109.469(2)^\circ$, $V = 4078.3(3)$ Å³, $Z = 1$, $D_c = 1.64$ Mg m⁻³, $\mu(\text{Mo K}_\alpha) = 0.553$ mm⁻¹, T = 173 K, 18 648 reflections collected. Refinement of 12 869 reflections (1180 parameters) with $I > 1.0 \sigma(I)$ converged at final $R1 = 0.0776$ ($R1$ all data = 0.1172), $wR2 = 0.0842$ ($wR2$ all data = (0.1214)), $gof = 1.0087$.

2. Crystal data for $[\text{Fe}(\mathbf{2})_2][\text{PF}_6]_2$

$\text{C}_{40}\text{H}_{28}\text{F}_{12}\text{FeN}_8\text{P}_2$, M= 966.49, Triclinic, space group $P-1$, $a = 9.3867(2)$, $b = 10.4130(2)$, $c = 21.3789(3)$ Å, $\alpha = 93.680(1)$, $\beta = 100.262(1)$, $\gamma = 110.4597(8)^\circ$, $V = 1908.30(6)$ Å³, $Z = 2$, $D_c = 1.682$ Mg m⁻³, $\mu(\text{Mo K}_\alpha) = 0.583$ mm⁻¹, T = 173 K, 18 394 reflections collected. Refinement of 5829 reflections (571 parameters) with $I > 2.0 \sigma(I)$ converged at final $R1 = 0.0375$ ($R1$ all data = 0.0648), $wR2 = 0.0434$ ($wR2$ all data = (0.0678)), $gof = 1.1183$.

3. Crystal data for $[\text{Fe}(\mathbf{3})_2][\text{PF}_6]_2 \cdot 2\text{MeCN}$

$\text{C}_{44}\text{H}_{34}\text{F}_{12}\text{FeN}_{10}\text{P}_2$, M= 1048.59, Tetragonal, space group $I4_1/a$, $a = b = 8.7704(2)$, $c = 56.525(1)$ Å, $\alpha = \beta = \gamma = 90^\circ$, $V = 4347.9(2)$ Å³, $Z = 2$, $D_c = 1.76$ Mg m⁻³, $\mu(\text{Mo K}_\alpha) = 0.52$ mm⁻¹, T = 173 K, 3188 reflections collected. Refinement of 2431 reflections (204 parameters) with $I > 3.0 \sigma(I)$ converged at final $R1 = 0.0998$ ($R1$ all data = 0.1160), $wR2 = 0.0578$ ($wR2$ all data = (0.0590)).

4. Crystal data for $[\text{Fe}(\mathbf{9})_2][\text{ClO}_4]_2 \cdot 2\text{MeOH} \cdot 0.5\text{H}_2\text{O}$

$\text{C}_{41}\text{H}_{33}\text{Cl}_2\text{FeN}_8\text{O}_9$, M= 916.50, triclinic, space group $P-1$, $a = 10.680(6)$, $b = 17.52(1)$, $c = 21.88(1)$ Å, $\alpha = 77.297(9)$, $\beta = 88.690(9)$, $\gamma = 72.752(9)^\circ$, $V = 3811(4)$ Å³, $Z = 4$, $D_c = 1.598$ Mg m⁻³, $\mu(\text{Mo K}_\alpha) = 0.609$ mm⁻¹, T = 150(2)K, 29279 reflections collected. Refinement of 12970 reflections (1073 parameters) with $I > 2\sigma(I)$ converged at final $R1 = 0.0850$ ($R1$ all data = 0.1490), $wR2 = 0.2282$ ($wR2$ all data = 0.2716), $gof = 1.031$.

5. Crystal data for $[\text{Fe}(\mathbf{38})_2][\text{PF}_6]_2$

$\text{C}_{50}\text{H}_{45}\text{F}_{12}\text{FeN}_{11}$, M = 1145.76, monoclinic, space group $C2/c$, $a = 26.179(5)$, $b = 11.920(2)$, $c = 19.026(4)$ Å, $\beta = 113.25(3)^\circ$, $V = 5454.8(19)$ Å³, $Z = 4$, $D_c = 1.395$ Mg

m^{-3} , $\mu(\text{Mo-K}_\alpha) = 0.421 \text{ mm}^{-1}$, $T = 223 \text{ K}$, 65680 reflections collected. Refinement of 7918 reflections (360 parameters) with $I > 2\sigma$ (I) converged at final $R1 = 0.0535$ ($R1$ all data 0.0578), $wR2 = 0.1461$ ($wR2$ all data = 0.1496), $gof = 1.147$.

6. Crystal data for $4\{\text{[Fe(39)}_2\text{][PF}_6\text{]}_2\}$ MeCN 2H₂O

$\text{C}_{154}\text{H}_{111}\text{F}_{48}\text{Fe}_4\text{N}_{41}\text{O}_2\text{P}_8, M = 3950.93$, triclinic, space group $P-1$, $a = 12.2234(4)$, $b = 16.2242(6)$, $c = 20.3558(7) \text{ \AA}$, $\alpha = 86.260(2)$, $\beta = 84.612(2)$, $\gamma = 79.4898(18)^\circ$, $V = 3946.8(2) \text{ \AA}^3$, $Z = 1$, $Z' = 0$, $D_c = 1.662 \text{ Mg m}^{-3}$, $\mu(\text{Mo K}_\alpha) = 0.568 \text{ mm}^{-1}$, $T = 173 \text{ K}$, 31963 reflections collected. Refinement of 12701 reflections (1261 parameters) with $I > 0.5\sigma(I)$ converged at final $R1 = 0.0905$ ($R1$ all data = 0.1306), $wR2 = 0.0844$ ($wR2$ all data = 0.1210), $gof = 1.0363$

7. Crystal data for $[\text{Fe(41)}_2\text{][PF}_6\text{]}_2$

$\text{C}_{40}\text{H}_{34}\text{F}_{12}\text{FeN}_{10}\text{P}_2, M = 1000.55$, monoclinic, space group $P2_1$, $a = 9.2578(6)$, $b = 13.1034(4)$, $c = 17.463(1) \text{ \AA}$, $\beta = 103.227(6)^\circ$, $V = 2062.2(2) \text{ \AA}^3$, $Z = 2$, $D_c = 1.611 \text{ Mg m}^{-3}$, $\mu(\text{Mo-K}_\alpha) = 0.544 \text{ mm}^{-1}$, $T = 173 \text{ K}$, 8566 reflections collected. Refinement of 6412 reflections (587 parameters) with $I > 2\sigma$ (I) converged at final $R1 = 0.0893$ ($R1$ all data = 0.1214), $wR2 = 0.0870$ ($wR2$ all data = 0.1243), $gof = 1.039$.

8. Crystal data for $[\text{Ru(33)}_2\text{][PF}_6\text{]}_2 \cdot 2\text{H}_2\text{O}$

$\text{C}_{40}\text{H}_{32}\text{F}_{12}\text{N}_8\text{O}_2\text{P}_2\text{Ru}, M = 1047.75$, triclinic, space group $P-1$, $a = 16.124(4)$, $b = 16.170(4)$, $c = 17.526(4) \text{ \AA}$, $\alpha = 94.305(5)$, $\beta = 99.731(4)$, $\gamma = 113.697(4)^\circ$, $V = 4071.9(16) \text{ \AA}^3$, $Z = 4$, $D_c = 1.768 \text{ Mg m}^{-3}$, $\mu(\text{Mo K}_\alpha) = 0.574 \text{ mm}^{-1}$, $T = 150(2) \text{ K}$, 18394 reflections collected. Refinement of 13 834 reflections (1157 parameters) with $I > 2.0\sigma(I)$ converged at final $R1 = 0.0598$ ($R1$ all data = 0.0838), $wR2 = 0.1536$ ($wR2$ all data = 0.1718), $gof = 1.030$.

9. Crystal data for $[\text{Ru(9)}_2\text{][PF}_6\text{]}_2$

$\text{C}_{40}\text{H}_{28}\text{F}_{12}\text{N}_8\text{P}_2\text{Ru}, M = 1011.71$, tetragonal, space group $I4_1/a$, $a = b = 8.774(4)$, $c = 57.731(1) \text{ \AA}$, $V = 4444(3) \text{ \AA}^3$, $Z = 4$, $D_c = 1.512 \text{ Mg m}^{-3}$, $\mu(\text{Mo K}_\alpha) = 0.514 \text{ mm}^{-1}$, $T = 173 \text{ K}$, 2558 reflections collected. Refinement of 1970 reflections (176 parameters) with $I > 3\sigma(I)$ converged at final $R1 = 0.0475$ ($R1$ all data = 0.0650), $wR2 = 0.0498$ ($wR2$ all data = 0.0549), $gof = 1.072$.

10. Crystal data for $[\text{Ru(9)}_2][\text{PF}_6][\text{NO}_3]$

$\text{C}_{40}\text{H}_{28}\text{F}_6\text{N}_9\text{O}_3\text{PRu}$, $M = 928.75$, triclinic, space group $P-1$, $a = 8.927(1)$, $b = 9.832(1)$, $c = 21.873(3)$ Å, $\alpha = 90.64(1)$, $\beta = 100.08(9)$, $\gamma = 102.03(9)^\circ$, $V = 1846.4(4)$ Å³, $Z = 2$, $D_c = 1.671$ Mg m⁻³, $\mu(\text{Mo K}_\alpha) = 0.554$ mm⁻¹, $T = 150(2)$ K, 20457 reflections collected. Refinement of 6373 reflections (519 parameters) with $I > 2\sigma(I)$ converged at final $RI = 0.0767$ (RI all data = 0.1045), $wR2 = 0.2130$ ($wR2$ all data = 0.2364), $gof = 1.063$.

11. Crystal data for $2\{\text{Ru(36)}_2\}[\text{PF}_6]_4 \cdot \text{H}_2\text{O}$

$\text{C}_{84}\text{H}_{70}\text{F}_{48}\text{N}_{16}\text{OP}_8\text{Ru}_2$, $M = 2679.41$, triclinic, space group $P-1$, $a = 8.5631(1)$, $b = 15.5219(2)$, $c = 19.7088(2)$ Å, $\alpha = 103.5494(7)$, $\beta = 97.4740(7)$, $\gamma = 101.6026(6)^\circ$, $V = 2451.09(5)$ Å³, $Z = 1$, $D_c = 1.815$ Mg m⁻³, $\mu(\text{Mo K}_\alpha) = 0.587$ mm⁻¹, $T = 173$ K, 11 707 reflections collected. Refinement of 8538 reflections (811 parameters) with $I > 3\sigma(I)$ converged at final $RI = 0.0364$ (RI all data = 0.0539), $wR2 = 0.0378$ ($wR2$ all data = 0.0481), $gof = 1.2304$.

12. Crystal data for $[\text{Ru(41)}_2][\text{PF}_6]_2$

$\text{C}_{40}\text{H}_{34}\text{F}_{12}\text{N}_{10}\text{P}_2\text{Ru}$, $M = 1045.77$, monoclinic, space group $P2_1$, $a = 9.3368(3)$, $b = 13.0679(4)$, $c = 17.5480(6)$ Å, $\beta = 103.341(2)^\circ$, $V = 2083.3(1)$ Å³, $Z = 2$, $D_c = 1.667$ Mg m⁻³, $\mu(\text{Mo K}_\alpha) = 0.553$ mm⁻¹, $T = 173$ K, 9271 reflections collected. Refinement of 7592 reflections (587 parameters) with $I > 3\sigma(I)$ converged at final $RI = 0.0440$ (RI all data = 0.0576), $wR2 = 0.0402$ ($wR2$ all data = 0.0453), $gof = 1.080$.

13. Crystal data for $\{2[\text{Ru(39)}_2][\text{PF}_6]_2\} \cdot \text{MeCN} \cdot \text{H}_2\text{O}$.

$\text{C}_{78}\text{H}_{57}\text{F}_{24}\text{N}_{21}\text{OP}_4\text{Ru}_2$, $M = 2086.44$, triclinic, space group $P-1$, $a = 12.1910(2)$, $b = 16.2789(2)$, $c = 20.6309(2)$ Å, $\alpha = 86.1650(7)$, $\beta = 83.6131(7)$, $\gamma = 80.5650(6)^\circ$, $V = 4008.93(9)$ Å³, $Z = 2$, $D_c = 1.729$ Mg m⁻³, $\mu(\text{Mo K}_\alpha) = 0.575$ mm⁻¹, $T = 173$ K, 19093 reflections collected. Refinement of 13339 reflections (1315 parameters) with $I > 1.5\sigma(I)$ converged at final $RI = 0.0441$ (RI all data = 0.0707), $wR2 = 0.0478$ ($wR2$ all data = 0.0604), $gof = 1.162$.

14. Crystal data for $[\text{Ni(9)}_2][\text{NO}_3]_2 \cdot 2\text{MeOH} \cdot 2\text{H}_2\text{O}$

$C_{42}H_{40}NiO_{10}$, $M = 903.55$, triclinic, space group $P-1$, $a = 10.960(4)$, $b = 12.628(4)$, $c = 15.545(5) \text{ \AA}$, $\alpha = 101.104(7)$, $\beta = 96.400(8)$, $\gamma = 98.498(7)^\circ$, $V = 2066(1) \text{ \AA}^3$, $Z = 2$, $D_c = 1.452 \text{ Mg m}^{-3}$, $\mu(\text{Mo K}_\alpha) = 0.542 \text{ mm}^{-1}$, $T = 150(2) \text{ K}$, 13989 reflections collected. Refinement of 9328 reflections (584 parameters) with $I > 2\sigma(I)$ converged at final $R1 = 0.0549$ ($R1$ all data = 0.0818), $wR2 = 0.1396$ ($wR2$ all data = 0.1530), $gof = 1.051$.

15. Crystal data for $\text{Fe}(\mathbf{41})_2[\text{PF}_6]_2$

$C_{40}H_{34}F_{12}\text{FeN}_{10}\text{P}_2$, $M = 1000.55$, monoclinic, space group $P2_1$, $a = 9.2578(6)$, $b = 13.1034(4)$, $c = 17.463(1) \text{ \AA}$, $\beta = 103.227(6)^\circ$, $V = 2062.2(2) \text{ \AA}^3$, $Z = 2$, $D_c = 1.611 \text{ Mg m}^{-3}$, $\mu(\text{Mo-K}_\alpha) = 0.544 \text{ mm}^{-1}$, $T = 173 \text{ K}$, 8566 reflections collected. Refinement of 6412 reflections (587 parameters) with $I > 2\sigma(I)$ converged at final $R1 = 0.0893$ ($R1$ all data = 0.1214), $wR2 = 0.0870$ ($wR2$ all data = 0.1243), $gof = 1.039$.

16. Crystal data for $[\text{Ru}(\mathbf{41})_2][\text{PF}_6]_2$

$C_{40}H_{34}F_{12}\text{N}_{10}\text{P}_2\text{Ru}$, $M = 1045.77$, monoclinic, space group $P2_1$, $a = 9.3368(3)$, $b = 13.0679(4)$, $c = 17.5480(6) \text{ \AA}$, $\beta = 103.341(2)^\circ$, $V = 2083.3(1) \text{ \AA}^3$, $Z = 2$, $D_c = 1.667 \text{ Mg m}^{-3}$, $\lambda(\text{Mo K}_\alpha) = 0.553 \text{ mm}^{-1}$, $T = 173 \text{ K}$, 9271 reflections collected. Refinement of 7592 reflections (587 parameters) with $I > 3\sigma(I)$ converged at final $R1 = 0.0440$ ($R1$ all data = 0.0576), $wR2 = 0.0402$ ($wR2$ all data = 0.0453), $gof = 1.080$.

17. Crystal data for $[\text{Pd}(\mathbf{9})\text{Cl}]\text{Cl}\cdot 3\text{H}_2\text{O}\cdot \text{DMF}$

$C_{23}H_{27}\text{Cl}_2\text{N}_4\text{PdC}_3\text{H}_7\text{NO}\cdot 3\text{H}_2\text{O}$, $M = 614.80$, triclinic, space group $P-1$, $a = 6.7306(3)$, $b = 13.4364(6)$, $c = 14.5910(6) \text{ \AA}$, $\alpha = 105.562(3)$, $\beta = 99.893(3)$, $\gamma = 90.163(2)^\circ$, $V = 1250.6(1) \text{ \AA}^3$, $Z = 2$, $D_c = 1.633 \text{ g cm}^{-3}$, $\mu(\text{Mo K}_\alpha) = 0.996 \text{ mm}^{-1}$, $T = 173 \text{ K}$, 7201 reflections collected. Refinement of 5378 reflections (317 parameters) with $I > 3.0\sigma(I)$ converged at final $R1 = 0.0730$ (0.0921 all data), $wR2 = 0.0836$ (0.1033 all data), $gof = 1.0487$. The crystal investigated was twinned, the twinning law is 1.000, 0.003, 0.000, 0.000, -1.000, 0.000, -0.750, -0.001, -1.000. Twin element scale factors refined to 0.614(3) and 0.386(3), respectively.

18. Crystal data for $[\text{Pd}(\mathbf{41})\text{Cl}]\text{PF}_6$

$C_{20}H_{17}\text{ClF}_6\text{N}_5\text{PPd}$, $M = 614.20$, triclinic, space group $P-1$, $a = 8.3796(2)$, $b = 10.8068(2)$, $c = 13.2536(3) \text{ \AA}$, $\alpha = 99.108(1)$, $\beta = 103.461(1)$, $\gamma = 110.1509(9)^\circ$, $V =$

$1057.73(4) \text{ \AA}^3$, $Z = 2$, $D_c = 1.928 \text{ Mg m}^{-3}$, $\mu(\text{Mo K}_\alpha) = 1.153 \text{ mm}^{-1}$, $T = 173 \text{ K}$, 6172 reflections collected. Refinement of 4716 reflections (361 parameters) with $I > 3\sigma(I)$ converged at final $R1 = 0.0308$ ($R1$ all data = 0.0441), $wR2 = 0.0337$ ($wR2$ all data = 0.0435), $gof = 1.148$.

19. Crystal data for $[\text{Cu(H41Cl}_2]\text{Cl}\cdot 3\text{H}_2\text{O}\cdot 0.5\text{EtOH}$

$\text{C}_{21}\text{H}_{21}\text{Cl}_3\text{CuN}_4\text{O}_4$, $M = 563.32$, triclinic, space group $P-1$, $a = 7.747(5)$, $b = 11.305(5)$, $c = 14.063(5) \text{ \AA}$, $\alpha = 102.087(5)$, $\beta = 96.866(5)$, $\gamma = 91.748(5)^\circ$, $V = 1193.74 \text{ \AA}^3$, $Z = 2$, $D_c = 1.567 \text{ Mg m}^{-3}$, $\mu(\text{Mo K}_\alpha) = 1.286 \text{ mm}^{-1}$, $T = 200 \text{ K}$, 25097 reflections collected.

Refinement of 6964 reflections (337 parameters) with $I > \sigma(I)$ converged at final $R1 = 0.044$ ($R1$ all data = 0.047), $wR2 = 0.121$ ($wR2$ all data = 0.123), $gof = 1.136$.

20. Crystal data for $[\text{Cu(H41Cl}_2]\text{Cl}\cdot 3\text{H}_2\text{O}$

$\text{C}_{20}\text{H}_{21}\text{Cl}_3\text{CuN}_4\text{O}_4$, $M = 551.30$, triclinic, space group $P-1$, $a = 7.7958(16)$, $b = 11.045(2)$, $c = 13.785(3) \text{ \AA}$, $\alpha = 88.48(3)$, $\beta = 85.04(3)$, $\gamma = 88.29(3)^\circ$, $V = 1181.7 \text{ \AA}^3$, $Z = 2$, $D_c = 1.549 \text{ Mg m}^{-3}$, $\mu(\text{Mo K}_\alpha) = 1.297 \text{ mm}^{-1}$, $T = 223 \text{ K}$, 22384 reflections collected. Refinement of 3804 reflections (310 parameters) with $I > \sigma(I)$ converged at final $R1 = 0.0647$ ($R1$ all data = 0.0693), $wR2 = 0.1722$ ($wR2$ all data = 0.1775), $gof = 1.089$.

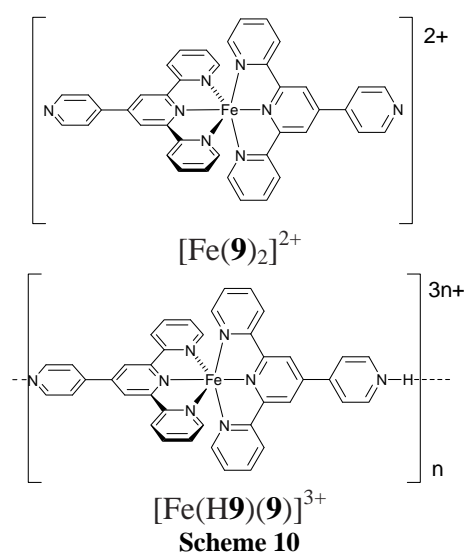
Chapter 5 Coordination polymers and networks

5.1. General considerations

Although the protonation and alkylation of the pendant pyridine in $[M(\textbf{9})_2]^{n+}$ is well established^{17, 166, 272, 273, 279, 280, 288, 292} and examples of discrete structures containing $[M(\textbf{9})_2]^{2+}$ bridging ligands have been reported^{91, 94, 169, 283-289} the formation of infinite networks and polymers containing this motif have proven elusive. This chapter reports the use of complexes introduced in chapter 3 as ‘expanded ligands’ to form to first crystallographically characterised coordination polymers and sheets incorporating $M(\text{tpy})_2$ units.

5.2. Self-complementary hydrogen-bonded polymers

We begin with the simplest cases, in which self-complementary hydrogen bonding is used to link together $[M(\textbf{9})_2]^{2+}$ complexes. Under certain conditions, protonation was found to be more favourable than coordination to a labile metal centre and this results in the prototypical hydrogen-bonded one-dimensional polymers in which $[M(\textbf{9})_2]^{2+}$ motifs are linked by protons bridging pendant 4-pyridyl groups (Scheme 10). This may be regarded as a coordination polymer in which a proton acts as the simplest ‘metal’ ion. Recently, an example of a similar system involving the related 2,6-bis(pyrazol-1-yl)-4-(4'-pyridyl)pyridine ligand has been reported.³⁵⁵



Our strategy for the preparation of iron(II) coordination polymers incorporating ligand **9** has involved the use of $[\text{Fe}(\mathbf{9})_2]^{2+}$ as a preformed building block and exposing the pendant N-donors to either Fe(II) or Fe(III). In each case, NH_4SCN was present to encourage complexation with Fe(II)/Fe(III) in the hope that this might facilitate the crystallization of coordination polymers.^{356, 357} An MeCN/H₂O solution of FeCl_3 and NH_4SCN or a EtOH/H₂O solution of $\text{Fe}(\text{ClO}_4)_2$ and NH_4SCN was allowed to diffuse into an MeCN/H₂O solution of $[\text{Fe}(\mathbf{1})_2][\text{PF}_6]_2$. The crystallization tubes were left to stand at room temperature. After ~3 weeks, dark red plates had grown from the reaction of $[\text{Fe}(\mathbf{9})_2][\text{PF}_6]_2$ with FeCl_3 and NH_4SCN , while the reaction of $[\text{Fe}(\mathbf{1})_2][\text{PF}_6]_2$ with $\text{Fe}(\text{ClO}_4)_2$ and NH_4SCN produced dark red-purple plates after a period of 2 months. Single crystal structure analysis of these products revealed them to be $[\text{Fe}(\mathbf{9})(\mathbf{H9})][\text{Fe}(\text{NCS})_6]\cdot 2\text{H}_2\text{O}$ or $[\text{Fe}(\mathbf{9})(\mathbf{H9})][\text{Fe}(\text{NCS})_6]\cdot \text{MeCN}$ (see Experimental section) and $[\text{Fe}(\mathbf{9})(\mathbf{H9})][\text{ClO}_4]_3\cdot \text{EtOH}$, respectively. Thus, under the conditions used, protonation of one pyridine ring occurs in preference to coordination to iron(II). The structure of an ion pair in $[\text{Fe}(\mathbf{9})(\mathbf{H9})][\text{Fe}(\text{NCS})_6]\cdot 2\text{H}_2\text{O}$ is shown in Figure 5-1.

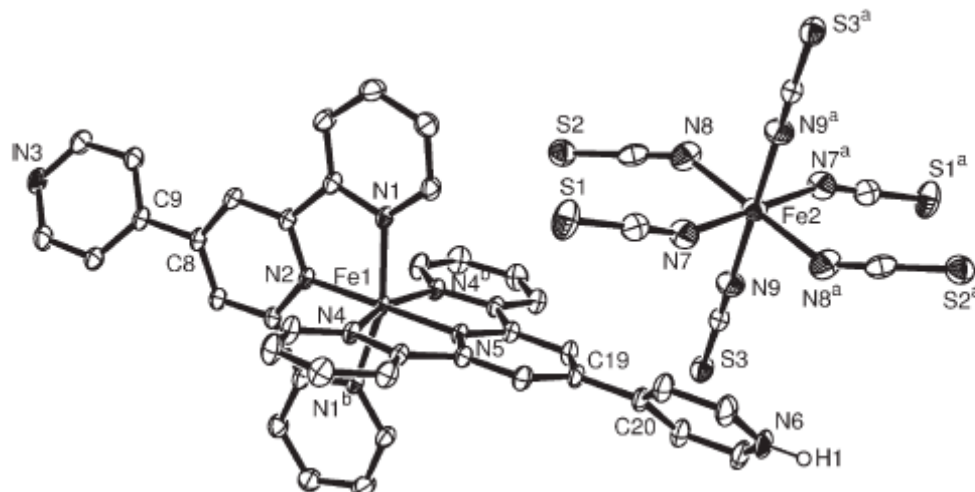


Figure 5-1 Molecular structure of an ion pair in $[\text{Fe}(\mathbf{9})(\mathbf{H9})][\text{Fe}(\text{NCS})_6]\cdot 2\text{H}_2\text{O}$ with thermal ellipsoids plotted at 40% probability level. Hydrogen atoms except for H1 are omitted. Symmetry codes: a = -x, -y, -z; b = 1 - x, y, 3/2 - z. Selected bond lengths and angles: $\text{Fe1}-\text{N1} = 1.976(1)$, $\text{Fe1}-\text{N2} = 1.879(2)$, $\text{Fe1}-\text{N4} = 1.981(1)$, $\text{Fe1}-\text{N5} = 1.879(2)$, $\text{Fe2}-\text{N7} = 2.044(2)$, $\text{Fe2}-\text{N8} = 2.064(2)$, $\text{Fe2}-\text{N9} = 2.065(2)$ Å; $\text{N1}-\text{Fe1}-\text{N2} = 81.05(4)$, $\text{N1}-\text{Fe1}-\text{N4} = 89.31(6)$, $\text{N2}-\text{Fe1}-\text{N4} = 99.05(4)$, $\text{N1}-\text{Fe1}-\text{N5} = 98.95(4)$, $\text{N4}-\text{Fe1}-\text{N5} = 80.95(4)$, $\text{N7}-\text{Fe2}-\text{N8} = 86.83(8)$, $\text{N7}-\text{Fe2}-\text{N9} = 91.69(8)$, $\text{N8}-\text{Fe2}-\text{N9} = 89.41(8)$, $\text{Fe2}-\text{N7}-\text{C23} = 155.6(2)$, $\text{Fe2}-\text{N8}-\text{C24} = 144.3(2)$, $\text{Fe2}-\text{N9}-\text{C25} = 172.3(2)$ °.

Atoms N6, C20, C19, N5, Fe1, N2, C8, C9 and N3 lie on a two-fold axis of the *Pbcn* space group. The cations are arranged in chains that run parallel to the crystallographic *b* axis (Figure 5-2) with an N6...N3*i* distance of 2.625(2) Å (symmetry code *i* = x, 1 + *y*, *z*). This short contact is consistent with the presence of an N–H...N hydrogen bonded

interaction and it was possible to locate atom H1 (which resides on a two-fold axis of the space group *Pbcn*) attached to N6 ($\text{N}-\text{H} = 0.88 \text{ \AA}$).

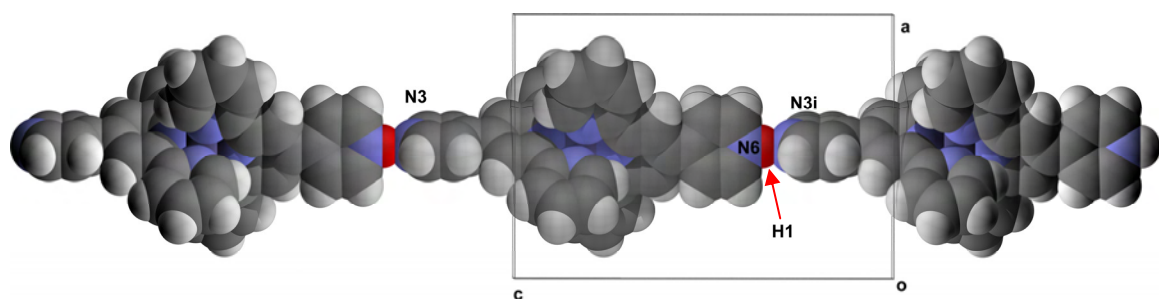


Figure 5-2 Part of one hydrogen-bonded chain of $[\text{Fe}(9)(\text{H9})]^{3+}$ cations in $[\text{Fe}(9)(\text{H9})][\text{Fe}(\text{NCS})_6]\cdot 2\text{H}_2\text{O}$. The unit cell is viewed down the *c* axis. Symmetry code $i = x, 1 + y, z$.

The coordination environment about Fe1 is unexceptional. Each pendant pyridine ring is twisted with respect to the tpy ligand to which it is bonded (the angles between the least squares planes of the rings containing N2 and N3, and N5 and N6 are 28.4(9) and 39.1(1) $^{\circ}$, respectively). The charge of the $[\text{Fe}(9)(\text{H9})]^{3+}$ cation is balanced by a $[\text{Fe}(\text{SCN})_6]^{3-}$ counter-ion in which both linear ($\text{Fe}_2-\text{N}9-\text{C}25 = 172.3(2)^{\circ}$) and bent ($\text{Fe}_2-\text{N}8-\text{C}24 = 144.3(2)$, $\text{Fe}_2-\text{N}7-\text{C}23 = 155.6(2)^{\circ}$) thiocyanate ligands are present. A search of the CSD¹⁹⁴ for structures containing $[\text{Fe}(\text{SCN})_6]^{3-}$ ions and analysis of the data using Mercury v. 1.4.2²² shows that the $\text{Fe}-\text{N}-\text{C}$ bond angles vary from 145.6(4) to 178.4(4) $^{\circ}$ (refcodes TMFETC³⁵⁸ and TMFETC01³⁵⁹), and such structural variation for metal coordinated [SCN] ligands has been discussed previously.³⁵⁹ Each $[\text{Fe}(\text{SCN})_6]^{3-}$ ion resides within a cavity created by six $[\text{Fe}(9)(\text{H9})]^{3+}$ ions (Figure 5-3), with the sulfur atoms involved in weak S...H-Ctpy interactions. The shortest contacts involve atoms S1 and S2 ($\text{C}7\text{H}71\dots\text{S}1 = 2.86 \text{ \AA}$, $\text{C}7\dots\text{S}1 = 3.706(2) \text{ \AA}$, angle $\text{C}7-\text{H}71\dots\text{S}1 = 152.0^{\circ}$, and $\text{C}11\text{H}111\dots\text{S}2 = 2.84 \text{ \AA}$, $\text{C}11\dots\text{S}2 = 3.712(2) \text{ \AA}$, angle $\text{C}11\text{H}111\dots\text{S}2 = 155.0^{\circ}$). While the role of S...H-C interactions in controlling molecular packing has received significantly less attention than that of O...H-C contacts,³³⁷ recent examples³⁶⁰⁻³⁶⁶ illustrate their importance in the solid state.

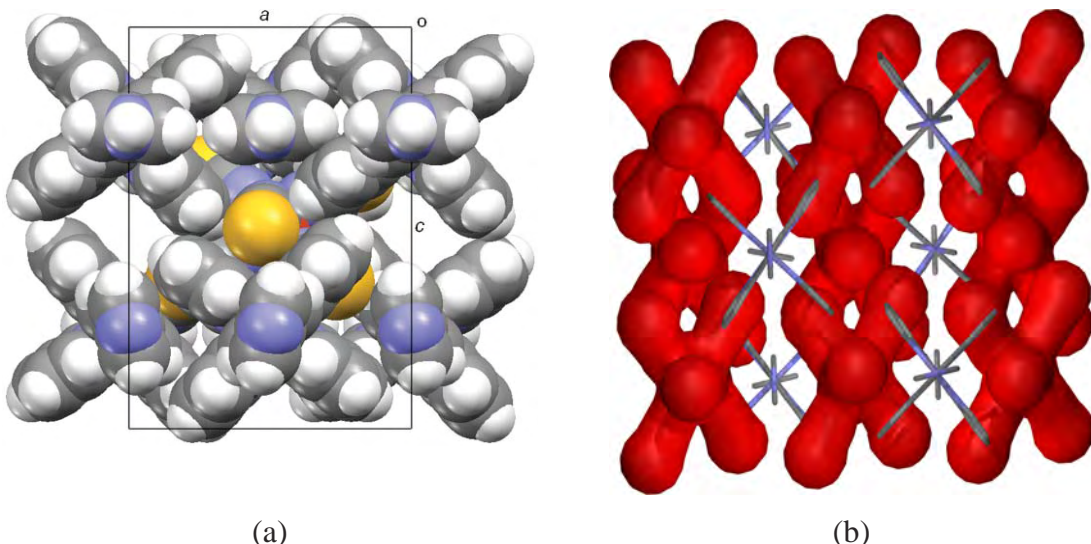


Figure 5-3 Unit cell of $[Fe(9)(H9)][Fe(NCS)_6] \cdot 2H_2O$ viewed down the b -axis showing (a) the encapsulation of an $[Fe(NCS)_6]^{3-}$ ion within six cations and (b) the cation chains held well apart by the steric bulk of the anions (anions in red, calculated (Weblabviewer Pro) solvent accessible surfaces shown).

The presence of the sterically demanding hexakis thiocyanatoiron(III) anions between the cationic polymer chains precludes any $[M(tpy)_2]$ embraces, as shown in Figure 5-3.³⁰¹ The two water molecules were modelled over four sites, each with a half occupancy. There is a weak hydrogen-bonded interaction between O1 and one pyridyl CH group ($C10H101 \dots O1 = 2.55 \text{ \AA}$, $C10 \dots O1 = 3.447(5) \text{ \AA}$, $C10H101 \dots O1 = 164^\circ$). The complex $[Fe(\mathbf{9})(H\mathbf{9})][Fe(NCS)_6] \cdot MeCN$ crystallizes in the same orthorhombic space group (*Pbcn*) as $[Fe(\mathbf{9})(H\mathbf{9})][Fe(NCS)_6] \cdot 2H_2O$. The packing of the cations and anions in the two structures is essentially identical. The acetonitrile solvent molecule in $[Fe(\mathbf{9})(H\mathbf{9})][Fe(NCS)_6] \cdot MeCN$ has been modelled over two sites with the central C atom on an inversion centre. This same inversion centre relates pairs of disordered water molecules in $[Fe(\mathbf{9})(H\mathbf{9})][Fe(NCS)_6] \cdot 2H_2O$. Subtle changes in packing on going from the dihydrate to the acetonitrile solvate result in only one significant change to the structure of either the complex cation or anion: the twisting of the pendant pyridine rings with respect to the central pyridine ring of the tpy unit. In $[Fe(\mathbf{9})(H\mathbf{9})][Fe(NCS)_6] \cdot MeCN$, the angles between the least squares planes of the rings containing N2 and N3, and N5 and N6 (atom numbering as in Fig. 1) are 31.4(2) and 34.8(2) $^\circ$, compared to 28.4(9) and 39.1(1) $^\circ$ in the dihydrate.

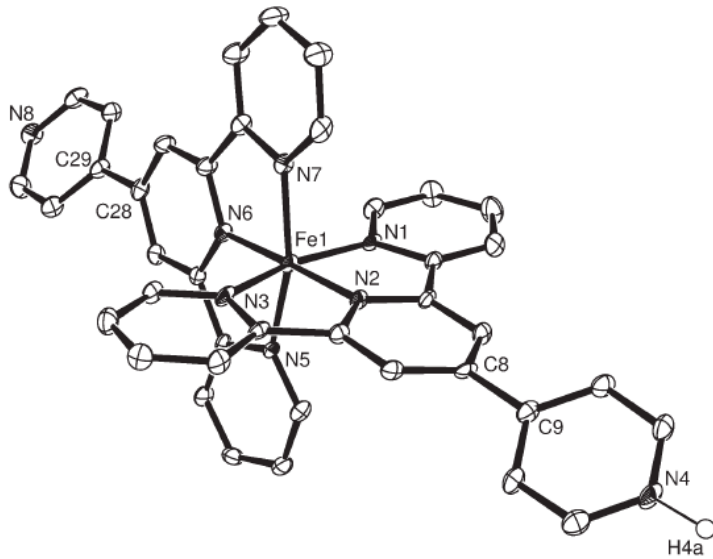


Figure 5-4 Molecular structure of the $[\text{Fe}(\mathbf{9})(\text{H9})]^{3+}$ ion in $[\text{Fe}(\mathbf{9})(\text{H9})][\text{ClO}_4]_3 \cdot \text{EtOH}$ with thermal ellipsoids plotted at 50% probability level. Hydrogen atoms except for H4a are omitted. Selected bond lengths and angles: Fe1–N1 = 1.973(4), Fe1–N2 = 1.892(3), Fe1–N3 = 1.964(4), Fe1–N5 = 1.979(3), Fe1–N6 = 1.892(3), Fe1–N7 = 1.971(3) Å; N1–Fe1–N2 = 80.37(13), N2–Fe1–N3 = 80.87(13), N5–Fe1–N6 = 80.83(14), N6–Fe1–N7 = 80.56(13)°

Polymeric chains formed by hydrogen-bonded $[\text{Fe}(\mathbf{9})(\text{H9})]^{3+}$ cations are also present in $[\text{Fe}(\mathbf{9})(\text{H9})][\text{ClO}_4]_3 \cdot \text{EtOH}$. The $[\text{Fe}(\text{tpy})_2]$ unit in the $[\text{Fe}(\mathbf{9})(\text{H9})]^{3+}$ ion (Figure 5-4) contains no unusual features. The deviation of each pendant pyridine ring from the plane of the central ring of the respective tpy unit (angles between the least squares planes of the rings containing N2 and N4, and N6 and N8 are 32.3(2) and 36.0(2)°, respectively) is similar to those observed in $[\text{Fe}(\mathbf{9})(\text{H9})][\text{Fe}(\text{NCS})_6] \cdot 2\text{H}_2\text{O}$ and $[\text{Fe}(\mathbf{9})(\text{H9})][\text{Fe}(\text{NCS})_6] \cdot \text{MeCN}$. In each cation in the latter compounds, the $\text{N}_{\text{py}} \dots \text{Fe} \dots \text{N}_{\text{py}}$ vector is constrained to being linear since it lies on a two-fold axis of the space group $Pbcn$. In contrast, there is significant bowing away from the ideal linear $\text{N4} \dots \text{N8}$ vector in the $[\text{Fe}(\mathbf{9})(\text{H9})]^{3+}$ cation in $[\text{Fe}(\mathbf{9})(\text{H9})][\text{ClO}_4]_3 \cdot \text{EtOH}$, and this resembles the conformation observed for $[\text{Ru}(\mathbf{9})_2]^{2+}$ in $[\text{Ru}(\mathbf{9})_2][\text{PF}_6][\text{NO}_3] \cdot \text{DMSO}$.²⁷⁵ The $\text{N4} \dots \text{N8i}$ (symmetry code $i = 1 + x, y, 1 + z$) distance between adjacent $[\text{Fe}(\mathbf{9})(\text{H9})]^{3+}$ cations in a hydrogen-bonded chain in $[\text{Fe}(\mathbf{9})(\text{H9})][\text{ClO}_4]_3 \cdot \text{EtOH}$ is 2.684(5) Å. Proton H4a was directly located ($\text{N4}–\text{H4a} = 0.93(2)$ Å, $\text{N4}–\text{H4a} \dots \text{N8i} = 177(4)$ °, symmetry code $i = 1 + x, y, 1 + z$). On going from $[\text{Fe}(\mathbf{9})(\text{H9})][\text{Fe}(\text{NCS})_6] \cdot 2\text{H}_2\text{O}$ or $[\text{Fe}(\mathbf{9})(\text{H9})][\text{Fe}(\text{NCS})_6] \cdot \text{MeCN}$ to $[\text{Fe}(\mathbf{9})(\text{H9})][\text{ClO}_4]_3 \cdot \text{EtOH}$, the cationic chains are relieved of the steric demands of the counter-ions and are able to approach one another more closely. This results in $[\text{Fe}(\text{tpy})_2]$ embraces³⁰¹ (Figure 5-5) with weak π-

stacking between pyridine rings containing atoms N1 and N3 (separation of rings = 3.34 Å) and weak edge-to-face interactions between C18H18 or C3H3 on either side of the pyridine ring containing N5 (H18...ring centroid 3.57 Å°, H18...ring centroid 3.42 Å).

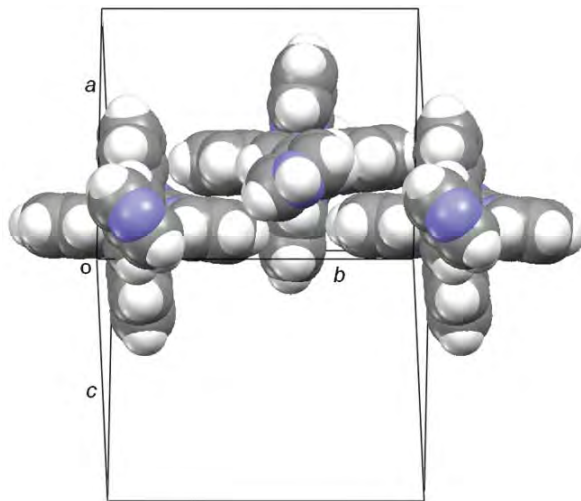


Figure 5-5 Looking down three chains of cations in $\text{Fe}(\mathbf{9})(\text{H9})][\text{ClO}_4]_3 \cdot \text{EtOH}$ showing $[\text{Fe}(\text{tpy})_2]$ embraces.

Perchlorate anions and EtOH molecules occupy the cavities between the $[\text{Fe}(\mathbf{9})(\text{H9})]^{3+}$ ions. One perchlorate ion is hydrogen bonded to the solvent molecule ($\text{O}13-\text{H}13\text{a}\dots\text{O}4 = 2.03(2)$, $\text{O}13\dots\text{O}4 = 2.896(5)$ Å, $\text{O}13-\text{H}13\text{a}\dots\text{O}4 = 166(5)^\circ$), and there are extensive interactions between perchlorate O atoms and aromatic C–H groups (Table 9).

Table 9 Hydrogen bonds between aromatic CH groups and perchlorate O atoms in $[\text{Fe}(\mathbf{9})(\text{H9})][\text{ClO}_4]_3 \cdot \text{EtOH}$

D–H...A	D–H/Å	H...A/Å	D...A/Å	D–H...A/°	Symmetry code
C1–H1...O12i	0.95	2.49	3.198(5)	131	x, 1/2 - y, -1/2 + z
C2–H2...O2	0.95	2.60	3.296(6)	131	
C11–H11...O3ii	0.95	2.55	3.456(6)	160	1 2x, 1 -y, 1 -z
C12–H12...O13iii	0.95	2.36	3.116(6)	136	1 + x, 1/2 - y, 1/2 + z
C14–H14...O11iv	0.95	2.46	3.391(5)	165	1 -x, -y, 1 -z
C17–H17...O10iv	0.95	2.36	3.182(5)	145	1 -x, -y, 1 -z
C19–H19...O3v	0.95	2.57	3.139(6)	119	x, -1+ y, z
C20–H20...O7i	0.95	2.43	3.335(5)	160	x, 1/2 -y, -1/2 + z
C22–H22...O8vi	0.95	2.53	3.198(6)	127	1 -x, -1/2 + y, 1/2 -z
C23–H23...O6vi	0.95	2.52	3.357(6)	147	1 -x, -1/2 + y, 1/2 -z
C30–H30...O8i	0.95	2.57	3.401(6)	146	x, 1/2 -y, -1/2 + z
C31–H31...O13i	0.95	2.48	3.365(6)	155	x, 1/2 -y, -1/2 + z
C32–H32...O3vii	0.95	2.41	3.349(6)	168	2x, 1 -y, z
C40–H40...O11vii	0.95	2.48	3.408(5)	165	2x, 1 -y, z

The validity of the expanded ligand model is seen by a comparison of the structures reported here with analogous 4,4'-bipyridine compounds. To the best of our knowledge,

no one-dimensional system of 4,4'-bipyridines linked by alternating metal ions and protons has been structurally characterised. However, one-dimensional chains of 4,4'-bipyridines linked by protons with N...N distances in the range of the compounds in this paper are well established (CSD¹⁹⁴ refcodes AYAFOV, BOQVEI, BOQVEI01, ECUZOS, FESBUB, ISUTAR, MUFMOP, OBOZIP, QURKUJ, UMAMOK, SETHAB, CEDDIZ, HUMDIC, LAHTUK, MEFNUK, SACDAC, SACDEG, UKIXUH).

5.3. *One dimensional coordination polymers*

The first two linear coordination polymers to use {M(**9**)₂} as an expanded ligand are reported here, using silver(I) and Cu(II) as bridging metals.

Silver(I) bridged coordination polymer

Described here is the first example of a coordination polymer in which [Ru(**9**)₂]²⁺ plays the role of a bridging bidentate ligand. The variety of coordination geometries and numbers available to silver(I) make this ion a common choice for the preparation of coordination networks and a variety of silver(I) complexes with 4,4'-bipyridine have been described.¹¹⁶ After numerous attempts at isolating heteronuclear compounds under various conditions, deep red X-ray quality plates of the compound {[Ru(**9**)₂](Ag(NO₃)(MeCN)(NO₃)₂(H₂O)} were grown via slow diffusion of an aqueous acetonitrile solution of AgNO₃ into a similar solution of [Ru(**9**)₂][PF₆]₂ in an H-cell. The lattice contains 1-D chains in which [Ru(**9**)₂]²⁺ expanded ligands are assembled into linear 1-D chains linked by {Ag(NO₃)(MeCN)} units (Figure 5-6). The N4...N8 distance is 17.84 Å and the complex is acting as an expanded 4,4'-bipyridine. The coordination geometry about the ruthenium is typical of a six-coordinate [Ru(tpy)₂] motif and closely resembles that in [Ru(**9**)₂]²⁺.²⁷⁵ There is no significant perturbation of the Ru–N interactions associated with coordination of the silver(I) to the pendant nitrogen.

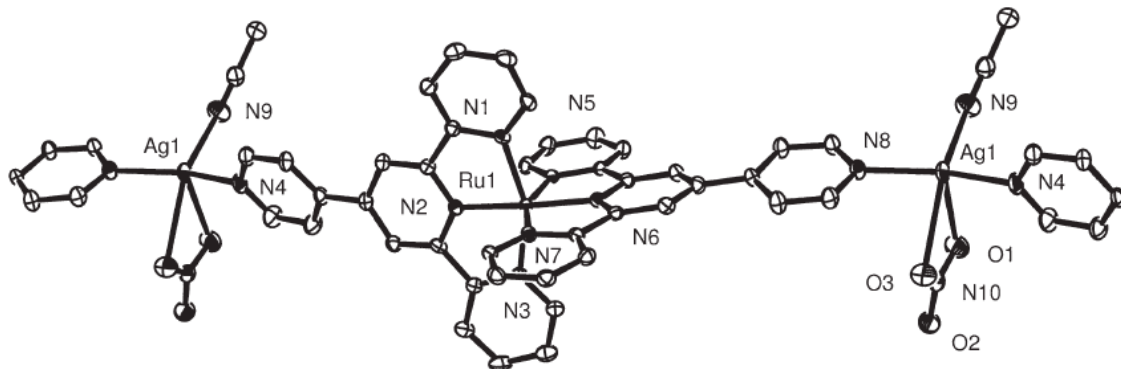


Figure 5-6 Part of the 1-D chain present in $\{(\text{Ru}(\mathbf{9})_2)(\text{Ag}(\text{NO}_3)_2(\text{MeCN})(\text{NO}_3)_2(\text{H}_2\text{O})\}$ showing the labelling of the non-carbon atoms. Hydrogen atoms, noncoordinated anions and the disordered solvent have been omitted for clarity; selected bond lengths Ag1–N4 2.241(4), Ag1–N8 2.244(4), Ag1–N9 2.404(4), Ru1–N6 1.978(3), Ru1–N2 1.981(3) Å, Ru1–N5 2.078(3), Ru1–N7 2.079(3), Ru1–N1 2.080(3), Ru1–N3 2.083(3) Å, N4–Ag1–N8 150.41(14), N4–Ag1–N9 101.35(15), N8–Ag1–N9 102.77(15), N6–Ru1–N2 175.82(13), N6–Ru1–N5 79.25(13), N2–Ru1–N5 96.89(13), N6–Ru1–N7 78.64(13), N2–Ru1–N7 105.22(13), N5–Ru1–N7 157.89(13), N6–Ru1–N1 99.37(13), N2–Ru1–N1 79.09(13), N5–Ru1–N1 92.47(13), N7–Ru1–N1 91.45(13), N6–Ru1–N3 103.25(13), N2–Ru1–N3 78.38(13), N5–Ru1–N3 92.26(13), N7–Ru1–N3 92.44(13), N1–Ru1–N3 157.38(13)°. Thermal ellipsoids at 50% probability.

The coordination environment of the silver(I) centre is less easily defined; the two shortest bonds are to the pyridine nitrogens N8 and N4a (generated by the symmetry operation $-x$, $-y$, $-z$) with bond lengths of 2.244(4) and 2.241(4) Å, respectively. A search of the CSD (Conquest Version 1.9, Quest, CSD version 5.28)²² revealed a total of 696 hits for silver with two pyridine donor ligands and the 1706 Ag–N bond length data ranged from 2.086–2.819 Å with a mean of 2.309 Å.

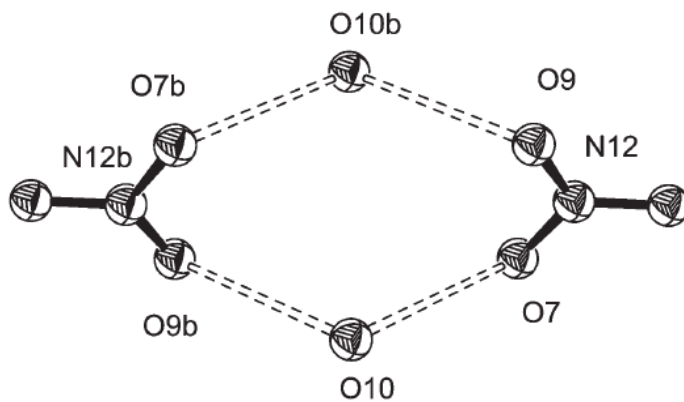


Figure 5-7 The cluster of water molecules and nitrate ions present in the lattice; O9–O10 2.919 Å, O7–O10 2.791 Å, /O7–O10–O9 105.04°. The atoms with the descriptor b are generated by the symmetry operation $-x$, $-y$, $-z$.

Accordingly, we can state that there are strong bonds between the pendant pyridine rings and the silver(I) centres. The N4a–Ag1–N8 angle of 150.4(1)° is sufficiently far

from linear that a description as a simple two-coordinate species seems inappropriate. The next shortest contact is of 2.404(5) Å to N9, to a coordinated acetonitrile ligand, which is short enough to be defined as an Ag–N bond.

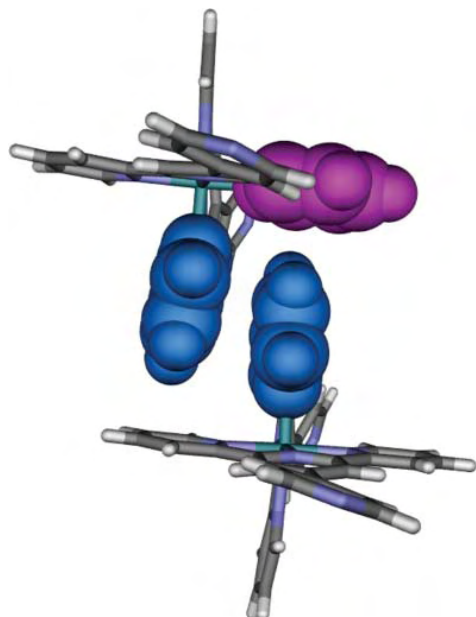


Figure 5-8 Face-to-face (blue–blue) and face-to-edge (blue–purple) $[M(\text{tpy})_2]$ embraces between chains of the same orientation lead to the formation of 2-D sheets.

The coordination sphere is completed by a longer contact to a monodentate nitrate anion with an Ag1–O1 distance of 2.623(4) Å. The result is a rather flattened tetrahedral geometry in which the flattening is associated with a further long contact of 2.774 Å to O3. Also present in the lattice is an ordered nitrate anion, a nitrate ion disordered over two sites, a water molecule and a disordered solvent molecule modelled simply with partial occupancy carbon atoms. The water molecules and the ordered nitrate ions form a $\{(\text{ONO}_2)(\text{OH}_2)_2(\text{O}_2\text{NO}\}$ cluster (O9–O10 2.919 Å, O7–O10 2.791 Å, /O7–O10–O9 105.04° (Fig. 3). One of the dominant interactions between adjacent chains are $\{M(\text{tpy})_2\}$ embraces³⁰¹ and both face-to-face and face-to-edge interactions are observed (Figure 5-8). These $[M(\text{tpy})_2]$ embraces result in the formation of 2-D sheets of the 1-D polymeric chains in which each chain has the same orientation (Figure 5-9).

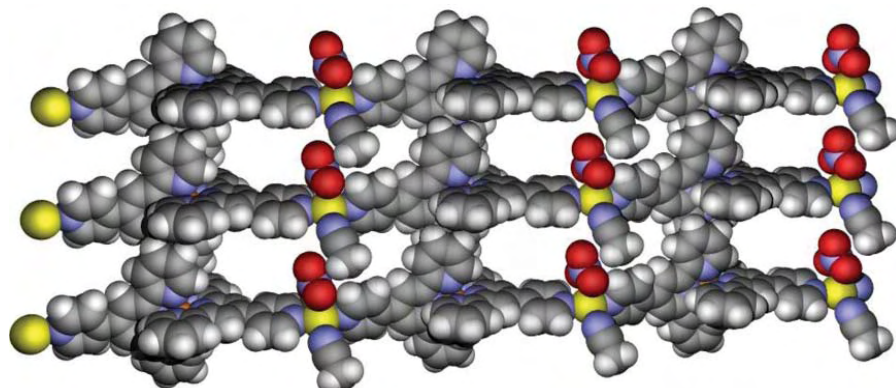


Figure 5-9 The two dimensional sheet resulting from the $\{\text{M(tpy)}_2\}$ embraces between chains of the same orientation (silver atoms in yellow).

Sheets in which the orientations of the Ag–NCMe vectors are opposite alternate and stack through pendant pyridine–tpy interactions to form a 3-D structure (Figure 5-10a). The extended lattice contains channels running along the crystallographic *b*-axis (Figure 5-10b) which are occupied by the non-coordinated anions and lattice solvent. Additional interactions involving nitrate and acetonitrile molecules link chains and sheets together.

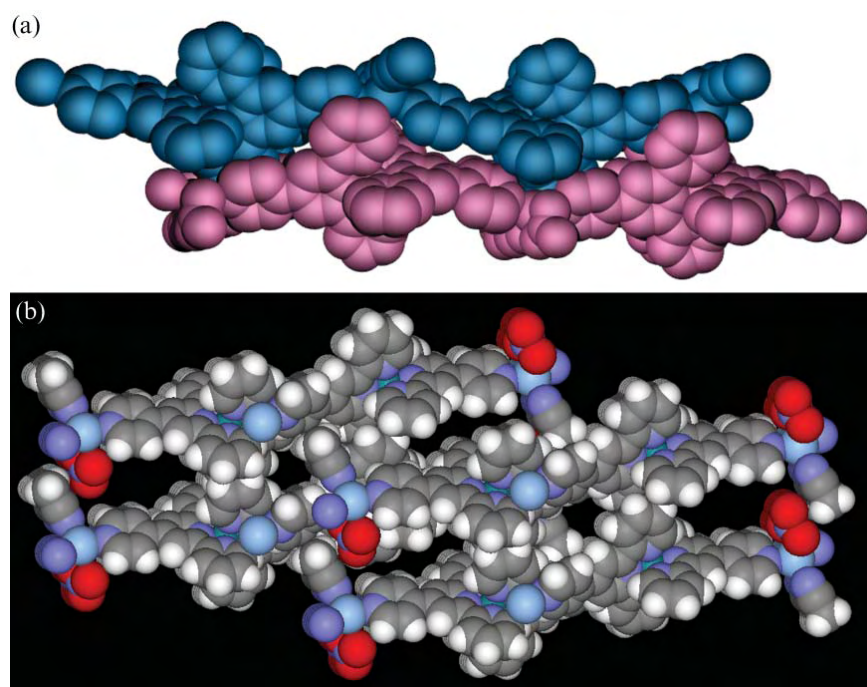


Figure 5-10 (a) Packing of adjacent layers of 1-D chains with opposite orientations. The principal interactions between the pink and blue layers with different orientation are tpy–pyridine stacking. (b) The linking of sheets and chains leads to channels along the crystallographic *b* axis that contain non-coordinated anions and disordered solvent.

A final point of interest relates to the orientation of the pendant pyridine rings with the central $\{\text{Ru(tpy)}_2\}$ moiety. Although the rings are expected to be twisted out of planarity about the interannular C–C bond to minimise the tpy H39 interactions with the

pyridine H3, there is a significant additional distortion. The tpy defined by N5, N6 and N7 is “normal” with the three rings approximately planar and the least squares planes of the rings containing N6 and N8 make an angle of 17.7° . In contrast, the tpy metal-binding domain defined by N1, N2 and N3 is very significantly distorted from planarity. The distortion is best described in terms of a bending of the central ring of the tpy out of the plane defined by the two terminal rings (Figure 5-11) with C8 lying 0.656 \AA out of this plane. This deviation is further amplified in the pendant pyridine ring and N4 lies 1.963 \AA from the plane. A very similar distortion of one of the two ligands is observed in $[\text{Ru}(\text{pytpy})_2][\text{PF}_6][\text{NO}_3]_2^{275}$ but not in other $\{\text{M}(\mathbf{9})_2\}$ derivatives (see chapter 4). The effect presumably originates from the asymmetry of anions and solvent within the lattice, although why this lattice pressure should manifest itself in a distortion of only one of the two **9** ligands is currently unclear.

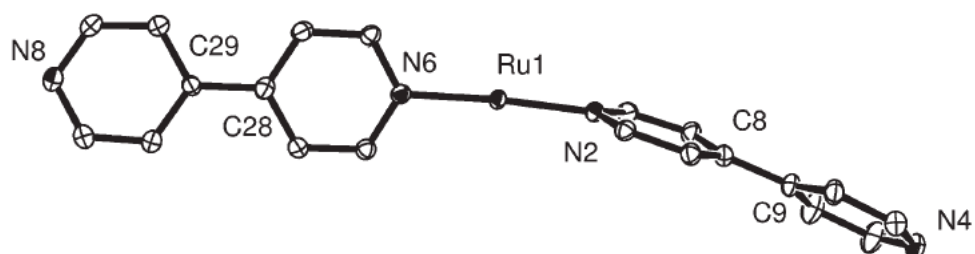


Figure 5-11 The tpy ligand containing N1, N2 and N3 and with the pendant ring containing N4 is significantly distorted from planarity.

Copper(II) bridged coordination polymer

The successful assembly of the one-dimensional polymer $[\{\text{Ru}(\mathbf{9})_2\}\{\text{AgNO}_3\}(\text{MeCN})(\text{NO}_3)_2(\text{H}_2\text{O})_2]_n$ by combining the preformed $[\text{Ru}(\mathbf{9})_2]^{2+}$ building block with Ag^+ ions, encouraged us to capitalize upon the strategy for the formation of related coordination polymers. The slow diffusion of an MeCN– H_2O solution of $\text{Cu}(\text{NO}_3)_2 \cdot 3\text{H}_2\text{O}$ into an MeCN– H_2O solution of $[\text{Fe}(\mathbf{9})_2][\text{PF}_6]_2$ produced purple crystals suitable for X-ray analysis. The structural analysis confirmed that $[\text{Fe}(\mathbf{9})_2]^{2+}$ acts as a bidentate ligand, coordinating to Cu^{2+} to form one-dimensional chains. Figure 5-12 shows the repeat unit in one chain. There are two crystallographically-independent iron(II) and copper(II) centres, although the coordination environments around Cu1 and Cu2 are very similar, as are those around

Fe1 and Fe2. Selected bond distances and angles are given in the caption to Figure 5-12. The $[\text{Fe}(\text{tpy})_2]$ units are unexceptional. Each pendant pyridine ring is twisted with respect to the central tpy ring to which it is connected. The twist angles fall within a relatively narrow range (the angles between the least-squares planes of the pyridine rings containing atoms N2 and N7, N5 and N8, N12 and N17, and N15 and N18 are $32.0(2)$, $42.9(2)$, $31.8(2)$ and $37.5(2)^\circ$, respectively). Each Cu(II) centre is bound by two pyridine donors which are

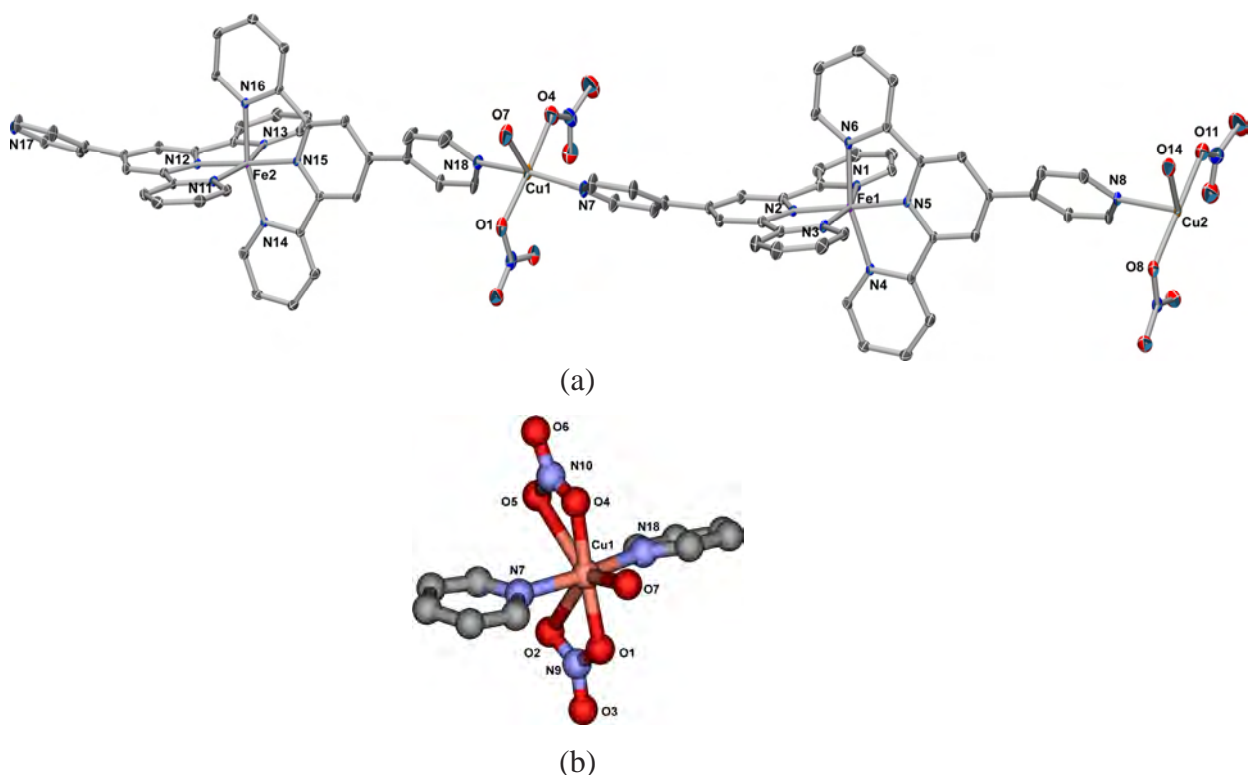


Figure 5-12 (a) The molecular structure of one repeating unit of the polymer chain in $\{(\text{H}_2\text{O})(\text{NO}_3)_2\text{CuFe}(\text{9})_2\}_2(\text{NO}_3)_4 \cdot 2.15\text{MeCN} \cdot 5.85\text{H}_2\text{O}\}_{\text{n}}$ with thermal ellipsoids plotted at the 30% probability level. Hydrogen atoms are omitted. Selected bond parameters: Cu1–N18 = 2.013(3), Cu1–O1 = 1.994(3), Cu1–O2 = 2.747(3), Cu1–O4 = 1.966(3), Cu1–O5 = 2.705(4), Cu1–O7 = 2.250(3), Cu2–N17a = 2.020(3), Cu2–N8 = 2.015(3), Cu2–O8 = 2.012(3), Cu2–O9 = 2.720(3), Cu2–O11 = 1.987(3), Cu2–O12 = 2.715(4), Cu2–O14 = 2.204(3), Fe1–N1 = 1.973(3), Fe1–N2 = 1.886(3), Fe1–N3 = 1.973(3), Fe1–N4 = 1.983(3), Fe1–N5 = 1.886(3), Fe1–N6 = 1.977(3), Fe2–N11 = 1.970(3), Fe2–N12 = 1.882(2), Fe2–N13 = 1.974(3), Fe2–N14 = 1.974(3), Fe2–N15 = 1.879(2), Fe2–N16 = 1.974(3) Å; N7–Cu1–N18 = 166.5(2), O1–Cu1–O2 = 51.7(1), O4–Cu1–O5 = 52.0(1), O1–Cu1–O7 = 90.0(1), O4–Cu1–O7 = 84.3(2), N7–Cu1–O7 = 95.5(1), N18–Cu1–O7 = 98.0(1), O8–Cu2–O9 = 52.1(1), O11–Cu2–O12 = 49.9(1), O8–Cu2–O14 = 91.7(1), O11–Cu2–O14 = 84.4(2), N17i–Cu2–O14 = 96.4(1), N8–Cu2–O14 = 97.1(1), N17i–Cu2–N8 = 166.5(1), N1–Fe1–N2 = 80.9(1), N2–Fe1–N3 = 81.0(1), N4–Fe1–N5 = 80.6(1), N5–Fe1–N6 = 81.3(1), N11–Fe2–N12 = 81.3(1), N12–Fe2–N13 = 80.9(1), N14–Fe2–N15 = 81.0(1), N15–Fe2–N16 = 81.3(1)°. Symmetry code: a = x, 1 + y, 21 + z. (b) The coordination sphere of Cu1.

trans to one another, and the coordination sphere is completed by two nitrate ions and a water ligand. The $[\text{NO}_3]_2$ ions are asymmetrically-bound with Cu–O bond distances in

the ranges 1.966(3) to 2.012(3), and 2.705(4) to 2.720(3) Å. The copper(II) coordination environment is best described as being square based pyramidal with the aqua ligand (O7 or O14) in the axial site; the angles O7–Cu1–O1, O7–Cu1–O4, O7–Cu1–N7 and O7–Cu1–N17 lie in the range 84.3(2) to 98.0(1)°, and angles O14–Cu2–O7, O14–Cu1–O8, O14–Cu1–N8 and O14–Cu1–N17i lie in the range 84.4(2) to 97.1(1)°. The second O-donor atom of each nitrate coordinates relatively weakly to the Cu(II) centre through the square-face of the primary coordination sphere (Figure 5-12b). The Cu1...Cu2 and Fe1...Fe2 distances are 21.699(3) and 21.696(3) Å respectively. The polymer chain in $\{(\text{H}_2\text{O})(\text{NO}_3)_2\text{CuFe}(\mathbf{9})_2\}_2(\text{NO}_3)_4 \cdot 2.15\text{MeCN} \cdot 5.85\text{H}_2\text{O}\}_{\text{n}}$ is similar to that in $[\text{Ru}(\mathbf{9})_2\{\text{AgNO}_3\} \cdot (\text{MeCN})(\text{NO}_3)_2(\text{H}_2\text{O})_2]_{\text{n}}$ only in terms of the presence of the bidentate $[\text{M}(\mathbf{9})_2]^{2+}$ ligand. In the copper(II) complex, the N–Cu–N units are closer to being linear (N7–Cu1–N18 = 166.5(2) Å and N17i–Cu2–N8 = 166.5(1) Å) than are the N–Ag–N units in the silver(I) complex (N–Ag–N = 150.4(1)°). As one would expect, the overall coordination geometries of the copper(II) centre (approximating to square based pyramidal) and silver(I) centre (flattened tetrahedral) are not equivalent.

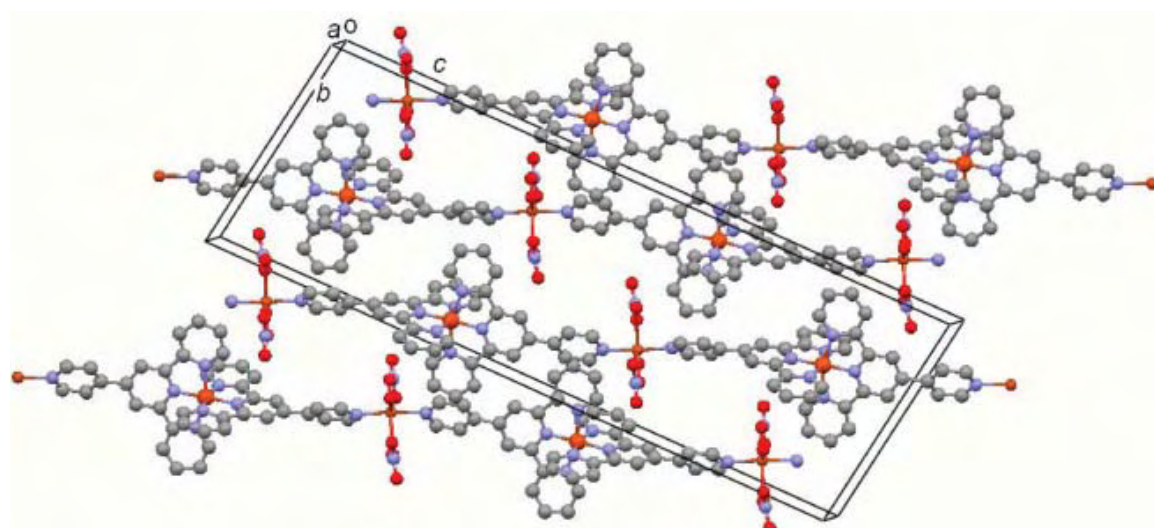


Figure 5-13 Relative orientations of the polymer chains in $\{(\text{H}_2\text{O})(\text{NO}_3)_2\text{CuFe}(\mathbf{9})_2\}_2(\text{NO}_3)_4 \cdot 2.15\text{MeCN} \cdot 5.85\text{H}_2\text{O}\}_{\text{n}}$ with solvent molecules and non-coordinated anions omitted.

Although one-, two- and three-dimensional assemblies based upon copper and 4,4'-bipyridine are well-established,^{367, 368} to the best of our knowledge no alternating heterometallic Fe–Cu systems based on 4,4'-bipyridine have been reported, and the expanded ligand strategy offers an almost unique approach to such species, which are expected to have novel magnetic and electronic properties. Somewhat surprisingly, the coordination environment of the copper(II) centre in $\{(\text{H}_2\text{O})(\text{NO}_3)_2\text{CuFe}(\mathbf{9})_2\}_2(\text{NO}_3)_4 \cdot 2.15\text{MeCN} \cdot 5.85\text{H}_2\text{O}\}_{\text{n}}$

$\text{CuFe(9)}_2\}{}_2(\text{NO}_3)_4 \cdot 2.15\text{MeCN} \cdot 5.85\text{H}_2\text{O}]_n$ is very rare. Although a few examples of copper complexes with two nitrate donors, one aqua ligand and two pyridine donors have been reported,^{153, 369-374} the majority have a cis-arrangement of pyridine donors and only in the case of an N,N'-bis-(2-pyridylmethyl)amine complex is a trans-configuration seen.³⁷⁴ The one-dimensional chains in $[(\text{H}_2\text{O})(\text{NO}_3)_2\text{CuFe(9)}_2\}{}_2(\text{NO}_3)_4 \cdot 2.15\text{MeCN} \cdot 5.85\text{H}_2\text{O}]_n$ run parallel to one another (Figure 5-13). Since the pendant pyridine rings all twist in the same direction relative to the axis of a polymer chain, the polymer is chiral. Both enantiomers are present in the crystal. One-dimensional polymers of one chirality form sheets and alternating sheets have opposite chirality (Figure 5-14).³⁷⁵ $[\text{Fe}(\text{tpy})_2]$ units within one sheet (e.g. a row of blue chains in Figure 5-14) engage in face-to-face π -stacking interactions (distance between the planes of the rings containing atoms N4 and N6, or N14 and N16 = 3.37 Å).

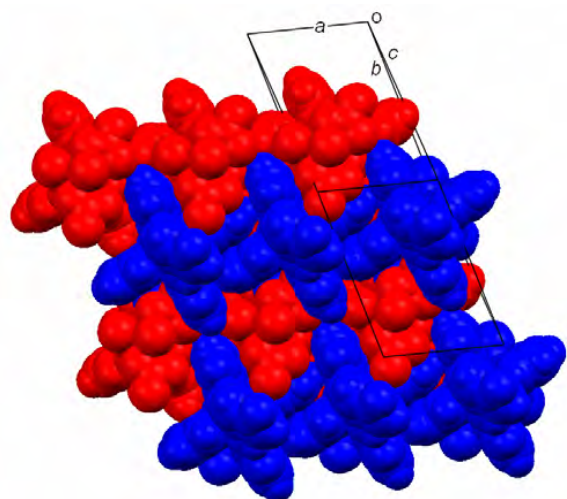


Figure 5-14 Packing of chiral polymer chains in $[(\text{H}_2\text{O})(\text{NO}_3)_2\text{CuFe(9)}_2\}{}_2(\text{NO}_3)_4 \cdot 2.15\text{MeCN} \cdot 5.85\text{H}_2\text{O}]_n$ (solvate and noncoordinated anions omitted). The red and blue chains are of opposite handedness.

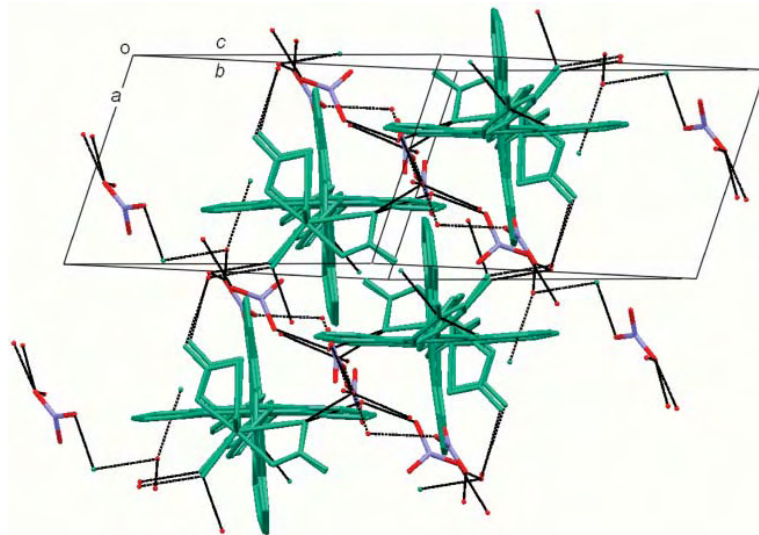


Figure 5-15 A partial packing diagram of $\{(\text{H}_2\text{O})(\text{NO}_3)_2\text{CuFe(9)}_2\}_2\cdot(\text{NO}_3)_4\cdot2.15\text{MeCN}\cdot5.85\text{H}_2\text{O}\}$ viewed down the coordination polymer chains (shown in green), and illustrating their interconnection by hydrogen-bonded networks of nitrate ions and water molecules. MeCN solvate is omitted from the figure.

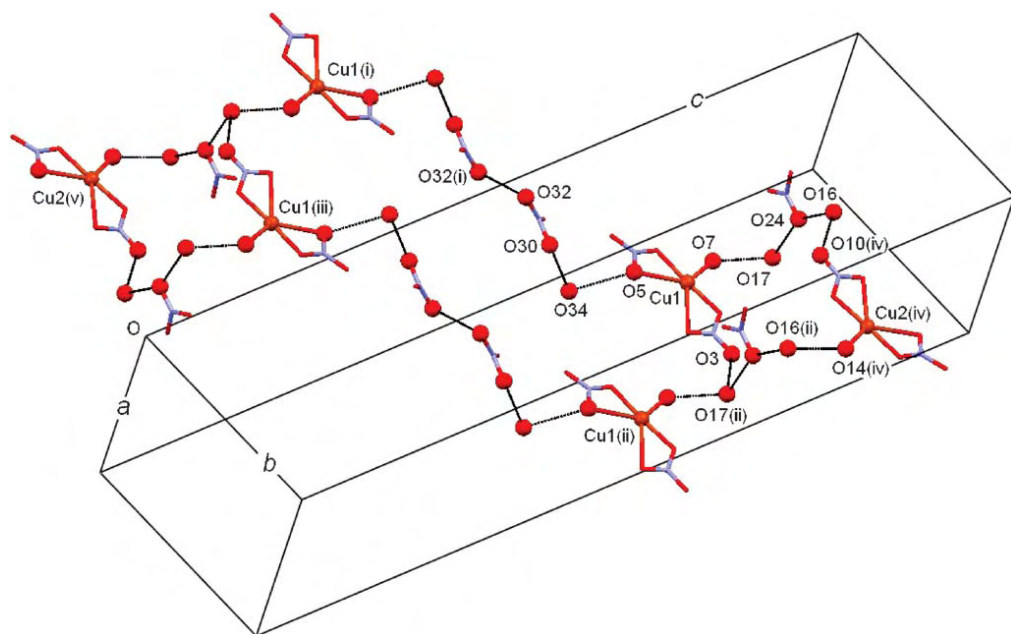


Figure 5-16 The repeating macrocyclic motifs that assemble into sheets in $\{(\text{H}_2\text{O})(\text{NO}_3)_2\text{CuFe(9)}_2\}_2\cdot(\text{NO}_3)_4\cdot2.15\text{MeCN}\cdot5.85\text{H}_2\text{O}\}$. One of the large and two of the small cyclic units are shown. Symmetry codes: (i) = $2x, 2y, 1 - z$; (ii) = $1 + x, y, z$; (iii) = $-x, 2 - y, 1 - z$; (iv) = $1 - x, 2 - y, 1 - z$; (v) = $x, -2 + y, z$. Atom O32 is shown as belonging to an $[\text{NO}_3]_2$, but is modelled as being disordered, 65% nitrate O and 35% water O (see text).

However, the $\{\text{Fe}(\text{tpy})_2\}$ units in the adjacent chains are prevented from participating in the extensive embraces typical of the packing in such systems³⁰¹ by hydrogen-bonded networks of water molecules, nitrate ions, the aqua ligands and coordinated nitrates (Figure 5-15). When viewed down the axes of the coordination polymers (Figure 5-15),

the packing diagram reveals that the copper-bound aqua and nitrate ligands are hydrogen bonded to non-coordinated nitrate ions or water molecules, leading to an array which interconnects the coordination polymer chains. The assembly can be interpreted in terms of repeating, copper(II)-containing sheets, each of which is made up of cyclic building blocks. Part of one sheet is shown in Figure 5-16, and comprises two differently-sized macrocyclic units (Table 10).

Table 10 Hydrogen-bonded O...O interactions present in the macrocyclic motifs in $\{(\text{H}_2\text{O})(\text{NO}_3)_2\text{CuFe}(\textbf{9})_2\}_2(\text{NO}_3)_4 \cdot 2.15\text{MeCN} \cdot 5.85\text{H}_2\text{O}\}_{\text{n}}$ (see Figure 5-16)

Small ring		Large ring	
Contacts ^a	Distance / Å	Contacts ^a	Distance / Å
O3...O17(ii)	2.901(6)	O3...O17(ii)	2.901(6)
O7...O17	2.711(5)	O5...O34	2.99(1)
O17...O24	2.915(5)	O30...O34	2.79(1)
O16...O24	2.969(5)	O32...O32(i)	2.95(1)
O16...O10(iv)	2.884(5)		
O14(iv)...O16(ii)	2.694(5)		

^a Symmetry codes: see Figure 5-16.

The nitrate ion containing atoms N26, O30, O31 and O32 is disordered over two sites (modelled with 65 and 35% occupancies) and atom O32 is also common to a disordered water molecule involving atoms O32 (35%) and O34 (65%). For clarity, Figure 5-16 shows only the major occupancy positions of the nitrate ion, and atom O34 for the position of the H₂O molecule. Each sheet is equivalent, but sheets are offset with respect to one another and are related as illustrated in Figure 5-17.

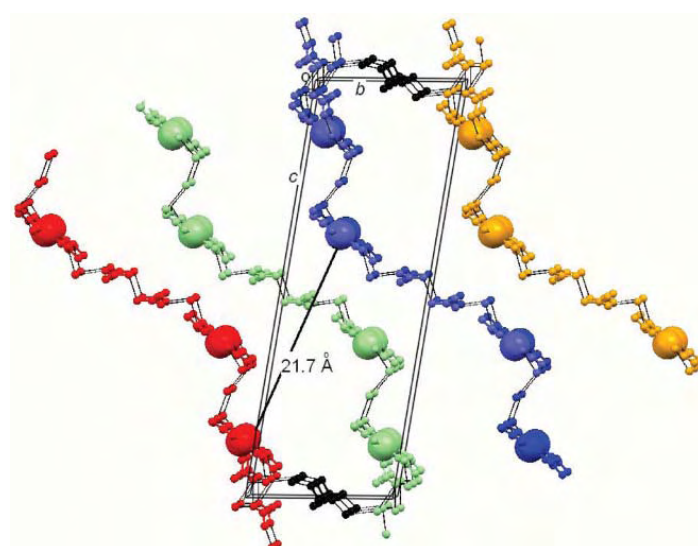


Figure 5-17 Four adjacent hydrogen-bonded sheets in $\{(\text{H}_2\text{O})(\text{NO}_3)_2\text{CuFe}(\textbf{9})_2\}_2(\text{NO}_3)_4 \cdot 2.15\text{MeCN} \cdot 5.85\text{H}_2\text{O}\}_{\text{n}}$. The Cu(II) centres are shown in space-filling representation, and nitrate ions and water O atoms in ball-and-stick representation. View approximately down the *a*-axis.

Hydrogen bonded chains shown in black connect adjacent sheets. Alternate sheets are connected via the polymer chains, indicated by the Cu...Cu separation of 21.699(3) Å.

Figure 5-17 shows a view of the unit cell down the crystallographic a axis, with parts of four adjacent sheets. The only part of the coordination polymers included in this diagram are the coordination spheres of the copper(II) centres. Adjacent sheets are connected via hydrogen-bonded $[\text{NO}_3^-]$ ions and H_2O molecules (shown in black), while alternate sheets are connected through the ...Cu{Fe(9)₂}Cu... chain of the coordination polymer. Each ...Cu{Fe(9)₂}Cu... chain is threaded through a hydrogen-bonded macrocycle. All sheets in the network are interconnected, and the system is not interpenetrating.^{158, 376-378} The topology of the network is shown in Figure 5-18, with the coordination polymer chains and hydrogen bonded sheets highlighted in yellow and red respectively.

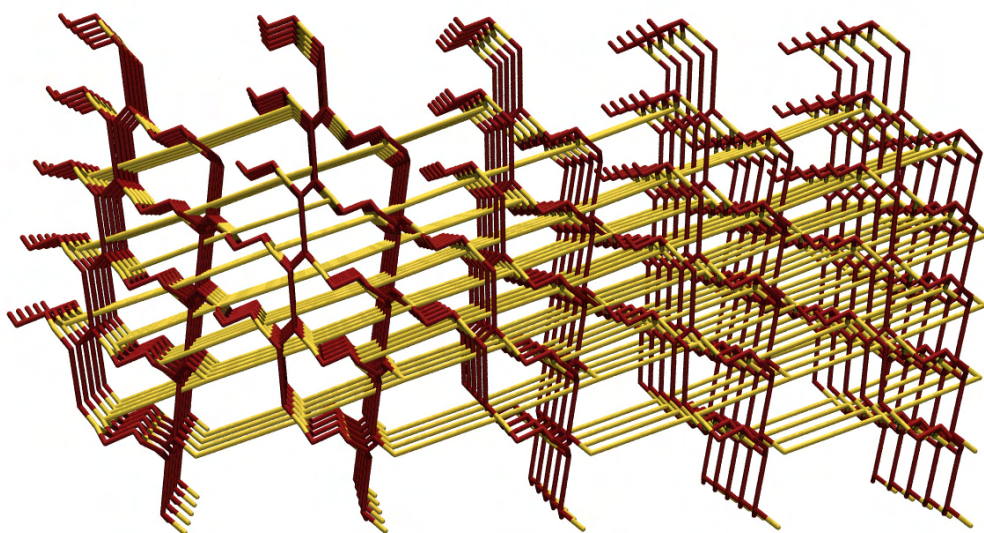
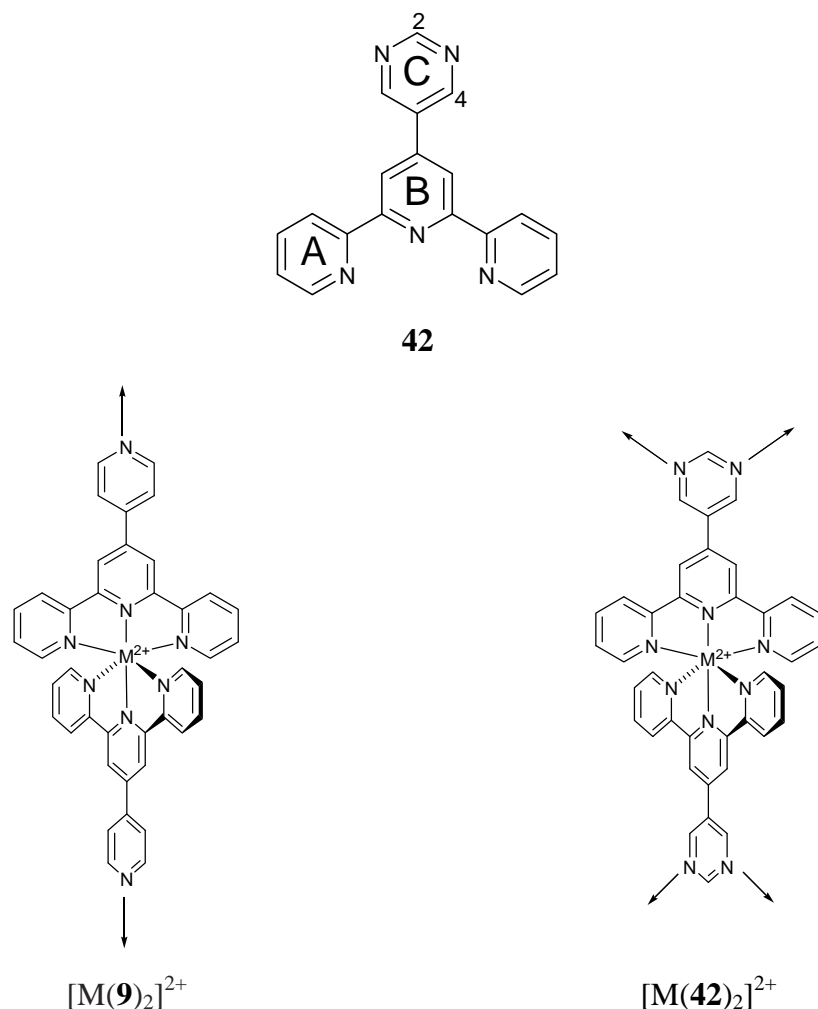


Figure 5-18 Topology of the hydrogen-bonded network through which coordination polymer chains are threaded in $\{(\text{H}_2\text{O})(\text{NO}_3)_2-\text{CuFe(9)}_2\}(\text{NO}_3)_4 \cdot 2.15\text{MeCN} \cdot 5.85\text{H}_2\text{O}\}_{\text{n}}$.

5.4. Two-dimensional coordination sheets



Scheme 11 Relationship between the directed coordination patterns of the homoleptic complexes of **9** and **42**.

Coordination networks formed by pyrimidine-bridged metal centres have been the topic of recent research efforts, a particular target being the development of magnetic materials. Pyrimidine bridged networks involving silver(I),^{287, 368, 379-382} copper(I),^{383, 384} and copper(II)^{95, 383, 385-389} have proved to be especially popular, although a range of other pyrimidine-based metal-containing networks^{368, 390-393} have also been reported. Many of these systems contain ligands with multiple metal ion-binding domains, but to date, none has included redox-active and luminescent $\{M(tpy)_2\}^{69}$ domains which could potentially be used as luminescent sensors or switches. (Scheme 1). Herein, is reported the synthesis of iron(II) and ruthenium(II) homoleptic complexes of 4'- (5-pyrimidinyl)-2,2':6',2''-terpyridine, **42**, and demonstrate that $[Ru(42)_2]^{2+}$ can be incorporated into a

two-dimensional coordination network bridged by copper(II) centres. In order to explore the utility of $[M(\mathbf{42})_2]^{2+}$ complexes as building blocks in the assembly of supramolecular architectures, we decided to study the reaction of $[Ru(\mathbf{42})_2][PF_6]_2$ with copper(II) chloride. Copper(II) was chosen on the basis that it is a flexible coordination centre allowing a plethora of distorted geometries and bond lengths and, as a consequence, the assembly of a coordination network would be primarily controlled by the spatial properties of the $[Ru(\mathbf{42})_2]^{2+}$ cation rather than the constraints of the second metal centre. Furthermore, the choice of the d⁹ centre allows the design of materials with emergent (magnetic) properties. Slow diffusion of a 5 : 1 MeCN : H₂O solution of CuCl₂·2H₂O into a similar solution of $[Ru(\mathbf{42})_2][PF_6]_2$ produced brown/black crystals of $\{[Ru(\mathbf{42})_2][CuCl_2(OH_2)] [CuCl_3]Cl \cdot MeCN \cdot 7H_2O\}_n$. The $[Ru(\mathbf{42})_2]^{2+}$ cations are connected through the pendant pyrimidine nitrogen atoms to copper(II) centres to form a (6,3) net (Fig. 2) which lies in the crystallographic ac plane. The local environment around each ruthenium(II) centre is not significantly different from that in $\{2[Ru(\mathbf{42})_2][PF_6]_2\} \cdot MeCN \cdot H_2O$ (see previous chapter) except for the extent to which each pyrimidine ring is twisted out of the plane of the tpy domain to which it is attached.

In $\{[Ru(\mathbf{42})_2][CuCl_2(OH_2)] [CuCl_3]Cl \cdot 3MeCN \cdot 7H_2O\}_n$, the angles between least squares planes of the rings containing N2 and N7/N8, and N5 and N9/ N10 are 41.0(2) and 40.5(2)^o, compared to 12.0(2) and 36.8(2)^o in $\{2[Ru(\mathbf{42})_2][PF_6]_2\} \cdot MeCN \cdot H_2O$. The near 45^o twist angles minimize steric repulsions between the pendant pyrimidine ring and the tpy domain to which it is bonded, while the near coplanarity of each pair of pyrimidine substituents in a $[Ru(\mathbf{42})_2]$ unit (angle between the least squares planes = 8.6(2)^o) in the coordination polymer is required to form a near-planar sheet (Figure 5-19).

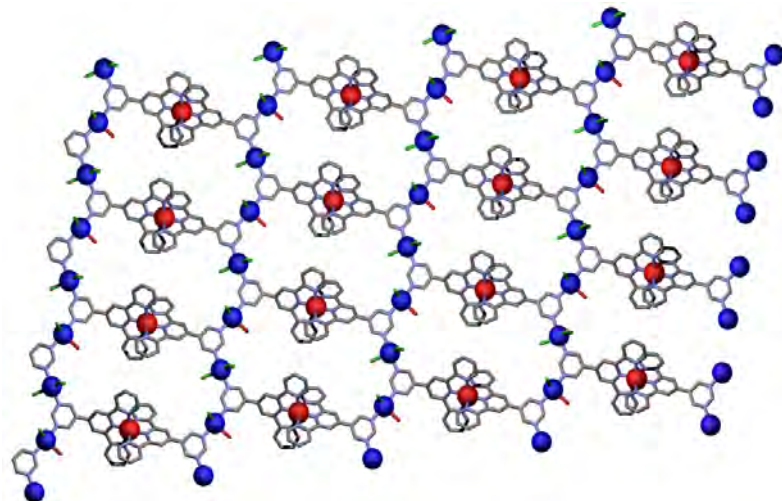


Figure 5-19 A single two-dimensional sheet in $\{[\text{Ru}(42)_2][\text{CuCl}_2(\text{OH}_2)][\text{CuCl}_3]\text{Cl}\cdot 3\text{MeCN}\cdot 7\text{H}_2\text{O}\}_n$; Ru(II) centres in red, Cu(II) in blue. Hydrogen atoms, solvent molecules and anions omitted.

The sheets are stacked together in an offset arrangement, with the closest direct contact between sheets involving Cl/H–C non-classical hydrogen bonds and Cl/C_{aromatic} interactions (Figure 5-20). Aryl embraces between [Ru(42)₂] domains of adjacent sheets are not observed, reminiscent of the one-dimensional coordination polymer of $\{(\text{H}_2\text{O})(\text{NO}_3)_2\text{CuFe}(9)_2\}\text{N}$ where adjacent chains are prevented from participating in embraces by hydrogen bonded networks of water and anions.

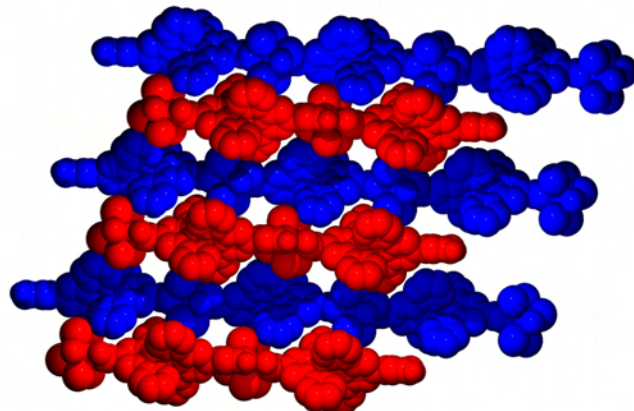


Figure 5-20 Alternating stacking of two-dimensional sheets in $\{[\text{Ru}(42)_2][\text{CuCl}_2(\text{OH}_2)][\text{CuCl}_3]\text{Cl}\cdot 3\text{MeCN}\cdot 7\text{H}_2\text{O}\}_n$. Closest inter-sheet contacts (C–H, C/Cl (Å), C–H/Cl (deg)) C2–H21/Cl1c = 2.80, 3.472(4), 127; C3–H31/Cl3c = 2.79, 3.740(4), 169; C18–H181/Cl4d = 2.81, 3.625(5), 143; C14–H141/Cle = 2.91, 3.846(3), 166; Cl/C_{aromatic} (Å) Cl2/C20e = 3.297(3), Cl2/C37y = 3.341(4), Cl2/C15f = 3.391(4), Cl4/C36g = 3.393(3), Cl5/C5c = 3.308(3), Cl5/C30c = 3.303(4), Cl5/C36g = 3.495(3). Symmetry codes: c = -x, -y, 2 - z; d = -x, 1 - y, 2 - z; e = 1 - x, 1 - y, 2 - z; f = 1 + x, y, 1 + z; g = x, y, 1 + z.

There are two structurally distinct copper(II) centres in $\{[\text{Ru}(42)_2][\text{CuCl}_2(\text{OH}_2)][\text{CuCl}_3]\text{Cl}\cdot 3\text{MeCN}\cdot 7\text{H}_2\text{O}\}_n$, a CuCl_3N_2 coordination sphere for

Cu1 and a CuCl₂N₂O environment for Cu2 (Figure 5-21). Both are distorted trigonal bipyramidal with near linear N – Cu – N units. The two-dimensional sheets have a low overall charge, +1 per ruthenium(II), a goal for the development of useful supramolecular materials.²⁶⁶ Despite the relatively large number of copper(II) bridged pyrimidine-based structures in the Cambridge Structural Database (217 pyrimidine–Cu–pyrimidine, 378 pyrimidine–Cu),¹⁹⁴ to the best of our knowledge, none contains either a pyrimidine–CuX₃–pyrimidine or pyrimidine– CuX₂(OH₂)–pyrimidine (X = halide) motif.

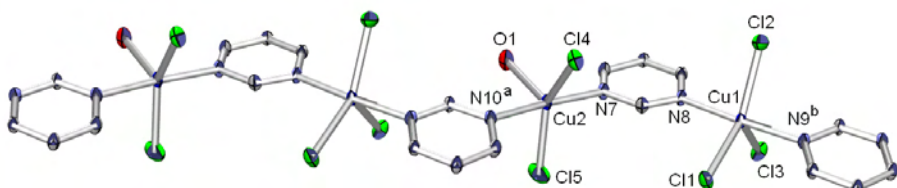


Figure 5-21 Pyrimidine rings in $[\text{Ru}(42)]_2^{2+}$ bridge copper(II) centres in $\{[\text{Ru}(42)]_2[\text{CuCl}_2(\text{OH}_2)][\text{CuCl}_3]\text{Cl}\cdot 3\text{MeCN}\cdot 7\text{H}_2\text{O}\}_n$; ellipsoids plotted at 50% probability level. Selected bond angles and lengths: Cu – Cl range 2.268(1)– 2.4699(9); Cu–N range 2.020(2) – 2.057(2), Cu2 – O1 = 2.239(2) Å; Cl1 – Cu1 – Cl2 = 135.12(4), Cl1 – Cu1 – Cl3 = 109.67(4), Cl2 – Cu1 – Cl3 = 115.21(4), N9b – Cu1 – N8 = 175.7(1), Cl4 – Cu2 – Cl5 = 147.53(5), N10a – Cu2 – N7 = 175.8(1), Cl4 – Cu2 – O1 = 114.91(8), Cl5 – Cu2 – O1 = 97.55(8)°. Symmetry code: a - x, y, 1 + z; b - 1 + x, y, 1 + z.

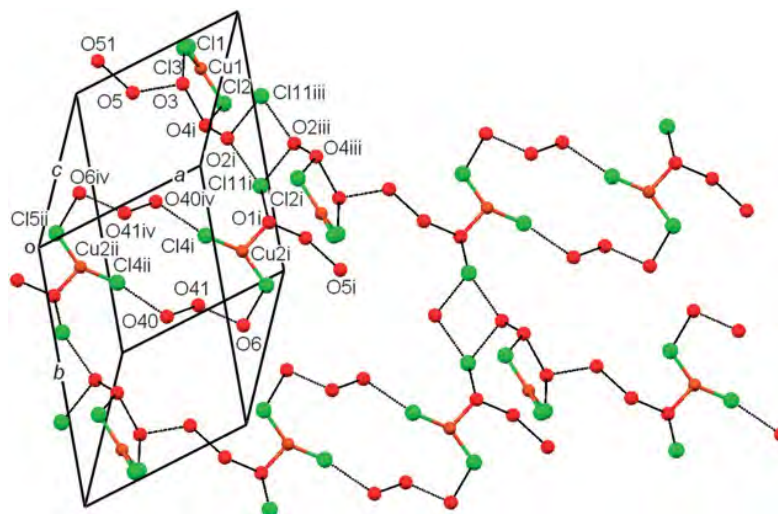


Figure 5-22 Part of one sheet of the hydrogen-bonded network in $\{[\text{Ru(42)}_2][\text{CuCl}_2(\text{OH}_2)][\text{CuCl}_3]\text{Cl}\cdot 3\text{MeCN}\cdot 7\text{H}_2\text{O}\}_n$. Symmetry codes: i = 1 -x, 1 -y, 2-z; ii = x, y, -1+z; iii = 1+x, y, z; iv = 1-x, 1-y, 1-z.

The non-coordinated chloride ion in $\{[\text{Ru(42)}_2][\text{CuCl}_2(\text{OH}_2)]$
 $[\text{CuCl}_3]\text{Cl}\cdot 3\text{MeCN}\cdot 7\text{H}_2\text{O}\}_{\text{n}}$ is involved in extensive hydrogen bonding between the two-dimensional coordination sheets which are connected by water molecules. The hydrogen-bonded networks involve both coordinated and non-coordinated water and

chloride ions (Figure 5-22), and they slice almost orthogonally through the coordination sheets as illustrated in Figure 5-23. Although the hydrogen bonded network shown in Figure 5-22 can be described in terms of a two-dimensional sheet, it is complicated by the fact that atoms O40 and O41 have partial (each modelled as 0.5) occupancies.

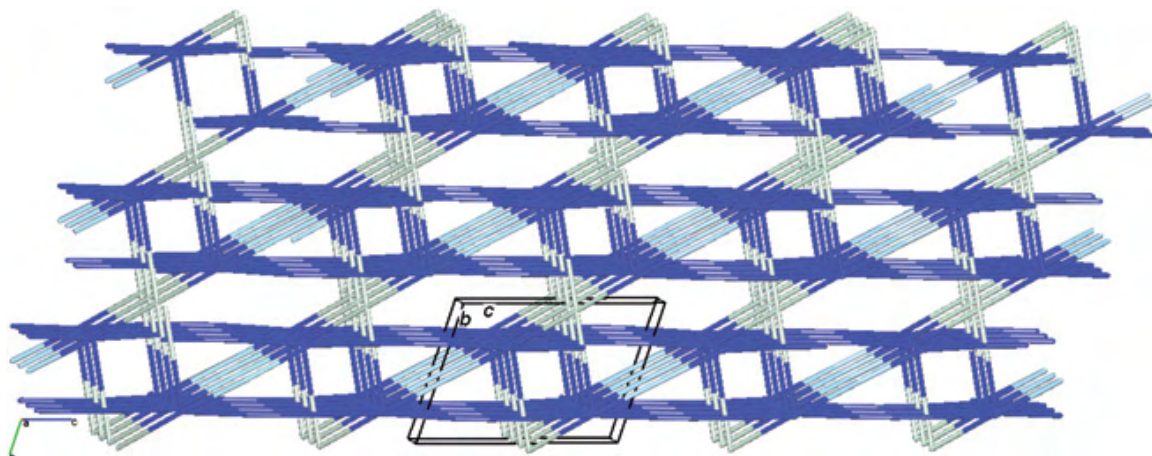


Figure 5-23 Interpenetrating networks of coordination polymer (in the ac plane) and hydrogen-bonded water molecules and chloride ions.

Magnetic measurements, and interpretation, were performed by Dr Tony Keene at the University of Bern. The magnetic susceptibility of $\{[\text{Ru(42)}_2][\text{CuCl}_2(\text{OH}_2)] [\text{CuCl}_3]\text{Cl}\cdot 3\text{MeCN}\cdot 7\text{H}_2\text{O}\}_n$ shows an increasing value on cooling from $1.3 \times 10^{-3} \text{ cm}^3 \text{ mol}^{-1}$ at 300 K to $135 \times 10^{-3} \text{ cm}^3 \text{ mol}^{-1}$ at 1.87 K. An inverse susceptibility plot shows linear behaviour above ~ 120 K, and fitting the Curie–Weiss equation to the data gave a Curie constant, $C = 0.416(1) \text{ cm}^3 \text{ K mol}^{-1}$ and a Weiss constant, $\theta = -2.3(5)$ K. The $\chi T(T)$ plot shows a linear behaviour above 120 K with an average value of $0.40 \text{ cm}^3 \text{ K mol}^{-1}$ before decreasing. Given the negative Weiss constant and the decreasing value of χT on cooling, it implies that there is a dominant antiferromagnetic interaction occurring in $\{[\text{Ru(42)}_2][\text{CuCl}_2(\text{OH}_2)][\text{CuCl}_3]\text{Cl}\cdot 3\text{MeCN}\cdot 7\text{H}_2\text{O}\}_n$. Inspection of the solid-state structure of $\{[\text{Ru(42)}_2][\text{CuCl}_2(\text{OH}_2)][\text{CuCl}_3]\text{Cl}\cdot 3\text{MeCN}\cdot 7\text{H}_2\text{O}\}_n$ shows that chains of $\{[\text{CuCl}_2(\text{H}_2\text{O})][\text{CuCl}_3] [\text{pyrimidine}]_2\}_\infty$ occur in the a -axis with the Cu atoms being connected through the pyrimidine rings. The bond spacings between the Cu atoms across the crystallographically independent pyrimidine rings are very similar, so for the treatment of the data, the polynomial for $S = \frac{1}{2}$ infinite antiferromagnetic chains by Feyerherm et al.³⁹⁴ will be appropriate (eqns (1) and (2), Figure 5-24).

$$H = -2J \sum_{i=1} (S_{Ai} \cdot S_{Ai+1}) \quad \text{eq. (1)}$$

$$\chi T = \frac{Ng^2\mu_B^2}{4k_B T} \cdot \frac{1 + 0.08516x + 0.23351x^2}{1 + 0.73382x + 0.13696x^2 + 0.53568x^3} \quad \text{eq. (2)}$$

where $x = |2J|/k_B T$.

Modelling the whole data set produces a poor fit and an unreasonably low g-value of 1.86. A feature at 7 K indicates the inclusion of an impurity species. By adjusting the data range to 15–300 K, the Feyerherm equation gives $g = 2.09(1)$ and $2J/k_B = -6.8(1)$ K. The g-value obtained is in good agreement with those derived from the Curie constant and the average high-temperature χT value (2.11 and 2.07, respectively).

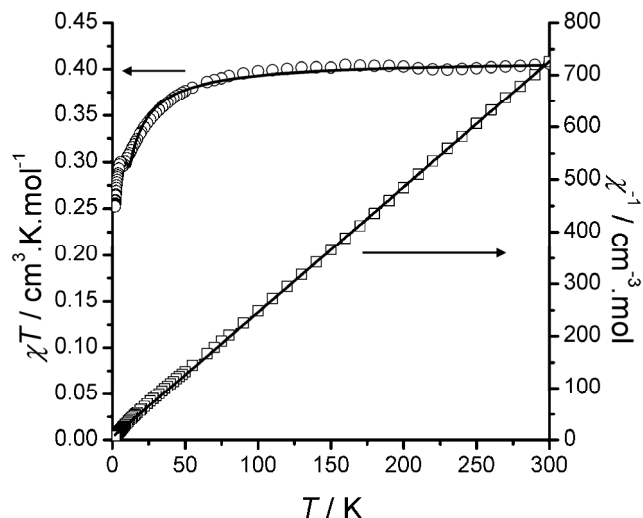


Figure 5-24 Plot of $\chi T(T)$ for $\{[\text{Ru(42)}_2][\text{CuCl}_2(\text{OH}_2)][\text{CuCl}_3]\text{Cl}\cdot 3\text{MeCN}\cdot 7\text{H}_2\text{O}\}_n$ (circles) with fit from Feyerherm equation between 15–300 K ($g = 2.09(1)$, $2J/k_B = -6.8(1)$ K) and of $\chi^{-1}(T)$ (squares) with Curie-Weiss fit ($C = 0.416(1)$ $\text{cm}^3 \text{K mol}^{-1}$ and $\theta = -2.3(5)$ K).

5.5. Conclusions

Under the conditions used for crystallization ($[\text{Fe(9)}_2]^{2+}$ with FeCl_3 , MeCN, H_2O and NH_4SCN , or $[\text{Fe(9)}_2]^{2+}$ with $\text{Fe}(\text{ClO}_4)_2$, EtOH, H_2O and NH_4SCN), one pendant pyridyl group of $[\text{Fe(9)}_2]^{2+}$ is protonated and the conjugate acid $[\text{Fe(9)(H9)}]^{3+}$ assembles into a one-dimensional hydrogen bonded polymer. In $[\text{Fe(9)(H9)}][\text{Fe}(\text{NCS})_6]\cdot 2\text{H}_2\text{O}$, $[\text{Fe(9)(H9)}][\text{Fe}(\text{NCS})_6]$ MeCN and $[\text{Fe(9)(H9)}][\text{ClO}_4]_3$ EtOH, the cationic chains lie parallel to one another, but are significantly closer together in the perchlorate salt, thus permitting the evolution of $[\text{Fe(tpy)}_2]$ embraces. In the hexakis thiocyanato iron(III) salt, the steric demands of the anions force the cationic chains apart, and the dominant interionic interactions are weak S...H–C_{tpy} contacts. The analogous hydrogen-bonded polymer with Ru(II), $[\text{Ru(9)(H9)}][\text{Fe}(\text{NCS})_6]\cdot 1.25\text{H}_2\text{O}$ was also prepared by colleagues at the University of Sydney¹⁶⁵ with the same packing arrangement, establishing the reproducibility of the packing motif.

We have demonstrated for the first time that complexes of the type $[\text{M(9)}_2]$ can not only act as an extended 4,4'-bipyridine in alkylation and protonation reactions, but also in the formation of coordination networks. The first two examples, using silver(I) and copper(II), have been successfully prepared, exemplifying $[\text{Fe(9)}_2]^{2+}$ as an expanded 4,4'-bipyridine ligand. The packing arrangements differ significantly, offering the opportunity to use solvent and anions choice to alter crystal packing for these types of structures. Following the publication of this structure, a related structure using a homoleptic ruthenium(II) complex of 4'-(3-pyridyl)-2,2':6',2"-terpyridine and silver(I) was reported,²⁹¹ showing the principle of these assemblies is not limited to the structures presented here. Extending the principle to the next dimension, the 4-connector $[\text{Ru(42)}_2]$ has been successfully used to assemble two-dimensional sheets with copper(II) illustrating the general nature of the ‘expanded ligand’ approach.

5.6. Experimental

Hydrogen bonded polymers

[Fe(**9**)(H**9**)][Fe(NCS)₆]·2H₂O and [Fe(**9**)(H**9**)][Fe(NCS)₆]·MeCN

Crystals of [Fe(**9**)(H**9**)][Fe(NCS)₆]·2H₂O or [Fe(**9**)(H**9**)][Fe(NCS)₆]·MeCN were grown by slow diffusion of an MeCN–H₂O solution of FeCl₃·6H₂O and NH₄SCN (1 : 2) into an MeCN–H₂O solution of [Fe(**9**)₂][PF₆]₂ over a period of ~3 weeks. The same complex crystallized as a hydrate or with MeCN solvate from a number of different experiments using different solution concentrations, for example, found: C, 50.55; H, 2.77; N, 18.68. C₄₆H₂₉Fe₂N₁₄S₆·CH₃CN·H₂O requires C, 50.53; H, 3.00; N, 18.41%.

[Fe(**9**)(H**9**)][ClO₄]₃·EtOH

Crystals of [Fe(**9**)(H**9**)][ClO₄]₃·EtOH were grown in an H-tube by slow diffusion of an EtOH–H₂O solution of Fe(ClO₄)₂·9H₂O and NH₄SCN (1 : 2) into an MeCN–H₂O solution of [Fe(**9**)₂][PF₆]₂ over a period of 2 months. Caution: perchlorate salts are potentially explosive.

Data for [Fe(**9**)(H**9**)][Fe(NCS)₆]·2H₂O and [Fe(**9**)(H**9**)][Fe(NCS)₆]·MeCN were collected on an Enraf Nonius Kappa CCD instrument; data reduction, solution and refinement used the programs COLLECT,²⁵² SIR92,²⁵³ DENZO/SCALEPACK²⁵⁶ and CRYSTALS.²⁵⁷ Data for [Fe(**9**)(H**9**)][ClO₄]₃·EtOH were collected on a Bruker SMART 1000 CCD diffractometer; data reduction, solution (by Patterson map) and refinement used the programs SAINT,⁷ SHELXS-97 and SHELXL-97.^{7, 258}

Crystal data for [Fe(**9**)(H**9**)][Fe(NCS)₆]·2H₂O

C₄₆H₃₃Fe₂N₁₄O₂S₆, M = 1117.95, orthorhombic, space group *Pbcn*, *a* = 13.1562(1), *b* = 20.3741(2), *c* = 18.8557(2) Å, V = 5054.19(8) Å³, Z = 4, *D_c* = 1.469 Mg m⁻³, μ (Mo K α) = 0.875 mm⁻¹, T = 173 K, 6034 reflections collected. Refinement of 3836 reflections (333 parameters) with I < 3.0σ(I) converged at final *R*1 = 0.0279 (*R*1 all data = 0.0445), *wR*2 = 0.0319 (*wR*2 all data = 0.0463), *gof* = 1.083.

Crystal data for [Fe(**9**)(H**9**)][Fe(NCS)₆]·MeCN

$C_{48}H_{32}Fe_2N_{15}S_6$, $M = 1122.97$, orthorhombic, space group $Pbcn$, $a = 13.3057(1)$, $b = 20.3495(2)$, $c = 18.4014(2)$ Å, $V = 4982.44(8)$ Å³, $Z = 4$, $D_c = 1.497$ Mg m⁻³, $\mu(\text{Mo K}_\alpha) = 0.886$ mm⁻¹, $T = 173$ K, 5914 reflections collected. Refinement of 4094 reflections (340 parameters) with $I < 3.0\sigma(I)$ converged at final $R1 = 0.0701$ ($R1$ all data = 0.0910), $wR2 = 0.0414$ ($wR2$ all data = 0.0432), $gof = 0.906$.

Crystal data for $[\text{Fe}(\mathbf{9})(\text{H9})][\text{ClO}_4]_3 \cdot \text{EtOH}$

$C_{42}H_{35}\text{Cl}_3\text{FeN}_8\text{O}_{13}$, $M = 1021.98$, monoclinic, space group $P2_1/c$, $a = 14.367(11)$, $b = 16.290(13)$, $c = 18.720(15)$ Å, $b = 105.060(14)^\circ$, $V = 4231(6)$ Å³, $Z = 4$, $D_c = 1.604$ Mg m⁻³, $\mu(\text{Mo K}_\alpha) = 0.625$ mm⁻¹, $T = 100(2)$ K, 41745 reflections collected. Refinement of 10085 reflections (612 parameters) with $I < 2.0\sigma(I)$ converged at final $R1 = 0.0615$ ($R1$ all data = 0.1488), $wR2 = 0.1120$ ($wR2$ all data = 0.1390), $gof = 0.974$.

Ag(I) polymer

Deep red X-ray quality plates were grown via slow diffusion of a 5 : 2 MeCN : H₂O solution of AgNO₃ into 5 : 2 MeCN : H₂O [Ru(**9**)₂][PF₆]₂ in a H-cell over one week. Analytical data for crystalline material dried in vacuum; Found: C, 45.3; H, 3.1; N, 14.5. Calculated for C₄₀H₂₈AgN₁₁O₉.2H₂O C, 45.7; H, 3.1; N, 14.7%

Crystal data and refinement

$C_{44}H_{36}\text{AgN}_{13}\text{O}_{10}\text{Ru}$, $M = 1115.80$, $T = 150(2)$ K, $\lambda = 0.71073$ Å, triclinic, space group $P-1$, $a = 8.827(3)$ Å, $b = 11.675(4)$ Å, $c = 21.160(7)$ Å, $\alpha = 96.847(6)^\circ$, $\beta = 100.776(6)^\circ$, $\gamma = 102.133(6)^\circ$, $V = 2065.7(11)$ Å³, $Z = 2$, $D_c = 1.794$ Mg m⁻³, $\mu = 0.921$ mm⁻¹, $F(000) = 1124$, Data/restr./param. 9540/1/610, GOOF on F2 = 1.041, $R1[I < 2\sigma(I)] = 0.0465$, $wR2[I < 2\sigma(I)] = 0.1289$.

Cu(II) polymer

[{(H₂O)(NO₃)₂CuFe(**9**)₂}₂(NO₃)₄·2.15MeCN·5.85H₂O]_n X-Ray quality single crystals (purple plates) of [{(H₂O)(NO₃)₂-CuFe(**9**)₂}₂(NO₃)₄·2.15MeCN·5.85H₂O]_n were grown by slow diffusion of an MeCN–H₂O (4 : 1) solution of Cu(NO₃)₂·3H₂O into an MeCN–H₂O (4 : 1) solution of [Fe(**9**)₂][PF₆]₂ over a period of 1 month. Insufficient crystalline material was obtained for elemental analysis.

Crystal structure determinations Data were collected on an Enraf Nonius Kappa CCD instrument; data reduction, solution and refinement used the programmes COLLECT,²⁵² SIR92,²⁵³ DENZO/ SCALEPACK²⁵⁶ and CRYSTALS.²⁵⁷ Hydrogen atoms on the water molecules could not be localized. The structure has been analysed using Mercury, ver. 1.4.2.

Crystal data for $\{(\text{H}_2\text{O})(\text{NO}_3)_2\text{CuFe(9)}_2\}_2(\text{NO}_3)_4 \cdot 2.15\text{MeCN} \cdot 5.85\text{H}_2\text{O}\}_{\text{n}}$
 $\text{C}_{84}\text{H}_{56}\text{Cu}_2\text{Fe}_2\text{N}_{24}\text{O}_{24}, M = 2201.88$, triclinic, space group $P-1$, $a = 8.6581(3)$, $b = 14.234(2)$, $c = 39.083(6)$ Å, $\alpha = 97.68(1)$, $\beta = 95.210(5)$, $\gamma = 104.377(5)^\circ$, $V = 4585.3(9)$ Å³, $Z = 2$, $D_c = 1.586$ Mg m⁻³, $\mu(\text{Mo K}_\alpha) = 0.868$ mm⁻¹, $T = 173$ K, 20844 reflections collected. Refinement of 14907 reflections (1414 parameters) with $I < 1.5\sigma(I)$ converged at final $R1 = 0.0685$ ($R1$ all data = 0.0997), $wR2 = 0.0602$ ($wR2$ all data = 0.0880), $gof = 1.024$.

Cu(II) coordination sheets

Data were collected on an Enraf Nonius Kappa CCD instrument; data reduction, solution and refinement used the programmes COLLECT,²⁵² SIR92,²⁵³ DENZO/SCALEPACK²⁵⁶ and CRYSTALS.²⁵⁷

Synthesis of $\{[\text{Ru(42)}_2]-[\text{CuCl}_2(\text{H}_2\text{O})][\text{CuCl}_3]\}(\text{MeCN})_3(\text{H}_2\text{O})_7\}_{\text{n}}$

A 4:1 MeCN/H₂O solution of [Ru(42)₂](PF₆)₂ was diffused slowly into a MeCN/H₂O solution (4:1) CuCl₂ over a period of 2 weeks to give intensely coloured block-like crystals.



$\text{C}_{44}\text{H}_{48}\text{Cl}_6\text{Cu}_2\text{N}_{13}\text{O}_8\text{Ru}$, $M = 1327.83$, triclinic, space group $P-1$, $a = 11.6465(1)$, $b = 14.5947(2)$, $c = 19.2504(2)$ Å, $\alpha = 98.9173(6)$, $\beta = 105.1056(6)$, $\gamma = 112.3198(6)^\circ$, $V = 2801.73(6)$ Å³, $Z = 2$, $D_c = 1.574$ Mg m⁻³, $\mu(\text{Mo K}_\alpha) = 1.365$ mm⁻¹, $T = 173$ K, 13380 reflections collected. Refinement of 10669 reflections (713 parameters) with $I > 3.0\sigma(I)$ converged at final $R1 = 0.0538$ ($R1$ all data = 0.0652), $wR2 = 0.0517$ ($wR2$ all data = 0.0549), $R_{\text{int}} = 0.031$, $gof = 1.000$. CCDC 681311.

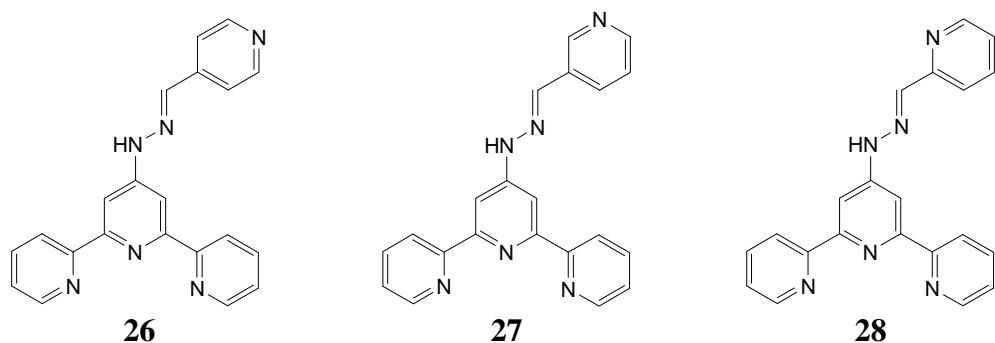
Magnetic measurements

Magnetic susceptibility measurements were performed on a Quantum Designs MPMS SQUID-XL magnetometer in an applied field of 5000 G from 300–1.87 K. 2.19 mg of $\{[\text{Ru}(\mathbf{42})_2] [\text{CuCl}_2(\text{OH}_2)][\text{CuCl}_3]\text{Cl}\cdot 3\text{MeCN}\cdot 7\text{H}_2\text{O}\}_n$ were prepared in a Saran film bag and placed in a plastic straw for insertion into the measurement chamber of the SQUID. Diamagnetic corrections were applied for the foil and the sample, initially using the approximate formula³⁹⁵ $0.4 \times \text{molecular weight} \times 10^{-6} \text{ cm}^3 \text{ mol}^{-1}$ and then iteratively adjusted by producing a linear plot in the high-temperature χT data ($560 \times 10^{-6} \text{ cm}^3 \text{ mol}^{-1}$).

Chapter 6 4'-Pyridyl hydrazone functionalised 2,2':6',2"-terpyridine ligands and their Fe(II) and Ru(II) complexes

6.1. General considerations

This chapter combines the use of 4'-hydrazone functionalised terpyridine ligands which have been presented in Chapter 2 with the ‘expanded ligands’ principles outlined in Chapter 3. The pyridyl hydrazone derivatives **1** to **3** and their Fe(II) and Ru(II) complexes were prepared. These complexes are the first examples of the use of M(tpy)₂ groups with additional donors attached by non-aromatic spacers.^{‡‡}



6.2. Synthesis of ligands

Ligands **26** to **28** were prepared and characterized in Chapter 2.

6.3. Synthesis and characterisation of Fe(II) complexes

Each of ligands **26** to **28** (L) reacts with FeCl₂ · 4H₂O in ethanol at room temperature to yield purple homoleptic complexes [FeL₂]²⁺ which were isolated as the hexafluorophosphate salts in >75% yields. The electrospray mass spectrum of each complex showed two peak envelopes at *m/z* 759 and 380 (base peak) which were assigned to [FeL₂ – 2PF₆ – H]⁺ and [FeL₂]²⁺, respectively. The isotope patterns were consistent with those simulated. The assignment of signals in the ¹H and ¹³C NMR spectra of the complexes was achieved by using COSY, NOESY, HMQC and HMBC techniques. The resonances for the tpy protons in the ¹H NMR spectra of [Fe(**26**)₂][PF₆]₂, [Fe(**27**)₂][PF₆]₂ and [Fe(**28**)₂][PF₆]₂ show little variation (Figure 6-1).

^{‡‡} Previous examples of M(tpy)₂ complexes with additional pendant donors are given in Chapter 4.

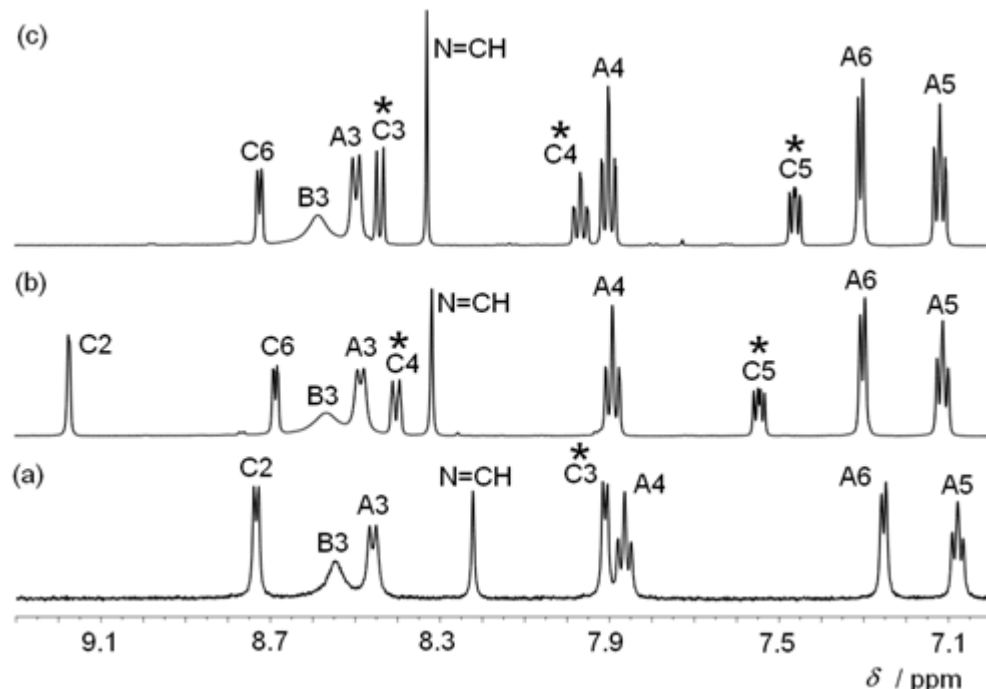


Figure 6-1 500 MHz ^1H NMR spectra of the complexes (a) $[\text{Fe}(\mathbf{1})_2][\text{PF}_6]_2$, (b) $[\text{Fe}(\mathbf{2})_2][\text{PF}_6]_2$ and (c) $[\text{Fe}(\mathbf{3})_2][\text{PF}_6]_2$ (500 MHz, CD_3CN , room temperature). The signals that are affected upon protonation of the complexes are marked with asterisks. See Scheme 3 for atom numbering.

The broadened signal for proton $\text{H}^{\text{B}3}$ is indicative of an increased energy barrier to rotation about the $\text{C}_{\text{pyridine}}-\text{N}$ bond on the NMR timescale compared to that in the free ligands. This dynamic process has been discussed in detail for a series of 4'-hydrazone-2,2':6',2"-terpyridine ligands and their protonated analogues (Chapter 2). NOESY experiments confirmed the *trans*-configuration of the imine bond in all cases. The reduced symmetry of the coordinated ligand on going from $[\text{Fe}(\mathbf{26})_2][\text{PF}_6]_2$ to $[\text{Fe}(\mathbf{2})_2][\text{PF}_6]_2$ and $[\text{Fe}(\mathbf{28})_2][\text{PF}_6]_2$ is apparent in the increase in the number of signals for protons on ring C. The addition of trifluoroacetic acid to CD_3CN solutions of $[\text{Fe}(\mathbf{26})_2][\text{PF}_6]_2$, $[\text{Fe}(\mathbf{27})_2][\text{PF}_6]_2$ and $[\text{Fe}(\mathbf{28})_2][\text{PF}_6]_2$ results in protonation of the pendant pyridine nitrogen atoms in each complex. This is deduced from changes in the ^1H NMR spectra. When $[\text{Fe}(\mathbf{26})_2][\text{PF}_6]_2$ is treated with trifluoroacetic acid, the signal for pyridine proton $\text{H}^{\text{C}3}$ shifts from δ 7.93 to 8.48 ppm. No other signals are significantly perturbed. Similarly, when trifluoroacetic acid is added to $[\text{Fe}(\mathbf{27})_2][\text{PF}_6]_2$ and $[\text{Fe}(\mathbf{28})_2][\text{PF}_6]_2$, only the pyridine protons attached to carbon atoms that are not adjacent to the nitrogen centre³⁹⁶ are affected (Figure 6-1b and c). The site of protonation in $[\text{Fe}(\mathbf{27})_2]^{2+}$ was also confirmed by a single crystal structural determination of $[\text{Fe}(\text{H27})(\mathbf{27})][\text{PF}_6]_3 \cdot 3.5\text{MeCN} \cdot 2.5\text{H}_2\text{O}$ (see later). Protonation also has a significant effect on the electronic absorption spectra of the purple iron(II) complexes. Aqueous acetonitrile

solutions of the unprotonated complexes exhibit an MLCT band at around 578 nm, as well as intense absorptions at higher energies arising from ligand $\pi^* \leftarrow \pi$ transitions (Table 11).

Table 11 UV-vis spectroscopic data for hexafluorophosphate salts of $[\text{FeL}_2]^{2+}$ in 1 : 5 MeCN : H₂O solution, and after the addition of excess CF₃CO₂H. Absorption λ_{\max} / nm ($\epsilon_{\max} / 10^3 \text{ dm}^3 \text{ mol}^{-1} \text{ cm}^{-1}$)

	Not protonated		Protonated	
	Ligand $\pi^* \leftarrow \pi$	MLCT	Ligand $\pi^* \leftarrow \pi$	MLCT
$[\text{Fe(26)}_2](\text{PF}_6)_2$	240 (31.4 sh), 274 (39.5), 287 (43.6), 297 (44.2), 308 (46.3), 355 (54.5),	520 (14.6, sh), 579 (26.5)	240 (45.3 sh) 279 (45.9), 309 (48.6), 329 (38.0), 369 (58.6), 430 (18.2)	520 (14.6 sh), 594 (36.2)
$[\text{Fe(27)}_2](\text{PF}_6)_2$	236 (38.8), 276 (42.5 sh), 285 (49.6), 308 (46.0), 357 (49.1),	520 (12.5 br), 578 (21.8)	240 (42.5), 275 (40.9 sh), 284 (42.8), 297 (44.6), 308 (47.0), 349 (50.8),	520 (13.9 br), 581 (26.5)
$[\text{Fe(28)}_2](\text{PF}_6)_2$	238 (40.4), 276 (45.2 sh,), 285 (49.4), 298 (47.3), 308 (49.4), 357 (57.0),	520 (14.4 br), 578 (26.1)	240 (39.8), 270 (37.0 sh), 283 (42.6), 307 (43.2), 368 (52.5), 430 (br 15.3)	520 (13.9 br), 591 (34.0).
$[\text{Ru(26)}_2](\text{PF}_6)_2$	236 (38.3), 273 (44.2), 286 (45.6), 300 (50.8), 355 (37.8)	506 (25.5)	272 (48.3), 301 (46.1), 354 (33.5), 410 (18.1 br)	523 (32.7)
$[\text{Ru(27)}_2](\text{PF}_6)_2$	234 (36.2), 273 (39.0 sh), 287 (45.8 sh), 300 (52.6), 355 (41.7)	508 (25.0)	273 (36.6), 300 (50.7), 335 (38.4),	512 (29.2).

Upon the addition of trifluoroacetic acid, a visual colour change from purple to blue is observed, consistent with the observation that the MLCT band shifts to lower energy (Table 11). Spectrophotometric titrations showed that an excess of acid was required to reach the fully protonated state. For conversion of $[\text{Fe(26)}_2]^{2+}$ to $[\text{Fe(H26)}_2]^{4+}$, approximately 50 equivalents of TFA were required, whereas for the corresponding protonations of $[\text{Fe(27)}_2]^{2+}$ and $[\text{Fe(28)}_2]^{2+}$, approximately 200 and 300 equivalents of acid were needed. This is somewhat surprising as the pKa values of 2, 3 and 4-picoline are 5.96, 5.63 and 5.98 (H₂O)³⁹⁷ and 6.11, 5.82, 6.16 (MeOH).³⁹⁸ That is, both 2- and 4-substituted pyridine are expected to have very similar pKa values, with the 3-pyridyl derivative being lower. However, for the complexes presented here the 2-pyridyl derivative has the lowest pKa by a substantial margin, indicating that steric effects must play a significant role. The possibility of intramolecular hydrogen bonding resulting from the formation of the *cis*-isomer (Figure 6-2) was eliminated by NOESY NMR experiments which showed strong cross peaks between the amino NH and imino CH, confirming only the *trans*-isomer is formed.

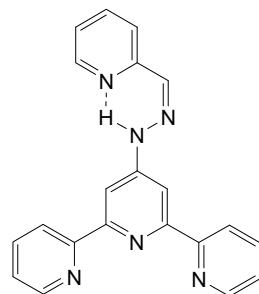


Figure 6-2 Possible intramolecular hydrogen bonding of **28** if the *cis*-isomer was formed

The UV-vis spectra of $[\text{Fe(26)}_2](\text{PF}_6)_2$, $[\text{Fe(27)}_2](\text{PF}_6)_2$ and $[\text{Fe(28)}_2](\text{PF}_6)_2$ with and without TFA addition are shown in Figure 6-4. The most notable feature is that on protonation, both the 2-pyridyl (**28**) and 4-pyridyl (**26**) derivatives experience similar shifts of the MLCT band to lower energy (13nm and 15nm respectively), whereas the 3-pyridyl derivative (**27**) shows only a small shift in wavelength (3nm). The origin of these changes can be explained with simple resonance structures (Figure 6-3). In the case of the 2-pyridyl and 4-pyridyl derivatives, the positive charge on the nitrogen can be delocalised as far as the tpy. However, in the case of the 3-pyridyl derivative, the charge is isolated on the pendant ring, accounting for the less significant influence on the MLCT absorption.

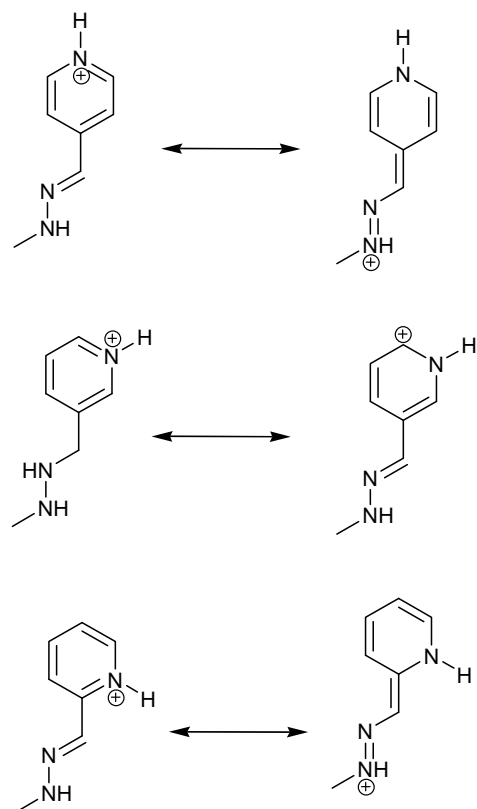


Figure 6-3 Resonance structures showing possible distributions of charge in $[\text{Fe(26)}_2](\text{PF}_6)_2$, $[\text{Fe(27)}_2](\text{PF}_6)_2$ and $[\text{Fe(28)}_2](\text{PF}_6)_2$

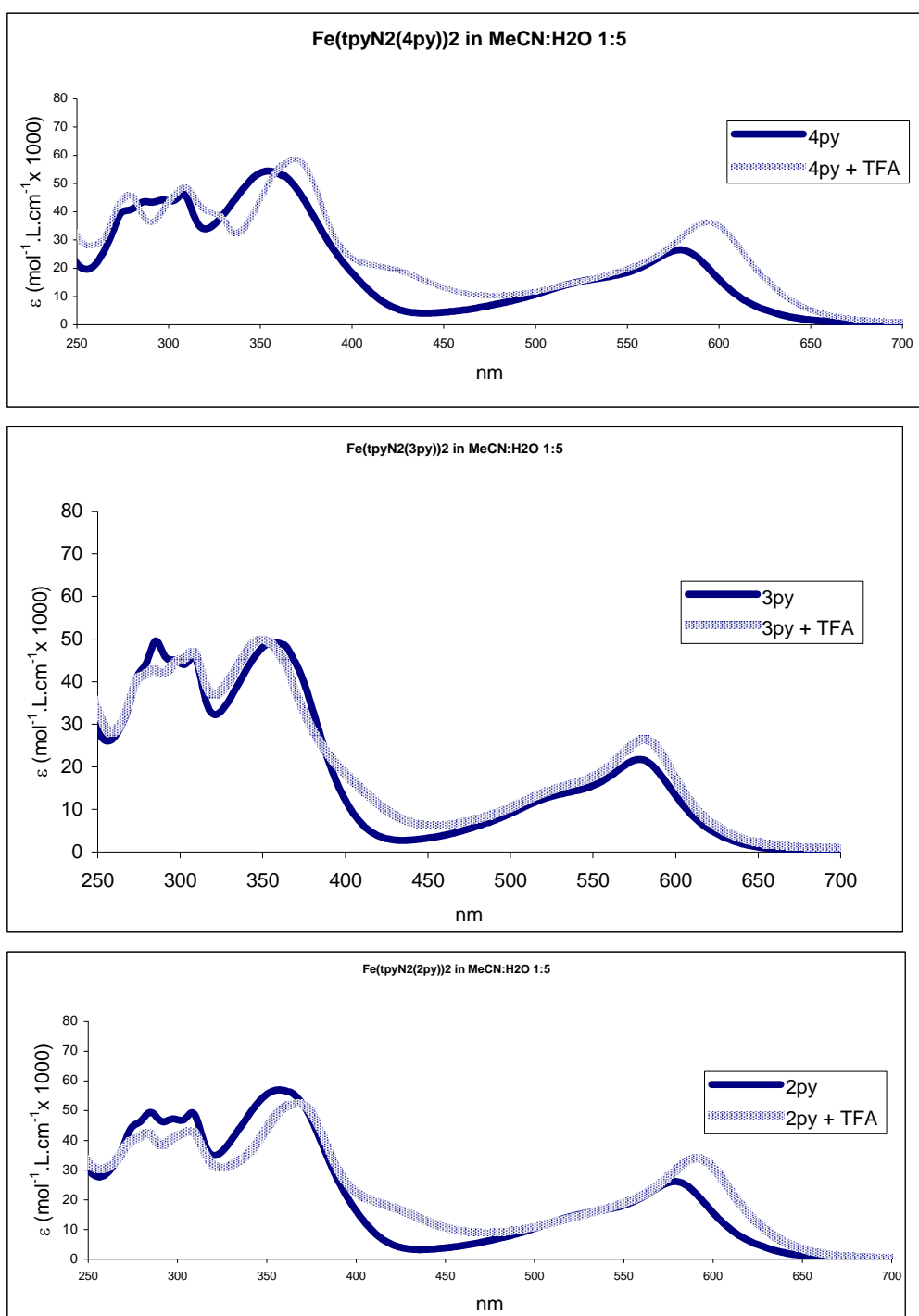


Figure 6-4 UV-visible spectra (1:5 MeCN:H₂O), of [Fe(**26**)₂](PF₆)₂, [Fe(**27**)₂](PF₆)₂ and [Fe(**28**)₂](PF₆)₂ with and without TFA addition.

6.4. Synthesis and characterisation of Ru(II) complexes

The ruthenium(II) complexes $[\text{Ru}(\mathbf{26})_2]\text{[PF}_6\text{]}_2$ and $[\text{Ru}(\mathbf{27})_2]\text{[PF}_6\text{]}_2$ were prepared by the reaction of $[\text{Ru(DMSO)}_4\text{Cl}_2]$ and ligands **26** and **27**, respectively, in ethane- 1,2-diol under microwave heating. After anion exchange and purification, $[\text{Ru}(\mathbf{26})_2]\text{[PF}_6\text{]}_2$ was obtained in 86 % yield, but only a moderate yield (38%) of $[\text{Ru}(\mathbf{27})_2]\text{[PF}_6\text{]}_2$ was achieved. Efforts to improve the yield by increasing the reaction times resulted in significant degradation of the product. Despite numerous attempts, the reaction of $[\text{Ru(DMSO)}_4\text{Cl}_2]$ or $\text{RuCl}_3\cdot 3\text{H}_2\text{O}$ with ligand **3** followed by anion exchange resulted in an intractable mixture of products. The electrospray mass spectra of $[\text{Ru}(\mathbf{26})_2]\text{[PF}_6\text{]}_2$ and $[\text{Ru}(\mathbf{27})_2]\text{[PF}_6\text{]}_2$ exhibited peaks at m/z 805 and 403. The observed isotope patterns were consistent with assignments to $[\text{M} - 2\text{PF}_6 - \text{H}]^+$ and $[\text{M} - 2\text{PF}_6]^{2+}$, respectively. The ^1H NMR spectra of $[\text{Ru}(\mathbf{26})_2]\text{[PF}_6\text{]}_2$ and $[\text{Ru}(\mathbf{27})_2]\text{[PF}_6\text{]}_2$ confirmed a single ligand environment in each complex, and the spectroscopic signatures for the two complexes are similar to those of their iron(II) analogues. However, compared to the latter, the signal for $\text{H}^{\text{B}3}$ is broadened, indicating that the energy barrier to rotation about the $\text{C}_{\text{pyridine}}-\text{N}$ bond is greater in $[\text{RuL}_2]^{2+}$ than in $[\text{FeL}_2]^{2+}$.

6.5. Solution behaviour of Ru(II) complexes: UV-vis

UV-vis spectroscopic data for aqueous acetonitrile solutions of the hexafluorophosphate salts of $[\text{Ru}(\mathbf{26})_2]^{2+}$ and $[\text{Ru}(\mathbf{27})_2]^{2+}$ are listed in Table 1. Each complex exhibits an MLCT band at around 507 nm, and intense higher-energy absorptions arising from ligand $\pi^*\leftarrow\pi$ transitions. Upon protonation with trifluoroacetic acid, the MLCT band shifts to longer wavelength (Table 11), leading to an observed colour change from cherry-red to Barbie pink. The peak shifts for the ruthenium(II) and iron(II) complexes are similar (for $[\text{M}(\mathbf{26})_2]^{2+}$, 15 nm and 17 nm for M = Fe and Ru, respectively, and for $[\text{M}(\mathbf{27})_2]^{2+}$, 3 nm and 4 nm for M = Fe and Ru, respectively). Complete protonation of $[\text{Ru}(\mathbf{26})_2]^{2+}$ to $[\text{Ru}(\text{H26})_2]^{4+}$, and $[\text{Ru}(\mathbf{27})_2]^{2+}$ to $[\text{Ru}(\text{H27})_2]^{4+}$, required approximately 50 and 200 equivalents of TFA, respectively, i.e. the same as for the corresponding iron(II) complexes.

UV-Vis titrations

When solutions of the complexes were passed through a small plug of NaHCO_3 their NMR spectra indicated that the pendant pyridyl rings were no longer protonated.

However, in pure acetonitrile the UV-vis spectra indicated the presence of multiple MLCT absorption bands, suggesting multiple (metal-containing) species in solution. Addition water resulted in spectra consistent with a single species and the addition of base (aqueous NaOH) resulted in an increase of the peaks observed at 440 nm and 635 nm for $\text{Fe(26)}_2(\text{PF}_6)_2$, reminiscent of the situation discussed in Chapter 3 for deprotonation of related complexes. It has been previously established that, protonation effects aside, the UV-visible spectrum of Fe(tpy)_2 and Ru(tpy)_2 complexes varies very little between acetonitrile and water²⁷⁹ and this was also found to be the case for the complexes presented here. As the pK_a of the hydrazone amine is expected to be relatively low, UV-vis measurements were conducted in 1:5 MeCN: H₂O to ensure that the complexes were not partially deprotonated. The addition of TFA resulted in the smooth protonation of the complexes, with absorbance changes as discussed above. Sample titrations for $[\text{Fe(26)}_2](\text{PF}_6)_2$ and $[\text{Fe(28)}_2](\text{PF}_6)_2$ are shown in Figure 6-5 and Figure 6-6.

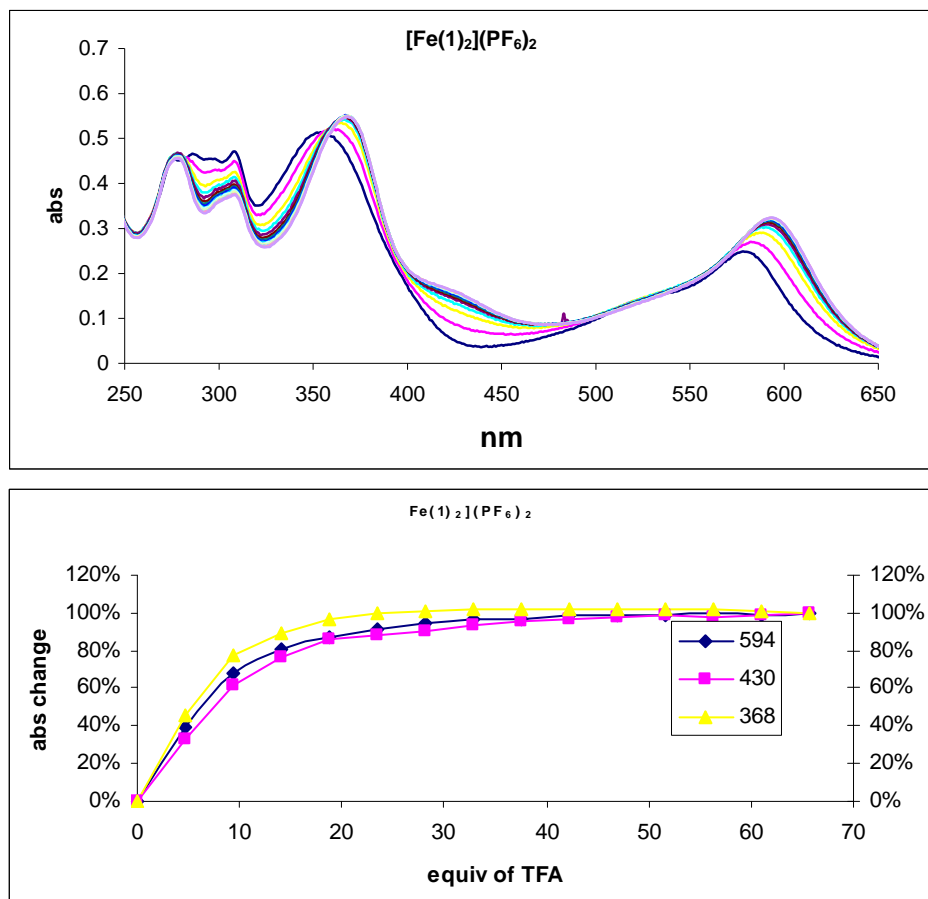


Figure 6-5 $[\text{Fe(26)}_2](\text{PF}_6)_2$ in 1:5 MeCN:H₂O (9.52×10^{-6} M) with 5 μ l additions of an aqueous TFA solution (27 mM). Curves shown for 3 different wavelengths: the protonated species MLCT (594 nm), the rising peak at 430 nm and the shift in the ligand centred transition at 368 nm.

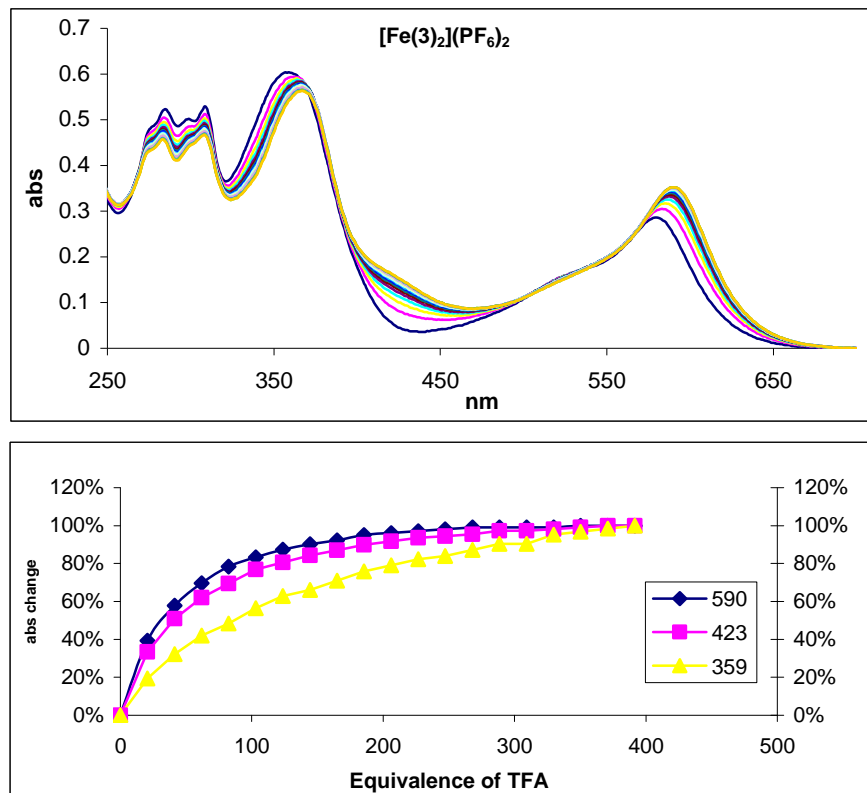


Figure 6-6 **2py** $[\text{Fe(28)}_2](\text{PF}_6)_2$ in 1:5 MeCN:H₂O (1.09×10^{-5} M) with 5 μ l additions of an aqueous TFA solution (134 mM). Curves shown for 3 different wavelengths: the protonated species MLCT (590 nm), the rising peak at 423 nm and the shift in the ligand centred transition at 359 nm..

6.6. Crystal structures of complexes of pyridyl derivatives 26 and 27

X-Ray quality single crystals of $2\{[\text{Fe(26)}_2]\text{PF}_6\}_2 \cdot 5\text{MeCN}$ and $[\text{Ru(26)}_2]\text{PF}_6$ were grown by slow evaporation of a MeCN/H₂O solution of each complex, while those of $[\text{Ru(26)}_2]\text{NO}_3 \cdot 4.25\text{H}_2\text{O}$ were grown by slow evaporation of a MeCN : H₂O : saturated aqueous KNO₃ 7 : 2 : 2 solution of $[\text{Ru(26)}_2]\text{PF}_6$, collected after chromatographic separation of the complex. The cations in each compound are depicted in Figure 6-7 to Figure 6-9.

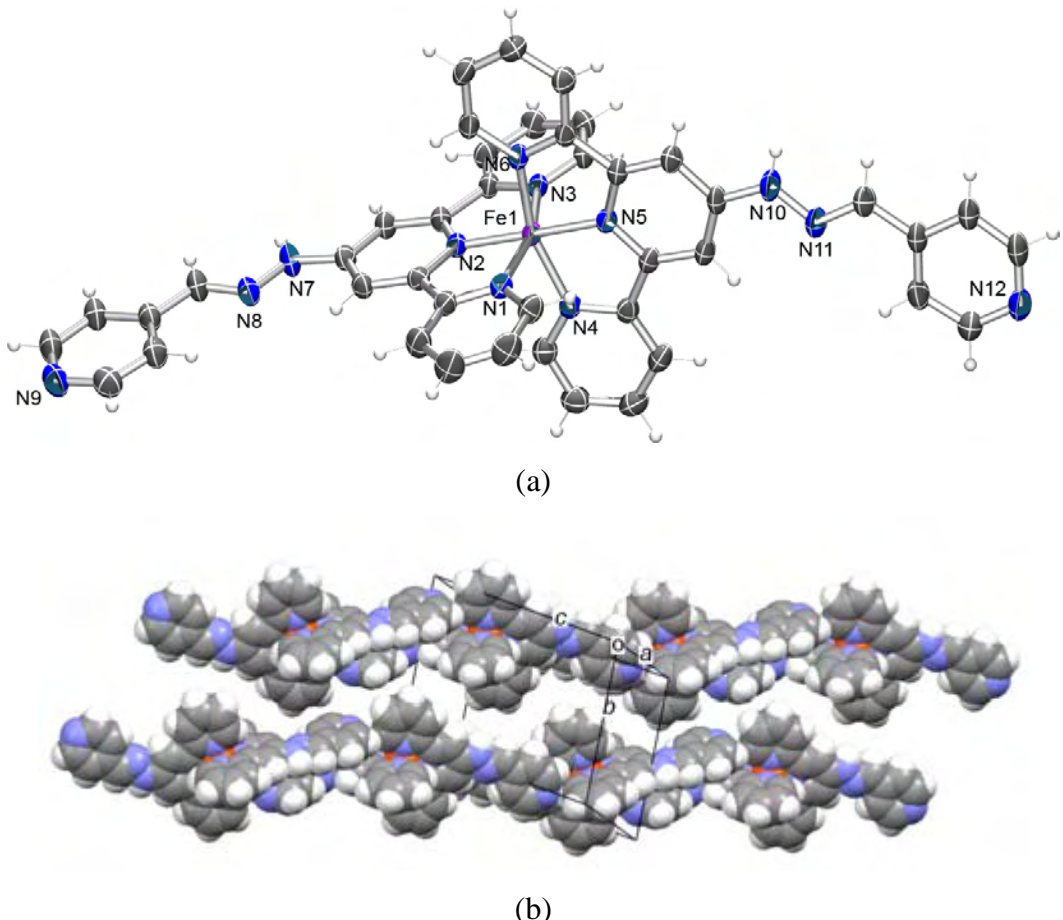


Figure 6-7 (a) Molecular structure of the $[\text{Fe}(\mathbf{26})_2]^{2+}$ cation in $2\{[\text{Fe}(\mathbf{26})_2](\text{PF}_6)_2\}.5\text{MeCN}$ with ellipsoids plotted at the 50% probability level. Selected bond parameters: $\text{Fe1-N1} = 1.975(2)$, $\text{Fe1-N2} = 1.884(2)$, $\text{Fe1-N3} = 1.981(2)$, $\text{Fe1-N4} = 1.970(2)$, $\text{Fe1-N5} = 1.881(2)$, $\text{Fe1-N6} = 1.979(2)$, $\text{N7-N8} = 1.358(3)$, $\text{N7-C8} = 1.369(3)$, $\text{N10-N11} = 1.358(3)$, $\text{N10-C23} = 1.367(3)$ Å; $\text{N1-Fe1-N2} = 80.78(9)$, $\text{N2-Fe1-N3} = 80.83(9)$, $\text{N4-Fe1-N5} = 80.51(9)$, $\text{N5-Fe1-N6} = 81.01(9)$, $\text{N8-N7-C8} = 121.3(2)$, $\text{N7-N8-C31} = 115.6(2)$, $\text{N11-N10-C23} = 121.4(2)$, $\text{N10-N11-C37} = 115.3(3)$ °. (b) Assembly of $[\text{Fe}(\mathbf{26})_2]^{2+}$ cations into chains in $2\{[\text{Fe}(\mathbf{26})_2](\text{PF}_6)_2\}.5\text{MeCN}$.

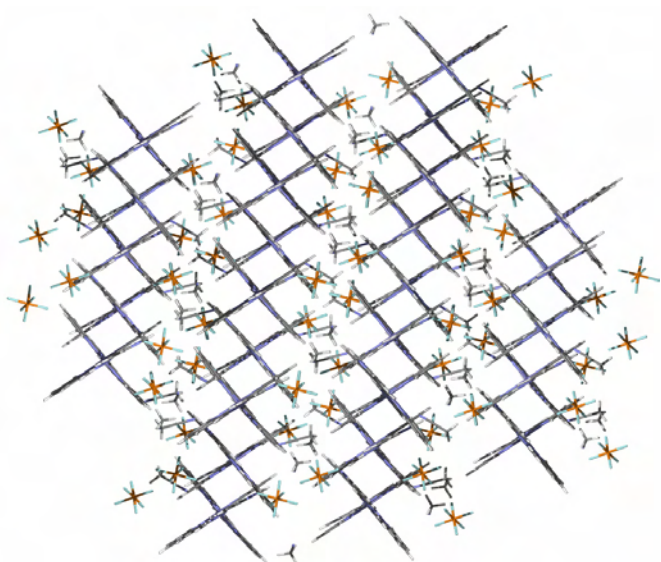


Figure 6-8 X-ray crystal structure of $2\{[\text{Fe}(\mathbf{26})_2](\text{PF}_6)_2\}.5\text{MeCN}$ showing crystal packing. Solvent and anions are fitted between rows of complexes which are tightly π - π stacked.

In each, the coordination environment about the metal(II) centre is unexceptional. A comparison of the three structures illustrates that the angle $N_{\text{pyridine}} \dots M \dots N_{\text{pyridine}}$ varies little, being 154.7° in the $[\text{Fe}(\mathbf{26})_2]^{2+}$ ion, and 156.5 and 159.0° , respectively, in the hexafluorophosphate and nitrate salts of $[\text{Ru}(\mathbf{26})_2]^{2+}$. This obtuse angle becomes the key to the topology of the coordination polymer described later. In each complex, the pendant pyridine ring is close to being coplanar with the tpy unit to which it is connected (angles between the least squares planes of the pendant pyridine and central ring of the tpy unit are $7.2(1)$ and $4.5(1)^\circ$ in $2\{[\text{Fe}(\mathbf{26})_2][\text{PF}_6]_2\}.5\text{MeCN}$, $7.9(3)^\circ$ (twice) in $[\text{Ru}(\mathbf{26})_2][\text{PF}_6]_2$, and $13.1(2)$ and $10.7(3)$ in $[\text{Ru}(\mathbf{26})_2][\text{NO}_3]_2 \cdot 4.25\text{H}_2\text{O}$). In $2\{[\text{Fe}(\mathbf{26})_2][\text{PF}_6]_2\}.5\text{MeCN}$, the cations assemble into chains by virtue of π -stacking interactions between the pyridyl hydrazone units. Taking least squares planes through sets of nine atoms in the $\text{NC}_5\text{C}=\text{NN}$ units, the cations associate through pairs of orthogonal interactions with the distances between planes containing $\text{N}9$, $\text{N}8$ and $\text{N}7$ and $\text{N}9\text{i}$, $\text{N}8\text{i}$ and $\text{N}7\text{i}$ (symmetry code $i = -1 - x, 1 - y, 2 - z$) of 3.38 \AA , and between planes containing $\text{N}12$, $\text{N}11$ and $\text{N}10$ and $\text{N}12\text{ii}$, $\text{N}11\text{ii}$ and $\text{N}10\text{ii}$ (symmetry code $\text{ii} = 2 - x, -y, 1 - z$) of 3.41 \AA . The chains are further stabilized by non-classical hydrogen bonds involving the pendant pyridine N and outer terpyridine ring CH ($\text{N}9 \dots \text{H}301\text{iC}30\text{i} = 2.69 \text{ \AA}$, $\text{N}9 \dots \text{C}30\text{i} = 3.495(4) \text{ \AA}$, $\text{N}9 \dots \text{H}301\text{i-C}30\text{i} = 143^\circ$; $\text{N}12 \dots \text{H}151\text{iiC}15\text{ii} = 2.45 \text{ \AA}$, $\text{N}12 \dots \text{C}15\text{ii} = 3.241(4) \text{ \AA}$, $\text{N}12 \dots \text{H}151\text{ii-C}15\text{ii} = 142^\circ$; symmetry codes as above). The chains lie parallel to one another as shown in Figure 6-7b, with anions and solvent molecules packed between them (Figure 6-8). Chain formation is also a feature of the solid state packing in $[\text{Ru}(\mathbf{26})_2][\text{PF}_6]_2$, again through π -interactions between the pyridyl hydrazone units and $\text{N}_{\text{pyridine}} \dots \text{HC}_{\text{tpy}}$ hydrogen bonds ($\text{N}6 \dots \text{H}15\text{AiC}15\text{i} = 2.53 \text{ \AA}$, $\text{N}6 \dots \text{C}15\text{i} = 3.366(8) \text{ \AA}$, $\text{N}6 \dots \text{H}15\text{Ai-C}15\text{i} = 148^\circ$; symmetry code $i = 1/2 + x, 3/2 - y, 3/2 + z$). In contrast to $2\{[\text{Fe}(\mathbf{26})_2][\text{PF}_6]_2\}.5\text{MeCN}$ where chains are held apart from one another, the lack of solvent molecules in $[\text{Ru}(\mathbf{26})_2][\text{PF}_6]_2$ allows the chains to approach closely.

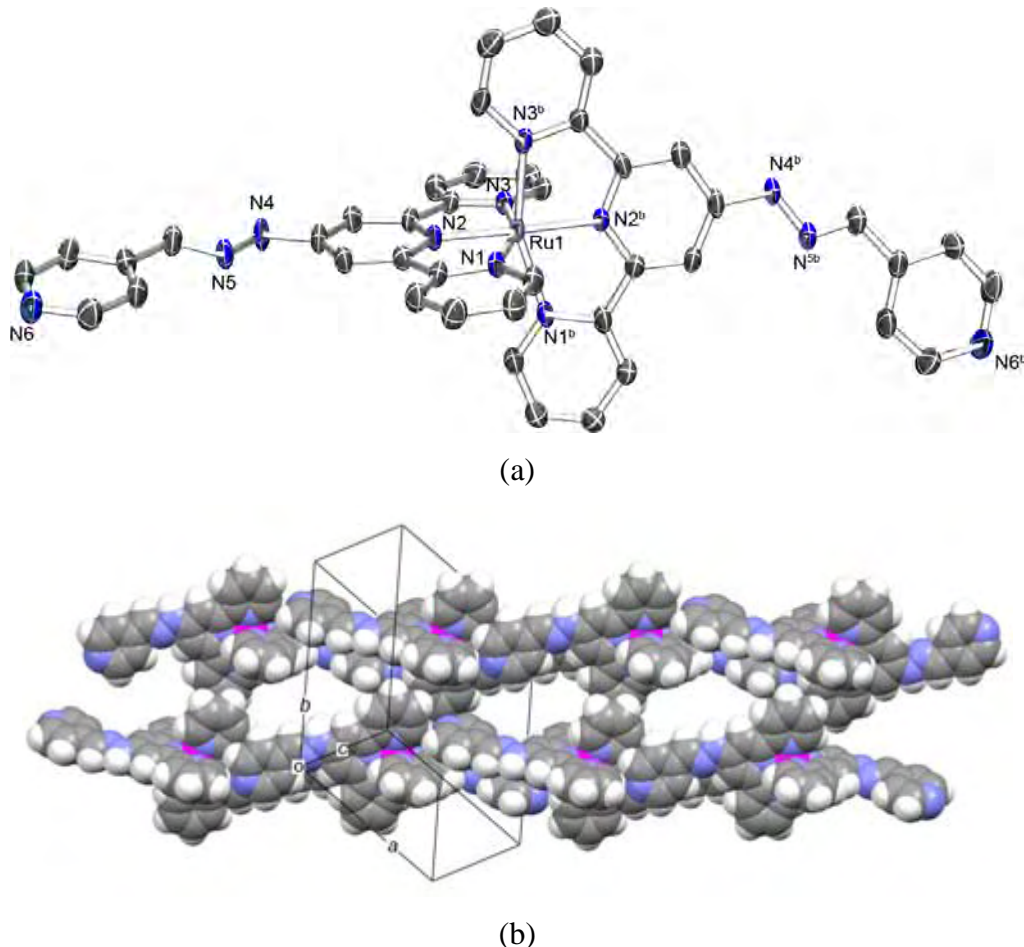


Figure 6-9 (a) Molecular structure of the $[\text{Ru}(26)_2]^{2+}$ cation in $[\text{Ru}(26)_2](\text{PF}_6)_2$ with ellipsoids plotted at the 50% probability level; hydrogen atoms omitted. Symmetry code $b = -x, y, -z + 1/2$. Selected bond parameters: $\text{Ru1}-\text{N}1 = 2.069(5)$, $\text{Ru1}-\text{N}2 = 1.986(4)$, $\text{Ru1}-\text{N}3 = 2.075(5)$, $\text{N}4-\text{N}5 = 1.365(7)$ Å; $\text{N}2-\text{Ru1}-\text{N}1 = 78.4(2)$, $\text{N}2-\text{Ru1}-\text{N}3 78.7(2)$, $\text{N}5-\text{N}4-\text{C}8 = 119.8(5)$, $\text{C}16-\text{N}5-\text{N}4 = 116.4(5)^\circ$. (b) Parts of two adjacent chains of cations in $[\text{Ru}(26)_2](\text{PF}_6)_2$, illustrating the face-to-face π -stacking than associates the chains into a sheet.

Firstly, the presence of face-to-face interactions between pendant pyridine rings and tpy rings of adjacent molecules results in the chains assembling into sheet-like arrays. Secondly, sheets interact through pairs of outer tpy rings containing N1 and N1ii (symmetry code $ii = 1 - x, 2 - y, 2 - z$) engaging in face-to face π -stacking. Figure 6-9 illustrates the latter contacts between two adjacent chains. The π -stacking of pyridyl hydrazone units is also a dominant factor in the packing $[\text{Ru}(26)_2]^{2+}$ cations in $[\text{Ru}(26)_2](\text{NO}_3)_2 \cdot 4.25\text{H}_2\text{O}$. However, in contrast to the hexafluorophosphate salts described above, each pendant pyridine N-donor in $[\text{Ru}(26)_2](\text{NO}_3)_2 \cdot 4.25\text{H}_2\text{O}$ is hydrogen bonded to a water molecule rather than to an aromatic CH unit of an adjacent cation (Figure 6-13a). Each imine NH unit is also involved in hydrogen bonding, either

to a water molecule or a nitrate ion. Additional hydrogen bonding between water molecules and nitrate ions contributes to the overall packing.

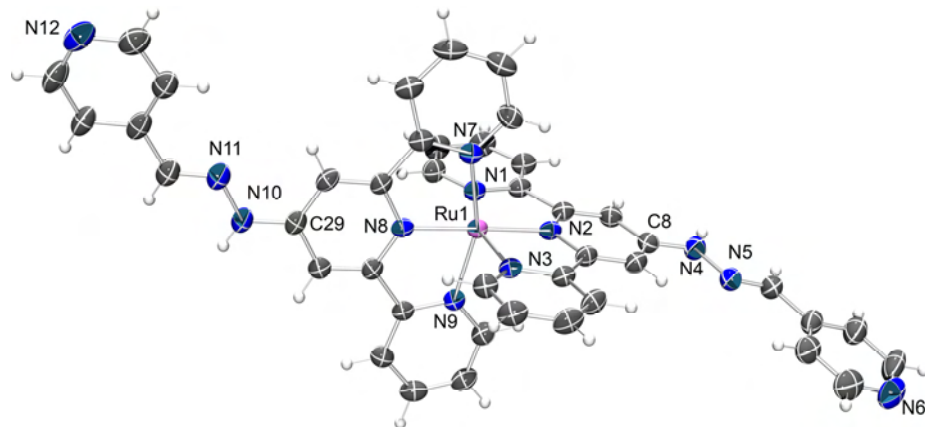


Figure 6-10 Molecular structure of the $[\text{Ru}(26)_2]^{2+}$ cation in $[\text{Ru}(26)_2]\text{[NO}_3\text{]}_4 \cdot 4.25\text{H}_2\text{O}$ with ellipsoids plotted at the 40% probability level; H atoms are omitted. Selected bond parameters: $\text{Ru1}-\text{N}2 = 1.972(4)$, $\text{Ru1}-\text{N}8 = 1.973(4)$, $\text{Ru1}-\text{N}9 = 2.061(4)$, $\text{Ru1}-\text{N}7 = 2.062(4)$, $\text{Ru1}-\text{N}1 = 2.074(3)$, $\text{Ru1}-\text{N}3 = 2.075(3)$, $\text{N}4-\text{N}5 = 1.366(5)$, $\text{N}10-\text{N}11 = 1.357(5)$ Å; $\text{N}1-\text{Ru1}-\text{N}2 = 79.0(1)$, $\text{N}2-\text{Ru1}-\text{N}3 = 79.0(1)$, $\text{N}8-\text{Ru1}-\text{N}7 = 79.0(1)$, $\text{N}8-\text{Ru1}-\text{N}9 = 79.4(1)$, $\text{C}8-\text{N}4-\text{N}5 = 118.9(4)$, $\text{C}16-\text{N}5-\text{N}4 = 116.3(4)$, $\text{N}11-\text{N}10-\text{C}29 = 118.5(4)$, $\text{C}37-\text{N}11-\text{N}10 = 117.0(4)^\circ$.

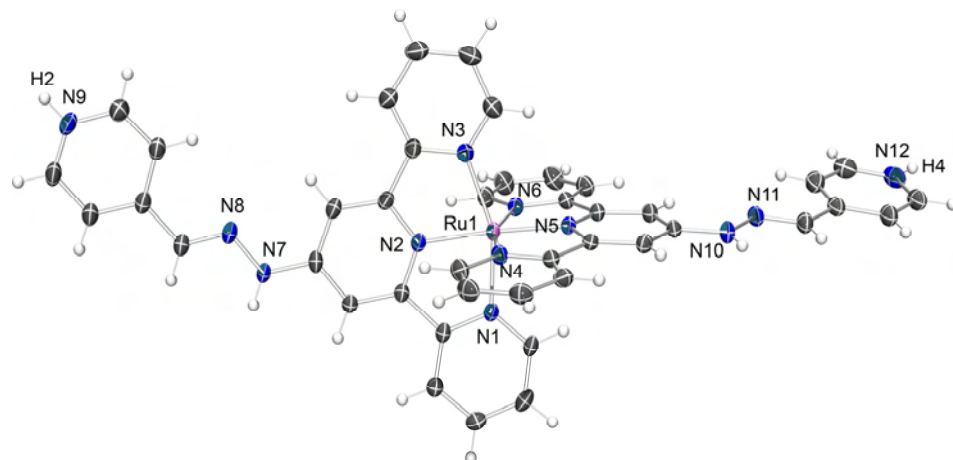


Figure 6-11 (a) Molecular structure of the $[\text{Ru}(\text{H26})_2]^{4+}$ cation in $[\text{Ru}(\text{H26})_2]\text{[NO}_3\text{]}_4 \cdot 3\text{H}_2\text{O}$ with ellipsoids plotted at the 50% probability level.. Selected bond parameters: $\text{Ru1}-\text{N}1 = 2.071(1)$, $\text{Ru1}-\text{N}2 = 1.982(1)$, $\text{Ru1}-\text{N}3 = 2.079(2)$, $\text{Ru1}-\text{N}4 = 2.057(1)$, $\text{Ru1}-\text{N}5 = 1.977(1)$, $\text{Ru1}-\text{N}6 = 2.059(1)$, $\text{N}7-\text{N}8 = 1.341(2)$, $\text{N}10-\text{N}11 = 1.347(2)$ Å; $\text{N}1-\text{Ru1}-\text{N}2 = 79.42(6)$, $\text{N}2-\text{Ru1}-\text{N}3 = 78.65(6)$, $\text{N}4-\text{Ru1}-\text{N}5 = 79.58(6)$, $\text{N}5-\text{Ru1}-\text{N}6 = 78.93(6)$, $\text{N}8-\text{N}7-\text{C}8 = 119.1(2)$, $\text{N}7-\text{N}8-\text{C}31 = 117.4(2)$, $\text{N}11-\text{N}10-\text{C}23 = 119.5(2)$, $\text{N}10-\text{N}11-\text{C}37 = 116.9(2)^\circ$.

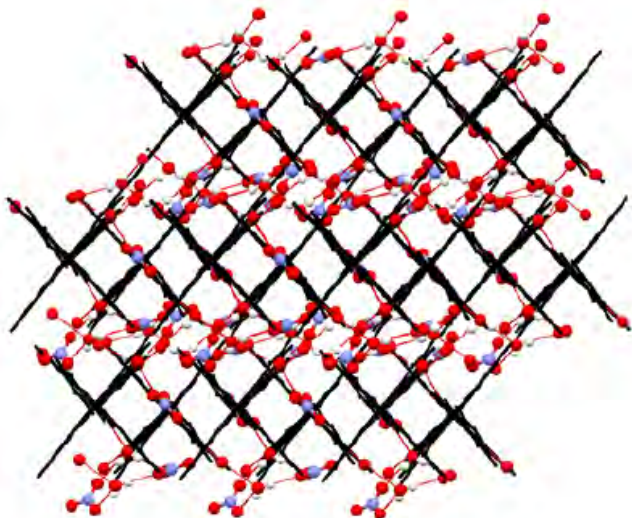


Figure 6-12 Packing of $[\text{Ru}(\text{H26})_2]^{4+}$ cations in $[\text{Ru}(\text{H26})_2][\text{NO}_3]_4 \cdot 3\text{H}_2\text{O}$ (shown in black, stick representation) with hydrogen bonded nitrate ions and water molecules.

X-Ray quality crystals of $[\text{Ru}(\text{H26})_2][\text{NO}_3]_4 \cdot 3\text{H}_2\text{O}$ were grown from slow diffusion of a MeCN– H_2O (5 : 1) solution of AgNO_3 into a similar solution of $[\text{Ru}(\text{26})_2][\text{PF}_6]_2$. The structure of the $[\text{Ru}(\text{H26})_2]^{4+}$ cation is shown in Figure 6-11a, and the coordination environment about the ruthenium(II) centre is as expected. Both pendant pyridine rings are protonated. The hydrogen atoms bonded to N and O have been localized in the difference map and optimized; their presence is also consistent with the short $\text{N}_{\text{py}} \dots \text{O}$ contacts to water or nitrate ion oxygen atoms (Figure 6-13b). Thus, in addition to the imine NH, the protonated pyridine rings are involved in hydrogen bonding to small clusters of water molecules and nitrate ions which reside in pockets within the efficiently π -stacked array of $[\text{Ru}(\text{H26})_2]^{4+}$ cations Figure 6-11b. Once again, the latter associate through face-to-face contacts between adjacent pyridyl–hydrazone–tpy units. A comparison of the structures of the cations in $[\text{Ru}(\text{26})_2][\text{NO}_3]_2 \cdot 4.25\text{H}_2\text{O}$ and $[\text{Ru}(\text{H26})_2][\text{NO}_3]_4 \cdot 3\text{H}_2\text{O}$ shows that on going from $[\text{Ru}(\text{26})_2]^{2+}$ to $[\text{Ru}(\text{H26})_2]^{4+}$, there is a small, but significant, shortening of the $\text{C}_{\text{py}}-\text{N}_{\text{imine}}$ bond (a change of 0.021 Å), consistent with there being greater conjugation between the central ring of the tpy unit and the hydrazone substituent.

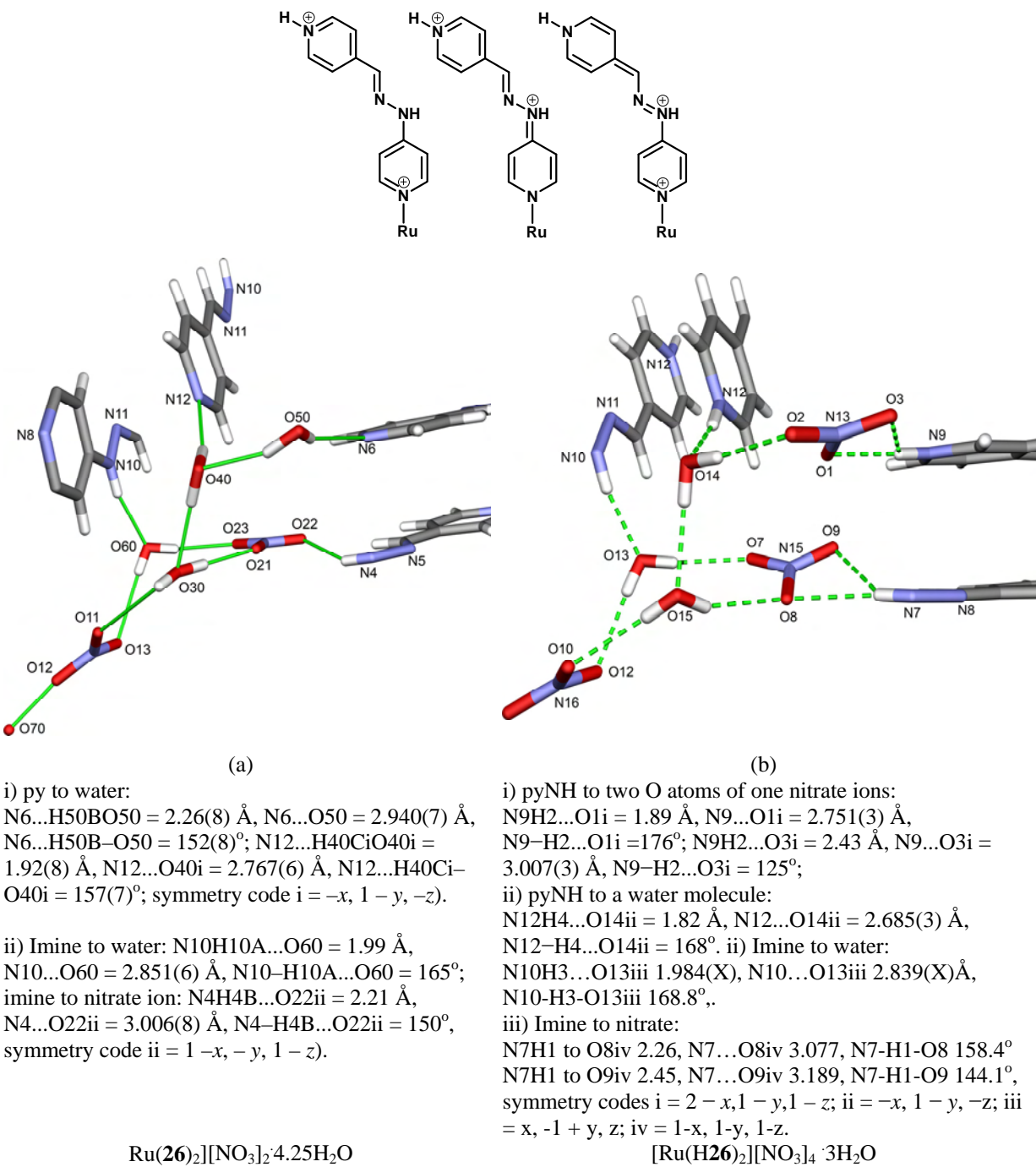


Figure 6-13 Comparison of hydrogen-bonded pockets of anions and water molecules in $\text{Ru}(\text{26})_2[\text{NO}_3]_2 \cdot 4.25\text{H}_2\text{O}$ and $[\text{Ru}(\text{H26})_2][\text{NO}_3]_4 \cdot 3\text{H}_2\text{O}$.

6.7. Extended structures: A hydrogen bonded polymer and a coordination polymer

Both NMR and electronic spectroscopic data provide evidence for the protonation of the pendant pyridine rings in $[\text{Fe}(\mathbf{26})_2]^{2+}$, $[\text{Fe}(\mathbf{27})_2]^{2+}$ and $[\text{Fe}(\mathbf{28})_2]^{2+}$. Single crystals of $[\text{Fe}(\text{H}\mathbf{27})(\mathbf{27})][\text{PF}_6]_3 \cdot 3.5\text{MeCN} \cdot 2.5\text{H}_2\text{O}$ were grown by slow evaporation of a MeCN solution of a partially protonated sample. Problems with disordered solvent molecules and hexafluorophosphate ions (the reasons for which become apparent from a study of the packing, see below) mean that the quality of the structure is not ideal. The fact that the $[\text{Fe}(\text{H}\mathbf{27})(\mathbf{27})]^{3+}$ cations (Figure 6-14a) are present is clear from (i) the presence of three $[\text{PF}_6]^-$ ions per cation, and (ii) the organization of the cations into polymeric chains with short intercation $\text{N}_{\text{py}} \dots \text{N}_{\text{py}}$ distances (Figure 6-14b). This close approach is consistent with the presence of $\text{N}-\text{H} \dots \text{N}$ hydrogen bonds ($\text{N}6\text{H}6 \dots \text{N}12i = 1.8(1)$ Å, $\text{N}6 \dots \text{N}12i = 2.706(9)$, $\text{N}6-\text{H}6 \dots \text{N}12i = 168(11)^\circ$; symmetry code $i = -1 + x, y, -1 + z$). Similar to the one-dimensional polymers based upon $[\text{Fe}(\text{pytpy})(\text{Hpytpy})]^{3+}$ and $[\text{Ru}(\text{pytpy})(\text{Hpytpy})]^{3+}$ (pytpy = 4'-(4-pyridyl)-2,2':6',2"-terpyridine) presented in the previous Chapter in which protons can be regarded as the simplest 'metal' ions within the coordination polymers. In these examples, the polymer chains are essentially linear. In $[\text{Fe}(\text{H}\mathbf{27})(\mathbf{27})]^{3+}$, a combination of the 3-pyridyl substituent and the hydrazone spacer results in each polymer chain possessing a wave-like backbone, while remaining topologically linear. Their packing (which is supported by extensive π -stacking) leads to the generation of a porous framework with channels of elliptical cross section (approximately 12×18 Å) running parallel to the crystallographic a axis (Figure 6-14c). The channels are occupied by $[\text{PF}_6]^-$ anions, acetonitrile and water solvent molecules. The presence of the undulating backbone in the one dimensional, hydrogen-bonded polymer $\{[\text{Fe}(\text{H}\mathbf{27})(\mathbf{27})]^{3+}\}_n$ illustrates that $[\text{Fe}(\mathbf{26})_2]^{2+}$, $[\text{Fe}(\mathbf{27})_2]^{2+}$, $[\text{Fe}(\mathbf{28})_2]^{2+}$, $[\text{Ru}(\mathbf{26})_2]^{2+}$ and $[\text{Ru}(\mathbf{27})_2]^{2+}$ are attractive expanded ligands¹⁶⁵ for the construction of novel coordination polymers.

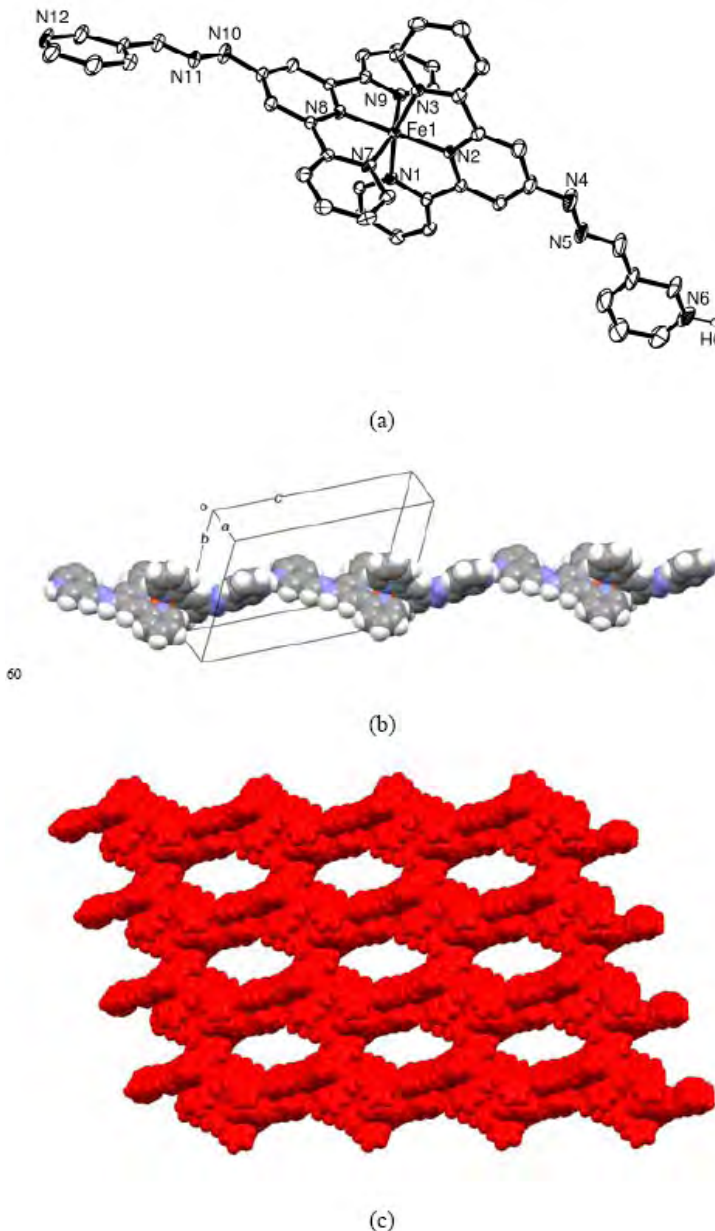


Figure 6-14 (a) Molecular structure of the $[Fe(H27)(27)]^{3+}$ cation in $[Fe(H27)(27)][PF_6]_3 \cdot 5.5\text{MeCN} \cdot 2.5\text{H}_2\text{O}$ with ellipsoids plotted at the 30% probability level; H atoms are omitted. Selected bond parameters: Fe1–N2 = 1.887(4), Fe1–N8 = 1.887(4), Fe1–N1 = 1.971(4), Fe1–N9 = 1.976(4), Fe1–N3 = 1.981(4), Fe1–N7 = 1.988(4), N4–N5 = 1.362(8), N10–N11 = 1.358(6) Å; N1–Fe1–N2 = 81.0(2), N2–Fe1–N3 = 80.4(2), N8–Fe1–N7 = 80.8(2), N8–Fe1–N9 = 80.6(2), C8–N4–N5 = 119.9(6), C16–N5–N4 = 116.7(6)°. (b) Assembly of a chain of $[Fe(H2)(2)]^{3+}$ cations, supported by $N_{py}-H \dots N_{py}$ hydrogen bonds. (c) Packing of chains showing channels that run through the crystal lattice (viewed down the *a* axis).

As a representative example, the pendant *N*-donors in $[\text{Ru}(26)_2]^{2+}$ were combined with iron(II) ions in the presence of NH_4SCN ^{356, 357, 399} in a mixture of acetonitrile, ethanol and water. After a period of 3 weeks, dark red plate-like crystals had formed, single crystal X-ray diffraction studies of which revealed them to consist of the coordination polymer $\{[\text{Fe}(\text{NCS})_2(\text{Ru}(26)_2)][\text{Fe}_2(\text{NCS})_6(\text{OEt})_2(\text{EtOH})_2][\text{NCS}]_2 \cdot 4\text{EtOH} \cdot \text{H}_2\text{O}\}_n$. The

repeat unit of the polymer is a heterometallomacrocycle and is shown in Figure 6-15a. The repeat unit in the polymer consists of two $[\text{Ru}(\mathbf{26})_2]^{2+}$ cations (related by a centre of inversion) bridging two high-spin iron(II) centres, each of which also carries two thiocyanate ligands. The local coordination environment of atom Fe1 is therefore $\{\text{trans-Fe}(\text{NCS})_2(\text{py})_4\}$. The thiocyanate ligand adopts a linear rather than bent mode (angle N13–C50–S1 = $179.0(10)^\circ$).^{165, 359}

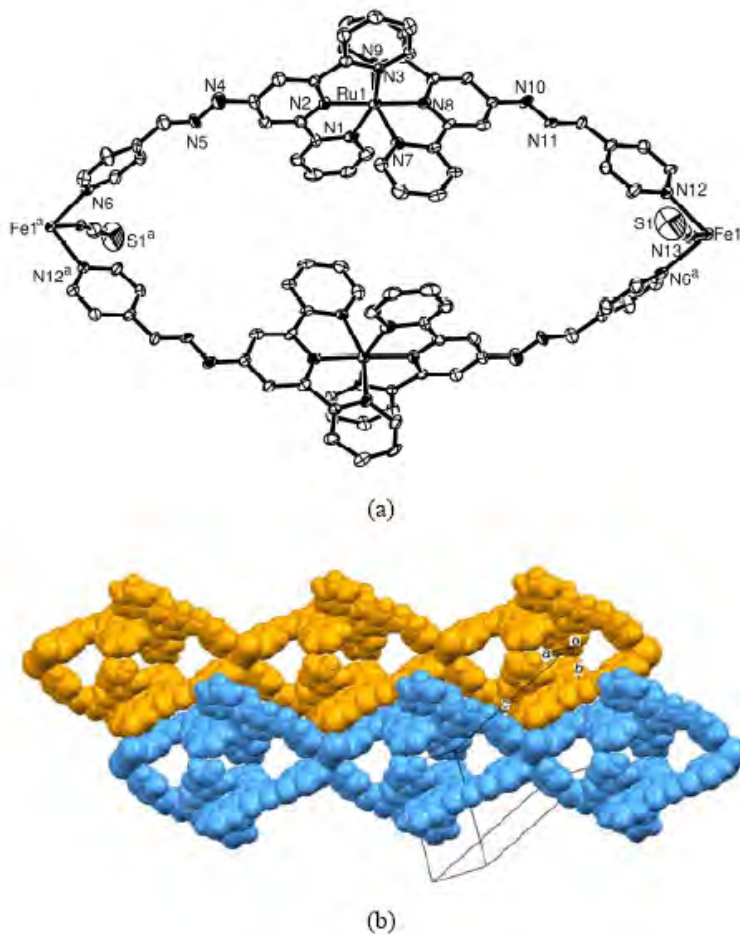


Figure 6-15 (a) One repeat unit in a $\{[\text{Fe}(\text{NCS})_2(\text{Ru}(\mathbf{26})_2)_2]\}_n^{4n+}$ polymer chain in $\{[\text{Fe}(\text{NCS})_2(\text{Ru}(\mathbf{26})_2)_2][\text{Fe}_2(\text{NCS})_6(\text{OEt})_2(\text{EtOH})_2][\text{NCS}]_2\text{4EtOH}\cdot\text{H}_2\text{O}\}_n$; atom Fe1 is shared between repeat units. Ellipsoids are plotted at the 40% probability level, and H atoms are omitted. Symmetry code a = $1 - x, -y, 2 - z$. Selected bond parameters: Ru1–N1 = 2.059(7), Ru1–N2 = 1.970(7), Ru1–N3 = 2.043(7), Ru1–N7 = 2.053(7), Ru1–N8 = 1.958(7), Ru1–N9 = 2.056(7), Fe1–N13 = 2.117(8), Fe1–N12 = 2.171(7), Fe1–N6a = 2.245(7) Å; N13–Fe1–N12 = 89.1(3), N12a–Fe1a–N6 = 87.4(2), N13a–Fe1a–N6 = 89.1(3), N13–C50–S1 = $179.0(10)^\circ$. (b) packing of two adjacent polymer chains, illustrating the π -stacking between pyridine–hydrazone–tpy units.

The $[\text{Ru}(\mathbf{26})_2]^{2+}$ cation clearly has some degree of flexibility, since the angle subtended by atoms N6 and N12 at atom Ru1 is 145.8° compared with 156.5 and 159.0° in the two salts of $[\text{Ru}(\mathbf{26})_2]^{2+}$ described above. This deformation of the expanded ligand allows atom Fe1 to reside comfortably in a close to ideal octahedral environment. The

Fe1...Fe1a and Ru1...Ru1a distances across the metallomacrocyclic cavity are 24.5 and 9.7 Å, respectively. The macrocyclic cavity is empty, and the relative orientations of the two $\{\text{Ru(26)}_2\}$ units preclude there from being any π -stacking interactions. In contrast, there are repulsive tpy H...H contacts across the ring ($\text{H}3\ldots\text{H}24\text{a} = 2.48$ Å, $\text{H}2\ldots\text{H}23\text{a} = 2.84$ Å, symmetry code $a = 1 - x, -y, 2 - z$). The polymer chains pack parallel to each other, but are offset as a consequence of face-to-face π -stacking between pyridine–hydrazone–tpy units of adjacent chains (Figure 6-15b). These interactions therefore pervade each of the structures described in this paper, and are clearly an important packing motif in both the free ligand and metal complexes.

The $[\text{Fe}_2(\text{NCS})_6(\text{OEt})_2(\text{EtOH})_2]^{2-}$ anion (Figure 6-16) present in $\{[\text{Fe}(\text{NCS})_2(\text{Ru(26)}_2)_2][\text{Fe}_2(\text{NCS})_6(\text{OEt})_2(\text{EtOH})_2][\text{NCS}]_2 \cdot 4\text{EtOH}\cdot\text{H}_2\text{O}\}_n$ is of interest in its own right. The anion is a centrosymmetric dimer, with two ethoxy ligands bridging the two iron(III) centres ($\text{Fe}2\ldots\text{Fe}2\text{a} = 3.129(4)$ Å, symmetry code $a = -x, -y, 2 - z$). The octahedral coordination environment of each Fe2 atom is completed by three linear thiocyanate ligands and an ethanol molecule. The assignment of the terminal ligand as EtOH rather than $[\text{EtO}]^-$ has been made on the grounds of charge balance; no OH proton was located.

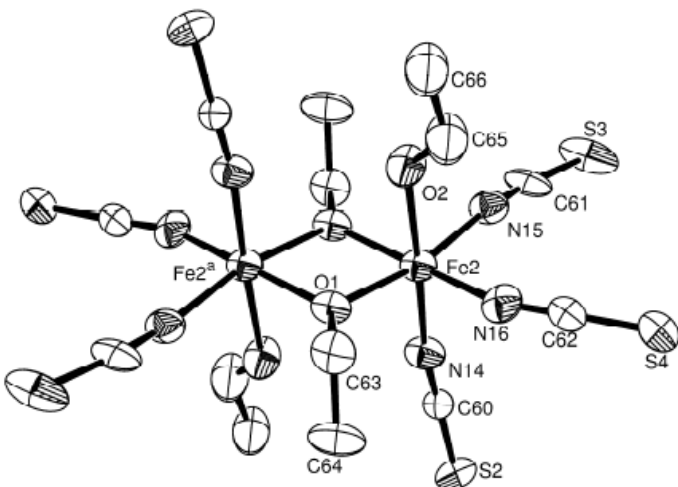


Figure 6-16 The molecular structure of $[\text{Fe}_2(\text{NCS})_6(\text{OEt})_2(\text{EtOH})_2]^{2-}$ anion in $\{[\text{Fe}(\text{NCS})_2(\text{Ru(26)}_2)_2][\text{Fe}_2(\text{NCS})_6(\text{OEt})_2(\text{EtOH})_2][\text{NCS}]_2 \cdot 4\text{EtOH}\cdot\text{H}_2\text{O}\}_n$ with ellipsoids are plotted at the 30% probability level; H atoms are omitted. Selected bond parameters: $\text{Fe}2-\text{O}1 = 1.984(7)$, $\text{Fe}2-\text{N}16 = 2.01(1)$, $\text{Fe}2-\text{N}14 = 2.02(1)$, $\text{Fe}2-\text{N}15 = 2.03(1)$, $\text{Fe}2-\text{O}2 = 2.16(8)$ Å; $\text{O}1-\text{Fe}2-\text{O}1\text{a} = 75.3(3)$, $\text{O}1-\text{Fe}2-\text{N}16 = 97.1(4)$, $\text{O}1-\text{Fe}2-\text{N}14 = 92.9(3)$, $\text{N}16-\text{Fe}2-\text{N}14 = 93.1(4)$, $\text{N}16-\text{Fe}2-\text{N}15 = 92.7(4)$, $\text{N}14-\text{Fe}2-\text{N}15 = 93.3(4)$, $\text{O}1\text{a}-\text{Fe}2-\text{O}2 = 83.4(3)$, $\text{O}1-\text{Fe}2-\text{O}2 = 85.2(3)$, $\text{N}16-\text{Fe}2-\text{O}2 = 88.5(4)$, $\text{N}15-\text{Fe}2-\text{O}2 = 88.3(4)$, $\text{N}14-\text{C}60-\text{S}2 = 179(1)$, $\text{N}15-\text{C}61-\text{S}3 = 174(2)$, $\text{N}16-\text{C}62-\text{S}4 = 178(1)^\circ$. Symmetry code $a = -x, -y, 2 - z$.

6.8. Experimental

General methods

¹H and ¹³C NMR spectra were recorded on a Bruker Avance DRX 500 spectrometer; the numbering scheme adopted for the ligands is shown in Scheme 3. Chemical shifts for ¹H and ¹³C NMR spectra are referenced to residual solvent peaks with respect to TMS = δ 0 ppm. For the NMR spectra of complexes containing ligands **26**, **27** or **28**, each solution was passed through a plug of KHCO₃ to confirm that the coordinated ligands were fully deprotonated. Electrospray (ESI) mass spectra were recorded using a Finnigan MAT LCQ mass spectrometer. Electronic absorption spectra were recorded on an Agilent 8453 UV-Visible Spectrophotometer.

Fe(II) complexes:

[Fe(**26**)₂][PF₆]₂

Ligand **26** (0.21 g, 0.60 mmol) and FeCl₂·4H₂O (0.059 g, 0.30 mmol) were dissolved in EtOH (70 mL) and the reaction mixture was stirred at room temperature for 1 h. Excess ethanolic NH₄PF₆ was added, and the resulting purple precipitate was collected on Celite and washed well with water (3 × 100 mL), EtOH (2 × 10 mL) and Et₂O (100 mL). The residue was dissolved in MeCN and the solvent removed to give

[Fe(**26**)₂][PF₆]₂ as a purple powder (0.24 g, 0.23 mmol, 78%). ¹H NMR (500 MHz, CD₃CN) δ / ppm 10.45 (s, 2H, NH), 8.76 (dd, *J* 4.6, 1.6 Hz, 4H, H^{C2}), 8.58 (br s, 4H, H^{B3}), 8.49 (d, *J* 7.9 Hz, 4H, H^{A3}), 8.25 (s, 4H, H^{N=CH}), 7.93 (dd, *J* 4.6, 1.5 Hz, 4H, H^{C3}), 7.90 (td, 8.0, 1.4, 4H, H^{A4}), 7.29 (d, 5.5, 4H, H^{A6}), 7.11 (ddd, *J* 6.9, 5.7, 1.1 Hz, 4H, H^{A5}). ¹³C{¹H} NMR (125 MHz, CD₃CN) δ / ppm 160.8 (C^{B2}), 159.3 (C^{A2}), 35 154.4 (C^{A6}), 153.7 (C^{B4}), 151.4 (C^{C2}), 142.7 (C^{C4}), 142.6 (C^{CH=N}), 139.2 (C^{A4}), 128.0 (C^{A5}), 124.3 (C^{A3}), 121.9 (C^{C3}), 108.5 (C^{B3}). ESI-MS *m/z* 759.2 [M – 2PF₆ – H]⁺, 380.3 [M – 2PF₆]²⁺. Found C 47.41, H 3.16, N 15.68 %. C₄₂H₃₂F₁₂FeN₁₂P₂ ·H₂O requires C 47.21, H 3.21, N 15.73 %.

Protonated: [Fe(**26**)₂](PF₆)₂ in MeCN-*d*₃ + TFA-*d*₁

¹H NMR (500 MHz, CD₃CN) δ 11.14 (s, 2H, NH), 8.73 (d, *J* 6.9 Hz, 4H, H^{C2}), 8.66 (s, 4H, H^{B3}), 8.50 (d, *J* 8.0 Hz, 4H, H^{A3}), 8.48 (d, *J* 6.9 Hz, 4H, H^{C3}), 8.35 (s, 2H, N=CH), 7.89 (td, *J* 1.2, 7.8 Hz, 4H, H^{A4}), 7.24 (d, *J* 5.5 Hz, 4H, H^{A6}), 7.09 (ddd, *J* 1.0, 5.7, 7.1

Hz, 4H, H^{A5}). ¹³C{¹H} 159.0 (C^{A2/B2}), 158.7 (C^{A2/B2}), 154.4 (C^{A6}), 153.0 (C^{C4}), 142.5 (C^{C2}), 139.4 (CA4), 138.3 (C^{CH=N}), 128.2 (C^{A5}), 124.6 (C^{A3}), 124.5 (C^{C3}), 109.3 (C^{B3}).

[Fe(27)₂][PF₆]₂

Ligand **27** (0.10 g, 0.29 mmol) and FeCl₂ ·4H₂O (0.029 g, 0.15 mmol) were dissolved in EtOH (40 mL). The method of preparation was as for [Fe(**26**)₂][PF₆]₂. [Fe(**27**)₂](PF₆)₂ was isolated as a purple powder (0.14 g, 0.13 mmol, 90%). ¹H NMR (500 MHz, CD₃CN) δ / ppm 10.23 (s, 2H, NH), 9.14 (s, 2H, H^{C2}), 8.65 (dd, *J* 4.9, 1.4 Hz, 2H, H^{C6}), 8.53 (br s, 4H, H^{B3}), 8.45 (d, *J* 7.2 Hz, 4H, H^{A3}), 8.37 (dd, *J* 8.0, 1.6 Hz, 2H, H^{C4}), 8.28 (s, 2H, H^{CH=N}), 7.86 (td, *J* 7.9, 1.3 Hz, 4H, H^{A4}), 7.51 (dd, *J* 8.0, 4.9 Hz, 2H, H^{C5}), 7.27 (d, *J* 5.4 Hz, 4H, H^{A6}), 7.08 (t, *J* 6.3 Hz, 4H, H^{A5}). ¹³C{¹H} NMR (125 Hz, CD₃CN) δ / ppm 159.5 (C^{A2+B2}), 154.4 (C^{A6}), 151.5 (C^{C6}), 149.7 (C^{C2}), 142.4 (C^{CH=N}), 139.1 (C^{A4}), 134.7 (C^{C4}), 131.5 (C^{C3}), 127.9 (C^{A5}), 124.9 (C^{C5}), 124.1 (C^{A3}), 108.3 (C^{B3}). C^{B4} not observed. ESI-MS *m/z* 759.2 [M – 2PF₆ – H]⁺, 380.0 [M – 2PF₆]²⁺. Found C 46.29, H 3.37, N 15.55 %. C₄₂H₃₂F₁₂FeN₁₂P₂ ·2H₂O requires C 46.43, H 3.34, N 15.47 %.

Protonated: [Fe(**27**)₂](PF₆)₂ in MeCN-*d*₃ + TFA-*d*₁

¹H NMR (500 MHz, CD₃CN) δ 10.75 (s, 2H, NH), 9.24 (s, 4H, H^{C2}), 9.14 (d, *J* 8.2 Hz, 2H, H^{C4}), 8.73 (d, *J* 5.7, 2H, H^{C6}), 8.60 (br s, 4H, H^{B3}), 8.48 (d, *J* 7.6 Hz, 4H, H^{A3}), 8.36 (s, 2H, N=CH), 8.16 (dd, *J* 5.8, 8.0 Hz, 2H, H^{C5}), 7.88 (t, *J* 7.6, 4H, H^{A4}), 7.25 (d, *J* 5.2 Hz, 4H, H^{A6}), 7.09 (dd, *J* = 5.8, 6.9 Hz, 4H, H^{A5}). ¹³C{¹H} NMR (126 MHz, CD₃CN) δ 159.2 (C^{A2/B2}), 154.5 (C^{A6}), 153.4 (C^{B4}), 144.7 (C^{C4}), 141.9 (C^{C6}), 140.7 (C^{C2}), 139.4 (C^{A4}), 137.4 (C^{CH=N}), 136.2 (C^{C3}), 128.8 (C^{C5}), 128.1 (C^{A5}), 124.4 (C^{A3}), 108.8 C^{B3}.

[Fe(**28**)₂][PF₆]₂

Ligand **3** (0.11 g, 0.32 mmol) and FeCl₂ ·4H₂O (0.032 g, 0.16 mmol) were dissolved in EtOH (45 mL). The method of preparation was as for [Fe(**26**)₂][PF₆]₂. [Fe(**3**)₂](PF₆)₂ was isolated as a purple powder (0.14 g, 0.14 mmol, 84%). ¹H NMR (500 MHz, CD₃CN) δ / ppm 10.29 (s, 2H, NH), 8.69 (d, *J* 4.4 Hz, 2H, H^{C6}), 8.55 (br s, 4H, H^{B3}), 8.46 (d, *J* 7.9 Hz, 4H, H^{A3}), 8.42 (s, 2H, H^{CH=N}), 8.40 (d, *J* 8.0 Hz, 2H, H^{C3}), 7.93 (td, *J* 7.9, 1.4 Hz, 2H, H^{C4}), 7.86 (t, *J* 7.8 Hz, 4H, H^{A4}), 7.42 (ddd, *J* 7.2, 4.9, 0.7 Hz, 2H, H^{C5}), 7.27 (d, *J* 6.3 Hz, 4H, H^{A6}), 7.08 (t, *J* 6.3 Hz, 4H, H^{A5}). ¹³C{¹H} NMR (125

MHz, CD₃CN) δ / ppm 160.8 (C^{B2}), 159.4 (C^{A2}), 154.4 (H^{A6}), 153.8 (C^{C2}), 150.8 (C^{C6}), 145.7 (C^{CH=N}), 139.2 (C^{A4}), 137.7 (C^{C4}), 128.0 (C^{A5}), 125.2 (C^{C5}), 124.2 (C^{A3}), 121.3 (C^{C3}), 108.4 (C^{B3}), C^{B4} not observed. ESI-MS *m/z* 759.2 [M – 2PF₆ – H]⁺, 380.1 [M – 2PF₆]²⁺. Found C 47.02, H 3.25, N 15.61 %. C₄₂H₃₂F₁₂FeN₁₂P₂.H₂O requires C 47.21, H 3.21, N 15.73 %.

[Fe(**28**)₂](PF₆)₂ in MeCN-*d*₃ + TFA-*d*₁

¹H NMR (500 MHz, CD₃CN) δ 11.12 (s, 2H, NH), 8.82 (d, *J* 5.5 Hz, 2H, C^{C6}), 8.70 (br s, 4H, H^{B3}), 8.68 (td, *J* 1.2, 8.1 Hz, 2H, H^{C4}), 8.48 (d, *J* 8.0 Hz, 4H, H^{A3}), 8.35 (s, 2H, H^{CH=N}), 8.32 (d, *J* 8.2 Hz, 2H, H^{C3}), 8.02 (t, *J* 6.5 Hz, 2H, H^{C5}), 7.91 (t, *J* 7.3 Hz, 4H, H^{A4}), 7.25 (d, *J* 5.2 Hz, 4H, H^{A6}), 7.10 (t, *J* 6.1 Hz, 4H, H^{A5}). ¹³C{¹H} 159.1 (C^{A2/B2}), 154.5 (C^{A6}), 149.1 (C^{C4}), 142.9 (C^{C6}), 139.6 (C^{A4}), 133.0 (C^{CH=N}), 128.3 (C^{A5}), 127.7 (C^{C3/C5}), 127.6 (C^{C3/C5}), 124.5 (C^{A3}), 109.5 (C^{B3}).

Ru(II) complexes

[Ru(**26**)₂][PF₆]₂

Ligand **26** (0.11 g, 0.31 mmol) and [Ru(DMSO)₄Cl₂] (0.076 g, 0.16 mmol) were suspended in ethane-1,2-diol (75 cm³) and heated in a conventional microwave (800 W, 5 min). The deep red solution was cooled to room temperature and poured into excess aqueous NH₄PF₆ (700 cm³). The resulting red precipitate was collected on Celite and washed well with water (3 × 100 cm³), EtOH (2 × 10 cm³) and Et₂O (50 cm³). The remaining residue was dissolved in MeCN and the solvent removed to give

[Ru(**26**)₂][PF₆]₂ as a deep red powder (0.27 g, 0.24 mmol, 86%). This was purified by column chromatography (SiO₂, MeCN : H₂O : saturated aqueous KNO₃ 7 : 2 : 2). The centre of the main red band was collected, excess aqueous NH₄PF₆ was added and the volume reduced to precipitate the hexafluorophosphate salt (0.060 g, 0.055 mmol, 38%). ¹H NMR (500 MHz, CD₃CN) δ / ppm 10.41 (s, 2H, NH), 8.71 (dd, *J* 4.6, 1.6 Hz, 4H, H^{C2}), 8.48 (d, *J* 8.0 Hz, 4H, H^{A3}), 8.44 (br s, 4H, H^{B3}), 8.17 (s, 2H, H^{HC=N}), 7.90 (td, *J* 8.0, 1.4 Hz, 4H, H^{A4}), 7.86 (dd, 4.6, 1.4, 4H, H^{C3}), 7.46 (d, 4.9, 4H, H^{A6}), 7.15 (ddd, *J* 7.1, 5.7, 1.2 Hz, 2H, H^{A5}). ¹³C{¹H} NMR (125 MHz, CD₃CN) δ / ppm 159.6 (C^{A2}), 156.6 (C^{B2}), 153.5 (C^{A6}), 151.4 (C^{C2}), 142.7 (C^{C4}), 142.0 (CN=CH), 138.5 (C^{A4}), 128.2 (C^{A5}), 125.1 (C^{A3}), 121.8 (C^{C3}), 108.1 (C^{B3}), C^{B4} not observed. ESI-MS *m/z* 805.1 [M – 2PF₆ – H]⁺, 403.0 [M – 2PF₆]²⁺. Found: C 44.28, H 3.11, N 14.65 %. C₄₂H₃₂F₁₂N₁₂P₂Ru·2.5H₂O requires C 44.22, H 3.27, N 14.37

The method was as for $[\text{Ru}(\mathbf{26})_2][\text{PF}_6]_2$ starting with **27** (0.11 g, 0.31 mmol) and $[\text{Ru}(\text{DMSO})_4\text{Cl}_2]$ (0.076 g, 0.16 mmol). $[\text{Ru}(\mathbf{27})_2][\text{PF}_6]_2$ was isolated as a deep red powder (0.065 g, 0.059 mmol, 38%). ^1H NMR (500 MHz, CD_3CN): 10.11 (s, 1H, NH), 9.09 (s, 1H, $\text{H}^{\text{C}2}$), 8.62 (d, 3.5 Hz, 1H, $\text{H}^{\text{C}6}$), 8.47 (d, 7.9 Hz, 2H, $\text{H}^{\text{A}3}$), 8.39 (br s, 2H, $\text{H}^{\text{B}3}$), 8.34 (d, 7.9 Hz, 1H, $\text{H}^{\text{C}4}$), 8.21 (s, 1H, N=CH), 7.89 (t, 7.3 Hz, 2H, $\text{H}^{\text{A}4}$), 7.49 (m, 3H, $\text{H}^{\text{A}6+\text{C}5}$), 7.15 (t, 6.3 Hz, 2H, $\text{H}^{\text{A}5}$). $^{13}\text{C}\{\text{H}\}$ (125MHz, CD_3CN): 159.6 ($\text{C}^{\text{A}2}$), 156.5 ($\text{C}^{\text{B}2}$), 153.5 ($\text{C}^{\text{A}6}$), 152.1 ($\text{C}^{\text{B}4}$), 151.5 ($\text{C}^{\text{C}6}$), 149.6 ($\text{C}^{\text{C}2}$), 141.8 (C=NH), 138.5 ($\text{C}^{\text{A}4}$), 134.6 ($\text{C}^{\text{C}4}$), 131.4 ($\text{C}^{\text{C}3}$), 128.2 ($\text{C}^{\text{A}5}$), 125.0 ($\text{C}^{\text{A}3}$), 124.8 ($\text{C}^{\text{C}5}$), 107.8 ($\text{C}^{\text{B}3}$). ESI-MS m/z 805.1 [$\text{M} - 2\text{PF}_6 - \text{H}]^+$, 403.0 [$\text{M} - 2\text{PF}_6]^{2+}$. Found C 43.60, H 3.33, N 14.07 %. $\text{C}_{42}\text{H}_{32}\text{F}_{12}\text{N}_{12}\text{P}_2\text{Ru} \cdot 3\text{H}_2\text{O}$ requires C 43.87, H 3.33, N 14.62 %.

Table 12 Comparison of bond lengths in $[\text{Ru}(\mathbf{26})_2]^{2+}$ and its protonated species, only C-NH is significantly different.

	$[\text{Ru}(\mathbf{26})_2][\text{NO}_3]_2 \cdot 4.25\text{H}_2\text{O}$	$[\text{Ru}(\mathbf{H26})_2][\text{NO}_3]_4 \cdot 3\text{H}_2\text{O}$
Ru1-N2	1.972(4)	1.982(1)
N2-C6	1.362(5)	1.349(2)
C6-C7	1.370(6)	1.383(2)
C7-C8	1.406(6)	1.396(3)
C8-N4	1.359(6)	1.386(2)
N4-N5	1.366(6)	1.341(2)
N5=C16	1.276(7)	1.289(2)

Curriculum Vitae

Dr JONATHON E. BEVES

PERSONAL INFORMATION

Full Name Jonathon Edward Beves
Date of Birth 24 August 1979
Nationality Australian
Address Department of Chemistry
University of Basel
Spitalstrasse 51
4056 Basel, Switzerland
Email jonathon.beves@unibas.ch

EDUCATIONAL HISTORY

2005-2008	<i>University</i>	The University of Basel (Switzerland)
	<i>Degree</i>	PhD
	<i>Supervisors</i>	<i>Prof. Edwin C. Constable</i> <i>Prof. Catherine E. Housecroft</i>
	<i>Thesis Title</i>	Crystal Engineering with 2,2':6',2''-Terpyridine Derivatives: From Simple Ligands to Networks
2003-2004	<i>University</i>	The University of Sydney (Australia)
	<i>Degree</i>	Master of Science
	<i>Supervisor</i>	Prof. Leonard F. Lindoy, FAA
	<i>Thesis Title</i>	An Investigation of Self-Assembled Metallosupramolecular Squares
1998-2002	<i>University</i>	The University of Sydney (Australia)
	<i>Degree</i>	Bachelor of Science (Honours)
	<i>Major</i>	Chemistry
	<i>Honours Class</i>	First Class
	<i>Supervisor</i>	Prof. Leonard F. Lindoy, FAA
	<i>Thesis Title</i>	New Supramolecular Systems Incorporating a Novel Ditopic Macrocyclic Ligand

PUBLICATIONS

- 16) **Curly-curly, loop-loop: homoleptic metal(II) complexes of pyridinecarbaldehyde 4'-(2,2':6',2''-terpyridyl)hydrazones and their coordination polymers**, J. E. Beves, E. C. Constable, C. E. Housecroft, C. J. Kepert, M. Neuburger, D. J. Price, S. Schaffner, *Dalton Trans.*, **2008**, 47, 6742.
- 15) **All-optical integrated logic operations based on chemical communication between molecular switches**, S. Silvi, E. C. Constable, C. E. Housecroft, J. E. Beves, E. L. Dunphy, M. Tomasulo, F. M. Raymo, A. Credi, *Chem. - Eur. J.*, accepted.
- 14) **A new polymorph of 4'-tolyl-2,2':6',2''-terpyridine (tppy) and the single crystal structures of $\text{Fe}(\text{tppy})_2](\text{PF}_6)_2$ and $[\text{Ru}(\text{tppy})_2](\text{PF}_6)_2$** , J. E. Beves, P. A. Chwalisz, E. C. Constable, C. E. Housecroft, M. Neuburger, S. Silvia Schaffner, J. A. Zampese, *Inorg. Chem. Commun.*, **2008**, 11, 1009.
- 13) **4'-Chloro-2,2':6',2''-terpyridine (L): ethyl sulfate salt of $[\text{H}_2\text{L}]^{2+}$ and the single crystal structures of $[\text{H}_2\text{L}][\text{EtOSO}_3]\text{Cl}\cdot\text{H}_2\text{O}$ and $[\text{ML}_2][\text{PF}_6]_2$ with M = Fe and Ru**, J. E. Beves, E. C. Constable, C. E. Housecroft, M. Neuburger, S. Silvia Schaffner, J. A. Zampese, *Inorg. Chem. Commun.*, **2008**, 11, 1006.
- 12) **4'-Hydrazone derivatives of 2,2':6',2''-terpyridine: protonation and substituent effects**, J. E. Beves, E. C. Constable, C. E. Housecroft, M. Neuburger, S. Schaffner, J. A. Zampese, *Eur. J. Org. Chem.*, **2008**, 3569.
- 11) **Homoleptic metal complexes of 4'-(5-pyrimidinyl)-2,2':6',2''-terpyridine: tetrafurcated expanded ligands**, J. E. Beves, E. C. Constable, S. Decurtins, E. L. Dunphy, C. E. Housecroft, T. D. Keene, M. Neuburger, S. Schaffner, *CrystEngComm*, **2008**, 10, 986.
- 10) **A pyrazolyl-terminated 2,2':6',2''-terpyridine ligand: iron(II), ruthenium(II) and palladium(II) complexes of 4'-(3,5-dimethylpyrazol-1-yl)-2,2':6',2''-terpyridine**, J. E. Beves, E. C. Constable, C. E. Housecroft, M. Neuburger and S. Schaffner, *Polyhedron*, **2008**, 27, 2395.
- 9) **Expanding the 4,4'-bipyridine ligand: structural variation in $\{\text{M}(\text{pytpy})_2\}^{2+}$ complexes ($\text{pytpy} = 4'-(4\text{-pyridyl})-2,2':6',2''\text{-terpyridine}$, M = Fe, Ni, Ru) and assembly of the hydrogen-bonded, one-dimensional polymer $\{[\text{Ru}(\text{pytpy})(\text{Hpytpy})]\}_n^{3n+}$** , J. E. Beves, D. J. Bray, J. K. Clegg, E. C. Constable, C. E. Housecroft, K. A. Jolliffe, C. J. Kepert, L. F. Lindoy, M. Neuburger, D. J. Price, S. Schaffner, F. Schaper, *Inorg. Chim. Acta*, **2008**, 361, 2582.
- 8) **A one-dimensional copper(II) coordination polymer containing $[\text{Fe}(\text{pytpy})_2]^{2+}$ ($\text{pytpy} = 4'-(4\text{-pyridyl})-2,2':6',2''\text{-terpyridine}$) as an expanded 4,4'-bipyridine ligand: a hydrogen-bonded network penetrated by rod-like polymers**, J. E. Beves, E. C. Constable, C. E. Housecroft, M. Neuburger and S. Schaffner, *CrystEngComm*, **2008**, 10, 344.
- 7) **Vectorial property dependence in bis{4'-(n-pyridyl)-2,2':6',2''-terpyridine}iron(II) and ruthenium(II) complexes with n = 2, 3 and 4**, J. E. Beves, E. L. Dunphy, E. C. Constable, C. E. Housecroft, C. J. Kepert, M. Neuburger, D. J. Price and S. Schaffner, *Dalton Trans.*, **2008**, 3, 386.

- 6) **The conjugate acid of bis{4'-(4-pyridyl)-2,2':6',2''-terpyridine}iron(II) as a self-complementary hydrogen-bonded building block**, J. E. Beves, E. C. Constable, C. E. Housecroft, C. J. Kepert, M. Neuburger, D. J. Price and S. Schaffner, *CrystEngComm*, **2007**, 9, 1073.
- 5) **A palladium(II) complex of 4'-(4-pyridyl)-2,2':6',2''-terpyridine : lattice control through an interplay of stacking and hydrogen bonding effects**, J. E. Beves, E. C. Constable, C. E. Housecroft, M. Neuburger, S. Schaffner, *Inorg. Chem. Commun.*, **2007**, 10, 1185.
- 4) **The first example of a coordination polymer from the expanded 4,4'-bipyridine ligand [Ru(pytpy)₂]²⁺ (pytpy = 4'-(4-pyridyl)-2,2':6',2''-terpyridine**, J. E. Beves, E. C. Constable, C. E. Housecroft, C. J. Kepert, D. J. Price, *CrystEngComm*, **2007**, 9, 456.
- 3) **[n + n]-Heterometallomacrocyclic complexes (n > 2) prepared from platinum(II)-centred ditopic 2,2':6',2''-terpyridine ligands: dimensional cataloguing by pulsed-field gradient spin-echo NMR spectroscopy**, J. E. Beves, E. C. Constable, C. E. Housecroft, M. Neuburger, S. Schaffner, E. J. Shardlow, *Dalton Trans.*, **2007**, 6, 1593.
- 2) **4'-Chloro-2,2':6',2''-terpyridine**. J. E. Beves, E. C. Constable, C. E. Housecroft, M. Neuburger, S. Schaffner, *Acta Cryst., Sect. E*, **2006**, E62, o2497.
- 1) **New discrete metallocycles incorporating palladium(II) and platinum(II) corners and dipyridyldibenzotetraaza[14]annulene side units**, J. E. Beves, B. E. Chapman, P. W. Kuchel, L. F. Lindoy, J. McMurtrie, M. McPartlin, P. Thordarson, G. Wei, *Dalton Trans.*, **2006**, 5, 744.

References

1. I. Dance, *New J. Chem.*, 2003, **27**, 1-2.
2. C. A. Hunter and J. K. M. Sanders, *J. Am. Chem. Soc.*, 1990, **112**, 5525.
3. C. Janiak, *Dalton*, 2000, 3885-3896.
4. C. G. Claessens and J. F. Stoddart, *J. Phys. Org. Chem.*, 1997, **10**, 254-272.
5. S. Tsuzuki and A. Fujii, *Phys. Chem. Chem. Phys.*, 2008, **10**, 2584-2594.
6. B. L. Schottel, H. T. Chifotides and K. R. Dunbar, *Chem. Soc. Rev.*, 2008, **37**, 68-83.
7. M. Nishio, *CrystEngComm*, 2004, **6**, 130-158.
8. S. D. Zaric, *Eur. J. Inorg. Chem.*, 2003, 2197-2209.
9. J. C. Ma and D. A. Dougherty, *Chem. Rev.*, 1997, **97**, 1303-1324.
10. T. Steiner, *Angew. Chem., Int. Ed.*, 2002, **41**, 48-76.
11. J. L. Cook, C. A. Hunter, C. M. R. Low, A. Perez-Velasco and J. G. Vinter, *Angew. Chem., Int. Ed.*, 2008, **47**, 6275-6277.
12. J. L. Cook, C. A. Hunter, C. M. R. Low, A. Perez-Velasco and J. G. Vinter, *Angew. Chem., Int. Ed.*, 2007, **46**, 3706-3709.
13. C. A. Hunter, *Angew. Chem., Int. Ed.*, 2004, **43**, 5310-5324.
14. L. Lindoy and Editor, *Special Issue: Metallocsupramolecular Chemistry. [In: Coord. Chem. Rev., 2008; 252(8+9)]*, 2008.
15. S. Leininger, B. Olenyuk and P. J. Stang, *Chem. Rev.*, 2000, **100**, 853-907.
16. L. F. Lindoy and I. M. Atkinson, *Self Assembly in Supramolecular Systems*, Cambridge, UK, 2000.
17. E. C. Constable, M. J. Hannon, A. J. Edwards and P. R. Raithby, *J. Chem. Soc., Dalton Trans.*, 1994, 2669-2677.
18. B. W. Clare and D. L. Kepert, in *Encyclopedia of Inorganic Chemistry*, ed. R. B. King, Wiley, New York, Editon edn., 1994, vol. 2, p. 795.
19. M.Cesario, C.O.Dietrich-Buchecker, J.Guilhem, C.Pascard and J.P.Sauvage, *Chem. Commun.*, 1985, 244.
20. C. E. Housecroft and A. G. Sharpe, *Inorganic Chemistry*, 3 edn., Pearson Education.

21. V. Chaurin, E. C. Constable and C. E. Housecroft, *New J. Chem.*, 2006, **30**, 1740-1744.
22. M. Fujita, M. Tominaga, A. Hori and B. Therrien, *Acc. Chem. Res.*, 2005, **38**, 369-378.
23. C. O. Dietrich-Buchecker, J.-P. Sauvage and J.-M. Kern, *J. Am. Chem. Soc.*, 1984, **106**, 3043.
24. J. M. Lehn, A. Rigault, J. Siegel, J. Harrowfield, B. Chevrier and D. Moras, *Proc. Nat. Acad. Sci. USA*, 1987, **84**, 2565-2569.
25. E. C. Constable, M. D. Ward and D. A. Tocher, *J. Chem. Soc., Dalton Trans.*, 1991, 1675-1683.
26. E. C. Constable, M. D. Ward and D. A. Tocher, *J. Am. Chem. Soc.*, 1990, **112**, 1256-1258.
27. K. Umemoto, H. Tsukui, T. Kusukawa, K. Biradha and M. Fujita, *Angew. Chem., Int. Ed.*, 2001, **40**, 2620-2622.
28. M. Fujita, K. Umemoto, M. Yoshizawa, N. Fujita, T. Kusukawa and K. Biradha, *Chem. Commun.*, 2001, 509-518.
29. M. Fujita, O. Sasaki, T. Mitsuhashi, T. Fujita, J. Yazaki, K. Yamaguchi and K. Ogura, *Chem. Commun.*, 1996, 1535-1536.
30. A. Sautter, D. G. Schmid, G. Jung and F. Wuerthner, *J. Am. Chem. Soc.*, 2001, **123**, 5424-5430.
31. M. Fujita and K. Ogura, *Coord. Chem. Rev.*, 1996, **148**, 249-264.
32. B. Olenyuk, A. Fechtenkotter and P. J. Stang, *J. Chem. Soc., Dalton Trans.*, 1998, 1707-1728.
33. R.-D. Schnebeck, E. Freisinger and B. Lippert, *Eur. J. Inorg. Chem.*, 2000, 1193-1200.
34. T. Yamamoto, A. M. Arif and P. J. Stang, *J. Am. Chem. Soc.*, 2003, **125**, 12309-12317.
35. S. B. Lee, S. Hwang, D. S. Chung, H. Yun and J.-I. Hong, *Tetrahedr. Lett.*, 1998, **39**, 873-876.
36. C. A. Schalley, T. Muller, P. Linnartz, M. Witt, M. Schafer and A. Lutzen, *Chem.- Eur. J.*, 2002, **8**, 3538-3551.
37. M. Fujita, K. Umemoto, M. Yoshizawa, N. Fujita, T. Kusukawa and K. Biradha, *Chem. Commun.*, 2001, 509-518.

38. M. Tominaga, K. Suzuki, M. Kawano, T. Kusukawa, T. Ozeki, S. Sakamoto, K. Yamaguchi and M. Fujita, *Angew. Chem., Int. Ed.*, 2004, **43**, 5621.
39. K. Suzuki, J. Iida, S. Sato, M. Kawano and M. Fujita, *Angew. Chem., Int. Ed.*, 2008, **47**, 5780-5782.
40. R. M. Yeh, J. Xu, G. Seeber and K. N. Raymond, *Inorg. Chem.*, 2005, **44**, 6228-6239.
41. C. R. K. Glasson, G. V. Meehan, J. K. Clegg, L. F. Lindoy, P. Turner, M. B. Duriska and R. Willis, *Chem. Commun.*, 2008, 1190-1192.
42. M. Beyler, V. Heitz and J.-P. Sauvage, *Chem. Commun.*, 2008, 5396 - 5398.
43. D. Schultz, F. Biaso, A. R. M. Shahi, M. Geoffroy, K. Rissanen, L. Gagliardi, C. J. Cramer and J. R. Nitschke, *Chem.- Eur. J.*, 2008, **14**, 7180-7185.
44. E. Coronado, J. R. Galan-Mascaros, P. Gavina, C. Marti-Gastaldo, F. M. Romero and S. Tatay, *Inorg. Chem.*, 2008, **47**, 5197-5203.
45. M. W. Cooke and G. S. Hanan, *Chem. Soc. Rev.*, 2007, **36**, 1466-1476.
46. M. W. Cooke, D. Chartrand and G. S. Hanan, *Coord. Chem. Rev.*, 2008, **252**, 903-921.
47. P. W. N. van Leeuwen, *Supramolecular Catalysis*, Wiley-VCH, Weinheim, Germany, 2008.
48. S. Saha and J. F. Stoddart, *Chem. Soc. Rev.*, 2007, **36**, 77-92.
49. S. Bonnet and J.-P. Collin, *Chem. Soc. Rev.*, 2008, **37**, 1207-1217.
50. V. Balzani, *Photochem. Photobiol. Sci.*, 2003, **2**, 459-476.
51. E. Pardo, R. Ruiz-Garcia, J. Cano, X. Ottenwaelder, R. Lescouezec, Y. Journaux, F. Lloret and M. Julve, *Dalton Trans.*, 2008, 2780-2805.
52. M. L. Merlau, M. Del Pilar Mejia, S. T. Nguyen and J. T. Hupp, *Angew. Chem., Int. Ed.*, 2001, **40**, 4239-4242.
53. T. S. Koblenz, J. Wassenaar and J. N. H. Reek, *Chem. Soc. Rev.*, 2008, **37**, 247-262.
54. F. Wurthner, C.-C. You and R. Saha-Moller Chantu, *Chem. Soc. Rev.*, 2004, **33**, 133-146.
55. H. Uppadine Lindsay, J.-P. Gisselbrecht, N. Kyritsakas, K. Nattinen, K. Rissanen and J.-M. Lehn, *Chem.- Eur. J.*, 2005, **11**, 2549-2565.
56. E. J. O'Neil and B. D. Smith, *Coord. Chem. Rev.*, 2006, **250**, 3068-3080 and references therein.

57. C. R. Rice, *Coord. Chem. Rev.*, 2006, **250**, 3190-3199.
58. Y. J. Jang, E. J. Jun, Y. J. Lee, Y. S. Kim, J. S. Kim and J. Yoon, *J. Org. Chem.*, 2005, **70** 9603.
59. V. Balzani, M. Clemente-Leon, A. Credi, B. Ferrer, M. Venturi, A. H. Flood and J. F. Stoddart, *Proc. Nat. Acad. Sci.*, 2006, **103**, 1178-1183.
60. P. J. Lusby, *Ann. Rep. Prog. Chem., Sect. A: Inorg. Chem.*, 2008, **104**, 297-324.
61. C. P. Pradeep and L. Cronin, *Ann. Rep. Prog. Chem., Sect. A: Inorg. Chem.*, 2007, **103**, 287-332.
62. L. Cronin, *Ann. Rep. Prog. Chem., Sect. A: Inorg. Chem.*, 2006, **102**, 353-378.
63. L. Cronin, *Ann. Rep. Prog. Chem., Sect. A: Inorg. Chem.*, 2005, **101**, 348-374.
64. L. Cronin, *Ann. Rep. Prog. Chem., Sect. A: Inorg. Chem.*, 2004, **100**, 323-383.
65. L. Cronin, *Ann. Rep. Prog. Chem., Sect. A: Inorg. Chem.*, 2003, **99**, 289-347.
66. M. D. Ward, *Ann. Rep. Prog. Chem., Sect. A: Inorg. Chem.*, 2002, **98**, 285-320.
67. M. D. Ward, *Ann. Rep. Prog. Chem., Sect. A: Inorg. Chem.*, 2001, **97**, 293-329.
68. M. D. Ward, *Ann. Rep. Prog. Chem., Sect. A: Inorg. Chem.*, 2000, **96**, 345-385.
69. E. C. Constable, *Chem. Soc. Rev.*, 2007, **36**, 246-253.
70. A. A. Schilt and S. W. Wong, *J. Coord. Chem.*, 1984, **13**, 331-339.
71. J. I. Bullock and P. W. G. Simpson, *J. Chem. Soc., Faraday Trans. 1*, 1981, **77**, 1991-1997.
72. H. Hofmeier, A. El-Ghayoury, A. P. H. J. Schenning and U. S. Schubert, *Tetrahedron*, 2004, **60**, 6121-6128.
73. W.-L. Wong, K.-H. Huang, P.-F. Teng, C.-S. Lee and H.-L. Kwong, *Chem. Commun.*, 2004, 384-385.
74. S. Bernhard, J. I. Goldsmith, K. Takada and H. D. Abruna, *Inorg. Chem.*, 2003, **42**, 4389-4393.
75. D. Suhr, D. Lotscher, H. Stoeckli-Evans and A. von Zelewsky, *Inorg. Chim. Acta*, 2002, **341**, 17-24.
76. H. Jiang, S. J. Lee and W. Lin, *J. Chem. Soc., Dalton Trans.*, 2002, 3429-3433.
77. H.-L. Kwong, W.-L. Wong, W.-S. Lee, L.-S. Cheng and W.-T. Wong, *Tetrahed. Asym.*, 2001, **12**, 2683-2694.

78. G. Chelucci, A. Saba, D. Vignola and C. Solinas, *Tetrahedron*, 2001, **57**, 1099-1104.
79. E. C. Constable, T. Kulke, M. Neuburger and M. Zehnder, *New J. Chem.*, 1997, **21**, 1091-1102.
80. E. C. Constable, T. Kulke, M. Neuburger and M. Zehnder, *New J. Chem.*, 1997, **21**, 633-646.
81. S. Bernhard, I. Goldsmith Jonas, K. Takada and D. Abruna Hector, *Inorg. Chem.*, 2003, **42**, 4389-4393.
82. M. Maestri, N. Armaroli, V. Balzani, E. C. Constable and A. M. W. Cargill Thompson, *Inorg. Chem.*, 1995, **34**, 2759-2767.
83. A. Juris, V. Balzani, F. Barigelletti, S. Campagna, P. Belser and A. Von Zelewsky, *Coord. Chem. Rev.*, 1988, **84**, 85-277.
84. A. Abbotto, C. Barolo, L. Bellotto, F. De Angelis, M. Graetzel, N. Manfredi, C. Marinzi, S. Fantacci, J.-H. Yum and M. K. Nazeeruddin, *Chem. Commun.*, 2008, 5318-5320.
85. M. Graetzel, *Nature*, 2003, **421**, 586-587.
86. M. Gratzel, *Nature*, 2001, **414**, 338-344.
87. B. O'Regan and M. Graetzel, *Nature*, 1991, **353**, 737-740.
88. Y. Bai, Y. Cao, J. Zhang, M. Wang, R. Li, P. Wang, M. Zakeeruddin Shaik and M. Gratzel, *Nature Mater.*, 2008, **7**, 626-630.
89. P. Wang, M. Zakeeruddin Shaik, E. Moser Jacques, K. Nazeeruddin Mohammad, T. Sekiguchi and M. Gratzel, *Nature Mater.*, 2003, **2**, 402-407.
90. F. Loiseau, F. Nastasi, A.-M. Stadler, S. Campagna and J.-M. Lehn, *Angew. Chem., Int. Ed.*, 2007, **46**, 6144-6147, .
91. F. Fabrizi de Biani, E. Grigiotti, F. Laschi, P. Zanello, A. Juris, L. Prodi, K. S. Chichak and N. R. Branda, *Inorg. Chem.*, 2008, **47**, 5425-5440.
92. D. A. Jose, P. Kar, D. Koley, B. Ganguly, W. Thiel, H. N. Ghosh and A. Das, *Inorg. Chem.*, 2007, **46**, 5576-5584.
93. Z. Deng, H.-W. Tseng, R. Zong, D. Wang and R. Thummel, *Inorg. Chem.*, 2008, **47**, 1835-1848.
94. F. Liu, J. J. Concepcion, J. W. Jurss, T. Cardolaccia, J. L. Templeton and T. J. Meyer, *Inorg. Chem.*, 2008, **47**, 1727-1752.

95. G. R. Newkome, P. Wang, C. N. Moorefield, T. J. Cho, P. P. Mohapatra, S. Li, S.-H. Hwang, O. Lukyanova, L. Echegoyen, J. A. Palagallo, V. Iancu and S.-W. Hla, *Science*, 2006, **312**, 1782-1785.
96. J. D. Dunitz, *Pure App. Chem.*, 1991, **63**, 177-185.
97. G. R. Desiraju, *Angew. Chem., Int. Ed.*, 2007, **46**, 8342-8356.
98. J. McMurtrie and I. Dance, *CrystEngComm*, 2005, **7**, 216-229.
99. J. McMurtrie and I. Dance, *CrystEngComm*, 2005, **7**, 230-236.
100. M. L. Scudder, H. A. Goodwin and I. G. Dance, *New. J. Chem.*, 1999, **23**, 695-705.
101. K. Lashgari, M. Kritikos, R. Norrestam and T. Norrby, *Acta Crystallogr., Sect. C*, 1999, **55**, 64.
102. M. Kawano and M. Fujita, *Coord. Chem. Rev.*, 2007, **251**, 2592-2605.
103. Z. Xu, *Coord. Chem. Rev.*, 2006, **250**, 2745-2757.
104. P. Przychodzen, T. Korzeniak, R. Podgajny and B. Sieklucka, *Coord. Chem. Rev.*, 2006, **250**, 2234-2260.
105. B. Sieklucka, R. Podgajny, P. Przychodzen and T. Korzeniak, *Coord. Chem. Rev.*, 2005, **249**, 2203-2221.
106. L. Carlucci, G. Ciani and D. M. Proserpio, *Coord. Chem. Rev.*, 2003, **246**, 247-289.
107. M. Oh, G. B. Carpenter and D. A. Sweigart, *Acc. Chem. Res.*, 2004, **37**, 1-11.
108. N. R. Champness and M. Schroder, *Curr. Opin. Solid State Mat. Sci.*, 1998, **3**, 419-424.
109. T. K. Maji and S. Kitagawa, *Pure App. Chem.*, 2007, **79**, 2155-2177.
110. J. J. Vittal, *Coord. Chem. Rev.*, 2007, **251**, 1781-1795.
111. C. L. Cahill, D. T. de Lill and M. Frisch, *CrystEngComm*, 2007, **9**, 15-26.
112. M. Hong, *Cryst. Growth Des.*, 2007, **7**, 10-14.
113. K. Biradha, M. Sarkar and L. Rajput, *Chem. Commun.*, 2006, 4169-4179.
114. A. Y. Robin and K. M. Fromm, *Coord. Chem. Rev.*, 2006, **250**, 2127-2157.
115. S. Kitagawa, S.-i. Noro and T. Nakamura, *Chem. Commun.*, 2006, 701-707.
116. C.-L. Chen, B.-S. Kang and C.-Y. Su, *Aust. J. Chem.*, 2006, **59**, 3-18.

117. R. Dobrawa and F. Wuerthner, *J. Polymer Sci. A*, 2005, **43**, 4981-4995.
118. S. Kitagawa and K. Uemura, *Chem. Soc. Rev.*, 2005, **34**, 109-119.
119. D. Maspoch, D. Ruiz-Molina and J. Veciana, *J. Mater. Chem.*, 2004, **14**, 2713-2723.
120. S. Kitagawa, R. Kitaura and S.-i. Noro, *Angewandte Chemie, International Edition*, 2004, **43**, 2334-2375.
121. S. Kitagawa and S. Noro, *Comprehensive Coordination Chemistry II*, 2004, **7**, 231-261.
122. J. Y. Lu, *Coord. Chem. Rev.*, 2003, **246**, 327-347.
123. B. Kesanli and W. Lin, *Coord. Chem. Rev.*, 2003, **246**, 305-326.
124. A. Erxleben, *Coord. Chem. Rev.*, 2003, **246**, 203-228.
125. L. Carlucci, G. Ciani and D. M. Proserpio, *CrystEngComm*, 2003, **5**, 269-279.
126. C. Janiak, *Dalton Trans.*, 2003, 2781-2804.
127. S. R. Batten and K. S. Murray, *Aust. J. Chem.*, 2001, **54**, 605-609.
128. R. J. Puddephatt, *Coord. Chem. Rev.*, 2001, **216-217**, 313-332.
129. R. Robson, *Dalton*, 2000, 3735-3744.
130. S. R. Batten and R. Robson, *Molecular Catenanes, Rotaxanes and Knots*, 1999, 77-106.
131. M. P. Suh, Y. E. Cheon and E. Y. Lee, *Coord. Chem. Rev.*, 2008, **252**, 1007-1026.
132. J. C. Bailar Jr, *Prep. Inorg. React.*, 1964, **1**, 1.
133. A. F. Wells, *Structural Inorganic Chemistry*, 5th edn., Clarendon Press, Oxford, 1984.
134. B. F. Hoskins and R. Robson, *J. Am. Chem. Soc.*, 1990, **112**, 1546-1554.
135. B. F. Hoskins and R. Robson, *J. Am. Chem. Soc.*, 1989, **111**, 5962-5964.
136. A. Henschel, K. Gedrich, R. Krahnert and S. Kaskel, *Chem. Commun.*, 2008, 4192-4194.
137. M. H. Alkordi, Y. Liu, R. W. Larsen, J. F. Eubank and M. Eddaoudi, *J. Am. Chem. Soc.*, 2008, **130**, 12639-12641.
138. D. Jiang, T. Mallat, F. Krumeich and A. Baiker, *Journal of Catalysis*, 2008, **257**, 390-395.

139. U. Mueller, M. M. Schubert and O. M. Yaghi, *Handbook of Heterogeneous Catalysis (2nd Edition)*, 2008, **1**, 247-262.
140. U. Ravon, M. E. Domine, C. Gaudillere, A. Desmartin-Chomel and D. Farrusseng, *New J. Chem.*, 2008, **32**, 937-940.
141. S. Horike, M. Dinca, K. Tamaki and J. R. Long, *J. Am. Chem. Soc.*, 2008, **130**, 5854-5855.
142. F. X. Llabres i Xamena, O. Casanova, R. Galiasso Tailleur, H. Garcia and A. Corma, *J. Catal.*, 2008, **255**, 220-227.
143. K. C. Szeto, K. O. Kongshaug, S. Jakobsen, M. Tilset and K. P. Lillerud, *Dalton Trans.*, 2008, 2054-2060.
144. P. Przychodzen, T. Korzeniak, R. Podgajny and B. Sieklucka, *Coord. Chem. Rev.*, 2006, **250**, 2234-2260.
145. M. Eddaoudi, D. B. Moler, H. Li, B. Chen, T. M. Reineke, M. O'Keeffe and O. M. Yaghi, *Acc. Chem. Res.*, 2001, **34**, 319-330.
146. N. L. Rosi, M. Eddaoudi, J. Kim, M. O'Keeffe and O. M. Yaghi, *CrystEngComm*, 2002, **4**, 401-404.
147. J. L. C. Rowsell and O. M. Yaghi, *Angew. Chem., Int. Ed.*, 2005, **44**, 4670-4679.
148. O. M. Yaghi, *Nature Mater.*, 2007, **6**, 92-93.
149. O. M. Yaghi, M. O'Keeffe, N. W. Ockwig, H. K. Chae, M. Eddaoudi and J. Kim, *Nature*, 2003, **423**, 705-714.
150. J. Rieter William, M. L. Taylor Kathryn and W. Lin, *J. Am. Chem. Soc.*, 2007, **129**, 9852-9853.
151. W. J. Rieter, K. M. L. Taylor and W. Lin, *J. Am. Chem. Soc.*, 2007, **129**, 9852-9853.
152. B. V. Harbuzaru, A. Corma, F. Rey, P. Atienzar, J. L. Jordà, H. Garcia, D. Ananias, L. D. Carlos and J. Rocha, *Angew. Chem., Int. Ed.*, 2008, **47**, 1080-1083.
153. N. Li, S. Chen and S. Gao, *J. Coord. Chem.*, 2007, **60**, 117.
154. W. You, X. Y. Yang, C. Yao and W. Huang, *Acta Crystallogr. Sect. E*, 2008, **E64**, m79.
155. L.-G. Qiu, Z.-Q. Li, Y. Wu, W. Wang, T. Xu and X. Jiang, *Chem. Commun.*, 2008, 3642-3644.
156. R. W. Gable, B. F. Hoskins and R. Robson, *Chem. Commun.*, 1990, 1677.

157. S. Noro, R. Kitaura, M. Kondo, S. Kitagawa, T. Ishii, H. Matsuzaka and M. Yamashita, *J. Am. Chem. Soc.*, 2002, **124**, 2568.
158. S. R. Batten and R. Robson, *Angew. Chem., Int. Ed.*, 1998, **37**, 1460.
159. L. Carlucci, G. Ciani and D. M. Proserpio, *Coord. Chem. Rev.*, 2003, **246**, 247.
160. R. Robson, in *Comprehensive Supramolecular Chemistry*, eds. J. L. Atwood, J. E. D. Davies, D. D. Macnicol and F. Voegtle, Pergamon, Editon edn., 1996, vol. 6, ch. 22, p. 733.
161. O. Ohmori and M. Fujita, *Chem. Commun.*, 2004, 1586-1587.
162. H. Li, M. Eddaoudi, M. O'Keeffe and M. Yaghi, *Nature*, 1999, **402**, 276-279.
163. D. J. Tranchemontagne, Z. Ni, M. O'Keeffe and O. M. Yaghi, *Angew. Chem., Int. Ed.*, 2008, **47**, 5136-5147.
164. <http://www.bASF-futurebusiness.com/en/projects/gas-storage.html>.
165. J. E. Beves, D. J. Bray, J. K. Clegg, E. C. Constable, C. E. Housecroft, K. A. Jolliffe, C. J. Kepert, L. F. Lindoy, M. Neuburger, D. J. Price, S. Schaffner and F. Schaper, *Inorg. Chim. Acta*, 2008, **accepted**.
166. E. C. Constable and A. M. W. C. Thompson, *J. Chem. Soc., Dalton Trans.*, 1992, 2947-2950.
167. E. C. Constable, E. L. Dunphy, C. E. Housecroft, M. Neuburger, S. Schaffner, F. Schaper and S. R. Batten, *Dalton Trans.*, 2007, 4323-4332.
168. L. Hou, D. Li, W.-J. Shi, Y.-G. Yin and S. W. Ng, *Inorg. Chem.*, 2005, **44**, 7825-7832.
169. J. Pitarch Lopez, W. Kraus, G. Reck, A. Thuenemann and D. G. Kurth, *Inorg. Chem. Commun.*, 2005, **8**, 281-284.
170. S. Hayami, K. Hashiguchi, G. Juhasz, M. Ohba, H. Okawa, Y. Maeda, K. Kato, K. Osaka, M. Takata and K. Inoue, *Inorg. Chem.*, 2004, **43**, 4124-4126.
171. A. Auffrant, A. Barbieri, F. Barigelletti, J.-P. Collin, L. Flamigni, C. Sabatini and J.-P. Sauvage, *Inorg. Chem.*, 2006, **45**, 10990-10997.
172. J. P. Collin, S. Guillerez, J. P. Sauvage, F. Barigelletti, L. De Cola, L. Flamigni and V. Balzani, *Inorg. Chem.*, 1991, **30**, 4230-4238.
173. F. Barigelletti, L. Flamigni, V. Balzani, J.-P. Collin, J.-P. Sauvage, A. Sour, E. C. Constable and A. M. W. Cargill Thompson, *J. Am. Chem. Soc.*, 1994, **116**, 7692-7699.

174. S. Bernhard, J. I. Goldsmith, K. Takada and H. D. Abruna, *Inorg. Chem.*, 2003, **42**, 4389-4393.
175. E. C. Constable and A. M. W. C. Thompson, *New J. Chem.*, 1996, **20**, 65-82.
176. E. C. Constable, M. J. Hannon and D. A. Tocher, *J. Chem. Soc., Dalton Trans.*, 1993, 1883-1890.
177. M. Abrahamsson, M. Jaeger, R. J. Kumar, T. Oesterman, P. Persson, H.-C. Becker, O. Johansson and L. Hammarstroem, *J. Am. Chem. Soc.*, 2008, **130**, 15533-15542.
178. F. S. Han, M. Higuchi and D. G. Kurth, *Adv. Mater.*, 2007, **19**, 3928-3931.
179. F. S. Han, M. Higuchi and D. G. Kurth, *J. Am. Chem. Soc.*, 2008, **130**, 2073-2081.
180. M. Kimura, T. Horai, T. Muto, K. Hanabusa and H. Shirai, *Chem. Lett.*, 1999, 1129-1130.
181. K. v. d. Schilden, F. Garcia, H. Kooijman, A. L. Spek, J. G. Haasnoot and J. Reedijk, *Angew. Chem., Int. Ed.*, 2004, **43** 5668.
182. J. Pitarch Lopez, W. Kraus, G. Reck, A. Thuenemann and D. G. Kurth, *Inorg. Chem. Commun.*, 2005, **8**, 281-284.
183. M. Schmittel, B. He, V. Kalsani and J. W. Bats, *Org. Biomol. Chem.*, 2007, **5**, 2395-2403.
184. S. Vaduvescu and P. G. Potvin, *Eur. J. Inorg. Chem.*, 2004, 1763-1769.
185. A. Winter, J. Hummel and N. Risch, *J. Org. Chem.*, 2006, **71**, 4862-4871.
186. C. Serbutoviez, C. Bosshard, G. Knoepfle, P. Wyss, P. Pretre, P. Guenter, K. Schenk, E. Solari and G. Chapuis, *Chem. Mater.*, 1995, **7**, 1198-1206.
187. D. Lupo, H. Ringsdorf, A. Schuster and M. Seitz, *J. Am. Chem. Soc.*, 1994, **116**, 10498-10506.
188. S. Roche, C. Haslam, S. L. Heath and J. A. Thomas, *Chem. Commun.*, 1998, **16**, 1681-1682.
189. L. Hunter and J. A. Marriott, *J. Chem. Soc.*, 1940, 166-170.
190. M. Kambe, Y. Hasegawa and E. Shindo, *Bunseki Kagaku*, 1963, **12**, 63-64.
191. M. Kambe, Y. Hasegawa and E. Shindo, *Bunseki Kagaku*, 1964, **13**, 1218-1223.
192. A. F. Hegarty, P. J. Moroney and F. L. Scott, *J. Chem. Soc., Perkin Trans. 2*, 1973, 1466-1471.
193. L. N. Yakhontov and M. F. Marshalkin, *Tetrahedr. Lett.*, 1973, 2807-2810.

194. K. S. Feldman, N. A. Porter and J. R. Allen, *Templated Organic Synthesis*, 2000, 219-248.
195. *Application: WO, WO Pat.*, 98-US18587, 9916746, 1999.
196. *Application: US, US Pat.*, 99-459046, 6479495, 2002.
197. *Application: WO, WO Pat.*, 97-US20591, 9829407, 1998.
198. *Application: WO, WO Pat.*, 2004-US37476, 2005046603, 2005.
199. *Application: WO, WO Pat.*, 2005-US40706, 2006053109, 2006.
200. J.-L. Schmitt, A.-M. Stadler, N. Kyritsakas and J.-M. Lehn, *Helv. Chim. Acta*, 2003, **86**, 1598-1624.
201. J.-l. Schmitt and J.-m. Lehn, *Helv. Chim. Acta*, 2003, **86**, 3417-3426.
202. X.-Y. Cao, J. Harrowfield, J. Nitschke, J. Ramirez, A.-M. Stadler, N. Kyritsakas-Gruber, A. Madalan, K. Rissanen, L. Russo, G. Vaughan and J.-M. Lehn, *Eur. J. Inorg. Chem.*, 2007, 2944-2965.
203. A.-M. Stadler, N. Kyritsakas and J.-M. Lehn, *Chem. Commun.*, 2004, 2024-2025.
204. A.-M. Stadler, N. Kyritsakas, G. Vaughan and J.-M. Lehn, *Chem. Eur. J.*, 2007, **13**, 59-68.
205. L. H. Uppadine, J.-P. Gisselbrecht and J.-M. Lehn, *Chem. Commun.*, 2004, 718-719.
206. H. Uppadine Lindsay and J.-M. Lehn, *Angew. Chem. Int. Ed.*, 2004, **43**, 240-243.
207. M. Ruben, J.-M. Lehn and G. Vaughan, *Chem. Commun.*, 2003, 1338-1339.
208. A.-M. Stadler, N. Kyritsakas, R. Graff and J.-M. Lehn, *Chem.- Eur. J.*, 2006, **12**, 4503-4522.
209. M. Barboiu, M. Ruben, G. Blasen, N. Kyritsakas, E. Chacko, M. Dutta, O. Radekovich, K. Lenton, D. J. R. Brook and J.-M. Lehn, *Eur. J. Inorg. Chem.*, 2006, 784-792.
210. A.-M. Stadler, F. Puntoriero, S. Campagna, N. Kyritsakas, R. Welter and J.-M. Lehn, *Chem.- Eur. J.*, 2005, **11**, 3997-4009.
211. H. E. Gottlieb, V. Kotlyar and A. Nudelman, *J. Org. Chem.*, 1997, **62**, 7512-7515.
212. E. E. Hamilton, P. E. Fanwick and J. J. Wilker, *J. Am. Chem. Soc.*, 2006, **128**, 3388-3395.

213. *Rodd's Chemistry of Carbon Compounds*, 2nd edn., Elsevier, Amsterdam, 1965.
214. A. J. Blake, P. Hubberstey, U. Suksangpanya and C. L. Wilson, *Dalton*, 2000, 3873-3880.
215. Y. N. Belokon, P. Carta, A. V. Gutnov, V. Maleev, M. A. Moskalenko, L. V. Yashkina, N. S. Ikonnikov, N. V. Voskoboev, V. N. Khrustalev and M. North, *Helv. Chim. Acta*, 2002, **85**, 3301-3312.
216. J. R. Deschamps, D. A. Knight, E. R. Goldman, J. B. Delehanty and E. L. Chang, *Acta Crystallogr. Sect. E*, 2003, **E59**, m916-m918.
217. G. J. Karabatsos and R. A. Taller, *Tetrahedron*, 1968, **24**, 3557-3568.
218. U. S. Schuber, H. Hofmeier and G. R. Newkome, *Modern Terpyridine Chemistry*, Wiley-VCH, Weinheim, 2006.
219. G. J. Karabatsos and C. E. Osborne, *Tetrahedron*, 1968, **24**, 3361-3368.
220. A. Hergold-Brundic, Z. Popovic and D. Matkovic-Calogovic, *Acta Crystallogr., Sect.C: Cryst. Struct. Commun.*, 1996, **52**, 3154.
221. A. Kochel, *Acta Crystallogr., Sect. E*, 2006, **62**, m37.
222. A. Jerschow and N. Muller, *J. Mag. Res.*, 1997, **125**, 372-375.
223. M. G. B. Drew, M. J. Hudson, P. B. Iveson, M. L. Russell, J.-O. Liljenzin, M. Sklberg, L. Spjuth and C. Madic, *J. Chem. Soc., Dalton Trans.*, 1998, 2973-2980.
224. SPARTAN '04, (1991-2004) Wavefunction Inc.
225. E. Farkas, E. A. Enyedy, G. Micera and E. Garribba, *Polyhedron*, 2000, **19**, 1727-1736.
226. M. G. B. Drew and G. R. Willey, *J. Chem. Soc., Perkin Trans. 2*, 1986, 215.
227. F. Kaberia, B. Vickery, G. R. Willey and M. G. B. Drew, *J. Chem. Soc., Perkin Trans. 1*, 1980, 1622-1626.
228. B. Vickery, G. R. Willey and M. G. B. Drew, *Acta Cryst.*, 1985, **C41**, 1072-1075.
229. L. Cook Joanne, A. Hunter Christopher, M. R. Low Caroline, A. Perez-Velasco and G. Vinter Jeremy, *Angew Chem Int Ed Engl FIELD Full Journal Title: Angewandte Chemie (International ed. in English)*, 2007, **46**, 3706-3709.
230. L. Lunazzi, C. Magagnoli, M. Guerra and D. Macciantelli, *Tetrahedron Lett.*, 1979, 3031-3032.
231. M. S. Gordon, S. A. Sojka and J. G. Krause, *J. Org. Chem.*, 1984, **49**, 97-100.

232. K. Neuvonen, F. Fueloep, H. Neuvonen, A. Koch, E. Kleinpeter and K. Pihlaja, *J. Org. Chem.*, 2003, **68**, 2151-2160.
233. P. W. Westerman, R. E. Botto and J. D. Roberts, *J. Org. Chem.*, 1978, **43**, 2590-2596.
234. C. Berthon and M. S. Grigoriev, *Acta Crystallogr., Sect. E*, 2005, **E61**, o1216-o1217.
235. C.J.Kepert, B.W.Skelton and A.H.White, *Aust.J.Chem.*, 1994, **47**, 391.
236. I. A. Charushnikova and C. Den Auwer, *Russ. J. Coord. Chem.*, 2004, **30**, 511-519.
237. W. Huang and H. Qian, *J. Mol. Struct.*, 2007, **832**, 108-116.
238. P. C. Junk, C. J. Kepert, L. I. Semenova, B. W. Skelton and A. H. White, *Z. Anorg. Allge. Chem.*, 2006, **632**, 1293-1302.
239. M.G.B.Drew, P.B.Iveson, M.J.Hudson, J.O.Liljenzin, L.Spjuth, P.-Y.Cordier, A.Enarsson, C.Hill and C.Madic, *J. Chem. Soc., Dalton Trans.*, 2000, 821.
240. K. N. Robertson, P. K. Bakshi, S. D. Lantos, T. S. Cameron and O. Knop, *Can. J. Chem.*, 1998, **76**, 583-611.
241. G. Tosi, L. Cardellini and G. Bocelli, *Acta Crystallogr., Sect. B*, 1988, **B44**, 55-63.
242. E. Chiba, K. Tani, M. Shuto, N. Haga and M. Tokonami, *Acta Crystallogr., Sect. C*, 1990, **C46**, 414-417.
243. M. Nagel and R. Allmann, *Crys. Struct. Commun.*, 1981, **10**, 905-908.
244. G. Tosi, P. Bruni, L. Cardellini and G. Bocelli, *Gaz. Chim. Ital.*, 1984, **114**, 111-115.
245. A.Kochel, *Acta Crystallogr., Sect.E:Struct.Rep.Online*, 2006, **62**, m37.
246. C. J. Kepert, W. Lu, B. W. Skelton and A. H. White, *Aust. J. Chem.*, 1994, **47**, 365-384.
247. W. Huang and H. Qian, *Journal of Molecular Structure*, 2007, **832**, 108-116.
248. G. J. Karabatsos and R. A. Taller, *J. Am. Chem. Soc.*, 1963, **85**, 3624-3629.
249. D.-J. X. Shang Shan, Jing-Yun Wu, Michael Y. Chiang, *Acta Crystallogr. Sect. E*, 2002, **E58**, o1333-o1335.
250. G. Lowe, A. S. Droz, T. Vilaivan, G. W. Weaver, L. Tweedale, J. M. Pratt, P. Rock, V. Yardley and S. L. Croft, *J. Med. Chem.*, 1999, **42**, 999-1006.

251. E. C. Constable and M. D. Ward, *J. Chem. Soc., Dalton Trans.*, 1990, 1405-1409.
252. *COLLECT Software*, (1997–2001) Nonius BV.
253. A. Altomare, M. C. Burla, M. Camalli, G. L. Cascarano, C. Giocavazzo, A. Guagliardi, A. G. C. Moliterni, G. Polidori and S. Spagna, *J. Appl. Crystallogr.*, 1999, **32**, 115.
254. *XRED v. 1.08*, (1996) XRED v. 1.08, Stoe & Cie Software.
255. G. M. Sheldrick and SHELXS86, Univ. of Göttingen, Germany, Editon edn., 1986.
256. Z. Otwinowski and W. Minor, *Methods in Enzymology*, Academic Press, New York, USA, 1997.
257. P. W. Betteridge, J. R. Carruthers, R. I. Cooper, K. Prout and D. J. Watkin, *J. Appl. Crystallogr.*, 2003, 1487.
258. G. M. Sheldrick, *Acta Crystallogr., Sect. A*, 2008, **A64**, 112-122.
259. P. O. D. Offenhartz, P. George and G. P. Haight, Jr., *J. Phys. Chem.*, 1963, **67**, 116-118.
260. E. C. Constable, E. Figgemeier, C. E. Housecroft, J. Olsson and Y. C. Zimmermann, *Dalton Trans.*, 2004, 1918-1927.
261. M. Sjoedin, J. Gaetjens, L. C. Tabares, P. Thuery, V. L. Pecoraro and S. Un, *Inorg. Chem.*, 2008, **47**, 2897-2908.
262. K. T. Potts, D. A. Usifer, A. Guadalupe and H. D. Abruna, *J. Am. Chem. Soc.*, 1987, **109**, 3961-3967.
263. L. M. E. Figgemeier, B. A. Hermann, Y. C. Zimmermann, C. E. Housecroft, H.-J. Guentherodt, E. C. Constable, *J. Phys. Chem. B*, 2003, **107**, 1157-1162.
264. A. S. I. P. Evans, and G. Wilkinson, *J. Chem. Soc., Dalton Trans.*, 1973, 204.
265. K. T. Potts, in *Organic Syntheses Collective*, Editon edn., 1990, vol. 7, p. 476.
266. P. H. Dinolfo and J. T. Hupp, *Chem. Mater.*, 2001, **13**, 3113-3125.
267. C. J. Kepert, *Chem. Commun.*, 2006, 695-700.
268. M. Ruben, J. Rojo, F. J. Romero-Salguero, L. H. Uppadine and J.-M. Lehn, *Angew. Chem., Int. Ed.*, 2004, **43**, 3644-3662.
269. A. P. Smith, C. L. Fraser, E. J. A. McCleverty and T. J. Meyer, *Comprehensive Coordination Chemistry II*, Elsevier, Oxford, 2004.
270. C. Laes, A. Katz and M. W. Hosseini, *Chem. Rev.*, 2000, **100**, 3553.

271. E. C. Constable, *Tetrahedron*, 1992, **48**, 10013-10059.
272. E. C. Constable and E. Schofield, *Chem. Commun.*, 1998, 403-404.
273. E. C. Constable, E. L. Dunphy, C. E. Housecroft, W. Kylberg, M. Neuburger, S. Schaffner, E. R. Schofield and C. B. Smith, *Chem. -Eur. J.*, 2006, **12**, 4600-4610.
274. E. C. Constable, C. E. Housecroft, M. Neuburger, S. Schaffner and F. Schaper, *Inorg. Chem. Commun.*, 2006, **9**, 433-436.
275. E. C. Constable, C. E. Housecroft, M. Neuburger, S. Schaffner and F. Schaper, *Inorg. Chem. Commun.*, 2006, **9**, 616-619.
276. R. P. Thummel, *Comprehensive Coordination Chemistry II*, Elsevier, Oxford, 2004.
277. E. C. Constable, A. M. W. C. Thompson and D. A. Tocher, *Supramolecular Chemistry*, Kluwer Academic Press, Dordrecht, 1992.
278. E. C. Constable and A. M. W. C. Thompson, *Journal of the Chemical Society, Dalton Transactions: Inorganic Chemistry (1972-1999)*, 1992, 3467-3475.
279. E. C. Constable, C. E. Housecroft, A. C. Thompson, P. Passaniti, S. Silvi, M. Maestri and A. Credi, *Inorg. Chim. Acta*, 2007, **360**, 1102-1110.
280. E. C. Constable, C. E. Housecroft, M. Neuburger, D. Phillips, P. R. Raithby, E. Schofield, E. Sparr, D. A. Tocher, M. Zehnder and Y. Zimmermann, *Dalton*, 2000, 2219-2228.
281. K. J. Arm and J. A. G. Williams, *Dalton Trans.*, 2006, 2172-2174.
282. H. Uppadine Lindsay, J.-P. Gisselbrecht and J.-M. Lehn, *Chem. Commun.*, 2004, 718-719.
283. S.-S. Sun and A. J. Lees, *Inorg. Chem.*, 2001, **40**, 3154-3160.
284. S.-S. Sun, A. S. Silva, I. M. Brinn and A. J. Lees, *Inorg. Chem.*, 2000, **39**, 1344-1345.
285. A. Winter and U. S. Schubert, *Polymer Preprints*, 2007, **48**, 693-694.
286. A. Winter and U. S. Schubert, *Macromol. Chem. Phys.*, 2007, **208**, 1956-1964.
287. C. V. K. Sharma, G. A. Broker, J. G. Huddleston, J. W. Baldwin, R. M. Metzger and R. D. Rogers, *J. Am. Chem. Soc.*, 1999, **121**, 1137-1144.
288. G. J. E. Davidson and S. J. Loeb, *Dalton Trans.*, 2003, 4319-4323.
289. C. R. Mayer, F. Dumur, F. Miomandre, E. Dumas, T. Devic, C. Fosse and F. Secheresse, *New. J. Chem.*, 2007, **31**, 1806-1814.

290. S. K. Padhi, R. Sahu and V. Manivannan, *Polyhedron*, 2008, **27**, 2221-2225.
291. C. M. Ollagnier, D. Nolan, C. M. Fitchett and S. M. Draper, *Inorg. Chem. Commun.*, 2007, **10**, 1045-1048.
292. W. Goodall and J. A. G. Williams, *Dalton*, 2000, 2893-2895.
293. M. Licini and J. A. G. Williams, *Chem. Commun.*, 1999, 1943-1944.
294. N. Masuhara, S. Hayami, N. Motokawa, A. Shuto, K. Inoue and Y. Maeda, *Chem. Lett.*, 2007, **36**, 90-91.
295. S. K. Padhi, D. Saha, R. Sahu, J. Subramanian and V. Manivannan, *Polyhedron*, 2008, **27**, 1714-1720.
296. N. Noshiranzadeh, A. Ramazani, A. Morsali, A. D. Hunter and M. Zeller, *Inorg. Chim. Acta*, 2007, **360**, 3603-3609.
297. N. Yoshikawa, S. Yamabe, N. Kanehisa, Y. Kai, H. Takashima and K. Tsukahara, *Eur. J. Inorg. Chem.*, 2007, 1911-1919.
298. H. Feng, X.-P. Zhou, T. Wu, D. Li, Y.-G. Yin and S. W. Ng, *Inorg. Chim. Acta*, 2006, **359**, 4027-4035.
299. R. Indumathy, S. Radhika, M. Kanthimathi, T. Weyhermuller and B. Unni Nair, *J. Inorg. Biochem.*, 2007, **101**, 434-443.
300. S.-S. Zhang, S.-Z. Zhan, M. Li, R. Peng and D. Li, *Inorg. Chem.*, 2007, **46**, 4365-4367.
301. J. E. Beves, B. E. Chapman, P. W. Kuchel, L. F. Lindoy, J. McMurtrie, M. McPartlin, P. Thordarson and G. Wei, *Dalton Trans.*, 2006, 744-750.
302. J. Wang, Y.-Q. Fang, G. S. Hanan, F. Loiseau and S. Campagna, *Inorg. Chem.*, 2005, **44**, 5-7.
303. Z.-J. Hu, J.-X. Yang, Y.-P. Tian, X.-T. Tao, L. Tian, H.-P. Zhou, G.-B. Xu, W.-T. Yu, Y.-X. Yan, Y.-H. Sun, C.-K. Wang, X.-Q. Yu and M.-H. Jiang, *Bull. Chem. Soc. Japan*, 2007, **80**, 986-993.
304. K. Ogura, T. Uchida, M. Noguchi, M. Minoguchi, A. Murata, M. Fujita and K. Ogata, *Tetrahed. Lett.*, 1990, **31**, 3331-3334.
305. O. Hagemann, M. Jorgensen and F. C. Krebs, *J. Org. Chem.*, 2006, **71**, 5546-5559.
306. E. M. Sussuchi, A. A. De Lima and W. F. De Giovani, *Polyhedron*, 2006, **25**, 1457-1463.
307. S. Tu, T. Li, F. Shi, Q. Wang, J. Zhang, J. Xu, X. Zhu, X. Zhang, S. Zhu and D. Shi, *Synthesis*, 2005, 3045-3050.

308. F. Tessore, D. Roberto, R. Ugo, M. Pizzotti, S. Quici, M. Cavazzini, S. Bruni and F. De Angelis, *Inorg. Chem.*, 2005, **44**, 8967-8978.
309. S. Tu, T. Li, F. Shi, F. Fang, S. Zhu, X. Wei and Z. Zong, *Chem. Lett.*, 2005, **34**, 732-733.
310. T. Mutai, J.-D. Cheon, S. Arita and K. Araki, *J. Chem. Soc., Perkin Trans. 2*, 2001, 1045-1050.
311. C. Chamchoumis and P. G. Potvin, *J. Chem. Res. (S)*, 1998, 180-181, 870-875.
312. P. Korall, A. Boerje, P.-O. Norrby and B. Aakermark, *Acta Chim. Scand.*, 1997, **51**, 760-766.
313. W. Spahni and G. Calzaferri, *Helv. Chim. Acta*, 1984, **67**, 450-454.
314. J. Sauer, D. K. Heldmann and G. R. Pabst, *Eur. J. Org. Chem.*, 1999, 313-321.
315. B. R. Manzano, F. A. Jalon, I. M. Ortiz, M. L. Soriano, F. Gomez de la Torre, J. Elguero, M. A. Maestro, K. Mereiter and T. D. W. Claridge, *Inorg. Chem.*, 2008, **47**, 413-428.
316. F. Texier-Boullet, B. Klein and J. Hamelin, *Synthesis*, 1986, 409-411.
317. R. Sreekumar and R. Padmakumar, *Synth. Commun.*, 1998, **28**, 1661-1665.
318. Y. Han and H. V. Huynh, *Chem. Commun.*, 2007, 1089-1091.
319. in *Rodd's Chemistry of Carbon Compounds, Part B, 2nd Ed., vol. 1*, ed. S. Coffey, Elsevier, Amsterdam, Editon edn., 1965, pp. 68-71.
320. J. S. Choi, C. W. Kang, K. Jung, J. W. Yang, Y.-G. Kim and H. Han, *J. Am. Chem. Soc.*, 2004, **126**, 8606-8607.
321. M. Ishihara, T. Tsuneya, M. Shiga, S. Kawashima, K. Yamagishi, F. Yoshida, H. Sato and K. Uneyama, *J. Agric. Food Chem.*, 1992, **40**, 1647-1655.
322. C. Mikel and P. G. Potvin, *Polyhedron*, 2002, **21**, 49-54.
323. I. P. Evans, A. Spencer and G. Wilkinson, *Journal of the Chemical Society, Dalton Transactions: Inorganic Chemistry (1972-1999)*, 1973, 204-209.
324. M. Lamsa, J. Huuskonen, K. Rissanen and J. Pursiainen, *Chem.- Eur. J.*, 1998, **4**, 84-92.
325. D. Chartrand, I. Theobald and G. S. Hanan, *Acta Crystallogr., Sect. E*, 2007, **E63**, m1561.
326. C. Coudret, *Synth. Commun.*, 1996, **26**, 3543-3547.
327. M. I. Arriortua, T. Rojo, J. M. Amigo, G. Germain and J. P. Declercq, *Bull. Soc. Chim. Belg.*, 1982, **91** 337.

328. G. U. Priimov, P. Moore, P. K. Maritim, P. K. Butalanyi and N. W. Alcock, *Dalton*, 2000, 445.
329. C. Alonso, L. Ballester, A. Gutierrez, M. F. Perpinan, A. E. Sanchez and M. T. Azcondo, *Eur. J. Inorg. Chem.*, 2005, 486.
330. N. W. Alcock, P. R. Barker, J. M. Haider, M. J. Hannon, C. L. Painting, Z. Pikramenou, E. A. Plummer, K. Rissanen and P. Saarenketo, *J. Chem. Soc., Dalton Trans.*, 2000, 1447.
331. R. K. M. Nayak, H. Stoeckli-Evans, S. Mohanta, *Cryst. Growth Design*, 2005, **5**.
332. N. D. Draper, R. J. Batchelor, P. M. Aguiar, S. Kroeker and D. B. Leznoff, *Inorg. Chem.*, 2004, **43** 6557.
333. E. C. Constable, J. Lewis, M. C. Liptrot and P. R. Raithby, *Inorganica Chimica Acta*, 1990, **178**, 47-54.
334. M.L. Calatayud, J. Sletten, M. Julve and I. Castro, *J. Mol. Struct.*, 2005, **741**, 121.
335. E. Freire, S. Baggio and R. Baggio, *Aust. J. Chem.*, 2001, **54** 131.
336. G. M. Intille, C. E. Pfluger and W. A. B. Jr, *Cryst. Struct. Commun.* , 1973, **2**, 217.
337. G. R. Desiraju and T. Steiner, *The Weak Hydrogen Bond*, Oxford University Press, Oxford, 1999.
338. R. Cini, A. Donati and R. Giannettoni, *Inorg. Chim. Acta*, 2001, **315**, 73.
339. J. D. Crowley, A. J. Goshe, I. M. Steele and B. Bosnich, *Chem. Eur. J.* , 2004, **10**, 1944.
340. A. J. Goshe, I. M. Steele and B. Bosnich, *Inorg. Chim. Acta* 2004, **357** 4544.
341. X. Liu, E. J. L. McInnes, C. A. Kilner, M. Thornton-Pett and M. A. Halcrow, *Polyhedron*, 2001, **20** 2889.
342. T. J. Wadas, Q.-M. Wang, Y.-J. Kim, C. Flaschenreim, T. N. Blanton and R. Eisenberg, *J. Am. Chem. Soc.*, 2004, **126** 16841.
343. R. Buchner, C. T. Cunningham, J. S. Field, R. J. Haines, D. R. McMillin and G. C. Summerton, *J. Chem. Soc., Dalton Trans.*, 1999, 711.
344. J. S. Field, J.-A. Gertenbach, R. J. Haines, L. P. Ledwaba, N. T. Mashapa, D. R. McMillin, O. Q. Munro and G. C. Summerton, *Dalton Trans.*, 2003, 1176.
345. J. S. Field, R. J. Haines, D. R. McMillin and G. C. Summerton, *J. Chem. Soc., Dalton Trans.*, 2002, 1369.

346. C. S. Angle, A. G. DiPasquale, A. L. Rheingold and L. H. Doerrer, *Acta Crystallogr., Sect. C*, 2006, **62** m340.
347. A. J. Goshe, I. M. Steele and B. Bosnich, *J. Am. Chem. Soc.*, 2003, **125** 444.
348. R. Okamura, T. Wada, K. Aikawa, T. Nagata and K. Tanaka, *Inorg. Chem.*, 2004, **43** 7210.
349. A. Sengul, *Turk. J. Chem.*, 2004, **28** 667.
350. A. Sengul, *Turk. J. Chem.*, 2005, **29** 571.
351. B.-C. Tzeng, G.-H. Lee and S.-M. Peng, *Inorg. Chem. Commun.*, 2003, **6** 1341.
352. J. A. Bailey, M. G. Hill, R. E. Marsh, V. M. Miskowski, W. P. Schaefer and H. B. Gray, *Inorg. Chem.*, 1995, **34** 4591.
353. J. Coleman Paul, M. Brashear Karen, C. Askew Ben, H. Hutchinson John, A. McVean Carol, T. Duong Le, P. Feuston Bradley, C. Fernandez-Metzler, A. Gentile Michael, D. Hartman George, B. Kimmel Donald, C.-T. Leu, L. Lipfert, K. Merkle, B. Pennypacker, T. Prueksaritanont, A. Rodan Gideon, A. Wesolowski Gregg, B. Rodan Sevgi and E. Duggan Mark, *J. Med. Chem.*, 2004, **47**, 4829-4837.
354. C. B. Smith, C. L. Raston and A. N. Sobolev, *Green Chem.*, 2005, **7**, 650-654.
355. C. Rajadurai, F. Schramm, S. Brink, O. Fuhr, M. Ghafari, R. Kruk and M. Ruben, *Inorg. Chem.*, 2006, **45**, 10019.
356. S. M. Neville, B. Moubaraki, K. S. Murray and C. J. Kepert, *Angew. Chem., Int. Ed.*, 2007, **46**, 2059.
357. G. J. Halder, C. J. Kepert, B. Moubaraki, K. S. Murray and J. D. Cashion, *Science*, 2002, **298**, 1762.
358. U. Mueller, *Acta Crystallogr., Sect. B*, 1977, **33**, 2197.
359. A. W. Addison, R. J. Butcher, Z. Homonnay, V. V. Pavlishchuk, M. J. Prushan and L. K. Thompson, *Eur. J. Inorg. Chem.*, 2005, 2404.
360. H. Borrmann, I. Persson, M. Sandstroem and C. M. V. Stalhandske, *J. Chem. Soc., Perkin Trans. 2*, 2000, 393.
361. W.-Y. Sun, X.-F. Shi, L. Zhang, J. Hu and J.-H. Wei, *J. Inorg. Biochem.*, 1999, **76**, 259.
362. Y. Tang, Y. Yao, L. Wu, Y. Qin, Y. Kang and Z. Li, *Chem. Lett.*, 2001, **30**, 542.
363. M.-C. Suen and J.-C. Wang, *J. Coord. Chem.*, 2007, **60**, 257.
364. S. H. Rahaman, R. Ghosh, G. Mostafa and B. K. Ghosh, *Inorg. Chem. Commun.*, 2005, **8**, 1137.

365. X.-J. Zhao, J.-H. Guo, H. Jian and M. Du, *Acta Crystallogr., Sect. E*, 2005, **E61**, m913.
366. M. Du, X.-J. Jiang and X.-J. Zhao, *Acta Crystallogr., Sect. E*, 2005, **E61**, m485.
367. K. Biradha, M. Sarkar and L. Rajput, *Chem. Commun.*, 2006, 4169.
368. S. A. Barnett and N. R. Champness, *Coord. Chem. Rev.*, 2003, **246**, 145.
369. E. Tynan, P. Jensen, A. C. Lees, B. Moubarak, K. S. Murray and P. E. Kruger, *CrystEngComm*, 2005, **7**, 90.
370. P. d. Hoog, P. Gamez, M. Lueken, O. Roubeau, B. Krebs and J. Reedijk, *Inorg. Chim. Acta*, 2004, **357**, 213.
371. W.-L. Jia, R.-Y. Wang, D. Song, S. J. Ball, A. B. McLean and S. Wang, *Chem.–Eur. J.*, 2005, **11**, 832.
372. H. E. Heldal and J. Sletten, *Acta Chem. Scand.*, 1997, **51**, 122.
373. A. M. Thomas, M. Nethaji, S. Mahadevan and A. R. Chakravorty, *J. Inorg. Biochem.*, 2003, **94**, 171.
374. S. S. Tandon, L. Chen, L. K. Thompson, S. P. Connors and J. N. Bridson, *Inorg. Chim. Acta*, 1993, **213**, 289.
375. A. Jouaiti, M. W. Hosseini and N. Kyritsakas, *Chem. Commun.*, 2002, 1898.
376. L. Carlucci, G. Ciani and D. M. Proserpio, *Coord. Chem. Rev.*, 2003, **246**, 247.
377. S. R. Batten, *CrystEngComm*, 2001, **3**, 67.
378. R. Robson, in *Comprehensive Supramolecular Chemistry*, eds. J. L. Atwood, J. E. D. Davies, D. D. Macnicol and F. Voegtle, Pergamon, Editon edn., 1996, vol. 6, ch. 22, p. 733.
379. A. Y. Robin and K. M. Fromm, *Coord. Chem. Rev.*, 2006, **250**, 2127-2157.
380. C. A. Black, L. R. Hanton and M. D. Spicer, *Chem. Commun.*, 2007, 3171-3173.
381. D. A. Beauchamp and S. J. Loeb, *Chem. Commun.*, 2002, 2484-2485.
382. A. B. Mallik, S. Lee and E. B. Lobkovsky, *Cryst. Growth Design*, 2005, **5**, 609-616.
383. F. Thebault, S. A. Barnett, A. J. Blake, C. Wilson, N. R. Champness and M. Schroeder, *Inorg. Chem.*, 2006, **45**, 6179-6187.
384. C. Naether and I. Jess, *Eur. J. Inorg. Chem.*, 2004, 2868-2876.
385. T. Kogane, N. Koyama, T. Ishida and T. Nogami, *Polyhedron*, 2007, **26**, 1811-1819.

386. S.-i. Ohkoshi, Y. Tsunobuchi, H. Takahashi, T. Hozumi, M. Shiro and K. Hashimoto, *J. Am. Chem. Soc.*, 2007, **129**, 3084-3085.
387. J. L. Manson, T. Lancaster, L. C. Chapon, S. J. Blundell, J. A. Schlueter, M. L. Brooks, F. L. Pratt, C. L. Nygren and J. S. Qualls, *Inorg. Chem.*, 2005, **44**, 989-995.
388. G. Beobide, O. Castillo, A. Luque, U. Garcia-Couceiro, J. P. Garcia-Teran and P. Roman, *Dalton Trans.*, 2007, 2669-2680.
389. T. Ishida, L. Yang and T. Nogami, *Chem. Lett.*, 2003, 1018-1019.
390. A. Galet, M. C. Munoz, A. B. Gaspar and J. A. Real, *Inorg. Chem.*, 2005, **44**, 8749-8755.
391. J. L. Manson, J. A. Schlueter and C. L. Nygren, *Dalton Trans.*, 2007, 646-652.
392. C. Naether, G. Bhosekar and I. Jess, *Inorg. Chem.*, 2007, **46**, 8079-8087.
393. G. Agusti, A. Belen Gaspar, M. C. Munoz and J. A. Real, *Inorg. Chem.*, 2007, **46**, 9646-9654.
394. R. Feyerherm, S. Abens, D. Guenther, T. Ishida, M. Meschke, T. Nogami and M. Steiner, *J. Phys.: Condens. Matter.*, 2000, **12**, 8495.
395. O. Kahn, *Molecular Magnetism*, Wiley VCH Publishers, New York, 1993.
396. T. J. Batterham, *NMR Spectra of Simple Heterocycles*, Wiley & Sons, New York, 1973.
397. R. J. L. Andon, J. D. Cox and E. F. G. Herington, *J. Chem. Soc., Trans. Faraday Soc.*, 1954, **50**, 918-927.
398. C. H. Rochester, *J. Chem. Soc., Sect. B*, 1967, **1**, 33-36.
399. S. M. Neville, G. J. Halder, K. W. Chapman, M. B. Duriska, P. D. Southon, J. D. Cashion, J.-F. Létard, B. Moubaraki, K. S. Murray and C. J. Kepert, *J. Am. Chem. Soc.*, 2008, **130**.

The end (you made it!)